# Petrographic study of well Zeerijp-3A (ZRP-3A)
# Final Report

**PanTerra Geoconsultants**

Date      November 2016

Editors    Clemens Visser, Jan van Elk & Dirk Doornhof

# General Introduction

Petrography focusses on the mineral content and the textural relationships within rocks. In this report, the results of a petrographic analysis of 25 samplesfrom well Zeerijp-3A (ZRP-3A) in the Groningen field is presented. The data in this report has been compared with other petrographic data from the Groningen field (Ref. 1). Well ZRP-3A was cored over a large section. The analytical program for the core not only includes this detailed petrographic description, but also extensive experiments to determine rock compaction and rupture.

Furthermore, the well has been equipped with a fibre-optic cable for temperature, compaction and seismic monitoring. All these studies will use the current report as a reference document.

Many of the important properties of the reservoir rock depend on the detailed mineral content and the textural relationships within the rock. An important example is rock permeability that impacts on the flow and pressure changes within the reservoir. The petrographic data obtained from this well have also been used to characterize the distribution of properties in the Groningen reservoir model.

This report is therefore important for geology studies and reservoir engineering studies (Ref. 2, 3 and 4).
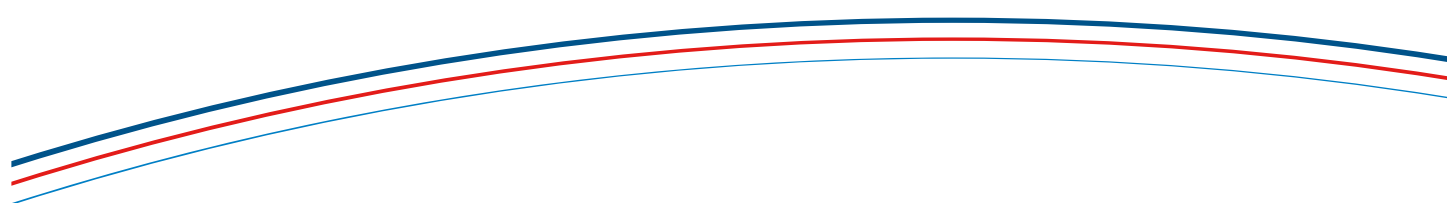
# References

1.   Petrographic Aspects of the Rotliegend of the Groningen Field, Inventory and quick-look analysis of petrographic data from the Groningen field, Clemens Visser, August 2016
2.   Supplementary Information to the Technical Addendum of the Winningsplan 2013, Nederlandse Aardolie Maatschappij BV (Jan van Elk and Dirk Doornhof, eds), December 2013.
3.   Groningen Field Review 2015 Subsurface Dynamic Modelling Report, Burkitov, Ulan, Van Oeveren, Henk, Valvatne, Per, May 2016.
4.   Technical Addendum to the Winningsplan Groningen 2016 - Production, Subsidence, Induced Earthquakes and Seismic Hazard and Risk Assessment in the Groningen Field, PART I – Summary and Production,

| Title | **Petrographic study of well Zeerijp-3A (ZRP-3A)** | | | **Date** | November 2016 |
|---|---|---|---|---|---|
| | | | | **Initiator** | NAM |
| **Autor(s)** | **PanTerra Geoconsultants** | | **Editors** | Clemens Visser, Jan van Elk Dirk Doornhof | |
| **Organisation** | PanTerra Geocnsultants | | **Organisation** | NAM | |
| **Place in the Study and Data Acquisition Plan** | <u>Study Theme:</u> Groningen Reservoir Model <br> <u>Comment:</u> <br> Petrography focusses on the mineral content and the textural relationships within the rock. In this report the petrographic data from well Zeerijp-3A (ZRP-3A) in the Groningen field is presented. The data in this report has been compiled with other petrographic data from the Groningen field (Ref. 1). The well was cored over a large section. This core was not only used for this detailed petrographic description, but also core experiment to determine rock compaction and rupture. <br> Furthermore, the well has been equipped with a fibre-optic cable for temperature, compaction and seismic minoring. All these studies will use the current report as a reference document. <br> Many of the important properties of the reservoir rock depend on the detailed mineral content and the textural relationships within the rock. An important example is rock permeability that impacts on the flow and pressure changes within the reservoir. The petrographic data obtained from this well has also been used to update the <br> This report is therefore important for geology studies and reservoir engineering studies (Ref. 2, 3 and 4). | | | | |
| **Directliy linked research** | (1) Reservoir engineering studies in the pressure depletion for different production scenarios. <br> (2) Subsidence and compaction studies. <br> (3) Studies on the core acquired in well Zeerijp-3A (ZRP-3A) | | | | |
| **Used data** | | | | | |
| **Associated organisation** | NAM | | | | |
| **Assurance** | PanTerra Geocnsultants and NAM | | | | |

# Petrographic study of well Zeerijp-3A (ZRP-3A)
## Final Report
September 2016

# Petrographic study of well Zeerijp-3A (ZRP-3A)

**Authors**
Resi Veeningen
Sven Könitzer

*Reviewed by*
Marita Felder

**Prepared for**
Nederlandse Aardolie Maatschappij B.V.
Postbus 28000
9400 HH Assen
The Netherlands

**Prepared by**
PanTerra Geoconsultants B.V.
Weversbaan 1-3
2352 BZ Leiderdorp
The Netherlands
T +31 (0)71 581 35 05
F +31 (0)71 301 08 02
info@panterra.nl

# Executive summary

At the request of NAM, 25 Slochteren Sandstone samples from the cored interval of well Zeerijp-3A (ZRP-3A) were studied petrographically. The samples were selected by NAM and to prevent a biased result, the depths and gas-water contact were only provided after the first interpretation phase.

Thin sections of all samples were described in detail and point counted. On the same samples XRD (WR and CF), SEM and BSEM was performed. The main objectives were (1) to study diagenetic variations between the samples and (2) investigate whether indications can be found for recent deformation (i.e. compaction in this case) due to gas extraction and related pore pressure reduction.

The sandstone samples are classified as sublitharenites. In all samples quartz is the dominant phase and they contain feldspar (both albite and microcline; based on XRD) and various rock fragments (sedimentary, metamorphic and igneous rock fragments). Feldspar and some types of rock fragments are commonly leached, leaving secondary (micro)pores. The total contents of the individual components vary between the samples.

Authigenic minerals comprise quartz, dolomite, siderite, barite and various clay minerals, including illite, chlorite and kaolinite. Authigenic clay is both pore-filling (intergranular) and replacive (intragranular). All samples contain clay coatings, which strongly vary in type, composition and thickness. These coatings comprise tangential illite, radial illitic clay (locally mixed with chlorite) and, mainly in the water lag, coarser crystalline chlorite rosettes. Some samples have clay coatings that are detached from the detrital grain, with coarse crystalline chlorite rosettes formed in between the detrital grain and the illitic clay coating.

On thin section scale there is no evidence that deformation occurred due to gas extraction. Local quartz cement and chlorite between detached clay coatings and detrital grains argue strongly against recent grain movement and there is no evidence that the cements precipitated at production time scales. Also the fracturing of grains occurred during burial diagenesis, as locally cement (mostly quartz) formed on the fracture surfaces. Grain dissolution pores are not significantly deformed or collapsed and illite fibres that bridge pore throats are not deformed or broken. Thus the compaction observed at the surface was not confined to short depth intervals but occurred most likely over a significant depth range or within a different type of lithology. An open question is whether thick shale units could alternatively have been compacted.

Feldspar and rock fragments content increase towards the top, indicating a change in provenance. The lack of a trend in authigenic (feldspar replacing) clay indicates that this is not (only) linked to diagenesis or the position of the gas water contact. In how much the depositional environment plays a role cannot be judged as a core description is not available. Fe-rich chlorite rosettes are largely restricted to the present day water lag, but results are not consistent with the pre-production gas water contact. Why this is the case cannot be evaluated based on the existing data.
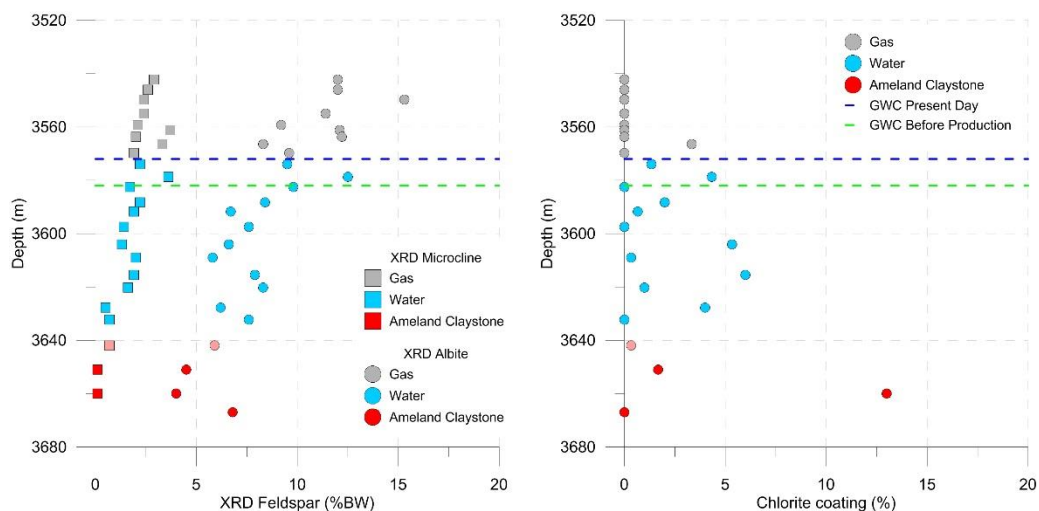


**Feldspar content and chlorite coating content show the most significant depth trends of the sample set. Dashed coloured lines indicate the past (green) and present-day gas-water contact depth.**

# Index of figures

# Index of tables

# Contents

# 1 Introduction

## 1.1 General

At the request of the Nederlandse Aardolie Maatschappij B.V. (NAM), PanTerra Geoconsultants B.V. (PanTerra) performed a detailed petrographic study on 25 trimend samples from the cored interval of well Zeerijp-3A (ZRP-3A; Onshore, The Netherlands (Figure 1-1)). These 25 samples are equally distributed over the gas leg and the water leg within the Rotliegend Group.
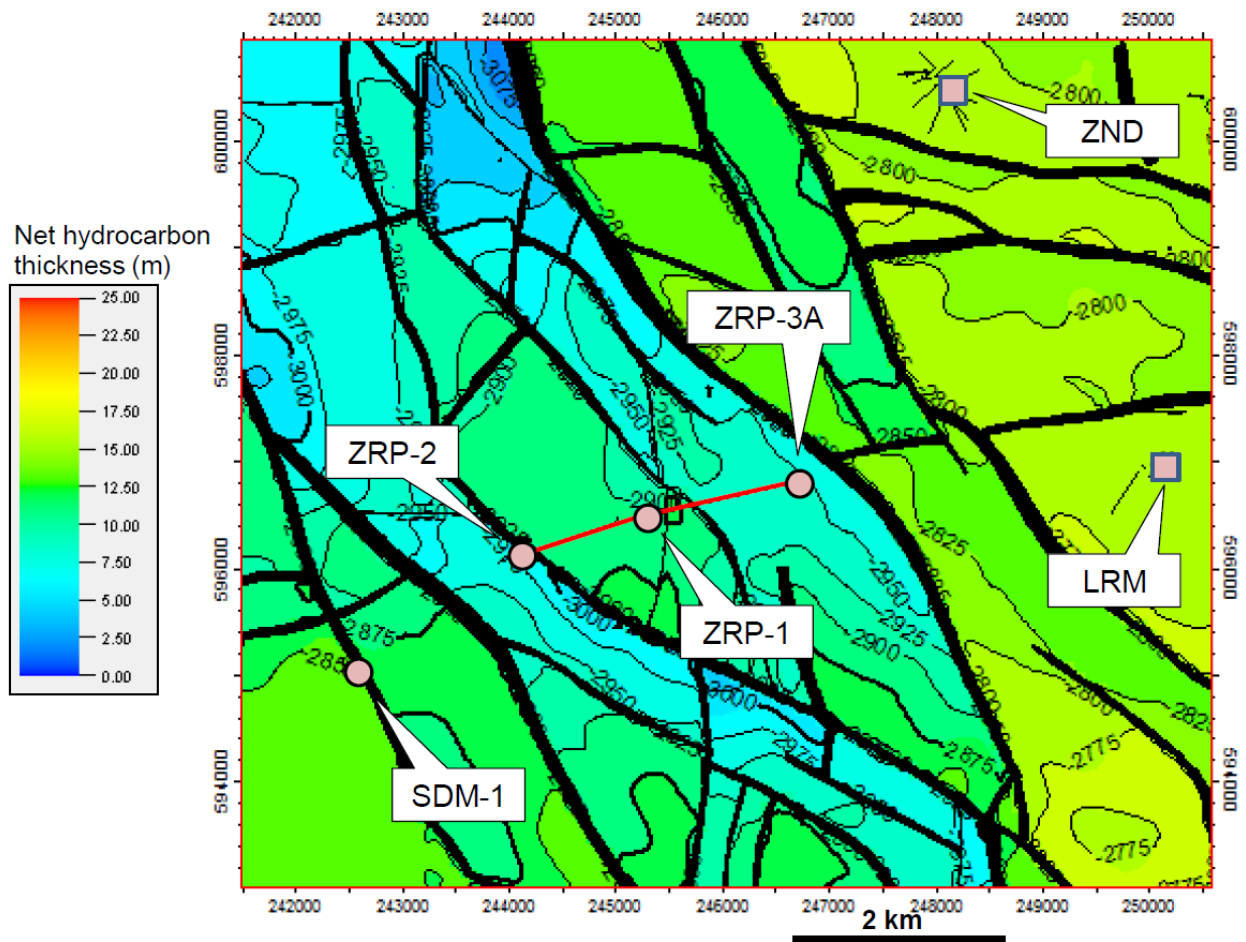


**Figure 1-1: Structural model of the Loppersum Area showing the Zeerijp-3A (ZRP-3A) well location. Image from Winningsplan 2016, Nederlandse Aardolie Maatschappij B.V.**

## 1.2 Objectives

The main objectives of this petrographic study were to:

- Characterise the mineralogy and diagenetic history of the sandstone samples.
- Check for petrographic evidence of grain movement due to gas extraction in the recent times. A special focus lied on the grain contacts and fractured grains.
- Define the (mostly very subtle) differences between the samples or groups of samples. The hypothesis is that there is a (minor) difference between the gas vs. water leg. To prevent a biased interpretation, the initial sample numbers were coded and depths were unknown. These depths were provided after the draft report has been compiled.
- The depth and the position of the samples will be compared with the observations and data to distinguish possible difference related to the gas vs. water leg from other depth related difference, such as composition.

## 1.3 Analytical work

Thin sections were prepared from the 25 trim-ends that were provided by NAM. These thin sections were used to quantify the mineralogy (including authigenic minerals) and porosity by point counting. Scanning Electron Microscopy (SEM & BSEM) on the 25 samples was performed on rock chips (for SEM) and impregnated blocks (for BSEM), to study the mineralogical composition, the grain contacts and the diagenetic history in detail, with a special focus on the clay coatings. EDX, attached to the SEM, aids in the identification of the minerals. Additionally, whole-rock (WR) and clay-fraction (CF) X-ray diffraction (XRD) was performed on the 25 samples. To better understand the diagenetic history, a paragenetic sequence is constructed, based on the observations done under the microscopes.

## 1.4 Samples

A sample list with the plug data, as provided by NAM is shown in Table 1.1. For each sample, there are two sample numbers; a P-number and an R-number. R-numbers are NAM internal numbers (and sorted by depth), whereas the P-number is the number provided by NAM (with a random depth order) prior to the draft report.

| Well | Sample number | Sample No. NAM* | Depth (m)* | Depth (m) | Porosity (%) | Permeability (Kk; mD) | Grain Density (g/cm³) |
|---|---|---|---|---|---|---|---|
| ZRP-3A | P1 | R246 | 3582.50 | n/a | 25.3 | n/a | 2.65 |
| ZRP-3A | P2 | R085 | 3542.25 | n/a | 18.2 | 17.0 | 2.66 |
| ZRP-3A | P3 | R378 | 3615.50 | n/a | 28.5 | 189 | 2.66 |
| ZRP-3A | P4 | R212 | 3574.00 | n/a | 26.1 | 185 | 2.65 |
| ZRP-3A | P5 | R283 | 3591.75 | n/a | 26.3 | 233 | 2.66 |
| ZRP-3A | P6 | R182 | 3566.46 | n/a | 20.8 | 72.0 | 2.64 |
| ZRP-3A | P7 | R100 | 3546.00 | n/a | 20.7 | 176 | 2.65 |
| ZRP-3A | P8 | R352 | 3609.00 | n/a | 25.2 | 77.0 | 2.66 |
| ZRP-3A | P9 | R231 | 3578.75 | n/a | 27.3 | n/a | 2.65 |
| ZRP-3A | P10 | R161 | 3561.25 | n/a | 22.0 | 105 | 2.65 |
| ZRP-3A | P11 | R332 | 3604.00 | n/a | 24.4 | n/a | 2.64 |
| ZRP-3A | P12 | R171 | 3563.71 | n/a | 17.4 | 25.0 | 2.66 |
| ZRP-3A | P13 | R154 | 3559.32 | n/a | 27.2 | n/a | 2.64 |
| ZRP-3A | P14 | R306 | 3597.50 | n/a | 21.0 | 31.0 | 2.66 |
| ZRP-3A | P15 | R269 | 3588.25 | n/a | 21.7 | n/a | 2.64 |
| ZRP-3A | P16 | R195 | 3569.75 | n/a | 22.8 | n/a | 2.66 |
| ZRP-3A | P17 | R484 | 3641.95 | n/a | 21.8 | 107 | 2.65 |
| ZRP-3A | P18 | R584 | 3667.03 | n/a | 17.7 | 7.0 | 2.65 |
| ZRP-3A | P19 | R397 | 3620.24 | n/a | 21.7 | n/a | 2.65 |
| ZRP-3A | P20 | R115 | 3549.75 | n/a | 18.1 | 53.0 | 2.66 |
| ZRP-3A | P21 | R556 | 3660.00 | n/a | 20.8 | 41.0 | 2.66 |
| ZRP-3A | P22 | R427 | 3627.74 | n/a | 17.3 | 11.0 | 2.66 |
| ZRP-3A | P23 | R520 | 3651.00 | n/a | 14.4 | 2.2 | 2.67 |
| ZRP-3A | P24 | R136 | 3555.05 | n/a | 24.1 | n/a | 2.66 |
| ZRP-3A | P25 | R445 | 3632.25 | n/a | 17.9 | 14.0 | 2.67 |

*Depth and sample no. obtained after draft

**Table 1.1: Sample list including the core analysis data.**

# 2  Petrography

This chapter describes the petrography of 25 plug trim-ends from well ZRP-3A, selected by NAM with a random depth order. The depths are unknown by the petrographer during the analysis and were provided after the compilation of the draft report. Therefore the quantitative results and descriptions are unbiased.

The quantitative point count results can be found in Appendix 2. The descriptions per sample and the thin section photoplates are presented in Appendix 4 and the SEM and BSEM images per sample can be found in Appendix 5. For the semi quantitative XRD results and diffractograms, see Appendix 7.

## 2.1  Texture

The textural properties, including sedimentary structures, grain size and grain shape are summarised in Table 2.1. These properties can also be found per individual thin section on the description page of Appendix 4. The textural properties discussed below are all on the thin section scale.

**Lamination:** Most of the 25 studied samples show, on the thin section scale, either a faint lamination or a distinct lamination. 7 samples are structureless, whereas one sample (P2) shows a very faint grain alignment. The lamination is either characterised by a clear grain size variation or variations in the clay content. Those with a very distinct grain size variations (e.g. P7), have two modal grain sizes indicated in Table 2.1, which cover two grain size classes. These samples are regarded as more typical for aeolian depositional environments, while those with less distinct grain size variations are rather fluvial. Sample P17 is not laminated, but it does show a ~1 cm diameter patch enriched in dolomite.

**Grain size:** The grain size is expressed as modal grain size, minimum grain size and maximum grain size. The modal grain size in the sample set varies from very fine grained (U) sand (sample P25), to medium grained (U) sand in some coarser laminae. The structureless sandstone samples are fine (U) or medium (L) grained sandstones, whereas the laminated sandstones vary from very fine grained (U) to medium grained (U) laminae (samples P7, P19). The minimum grain size varies from fine silt (P20) to very fine sand (P2, P6, P8). Most samples have minimum grain size between 31 and 62.5 µm (coarse silt). The maximum grain size ranges from medium grained sand (U), e.g. sample P1, to very coarse grained sand (L), e.g. sample P2.

**Grain shape:** The detrital quartz grains are all sub-angular (SA) to sub-rounded (SR), with little variations between the different samples. Due to small quartz outgrowths, some quartz grains have a more angular appearance. This is especially visible in the samples with detached clay coatings (discussed in the next section), where quartz could form between the coating and the detrital grain, e.g. sample P25. Feldspar grains, which sometimes have a clear cleavage, are locally more elongated, parallel to the cleavage.

**Fractures:** Natural fractures and associated grain breakage are not observed in the sample set. Some samples (e.g. sample P3) have artificial (dilatational) fractures which have formed during sampling or sample preparation. These artificially fractured samples are commonly more friable. Compaction related intragranular fractures do occur in most samples. These vary from a single fracture cutting through a grain (both quartz and feldspar grains) to complete shattering of the grains (mostly mechanically weaker feldspar grains).

| Well | Sample No. | Sample No. NAM* | Depth (m)* | Min (μm) | Max (μm) | Mode (μm) (fine/coarse laminae) | Mode Class (fine/coarse laminae) | Sorting | Roundness | Grain contacts, rigid grains | Grain contacts, ductile grains | Texture | Sample heterogeneity | Fractures | Pore filling Cement (%) | Minus cement porosity (%) | IGV (%) | COPL (%) | CEPL (%) |
|---|---|---|---|---|---|---|---|---|---|---|---|---|---|---|---|---|---|---|---|
| ZRP-3A | P1 | R246 | 3582.50 | 31-62.5 | 350-500 | 177-250 | fine sand (U) | P | SR | P | L-CC | faintly laminated | low to moderate | none | 10.0 | 20.7 | 21 | 31 | 7 |
| ZRP-3A | P2 | R085 | 3542.25 | 88-125 | 1-1.41 mm | 177-250 | fine sand (U) | M-P | SA-SR | P-L | CC | grain alignment | low to moderate | none | 14.0 | 17.7 | 18 | 33 | 9 |
| ZRP-3A | P3 | R378 | 3615.50 | 31-62.5 | 500-710 | 177-250 | fine sand (U) | MG-M | SA-SR | P | L-CC | faintly laminated | low to moderate | artificial | 15.3 | 22.7 | 23 | 29 | 11 |
| ZRP-3A | P4 | R212 | 3574.00 | 62.5-88 | 710-1000 | 250-350 | medium sand (L) | MG-M | SR | P | L-CC | faintly laminated | low to moderate | none | 11.7 | 17.3 | 17 | 33 | 8 |
| ZRP-3A | P5 | R283 | 3591.75 | 62.5-88 | 710-1000 | 250-350 | medium sand (L) | M | SR | P-L | CC | faintly laminated | moderate | none | 10.0 | 20.3 | 20 | 31 | 7 |
| ZRP-3A | P6 | R182 | 3566.46 | 88-125 | 500-710 | 177-250 | fine sand (U) | MG | SA-SR | P-L | L-CC | structureless | low | none | 15.3 | 24.3 | 24 | 27 | 11 |
| ZRP-3A | P7 | R100 | 3546.00 | 31-62.5 | 1-1.41 mm | 125-177/350-500 | fine (L) / medium (U) sand | MG-B | SA | P | L-CC | laminated | moderate | none | 8.3 | 22.0 | 22 | 29 | 6 |
| ZRP-3A | P8 | R352 | 3609.00 | 88-125 | 500-710 | 250-350 | medium sand (L) | MG | SR | P-L | L-CC | structureless | low | none | 12.3 | 17.0 | 17 | 34 | 8 |
| ZRP-3A | P9 | R231 | 3578.75 | 62.5-88 | 500-710 | 177-250 | fine sand (U) | M | SR | P | L | structureless | low to moderate | artificial | 14.0 | 21.3 | 21 | 30 | 10 |
| ZRP-3A | P10 | R161 | 3561.25 | 31-62.5 | 500-710 | 177-250 | fine sand (U) | M-P | SA-SR | P-L | CC | faintly laminated | moderate | none | 9.3 | 14.7 | 15 | 36 | 6 |
| ZRP-3A | P11 | R332 | 3604.00 | 62.5-88 | 710-1000 | 177-250 | fine sand (U) | P | SA-SR | P | CC | laminated | moderate to high | none | 13.3 | 18.7 | 19 | 32 | 9 |
| ZRP-3A | P12 | R171 | 3563.71 | 62.5-88 | 710-1000 | 125-177 | fine sand (L) | P | SA-SR | P-L | CC | irregular lamination | moderate to high | none | 14.3 | 21.3 | 21 | 30 | 10 |
| ZRP-3A | P13 | R154 | 3559.32 | 31-62.5 | 500-710 | 177-250 | fine sand (U) | MG-M | SA-SR | P | L | structureless | low | artificial | 4.7 | 21.0 | 21 | 30 | 3 |
| ZRP-3A | P14 | R306 | 3597.50 | 62.5-88 | 350-500 | 177-250 | fine sand (U) | MG | SA-SR | P | L-CC | structureless | low | none | 18.0 | 23.0 | 23 | 29 | 13 |
| ZRP-3A | P15 | R269 | 3588.25 | 31-62.5 | 710-1000 | 88-125/250-350 | v.fine (U) / medium (L) sand | MG-B | SA-R | P | L-CC | laminated | moderate | none | 12.7 | 16.7 | 17 | 34 | 8 |
| ZRP-3A | P16 | R195 | 3569.75 | 31-62.5 | 710-1000 | 250-350 | medium sand (L) | P | SA-SR | P-L | CC | faintly laminated | low to moderate | none | 9.7 | 15.3 | 15 | 35 | 6 |
| ZRP-3A | P17 | R484 | 3641.95 | 31-62.5 | 710-1000 | 177-250 | fine sand (U) | MG-M | SA-SR | P | L-CC | structureless | moderate to high | none | 13.7 | 21.3 | 21 | 30 | 10 |
| ZRP-3A | P18 | R584 | 3667.03 | 62.5-88 | 350-500 | 177-250 | fine sand (U) | G-MG | SA-SR | P-L | L-CC | faintly laminated | low to moderate | artificial microfracs | 22.0 | 23.7 | 24 | 28 | 16 |
| ZRP-3A | P19 | R397 | 3620.24 | 31-62.5 | 500-710 | 125-177/350-500 | fine (L) / medium (U) sand | MG-B | SA-SR | P-L | L-CC | laminated | moderate | none | 11.0 | 22.3 | 22 | 29 | 8 |
| ZRP-3A | P20 | R115 | 3549.75 | 4-31 | 710-1000 | 88-125/250-350 | v. fine (U) / medium (L) sand | P-B | SA-SR | P | L | irregular lamination | moderate to high | none | 12.7 | 19.7 | 20 | 32 | 9 |
| ZRP-3A | P21 | R556 | 3660.00 | 31-62.5 | 1-1.41 mm | 177-250 | fine sand (U) | M | SA-SR | P-L | L | laminated | low to moderate | none | 20.7 | 25.0 | 25 | 27 | 15 |
| ZRP-3A | P22 | R427 | 3627.74 | 31-62.5 | 500-710 | 88-125/177-250 | v. fine (U) / fine (U) sand | M | SA-SR | P | CC | laminated | moderate | none | 14.3 | 21.3 | 21 | 30 | 10 |
| ZRP-3A | P23 | R520 | 3651.00 | 31-62.5 | 1-1.41 mm | 88-125/250-350 | v. fine (U) / medium (L) sand | P | A-SR | P-L | L-PS | laminated | moderate to high | artificial microfracs | 16.3 | 20.7 | 21 | 30 | 11 |
| ZRP-3A | P24 | R136 | 3555.05 | 31-62.5 | 710-1000 | 250-350 | medium sand (L) | MG | SR | P | L-CC | structureless | low to moderate | none | 11.3 | 22.3 | 21 | 31 | 8 |
| ZRP-3A | P25 | R445 | 3632.25 | 31-62.5 | 710-1000 | 88-125 | v.fine sand (U) | M | SA-SR | P-L | CC | laminated | moderate | none | 17.7 | 22.3 | 22 | 29 | 13 |

*Depth and sample no. obtained after draft

**Table 2.1: Textural and compactional properties of 25 samples from ZRP-3A.**

## 2.2 Compaction

The degree of compaction in the samples is assessed by observing the grain contacts and quantifying compactional porosity loss (COPL), cementational porosity loss (CEPL) and intergranular volume (IGV). The equations for calculating COPL and CEPL can be found in Appendix 1. The grain contacts and the values for IGV, COPL and CEPL can also be found in Table 2.1.

**Grain contacts:** In order to qualitatively assess the degree of compaction, the nature of the grain contacts between two types of grains was described: (1) between individual rigid grains and (2) between rigid grains and ductile (clay-rich) grains. The grain contacts between individual rigid grains, mostly quartz grains, vary from point to long grain, indicating a comparatively low to moderate degree of compaction for a given burial depth of more than 2-3 km. Very locally, the grain contacts are sutured, indicating that under the right circumstances, chemical compaction (i.e. pressure solution) occurred. There are however no distinct stylolitic seams present in the sample set, except for maybe in sample P25 (see Appendix 4, TS plate B). Ductile grains are relatively rare in the sample set. The grain contacts between ductile grains and clay-rich grains are however mostly long to concavo-convex. Pseudomatrix (i.e. a completely deformed clay-rich grain, pressed in the intergranular pores) is very rare, occurring with some certainty in sample P23. Note that pseudomatrix is in some samples (e.g. sample P4) difficult to differentiate from authigenic pore-filling clay.

**IGV:** The intergranular volume (IGV) is an index for the degree of compaction for grain-supported sandstones (e.g. Paxton et al., 2002) as is the case for the 25 sandstone samples studied here. The IGV is calculated by summing up the detrital matrix (which is absent in this sample set), the intergranular pore-filling cements and intergranular (primary) porosity. The main assumption is that the IGV is 45% during deposition, which is a valid assumption for moderate to well sorted sands. Note that in poorly sorted sandstone samples, the initial IGV was likely below 45%, and that for the present day situation, the IGV should also be lower. IGV in the ZRP-3A sample set varies from 15% (e.g. sample P10) to 25% (sample P21) with an average of 20.5%. This indicates that compaction has in all cases reached more than the maximum mechanical compaction that was possible and is therefore defined as moderate. This roughly corresponds with the observed grain contacts discussed above.

For the given true burial depth of probably more than 2500m, the range in IGV is relatively significant and only a weak tendency can be observed where the better sorted samples have a higher IGV. This indicates that also diagenetic differences must have influenced the IGV.

**COPL and CEPL:** Porosity loss of a sediment is due to compaction and/or cementation. The equations (after Lundegard, 1992) for calculating the relative importance of compactional porosity loss (COPL) and cementational porosity loss (CEPL) can be found in Appendix 1, and require sandstone samples with less than 10% clay matrix. The latter is the case for all 25 sandstone samples studied here. Calculated COPL ranges from 27% (P6, P21) to 36% (P10) whereas CEPL ranges from 3% (P13) to 16% (P18). This indicates that for all samples, porosity loss was mainly due to compaction rather than cementation (Figure 2-1). It also shows that the range of compactional porosity loss within the sample set is partially related to the degree of cementation.

In this figure also roughly two trends are visible: (1) a flat trend with ~30% COPL, including sample P7 and P13 and (2) a steeper (parallel to the lines of equal porosity) trend, including samples P10 and P16. Distinct differences in composition and reservoir quality are not observed.

As samples P7 and P10, both have a comparatively low degree of compaction and of cementation, these samples might have been most prone to late (production related) compaction as they are assumed to be mechanically most unstable. The assumption will be further discussed in the following sections.
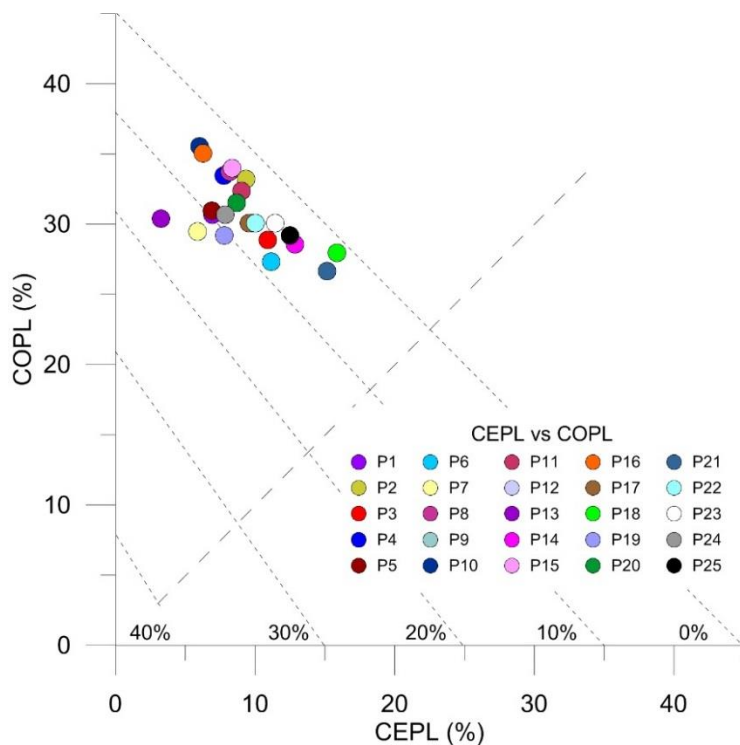
**Figure 2-1: CEPL vs COPL (after Lundegard, 1992) for the 25 sandstone samples. An initial porosity of 45% is assumed. Fine dashed lines are lines of equal porosity. These are not parallel due to the reduction of bulk rock volume by compaction. Coarse dashed line is the line of equal porosity loss by compaction and cementation.**

## 2.3 Detrital composition

The point-counted detrital composition of the 25 sandstone samples (in volume %) is presented in Table 2.3 and Appendix 2. The main detrital components are quartz, feldspar and various types of rock fragments, including sedimentary, igneous and metamorphic rock fragments.

Since all sandstone samples contain less than 15% detrital clay matrix, all samples are defined as arenites. By plotting the feldspar, quartz and rock fragment (incl. chert) content in the sandstone classification diagram (see Figure 2-2; after Pettijohn, 1975), it is visible that all sandstone samples are sublitharenites. Note that the feldspar content is likely to be underestimated in point counting (as they could not all be identified in the thin section due to the optical similarities with quartz), and that some samples might actually be subarkoses. The main characteristics of the detrital grains will be discussed below.
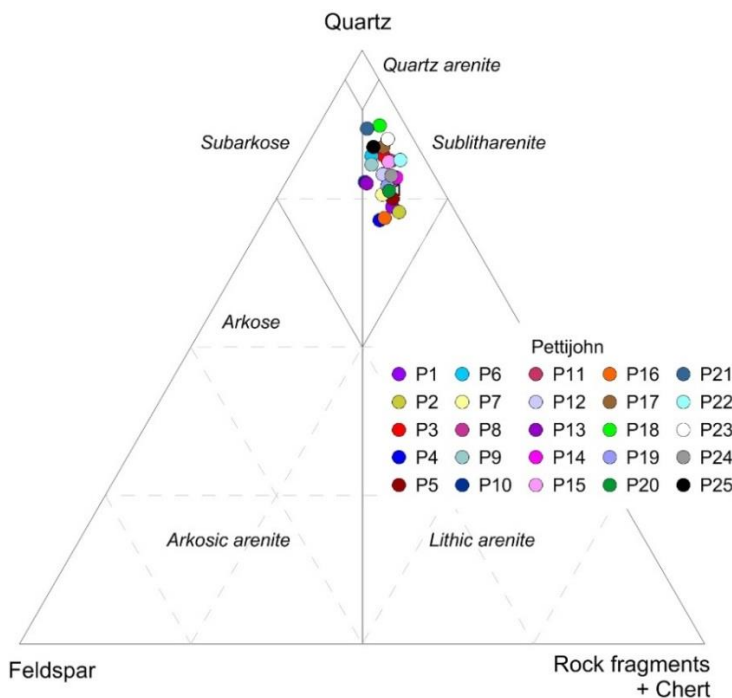


**Figure 2-2: Sandstone classification diagram after Pettijohn (1975) for sandstones with less than 15% clay matrix.**

| G1220 Well | Sample No. | Sample No. NAM* | Depth (m)* | Sample Type | Whole Rock (%BW) Quartz | Illite/Smectite | Kaolinite/Chlorite | Microcline | Albite | Dolomite | Fe-dolomite | Siderite | Barite | TOTAL % (WR) | Clay Fraction (%BW) Illite | Kaolinite | Chlorite | TOTAL % (CF) |
|---|---|---|---|---|---|---|---|---|---|---|---|---|---|---|---|---|---|---|
| ZRP-3A | P1 | R246 | 3582.5 | Trimend | 81 | 4 | 4 | 2 | 10 | 0 | 0 | Tr | 0 | 100 | 47 | 20 | 33 | 100 |
| ZRP-3A | P2 | R085 | 3542.3 | Trimend | 71 | 3 | 8 | 3 | 12 | 1 | 2 | Tr | 0 | 100 | 43 | 43 | 14 | 100 |
| ZRP-3A | P3 | R378 | 3615.5 | Trimend | 82 | 2 | 5 | 2 | 8 | 0 | 0 | Tr | Tr | 100 | 21 | 20 | 59 | 100 |
| ZRP-3A | P4 | R212 | 3574.0 | Trimend | 78 | 2 | 8 | 2 | 10 | 0 | 0 | 0 | 1 | 100 | 58 | 15 | 27 | 100 |
| ZRP-3A | P5 | R283 | 3591.8 | Trimend | 79 | 3 | 9 | 2 | 7 | 0 | 0 | Tr | Tr | 100 | 48 | 23 | 29 | 100 |
| ZRP-3A | P6 | R182 | 3566.5 | Trimend | 86 | Tr | 2 | 3 | 8 | 0 | 0 | Tr | 1 | 100 | 31 | 27 | 42 | 100 |
| ZRP-3A | P7 | R100 | 3546.0 | Trimend | 74 | 5 | 4 | 3 | 12 | 1 | 1 | 0 | Tr | 100 | 49 | 35 | 16 | 100 |
| ZRP-3A | P8 | R352 | 3609.0 | Trimend | 82 | 2 | 7 | 2 | 6 | 0 | 0 | Tr | 1 | 100 | 36 | 12 | 52 | 100 |
| ZRP-3A | P9 | R231 | 3578.8 | Trimend | 78 | 3 | 3 | 4 | 13 | 0 | 0 | 0 | 1 | 100 | 29 | 27 | 43 | 100 |
| ZRP-3A | P10 | R161 | 3561.3 | Trimend | 74 | 3 | 5 | 4 | 12 | 1 | 1 | Tr | 1 | 100 | 49 | 34 | 16 | 100 |
| ZRP-3A | P11 | R332 | 3604.0 | Trimend | 85 | 3 | 4 | 1 | 7 | 0 | 0 | Tr | 0 | 100 | 14 | 20 | 65 | 100 |
| ZRP-3A | P12 | R171 | 3563.7 | Trimend | 74 | 4 | 4 | 2 | 12 | 2 | 1 | 0 | Tr | 100 | 38 | 22 | 41 | 100 |
| ZRP-3A | P13 | R154 | 3559.3 | Trimend | 83 | 2 | 4 | 2 | 9 | 0 | 0 | 0 | Tr | 100 | 55 | 38 | 7 | 100 |
| ZRP-3A | P14 | R306 | 3597.5 | Trimend | 75 | 2 | 7 | 1 | 8 | 3 | 3 | Tr | 1 | 100 | 47 | 26 | 27 | 100 |
| ZRP-3A | P15 | R269 | 3588.3 | Trimend | 83 | Tr | 4 | 2 | 8 | Tr | 1 | Tr | 1 | 100 | 34 | 19 | 47 | 100 |
| ZRP-3A | P16 | R195 | 3569.8 | Trimend | 79 | 2 | 5 | 2 | 10 | 2 | 1 | 0 | Tr | 100 | 39 | 36 | 25 | 100 |
| ZRP-3A | P17 | R484 | 3642.0 | Trimend | 83 | 2 | 7 | 1 | 6 | Tr | Tr | Tr | 1 | 100 | 39 | 16 | 45 | 100 |
| ZRP-3A | P18 | R584 | 3667.0 | Trimend | 84 | 3 | 5 | Tr | 7 | 0 | 0 | 0 | 1 | 100 | 27 | 25 | 49 | 100 |
| ZRP-3A | P19 | R397 | 3620.2 | Trimend | 79 | 5 | 4 | 2 | 8 | 1 | 1 | Tr | 1 | 100 | 28 | 33 | 39 | 100 |
| ZRP-3A | P20 | R115 | 3549.8 | Trimend | 72 | 4 | 3 | 2 | 15 | 2 | 1 | 0 | 0 | 100 | 42 | 14 | 45 | 100 |
| ZRP-3A | P21 | R556 | 3660.0 | Trimend | 92 | Tr | 3 | Tr | 4 | 0 | 0 | Tr | 1 | 100 | 15 | 3 | 82 | 100 |
| ZRP-3A | P22 | R427 | 3627.7 | Trimend | 84 | 3 | 4 | 1 | 6 | 1 | Tr | Tr | 1 | 100 | 20 | 5 | 75 | 100 |
| ZRP-3A | P23 | R520 | 3651.0 | Trimend | 84 | 4 | 4 | Tr | 5 | 2 | 1 | Tr | 1 | 100 | 46 | 46 | 9 | 100 |
| ZRP-3A | P24 | R136 | 3555.1 | Trimend | 76 | 0 | 7 | 2 | 11 | 1 | 2 | Tr | Tr | 100 | 33 | 5 | 62 | 100 |
| ZRP-3A | P25 | R445 | 3632.3 | Trimend | 78 | 3 | 6 | 1 | 8 | 2 | 1 | Tr | 1 | 100 | 42 | 15 | 43 | 100 |

Tr = Trace amounts (<0.5%BW)          *Depth and sample no. obtained after draft

**Table 2.2: Semi-quantitative results of the whole rock and clay fraction (<2µm) XRD analysis on sandstone samples from well ZRP-3A. The whole rock composition gives the relative weight percent of each mineral in the bulk rock; the clay fraction composition gives the relative weight percent of each clay mineral in the extracted clay fraction.**

**Quartz (49.7-63.3%):** Detrital quartz grains are the most abundant phase in all 25 sandstone samples. Both monocrystalline (37.0-50.7%) and polycrystalline (7.0-20.3%) quartz occur. Most of the coarser grained sandstone samples have a relative higher abundance of polycrystalline quartz grains, which is as expected as the coarser polycrystalline quartz grains have not been broken up completely into individual monocrystalline quartz grains. Note that the XRD results (Table 2.2 and Appendix 7) indicate a higher quartz content compared to the thin section point counts, which is partially due to the occurrence of quartz as cement and within rock fragments.

**Feldspar (2.7-8.3%)**: During point counting, a distinction between unleached feldspar (1.0-4.7%) and leached feldspar (Tr-4.7%) was made. Unleached feldspar is recognized by the twinning and occurrence of a cleavage. Since not all feldspar grains exhibit twinning, and then look very similar as quartz grains, it likely that the feldspar content is underestimated. This is also suggested by the higher feldspar content in the XRD results (Appendix 7) and illustrated in Figure 2-3, where all (except for sample P21) results plot left of the 1:1 line, even after normalisation (e.g. vol% to %BW correction; Figure 2-3 (right)). The higher the feldspar content, the more the point counted result deviates from the XRD results. Sample P2 comprises the most albite (from XRD) whereas sample P9 and P10 are relatively rich in microcline (from XRD). Samples P4, P16 and P10 comprise most point counted feldspar (in vol%), with an approximately 50/50 division between leached and unleached feldspar. P18, P22 and P23 comprise the least (identifiable) feldspar, where both P18 and P23 have only trace amounts (Tr) of leached feldspar. In XRD, the latter (low amount) samples have total feldspar content below 10% (BW) whereas the first (high amount) have total feldspar content (%BW) significantly above 10% (BW). From the XRD results, Table 2.2, both albite and microcline are observed, where albite is commonly more dominant. This is also observed in the BSEM. Variations in feldspar composition might be related to different sandbodies that have a different depositional background.
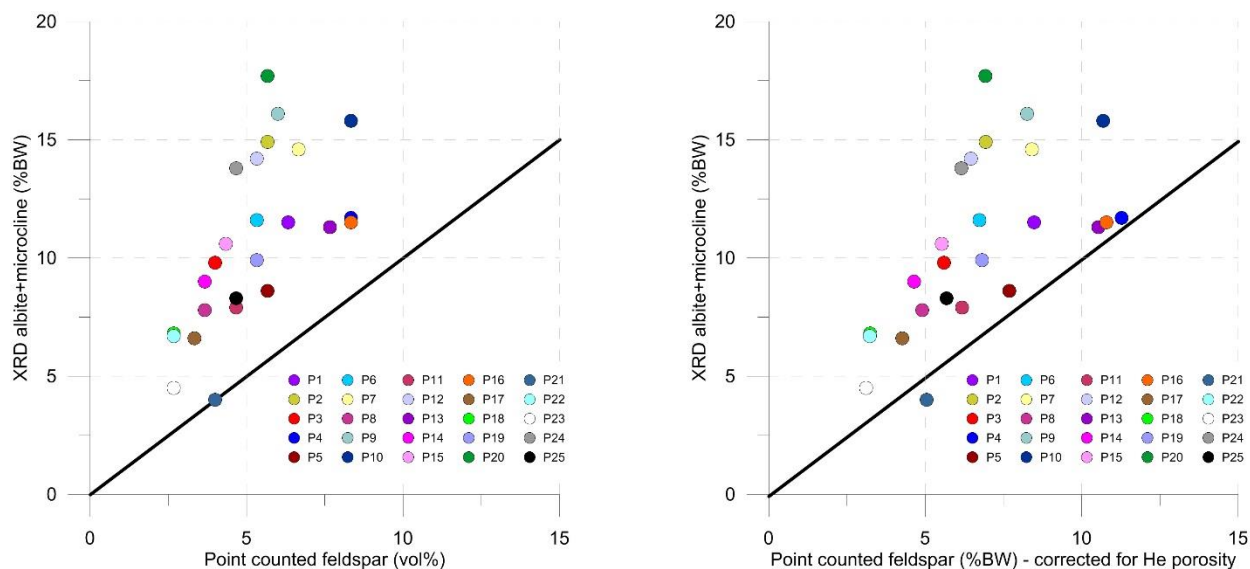
**Figure 2-3: Comparison of the feldspar composition as point counted (x-axes) and determined in XRD (y-axes). Note: the point count results are vol% whereas the XRD results are in %BW (left). To correct for this, the He-porosity is subtracted from the point count results and point-counted feldspar composition is normalized (right). Black line is 1:1 ratio.**

**Rock fragments (5.0-13.3%)**: Different types of rock fragments are identified, including sedimentary rock fragments (0-2.7%), metamorphic rock fragments (0-1.0%), igneous rock fragments (0.3-4.7%) and claystone fragments (0-2.3%). Some of the claystone fragments are strongly deformed. Sedimentary rock fragments are defined as siltstone and sandstone fragments. Most common are the rock fragments that could not be identified. This includes non-porous (1.3-6.0%) and microporous rock fragments (0-4.0%). Sample P16 comprises the most rock fragments, of which most are igneous (4.7%) or unidentified (4.3+1.3%). Some igneous rock fragments are coarse crystalline, with clear quartz, feldspar and possibly pyroxene crystals. Most igneous rock fragments have a felsic composition. In some cases, feldspar in these igneous rock fragments is (partially) leached. Chert, which occurs in most samples, is mostly rare (0-2.0%)

**Accessory minerals (Tr-1.0%):** Accessory minerals include muscovite, heavy minerals (zircon, tourmaline etc.), glauconite and opaque minerals (e.g. pyrite). Most of these minerals occur in trace amounts. Muscovite and zircon are slightly more common (though still <1%) in sample P20, where especially small zircon grains are enriched in the finer grained laminae. Glauconite type grains (see glossary; Appendix 3) occur in sample P15 and P19. This is remarkable for the continental Rotliegend deposits as glauconite is supposed to be a marine indicator.

| Well | Sample No. | Sample No. NAM* | Depth (m)* | Rock Classification: Pettijohn (1975) | Detrital Components (%) | | | | | | | | | | | | Accessories | | | |
|---|---|---|---|---|---|---|---|---|---|---|---|---|---|---|---|---|---|---|---|---|
| | | | | | Quartz | | FSP | | Rock Fragments | | | | | | | | | | | |
| | | | | | Monocrystalline quartz | Polycrystalline quartz | Feldspar, unleached | Feldspar, leached/microporous | Chert | Claystone | Claystone, ductile | Sedimentary rock fragment | Metamorphic, indeterminate | Igneous, indeterminate | Rock fragment, indeterminate | Rock fragment, microporous | Muscovite | Heavy minerals (zircon, tourmaline) | Glauconite | Opaque mineral |
| ZRP-3A | P1 | R246 | 3582.50 | Sublitharenite | 44.0 | 9.0 | 3.3 | 3.0 | 0.3 | 1.3 | 0 | 2.7 | 1.0 | 1.0 | 4.7 | 1.7 | 0 | Tr | 0 | 0 |
| ZRP-3A | P2 | R085 | 3542.25 | Sublitharenite | 40.3 | 9.3 | 3.0 | 2.7 | 1.0 | Tr | 0 | 1.3 | 1.0 | 3.7 | 4.7 | 1.3 | Tr | Tr | 0 | Tr |
| ZRP-3A | P3 | R378 | 3615.50 | Sublitharenite | 44.3 | 12.7 | 2.0 | 2.0 | 1.3 | 0 | 0.3 | 0.7 | 0 | 1.0 | 3.3 | 1.7 | 0 | Tr | 0 | 0 |
| ZRP-3A | P4 | R212 | 3574.00 | Sublitharenite | 38.7 | 12.0 | 4.3 | 4.0 | 0.7 | 0 | Tr | 1.3 | 0.3 | 0.3 | 6.0 | 3.3 | 0 | Tr | 0 | 0 |
| ZRP-3A | P5 | R283 | 3591.75 | Sublitharenite | 37.0 | 16.0 | 2.3 | 3.3 | 0.7 | 0 | 0 | 1.7 | Tr | 2.3 | 3.7 | 3.7 | Tr | 0 | 0 | 0 |
| ZRP-3A | P6 | R182 | 3566.46 | Sublitharenite | 48.0 | 10.3 | 1.7 | 3.7 | 0.3 | 0.3 | 0 | 1.0 | Tr | 1.0 | 2.7 | 2.0 | 0 | 0 | 0 | Tr |
| ZRP-3A | P7 | R100 | 3546.00 | Sublitharenite | 46.0 | 9.0 | 4.7 | 2.0 | 0.7 | 1.7 | 0 | 0.7 | 0 | 3.3 | 3.0 | 1.7 | Tr | Tr | 0 | 0.3 |
| ZRP-3A | P8 | R352 | 3609.00 | Sublitharenite | 44.7 | 13.3 | 1.3 | 2.3 | 0.7 | 0.3 | 0 | 0.7 | 0.3 | 1.7 | 3.0 | 3.0 | Tr | 0 | 0 | 0 |
| ZRP-3A | P9 | R231 | 3578.75 | Sublitharenite | 42.0 | 16.7 | 4.0 | 2.0 | 0.7 | 1.0 | 0 | 0.3 | 0 | 3.0 | 2.7 | 0.3 | 0 | Tr | 0 | Tr |
| ZRP-3A | P10 | R161 | 3561.25 | Sublitharenite | 50.0 | 10.7 | 3.7 | 4.7 | 0.3 | 1.3 | 0 | 1.0 | 0.3 | 1.0 | 3.0 | 2.0 | Tr | Tr | 0 | 0 |
| ZRP-3A | P11 | R332 | 3604.00 | Sublitharenite | 43.0 | 16.3 | 2.3 | 2.3 | 1.7 | 1.3 | 0 | 2.0 | 0.3 | 1.7 | 4.0 | 0.7 | 0 | Tr | 0 | 0 |
| ZRP-3A | P12 | R171 | 3563.71 | Sublitharenite | 49.7 | 7.0 | 3.0 | 2.3 | 0.7 | 1.7 | 0.7 | 0 | 0 | 1.3 | 4.0 | 1.3 | Tr | 0.3 | 0 | 0 |
| ZRP-3A | P13 | R154 | 3559.32 | Sublitharenite | 44.3 | 12.0 | 4.0 | 3.7 | 0 | 1.0 | 0 | 0.3 | 0.3 | 1.7 | 1.3 | 4.0 | 0 | Tr | 0 | 0 |
| ZRP-3A | P14 | R306 | 3597.50 | Sublitharenite | 38.7 | 11.3 | 1.0 | 2.7 | 0.7 | Tr | 0 | 1.3 | Tr | 2.3 | 2.3 | 3.3 | 0 | 0 | 0 | Tr |
| ZRP-3A | P15 | R269 | 3588.25 | Sublitharenite | 50.7 | 12.7 | 3.0 | 1.3 | 0.3 | 0.7 | 0 | 0.3 | 0.3 | 1.3 | 4.0 | 3.3 | 0 | Tr | Tr | 0 |
| ZRP-3A | P16 | R195 | 3569.75 | Sublitharenite | 42.0 | 13.0 | 4.7 | 3.7 | 0.3 | 1.3 | 0 | 0.7 | 0.7 | 4.7 | 4.3 | 1.3 | 0 | 0 | 0 | Tr |
| ZRP-3A | P17 | R484 | 3641.95 | Sublitharenite | 44.7 | 10.0 | 2.0 | 1.3 | 0.3 | Tr | 0 | 1.3 | 0.3 | 1.7 | 3.7 | 0 | Tr | Tr | 0 | Tr |
| ZRP-3A | P18 | R584 | 3667.03 | Sublitharenite | 46.3 | 15.7 | 2.7 | Tr | 0 | 0.3 | 0 | 0.7 | 0 | 1.0 | 3.3 | 1.0 | 0 | Tr | 0 | 0 |
| ZRP-3A | P19 | R397 | 3620.24 | Sublitharenite | 40.7 | 12.0 | 2.0 | 3.3 | 2.0 | 0.7 | 0 | 0 | 0.7 | 0.7 | 4.0 | 2.3 | 0 | Tr | Tr | Tr |
| ZRP-3A | P20 | R115 | 3549.75 | Sublitharenite | 45.7 | 9.0 | 2.3 | 3.3 | 0.7 | 0 | 2.0 | 0.3 | 1.0 | 1.3 | 4.3 | 1.7 | 0.7 | 0.3 | 0 | 0 |
| ZRP-3A | P21 | R556 | 3660.00 | Sublitharenite | 38.7 | 20.3 | 3.3 | 0.7 | 1.0 | Tr | 0.3 | 0.3 | 0 | 0.3 | 2.7 | 0.3 | Tr | Tr | 0 | Tr |
| ZRP-3A | P22 | R427 | 3627.74 | Sublitharenite | 40.7 | 18.0 | 1.3 | 1.3 | 0.7 | 1.3 | 0 | 0.7 | 0.7 | 1.0 | 4.7 | 1.7 | Tr | 0 | 0 | Tr |
| ZRP-3A | P23 | R520 | 3651.00 | Sublitharenite | 46.3 | 14.3 | 2.7 | Tr | 1.0 | 0.3 | 1.0 | 0.3 | 0 | 1.0 | 3.3 | 1.0 | 0.3 | Tr | 0 | Tr |
| ZRP-3A | P24 | R136 | 3555.05 | Sublitharenite | 40.0 | 18.3 | 2.3 | 2.3 | 1.3 | 0.3 | 0 | 0.3 | 0.3 | 1.3 | 4.0 | 3.3 | Tr | 0 | 0 | 0 |
| ZRP-3A | P25 | R445 | 3632.25 | Sublitharenite | 47.7 | 12.0 | 3.0 | 1.7 | 0 | 1.0 | 0.3 | 0 | 1.0 | 0.3 | 4.0 | 0.3 | Tr | Tr | 0 | Tr |

*Depth and sample no. obtained after draft

**Table 2.3: Detrital mineral and rock fragment composition of the 25 point-counted thin sections of well ZRP-3A, sorted by sample number. Tr = trace amounts (observed in the thin section but not point counted).**

## 2.4   Authigenic minerals and processes

An overview of the point counted authigenic mineral composition is shown in Table 2.4 and Appendix 2. A distinction between intergranular pore-filling (PF) authigenic minerals, and intragranular (replacive; REPL) authigenic minerals is made. Part of the PF authigenic mineral composition is the various types of clay rims that occur in the samples. A paragenetic sequence was constructed using microscopical observations and EDX analyses. This is further discussed in Section 2.6. The various authigenic minerals in the 25 samples from well ZRP-3A are discussed below.

| Well | Sample No. | Sample No. NAM* | Depth (m)* | Authigenic Components (%) | | | | | | | | | | | | | | | | | |
| --- | --- | --- | --- | --- | --- | --- | --- | --- | --- | --- | --- | --- | --- | --- | --- | --- | --- | --- | --- | --- | --- |
| | | | | Pore-Filling / Intergranular | | | | | | | | | | Replacive / Intragranular | | | | | | | |
| | | | | Quartz | Dolomite/Siderite | Barite | Illite | Chlorite | Kaolinite | Clay, indeterminate/mixed | Grain-rimming clay (mixed) | Grain-rimming (tangential & radial) illite | Grain-Rimming Chlorite | Quartz | Dolomite/Siderite | Feldspar | Opaque/Heavy mineral | Illite | Chlorite | Kaolinite | Clay, indeterminate/mixed |
| ZRP-3A | P1 | R246 | 3582.50 | 1.0 | 0 | 0.3 | 0 | 1.3 | 1.3 | 1.7 | 0 | 4.3 | 0 | 0.3 | 0 | 0 | 0.3 | 0 | 0 | 3.7 | 0.7 |
| ZRP-3A | P2 | R085 | 3542.25 | 2.0 | 3.3 | 0.3 | 0 | 0 | 1.7 | 3.7 | 0 | 3.0 | 0 | 2.0 | 0 | 0 | Tr | 0.7 | 0 | 6.7 | 1.3 |
| ZRP-3A | P3 | R378 | 3615.50 | 1.7 | 0.7 | 0 | 0 | 0.7 | 0 | 0.3 | 0 | 6.0 | 6.0 | 0.7 | 0.7 | 0 | 0.3 | 0 | 0 | 1.3 | 1.0 |
| ZRP-3A | P4 | R212 | 3574.00 | 0.3 | 0 | Tr | 0 | 0.3 | 0.3 | 6.0 | 0.7 | 2.7 | 1.3 | Tr | 0.3 | 0 | 0 | 0.3 | 0 | 4.3 | 3.3 |
| ZRP-3A | P5 | R283 | 3591.75 | 0.3 | 0 | 0 | 0.3 | 0 | 2.3 | 1.0 | 1.3 | 4.0 | 0.7 | 0.7 | 0 | 0 | 0 | 0 | 0 | 5.7 | 1.0 |
| ZRP-3A | P6 | R182 | 3566.46 | 3.7 | 0 | 0.3 | 0 | 0.3 | 0.3 | 1.0 | 0.7 | 5.7 | 3.3 | 0.3 | Tr | 0 | 0.3 | 0 | 0.3 | 0.7 | 1.3 |
| ZRP-3A | P7 | R100 | 3546.00 | 0.7 | 3.0 | 0.3 | 0 | 0 | 0.7 | 1.3 | 0 | 2.3 | 0 | 0.3 | 0 | 0 | 0 | 0 | 0 | 2.0 | 1.0 |
| ZRP-3A | P8 | R352 | 3609.00 | 1.0 | 0.7 | Tr | 0.3 | 0 | 0.3 | 3.7 | 3.7 | 2.3 | 0.3 | 0.3 | Tr | 0 | 0 | 0 | 1.0 | 5.7 | 1.3 |
| ZRP-3A | P9 | R231 | 3578.75 | Tr | 0 | 0.3 | 0 | 0.3 | 0.3 | 0 | 1.7 | 7.0 | 4.3 | 0.3 | Tr | 0 | 0.3 | 0 | 0.3 | 1.0 | 1.3 |
| ZRP-3A | P10 | R161 | 3561.25 | Tr | 1.3 | 0.3 | 0 | 0.3 | 0 | 2.7 | 0.7 | 4.0 | 0 | 0.3 | Tr | 0 | 0 | 0 | 0 | 3.3 | 1.3 |
| ZRP-3A | P11 | R332 | 3604.00 | 0.3 | 0 | 0.3 | 0 | 0 | 0 | 0.7 | 1.3 | 5.3 | 5.3 | 0 | 0.3 | 0 | 0 | 0 | 0 | 1.0 | 2.0 |
| ZRP-3A | P12 | R171 | 3563.71 | Tr | 5.3 | 0 | 1.0 | 0 | 0.7 | 1.7 | 0.7 | 5.0 | 0 | 0.7 | 0.3 | 0 | 0 | 0 | 0.3 | 1.7 | 2.0 |
| ZRP-3A | P13 | R154 | 3559.32 | Tr | 0.3 | Tr | 0 | 0 | 0.7 | 0 | 0 | 3.0 | 0 | 1.0 | 0 | 0 | 0 | 0.3 | 0 | 2.7 | 0 |
| ZRP-3A | P14 | R306 | 3597.50 | 0.3 | 5.3 | 0 | 0 | 0 | 2.0 | 6.3 | 1.0 | 3.0 | 0 | 0 | 0 | 0 | 0 | 0.3 | 0 | 5.7 | 3.7 |
| ZRP-3A | P15 | R269 | 3588.25 | Tr | 1.7 | 0 | 0 | 0 | 0.3 | 1.0 | 1.3 | 6.3 | 2.0 | 0.3 | 0.3 | 0 | 0 | 0 | 1.3 | 2.0 | 0.7 |
| ZRP-3A | P16 | R195 | 3569.75 | 1.0 | 1.3 | 0 | 0.3 | 0 | 0.3 | 2.0 | 1.7 | 3.0 | 0 | 0.7 | 1.0 | 0 | Tr | 0 | 0 | 3.3 | 1.3 |
| ZRP-3A | P17 | R484 | 3641.95 | 1.0 | 5.7 | 0 | 0 | 0 | 0.7 | 3.7 | 0.7 | 1.7 | 0.3 | 1.0 | Tr | 0.3 | 0.3 | 0.3 | 0.7 | 5.7 | 1.7 |
| ZRP-3A | P18 | R584 | 3667.03 | 1.3 | 0.3 | 0.7 | 0 | 0.3 | 1.0 | 9.3 | 4.3 | 4.7 | 0 | 1.0 | 0 | 0.3 | 0 | 0 | 0.3 | 1.3 | 1.3 |
| ZRP-3A | P19 | R397 | 3620.24 | 0.3 | 1.3 | 0.3 | 0 | 0.3 | 0.7 | 1.3 | 1.0 | 4.7 | 1.0 | 0.3 | 0.7 | 0 | Tr | 0.7 | 0.7 | 5.0 | 1.3 |
| ZRP-3A | P20 | R115 | 3549.75 | 1.0 | 4.7 | Tr | 0.7 | 0.7 | 0.3 | 2.3 | 0.7 | 2.3 | 0 | 0 | Tr | 0 | 0.7 | 0.3 | Tr | 2.3 | 2.7 |
| ZRP-3A | P21 | R556 | 3660.00 | 0.3 | 0.7 | 0 | 0 | 4.3 | 0 | 0 | 1.0 | 1.3 | 13.0 | 0.3 | Tr | 0 | 0 | 0.3 | 1.7 | 2.7 | 1.3 |
| ZRP-3A | P22 | R427 | 3627.74 | 2.3 | 1.7 | 0 | 0 | 4.3 | 0 | 1.0 | 0.7 | 0.3 | 4.0 | 0 | 0.3 | 0 | 0 | 0 | 1.7 | 2.0 | 0.7 |
| ZRP-3A | P23 | R520 | 3651.00 | 1.3 | 2.0 | 0.3 | 0.3 | 2.0 | 0 | 3.7 | 2.7 | 2.3 | 1.7 | 0.7 | Tr | 0 | 0.3 | 0.7 | 0.3 | 2.3 | 2.0 |
| ZRP-3A | P24 | R136 | 3555.05 | 0 | 3.0 | 0.3 | 0 | 0 | 1.0 | 6.0 | 0.7 | 0.3 | 0 | 0.3 | Tr | 0 | 0 | 0 | 0.3 | 2.7 | 1.3 |
| ZRP-3A | P25 | R445 | 3632.25 | 1.3 | 5.0 | 0 | 0 | 0.3 | 0 | 5.3 | 2.7 | 3.0 | 0 | 0.7 | Tr | 0 | 0 | 0 | 1.0 | 1.7 | 2.7 |

*Depth and sample no. obtained after draft

**Table 2.4: Authigenic mineral composition of the 25 point-counted thin sections of well ZRP-3A, sorted by sample number. Tr = trace amounts (observed in the thin section but not point counted).**

**Quartz (0.3-4.0%):** Authigenic quartz occurs both as an intergranular (0-3.7%) and a replacive mineral (0-2.0%). This is visible in SEM (e.g. SEM P1, plate C and P3, plate B) and in the thin sections (e.g. P9, TS plate B). Quartz outgrowths formed relatively large crystals in areas where a clay coating is thin or interrupted. Locally, quartz formed on top of a thicker clay coating. This could partially however be a 3D effect, because both a thin section and BSEM sample represent a 2D cut through 3D objects, where coating is thinner or interrupted in an area that is not included in the TS. There is however no distinct relation between the content of intergranular quartz cement and the amount of clay coatings (Figure 2-4; right). Replacive quartz formed in leached feldspar grains and rock fragments, locally filling up leached grains completely. The replacive quartz appears to have started to form in the areas where the leached grain was in contact with a quartz grain, without a distinct clay rim in between. Remarkable is that quartz cement could also locally form in between detrital quartz grains and detached clay coatings, giving the detrital quartz grain an irregular shape (e.g. P6, TS plate A). Very locally, quartz cement also formed on fracture surfaces in fractured grains (e.g. SEM P20, plate B).

**Dolomite/Siderite (0-5.7%):** Carbonate cement, which comprises mostly dolomite, occurs also as intergranular (0-5.7%) and replacive (0-1.0%) cement. The replacive dolomite and siderite is present in leached grains, mostly

feldspar grains. The outer rim of the pore-filling dolomite cement is commonly enriched in iron, as visible in BSEM pictures (e.g. P12, BSEM plate B). Sample P17 has a dolomite cement enriched nodule with a diameter of ~1 cm. This nodule negatively affects the reservoir quality in this thin section.

**Barite (0-0.7%):** 15 of the 25 samples contain trace amounts of barite cement, which is mostly pore-filling. Locally, barite occurs within leached grains. Since barite occurs in such little amounts, it does not affect the reservoir quality, the grain framework stability or the grain density significantly.

**Kaolinite (1.0-8.3%):** All 25 sandstones samples contain authigenic kaolinite, both identified in the thin section and with the XRD. Most of the kaolinite crystals occur in clusters and are the result of the complete leaching of grains. There is however no grain material remaining that is associated with the kaolinite. Literature has shown that kaolinite commonly replaces feldspar but can also replace mica (e.g. Bertier et al., 2009; Milliken, 2001). The shape of the clusters rather suggests feldspar replacement. Commonly, the kaolinite clusters are affected by continued compaction and the kaolinite crystals are dispersed through the pores, as is visible in sample P11 TS plate B. It has to be noted that the clay fraction XRD results might underestimate the kaolinite content as the kaolinite crystals are relatively coarse crystalline (>2µm) and therefore not incorporated in the clay fraction (<2µm). Kaolinite is the least common in samples P6 and P11 whereas sample P2 has 8.3% kaolinite, which is best visible in the BSEM images.

**Unidentified or mixed clay (0-10.7%):** Most of the 25 studied samples contain sparse to common unidentified or mixed clay, which occurs both as intergranular (0-9.3%) and replacive (0-3.7%) clay. This clay is commonly greenish to brownish in colour and is very fine crystalline. In cross polarised light (XPL), the mineral is characterized by low birefringence, with minor higher birefringence crystals in between, suggesting this unidentified clay is commonly a mixture of dominantly chlorite and subordinate illite. Sample P18 has the most common unidentified/mixed clay, occurring in the pore spaces. Some of this clay might be part of the thick clay rim occurring in this sample. Sample P14, which also contains unidentified/mixed clay, has the most replacive clay. This clay forms a greenish fine-crystalline mesh predominantly in leached parts of rock fragments. The pore-filling clay is blotchy in this sample. Sample P13 has no unidentified/mixed clay, as all the fine-crystalline clay is part of clay rims.
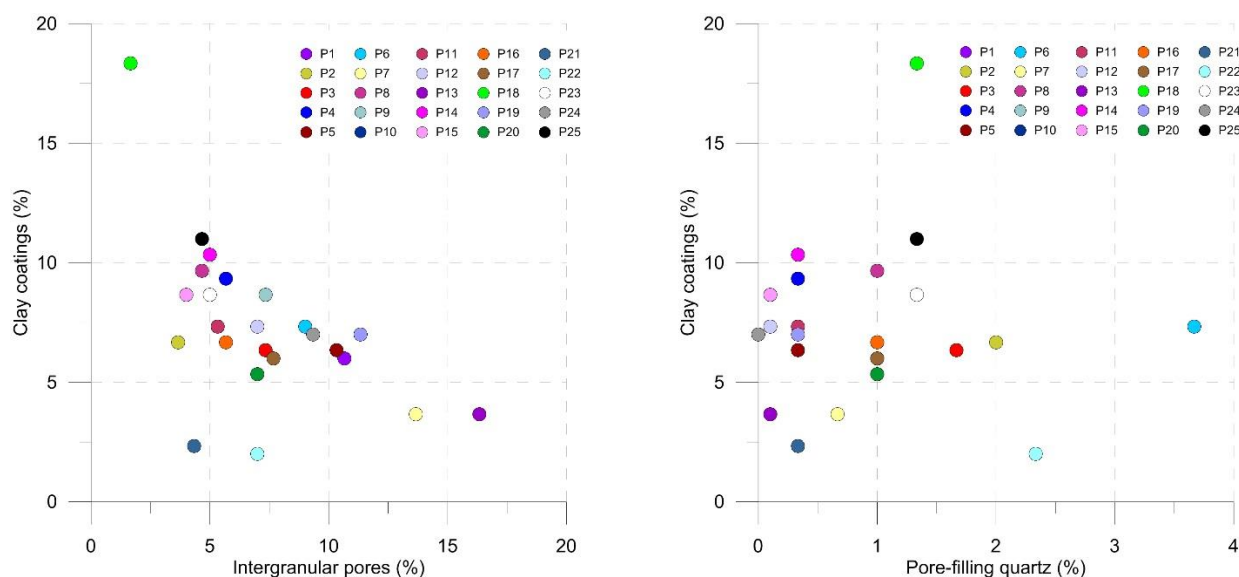


**Figure 2-4: Intergranular pores (left) and pore-filling quartz (right) against the total amount of clay coatings (including tangential and radial illite, and chlorite).**

**Clay coatings (1.0-15.3%):** All 25 sandstone samples contain various types of clay coatings. For detailed photographs of the coatings of each sample, see Appendix 6. During point counting, a distinction between grain-rimming illite (0.3-7.0%), grain-rimming chlorite (0-13.0%) and unidentified/mixed clay (0-4.3%) was made. A small portion of the grain-rimming illite (roughly 10%-30%) is tangential illite, which has high birefringence and occurs most commonly in the concave parts of grains, previously known as pellicle clay. Following strict definitions, tangential illite should be regarded as detrital as this coating developed shortly after sedimentation of the grains (e.g. Malicse & Mazullo, 1996). Such clay is common in soil and can survive short transport.

The rest of the grain-rimming illite is authigenic very fine crystalline radial illite (?), which is commonly mixed chlorite. Radial illite(-chlorite) occurs in most samples and is ~5μm thick (as visible in P25, SEM plate D). Note that TS observations argue for a dominance of chlorite according to low to bluish birefringence colours, while the SEM seems to favour an illitic composition by showing K instead of Fe or Mg peaks in the EDX spectra. A comparison to literature data and photos (Gaupp et al., 1993; Ziegler, 2006) suggests that the fine crystalline material is potentially mainly Mg-chlorite with illite fibres overgrowths. With crystal diameters significantly smaller than 5 microns, however, the clay is at or below the detection limit of the EDX and thus also surrounding material such as the tangential illite coat and/or feldspar may have been measured. These small sized crystals also may not give the high birefringence expected for aligned illite as visible for tangential illite. The absence of Fe-peaks in the EDX spectra would argue in favour of illite being the dominant mineral. Conventional XRD clay fraction analyses as performed here shows the presence of both illite and chlorite in variable amounts but lacks the spatial resolution to solve the issue. Thus, should the clay mineralogy be of importance, different methods need to be found for an unequivocal determination regarding the radial clay coatings.

The clay coating is in some samples detached from the detrital grain. This is likely the result of continued compaction. Clearly distinguishable coarser crystalline chlorite occurs in ~50% of the samples. This type of chlorite occurs mostly as distinct rosette-shaped clusters. Interesting is that chlorite in e.g. sample P6 (SEM Plate D) and P11 (SEM plate C) occurs in between the detrital grains and the detached radial clay rim. Other samples show a clay rim that comprises a mix of chlorite and illite, as is visible in e.g. sample P8 (SEM plate C&D). Sample P21 is an exception, as this sample contains very common and very thick greenish chlorite coatings, with only very sparse illite. As visible in Figure 2-4 (left), there is a direct (negative) relation between the amount of clay coatings and the intergranular pore volume.

## 2.5    Porosity

During point count analysis, four types of pores were differentiated (Appendix 2 and 6). These are:

- Intergranular pores
- Oversized pores (>1.2x the diameter of the maximum surrounding grain size)
- Mouldic pores (pores with a clear outline from a fully dissolved grain)
- Intragranular (secondary) pores (pores in partly dissolved grains or porous rock fragments)

Summing up these four types of pore spaces, results in the so-called total macroporosity, i.e. the total amount of pores visible under the optical light microscope. This macroporosity is compared with, and subtracted from the He-porosity of the plugs, which results in an estimate of the total microporosity (Table 2.5).

**Intergranular pores (1.7-16.3%):** The intergranular porosity varies significantly between the samples. Sample P13 has, besides a high intergranular macroporosity, also a good pore connectivity. Sample P18 has, besides a very poor intergranular macroporosity, also a poor pore connectivity due to significant intergranular clay. Intergranular porosity also varies within some samples, due to distinct lamination. This is the case in e.g. sample P15 and P23 (see TS scans, Appendix 4).

**Oversized pores (0-1.3%):** Oversized pores are pores that are larger than ~1.2x the maximum surrounding grain size. Oversized pores occur in trace amounts in most of the samples. As expected, there is a faint negative correlation between the total amount of oversized pores versus the total grain rimming clay, suggesting that oversized pores are partially the result of complete leaching of grains which had no (distinct) clay coating.

**Mouldic pores (0-1.3%):** Mouldic pores are the result of complete leaching of grains, where the grain coating is preserved, leaving a halo of the original grain. Due to the presence of significant clay coating in all samples, and the presence of feldspar minerals (which leach relatively easy), mouldic pores occur in most samples. Samples P8 and P14 contain the most mouldic pores. Mouldic pores are relatively little deformed, despite the fact that a framework grain is leached out, indicating that leaching postdates most of the mechanical compaction. Locally, mouldic pores are filled with secondary quartz and/or carbonate cement.

| Well | Sample No. | Sample No. NAM* | Depth (m) * | Porosity (%) | | | | | | | | |
|---|---|---|---|---|---|---|---|---|---|---|---|---|
| | | | | Point counted | | | | | Core analysis | | | |
| | | | | Intergranular | Oversized | Mouldic | Intragranular | SUM Macroporosity | Porosity (%) | Permeability (Kk; Md) | Grain Density (g/cm³) | Theoretical microporosity |
| ZRP-3A | P1 | R246 | 3582.50 | 10.7 | 0 | 0 | 2.3 | 13.0 | 25.3 | n/a | 2.65 | 12.3 |
| ZRP-3A | P2 | R085 | 3542.25 | 3.7 | 1.3 | 0 | 2.0 | 7.0 | 18.2 | 17.0 | 2.66 | 11.2 |
| ZRP-3A | P3 | R378 | 3615.50 | 7.3 | 0.7 | 1.0 | 2.3 | 11.3 | 28.5 | 189 | 2.66 | 17.2 |
| ZRP-3A | P4 | R212 | 3574.00 | 5.7 | 1.0 | 0.7 | 1.7 | 9.0 | 26.1 | 185 | 2.65 | 17.1 |
| ZRP-3A | P5 | R283 | 3591.75 | 10.3 | 0.3 | 0 | 1.3 | 12.0 | 26.3 | 233 | 2.66 | 14.3 |
| ZRP-3A | P6 | R182 | 3566.46 | 9.0 | 0 | 0 | 1.7 | 10.7 | 20.8 | 72.0 | 2.64 | 10.1 |
| ZRP-3A | P7 | R100 | 3546.00 | 13.7 | 0 | 0.7 | 1.0 | 15.3 | 20.7 | 176 | 2.65 | 5.4 |
| ZRP-3A | P8 | R352 | 3609.00 | 4.7 | 0.3 | 1.3 | 1.7 | 8.0 | 25.2 | 77.0 | 2.66 | 17.2 |
| ZRP-3A | P9 | R231 | 3578.75 | 7.3 | 0.3 | 0.7 | 1.7 | 10.0 | 27.3 | n/a | 2.65 | 17.3 |
| ZRP-3A | P10 | R161 | 3561.25 | 5.3 | 0.3 | 0.7 | 1.3 | 7.7 | 22.0 | 105 | 2.65 | 14.3 |
| ZRP-3A | P11 | R332 | 3604.00 | 5.3 | 0 | 1.3 | 1.0 | 7.7 | 24.4 | n/a | 2.64 | 16.7 |
| ZRP-3A | P12 | R171 | 3563.71 | 7.0 | 0.3 | Tr | 1.3 | 8.7 | 17.4 | 25.0 | 2.66 | 8.7 |
| ZRP-3A | P13 | R154 | 3559.32 | 16.3 | 1.0 | Tr | 1.3 | 18.7 | 27.2 | n/a | 2.64 | 8.5 |
| ZRP-3A | P14 | R306 | 3597.50 | 5.0 | 0.7 | 1.3 | 1.7 | 8.7 | 21.0 | 31.0 | 2.66 | 12.3 |
| ZRP-3A | P15 | R269 | 3588.25 | 4.0 | 0 | Tr | 0.7 | 4.7 | 21.7 | n/a | 2.64 | 17.0 |
| ZRP-3A | P16 | R195 | 3569.75 | 5.7 | 0.3 | Tr | 1.3 | 7.3 | 22.8 | n/a | 2.66 | 15.5 |
| ZRP-3A | P17 | R484 | 3641.95 | 7.7 | 0.3 | 0.3 | 2.7 | 11.0 | 21.8 | 107 | 2.65 | 10.8 |
| ZRP-3A | P18 | R584 | 3667.03 | 1.7 | 0 | 0.7 | 0.3 | 2.7 | 17.7 | 7.00 | 2.65 | 15.0 |
| ZRP-3A | P19 | R397 | 3620.24 | 11.3 | 0 | 0.7 | Tr | 12.0 | 21.7 | n/a | 2.65 | 9.7 |
| ZRP-3A | P20 | R115 | 3549.75 | 7.0 | 0.7 | 0.3 | 0.7 | 8.7 | 18.1 | 53.0 | 2.66 | 9.4 |
| ZRP-3A | P21 | R556 | 3660.00 | 4.3 | 0.3 | 0 | 0.3 | 5.0 | 20.8 | 41.0 | 2.66 | 15.8 |
| ZRP-3A | P22 | R427 | 3627.74 | 7.0 | 0.3 | 0 | 1.7 | 9.0 | 17.3 | 11.0 | 2.66 | 8.3 |
| ZRP-3A | P23 | R520 | 3651.00 | 5.0 | 0 | Tr | 0.7 | 5.7 | 14.4 | 2.20 | 2.67 | 8.7 |
| ZRP-3A | P24 | R136 | 3555.05 | 9.3 | 0 | 0.3 | 0.3 | 10.0 | 24.1 | n/a | 2.66 | 14.1 |
| ZRP-3A | P25 | R445 | 3632.25 | 4.7 | 0.3 | 0 | 0 | 5.0 | 17.9 | 14.0 | 2.67 | 12.9 |

**Table 2.5: Porosity variation between the 25 point-counted thin sections of well ZRP-3A, ordered by sample number. Tr = trace amounts (observed in the thin section but not point counted). Core analysis data provided by NAM.**

*Depth and sample no. obtained after draft

**Intragranular pores (0-2.7%):** In the present sample set, intragranular pores are generally secondary pores that are the result of partial grain dissolution of either feldspar grains or rock fragments. Especially in the feldspar grains, intragranular pores can be relatively large. The connectivity of the pores is however poor due to the preserved clay coatings and the presence of remaining grain material.

**Micropores (He-porosity minus point counted (macro)porosity; 5.4-17.3%):** The theoretical microporosity is significant in all 25 studied samples. This is mainly because all samples contain significant micropore-rich clay (including kaolinite, chlorite and illite) and strongly leached rock fragments. Samples P3, P4, P8 and P9 all have a theoretical microporosity above 17%, which are all relatively clay-rich samples. Note however that a thin section might not be representative of the entire plug, and that therefore the microporosity might be overestimated. An example is sample P17 (10.8% theoretical microporosity), which contains in the TS a patch enriched in dolomite cement, which might be insignificant in the plug. Hence, the point-counted porosity is relatively low and therefore the theoretical microporosity relatively high. Figure 2-5 shows the microporous material (clay and microporous detrital material) versus the theoretical (calculated) microporosity. As expected, there is a relatively good linear relation, where the samples with more microporous material also have a higher microporosity. Note that e.g. kaolinite has a lower microporosity than illite. Thus the microporosity per mineral type would need to be taken into consideration to come to a better estimate. Theoretically, all samples should fall on the right side of the black 1:1 line. Sample P16 however has more theoretical micropores than microporous material. This could indicate that the thin section is not representative for the sample or that the sample contains (artificial) microcracks that increased the porosity.
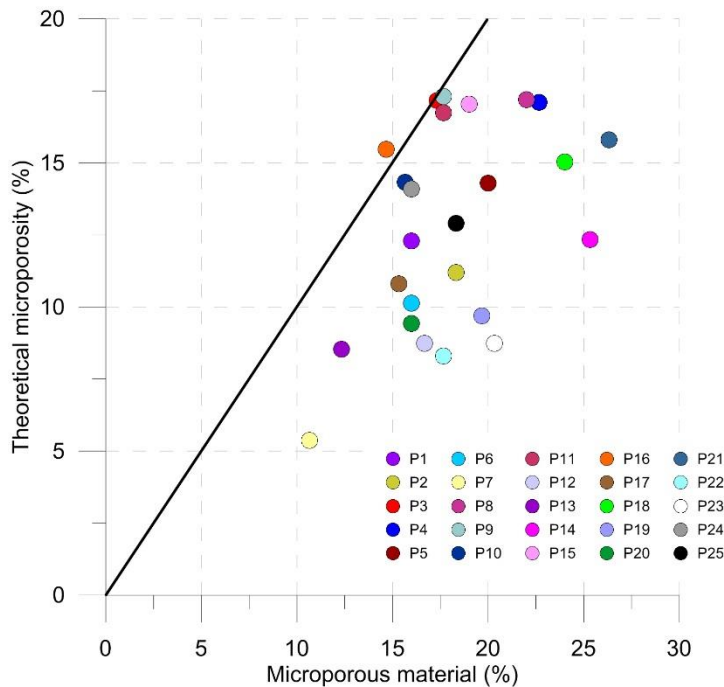
**Figure 2-5: Microporous material vs. theoretical microporosity plot. The black diagonal line represents the 1:1 line.**

## 2.6   Paragenetic sequence and porosity evolution

In order to assess the diagenetic history of the sandstone samples from well ZRP-3A, the observations made with the optical light microscope were combined with SEM and BSEM observations. A schematic summary of the diagenetic history is shown in Figure 2-6. Key images, which aided in the construction of the paragenetic sequence are shown in Figure 2-7. This paragenetic sequence is compared with the one presented by Gaupp and Okkerman (2011). A special focus in this study is on the potential evidence for recent deformation/compaction related to gas extraction.

| Diagenetic Product / *Process* | Diagenetic Evolution | | |
|---|---|---|---|
| | **Eodiagenesis** ⟶ | **Mesodiagenesis** ⟶ | |
| **Clay coating (illite/chlorite)** | Tangential    Radial | Chlorite rosettes formed after compaction and coating separation. | |
| **Kaolinite** | | Not always a coating present. Locally dispersed due to compaction. | |
| **Illite/chlorite (replacive)** | | Due to leaching of grains. Commonly likely mixed. | |
| **Quartz** | | After most compaction and leaching. Filling up intragranular pores. | |
| **Dolomite/Siderite** | | Mostly after quartz. Filling up intragranular pores.    Fe-enriched rims (late). | |
| **Barite/Ti-oxide** | | Latest stage cement. Overgrows kaolinite, quartz and carbonates. | |
| *Compaction* | Most mech. compaction prior to coatings | Detachment of clay coatings    Late stage: fracturing of grains | ? |
| *Dissolution* | | Replaced by kaolinite    Late stage postdates clay coating | |

| Enhances res. qual. | Strongly reduce res. Qual. | Reduces res. qual. | No significant effect |
|---|---|---|---|

**Figure 2-6: Inferred paragenetic sequence based on the microscopic observations on the 25 thin sections from well ZRP-3A. All diagenetic features are the result of burial diagenesis. Evidence for compaction/deformation (grey box with "?" symbol) due to gas production is absent or very minimal in some samples.**

**Compaction:**

Mechanical compaction was initiated almost instantly after deposition and continued after the first phases of leaching and kaolinite formation and the formation of clay rims. Continued leaching of mostly feldspar grains resulted in the formation of mouldic pores. This grain leaching postdates main compaction, as most mouldic pores and secondary pores show only minor indications of deformation (e.g. Figure 2-7, P11 and P24). Compaction is generally moderate as observed by the point to long grain contacts and the IGV values. Chemical compaction, which postdates mechanical compaction, is limited. Locally however, sutured grain contacts and very small stylolitic grain contacts indicate that chemical compaction (i.e. pressure solution) did occur. Mechanical compaction is the main factor for porosity (and therefore permeability) loss in the sampled interval, as visible by the COPL (vs. CEPL) values, Table 2.1.

Evidence for any gas production related compaction or deformation is absent or very minimal. The grain framework did not collapse after the complete leaching of grains. The pore-bridging illite coating is intact (i.e. not sheared) at the grain contacts, as visible in e.g. the SEM pictures (Appendix 5) of P19, Plate A & C, indicating that grains have not moved with respect to each other after clay coating formation. Some of the mouldic pores appear collapsed (e.g. Appendix 4; P18, TS Plate B), but this could have been caused by earlier compaction. Also fractured grains occur in all samples (e.g. Figure 2-7, P3). These grains are deformed due to compaction. This fracturing however likely occurred earlier during diagenesis as locally cement (mostly quartz) occurs on the fracture surfaces. Also fractured grains locally occur next to strongly leached grains, and if fracturing would be a result of gas production enhanced compaction, a strong deformation of the leached grains could be expected. This is however not observed.

**Grain rim formation:**

A special focus of this study was on the grain coatings, which formed early during diagenesis, during mechanical compaction and prior to most grain leaching. There is a strong variety between the samples regarding the thickness and the complexity of the grain rims, as visible in Appendix 6. Examples with relatively simple and thin clay coatings are P13 and P14. In these samples, tangential illite formed in the concave parts of grains, which is overgrown by a relatively thin layer of fibrous illite. The coating is not separated from the grains and chlorite in the coating is mostly absent.

Samples P9 and P11 are examples that have more complex clay rims. These clay rims are detached from the grain and comprise both tangential illite and radial clay, as well as fine and coarser crystalline chlorite. Tangential illite formed prior to radial clay, followed by clay coating detachment and the formation of chlorite in between the radial illite and the grain. The detachment of the clay coating did not occur (completely) as a result of compaction related to gas production. This is because locally, quartz cement formed in between the clay coating and detrital grain (e.g. Figure 2-7, P11). This quartz cementation process is assumed to be too slow for production time scale and did thus most likely occur as result of burial diagenesis.

**Cementation:**

Already during early mechanical compaction, grains started to leach and kaolinite started to form. The kaolinite clusters are locally slightly dispersed but commonly present in localised patches that resemble deformed grains (e.g. Figure 2-7, P13 and P24) due to continued mechanical compaction. Other cements formed mostly after mechanical compaction, including quartz, dolomite, siderite and barite. After the illite coating formation and kaolinite formation, quartz was the first pore-filling cement to form. There appears to be an overlap with early (Fe-poor) dolomite cementation. Dolomite shows zonation (Figure 2-7, P14), with Fe-rich dolomite (brighter in BSEM) postdating Fe-poor dolomite. Both dolomite and quartz appear to have formed during a relatively long period of time, as these cements also occur in secondary pores (Figure 2-7, P1, P9 and P24) and in between grain coatings and detrital grains (Figure 2-7, P11). Quartz also locally occurs on fracture surfaces or within intragranular fracture porosity (e.g. Figure 2-7, P16), indicating that quartz cementation continued after most mechanical compaction. Siderite postdates quartz as it overgrows replacive quartz cements. Barite formed at a later stage during diagenesis, overgrowing dolomite, quartz and kaolinite (Figure 2-7, P14).
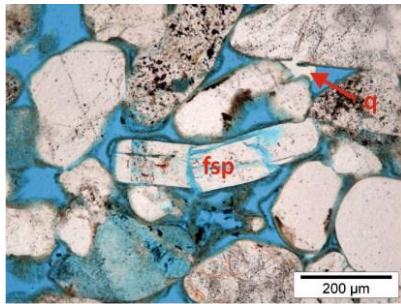
P3: Feldspar (FSP) breakage. Coating detachment. Qtz (q) cementation.
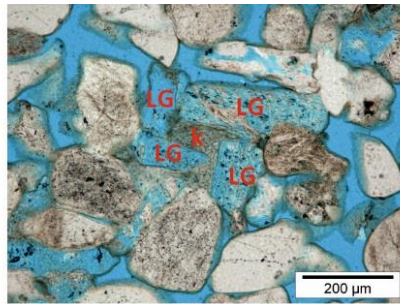
P13: Kaolinite (k) dispersion. Grain leaching (LG). No leached grain deformation.
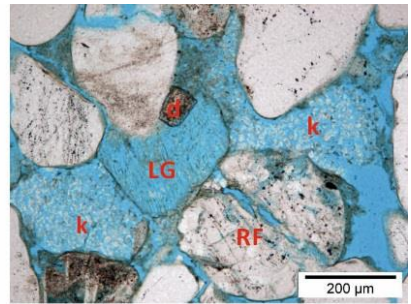
P24: Grain breakage (in RF), dolomite (d) in leached grain (LG). Kaolinite (k), partially dispersed.
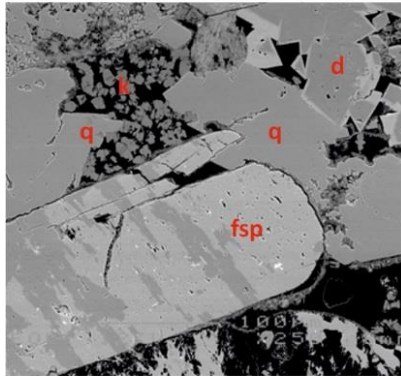
P16: Feldspar (fsp) breakage with qtz (q) cement. Qtz overgrows dolomite (d) & kaolinite (k).
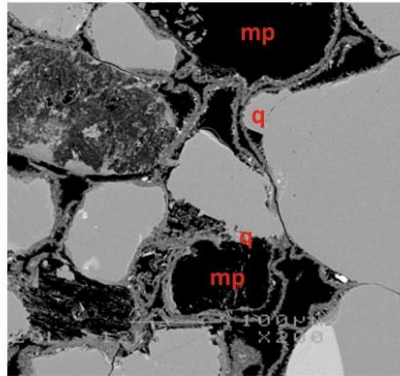
P11: Mouldic pores (MP). Coatings detachment. Qtz (q) between coating and grain.
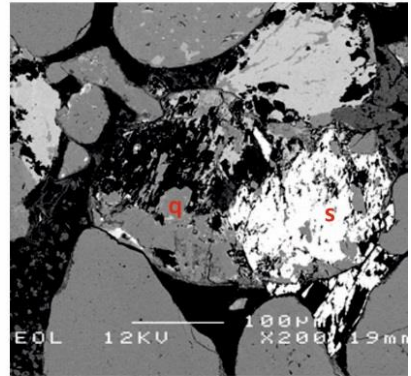
P1: Siderite (s) within and outside leached grain. Overgrows qtz (q) cement.
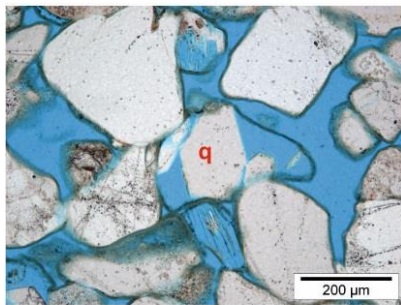
P9: Qtz (q) in mouldic pore. No Deformation. Uniform clay coating.
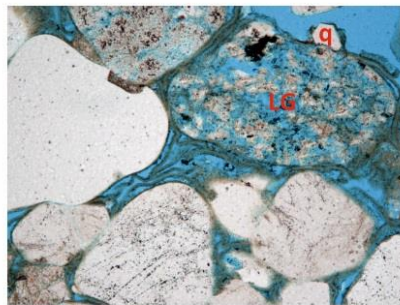
P11: Complex clay coating, detached. Leached grain (LG). Qtz (q) overgrowth with some PF clay.
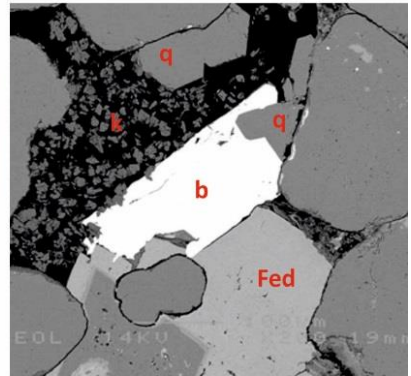
P14: Barite (b) overgrowing kaolinite, qtz & Fe dolomite (Fed). Qtz (q) also overgrows kaolinite (k).

**Figure 2-7: Photo summary of the main diagenetic features (compaction and cementation) observed in the thin sections using optical light microscopy (coloured images) and BSEM (greyscale images). Notes are written below each image. Qtz = quartz.**

# 3 Sample comparison and discussion

## 3.1 Comparison of the 25 sandstone samples

Detrital and authigenic composition of the 25 samples are compared in this section. Depth data was provided after the compilation of the draft report. A chapter dedicated to depth trends can be found in section 0. The depositional environments are unknown and could therefore not (yet) linked.

Between the sandstone samples studied here no general compositional differences exist, while the contents of the individual components vary. All samples comprise mainly quartz, feldspar and a variety of rock fragments, including igneous rock fragments. What is varying is the total content of the individual components, with e.g. feldspar ranging from 2.7% to 8.3% and rock fragments ranging from 5% to 13.3%. The sum of pore-filling authigenic material ranges from 4.7% to 22%, whereby only quartz and dolomite (0.3% to 6.3%) can be regarded as grain stabilizing components. Samples with a finer grain size, or finer grained laminae, generally have smaller pore diameters and more poorly connected pore throats. Theoretically, authigenic components are thought to be less common in finer grained samples as fluids cannot efficiently migrate through the finer grained areas and therefore cements cannot precipitate. A trend is however not observed and therefore it is likely that cement precipitation is due to a closed fluid circuit where precipitation took place from saturated fluids that were already in place.

The main authigenic components are the clay coatings. They are commonly pore throat bridging and locally even completely pore-filling. They however do not block the pores but rather form a meshwork that reduces porosity to microporosity. The fine crystals increase the surface significantly and thus the irreducible water content. Why the clay coatings vary in thickness and composition between the different samples cannot be explained by one factor only. Considering that illite is potassium (K) bearing, while chlorites are Mg and/or Fe bearing, the availability of the according ions must be given. While potassium might be sourced from K-Feldspar, Mg and Fe can be sourced by the volcanics (pyroxene, amphibole) and/or evaporite minerals or iron oxides as they are common in desert systems. According to literature data (Gaupp & Okkerman, 2011) one main source of the chlorite are the volcanites. However, based on the present dataset also other sources cannot be excluded.

Whole rock XRD data does not help much to determine chlorite relative to illite, due to the overlapping peak positions of chlorite and kaolinite and the random orientation (thus relatively broad peak) of crystals in the whole rock samples. Figure 3-1 shows the clay fraction composition in a ternary diagram. Even though it is not representative for the total clay content as only clay minerals of less than 2 microns diameter were analysed and normalised, there is a clear range in composition visible. Chlorite-rich samples are poor in illite and kaolinite, while illite-rich samples can also contain significant kaolinite. The negative correlation between chlorite and kaolinite is also to some extent observed in thin sections.

A significant compositional variation without distinct relationships, which is typical for the sample set, is evidence for different influencing parameters. These parameters could be e.g. the initial composition with more volcanites leading to a more chlorite-rich sample set. However, rock fragments are difficult to interpret if very small and thus no quantitative evaluation can be done. Additionally potentially present volcanic ash tends to dissolved and can thus not be reconstructed. Alternatively, diagenesis might have changed after the gas charge, because in the gas leg diffusion of ions is likely to be different.
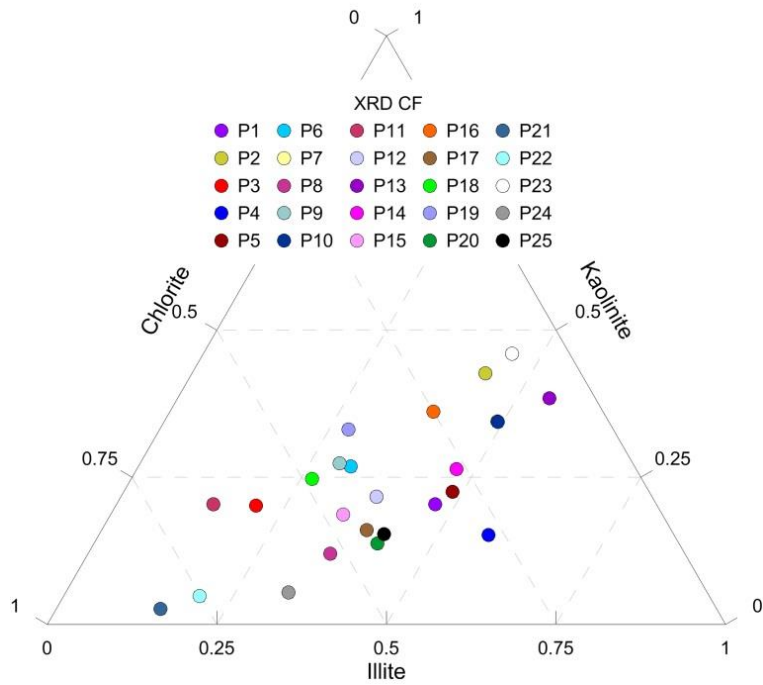
**Figure 3-1: Ternary diagram of the XRD clay fraction results.**

### 3.1.1 Grain rimming clay

The clay coatings vary significantly between individual samples. In order to facilitate a comparison of the different aspects representative photos of the clay coatings for each sample can be found in Appendix 6.

The different types of clay coatings can be grouped in roughly 4 different types (Table 3.1):

- Irregular clay coatings with cloudy pore-filling clay
- Homogeneous (thickness & textural) clay coatings, tangential illite and radial illite (+chlorite)
- Thick clay coating, commonly detached, illite + chlorite
- Other (e.g. nearly absent clay coating or pure chlorite coating)

Most of the clay coatings are illitic with either a homogeneous thickness or a more irregular to cloudy appearance. Detached coatings are most common in 4 samples, whereas 3 samples could not be grouped (Table 3.1). Note that some samples overlap. E.g. sample P25 has locally some detachment of the clay coating and sample has some clay coatings that have a more cloudy appearance.

| cloudy/irregular | homogenous, illitic | Thick, detached, chlorite | Other | |
|---|---|---|---|---|
| P2 | P1 | P3 | P20 | Thin to absent |
| P4 | P5 | P11 | P21 | Thick, mostly chl., traces of illite |
| P6 | P7 | P18 | P22 | Thin, mostly chl. |
| P8 | P10 | P19 | | |
| P9 | P12 | | | |
| P14 | P13 | | | |
| P15 | P16 | | | |
| P23 | P17 | | | |
| P24 | P25 | | | |

**Table 3.1: Grouping of sample per clay coating type.**

### 3.1.2 Other authigenic and detrital components

In order to exemplify the characteristics of the sample set, Figure 3-2 shows a typical compositional diagenetic-product plot for the sample set. Albite (from XRD results) is plotted against kaolinite (point counted) as it is assumed that albite is the potential Si and Al source for kaolinite. If albite was the only source for kaolinite, and if albite content was approximately equal for all samples prior to leaching, it is expected that with a decrease of albite (leaching) an increase of kaolinite is observed. If approximately the same relative amounts of albite is leached (with variable amounts prior to leaching), an increase in kaolinite with (remaining) albite is expected. When looking at the plot one has the idea that for part of the sample set a very faint (negative) trend may be present, but when looking at the entire set, no distinct trend can be observed. Thus it can be assumed that changes in feldspar composition, but also other Si and Al sources (e.g. muscovite) for kaolinite had an additional influence. Alternatively, the fluid composition, temperature or other parameters may have also influenced kaolinite formation.

Based on the previous discussion it becomes evident that a higher number of variables are likely to have influenced the present day diagenetic composition than can be evaluated at the present stage of the study. In order to minimize the number of unknown variables also gas vs. water leg, sedimentology and depth need to be known to better understand that diagenesis of the studied well.
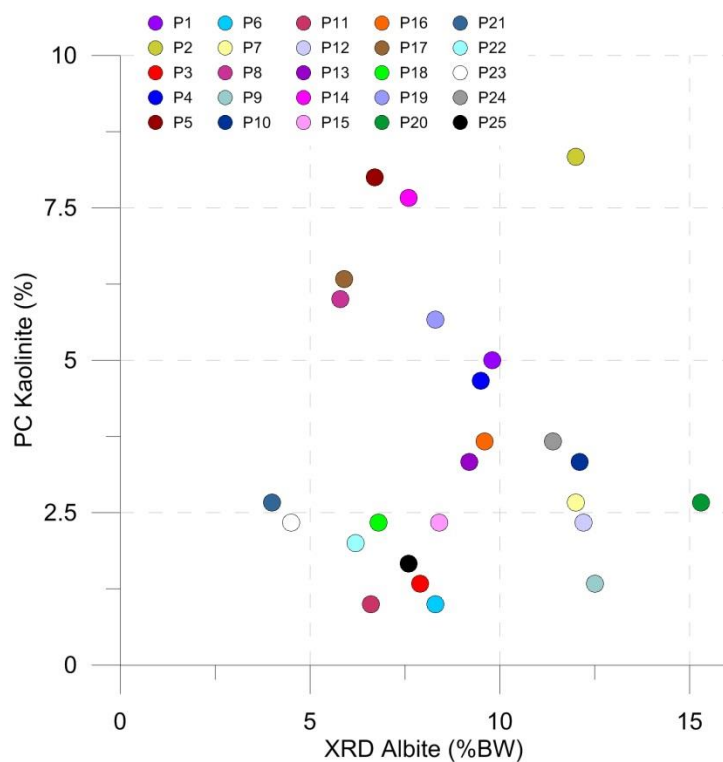


**Figure 3-2: XRD (WR) albite content vs. point counted kaolinite content. Albite is a potential source for kaolinite precipitation.**

## 3.2 Reservoir quality and sandstone compactibility

Even though studying reservoir quality is not the main purpose for this study, it might be of high importance as it is likely that high reservoir quality sandstones (e.g. sample P3 and P5; Figure 3-3) are also most prone to late stage compaction. This is because the grain framework is only mechanically stable below ~26% porosity in well sorted sands (less in poorly sorted sand). Cementation, e.g. by quartz can increase stability in such high porous samples while the presence of mechanically weaker feldspar grains and clay coatings may decrease it. The latter is potentially the case in the sample set as can be seen from a decrease of intergranular porosity with increasing clay coat content (Figure 2-4; left). Additionally grain leaching as can be seen in Figure 2-7 (P13) can destabilize a once stable grain framework.
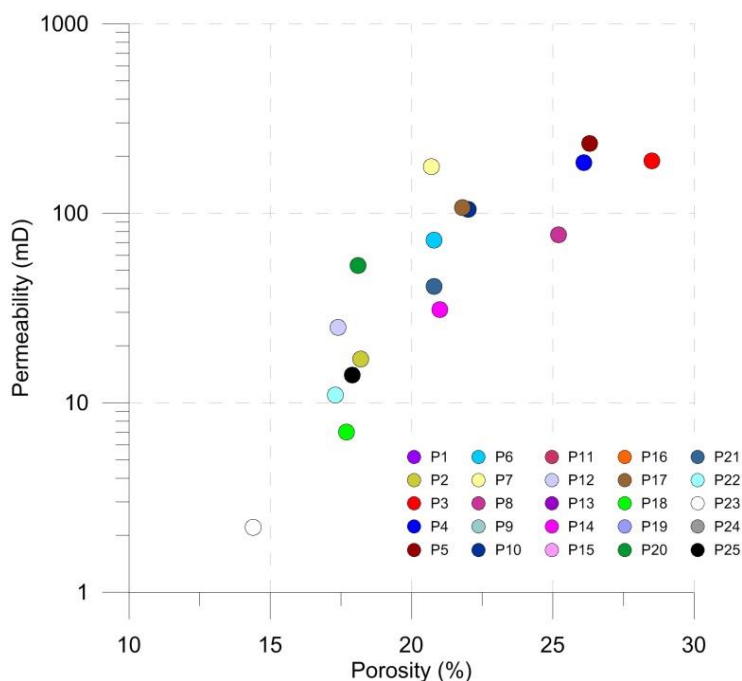
Figure 3-3: Porosity (linear) vs. Permeability (log) plot.

In addition to the influence of grain packing, porosity and permeability directly have an effect on the fluid flow potential and therefore they might have an effect on the diagenetic history for the varying sand intervals. The reservoir quality of a sandstone is controlled by both the detrital composition (hence the sedimentology) and the authigenic components, the latter being both determined by detrital composition and potential by fluid flow from external sources.

The main authigenic components that are affecting the reservoir quality are the clay coatings. They are commonly pore-throat bridging and locally even completely pore-filling. Other cements such as quartz, dolomite, siderite and barite only have a minor (negative) effect on the reservoir quality. Only dolomite is locally more abundant (e.g. sample P17), whereas quartz, siderite and barite are rare to sparse, only rarely filling up the pores completely.

As the observed compaction at the surface is not more than 30-50 cm, it depends on how the distribution of compaction is within the reservoir unit to understand how pronounced it is on the plug scale. If related only to high permeability intervals of few decimetres to meters thickness, a strong effect can be expected with grain collapse that is potentially visible on the thin section scale. Compaction over a larger vertical interval, such as the within the gas leg is assumed to be much more subtle and still probably linked to the best reservoir quality intervals. Thus depth information and the link of high reservoir quality to the depositional environment are important pieces of information in order to understand gas extraction related compaction at the studied scale.

## 3.3    Mechanical stability of the grains and evidence for recent grain movement

As discussed, the reservoir quality may be an indication of grain framework stability and sandstone compactibility. Additionally, the mechanical stability of sandstone is strongly dependent on the detrital composition. However, mainly mechanically stable grains are present and thus no significant difference between individual samples is expected based on the detrital composition, even though feldspar grains are mechanically less stable than quartz grains.

Secondary pores created due to the leaching of grains might result in instability of the grain framework and framework collapse, especially with reducing pore pressures during production. Even though secondary pores (due to the leaching of feldspar grains and rock fragments) including mouldic pores are relatively common, there is no evidence for significant framework collapse. The remaining feldspar is very fibrous but fibres are not deformed.

The clay coatings are in some samples detached from the grains, which is an indication for compaction after coating formation. Even though some of this detachment might be due to recent activity, most is however due to burial diagenesis. This is visible by the chlorite and quartz cement which formed in between the illite coating and

the detrital grain. Additionally pore throat bridging illite fibres appear intact (i.e. not sheared or broken), which also rather argues against production related compaction.

A potential alternative area where production related compaction might take place are mudstones and claystones in the subsiding reservoir. Are significant shales present? How would they react on the reduction of pore pressure? Could e.g. additionally dewatering occur? Considering the absence of production induced compaction indicators in the present sample set, it might be worthwhile to give this alternative some further thoughts.

## 3.4    Sample integration: Summary

Even though the detrital components are similar for all samples of ZRP-3A, the amounts are varying. The samples most prone to production related compaction are high reservoir quality samples with a high content of secondary intragranular pores (e.g. rich in leached feldspar) and common clay coats. Quartz and dolomite cements are likely to have stabilizing effect on the grain framework. The absence of clear evidence for production related compaction even in the samples with high compactibility implies that if the subsidence is related to compaction of Slochteren Sandstones, the subsidence is not focused on thin individual beds, but occurs over longer depth intervals and are therefore not distinctly visible on the thin section scale. Note that despite the lack of evidence, compaction at the grain scale due to reducing pore pressures (i.e. due to gas production) cannot be excluded. Variations in depositional environment (e.g. fluvial vs. aeolian settings), provenance differences and the proximity to volcanic rocks (at the time of deposition) may have influenced the composition and therefore the diagenetic differences (including clay coatings) and compactibility variations. Potential links to (variations in) compaction variations and variations above and below the gas-water contact might have been obscured.

# 4 Sample integration: Depth trends

## 4.1 Depth trend of detrital components

In order to assess the diagenetic variation between the samples above and below the gas-water contact, it is important to also investigate the variations in detrital components with depth. By plotting the Pettijohn sandstone classification diagram (Figure 4-1), colour coded for the depth interval, it is visible that the sandstone samples derived from the Ameland Claystones (base of the cored interval) are the closest to quartz arenites. There is however no distinct difference visible in this diagram between the Upper Slochteren sandstone above (grey) and below (blue) the gas-water contact.
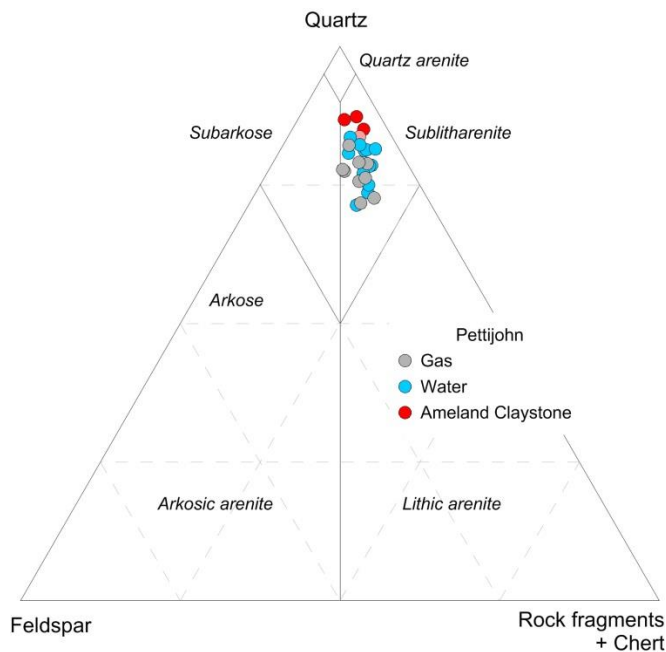


Figure 4-1: Sandstone classification diagram after Pettijohn (1975), similar to Figure 2-2, colour coded for relative depth (either in the gas leg; grey, water leg; blue, or in the Ameland Claystone interval; red).

In order to evaluate whether there are trends in the detrital composition, which would be provenance rather than diagenesis related, the rock fragment (Figure 4-2) and feldspar (Figure 4-3) content are plotted against depth. In these figures, a clear trend is visible. Especially for the total rock fragment content and the feldspar content (both in XRD results; left, and in point count results; right), there is a distinct trend with decreasing amount of rock fragments and feldspar with depth. For the rock fragments in the gas leg, there is a relative large scatter, especially when focussing on the igneous rock fragments only. There is however no distinct step above and below the gas-water contact, neither in the rock fragments, nor in the feldspar composition. Considering the similar trends in igneous rock fragment content and the feldspar content it is not unlikely that in the course of the Rotliegend more and more igneous basement was eroded. The absence of larger quantities of mica is most likely owed to the fact that due to its shape and cleavage, the mica is not deposited together with the other two components. A second possible explanation for the decreasing feldspar content with depth is diagenesis and feldspar dissolution, which will be discussed in section 4.3.

The compositional variability, which is especially prominent in the top part of the sampled interval might be related to sedimentological differences such as fluvial versus aeolian deposition, whereby it is assumed that the aeolian deposits are recycled more often and thus may have a lower feldspar content. This hypothesis, however would need to be validated. Other trends regarding e.g. grain size, sorting, quartz grain content or trends in accessory minerals are not observed.
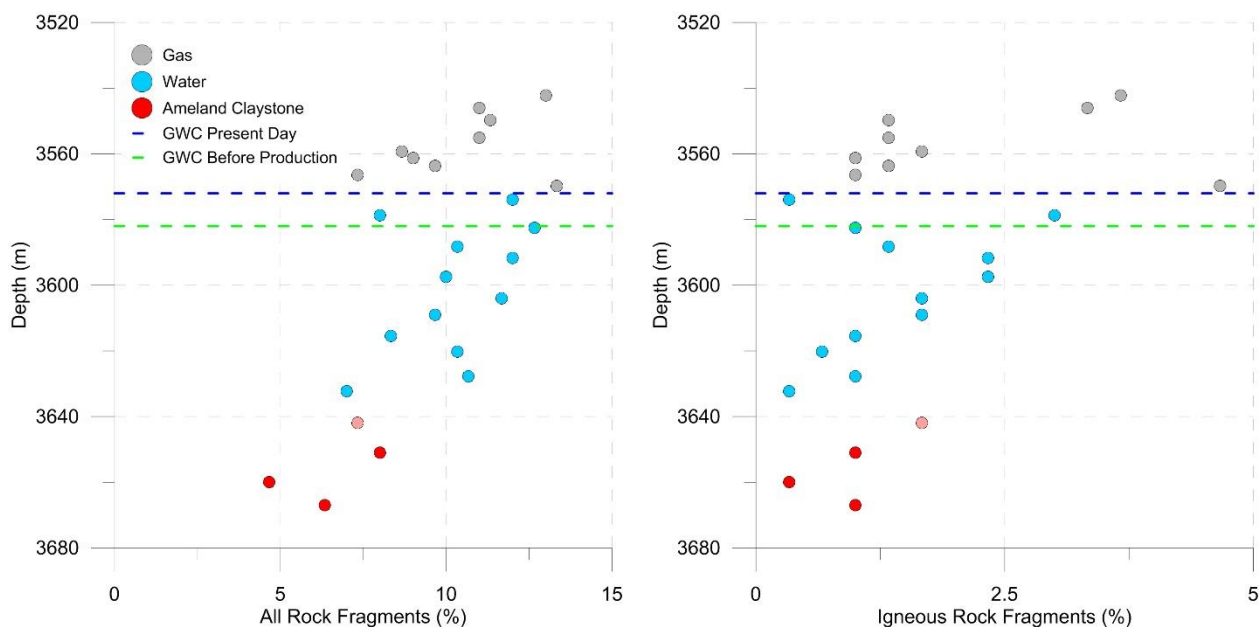
**Figure 4-2: Depth versus all the point counted rock fragments (left) or the igneous rock fragments (right), showing a decrease in rock fragments with depth. Coloured dashed lines indicate the depth of the gas water contact prior to production (green) and the present-day depth (blue).**
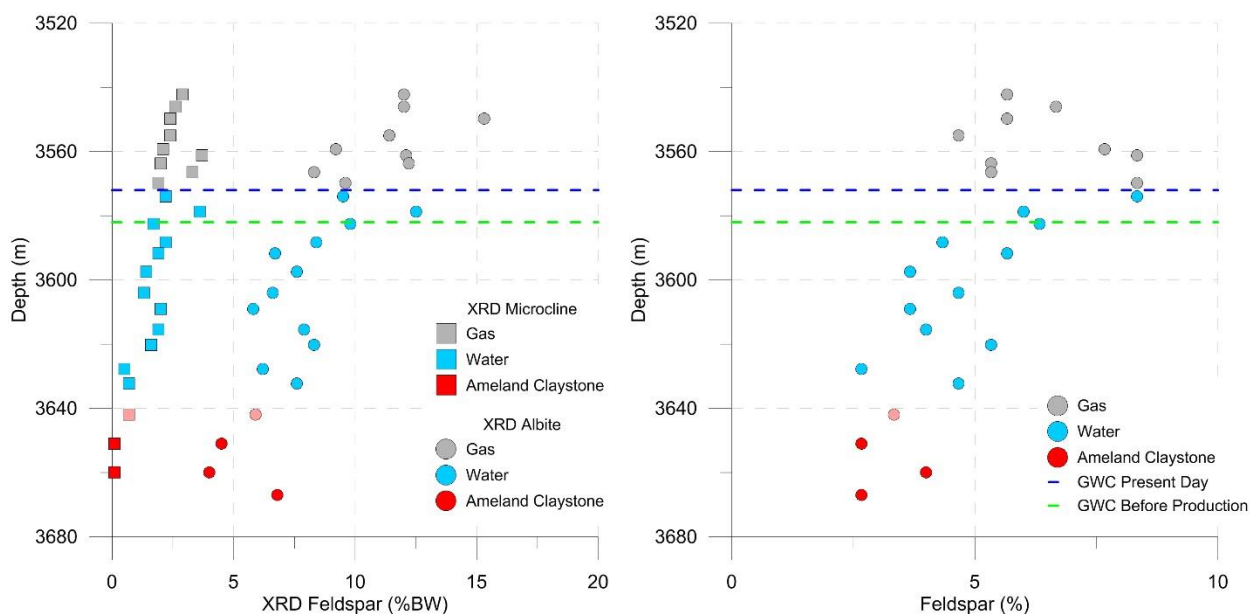


**Figure 4-3: Depth versus feldspar, with on the left side, the XRD results (separating microcline; cubes from albite; circles) and on the right side the point counted feldspar content. The results show distinct decrease in feldspar (both albite and microcline) with depth.**

## 4.2    Depth trend of compaction

In chapter 2 it is concluded that there is no visible evidence for additional compaction after gas extraction. Integrating compactional data with depth shows that there is a large variability of IGV at the top (in the gas leg) and a weak tendency where IGV decrease towards the top (Figure 4-4; left). It is striking that the IGV trend is approximately opposite to the feldspar content trend (Figure 4-4; right). Feldspar grains are mechanically more unstable compared to quartz and feldspar grains are often indented by quartz grains. Clay coatings (see Figure 2-4 and Bjorkum, 1996; Čyžienė et. Al. 2006) and other mechanically unstable rock fragments or grains enhance compaction and therefore obscure the direct IGV – feldspar content relationship. However, it is likely that the degree of compaction is linked to the composition, while the pressurized gas leg had no (significant) influence on the degree of compaction.
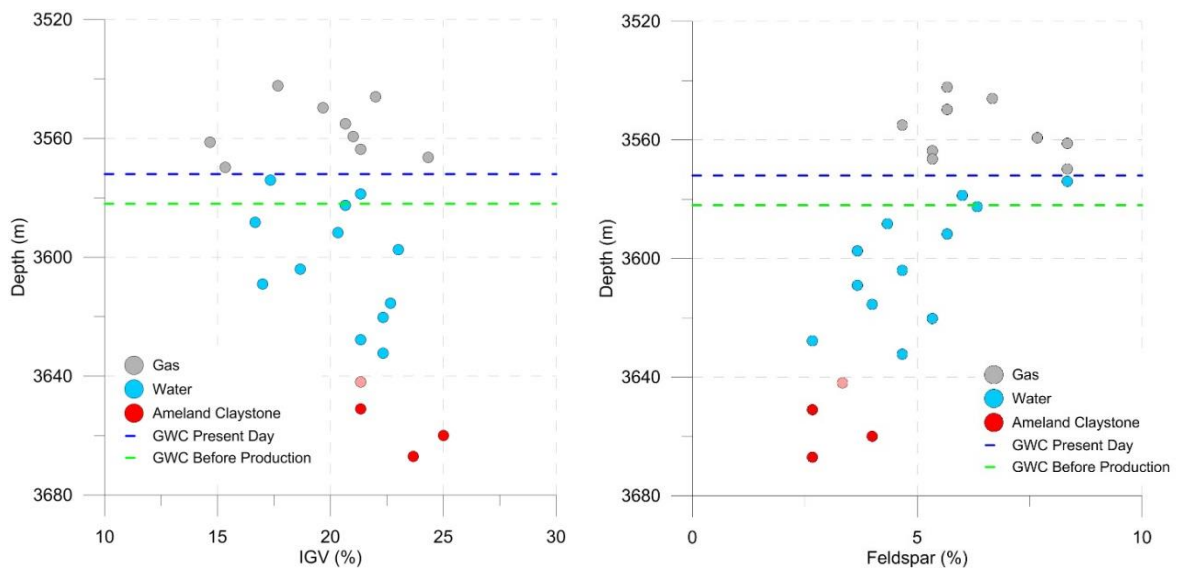
**Figure 4-4: IGV (left) and Point Counted feldspar (right) against depth. The gas leg is on average characterized by a lower IGV and a larger scatter compared to the water lag.**

## 4.3    Depth trend of authigenic components

Compared to the distinct depth trends visible for detrital feldspar and rock fragment content, depth trends of authigenic minerals are significantly less distinct. In the ternary diagram of the clay fraction XRD results (Figure 4-5; right) it is visible that for the samples selected from the Ameland Sandstone interval (base of the interval), there is a significant scatter. The samples from the gas leg appear to have slightly more kaolinite compared to the samples from the water leg. Considering the overall higher feldspar content, however, this might rather be provenance related with more albite present, which is regarded as source of the kaolinite. The scatter and therefore also the overlap in clay occurrence and composition is significant. Also the scatter in COPL vs CEPL (Figure 4-5; left) is large, and a difference between the samples from the gas or water leg is not significant; even though the samples from the water leg have on average a slightly higher CEPL.
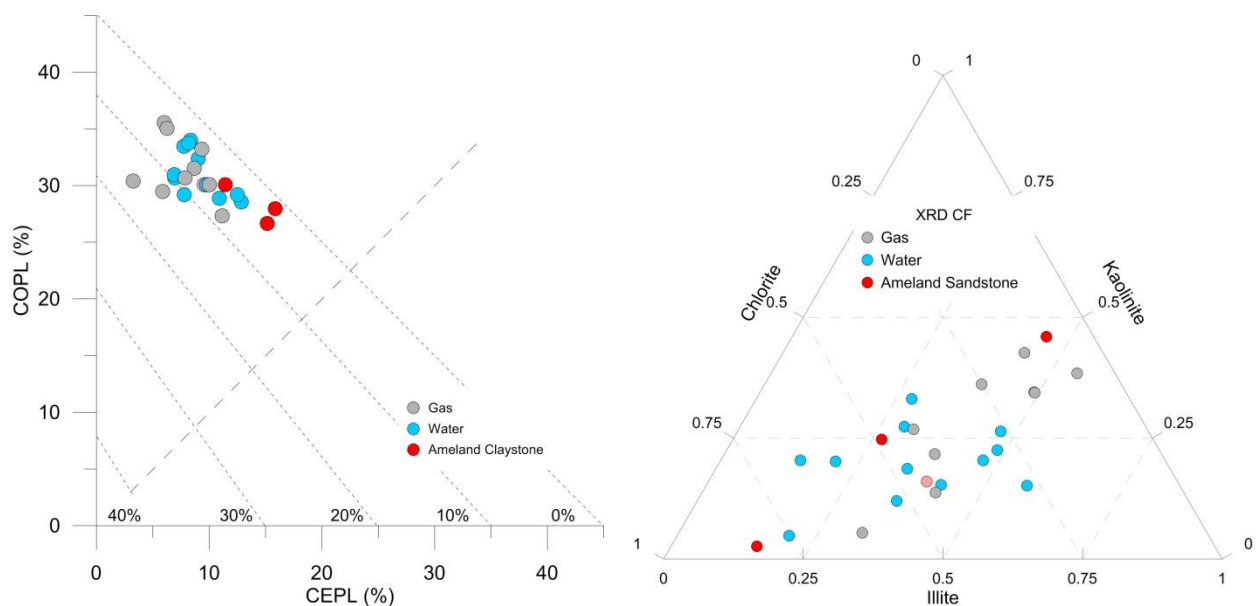


**Figure 4-5: (Left) CEPL vs COPL (as Figure 2-1) diagram and (right) clay fraction XRD results (as Figure 3-1), colour coded for the relative depth. Both diagrams show no distinct trend.**

As mentioned earlier, there is a large variation in clay coatings, both in thickness and composition. Both tangential illite, radial clay (mixed fine crystalline illite/chlorite) and rosette shaped chlorite occur. Plotting the clay coating content against depth shows that there is no distinct depth trend. Visible in Figure 4-6 (left) is that the chlorite

coating content (which comprises mostly the coarser crystalline chlorite rosettes) is becoming more scattered with increasing depth. The samples from above the present day gas-water contact mostly have no chlorite rosettes except for one sample (P6), which occurs near the base of the gas leg. The samples from the water leg have a scattered chlorite content, ranging from zero to 6% of chlorite (P3). However, the pre-production gas water contact was ~10 m below the present day contact at around 3582 m and in this interval the chlorite rosettes are present. Thus it might rather be coincidence that the rosettes disappear at a depth of around 3565 m. To test this, more samples from around the gas-ater contact could be studied. Note that it is the Fe-rich chlorite that is absent. Thus a link might exist to the presence or absence of hematite rich grain coatings as they are typical for large parts of the Rotliegend. This assumption is however speculative and not based on data from this well. What is known is that the area around Zeerijp is the only one in the Netherlands, where chlorite is common (see Gaupp & Okkerman 2011). Also note sample P21 (sampled from the Ameland Claystone interval) which has common chlorite. Sample P18 on the other hand has no chlorite coatings, even though it is sampled in the same Ameland Claystone interval, ~7 m below.

The total clay coatings content (Figure 4-6; right) shows the same pattern, with possibly a faint increase in the content of clay coatings with depth, but also an increase in scatter.
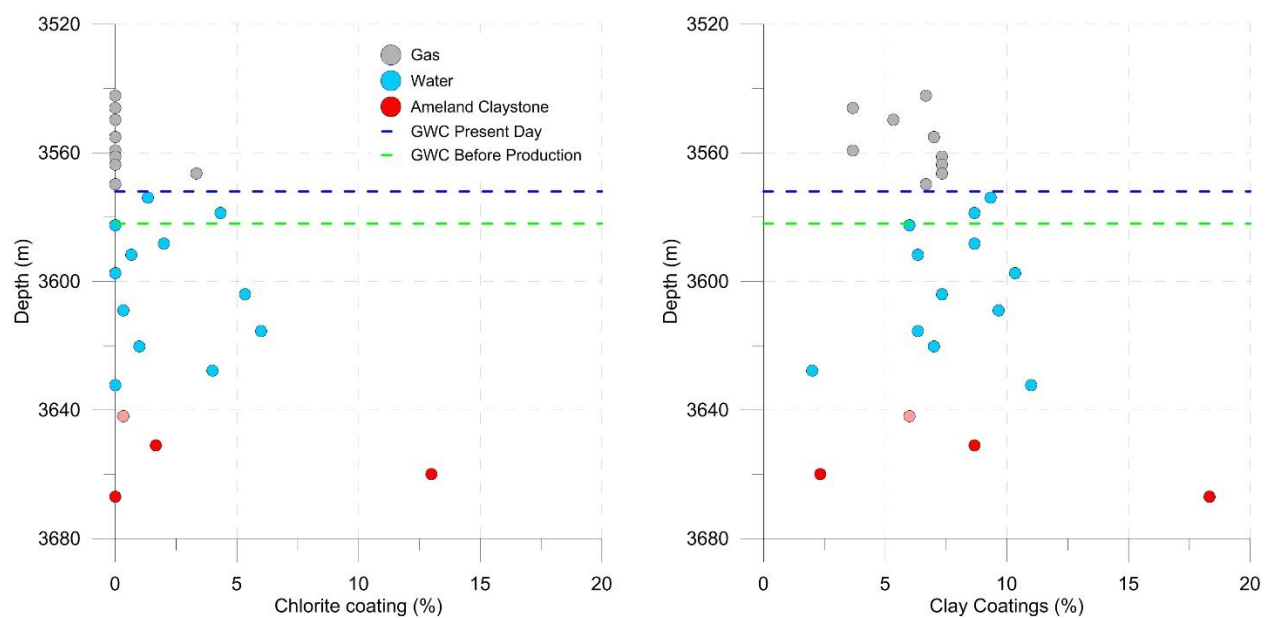


**Figure 4-6: Depth versus chlorite coating (left) and all clay coatings (right), showing a faint trend with increasing clay coatings and increasing scatter towards deeper sands. Dashed coloured lines indicate the past (green) and present-day (blue) gas-water contact.**

Also regarding other authigenic mineral components, there is no distinct depth trend observed. If feldspar was indeed more leached out with increasing depth, an increase in replacive clay minerals would be expected. The replacive clay mineral content is however dispersed with depth, as visible in Figure 4-7; left. When roughly estimating (reconstructing) the feldspar content prior to leaching (by adding up the current feldspar content, the replacive clay content and the authigenic kaolinite content) the decrease in feldspar with depth relation is remaining and results are becoming more scattered (Figure 4-7; right). Note these calculations only give a rough estimate and assumes that all feldspar has been replaced by clay in a closed system.
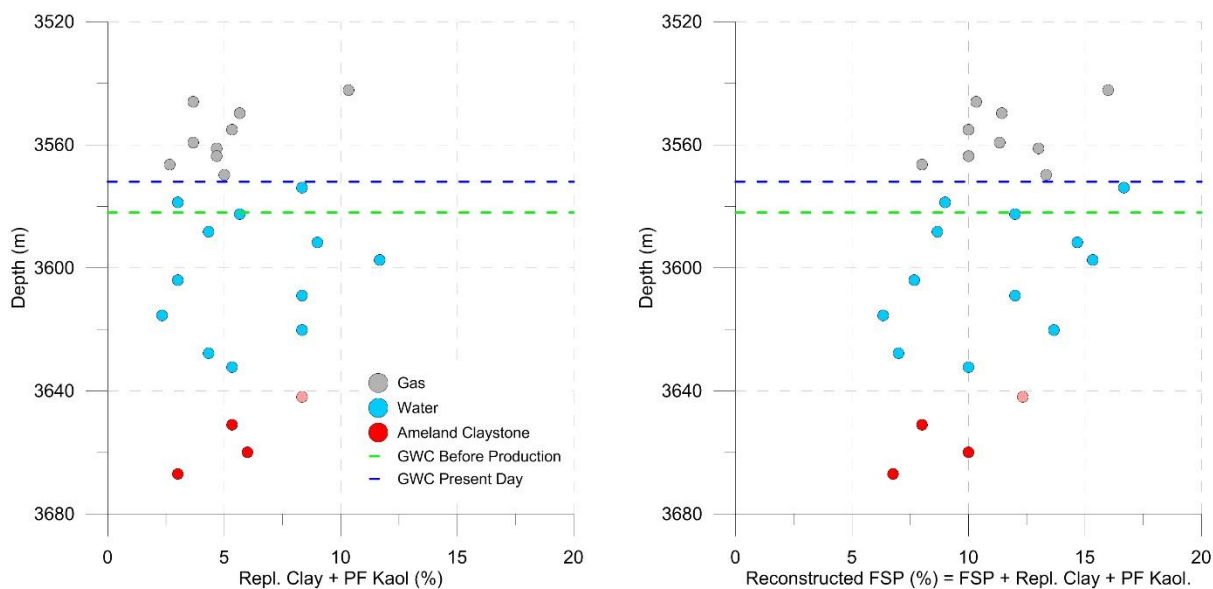
**Figure 4-7: Depth versus all replacive clay + PF kaolinite (left) and an estimate of the reconstructed feldspar (FSP) content (right). Note that PF kaolinite is included in the reconstructed feldspar calculations, as it is likely that kaolinite is dispersed through the sample (thus now pore-filling) after it formed. Hence all kaolinite is assumed to be derived from leaching of feldspar.**

Pore-filling cements such as quartz or dolomite do not show a convincing depth trend either. Due to the high porosity and permeability of the samples, pore connectivity is high and the fluids that lead to mineral precipitation could have migrated from a large distance, even though the amounts are small and local sources would probably be sufficient to explain the cements observed. Therefore it is possible that the depositional environment was (partially) controlling authigenic mineral precipitation rather than diagenetic conditions.

## 4.4    Depth trend: Summary

The main depth trends observed in the sample set are related to variations in detrital composition, especially in feldspar (both albite and microcline) composition. With depth, a distinct decrease in feldspar content and a faint increase in IGV is observed. For the feldspar trend two explanations are possible, either feldspar was deposited in higher amounts towards the top (due to e.g. a change in tectonic activity) or feldspar was leached less towards the top. The latter would be visible by an increase in replacive cements such as kaolinite. This is however not observed, and therefore it is likely that the increase in feldspar and rock fragment content (towards the top) is due to a change of provenance from a more mature to a more immature source. Such can be expected if e.g. an orogenic chain is continuously eroding. The feldspar content is possibly also explaining the decrease in IGV as the feldspar grains are mechanically relatively unstable, resulting in an increase in compaction and concavo-convex contacts with adjoining quartz grains.

Compositional variations above and below the gas-water contact are restricted to the clay coatings, especially chlorite. Most samples above the present day gas-water contact do not contain coarse crystalline chlorite rosettes whereas below the contact, such rosettes occur more commonly. However, this might be coincidence as there is no relation to the pre-production gas water contact. Considering that most likely the absence of $Fe^{2+}$ (and Mg) inhibited the last phase of chlorite formation, a possible explanation for the difference in chlorite rosette content could be the presence or absence of hematitic clay coats as iron source. Based on the available data, however, it is not possible to come to a meaningful interpretation of the observations. Other authigenic components do not show a possible relation with the gas-water contact.

The discussion implies that the gas water contact was stable in geological times. In case charging was not a short term single event, the contact might have shifted in geological times.

# 5 Recommendations

- In order to reduce the number of unknown variables that might affect the differences in detrital and diagenetic composition, it is useful to have better insights in the depositional environment and provenance. This is especially important to explain variations in the detrital content, which eventually overlaps the overall depth trend.

- A possible important parameter on the diagenetic history is the grain size and sorting of the sandstone samples. A well sorted sand and/or a coarse(r) grained sand are most likely better conduits for fluid flow. These fluids contribute to the minerals that precipitate and in the end affect the reservoir quality and the grain framework stability. For this study, the grain size and sorting are visually estimated, but it would be necessary to quantitatively point count the grain size in order to get a more detailed and representative estimate of the grain size and texture. Variations in diagenetic composition are possibly better explained once a more quantitative textural study is executed.

- In a second step, the sample set can be compared with samples from other wells which were drilled prior to production and/or to samples after deformation tests in order to have a comparison with mechanically undisturbed and/or disturbed samples. If the named steps do not help to explain the subsidence, a potential further approach can focus more on the mechanical behaviour of clay units during production.

# 6 Summary and conclusions

- A total of 25 samples were provided from the cored interval of well ZRP-3A, comprising sandstones from the Slochteren SST lithographic unit (Rotliegend). These samples were petrographically analysed. Thin section from the samples were point counted, imaged and described. Additionally, XRD (WR & CF), SEM and BSEM analyses were performed on the sample set.

- All samples are sublitharenites, comprising dominantly quartz. Feldspar (both albite and microcline) occur, as well as a variety of rock fragments. The most common identified rock fragment is igneous in origin. Feldspar, both as a grain and within rock fragments is commonly partially to fully leached, resulting in secondary porosity. Other detrital accessories comprise traces of muscovite, zircon, tourmaline, opaque minerals and glauconite. The latter is interesting as it would suggest a marine sedimentary environment rather than a continental setting.

- The main authigenic phases in the sandstone samples comprise quartz, carbonate minerals, kaolinite, illite and chlorite. Also traces of authigenic feldspar, barite and a Ti-oxide mineral (rutile?) occur in some samples. Most authigenic minerals occur as both pore-filling (intergranular) minerals and replacive (intragranular; filing secondary pores) minerals.

- The most striking authigenic features are the various types of clay coatings that occur in the sample set. All samples have coated grains, but the texture (e.g. coating thickness and heterogeneity) and mineralogical composition varies. Tangential illite occurs in most samples, and is thicker in the concave part of the grains. This is covered with a thin layer of authigenic radial clay. This radial clay is likely mostly illitic, mixed with chlorite.

- The clay coatings in some samples are detached from the detrital grain. This detachment is most likely due to compaction, where the (early formed) coatings are sheared from the grain. The presence of (undamaged) chlorite rosettes and authigenic quartz, which is independent from the geological gas water contact, indicates that this coating detachment occurred during diagenesis and is not the result of compaction due to pore pressure reduction related to gas extraction. Also the presence of quartz cement on the fracture surfaces of fractured grains indicate that grain fracturing also occurred during burial diagenesis. Grain leaching (resulting in secondary pores and mouldic pores) postdates most of the mechanical compaction as these pores are not further deformed, despite the removal of potential framework grains.

- Distinct to faint depth related trends only occur for the IGV, the feldspar and the rock fragment content as well as the authigenic clay composition and coating type. Apart from the variation in clay coating, these depth can be (partially) linked to sedimentological variations. A change in provenance of the sands is visible by the increase of feldspar grains and rock fragments with time. This provenance change has most likely also resulted in an increased compaction of the sediments towards the top of the studied succession. The compositional change is not diagenetic as there is no evidence for increased feldspar dissolution (i.e. an increase in replacive clay minerals and secondary pores) with increasing depth.

- Chlorite coatings are more commonly occurring (but more scattered) in the present-day water leg, whereas they are nearly absent in the present-day gas leg interval. This effect disappears when instead of the production related contact, the gas-water contact depth (~10 m deeper) prior to gas extraction is used. More research is necessary to understand the cause of the vertical distribution of the chlorite coatings. In first instance a core description may add information on depositional environment related changes, but also a more in-depth study on the chlorite and its distribution in Slochteren sandstones may be useful.

# 7 References

Study and Data Acquisition Plan Induced Seismicity in Groningen. Update Post-Winningsplan 2016. Nederlandse Aardolie Maatschappij B.V.

Bertier, P., Swennen, R., Lagrou, D., Laenen, B., Kemps, R. (2008): Palaeo-climate controlled diagenesis of the Westphalian C & D fluvial sandstones in the Campine Basin (north-east Belgium). Sedimentology, v. 55 (5), p. 1375-1417.

Bjorkum, P. A. (1996): How important is pressure in causing dissolution of quartz in sandstones? Journal of Sedimentary Research, 66(1), 147-154.

Čyžienė, J., Molenaar, N., Šliaupa, S. (2006): Clay-induced pressure solution as a Si source for quartz cement in sandstones of the Cambrian Deimena Group. Geologija, 53, 8-21.

Gaupp, R., Matter, A., Platt, J., Ramseyer, K., Walzebuck, J. (1993): Diagenesis and fluid evolution of deeply buried Permian Rotliegende) gas reservoirs, northwest Germany. AAPG Bulletin, v. 77 (7), p. 111-128.

Gaupp, R., Okkerman, J.A. (2011): Diagenesis and reservoir quality of Rotliegend sandstones in the northern Netherlands – A review. SEPM Special Publication, v. 98, p. 193-226.

Lundegard, P. D. (1992): Sandstone porosity loss - A "big picture" view of the importance of compaction. Journal of Sedimentary Petrology, v. 62, p. 250-260.

Malicse, A., Mazzullo, J. (1996): Early diagenesis and paleosol features of ancient desert sediments: Examples from the Permian Basin. Siliciclastic Diagenesis and Fluid Flow, v. 55, p. 151-161.

Milliken, K.L. (2001): Diagenetic heterogeneity in sandstone at the outcrop scale, Breathitt Formation (Pennsylvanian, Eastern Kentucky. AAPG Bulletin, v. 85 (5), p. 795-815.

Paxton, S. T., Szabo, J. O., Ajdukiewicz, J. M. & Klimentidis, R. E. (2002): Construction of an intergranular volume compaction curve for evaluating and predicting compaction and porosity loss in rigid-grain sandstone reservoirs. American Association of Petroleum Geologists Bulletin, v. 86 (12), p. 2047-2067.

Pettijohn, F. J. (1975): Sedimentary Rocks. Harper and Row, 628 pp.

Ziegler, K. (2006): Clay minerals in the Permian Rotliegend Group in the North Sea and adjacent areas. Clay minerals, v. 41 (1), p. 355-393.

# Appendices

# Appendix 1: Petrography methodology

This appendix describes the detailed methodology and terminology on the various methods applied for petrographic analysis (Chapter 2). This includes thin section preparation, description and imaging (including SEM), as well as X-ray diffraction (XRD) and the determination of compaction.

**Sample preparation**
Thin sections: Trimends from a total of 25 samples were received for thin section preparation. One trimend per sample was impregnated with blue-dyed epoxy resin to aid the identification of porosity. No stain colour was applied to the samples.

BSEM: The remaining impregnated blocks were polished for BSEM analysis, so that the observations done with the thin sections and in BSEM are similar. To make the samples conductive, the polished blocks were coated using a Polaron CC7650 carbon coater.

SEM: From the other trimend, a rough cube is broken off and glued with conductive carbon glue on aluminium stubs. These mounted stubs were coated with gold coating using a Biorad Sputter coater. To further improve electron conductivity, the sides of the stubs were painted with silver paint, in order to prevent electron loading on the sample surface during analysis.

**Qualitative description of thin sections**
Descriptive terms used throughout the petrographic study are listed below in Table A.2 and Table A.3. The percentages are visually estimated using the comparison charts in Flügel (2004) and where possible derived from the point counting results. Also the texture (sorting, roundness, grain contacts, heterogeneity) and the grain size (min, max, mode) were visually estimated under the optical microscope. For the samples that have clearly different grain sizes per laminae on the thin section scale, a distinction between fine-grained and coarse-grained laminae is made in order to visualise the difference between the coarse- and fine- grained laminae.

| Pore connectivity | |
|---|---|
| No pore interconnections observed | very poor |
| Some pores are interconnected | poor |
| Pores commonly show interconnections | moderate |
| Most pores show interconnections | good |
| Most pores show several interconnections | very good |

**Table A.2: Terminology for the description of pore connectivity.**

| Mineralogy (%) | | Porosity (%) | | Permeability (mD) | |
|---|---|---|---|---|---|
| Tr | Very rare | Tr | Very poor | <0.01 | Very poor |
| <1 | Rare | <1 | Poor | 0.01-0.1 | Poor |
| 1-2 | Very sparse | 1-2 | Very low | 0.1-1 | Very low |
| 2-5 | Sparse | 2-5 | Low | 1-10 | Low |
| 5-10 | Common | 5-10 | Fair | 10-100 | Fair |
| 10-20 | Abundant | 10-20 | High | 100-1000 | Good |
| 20-50 | Very abundant | 20-30 | Very high | 1000-5000 | Very good |
| >50 | Dominant | >30 | Extremely high | >5000 | Extremely good |

**Table A.3: Coding for the qualitative and quantitative description of the thin sections.**

**Quantitative petrographic analysis by point counting**
Quantification of the mineralogical composition and porosity was achieved by counting 300 points using a mechanical interval displacer connected to a counting machine. The interval displacer, in which the thin section was clamped, was fixed to the rotating stage of the optical microscope. By selecting the region of interest and pressing the master key, the thin section was moved a given distance along a transverse and the exact spot under the crosshair was identified and counted. These distances depended on the region of interest and were adjusted according to the grain-size of the sample so that after 300 points, the entire region of interest is covered. This way, the point counting is as representative as possible for the sample. Note that the outer rims of the thin section were

disregarded to avoid any preparation induced features such as fractures and plugged out materials. Based on their modal detrital composition quantified by point counting, the samples were classified using the sandstone classification scheme of Pettijohn (1975). Appendix 3 shows the different categories used for point counting and the point counting results of the samples.

**(Backscattered) Scanning Electron Microscopy ((B)SEM)**
The 25 gold coated stubs and carbon coated polished blocks were examined using a JEOL 6400 Scanning Electron Microscope. During SEM analysis, a topographic contrast (i.e. the shape and morphology) becomes clear, whereas for BSEM analysis, a compositional contrast (i.e. variations in atomic number or Z-value) is visualised. The variation in grey-scales between minerals in a BSEM image can thus be used for mineral distinction based on image analyses. The higher the atomic numbers of the mineral, the brighter it will be in the image. For both SEM and BSEM methods, an energy dispersive X-ray analysing system (EDX) was used to identify elements and therefore unknown minerals in the samples.

**X-ray diffraction (XRD)**
Additional to SEM analyses, whole rock and clay fraction (i.e. the fraction smaller than 2 μm) XRD was applied on all 25 samples. For whole rock XRD, a portion of each sample was ground to powder in a mill, using acetone to minimize structural grinding damage. The resulting slurry was dried and the powder packed firmly into a backloading powder mount.

For clay fraction XRD analysis, each sample was lightly crushed (to prevent damage of the clays) and mixed with a small amount of distilled water and 1ml peptisation solution ($Na_7P_2O_7$ + $Na_2CO_3$). A 6% hydrogenperoxide solution was added drop-wise to test the presence of organic material and, if necessary, remove the organic material present as this interferes with the clay measurements. After shaking the samples, the samples were placed in an ultrasonic bath for 20 minutes to release the maximum amount of clay into suspension. After settling of the larger than 2 μm fraction, the clay suspension was decanted off and then centrifuged to deposit the entire less than 2 μm fraction. This fraction was once again washed three times with distilled water by centrifugation and decanting. The cleaned clay fraction was then mixed with a small amount of distilled water and two drops of $MoS_2$ (molybdenite) suspension to make a thick slurry and applied onto a glass tile. The glass slide was left to dry at room temperature for a minimum of 16 hours. The $MoS_2$ is used as a reference peak to control the potential peak shift during analysis, and can be found back at 14.4°2θ.

The samples were scanned on a PANalytical CubixPro automated X-ray diffractometer using Ni-filtered CuK radiation. The powder samples were scanned at a rate of 4 seconds per 0.02° step width, using 0.2 mm slits from 5 to 70° 2θ. The clay tiles were scanned at a rate of 4 seconds per 0.02° step width, using 0.2 mm slits from 2 to 40° 2θ. The clay tiles were glycolated by placing them in a desiccator containing a layer of ethylene glycol at a temperature of 60°C for a minimum of 16 hours. The glycolated clay slides were rescanned from 2 to 26° within 1 hour after removal from the glycolation desiccator. The scans were repeated after heating for 4 hours at 300°C and after heating for 4 hours at 550°C.

The qualitative XRD analysis of a mineral composition is based on the identification of the main or primary peaks of the relevant mineral, keeping in mind the minerals identified under the microscopes. Every mineral is characterised by a specific pattern of peaks (primary, secondary and peaks of higher order) in a XRD spectrum, which allows the identification and differentiation from other components of the sample. Generally, primary peaks are the strongest peaks in a XRD spectrum and are used to identify and quantify minerals.

The quantification of a specific mineral is based on the integration of the area below its characteristic peaks. The resulting value is multiplied with a calibration factor, the so-called Reference Intensity Ratio (= RIR factor). This calibration factor is mineral depended and is usually determined by preparing a 50:50 mixture of the pure mineral with a reference mineral (PanTerra Geoconsultants uses corundum as reference mineral). The RIR factor is then the ratio of the main peak of the mineral phase and the main peak of corundum. This approach allows the quantification of (crystalline) mineral phases of a sample. The RIR factors for each identified mineral are applied to the peak areas of each identified mineral. The numbers so derived can be considered as the (normalised) relative contributions of each mineral to the XRD spectrum. By summing up of these relative contributions and dividing each contribution by the sum of the total contribution, the relative quantity of each mineral (by weight) is calculate as a fraction of 1 (in percentages). Percentage of illite in illite/smectite mixed layer was estimated using the data in Moore and Reynolds (1997).

**Compaction**

Important for the determination of compaction are the minus cement porosity and the IGV. Minus cement porosity is the porosity that would be present if no intergranular cements were occurring in the sandstone. The intergranular volume (IGV) is the sum of the volume percentages of all components between the original sand grains, including intergranular porosity, matrix and cements (Paxton et al. 2002).

Porosity loss by compaction and cementation was calculated using the method of Lundegard (1992):

$$compactional\ porosity\ loss\ COPL = Pi - \frac{(100 - Pi)\ \times Pmc}{100 - Pmc}$$

$$cementational\ porosity\ loss\ CEPL = (Pi - COPL)\ \times \frac{C}{Pmc}$$

In which Pi is the depositional porosity and Pmc the minus cement porosity. The latter is the sum of two petrographically determined parameters: Po, which is the primary intergranular porosity, and C, being the volume of the pore-filling cement. Following Lundegard (1992), a depositional porosity (Pi) of 45% is used for the calculations. Note that this is an average value and depositional porosities in sandstones can vary between about 27% and 55%.

The maximum degree of mechanical compaction due to grain rearrangement that can be obtained during diagenesis leads to an IGV value of 26%, but the exact value depends on the sorting. Values lower than 26% are either due to the deformation of mechanically unstable grains or a result of chemical compaction. To evaluate the maximum degree of compaction that sandstone has experienced during diagenesis, most commonly the method of Paxton et al. (2002) is used. These authors regard the intergranular volume (IGV) as approximation of the porosity at the maximum stage of compaction. Since the IGV is defined as the sum of intergranular porosity, intergranular cements and of the detrital clay matrix, a (perfectly sorted, mature) sandstone with an IGV below 26% is either also chemically compacted at grain-to-grain contacts and/or mechanically unstable grains are squashed.

**References**

Adams, A.E., MacKenzie, W.S. (1998): A Colour Atlas of Carbonate Sediments and Rocks under the Microscope. Oxford University Press. 180 pp.

Flügel, E. (2004): Microfacies of Carbonate Rocks Analysis, Interpretation and Application. Springer, Berlin-Heidelberg-New York, 976 pp.

Lundegard, P. D. (1992): Sandstone porosity loss - A "big picture" view of the importance of compaction. Journal of Sedimentary Petrology, v.62, p. 250-260.

Moore, D.M., Reynolds, R.C. (1997): X-Ray Diffraction and the Identification and Analysis of Clay Minerals, second edition. Oxford University Press. 378 pp.

Paxton, S. T., Szabo, J. O., Ajdukiewicz, J. M., and Klimentidis, R. E. (2002): Construction of an intergranular volume compaction curve for evaluating and predicting compaction and porosity loss in rigid-grain sandstone reservoirs. American Association of Petroleum Geologists Bulletin, v.86 (12), p. 2047-2067.

Pettijohn, F. J. (1975): Sedimentary Rocks. Harper and Row, 628 pp.

# Appendix 2: Compiled petrographic table

| Well | Sample No. | Sample No. NAM | Depth (m) | Grain Size non-laminated | | | | Texture | | | | | | | Compaction and Cementation | | | | |
|------|-----------|---------------|-----------|----------|----------|--------------------------------|----------------------------------|---------|-----------|------------------------------|-------------------------------|--------------------|----------------------|----------|------------------------|--------------------------|---------|----------|----------|
| | | | | Min (µm) | Max (µm) | Mode (µm) (fine/coarse laminae) | Mode Class (fine/coarse laminae) | Sorting | Roundness | Grain contacts, rigid grains | Grain contacts, ductile grains | Texture | Sample heterogeneity | Fractures | Pore filling Cement (%) | Minus cement porosity (%) | IGV (%) | COPL (%) | CEPL (%) |
| ZRP-3A | P1 | R246 | 3582.50 | 31-62.5 | 350-500 | 177-250 | fine sand (U) | P | SR | P | L-CC | faintly laminated | low to moderate | none | 10.0 | 20.7 | 21 | 31 | 7 |
| ZRP-3A | P2 | R085 | 3542.25 | 88-125 | 1-1.41 mm | 177-250 | fine sand (U) | M-P | SA-SR | P-L | CC | grain alignment | low to moderate | none | 14.0 | 17.7 | 18 | 33 | 9 |
| ZRP-3A | P3 | R378 | 3615.50 | 31-62.5 | 500-710 | 177-250 | fine sand (U) | MG-M | SA-SR | P | L-CC | faintly laminated | low to moderate | artificial | 15.3 | 22.7 | 23 | 29 | 11 |
| ZRP-3A | P4 | R212 | 3574.00 | 62.5-88 | 710-1000 | 250-350 | medium sand (L) | MG-M | SR | P | L-CC | faintly laminated | low to moderate | none | 11.7 | 17.3 | 17 | 33 | 8 |
| ZRP-3A | P5 | R283 | 3591.75 | 62.5-88 | 710-1000 | 250-350 | medium sand (L) | M | SR | P-L | CC | faintly laminated | moderate | none | 10.0 | 20.3 | 20 | 31 | 7 |
| ZRP-3A | P6 | R182 | 3566.46 | 88-125 | 500-710 | 177-250 | fine sand (U) | MG | SA-SR | P-L | L-CC | structureless | low | none | 15.3 | 24.3 | 24 | 27 | 11 |
| ZRP-3A | P7 | R100 | 3546.00 | 31-62.5 | 1-1.41 mm | 125-177/350-500 | fine (L) / medium (U) sand | MG-B | SA | P | L-CC | laminated | moderate | none | 8.3 | 22.0 | 22 | 29 | 6 |
| ZRP-3A | P8 | R352 | 3609.00 | 88-125 | 500-710 | 250-350 | medium sand (L) | MG | SR | P-L | L-CC | structureless | low | none | 12.3 | 17.0 | 17 | 34 | 8 |
| ZRP-3A | P9 | R231 | 3578.75 | 62.5-88 | 500-710 | 177-250 | fine sand (U) | M | SR | P | L | structureless | low to moderate | artificial | 14.0 | 21.3 | 21 | 30 | 10 |
| ZRP-3A | P10 | R161 | 3561.25 | 31-62.5 | 500-710 | 177-250 | fine sand (U) | M-P | SA-SR | P-L | CC | faintly laminated | moderate | none | 9.3 | 14.7 | 15 | 36 | 6 |
| ZRP-3A | P11 | R332 | 3604.00 | 62.5-88 | 710-1000 | 177-250 | fine sand (U) | P | SA-SR | P | CC | laminated | moderate to high | none | 13.3 | 18.7 | 19 | 32 | 9 |
| ZRP-3A | P12 | R171 | 3563.71 | 31-62.5 | 710-1000 | 125-177 | fine sand (L) | P | SA-SR | P-L | CC | irregular lamination | moderate to high | none | 14.3 | 21.3 | 21 | 30 | 10 |
| ZRP-3A | P13 | R154 | 3559.32 | 31-62.5 | 500-710 | 177-250 | fine sand (U) | MG-M | SA-SR | P | L | structureless | low | artificial | 4.7 | 21.0 | 21 | 30 | 3 |
| ZRP-3A | P14 | R306 | 3597.50 | 62.5-88 | 350-500 | 177-250 | fine sand (U) | MG | SA-SR | P | L-CC | structureless | low | none | 18.0 | 23.0 | 23 | 29 | 13 |
| ZRP-3A | P15 | R269 | 3588.25 | 31-62.5 | 710-1000 | 88-125/250-350 | v.fine (U) / medium (L) sand | MG-B | SA-R | P | L-CC | laminated | moderate | none | 12.7 | 16.7 | 17 | 34 | 8 |
| ZRP-3A | P16 | R195 | 3569.75 | 31-62.5 | 710-1000 | 250-350 | medium sand (L) | P | SA-SR | P-L | CC | faintly laminated | low to moderate | none | 9.7 | 15.3 | 15 | 35 | 6 |
| ZRP-3A | P17 | R484 | 3641.95 | 31-62.5 | 710-1000 | 177-250 | fine sand (U) | MG-M | SA-SR | P | L-CC | structureless | moderate to high | none | 13.7 | 21.3 | 21 | 30 | 10 |
| ZRP-3A | P18 | R584 | 3667.03 | 62.5-88 | 350-500 | 177-250 | fine sand (U) | G-MG | SA-SR | P-L | L-CC | faintly laminated | low to moderate | artificial microfracs | 22.0 | 23.7 | 24 | 28 | 16 |
| ZRP-3A | P19 | R397 | 3620.24 | 31-62.5 | 500-710 | 125-177/350-500 | fine (L) / medium (U) sand | MG-B | SA-SR | P-L | L-CC | laminated | moderate | none | 11.0 | 22.3 | 22 | 29 | 8 |
| ZRP-3A | P20 | R115 | 3549.75 | 4-31 | 710-1000 | 88-125/250-350 | v. fine (U) / medium (L) sand | P-B | SA-SR | P | L-CC | irregular lamination | moderate to high | none | 12.7 | 19.7 | 20 | 32 | 9 |
| ZRP-3A | P21 | R556 | 3660.00 | 62.5-88 | 1-1.41 mm | 177-250 | fine sand (U) | M | SA-SR | P | L | laminated | low to moderate | none | 20.7 | 25.0 | 25 | 27 | 15 |
| ZRP-3A | P22 | R427 | 3627.74 | 31-62.5 | 500-710 | 88-125/177-250 | v. fine (U) / fine (U) sand | M | SA-SR | P-L | CC | laminated | moderate | none | 14.3 | 21.3 | 21 | 30 | 10 |
| ZRP-3A | P23 | R520 | 3651.00 | 31-62.5 | 1-1.41 mm | 88-125/250-350 | v. fine (U) / medium (L) sand | P | A-SR | P-L | L-PS | laminated | moderate to high | none | 16.3 | 21.3 | 21 | 30 | 11 |
| ZRP-3A | P24 | R136 | 3555.05 | 31-62.5 | 710-1000 | 250-350 | medium sand (L) | MG | SR | P | L-CC | structureless | low to moderate | artificial microfracs | 11.3 | 20.7 | 21 | 31 | 8 |
| ZRP-3A | P25 | R445 | 3632.25 | 31-62.5 | 710-1000 | 88-125 | v.fine sand (U) | M | SA-SR | P-L | CC | laminated | moderate | none | 17.7 | 22.3 | 22 | 29 | 13 |

*Depth and sample no. obtained after draft

**Appendix 2, Part A: Textural description and compaction/cementation properties of the 25 sublitharenite samples from well ZRP-3A.**

Sorting: P = poor, M = Moderate, MG = Moderately Good, G = Good B = Bimodal

Roundness: SR = Subrounded, SA = Subangular

Grain contacts: P = Point, L = Long, CC = Concavo-convex, PS = Pseudomatrix

Appendix 2, Part B: Point count results table — well ZRP-3A sublitharenite samples.

| Well | Sample No. | Sample No. NAM* | Depth (m)* | Rock Classification (Pettijohn 1975) | Monocrystalline quartz | Polycrystalline quartz | Feldspar, unleached | Feldspar, leached/microporous | Chert | Claystone | Claystone, ductile | Sedimentary rock fragment | Metamorphic, indeterminate | Igneous, indeterminate | Rock fragment, indeterminate | Rock fragment, microporous | Muscovite | Heavy minerals (zircon, tourmaline) | Glauconite | Opaque mineral | Quartz (PF) | Dolomite/Siderite (PF) | Barite | Illite (PF) | Chlorite (PF) | Kaolinite (PF) | Clay, indeterminate/mixed (PF) | Grain-rimming clay (mixed) | Grain-rimming (tangential & radial) Illite | Grain-Rimming Chlorite | Quartz (R) | Dolomite/Siderite (R) | Feldspar (R) | Opaque/Heavy mineral | Illite (R) | Chlorite (R) | Kaolinite (R) | Clay, indeterminate/mixed (R) | Intergranular | Oversized | Mouldic | Intragranular | SUM Macroporosity |
|---|---|---|---|---|---|---|---|---|---|---|---|---|---|---|---|---|---|---|---|---|---|---|---|---|---|---|---|---|---|---|---|---|---|---|---|---|---|---|---|---|---|
| ZRP-3A | P1 | R246 | 3582.50 | Sublitharenite | 44.0 | 9.0 | 3.3 | 3.0 | 0.3 | 1.3 | 0 | 2.7 | 1.0 | 1.0 | 4.7 | 1.7 | 0 | Tr | 0 | 0 | 1.0 | 0 | 0.3 | 0 | 1.3 | 1.3 | 1.7 | 0 | 4.3 | 0 | 0.3 | 0 | 0 | 0.3 | 0 | 0 | 3.7 | 0.7 | 10.7 | 0 | 0 | 2.3 | 13.0 |
| ZRP-3A | P2 | R085 | 3542.25 | Sublitharenite | 40.3 | 9.3 | 3.0 | 2.7 | 1.0 | Tr | 0 | 1.3 | 1.0 | 3.7 | 4.7 | 1.3 | Tr | Tr | 0 | Tr | 2.0 | 3.3 | 0.3 | 0 | 0 | 1.7 | 3.7 | 0 | 3.0 | 0 | 2.0 | 0 | 0 | Tr | 0.7 | 0 | 6.7 | 1.3 | 3.7 | 1.3 | 0 | 2.0 | 7.0 |
| ZRP-3A | P3 | R378 | 3615.50 | Sublitharenite | 44.3 | 12.7 | 2.0 | 2.0 | 1.3 | 0 | 0.3 | 0.7 | 0 | 1.0 | 3.3 | 1.7 | 0 | Tr | 0 | 0 | 1.7 | 0.7 | 0 | 0 | 0.7 | 0 | 0.3 | 0 | 6.0 | 6.0 | 0.7 | 0.7 | 0 | 0.3 | 0 | 0 | 1.3 | 1.0 | 7.3 | 0.7 | 1.0 | 2.3 | 11.3 |
| ZRP-3A | P4 | R212 | 3574.00 | Sublitharenite | 38.7 | 12.0 | 4.3 | 4.0 | 0.7 | 0 | Tr | 1.3 | 0.3 | 0.3 | 6.0 | 3.3 | 0 | Tr | 0 | 0 | 0.3 | 0 | Tr | 0 | 0.3 | 0.3 | 6.0 | 0.7 | 2.7 | 1.3 | Tr | 0.3 | 0 | 0 | 0.3 | 0 | 4.3 | 3.3 | 5.7 | 1.0 | 0.7 | 1.7 | 9.0 |
| ZRP-3A | P5 | R283 | 3591.75 | Sublitharenite | 37.0 | 16.0 | 2.3 | 3.3 | 0.7 | 0 | 0 | 1.7 | Tr | 2.3 | 3.7 | 3.7 | Tr | 0 | 0 | 0 | 0.3 | 0 | 0 | 0.3 | 0 | 2.3 | 1.0 | 1.3 | 4.0 | 0.7 | 0.7 | 0 | 0 | 0 | 0 | 0 | 5.7 | 1.0 | 10.3 | 0.3 | 0 | 1.3 | 12.0 |
| ZRP-3A | P6 | R182 | 3566.46 | Sublitharenite | 48.0 | 10.3 | 1.7 | 3.7 | 0.3 | 0.3 | 0 | 1.0 | Tr | 1.0 | 2.7 | 2.0 | 0 | 0 | 0 | Tr | 3.7 | 0 | 0.3 | 0 | 0.3 | 0.3 | 1.0 | 0.7 | 5.7 | 3.3 | 0.3 | Tr | 0 | 0.3 | 0 | 0.3 | 0.7 | 1.3 | 9.0 | 0 | 0 | 1.7 | 10.7 |
| ZRP-3A | P7 | R100 | 3546.00 | Sublitharenite | 46.0 | 9.0 | 4.7 | 2.0 | 0.7 | 1.7 | 0 | 0.7 | 0 | 3.3 | 3.0 | 1.7 | Tr | Tr | 0 | 0.3 | 0.7 | 3.0 | 0.3 | 0 | 0 | 0.7 | 1.3 | 0 | 2.3 | 0 | 0.3 | 0 | 0 | 0 | 0 | 0 | 2.0 | 1.0 | 13.7 | 0 | 0.7 | 1.0 | 15.3 |
| ZRP-3A | P8 | R352 | 3609.00 | Sublitharenite | 44.7 | 13.3 | 1.3 | 2.3 | 0.7 | 0.3 | 0 | 0.7 | 0.3 | 1.7 | 3.0 | 3.0 | Tr | 0 | 0 | 0 | 1.0 | 0.7 | Tr | 0.3 | 0 | 0.3 | 3.7 | 3.7 | 2.3 | 0.3 | 0.3 | Tr | 0 | 0 | 0 | 1.0 | 5.7 | 1.3 | 4.7 | 0.3 | 1.3 | 1.7 | 8.0 |
| ZRP-3A | P9 | R231 | 3578.75 | Sublitharenite | 42.0 | 16.7 | 4.0 | 2.0 | 0.7 | 1.0 | 0 | 0.3 | 0 | 3.0 | 2.7 | 0.3 | 0 | Tr | 0 | Tr | Tr | 0 | 0 | 0.3 | 0.3 | 0 | 1.7 | 7.0 | 4.3 | 0 | 0.3 | Tr | 0 | 0.3 | 0 | 0.3 | 1.0 | 1.3 | 7.3 | 0.3 | 0.7 | 1.7 | 10.0 |
| ZRP-3A | P10 | R161 | 3561.25 | Sublitharenite | 50.0 | 10.7 | 3.7 | 4.7 | 0.3 | 1.3 | 0 | 1.0 | 0.3 | 1.0 | 3.0 | 2.0 | Tr | Tr | 0 | 0 | Tr | 1.3 | 0.3 | 0 | 0.3 | 0 | 2.7 | 0.7 | 4.0 | 0 | 0.3 | Tr | 0 | 0 | 0 | 0 | 3.3 | 1.3 | 5.3 | 0.3 | 0.7 | 1.3 | 7.7 |
| ZRP-3A | P11 | R332 | 3604.00 | Sublitharenite | 43.0 | 16.3 | 2.3 | 2.3 | 1.7 | 1.3 | 0 | 2.0 | 0.3 | 1.7 | 4.0 | 0.7 | 0 | Tr | 0 | 0 | 0.3 | 0 | 0.3 | 0 | 0 | 0 | 0.7 | 1.3 | 5.3 | 5.3 | 0 | 0.3 | 0 | 0 | 0 | 0 | 1.0 | 2.0 | 5.3 | 0 | 1.3 | 1.0 | 7.7 |
| ZRP-3A | P12 | R171 | 3563.71 | Sublitharenite | 49.7 | 7.0 | 3.0 | 2.3 | 0.7 | 1.7 | 0.7 | 0 | 0 | 1.3 | 4.0 | 1.3 | Tr | 0.3 | 0 | 0 | Tr | 5.3 | 0 | 1.0 | 0 | 0.7 | 1.7 | 0.7 | 5.0 | 0 | 0.7 | 0.3 | 0 | 0 | 0 | 0.3 | 1.7 | 2.0 | 7.0 | 0.3 | Tr | 1.3 | 8.7 |
| ZRP-3A | P13 | R154 | 3559.32 | Sublitharenite | 44.3 | 12.0 | 4.0 | 3.7 | 0 | 1.0 | 0 | 0.3 | 0.3 | 1.7 | 1.3 | 4.0 | 0 | Tr | 0 | 0 | Tr | 0.3 | Tr | 0 | 0 | 0.7 | 0 | 0.7 | 3.0 | 0 | 1.0 | 0 | 0 | 0 | 0.3 | 0 | 2.7 | 0 | 16.3 | 1.0 | Tr | 1.3 | 18.7 |
| ZRP-3A | P14 | R306 | 3597.50 | Sublitharenite | 38.7 | 11.3 | 1.0 | 2.7 | 0.7 | Tr | 0 | 1.3 | Tr | 2.3 | 2.3 | 3.3 | 0 | 0 | 0 | Tr | 0.3 | 5.3 | 0 | 0 | 0 | 2.0 | 6.3 | 1.0 | 3.0 | 0 | 0 | 0 | 0 | 0 | 0.3 | 0 | 5.7 | 3.7 | 5.0 | 0.7 | 1.3 | 1.7 | 8.7 |
| ZRP-3A | P15 | R269 | 3588.25 | Sublitharenite | 50.7 | 12.7 | 3.0 | 1.3 | 0.3 | 0.7 | 0 | 0.3 | 0.3 | 1.3 | 4.0 | 3.3 | 0 | Tr | Tr | 0 | Tr | 1.7 | 0 | 0 | 0 | 0.3 | 1.0 | 1.3 | 6.3 | 2.0 | 0.3 | 0.3 | 0 | 0 | 0 | 1.3 | 2.0 | 0.7 | 4.0 | 0 | Tr | 0.7 | 4.7 |
| ZRP-3A | P16 | R195 | 3569.75 | Sublitharenite | 42.0 | 13.0 | 4.7 | 3.7 | 0.3 | 1.3 | 0 | 0.7 | 0.7 | 4.7 | 4.3 | 1.3 | 0 | 0 | 0 | Tr | 1.0 | 1.3 | 0 | 0.3 | 0 | 0.3 | 2.0 | 1.7 | 3.0 | 0 | 0.7 | 1.0 | 0 | Tr | 0 | 0 | 3.3 | 1.3 | 5.7 | 0.3 | Tr | 1.3 | 7.3 |
| ZRP-3A | P17 | R484 | 3641.95 | Sublitharenite | 44.7 | 10.0 | 2.0 | 1.3 | 0.3 | Tr | 0 | 1.3 | 0.3 | 1.7 | 3.7 | 0 | Tr | Tr | 0 | Tr | 1.0 | 5.7 | 0 | 0 | 0 | 0.7 | 3.7 | 0.7 | 1.7 | 0.3 | 1.0 | Tr | 0.3 | 0 | 0.3 | 0.7 | 5.7 | 1.7 | 7.7 | 0 | 0.3 | 2.7 | 11.0 |
| ZRP-3A | P18 | R584 | 3667.03 | Sublitharenite | 46.3 | 15.7 | 2.7 | Tr | 0 | 0.3 | 0 | 0.7 | 0 | 1.0 | 3.3 | 1.0 | 0 | Tr | 0 | 0 | 1.3 | 0.3 | 0.7 | 0 | 0.3 | 1.0 | 9.3 | 4.3 | 4.7 | 0 | 1.0 | 0 | 0.3 | 0 | 0 | 0.3 | 1.3 | 1.3 | 1.7 | 0 | 0.7 | 0.3 | 2.7 |
| ZRP-3A | P19 | R397 | 3620.24 | Sublitharenite | 40.7 | 12.0 | 2.0 | 3.3 | 2.0 | 0.7 | 0 | 0 | 0.7 | 0.7 | 4.0 | 2.3 | 0 | Tr | Tr | Tr | 0.3 | 1.3 | 0.3 | 0 | 0.3 | 0.7 | 1.3 | 1.0 | 4.7 | 1.0 | 0.3 | 0.7 | 0 | Tr | 0.7 | 0.7 | 5.0 | 1.3 | 11.3 | 0 | 0.7 | Tr | 12.0 |
| ZRP-3A | P20 | R115 | 3549.75 | Sublitharenite | 45.7 | 9.0 | 2.3 | 3.3 | 0.7 | 0 | 2.0 | 0.3 | 1.0 | 1.3 | 4.3 | 1.7 | 0.7 | 0.3 | 0 | 0 | 1.0 | 4.7 | Tr | 0.7 | 0.7 | 0.3 | 2.3 | 0.7 | 2.3 | 0 | 0 | Tr | 0 | 0.7 | 0.3 | Tr | 2.3 | 2.7 | 7.0 | 0.3 | 0.7 | 0.7 | 8.7 |
| ZRP-3A | P21 | R556 | 3660.00 | Sublitharenite | 38.7 | 20.3 | 3.3 | 0.7 | 1.0 | Tr | 0.3 | 0.3 | 0 | 0.3 | 2.7 | 0.3 | Tr | Tr | 0 | 0 | 0.3 | 0.7 | 0 | 0 | 4.3 | 0 | 0 | 1.0 | 1.3 | 13.0 | 0.3 | Tr | 0 | 0 | 0.3 | 1.7 | 2.7 | 1.3 | 4.3 | 0.3 | 0 | 0.3 | 5.0 |
| ZRP-3A | P22 | R427 | 3627.74 | Sublitharenite | 40.7 | 18.0 | 1.3 | 1.3 | 0.7 | 1.3 | 0 | 0.7 | 0.7 | 1.0 | 4.7 | 1.7 | Tr | 0 | 0 | Tr | 2.3 | 1.7 | 0 | 0 | 4.3 | 0 | 1.0 | 0.7 | 4.0 | 0 | 0.3 | 0 | 0 | 0 | 0 | 1.7 | 2.0 | 0.7 | 7.0 | 0.3 | 0 | 1.7 | 9.0 |
| ZRP-3A | P23 | R520 | 3651.00 | Sublitharenite | 46.3 | 14.3 | 2.7 | Tr | 1.0 | 0.3 | 1.0 | 0.3 | 0 | 1.0 | 3.3 | 1.0 | 0.3 | 0 | 0 | Tr | 1.3 | 2.0 | 0.3 | 0.3 | 2.0 | 0 | 3.7 | 2.7 | 2.3 | 1.7 | 0.7 | Tr | 0 | 0.3 | 0.7 | 0.3 | 2.3 | 2.0 | 5.0 | 0 | Tr | 0.7 | 5.7 |
| ZRP-3A | P24 | R136 | 3555.05 | Sublitharenite | 40.0 | 18.3 | 2.3 | 2.3 | 1.3 | 0.3 | 0 | 0.3 | 0.3 | 1.3 | 4.0 | 3.3 | Tr | 0 | 0 | 0 | 0 | 3.0 | 0.3 | 0 | 0 | 1.0 | 6.0 | 0.7 | 0.3 | 0 | 0.3 | Tr | 0 | 0 | 0 | 0.3 | 2.7 | 1.3 | 9.3 | 0 | 0.3 | 0.3 | 10.0 |
| ZRP-3A | P25 | R445 | 3632.25 | Sublitharenite | 47.7 | 12.0 | 3.0 | 1.7 | 0 | 1.0 | 0.3 | 0 | 1.0 | 0.3 | 4.0 | 0.3 | Tr | Tr | 0 | Tr | 1.3 | 5.0 | 0 | 0 | 0.3 | 0 | 5.3 | 2.7 | 3.0 | 0 | 0.7 | Tr | 0 | 0 | 0 | 1.0 | 1.7 | 2.7 | 4.7 | 0.3 | 0 | 0 | 5.0 |

*Depth and sample no. obtained after draft

**Appendix 2, Part B: Point count results of the 25 sublitharenite samples from well ZRP-3A. Tr = trace amount (observed in the thin section but not point counted).**

# Appendix 3: Point count glossary

This appendix contains photographs of key components. These photographs are used as a reference for thin section point counting and descriptions. The red crosses on the images point out the respective mineral.

## Detrital Grains

The main detrital mono-mineralic constituents comprise quartz and feldspar.

**Monocrystalline quartz**



**Polycrystalline quartz**
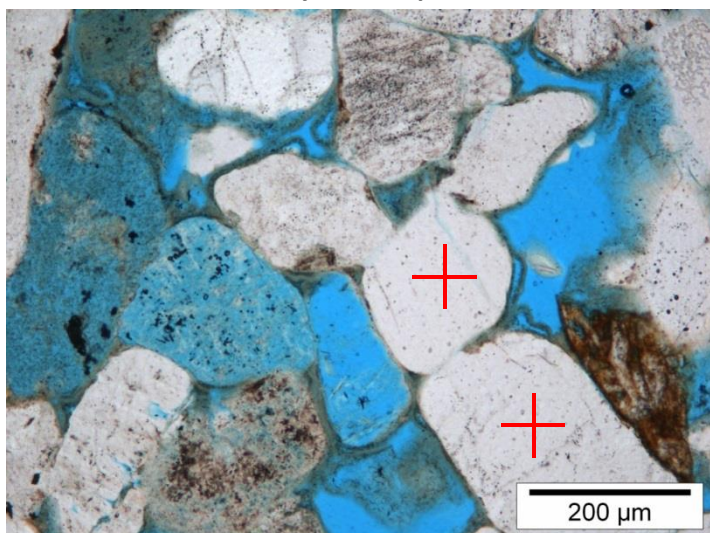


**Feldspar, unleached**
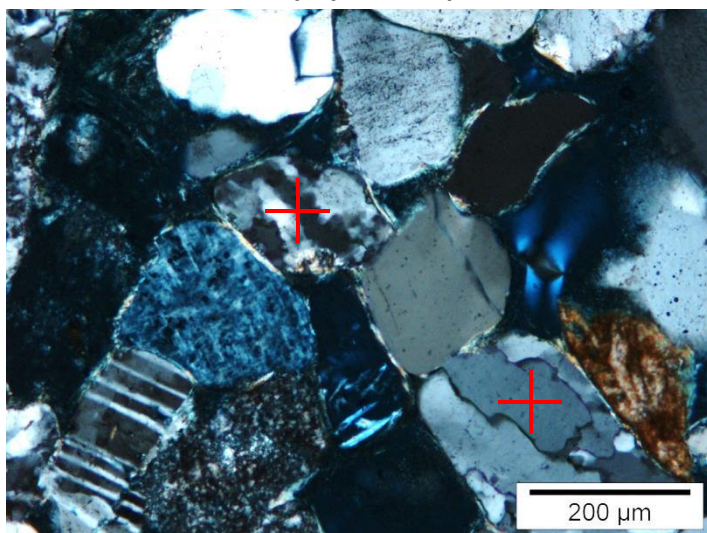
**Feldspar, leached/microporous**

Left: Feldspar identification is mostly based on the presence of a clear cleavage or, if present, twinning of the grain in XPL. Right: A microporous feldspar is identified when the crosshair points on a microporous-rich area. If the crosshair points on larger intragranular pores, it is defined as an intragranular pore.





.
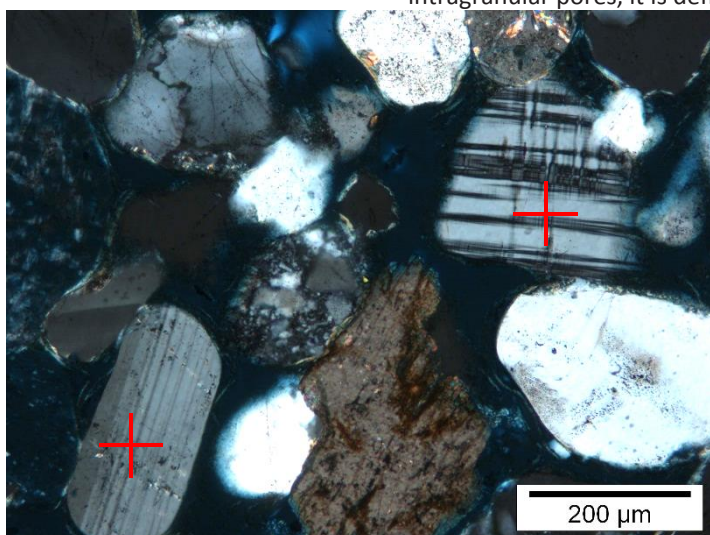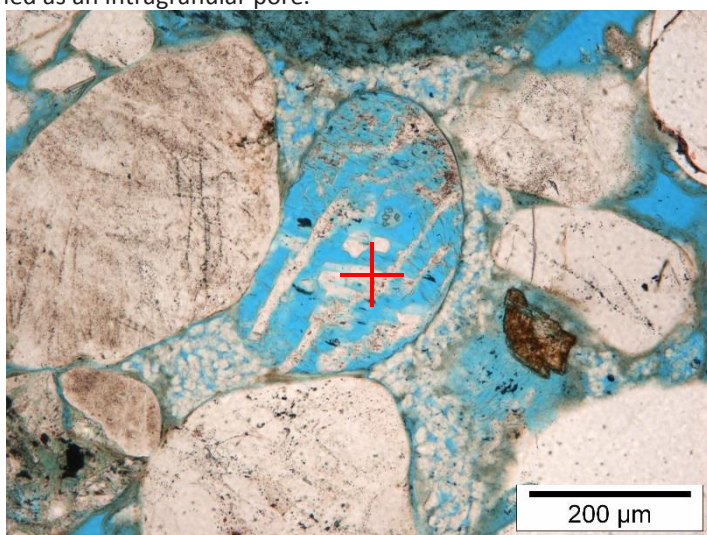
# Detrital Grains – Rock Fragments

Most rock fragments are rigid. Leached (microporous) rock fragments and claystone fragments are however commonly deformed due to compaction.

## Chert



## Claystone (ductile)  ·  Sedimentary rock fragment (SRF)
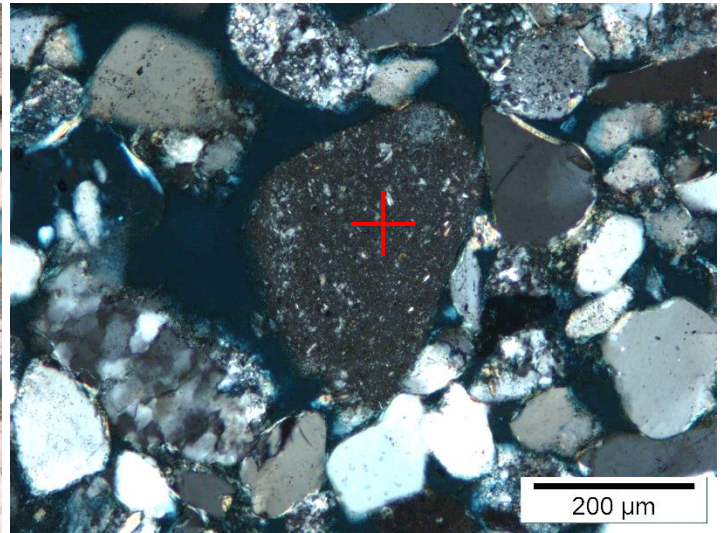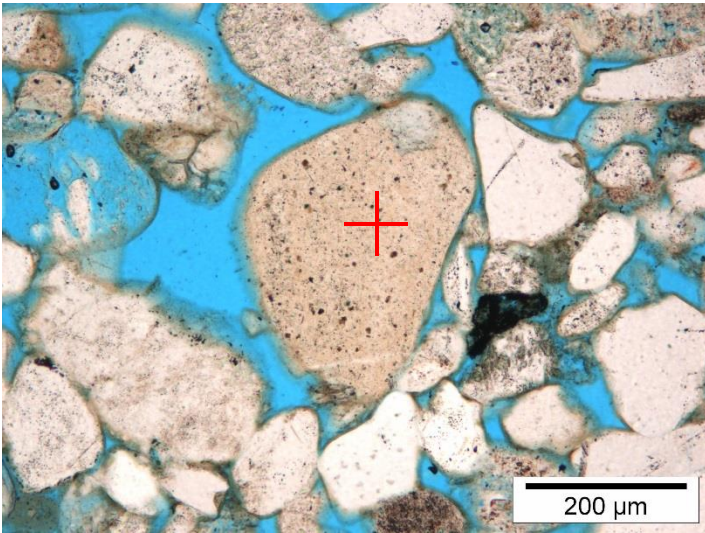
Left: Most claystone grains are strongly deformed due to compaction. Right: SRF comprise mostly siltstone and sandstone fragments.
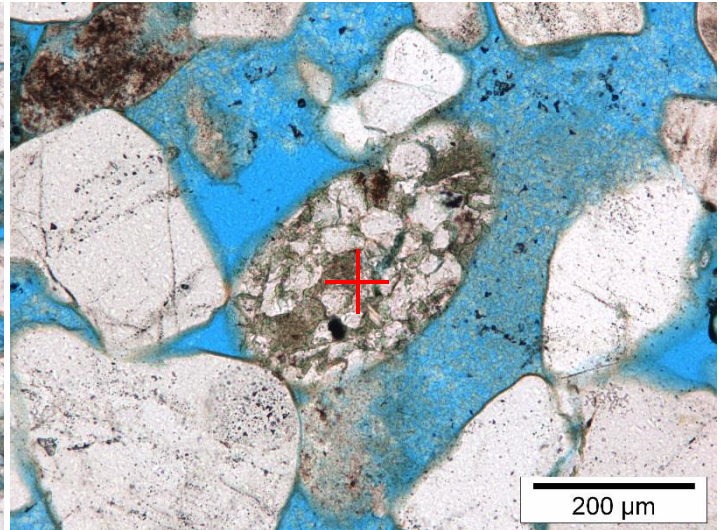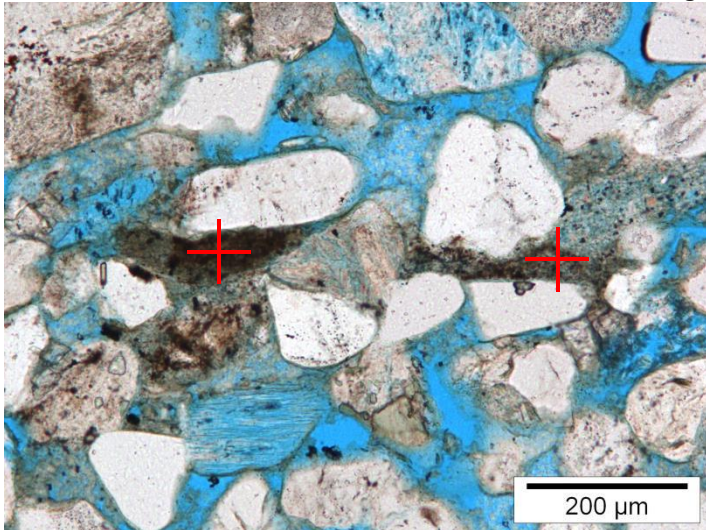
## Metamorphic rock fragment (MRF)

Grains with a clear foliation (example is schist-like). Grains are often elongated.
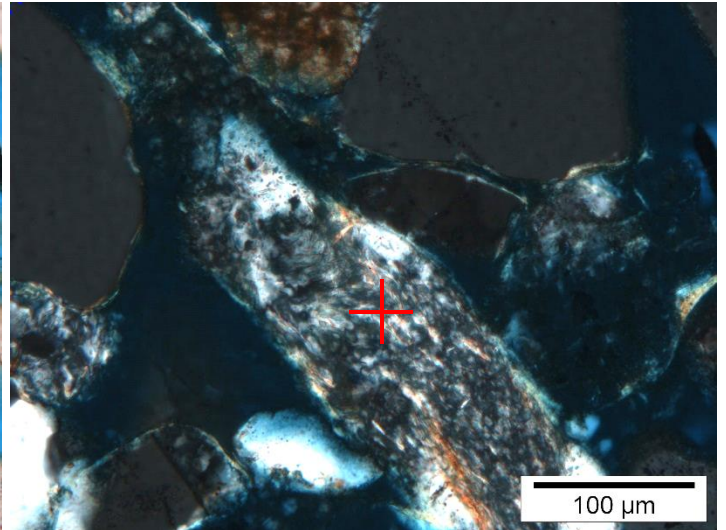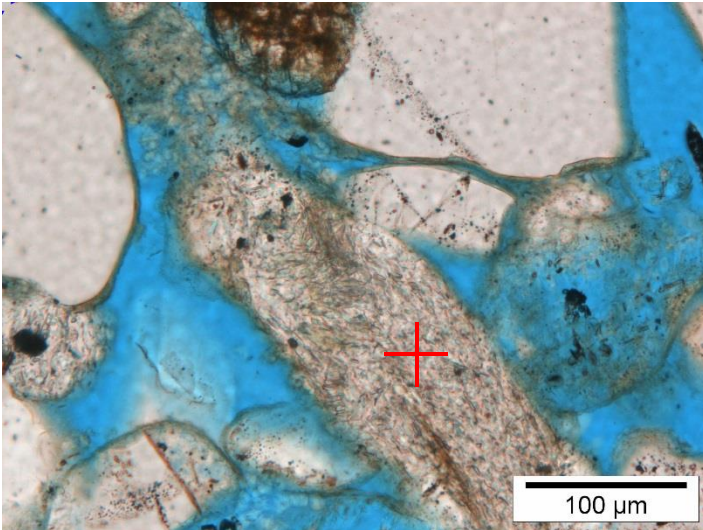



## Igneous rock fragment (IRF)          ## Rock fragment, indeterminate (RF)

Left: Commonly, the IRF are partially altered, containing greenish chlorite and micropores. The relatively coarse-crystalline nature (intrusive) is often still visible. Sometimes, the feldspar grains are leached. Right: RF vary from quartz rich (light) to dark (as shown here).
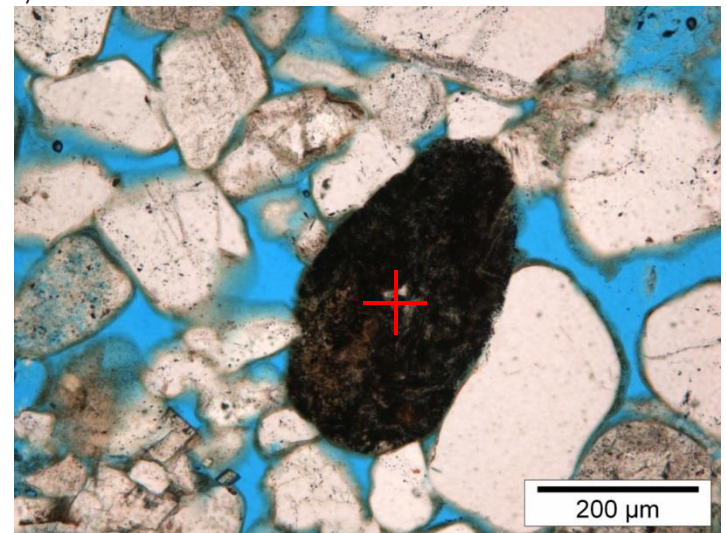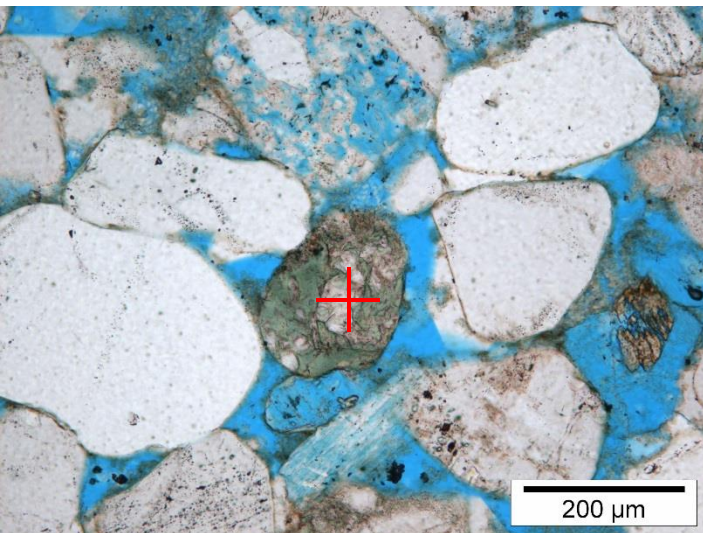
## Rock fragment, microporous

This category comprises strongly leached igneous and sedimentary rock fragments, and are rich in authigenic unidentified clay. Locally, other authigenic cements occurs.
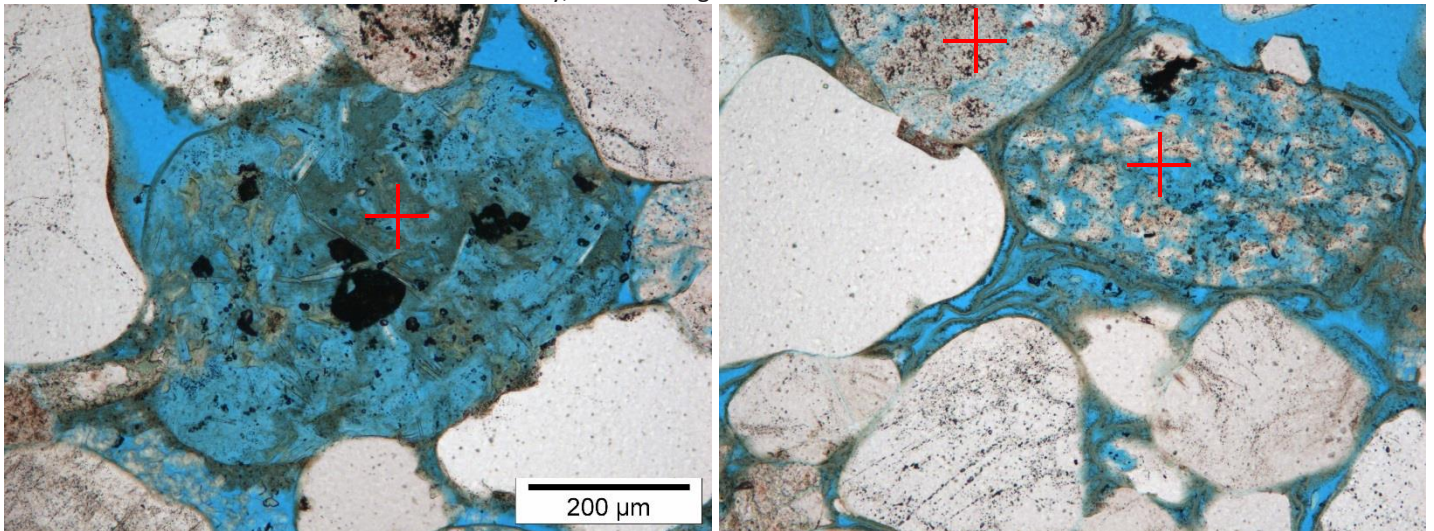


## Detrital Grains – Accessories

Accessory minerals are often not encountered during point counting, but trace amounts do occur in most samples. Glauconite (right) has a higher, and brighter green birefringence compared to chlorite.
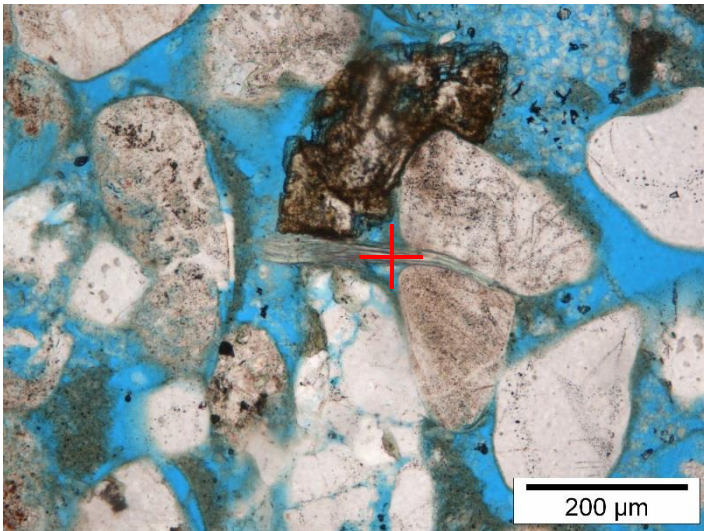
**Muscovite**                    **Glauconite**
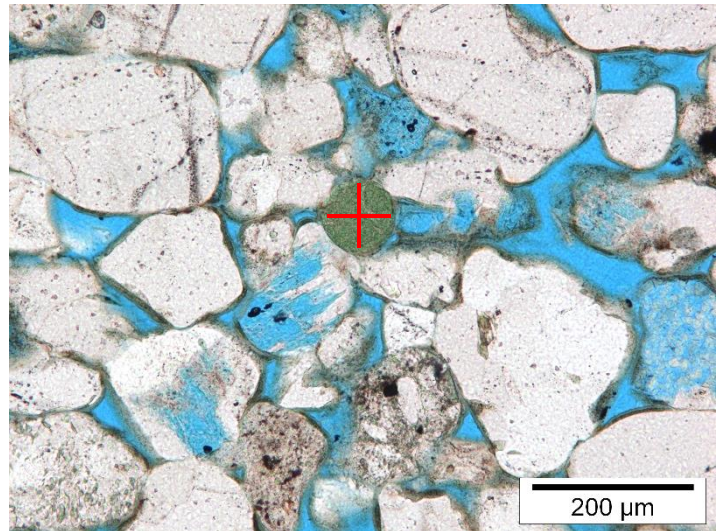
**Heavy minerals (e.g. zircon, tourmaline)**

Zircon
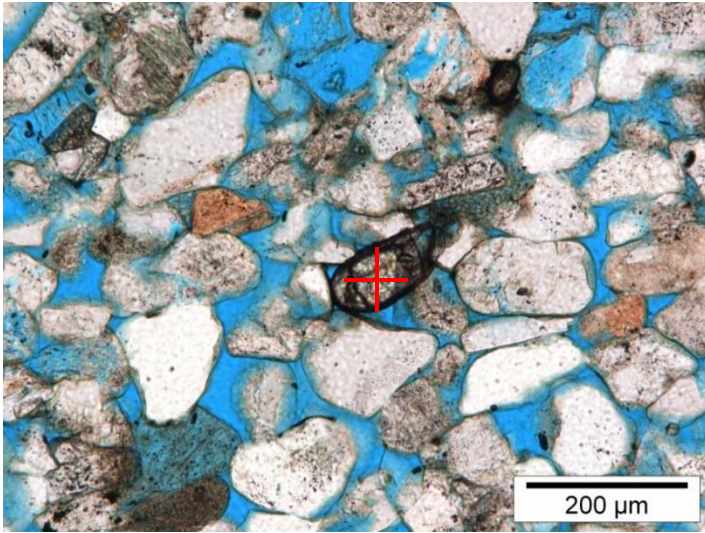
Tourmaline
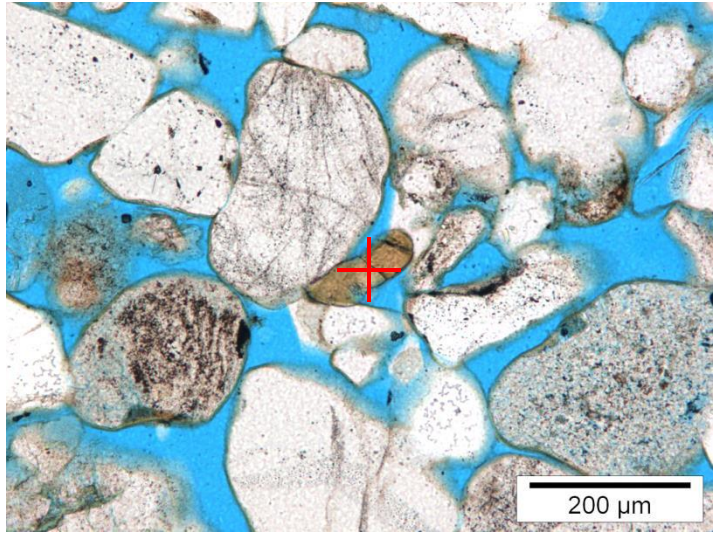


**Opaque minerals**
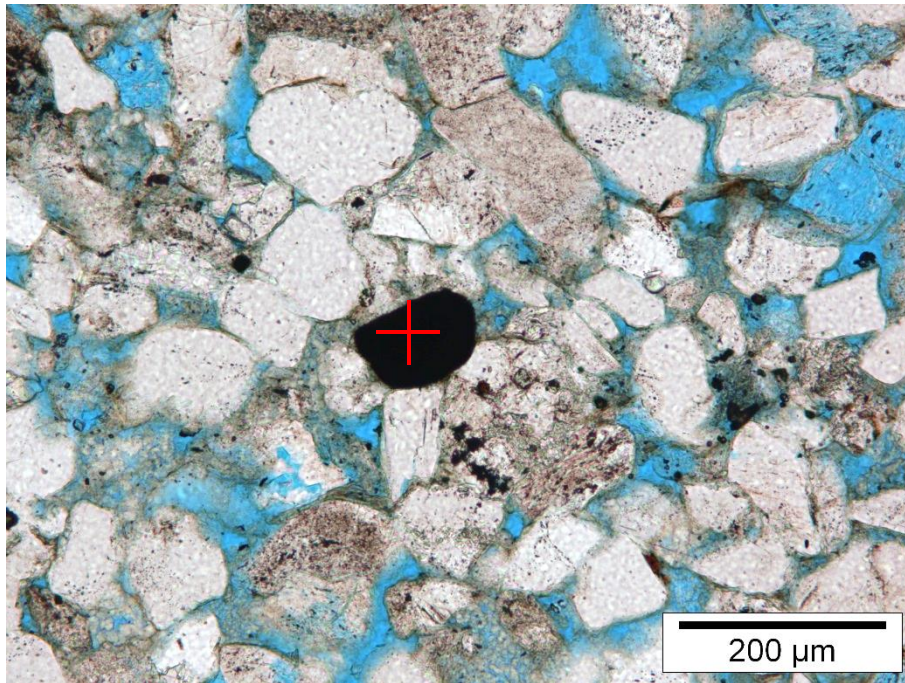
# Authigenic Components – Intergranular, pore-filling

## Quartz

Left: quartz formed on top of a clay coating. Coating not interrupted in this field of view. This is possibly a 3D effect. Right: Locally, PF quartz formed in between the clay rim and the detrital grain (right photo)



200 µm



200 µm
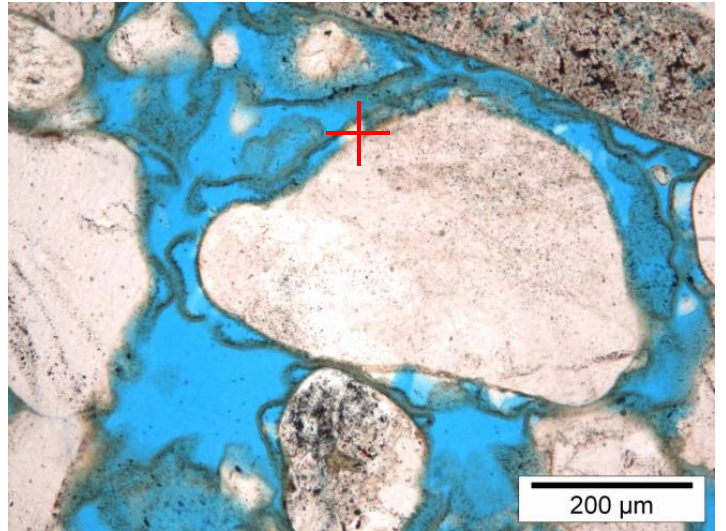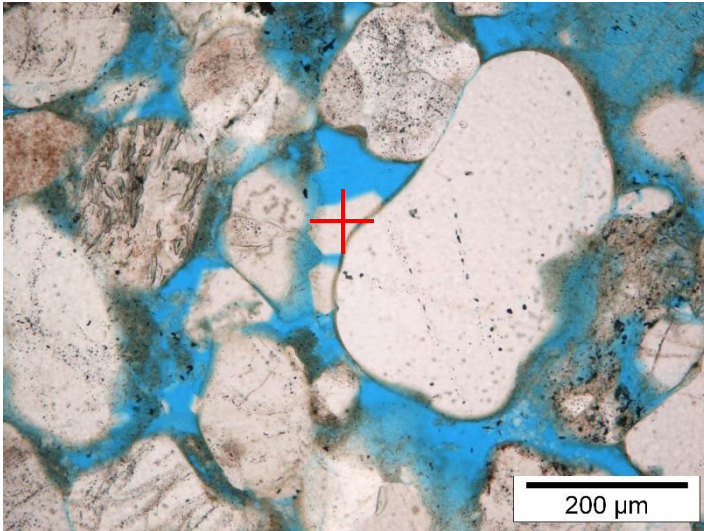
## Dolomite / Siderite

Can be both inclusion rich and inclusion poor (as shown here). Most dolomite shows zonation, commonly related to the Fe-content (visible in EDX). Siderite is differentiated from dolomite in the XRD and EDX.



200 µm
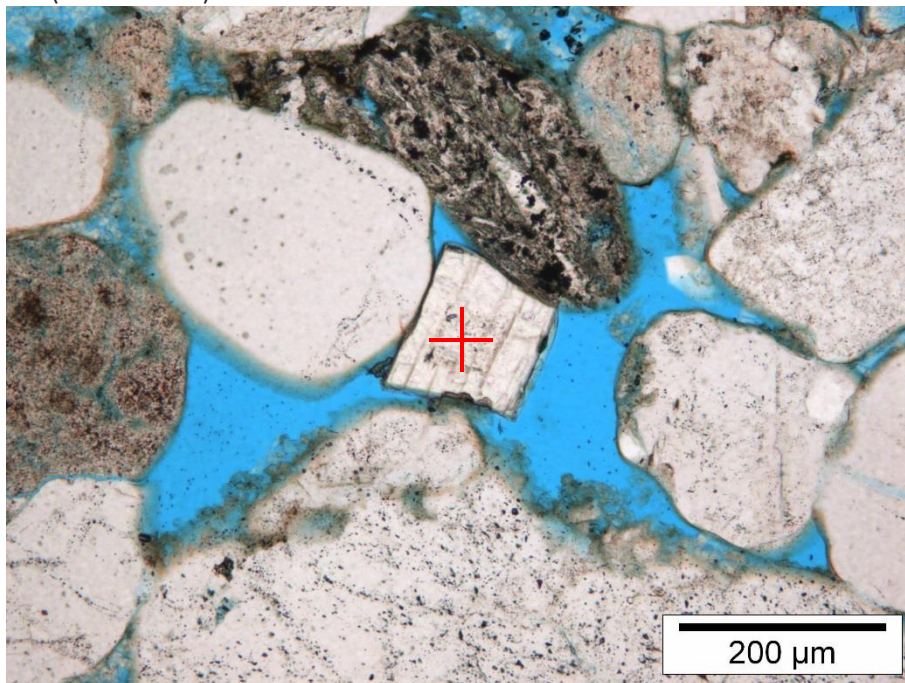
**Barite**
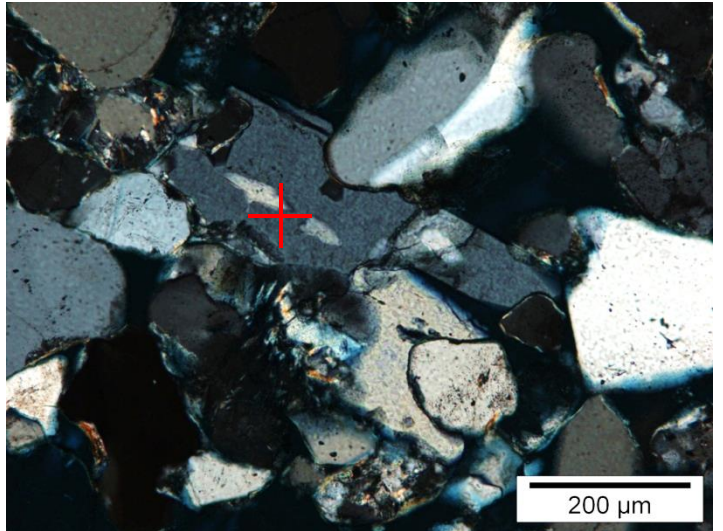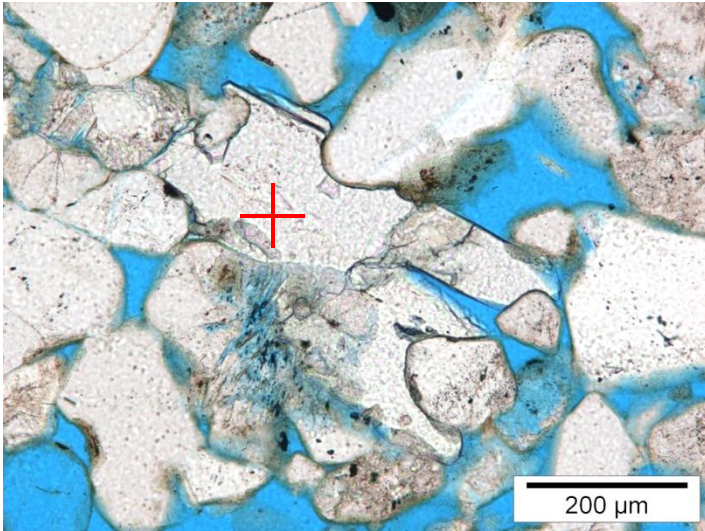




**Chlorite**

Commonly greenish in PPL. In XPL, low birefringence with a faint greenish hue. Possibly partially mixed with other clay.
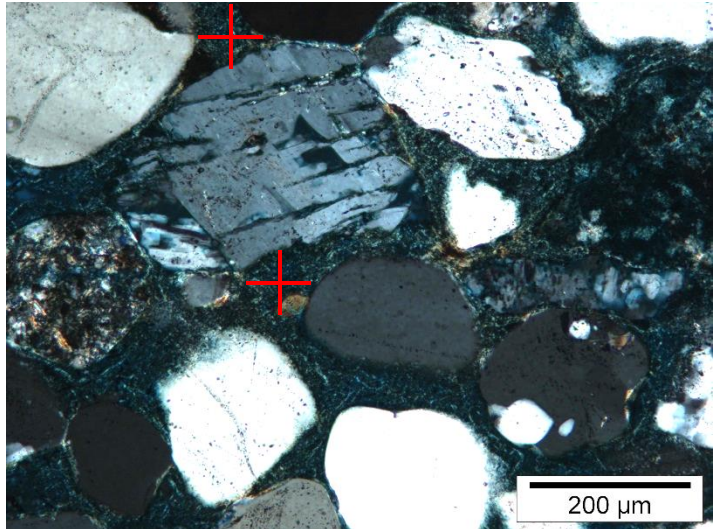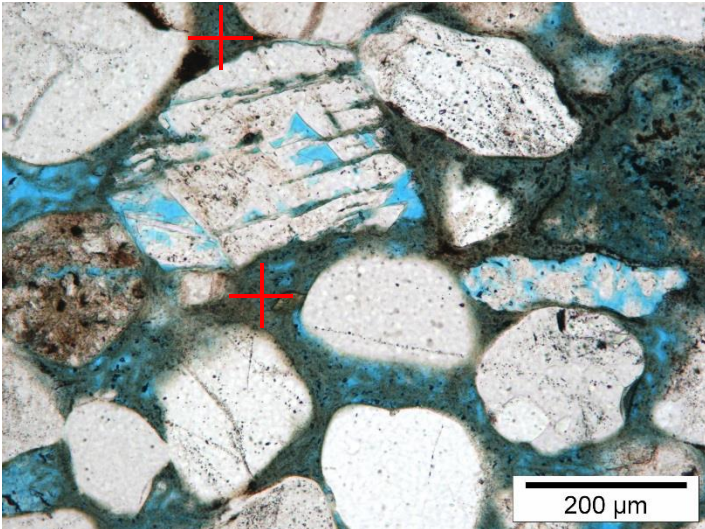
## Kaolinite

Left: In XPL, kaolinite has a low birefringence (white-greyish). Booklet shapes visible in both PPL and XPL. Right: Unidentified clay is very fine crystalline commonly greenish and has both low and higher birefringence minerals (mixed chlorite/illite?)

## Clay, indeterminate / mixed
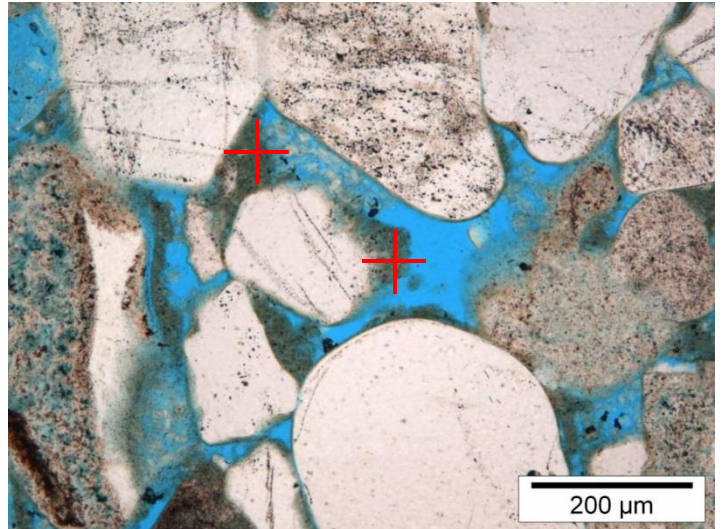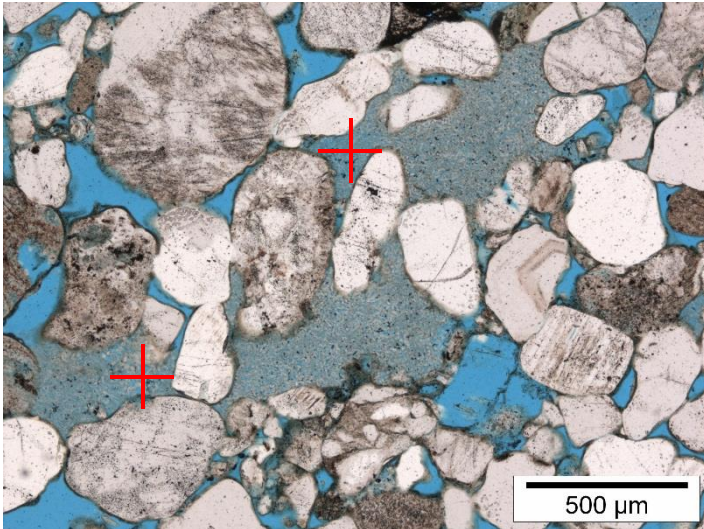




## Authigenic Components – Grain-rimming clay

Grain rimming clay occurs in all samples, but the thickness and clay types vary per sample. Identification of the minerals is mostly based on the birefringence colour, the SEM/BSEM images and the XRD results.

### Grain rimming illite, mostly tangential

Bright birefringence colour, thicker in the concave parts of the grain. Could have formed prior to final deposition, during rolling of the grains. Commonly covered with radial illitic clay.
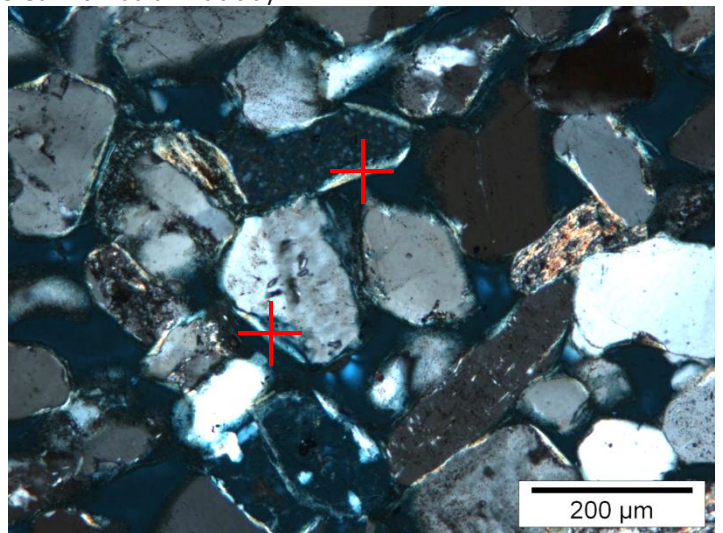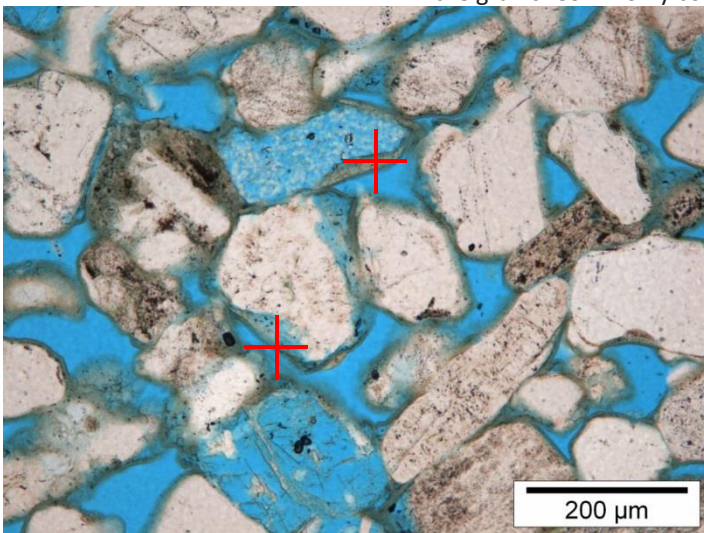
# Grain rimming chlorite

Coarser crystalline fibres (in 2D). Low birefringence colour, partially dull blueish to greenish. Formed often between grain and the radial clay coating, likely after clay coating detachment.



100 µm



100 µm
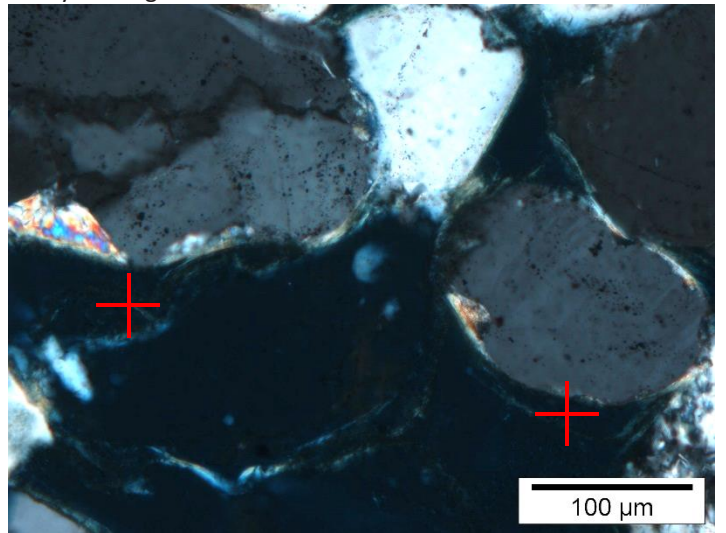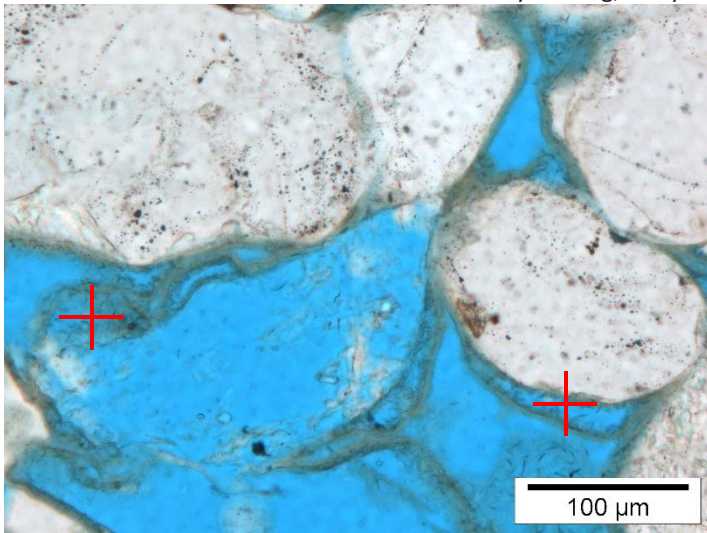
# Grain rimming clay, mixed and mostly radial

Fine crystalline, likely mixed illite/chlorite. Generally low birefringence. Covers tangential illite and is purely authigenic.



100 µm



100 µm
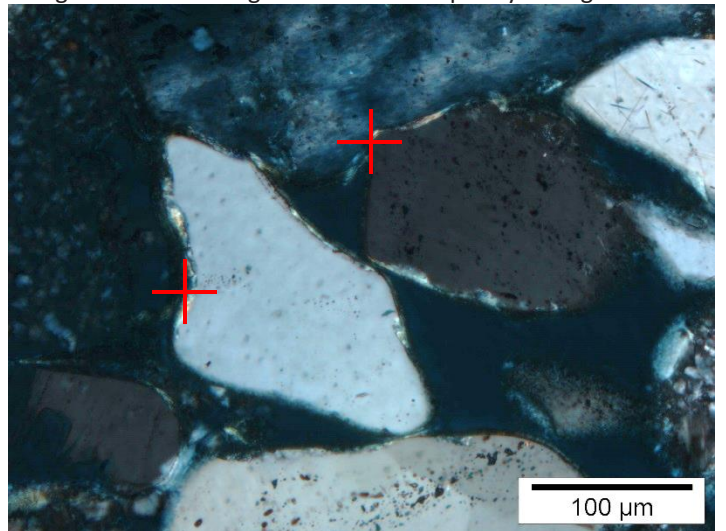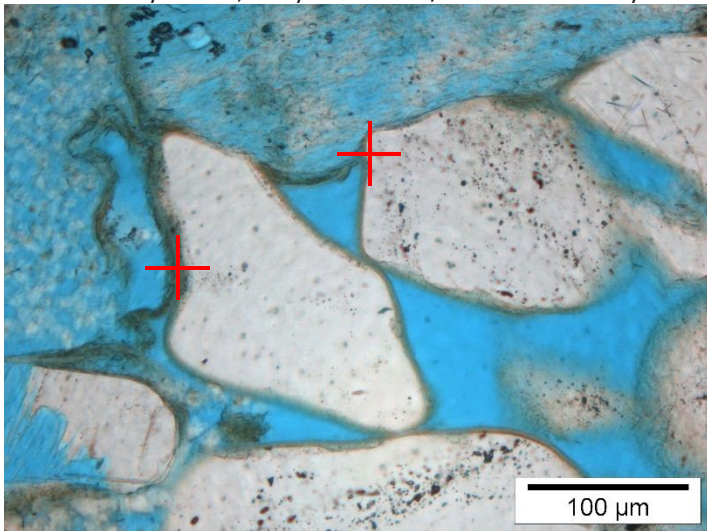
# Authigenic Components – Replacive

## Quartz

## Feldspar

Left: Quartz locally formed in leached grains, mostly in areas where grain was in contact with a quartz grain, and where the clay coating is lacking. Right: Authigenic feldspar is rare (according to BSEM & EDX) and difficult to distinguish from replacive quartz. Overgrowths are commonly small.



200 µm



200 µm

## Dolomite / Siderite
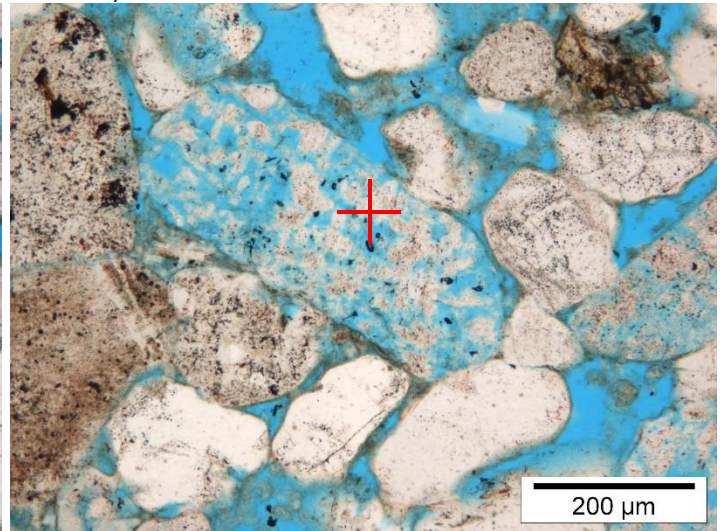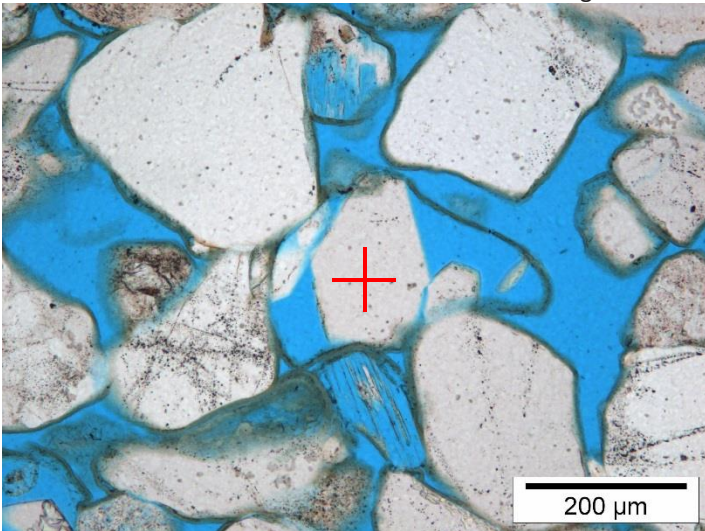
## Opaque / Heavy mineral (e.g. rutile)

Right: Relatively fine crystalline rutile. Intergrown crystals result a fractured appearance.



200 µm



200 µm
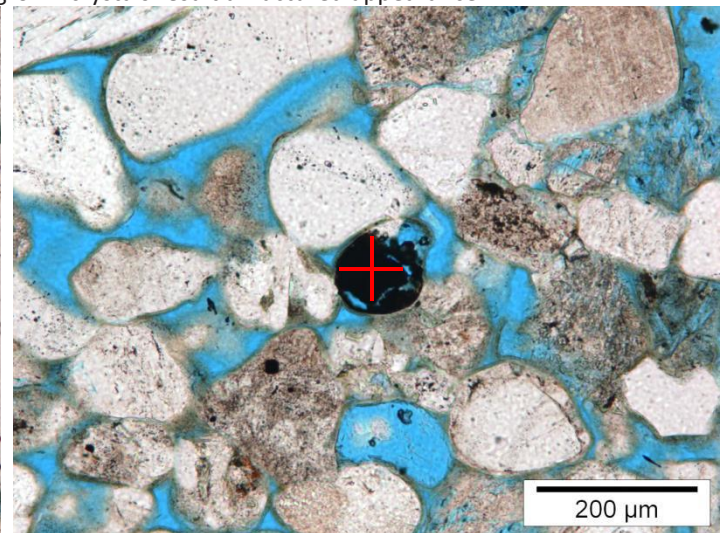
## Illite

Rare. Idientified by the high birefringence colour.
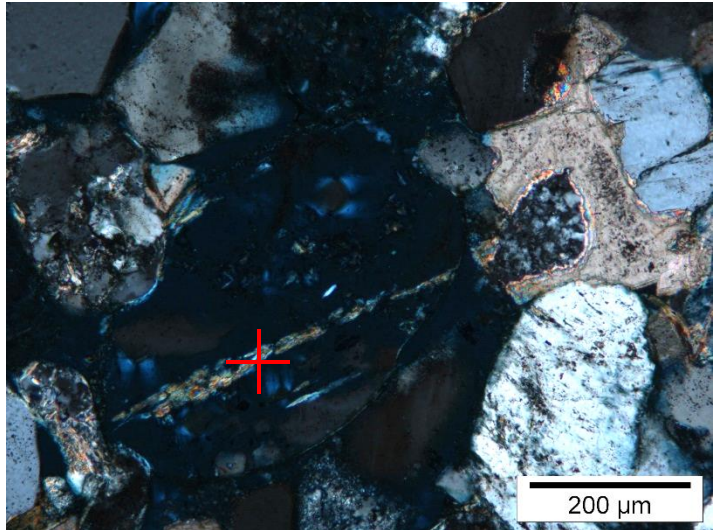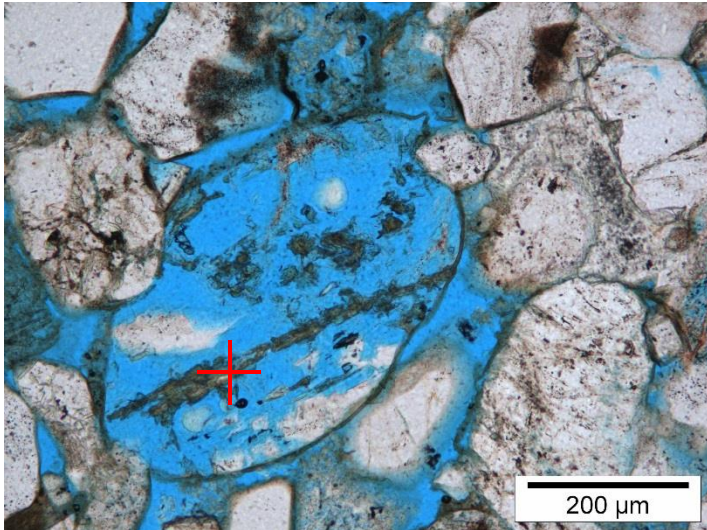




## Chlorite                                    Kaolinite

Left: Chlorite is identified by the fibrous nature of the crystals (in XPL: low birefringence, dull greenish). Right: Replacive kaolinite is identified as booklet shaped clusters (in XPL: low birefringence, grey)
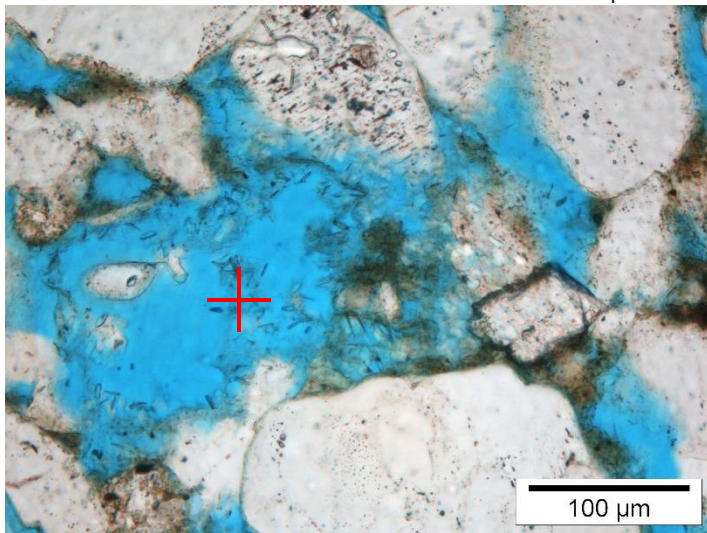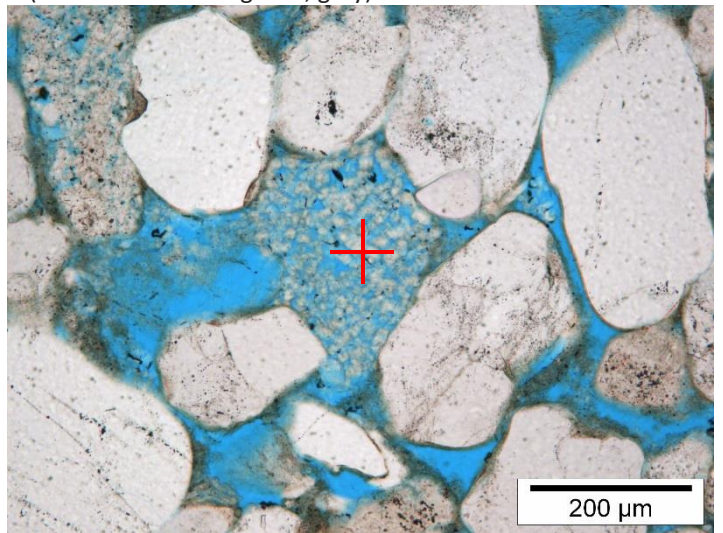
## Clay, indeterminate / mixed

Very fine crystalline. Generally low birefringence colour and therefore likely to be dominantly chlorite.
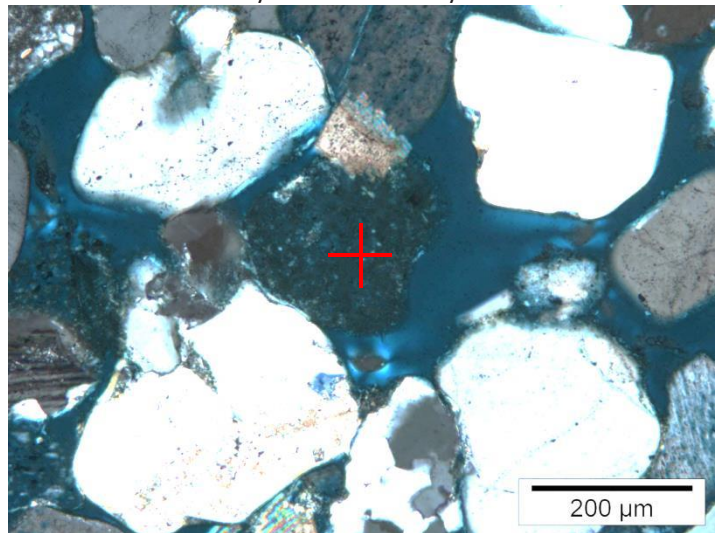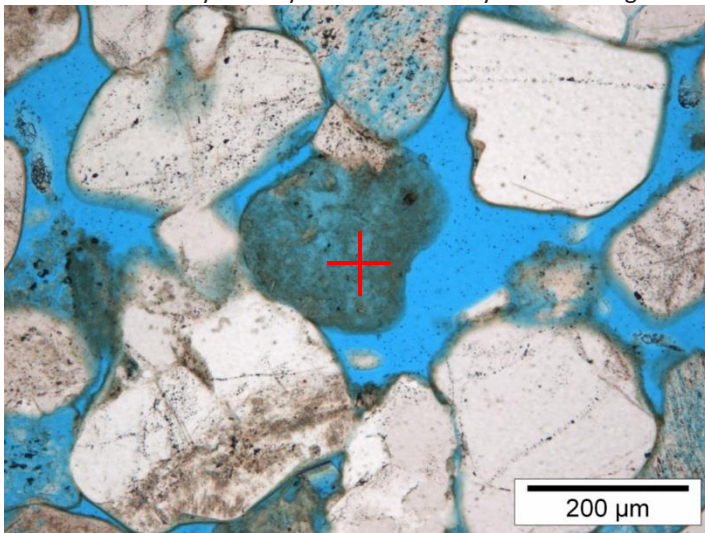


## Porosity

Included in the porosity determination during point counting are all pores that are free of clay. In cases these are filled with kaolinite, illite or chlorite, they are point counted as the according mineral. This is because the crystals are significantly smaller than the thin section thickness (20 µm) and therefore the relative content of pore space and mineral is difficult to quantify. The (micro)pores in between the clay crystals, which can be significant, are integrated by subtracting the point-counted porosity from the total He-porosity.

### Intergranular (primary)                    Oversized

Left: Intergranular pores which are free of clay. Right: Strictly speaking, oversized pores have sizes >1.2x larger than the surrounding grains and do not contain any relict coating, as is visible on the right side of the pore. The left part can be considered as an oversized pore as the coating is absent.
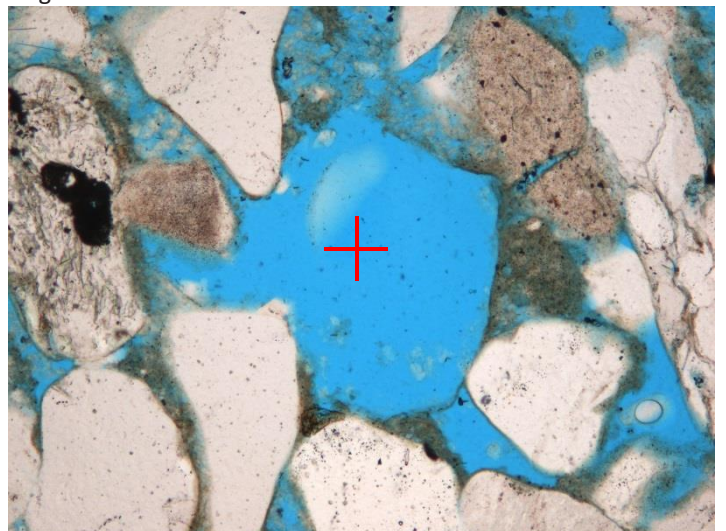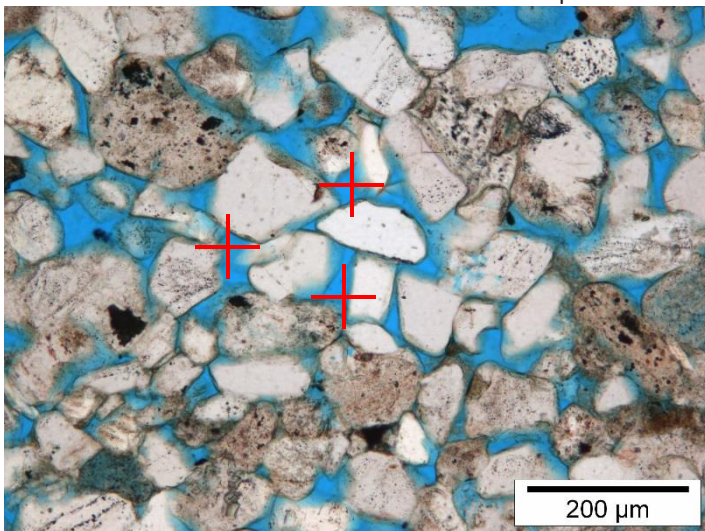
## Intragranular (mostly secondary)

Can be either fracture porosity (left) or dissolution porosity (right). The latter is significantly more common.



200 μm



200 μm
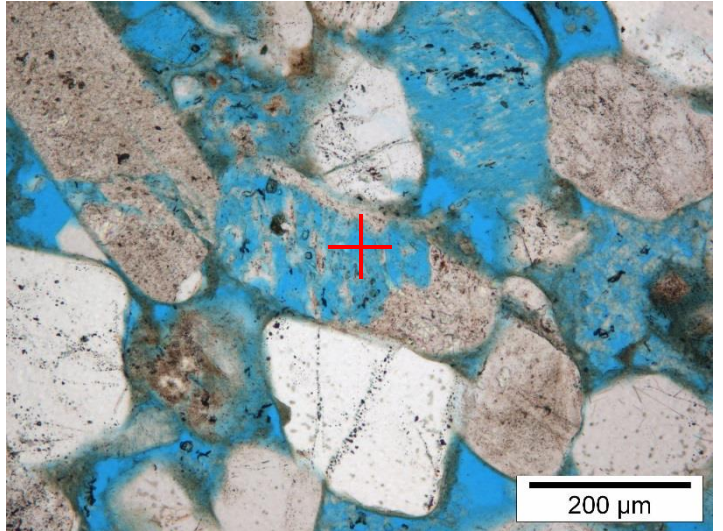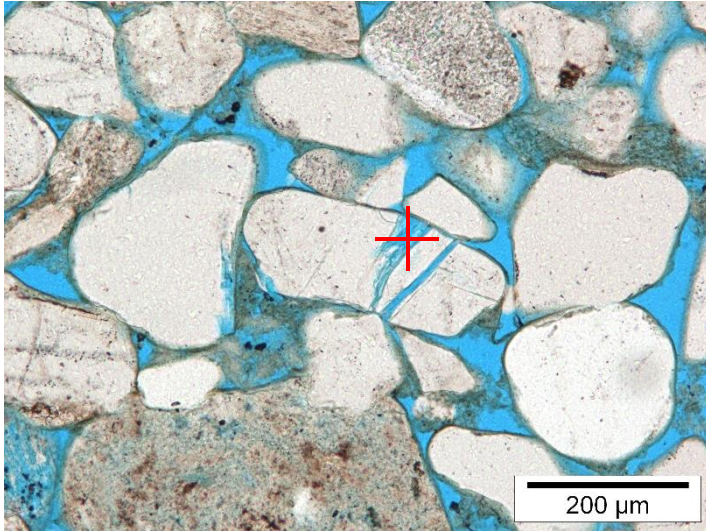
## Mouldic

The result of leaching of grains. The remaining clay rim reveals the size and shape of the leached grain.



200 μm
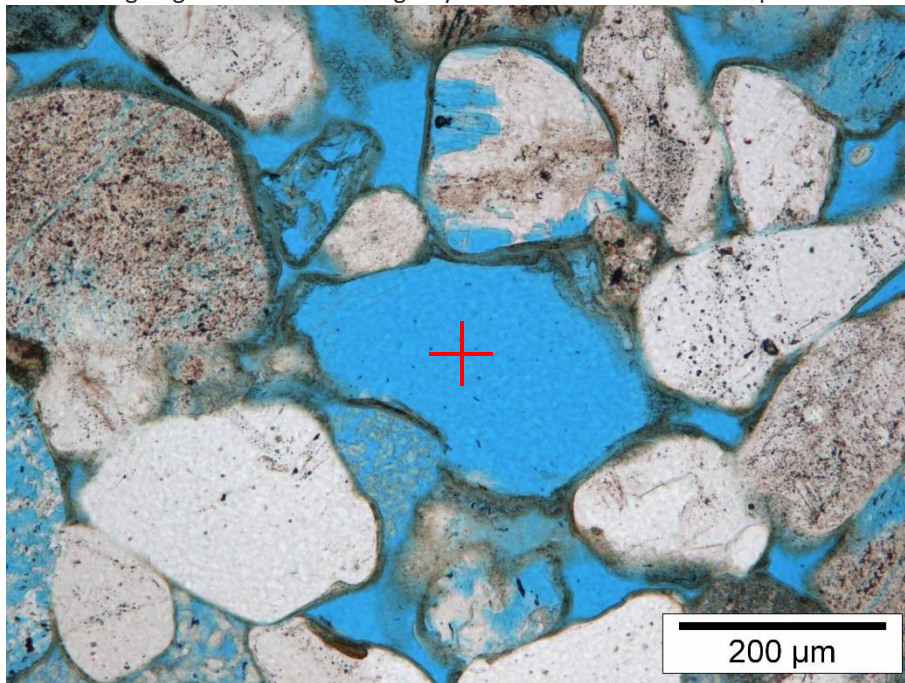
# Appendix 4: Thin section descriptions and photoplates

| Abbreviations | |
|---|---|
| **Roundness** | **Sorting** |
| SA — Subangular | G — Good |
| SR — Subrounded | MG — Moderately good |
| R — Rounded | M — Moderate |
| | P — Poor |
| **Grain contacts** | B — Bimodal |
| P — Point | |
| L — Long | |
| CC — Concavo-convex | |
| **PS** — Pseudomatrix | |
| **Compaction** | **Optical light microscopy** |
| IGV — Intergranular volume | PPL — Plane Polarised Light |
| COPL — Compactional porosity loss | XPL — Cross Polarised Light |
| CEPL — Cementational porosity loss | |
| **Detrital minerals** | **Authigenic minerals and porosity** |
| Q — Quartz grain | i — Illite (grain coating) |
| R — Removed grain (SEM) | chl — Chlorite |
| FSP — Feldspar (general) | q — Quartz |
| ALB — Albite | d — Dolomite |
| CG — Clay-rich grain | fsp — Feldspar |
| RF — Rock fragment | k — Kaolinite |
| M — Mica | b — Barite |
| IG — Igneous grain | c — Clay (unidentified) |
| Z — Zircon | s — Siderite |
| DG — Deformed grain | op — Opaque cement |
| LG — Leached grain | TiO — TiO mineral cement |
| O — Opaque grain | |
| SRF — Sedimentary RF | PP — Intergranular / Primary pore |
| CA — Carbonate grain | IP — Intragranular / Dissolution pore |
| CaP — Calc Phosphate (Apatite) | MP — Mouldic pore |

Abbreviations for the texture (description pages), minerals and pore types (photoplates, SEM & BSEM).
Pores, detrital grains and minerals are in capital letters, whereas the authigenic components have small letters.

**Sample Type:** Plug Trimend  **Rock Classification (Pettijohn, 1975):** Sublitharenite

## Texture

| Texture | faintly laminated | Grain size (modal) | fine sand (U) | Roundness | SR |
|---|---|---|---|---|---|
| Sample heterogeneity | low to moderate | Grain size (min) | 31-62.5 μm | Sorting | P |
| | | Grain size (max) | 350-500 μm | | |

**Remarks:** Despite the relatively poor sorting, the sample does not contain coarse sand grains.

## Compaction

| Grain contacts - Rigid | P | COPL (%) | 31 | IGV (%) | 21 |
|---|---|---|---|---|---|
| Grain contacts - Ductile | L-CC | CEPL (%) | 7 | | |

**Remarks:** Compaction is low to moderate, as indicated by the grain contacts and the IGV.

## Detrital components (%)

| Monoquartz | 44.0 | Feldspar | 3.3 | Rigid RF | 9.7 | Microporous RF | 1.7 |
|---|---|---|---|---|---|---|---|
| Polyquartz | 9.0 | Leached feldspar | 3.0 | Ductile RF | 1.3 | Accessories | Tr |

**Remarks:** Most rock fragments are indeterminate (4.7%). Sedimentary rock fragments are sparse (2.7%). Traces comprise heavy minerals.

## Authigenic components (%)

| Quartz | 1.3 | Grain rimming illite | 4.3 | Pore-filling kaolinite | 1.3 |
|---|---|---|---|---|---|
| Dolomite/Siderite | - | Grain rimming clay (mix) | - | Replacive kaolinite | 3.7 |
| Barite | 0.3 | Grain rimming chlorite | - | Replacive chlorite | - |
| | | Pore-filling clay (indet/mix) | 1.7 | Replacive clay (indet/mix) | 0.7 |

**Remarks:** Quartz cement is mostly pore-filling. Grain-rimming clay is mostly radial. Note the absence of authigenic carbonate.

*Spatial relationships (Paragenetic sequence):*
- No clay at grain contacts (Coating prior to most compaction)
- Quartz cement on top of grain coating
- Quartz and siderite cement in leached feldspar

## Point counted porosity (%)

| Intergranular | 10.7 | Intragranular | 2.3 |
|---|---|---|---|
| Oversized | - | Mouldic | - |
| Macroporosity (visible porosity) | | 13.0 | |
| Microporosity (He-porosity minus macroporosity) | | 12.3 | |

**Remarks:** Micropores occur in the leached grains and authigenic clay.

## Reservoir properties

| He-Porosity (%) | 25.3 |
|---|---|
| Permeability (mD) | n/a |
| Grain density (g/cm$^3$) | 2.65 |
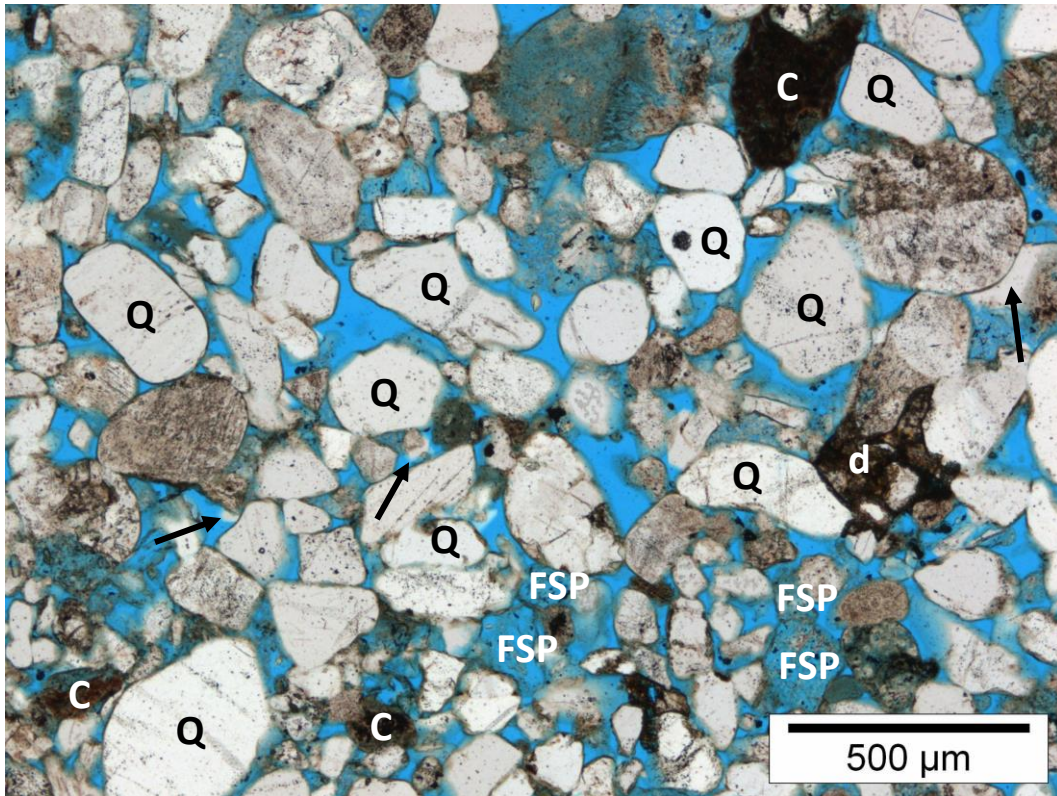


*Thin section scan (width ~2.5 cm)*

**A. Magnification 45x**                                              **Plane Polarised Light**
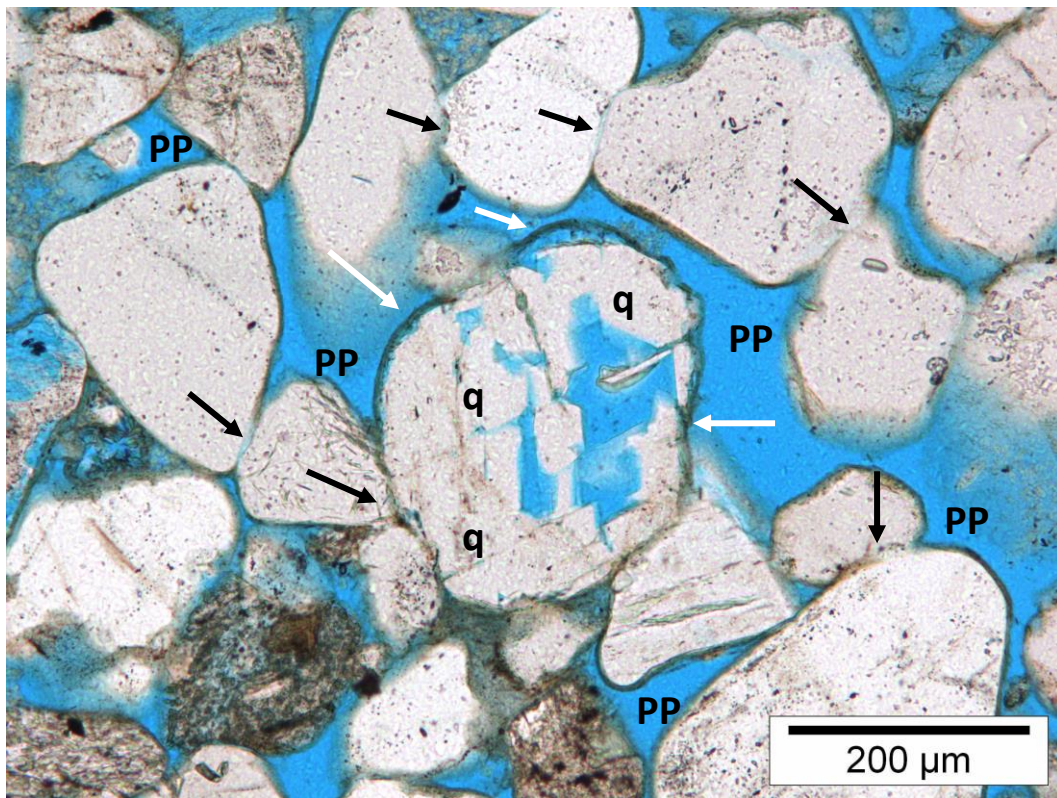


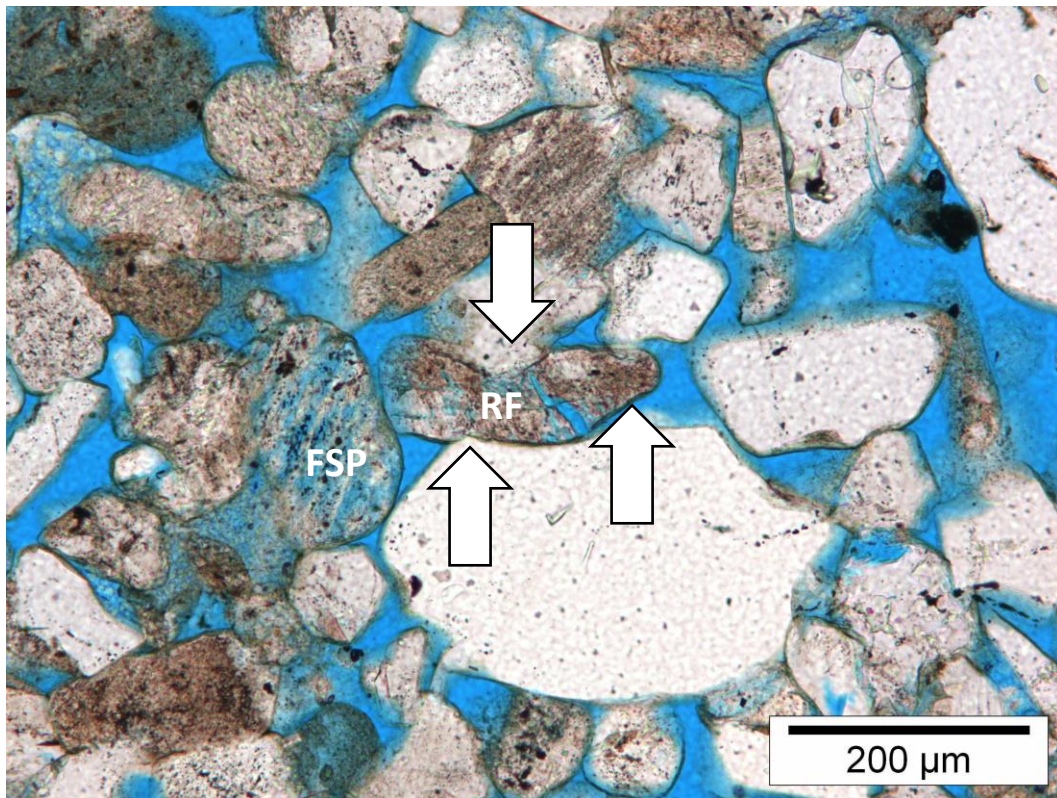**B. Magnification 113x**                                             **Plane Polarised Light**

**Plate A:** The detrital quartz grains (Q) in this poorly sorted sandstone are covered with a thin, brownish clay rim. Rarely, quartz overgrowths (arrows) formed. Note the dark dolomite cement (d), clay-rich grains (C) and leached feldspar grains (FSP). **Plate B:** Some leached (feldspar?) grains are filled with secondary quartz (q). The original clay rim remained present (white arrows). Pores (PP) in this field of view are relatively large and well connected. Grain contacts are mostly point contacts, with no authigenic clay in between (black arrows).

**Sample Type:** Plug Trimend

**Rock Classification (Pettijohn, 1975):** Sublitharenite

## Texture

| Texture | grain alignment | Grain size (modal) | fine sand (U) | Roundness | SA-SR |
|---|---|---|---|---|---|
| Sample heterogeneity | low to moderate | Grain size (min) | 88-125 µm | Sorting | M-P |
| | | Grain size (max) | 1-1.41 mm | | |

**Remarks:** Lamination on the TS scale is not observed.

## Compaction

| Grain contacts - Rigid | P-L | COPL (%) | 33 | IGV (%) | 18 |
|---|---|---|---|---|---|
| Grain contacts - Ductile | CC | CEPL (%) | 9 | | |

**Remarks:** Note that ductile grains are very rare and that the grain contacts between ductile and rigid grains are therefore also rare. The IGV below average (for this sample set) indicates moderate compaction.

## Detrital components (%)

| Monoquartz | 40.3 | Feldspar | 3.0 | Rigid RF | 11.7 | Microporous RF | 1.3 |
|---|---|---|---|---|---|---|---|
| Polyquartz | 9.3 | Leached feldspar | 2.7 | Ductile RF | Tr | Accessories | Tr |

**Remarks:** Igneous rock fragments are relatively common for this sample set (2.7%). Some are strongly leached. Accessory minerals include muscovite, heavy minerals and opaque grains.

## Authigenic components (%)

| Quartz | 4.0 | Grain rimming illite | 3.0 | Pore-filling kaolinite | 1.7 |
|---|---|---|---|---|---|
| Dolomite/Siderite | 3.3 | Grain rimming clay (mix) | - | Replacive kaolinite | 6.7 |
| Barite | 0.3 | Grain rimming chlorite | - | Replacive chlorite | - |
| | | Pore-filling clay (indet/mix) | 3.7 | Replacive clay (indet/mix) | 1.3 |

**Remarks:** Quartz cement occurs both as a replacive, locally replacing feldspar grains and as intergranular pore-filling cement. Note the common replacive kaolinite, also identified in the XRD (8%).

*Spatial relationships (Paragenetic sequence):*
- Tangential clay coating covered by radial clay coating
- Siderite in leached grains
- Barite has overgrown dolomite

## Point counted porosity (%)

| Intergranular | 3.7 | Intragranular | 2.0 |
|---|---|---|---|
| Oversized | 1.3 | Mouldic | - |
| Macroporosity (visible porosity) | | | 7.0 |
| Microporosity (He-porosity minus macroporosity) | | | 11.2 |

**Remarks:** Pores are commonly filled with authigenic clay, hence the low intergranular macroporosity.

## Reservoir properties

| He-Porosity (%) | 18.2 |
|---|---|
| Permeability (mD) | 17 |
| Grain density (g/cm$^3$) | 2.66 |

**Remarks:** Relatively low permeability due to authigenic clay content.
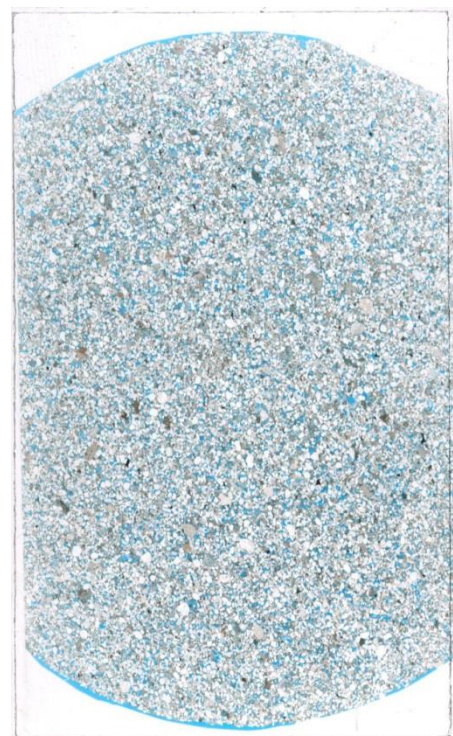


*Thin section scan (width ~2.5 cm)*
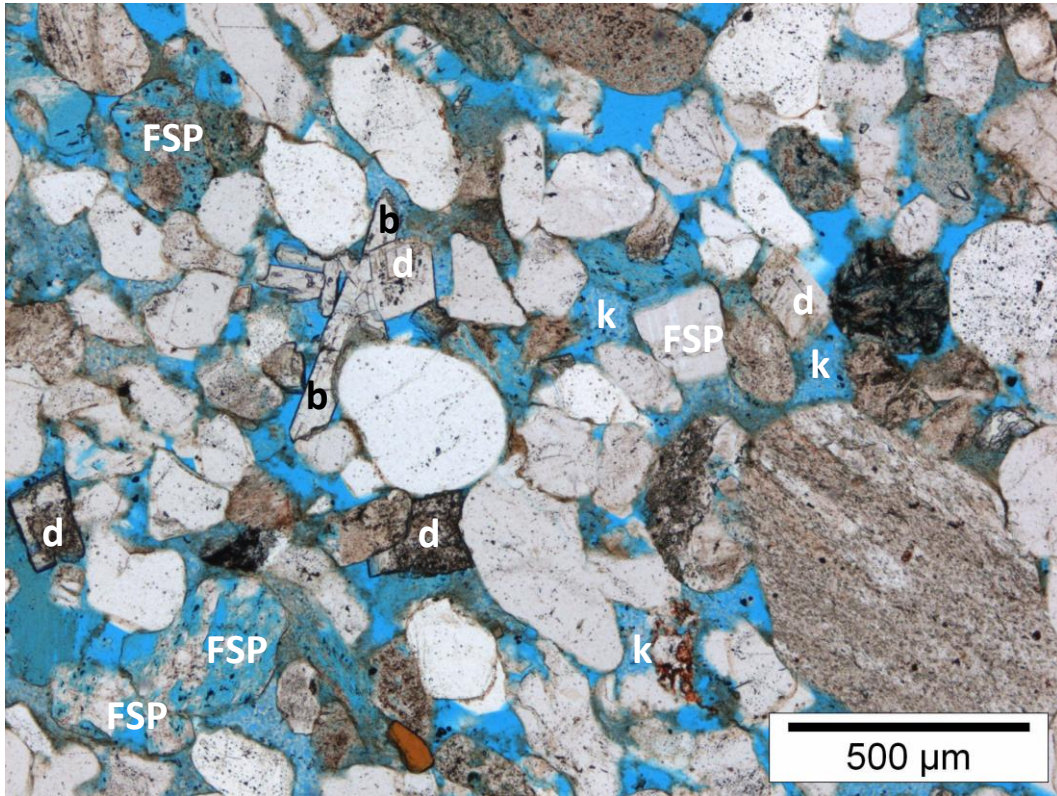
**A. Magnification 45x**          **Plane Polarised Light**
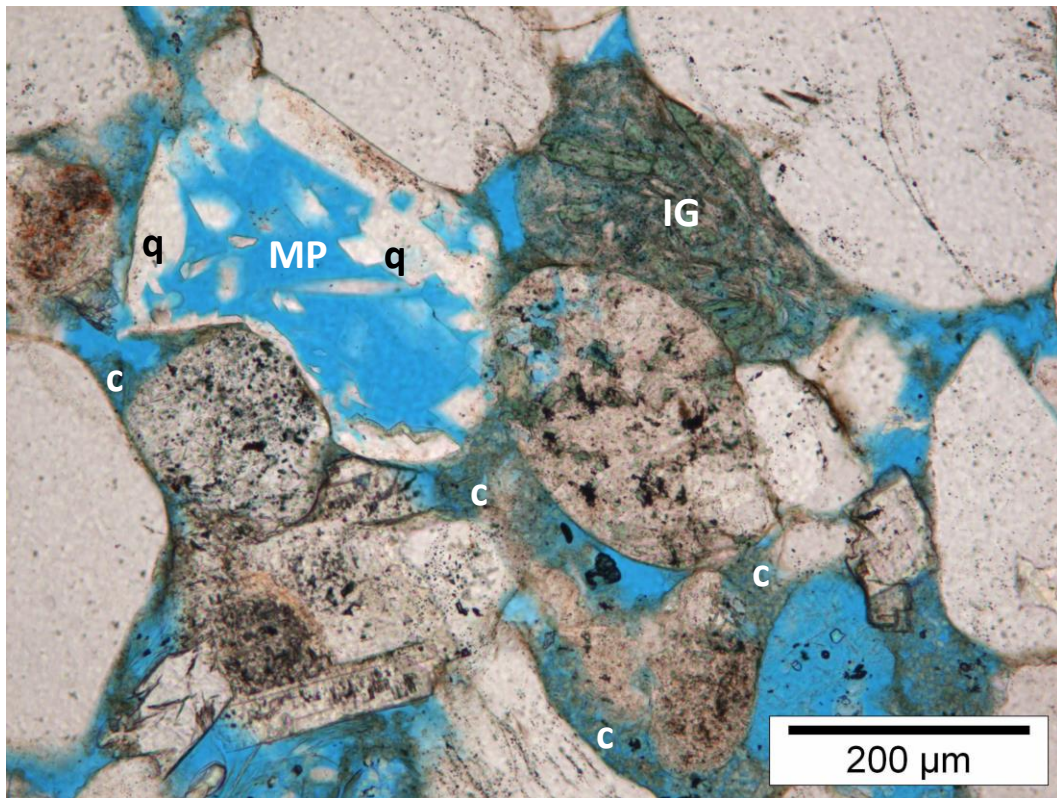


**B. Magnification 113x**          **Plane Polarised Light**

**Plate A:** Locally, authigenic kaolinite (k) occurs in this poorly sorted sandstone. Quartz overgrowths (q) are locally well developed, despite the thin clay rim. The preservation status of Feldspar (FSP) ranges from strongly leached to unleached. When unleached, feldspar is best identified by the twinning (visible in XPL). Note the authigenic barite (b) and dolomite (d).
**Plate B:** Detailed image of an altered igneous grain (IG) which is slightly deformed, as well as a deformed mouldic pore (MP), which is partially filled with authigenic quartz (q). Intergranular clay (c) is common in this field of view.

**Sample Type:** Plug Trimend        **Rock Classification (Pettijohn, 1975):** Sublitharenite

## Texture

| | | | | | |
|---|---|---|---|---|---|
| Texture | faintly laminated | Grain size (modal) | fine sand (U) | Roundness | SA-SR |
| Sample heterogeneity | low to moderate | Grain size (min) | 31-62.5 μm | Sorting | MG-M |
| | | Grain size (max) | 500-710 μm | | |

## Compaction

| | | | | | |
|---|---|---|---|---|---|
| Grain contacts - Rigid | P | COPL (%) | 29 | IGV (%) | 23 |
| Grain contacts - Ductile | L-CC | CEPL (%) | 11 | | |

**Remarks:** The thick clay coatings are commonly detached. This might be due to continued compaction. Total mechanical compaction is low to moderate.

## Detrital components (%)

| | | | | | | | |
|---|---|---|---|---|---|---|---|
| Monoquartz | 44.3 | Feldspar | 2.0 | Rigid RF | 6.3 | Microporous RF | 1.7 |
| Polyquartz | 12.7 | Leached feldspar | 2.0 | Ductile RF | 0.3 | Accessories | Tr |

**Remarks:** Note that the sparse amount of identified feldspar (especially albite) is likely to be underestimated due to similarities with quartz and because the feldspar was not stained for recognition, both in PPL and XPL. XRD suggests ~10% feldspar

## Authigenic components (%)

| | | | | | |
|---|---|---|---|---|---|
| Quartz | 2.3 | Grain rimming illite | 6.0 | Pore-filling kaolinite | - |
| Dolomite/Siderite | 1.3 | Grain rimming clay (mix) | - | Replacive kaolinite | 1.3 |
| Barite | - | Grain rimming chlorite | 6.0 | Replacive chlorite | - |
| | | Pore-filling clay (indet/mix) | 0.3 | Replacive clay (indet/mix) | 1.0 |

**Remarks:** Note the common clay coating, comprising both illite and chlorite. Kaolinite on the other hand is very sparse.

*Spatial relationships (Paragenetic sequence):*

- Clay coating at grain-to-grain contacts. Coatings fractured together with breakage (compaction) of grains.
- (Some) quartz cement and chlorite crystals between detached clay coat and detrital quartz grains.

## Point counted porosity (%)

| | | | |
|---|---|---|---|
| Intergranular | 7.3 | Intragranular | 2.3 |
| Oversized | 0.7 | Mouldic | 1.0 |
| Macroporosity (visible porosity) | | 11.3 | |
| Microporosity (He-porosity minus macroporosity) | | 17.2 | |

**Remarks:** Traces of intergranular pores between clay rim and grain.

## Reservoir properties

| | |
|---|---|
| He-Porosity (%) | 28.5 |
| Permeability (mD) | 189 |
| Grain density (g/cm$^3$) | 2.66 |
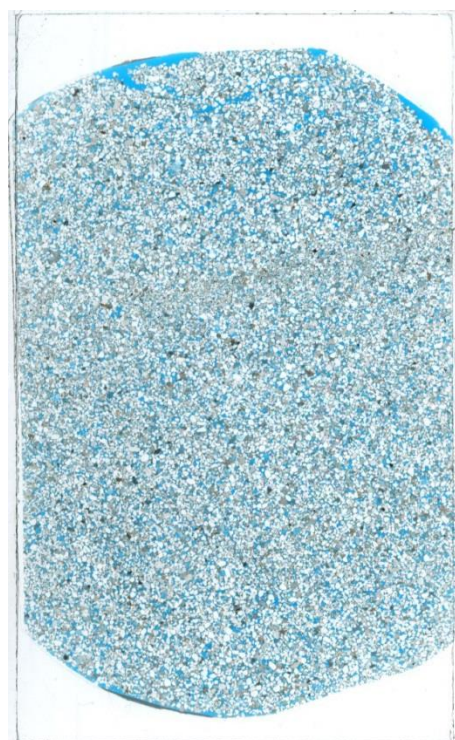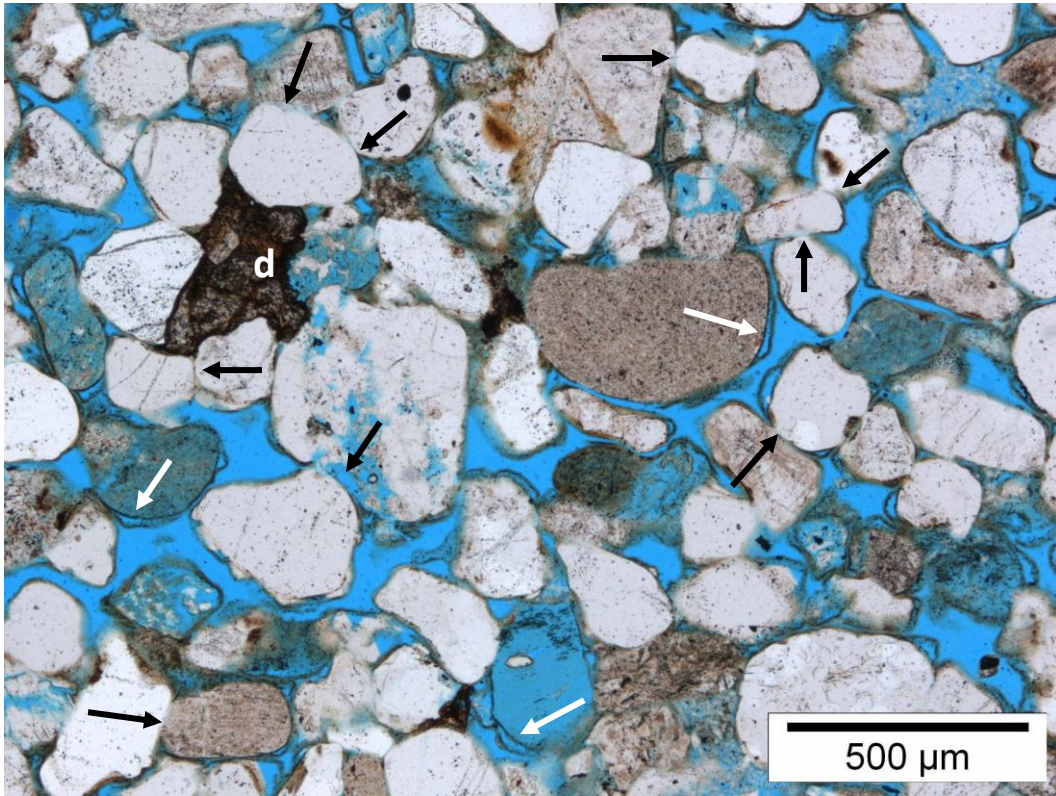


*Thin section scan (width ~2.5 cm)*

**A. Magnification 45x**        **Plane Polarised Light**
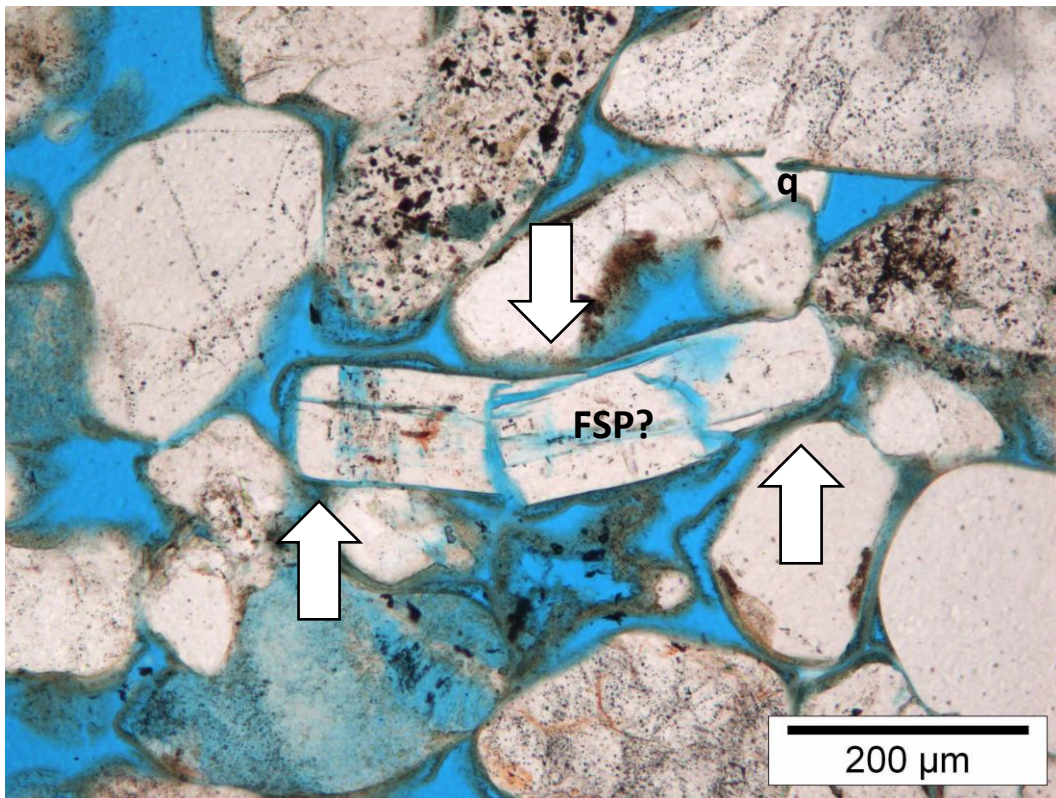


**B. Magnification 113x**        **Plane Polarised Light**

**Plate A:** The detrital grains in this fine grained sandstone are relatively well rounded and covered with a thick clay coating. The coatings are locally separated from the detrital grains (white arrows). The clay coatings are locally absent, but locally also present at the grain contacts, indicating that these have formed during or shortly after mechanical compaction. Note the dark dolomite cement (d). **Plate B:** Due to continued mechanical compaction (large arrows), this elongated feldspar (FSP) is broken, as is the clay rim. Note the quartz cement (q) which has formed there where the clay rim is interrupted.

**Sample Type:** Plug Trimend                    **Rock Classification (Pettijohn, 1975):** Sublitharenite

## Texture

| | | | | | |
|---|---|---|---|---|---|
| Texture | faintly laminated | Grain size (modal) | medium sand (L) | Roundness | SR |
| Sample heterogeneity | low to moderate | Grain size (min) | 62.5-88 µm | Sorting | MG-M |
| | | Grain size (max) | 710-1000 µm | | |

**Remarks:** Some grain size variation between the laminae. Detrital clay content does not vary.

## Compaction

| | | | | | |
|---|---|---|---|---|---|
| Grain contacts - Rigid | P | COPL (%) | 33 | IGV (%) | 17 |
| Grain contacts - Ductile | L-CC | CEPL (%) | 8 | | |

**Remarks:** The relatively low IGV is mostly due to the low intergranular macroporosity. Deformed rock fragments, quartz and feldspar grains indicate moderate compaction.

## Detrital components (%)

| | | | | | | | |
|---|---|---|---|---|---|---|---|
| Monoquartz | 38.7 | Feldspar | 4.3 | Rigid RF | 8.7 | Microporous RF | 3.3 |
| Polyquartz | 12.0 | Leached feldspar | 4.0 | Ductile RF | Tr | Accessories | Tr |

**Remarks:** Rock fragments (RF) are mostly indeterminable, amongst them sparse microporous RF.

## Authigenic components (%)

| | | | | | |
|---|---|---|---|---|---|
| Quartz | 0.3 | Grain rimming illite | 2.7 | Pore-filling kaolinite | 0.3 |
| Dolomite/Siderite | 0.3 | Grain rimming clay (mix) | 0.7 | Replacive kaolinite | 4.3 |
| Barite | Tr | Grain rimming chlorite | 1.3 | Replacive chlorite | - |
| | | Pore-filling clay (indet/mix) | 6.0 | Replacive clay (indet/mix) | 3.3 |

**Remarks:** Barite occurs locally as a replacive mineral. Most of the indeterminate/mixed clay is likely to be illite, based on the XRD results. Authigenic quartz mostly forms microcrystalline overgrowths.

*Spatial relationships (Paragenetic sequence):*

- Some clay coatings at grain-to-grain contacts (prior to main compaction)
- Undeformed leached grains (compaction prior to grain leaching)
- Quartz and barite cement in leached grains (postdates leaching)

## Point counted porosity (%)

| | | | |
|---|---|---|---|
| Intergranular | 5.7 | Intragranular | 1.7 |
| Oversized | 1.0 | Mouldic | 0.7 |
| Macroporosity (visible porosity) | | 9.0 | |
| Microporosity (He-porosity minus macroporosity) | | 17.1 | |

**Remarks:** Traces of intragranular porosity is due to fractured grains.

## Reservoir properties

| | |
|---|---|
| He-Porosity (%) | 26.1 |
| Permeability (mD) | 185 |
| Grain density (g/cm$^3$) | 2.65 |
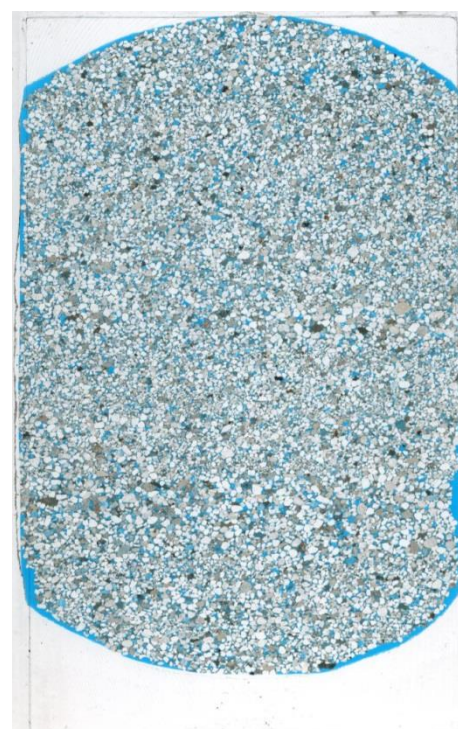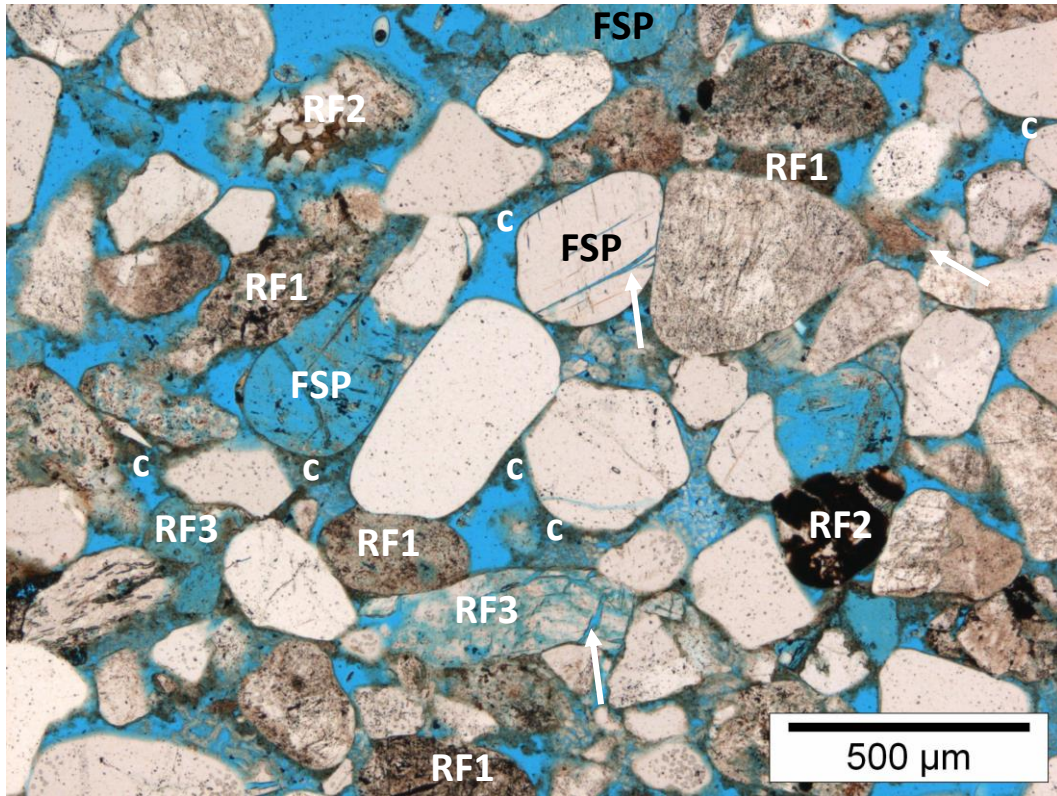


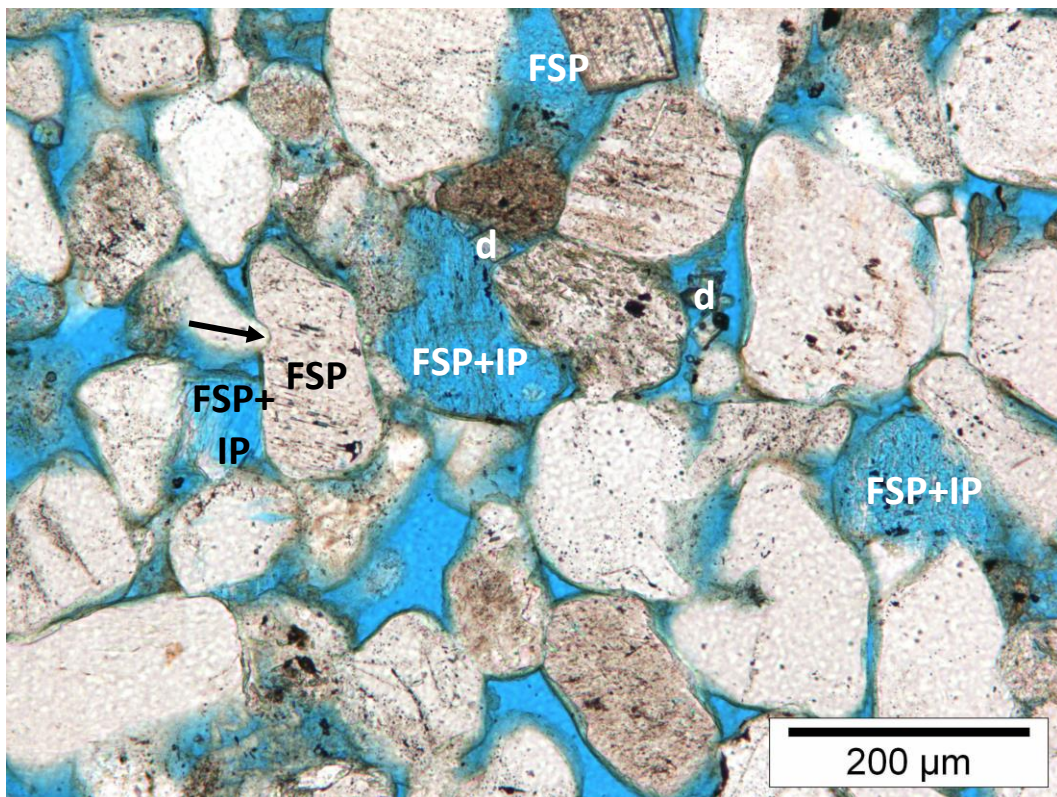*Thin section scan (width ~2.5 cm)*

**A. Magnification 45x**      **Plane Polarised Light**
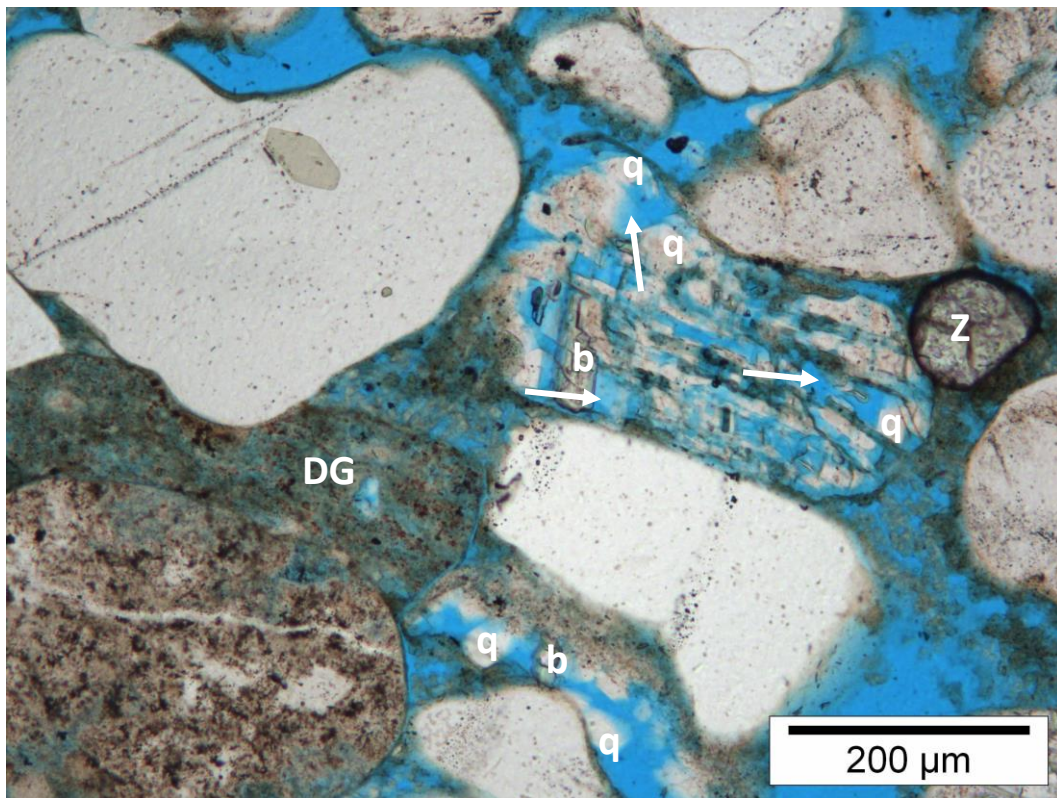


**B. Magnification 113x**      **Plane Polarised Light**

**Plate A:** Rock fragments (RF) are common, ranging from clay-rich (RF1) to possibly igneous (RF2) and strongly leached (RF3). Also both strongly leached and unleached feldspar occur (FSP). Note the fracturing of detrital grains (arrows) due to compaction. Intergranular fine-crystalline clay (c; likely chlorite rich) is relatively common. **Plate B:** Secondary porosity (arrows), authigenic barite (b) and quartz (q) have formed in a leached feldspar grain. Quartz cement is also present in intergranular pores. The relatively strong compaction is visible by the deformed microporous grain (DG) and long grain-to-grain contacts. Note the detrital zircon (Z).

**Sample Type:** Plug Trimend

**Rock Classification (Pettijohn, 1975):** Sublitharenite

## Texture

| | | | | | |
|---|---|---|---|---|---|
| Texture | faintly laminated | Grain size (modal) | medium sand (L) | Roundness | SR |
| Sample heterogeneity | moderate | Grain size (min) | 62.5-88 µm | Sorting | M |
| | | Grain size (max) | 710-1000 µm | | |

**Remarks:** Thin finer grained laminae alternate with thick (on the TS level) coarser grained laminae.

## Compaction

| | | | | | |
|---|---|---|---|---|---|
| Grain contacts - Rigid | P-L | COPL (%) | 31 | IGV (%) | 20 |
| Grain contacts - Ductile | CC | CEPL (%) | 7 | | |

**Remarks:** Both the grain contacts and the IGV suggest low to moderate compaction.

## Detrital components (%)

| | | | | | | | |
|---|---|---|---|---|---|---|---|
| Monoquartz | 37.0 | Feldspar | 2.3 | Rigid RF | 8.3 | Microporous RF | 3.7 |
| Polyquartz | 16.0 | Leached feldspar | 3.3 | Ductile RF | - | Accessories | Tr |

**Remarks:** The coarser grained quartz grains are more commonly polycrystalline rather than monocrystalline. Rock fragments are relatively commonly leached, containing micropores.

## Authigenic components (%)

| | | | | | |
|---|---|---|---|---|---|
| Quartz | 1.0 | Grain rimming illite | 4.0 | Pore-filling kaolinite | 2.3 |
| Dolomite/Siderite | - | Grain rimming clay (mix) | 1.3 | Replacive kaolinite | 5.7 |
| Barite | - | Grain rimming chlorite | 0.7 | Replacive chlorite | - |
| | | Pore-filling clay (indet/mix) | 1.0 | Replacive clay (indet/mix) | 1.0 |

**Remarks:** Quartz is mostly replacive. Note the common kaolinite. This kaolinite is often relatively loosely packed. Very locally, the clay coating is detached from the grain.

*Spatial relationships (Paragenetic sequence):*

- Quartz and siderite engulf kaolinite (postdates kaolinite formation)
- Quartz and dolomite in leached grains (postdates leaching)

## Point counted porosity (%)

| | | | |
|---|---|---|---|
| Intergranular | 10.3 | Intragranular | 1.3 |
| Oversized | 0.3 | Mouldic | - |
| Macroporosity (visible porosity) | | 12.0 | |
| Microporosity (He-porosity minus macroporosity) | | 14.3 | |

## Reservoir properties

| | |
|---|---|
| He-Porosity (%) | 26.3 |
| Permeability (mD) | 233 |
| Grain density (g/cm$^3$) | 2.66 |

**Remarks:** Note the good permeability, which is partially related to the clay content and the relatively coarse grain size.
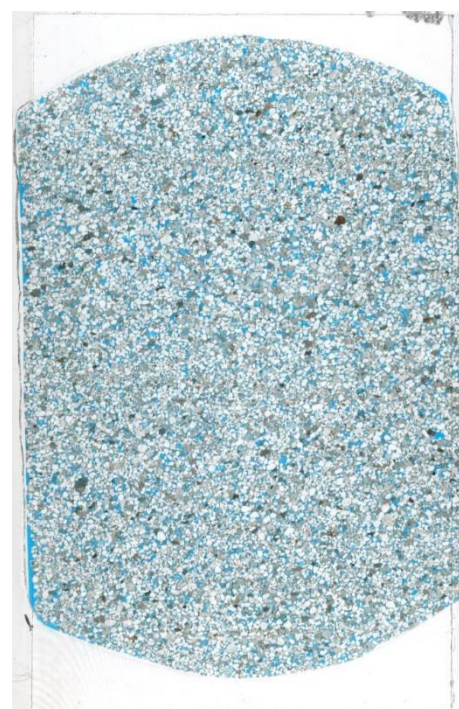


*Thin section scan (width ~2.5 cm)*
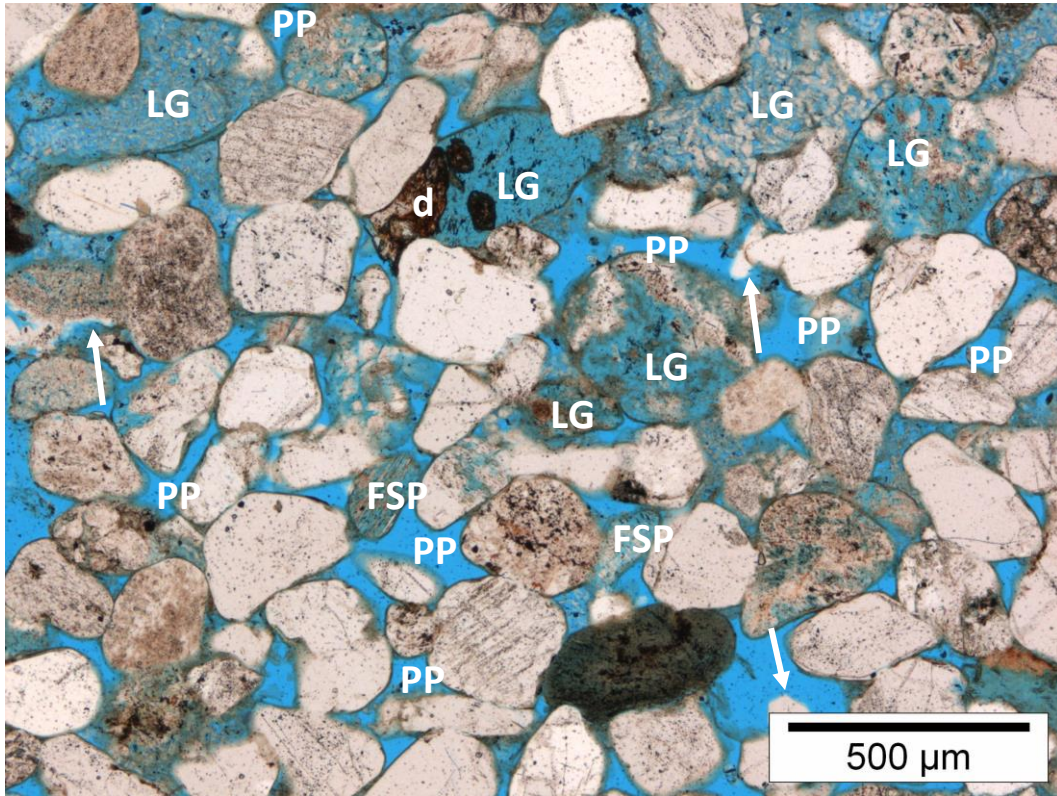
**A. Magnification 45x**                                                    **Plane Polarised Light**
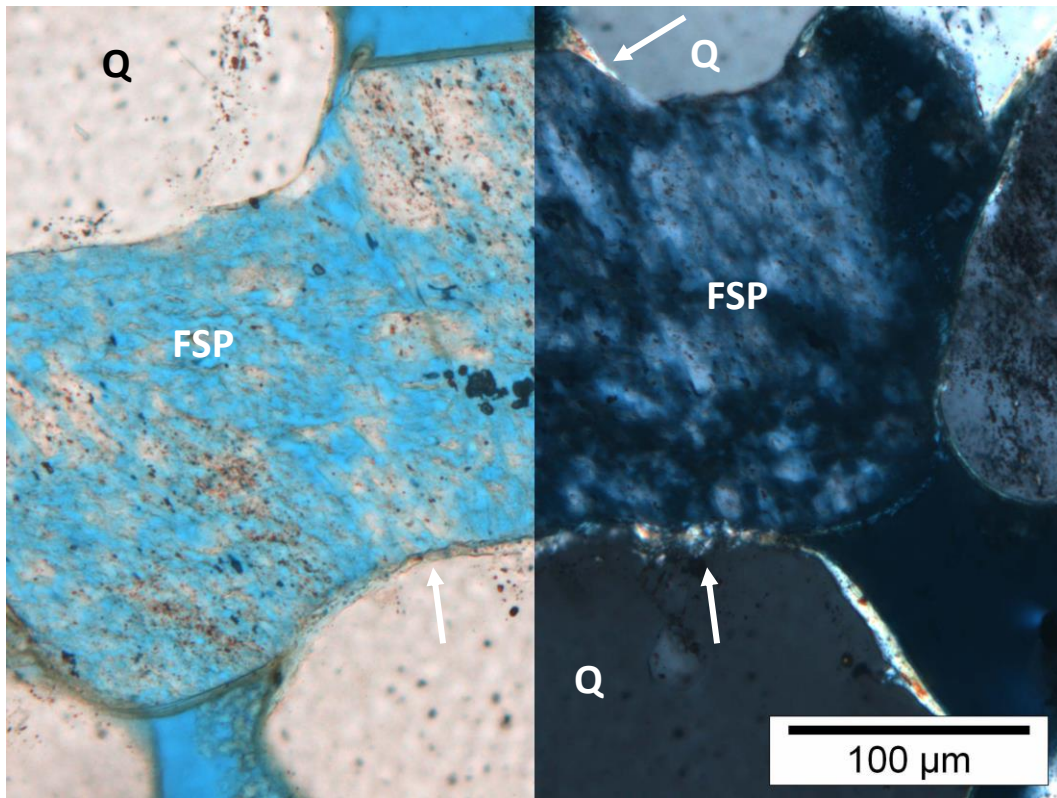


**B. Magnification 225x**                                    **Plane Polarised Light/Crossed Nicols**

**Plate A:** Authigenic radial clay coatings in this medium grained sandstone are covering all detrital grains, also outlining the leached grains. Leached grains include feldspar grains (FSP; visible by the remaining lamellae) but also rock fragments (LG). Dolomite (d) has replaced part of a leached grain. Locally, small quartz overgrowths occur (arrows). Intergranular pores (PP) are relatively free of authigenic clay. **Plate B:** Detailed image of a deformed leached feldspar grain (FSP), showing the indentation of quartz grains (Q). Some tangential clay coatings (arrows) occur in between the detrital grains, indicating compaction after coating formation.

**Sample Type:** Plug Trimend　　　　　　　　　**Rock Classification (Pettijohn, 1975):** Sublitharenite

## Texture

| Texture | structureless | Grain size (modal) | fine sand (U) | Roundness | SA-SR |
|---|---|---|---|---|---|
| Sample heterogeneity | low | Grain size (min) | 88-125 µm | Sorting | MG |
| | | Grain size (max) | 500-710 µm | | |

**Remarks:** Quartz grains have an angular appearance due to local quartz cement overgrowths.

## Compaction

| Grain contacts - Rigid | P-L | COPL (%) | 27 | IGV (%) | 24 |
|---|---|---|---|---|---|
| Grain contacts - Ductile | L-CC | CEPL (%) | 11 | | |

**Remarks:** Compared to most samples in the sample set, COPL is relatively low, whereas the CEPL is relatively high.

## Detrital components (%)

| Monoquartz | 48.0 | Feldspar | 1.7 | Rigid RF | 5.0 | Microporous RF | 2.0 |
|---|---|---|---|---|---|---|---|
| Polyquartz | 10.3 | Leached feldspar | 3.7 | Ductile RF | 0.3 | Accessories | Tr |

**Remarks:** Rock fragments (mostly indeterminate) are relatively rare. Accessories comprise only opaque minerals.

## Authigenic components (%)

| Quartz | 4.0 | Grain rimming illite | 5.7 | Pore-filling kaolinite | 0.3 |
|---|---|---|---|---|---|
| Dolomite/Siderite | Tr | Grain rimming clay (mix) | 0.7 | Replacive kaolinite | 0.7 |
| Barite | 0.3 | Grain rimming chlorite | 3.3 | Replacive chlorite | 0.3 |
| | | Pore-filling clay (indet/mix) | 1.0 | Replacive clay (indet/mix) | 1.3 |

**Remarks:** Kaolinite is rare, both in the point count results and in the XRD results. Fine crystalline clay coatings are commonly detached, with coarse crystalline chlorite in between the grain and the fine crystalline radial (illite) coating. Quartz cement locally occurs between coating and grain.

*Spatial relationships (Paragenetic sequence):*

- Clay coating broken together with broken grains
  (predates endstage mechanical compaction)
- Quartz cement between detrital grain and detached coating
- Chlorite rosettes overgrows radial clay (postdates radial clay)

## Point counted porosity (%)

| Intergranular | 9.0 | Intragranular | 1.7 |
|---|---|---|---|
| Oversized | - | Mouldic | - |
| Macroporosity (visible porosity) | | 10.7 | |
| Microporosity (He-porosity minus macroporosity) | | 10.1 | |

## Reservoir properties

| He-Porosity (%) | 20.8 |
|---|---|
| Permeability (mD) | 72 |
| Grain density (g/cm$^3$) | 2.64 |

**Remarks:** Clay coatings and quartz cement locally obstruct pore throats.
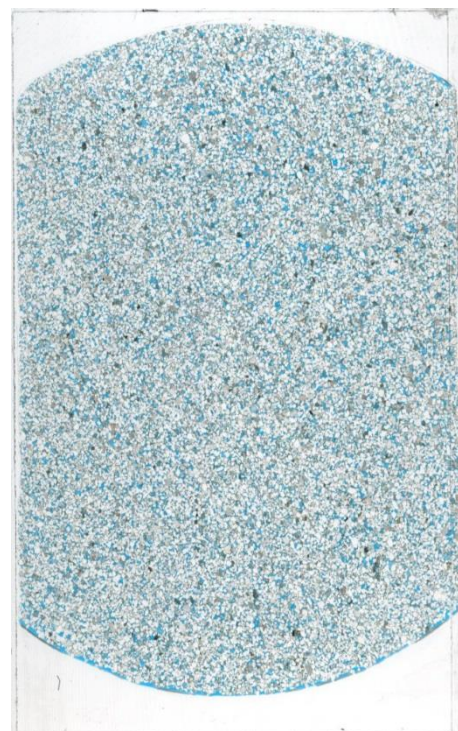


*Thin section scan (width ~2.5 cm)*
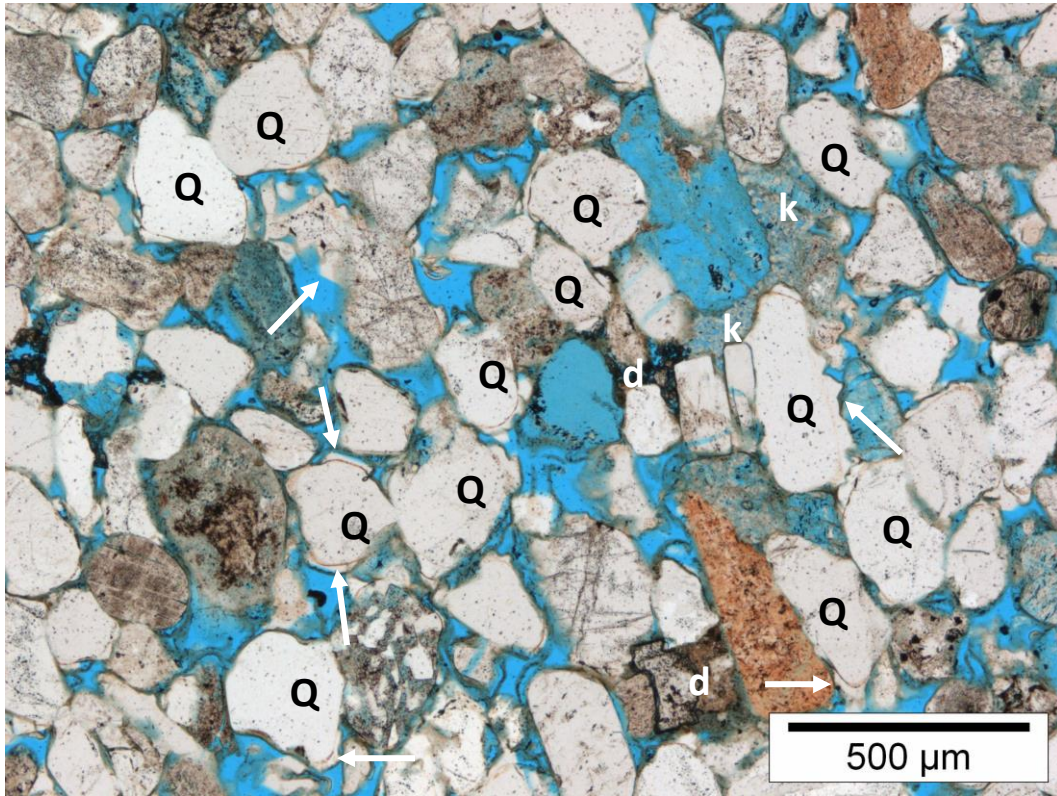
A. Magnification 45x      Plane Polarised Light
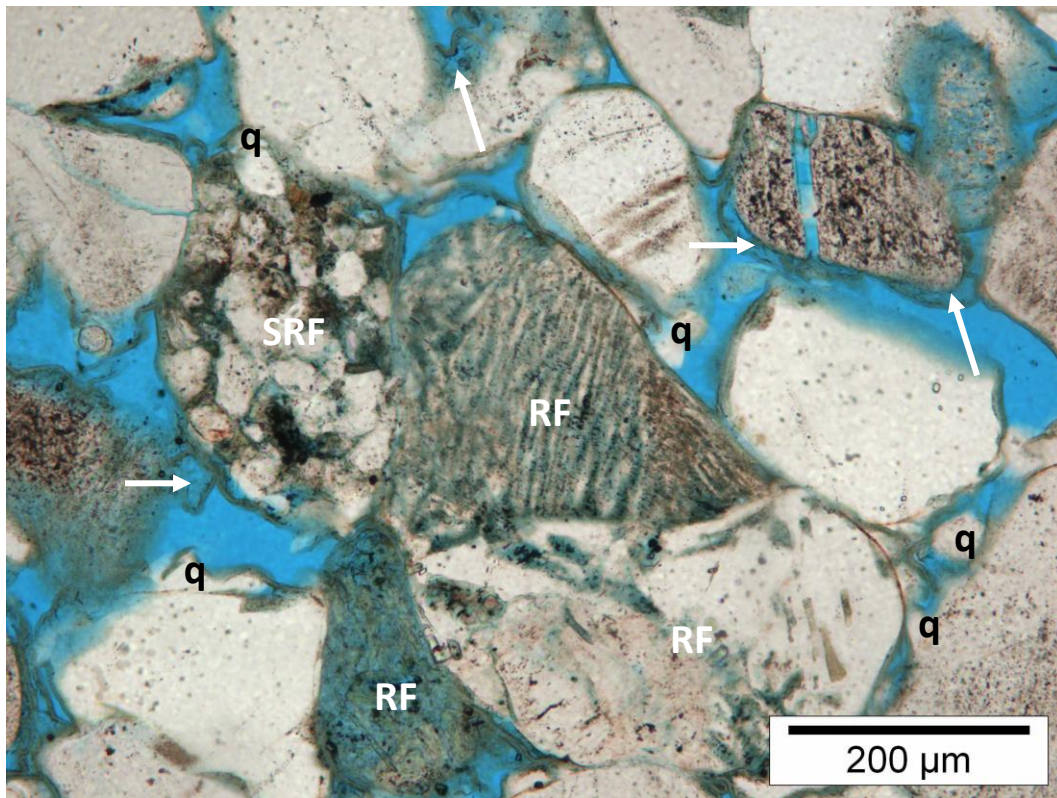


B. Magnification 113x      Plane Polarised Light

**Plate A:** The irregular shape of the quartz grains in this structureless sandstone is due to significant quartz overgrowths (arrows) that have locally formed between the detached radial? Mixed clay rims and quartz (Q) grains. Also note the dolomite cement (d) and authigenic kaolinite (k). **Plate B:** Multiple rock fragments (RF; including a sedimentary rock fragment; SRF) with a partially detached clay coating. The coating comprises illite (green high birefringence in XPL)) and chlorite (fibres in 2D, low birefringence in XPL; arrows). Note the quartz cement (q).

**Sample Type:** Plug Trimend

**Rock Classification (Pettijohn, 1975):** Sublitharenite

## Texture

| | | | | | |
|---|---|---|---|---|---|
| Texture | laminated | Grain size (modal) | f sand (L) / m sand (U) | Roundness | SA |
| Sample heterogeneity | moderate | Grain size (min) | 31-62.5 µm | Sorting | MG-B |
| | | Grain size (max) | 1-1.41 mm | | |

**Remarks:** Top and base of thin section are significantly coarser grained (hence the 2 modal grain sizes). The finer grained area is also laminated.

## Compaction

| | | | | | |
|---|---|---|---|---|---|
| Grain contacts - Rigid | P | COPL (%) | 29 | IGV (%) | 22 |
| Grain contacts - Ductile | L-CC | CEPL (%) | 6 | | |

**Remarks:** Compaction is low to moderate, despite the traces of broken grains.

## Detrital components (%)

| | | | | | | | |
|---|---|---|---|---|---|---|---|
| Monoquartz | 46.0 | Feldspar | 4.7 | Rigid RF | 7.7 | Microporous RF | 1.7 |
| Polyquartz | 9.0 | Leached feldspar | 2.0 | Ductile RF | 1.7 | Accessories | 0.3 |

**Remarks:** Igneous rock fragments are the most common rock fragments (3.3%). Feldspar is relatively commonly identified. Feldspar content is however underestimated (XRD results; 19%) due to the similarity with quartz.

## Authigenic components (%)

| | | | | | |
|---|---|---|---|---|---|
| Quartz | 1.0 | Grain rimming illite | 2.3 | Pore-filling kaolinite | 0.7 |
| Dolomite/Siderite | 3.0 | Grain rimming clay (mix) | - | Replacive kaolinite | 2.0 |
| Barite | 0.3 | Grain rimming chlorite | - | Replacive chlorite | - |
| | | Pore-filling clay (indet/mix) | 1.3 | Replacive clay (indet/mix) | 1.0 |

**Remarks:** Quartz is mostly pore-filling, as is dolomite. Note the sparse kaolinite. Clay coatings are thin and mostly illitic.

*Spatial relationships (Paragenetic sequence):*

- Kaolinite is overgrown by quartz cement (quartz postdates kaolinite)
- Siderite and dolomite in leached grain (postdates leaching)
- Clay coating remain where feldspar is leached (predates leaching)

## Point counted porosity (%)

| | | | |
|---|---|---|---|
| Intergranular | 13.7 | Intragranular | 1.0 |
| Oversized | - | Mouldic | 0.7 |
| Macroporosity (visible porosity) | | 15.3 | |
| Microporosity (He-porosity minus macroporosity) | | 5.4 | |

**Remarks:** Microporosity is relatively low and is related to the low clay content.

## Reservoir properties

| | |
|---|---|
| He-Porosity (%) | 20.7 |
| Permeability (mD) | 176 |
| Grain density (g/cm$^3$) | 2.65 |
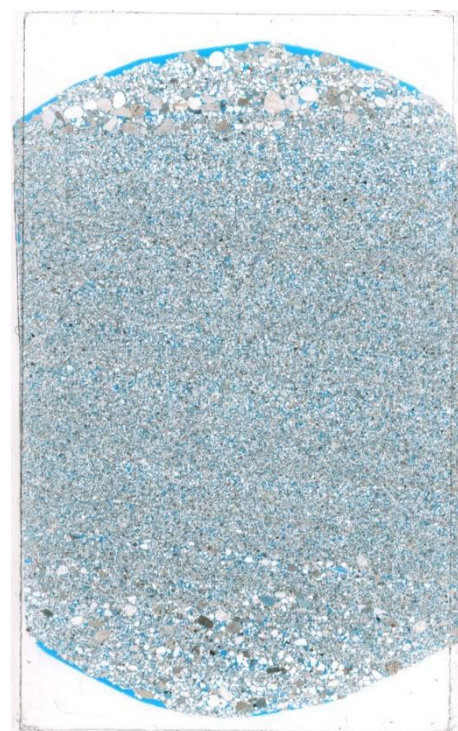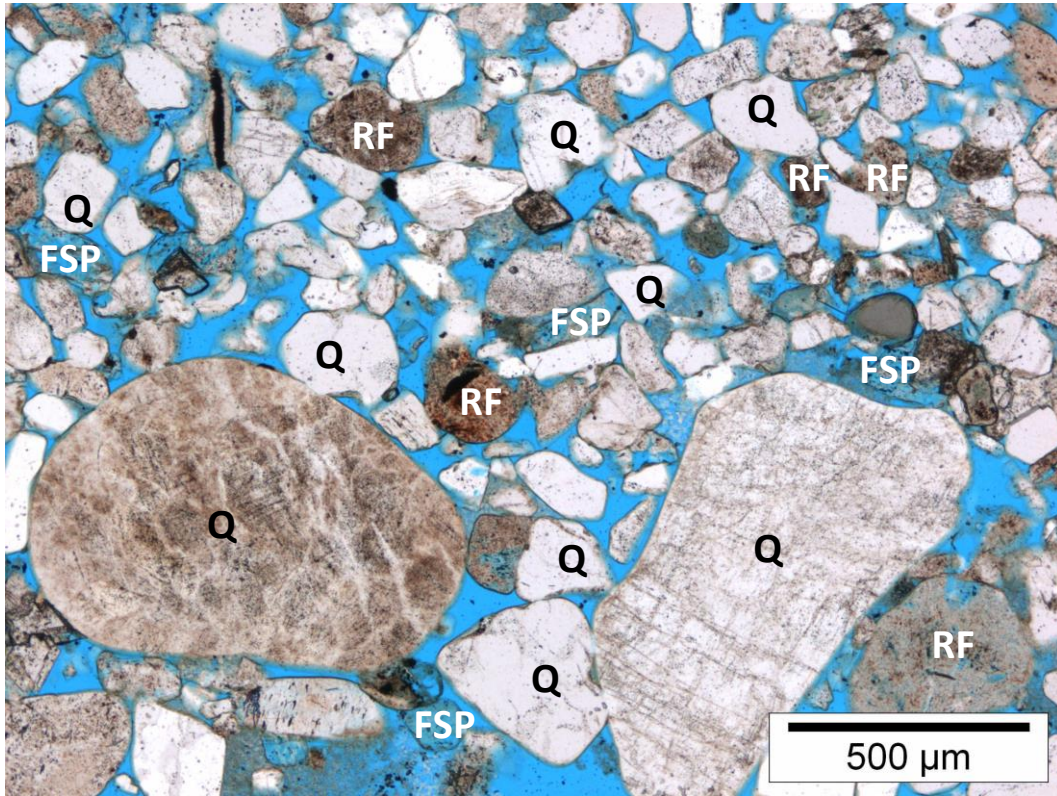


*Thin section scan (width ~2.5 cm)*

**A. Magnification 45x**                                    **Plane Polarised Light**



**B. Magnification 113x**                                    **Plane Polarised Light**

**Plate A:** Laminae with coarse-grained quartz grains (Q) occur in this fine grained sample. Clay coatings are present but fairly thin, locally outlining (partially) dissolved feldspar (FSP) grains. Pores are well connected and porosity is high. Rock fragments (RF) are often clay rich and fairly undeformed. **Plate B:** Compaction (large arrows) resulted in deformation and fracturing of this rock fragment (RF). The strongly leached feldspar (FSP) is however not deformed, due to the position and orientation of the grain. Grain leaching postdates most of the mechanical compaction as indicated by the undeformed nature of the leached grains.

**Sample Type:** Plug Trimend

**Rock Classification (Pettijohn, 1975):** Sublitharenite

## Texture

| | | | | | |
|---|---|---|---|---|---|
| Texture | structureless | Grain size (modal) | medium sand (L) | Roundness | SR |
| Sample heterogeneity | low | Grain size (min) | 88-125 µm | Sorting | MG |
| | | Grain size (max) | 500-710 µm | | |

**Remarks:** Relatively coarse grained sandstone sample.

## Compaction

| | | | | | |
|---|---|---|---|---|---|
| Grain contacts - Rigid | P-L | COPL (%) | 34 | IGV (%) | 17 |
| Grain contacts - Ductile | L-CC | CEPL (%) | 8 | | |

**Remarks:** The high COPL and relatively low IGV suggest relatively strong compaction. This is also shown by the occurrence of broken grains; both feldspar and quartz grains.

## Detrital components (%)

| | | | | | | | |
|---|---|---|---|---|---|---|---|
| Monoquartz | 44.7 | Feldspar | 1.3 | Rigid RF | 6.3 | Microporous RF | 3.0 |
| Polyquartz | 13.3 | Leached feldspar | 2.3 | Ductile RF | 0.3 | Accessories | Tr |

**Remarks:** Among the accessory minerals is muscovite. Observed feldspar content is relatively low.

## Authigenic components (%)

| | | | | | |
|---|---|---|---|---|---|
| Quartz | 1.3 | Grain rimming illite | 2.3 | Pore-filling kaolinite | 0.3 |
| Dolomite/Siderite | 0.7 | Grain rimming clay (mix) | 3.7 | Replacive kaolinite | 5.7 |
| Barite | Tr | Grain rimming chlorite | 0.3 | Replacive chlorite | 1.0 |
| | | Pore-filling clay (indet/mix) | 3.7 | Replacive clay (indet/mix) | 1.3 |

**Remarks:** Quartz and carbonate cement are mostly pore-filling. A significant amount of the minerals in the clay coating is indeterminable or mixed, as visible in SEM plate C & D.

*Spatial relationships (Paragenetic sequence):*

- Traces of clay coating on grain fracture surface (some coating after fracturing)
- Dolomite and siderite in leached grains
- Mouldic pores are undeformed (postdates most mechanical compaction)

## Point counted porosity (%)

| | | | |
|---|---|---|---|
| Intergranular | 4.7 | Intragranular | 1.7 |
| Oversized | 0.3 | Mouldic | 1.3 |
| Macroporosity (visible porosity) | | 8.0 | |
| Microporosity (He-porosity minus macroporosity) | | 17.2 | |

## Reservoir properties

| | |
|---|---|
| He-Porosity (%) | 25.2 |
| Permeability (mD) | 77 |
| Grain density (g/cm³) | 2.66 |

**Remarks:** Permeability is relatively low, compared to the porosity. This is partly because micropores do not contribute significantly to the permeability.
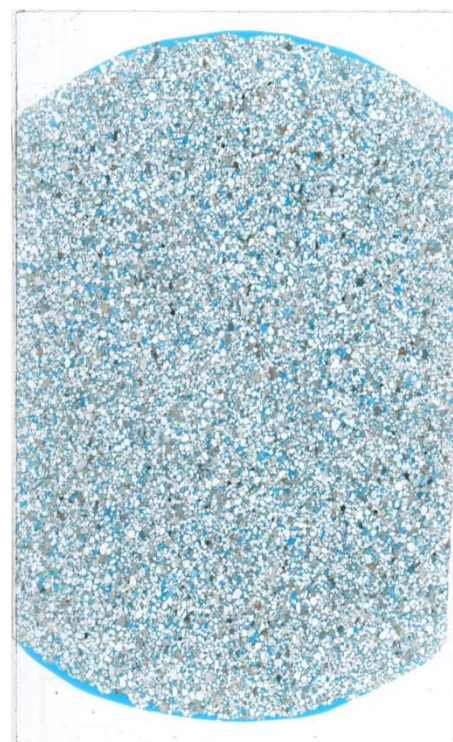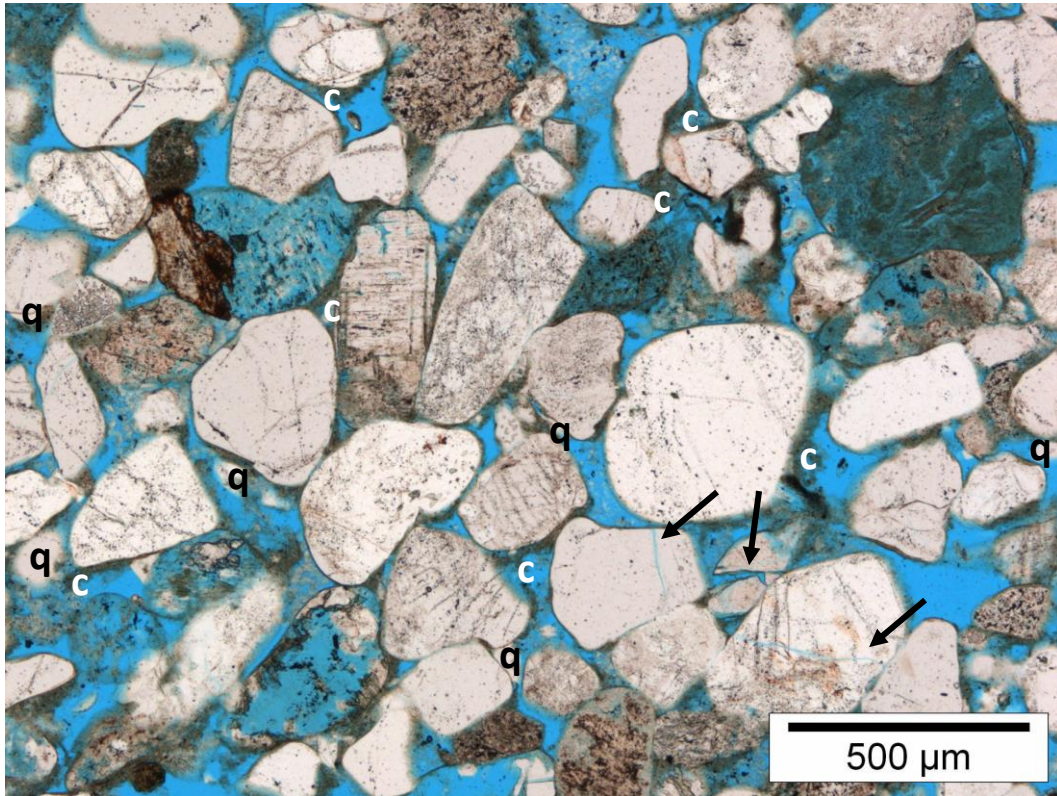


*Thin section scan (width ~2.5 cm)*

**A. Magnification 45x**                                    **Plane Polarised Light**
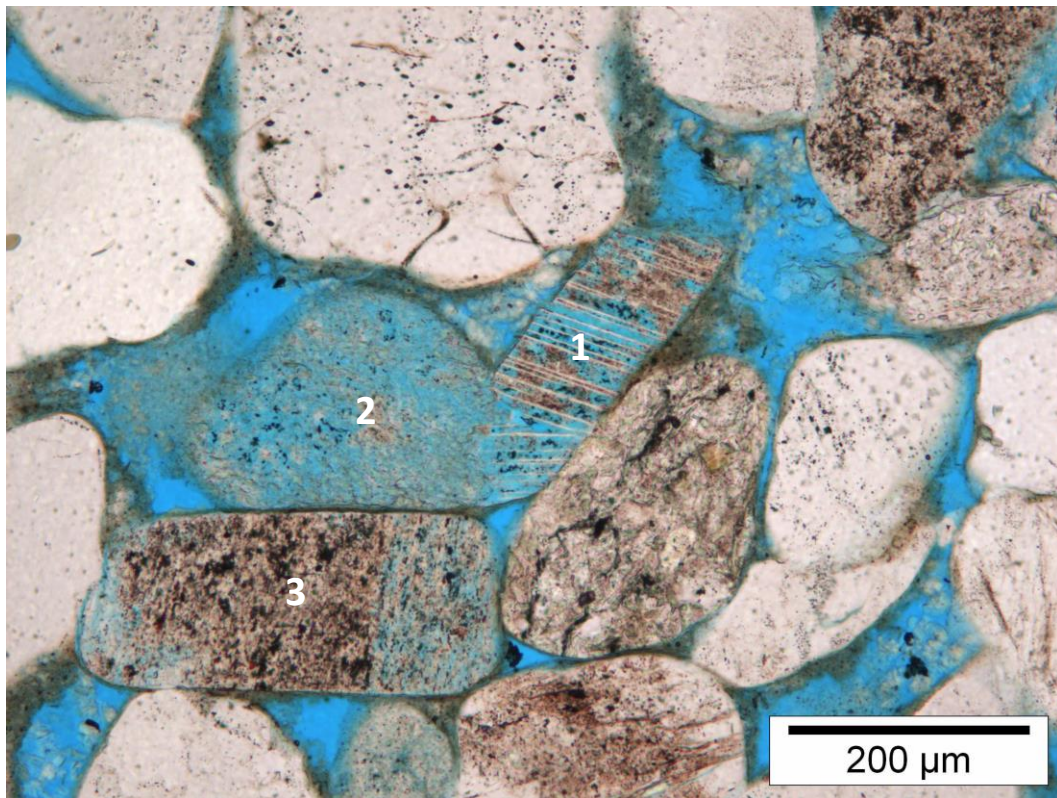


**B. Magnification 113x**                                   **Plane Polarised Light**

**Plate A:** The permeability in this relatively coarse grained sandstone is reduced by the occurrence of common intergranular randomly oriented clay (c; chloritic?) and (more rarely) the cementation of quartz (q), which clogg the pore throats. Multiple grains show compaction related fracturing (arrows). **Plate B:** The three feldspar grains (1-3) visible here show various degrees of leaching, which is related to the variations in feldspar composition. In feldspar 1, the original lamellae are well visible due to partial dissolution. Note the relative undeformed nature of the leached feldspar grains.

**Sample Type:** Plug Trimend

**Rock Classification (Pettijohn, 1975):** Sublitharenite

## Texture

| | | | | | |
|---|---|---|---|---|---|
| Texture | structureless | Grain size (modal) | fine sand (U) | Roundness | SR |
| Sample heterogeneity | low to moderate | Grain size (min) | 62.5-88 µm | Sorting | M |
| | | Grain size (max) | 500-710 µm | | |

**Remarks:** An artificial fracture cuts through the thin section. The sample is fairly unconsolidated.

## Compaction

| | | | | | |
|---|---|---|---|---|---|
| Grain contacts - Rigid | P | COPL (%) | 30 | IGV (%) | 21 |
| Grain contacts - Ductile | L | CEPL (%) | 10 | | |

**Remarks:** The mouldic pores (see TS plate A) are open and have retained the original shape, indicating that compaction did not continue significantly after grain leaching, despite the limited lithification.

## Detrital components (%)

| | | | | | | | |
|---|---|---|---|---|---|---|---|
| Monoquartz | 42.0 | Feldspar | 4.0 | Rigid RF | 6.7 | Microporous RF | 0.3 |
| Polyquartz | 16.7 | Leached feldspar | 2.0 | Ductile RF | 1.0 | Accessories | Tr |

**Remarks:** Note the relatively high content of polycrystalline quartz grains. Rigid rock fragments comprise mostly igneous rock fragments.

## Authigenic components (%)

| | | | | | |
|---|---|---|---|---|---|
| Quartz | 0.3 | Grain rimming illite | 7.0 | Pore-filling kaolinite | 0.3 |
| Dolomite/Siderite | Tr | Grain rimming clay (mix) | 1.7 | Replacive kaolinite | 1.0 |
| Barite | 0.3 | Grain rimming chlorite | 4.3 | Replacive chlorite | 0.3 |
| | | Pore-filling clay (indet/mix) | - | Replacive clay (indet/mix) | 1.3 |

**Remarks:** Authigenic quartz is almost entirely replacive. Clay rims are thick, double layered and contain both illite and chlorite.

*Spatial relationships (Paragenetic sequence):*

- Coating preserved after feldspar leaching
- Quartz cement covers clay coating
- Barite overgrew quartz cement (postdates quartz cement)

## Point counted porosity (%)

| | | | |
|---|---|---|---|
| Intergranular | 7.3 | Intragranular | 1.7 |
| Oversized | 0.3 | Mouldic | 0.7 |
| Macroporosity (visible porosity) | | 10.0 | |
| Microporosity (He-porosity minus macroporosity) | | 17.3 | |

## Reservoir properties

| | |
|---|---|
| He-Porosity (%) | 27.3 |
| Permeability (mD) | n/a |
| Grain density (g/cm$^3$) | 2.65 |

**Remarks:** Artificial microfractures might have resulted in a slight overestimation of porosity.



*Thin section scan (width ~2.5 cm)*
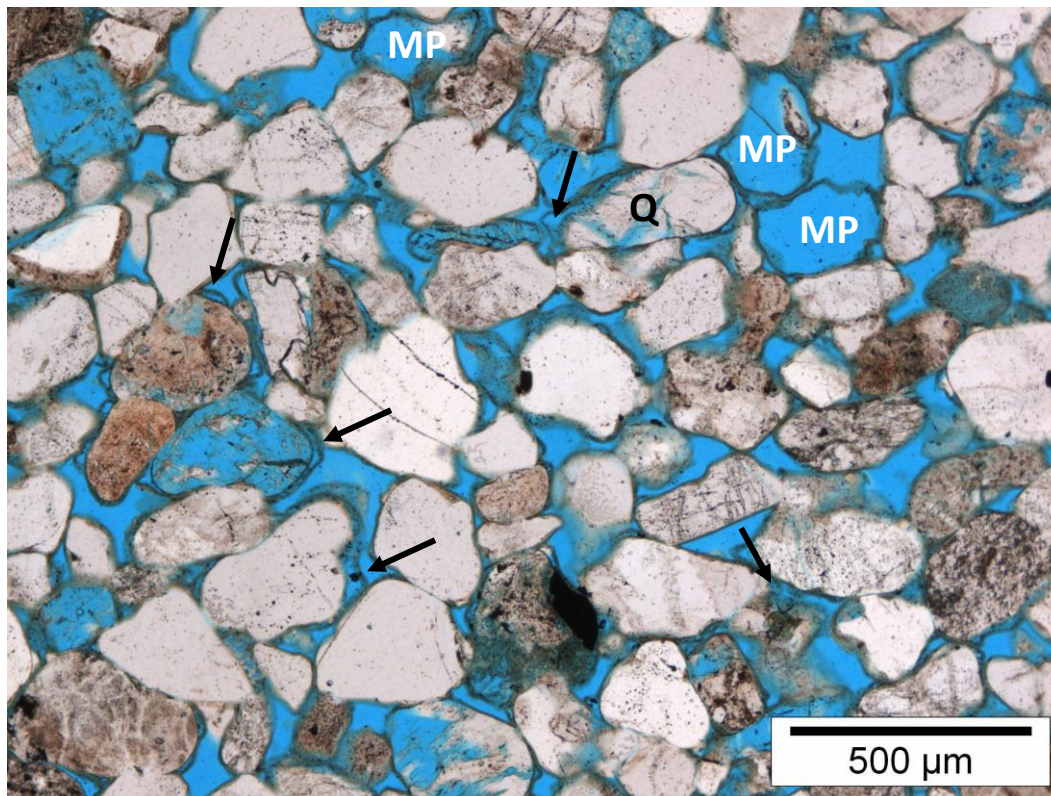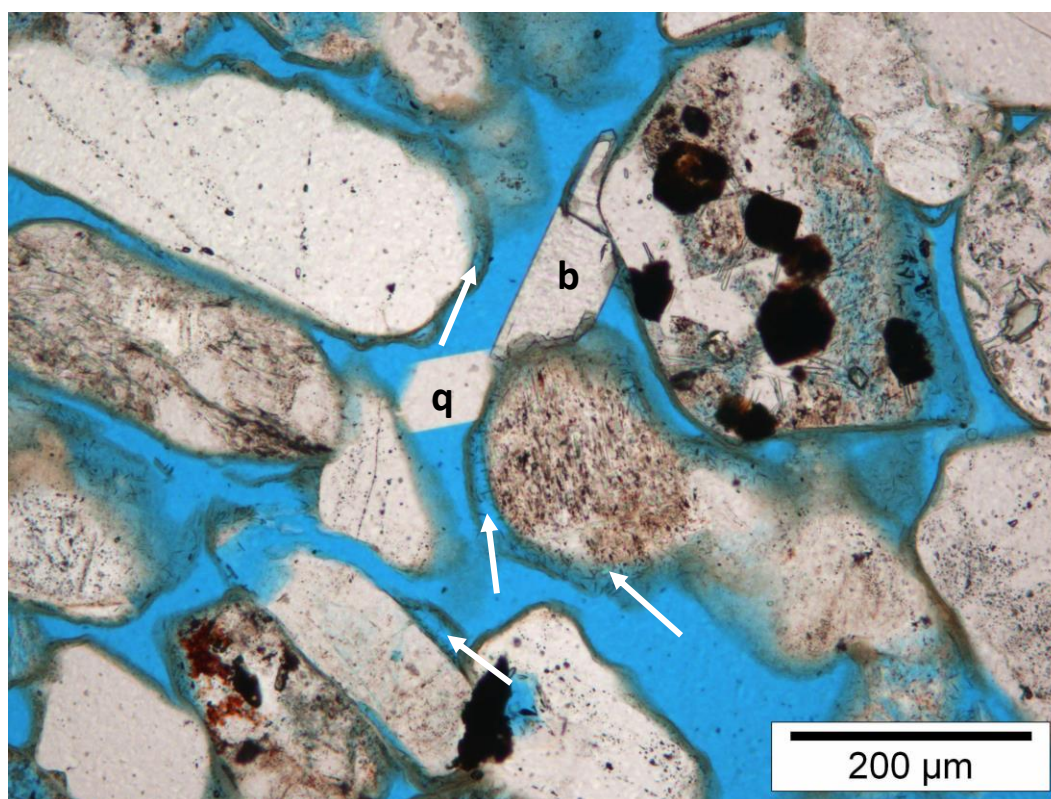
A. Magnification 45x — Plane Polarised Light



B. Magnification 113x — Plane Polarised Light

**Plate A:** The detrital grains are covered with a thick layer of grain rimming clay, which locally is separated from the detrital grains (arrows). Due to the clay rim, mouldic pores (MP) are easy to distinguish. Locally, some feldspar is remaining (FSP). Since the shape of these mouldic pores does not show indications of significant deformation, compaction likely occurred mostly prior to leaching. Note the strongly fractured quartz grain (Q). **Plate B:** In this porous area, some low relief quartz cement (q) and high relief barite (b) occurs. Note the chlorite which occurs in between the thick clay rim and the detrital grains (arrows).

**Sample Type:** Plug Trimend          **Rock Classification (Pettijohn, 1975):** Sublitharenite

## Texture

| | | | | | |
|---|---|---|---|---|---|
| Texture | faintly laminated | Grain size (modal) | fine sand (U) | Roundness | SA-SR |
| Sample heterogeneity | moderate | Grain size (min) | 31-62.5 µm | Sorting | M-P |
| | | Grain size (max) | 500-710 µm | | |

**Remarks:** Lamination is characterised by minor variations in grain size. Lamellae have approximately equal thicknesses.

## Compaction

| | | | | | |
|---|---|---|---|---|---|
| Grain contacts - Rigid | P-L | COPL (%) | 36 | IGV (%) | 15 |
| Grain contacts - Ductile | CC | CEPL (%) | 6 | | |

**Remarks:** Relatively little CEPL, indicating that most of the porosity loss was due to compaction.

## Detrital components (%)

| | | | | | | | |
|---|---|---|---|---|---|---|---|
| Monoquartz | 50.0 | Feldspar | 3.7 | Rigid RF | 5.7 | Microporous RF | 2.0 |
| Polyquartz | 10.7 | Leached feldspar | 4.7 | Ductile RF | 1.3 | Accessories | Tr |

**Remarks:** Most rock fragments are undetermined. Feldspar is commonly identified due to leaching and twinning.

## Authigenic components (%)

| | | | | | |
|---|---|---|---|---|---|
| Quartz | 0.3 | Grain rimming illite | 4.0 | Pore-filling kaolinite | - |
| Dolomite/Siderite | 1.3 | Grain rimming clay (mix) | 0.7 | Replacive kaolinite | 3.3 |
| Barite | 0.3 | Grain rimming chlorite | - | Replacive chlorite | - |
| | | Pore-filling clay (indet/mix) | 2.7 | Replacive clay (indet/mix) | 1.3 |

**Remarks:** There is only very sparse replacive clay. Most authigenic clay occurs either in detrital rock fragments or as pore-filling (grain rimming) clay.

*Spatial relationships (Paragenetic sequence):*

- Some tangential clay in between grain contacts (predates final compaction)
- Quartz cement in between detrital grain and coating (postdates coating detachment)
- Dolomite and quartz cement in leached grains (postdates leaching)

## Point counted porosity (%)

| | | | |
|---|---|---|---|
| Intergranular | 5.3 | Intragranular | 1.3 |
| Oversized | 0.3 | Mouldic | 0.7 |
| Macroporosity (visible porosity) | | | 7.7 |
| Microporosity (He-porosity minus macroporosity) | | | 14.3 |

**Remarks:** Intergranular pores are relatively small.

## Reservoir properties

| | |
|---|---|
| He-Porosity (%) | 22 |
| Permeability (mD) | 105 |
| Grain density (g/cm$^3$) | 2.65 |
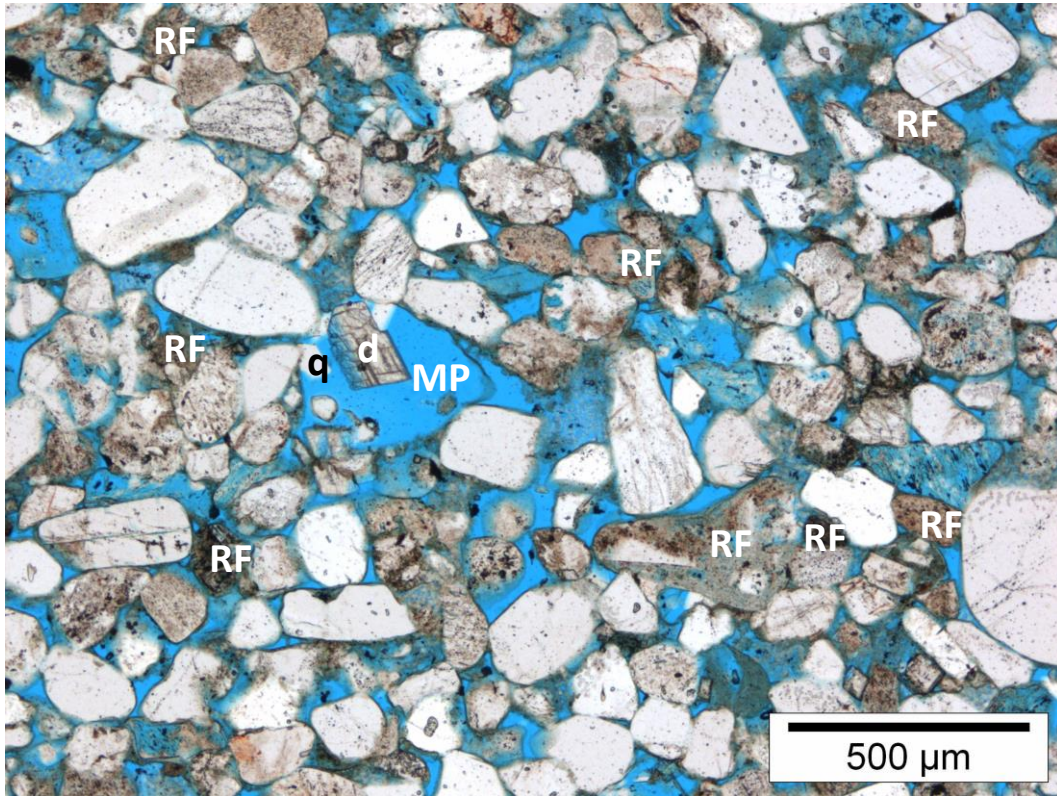


*Thin section scan (width ~2.5 cm)*

**A. Magnification 45x**          **Plane Polarised Light**



**B. Magnification 113x**          **Plane Polarised Light**

**Plate A:** Permeability in this fine grained sandstone is likely to be relatively low due to the absence of well-connected pores and occurrence of authigenic clay, probably chlorite-rich. A large mouldic pore (MP) is filled with both quartz cement (q) and dolomite cement (d). Rock fragments (RF) are common. **Plate B:** Detailed photo showing the mostly point to long rigid grain contacts in this sample. Note how a quartz grain is indenting (arrow) an unleached feldspar grain (FSP). Locally, very fine crystalline dolomite (d) occurs. Strongly leached feldspar grains (FSP+IP) show limited deformation.

**Sample Type:** Plug Trimend　　　　　　　　**Rock Classification (Pettijohn, 1975):** Sublitharenite

## Texture

| | | | | | |
|---|---|---|---|---|---|
| Texture | laminated | Grain size (modal) | fine sand (U) | Roundness | SA-SR |
| Sample heterogeneity | moderate to high | Grain size (min) | 62.5-88 µm | Sorting | P |
| | | Grain size (max) | 710-1000 µm | | |

**Remarks:** The thickness of laminae varies. Grain size variation varies strongly, hence the poor sorting.

## Compaction

| | | | | | |
|---|---|---|---|---|---|
| Grain contacts - Rigid | P | COPL (%) | 32 | IGV (%) | 19 |
| Grain contacts - Ductile | CC | CEPL (%) | 9 | | |

**Remarks:** Due to the poor sorting, the grains were possibly more closely packed at the time of deposition and therefore the IGV likely represents a rather low compaction as can also be inferred from the low content ductile grains and the point contacts between rigid grains.

## Detrital components (%)

| | | | | | | | |
|---|---|---|---|---|---|---|---|
| Monoquartz | 43.0 | Feldspar | 2.3 | Rigid RF | 9.7 | Microporous RF | 0.7 |
| Polyquartz | 16.3 | Leached feldspar | 2.3 | Ductile RF | 1.3 | Accessories | Tr |

**Remarks:** Note the high polycrystalline quartz content and rigid rock fragment content.

## Authigenic components (%)

| | | | | | |
|---|---|---|---|---|---|
| Quartz | 0.3 | Grain rimming illite | 5.3 | Pore-filling kaolinite | - |
| Dolomite/Siderite | 0.3 | Grain rimming clay (mix) | 1.3 | Replacive kaolinite | 1.0 |
| Barite | 0.3 | Grain rimming chlorite | 5.3 | Replacive chlorite | - |
| | | Pore-filling clay (indet/mix) | 0.7 | Replacive clay (indet/mix) | 2.0 |

**Remarks:** Grain rimming clay is common, with distinct illite and chlorite. Coatings are commonly detached.

*Spatial relationships (Paragenetic sequence):*

- Kaolinite crystals wrap around leached grain (predates some FSP leaching)
- Dolomite cement in leached FSP grain
- Quartz cement between detrital grain and detached clay rim

## Point counted porosity (%)

| | | | |
|---|---|---|---|
| Intergranular | 5.3 | Intragranular | 1.0 |
| Oversized | - | Mouldic | 1.3 |
| Macroporosity (visible porosity) | | 7.7 | |
| Microporosity (He-porosity minus macroporosity) | | 16.7 | |

**Remarks:** Microporosity is high due to the high clay content.

## Reservoir properties

| | |
|---|---|
| He-Porosity (%) | 24.4 |
| Permeability (mD) | n/a |
| Grain density (g/cm$^3$) | 2.64 |
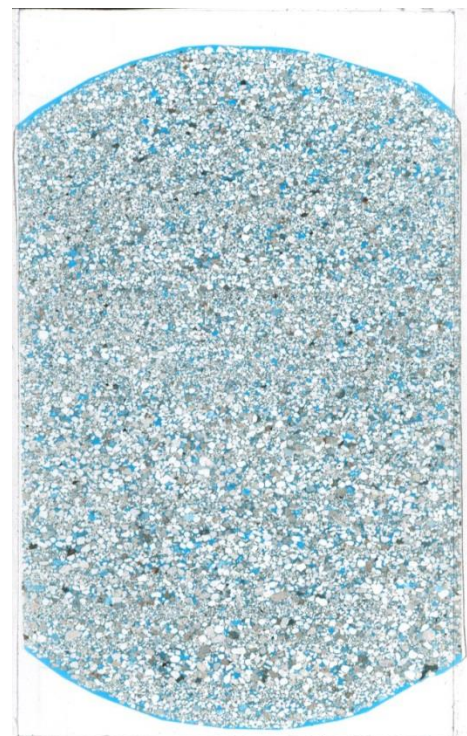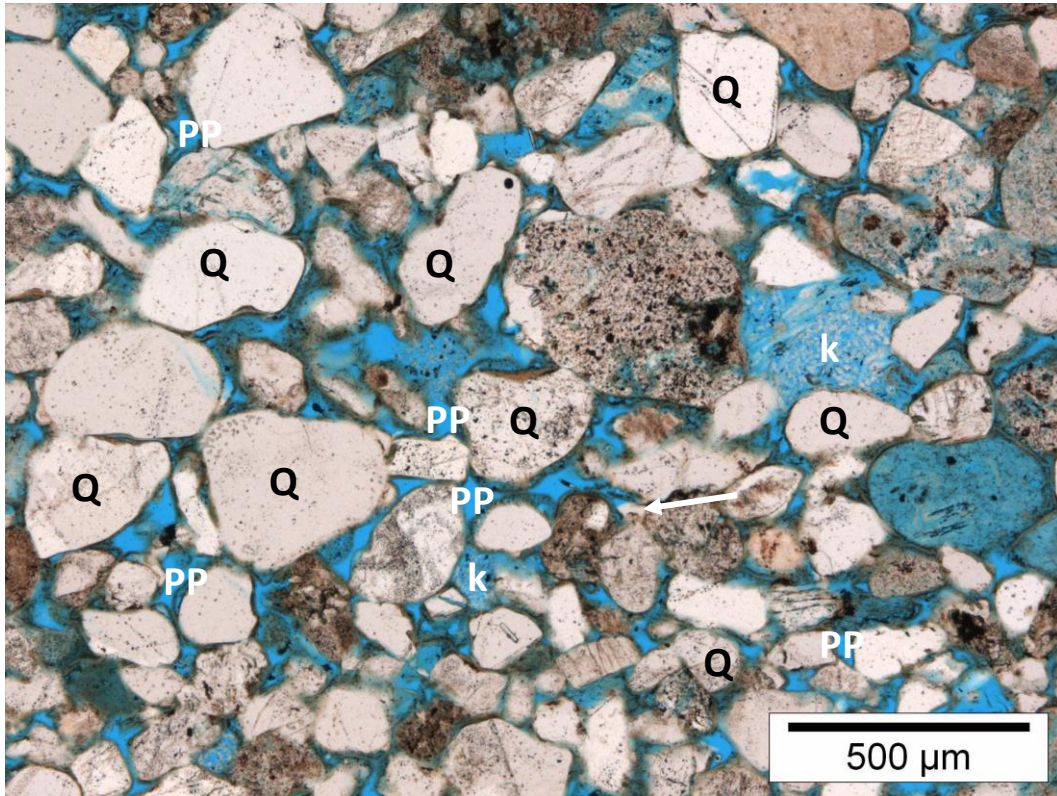


*Thin section scan (width ~2.5 cm)*

**A. Magnification 45x**        **Plane Polarised Light**
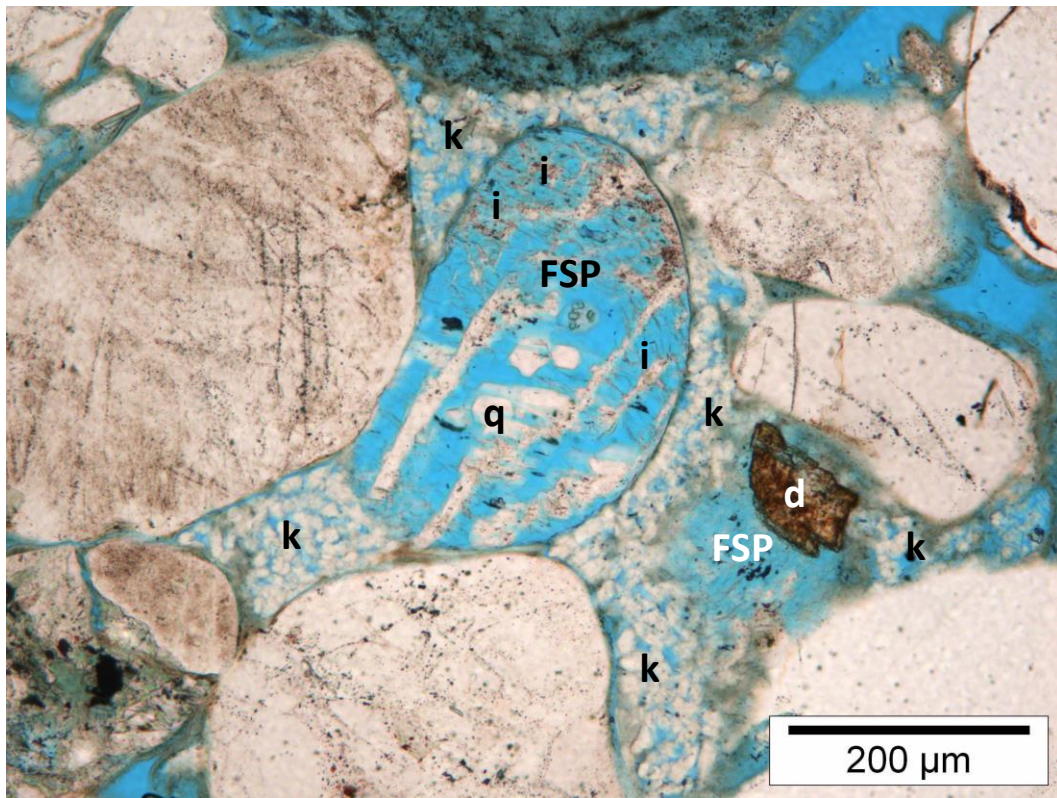


**B. Magnification 113x**        **Plane Polarised Light**

**Plate A:** The detrital grains (mostly quartz; Q) in this poorly sorted sublitharenite are covered with authigenic clay coats. Rare quartz cement locally formed (arrow). Note also that the clay rims are commonly detached from the underlying detrital grain. Locally, pores are filled with authigenic kaolinite (k), which often is not covered with a darker authigenic clay rim. Intergranular pores (PP) are poorly connected. **Plate B:** Leached feldspar grains (FSP), with replacive quartz (q) and illite (i) are surrounded by dispersed authigenic kaolinite (k), which is absent in the grain dissolution pore. Note the dark dolomite cement (d).

**Sample Type:** Plug Trimend

**Rock Classification (Pettijohn, 1975):** Sublitharenite

## Texture

| | | | | | |
|---|---|---|---|---|---|
| Texture | irregular lamination | Grain size (modal) | fine sand (L) | Roundness | SA-SR |
| Sample heterogeneity | moderate to high | Grain size (min) | 31-62.5 µm | Sorting | P |
| | | Grain size (max) | 710-1000 µm | | |

**Remarks:** Generally fine grained sample with locally coarse grains, including quartz and rock fragments.

## Compaction

| | | | | | |
|---|---|---|---|---|---|
| Grain contacts - Rigid | P-L | COPL (%) | 30 | IGV (%) | 21 |
| Grain contacts - Ductile | CC | CEPL (%) | 10 | | |

**Remarks:** Some of the clay in the finer grained laminae might be deformed rock fragments and thus pseudomatrix.

## Detrital components (%)

| | | | | | | | |
|---|---|---|---|---|---|---|---|
| Monoquartz | 49.7 | Feldspar | 3.0 | Rigid RF | 6.0 | Microporous RF | 1.3 |
| Polyquartz | 7.0 | Leached feldspar | 2.3 | Ductile RF | 2.3 | Accessories | 0.3 |

**Remarks:** Claystone rock fragments (which are mostly ductile) are relatively common.

## Authigenic components (%)

| | | | | | |
|---|---|---|---|---|---|
| Quartz | 0.7 | Grain rimming illite | 5.0 | Pore-filling kaolinite | 0.7 |
| Dolomite/Siderite | 5.7 | Grain rimming clay (mix) | 0.7 | Replacive kaolinite | 1.7 |
| Barite | - | Grain rimming chlorite | - | Replacive chlorite | 0.3 |
| | | Pore-filling clay (indet/mix) | 1.7 | Replacive clay (indet/mix) | 2.0 |

**Remarks:** Zoned dolomite with Fe-rich outer rims, is common. Siderite occurs at levels below XRD detection limits. Clay is most common in the finer-grained laminae.

*Spatial relationships (Paragenetic sequence):*

- Tangential illite coating prior to grain leaching.
- Quartz cementation after grain leaching & mouldic pore formation.
- Siderite & Fe-dolomite cementation after quartz cementation.

## Point counted porosity (%)

| | | | |
|---|---|---|---|
| Intergranular | 7.0 | Intragranular | 1.3 |
| Oversized | 0.3 | Mouldic | Tr |
| Macroporosity (visible porosity) | | 8.7 | |
| Microporosity (He-porosity minus macroporosity) | | 8.7 | |

**Remarks:** Visually, intergranular pores are generally poorly to moderately connected.

## Reservoir properties

| | |
|---|---|
| He-Porosity (%) | 17.4 |
| Permeability (mD) | 25 |
| Grain density (g/cm$^3$) | 2.66 |
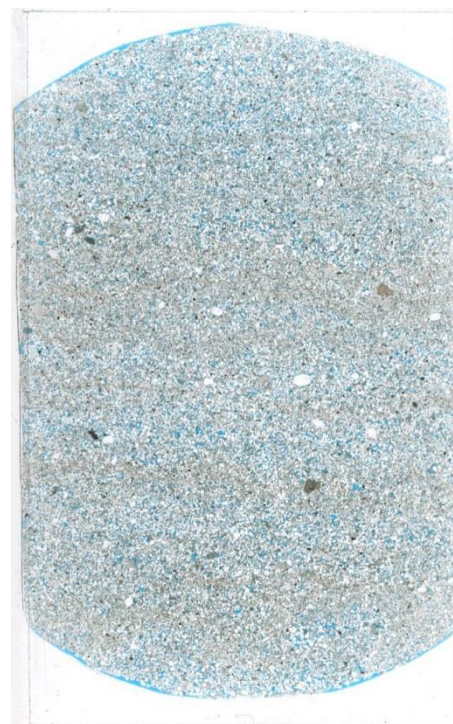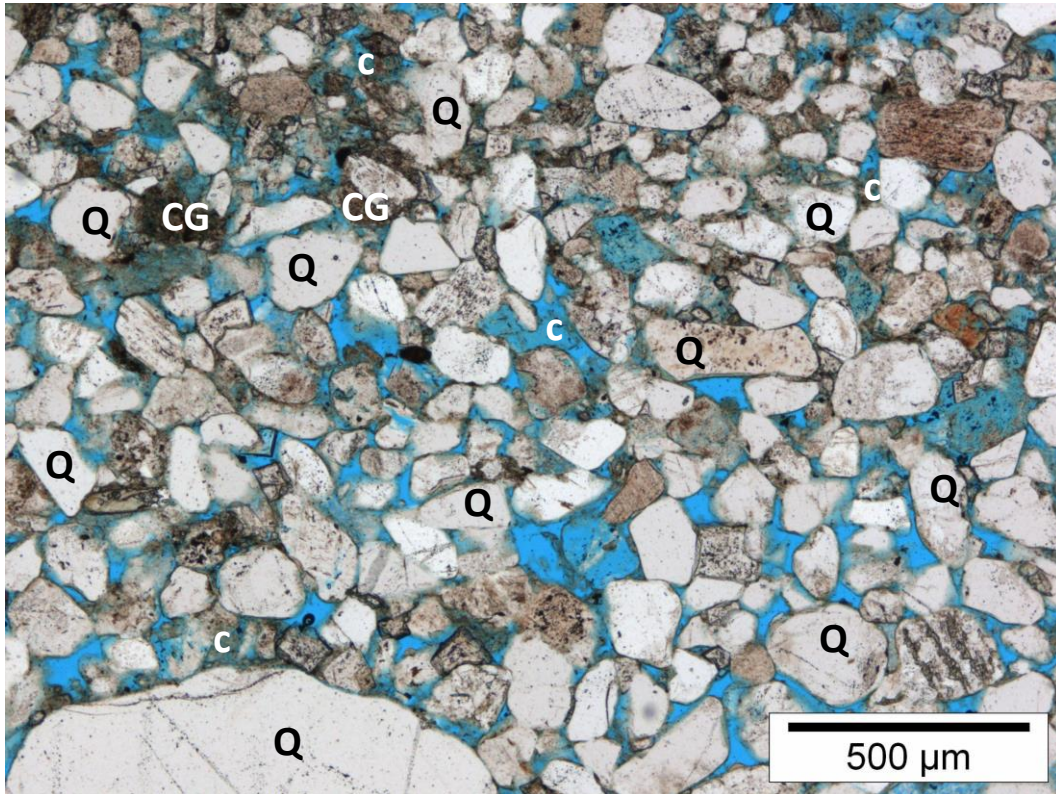


*Thin section scan (width ~2.5 cm)*

**A. Magnification 45x**          Plane Polarised Light
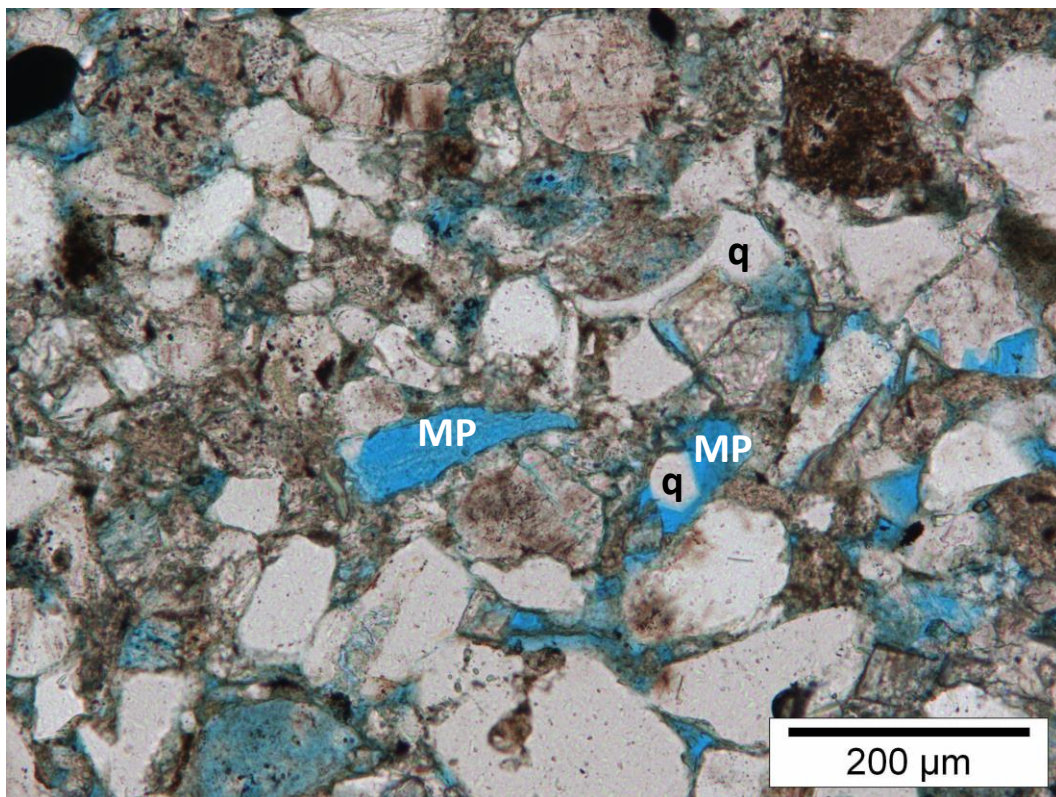


**B. Magnification 113x**          Plane Polarised Light

**Plate A:** The detrital quartz grains (Q) in this sandstone are subrounded to subangular. The sandstone is rich in clay, which occurs both as clay-rich grains (CG) as well as (dispersed) authigenic clay (c). The clay content varies per lamina; the top of the field of view is more clay rich (i.e. less porous) compared to the base. This is well visible in the TS scan (shown the page before). **Plate B:** Macropores in the clay-rich areas are rare. Locally mouldic pores (MP) and intragranular pores (IP; secondary) occur. Quartz cementation (q) reduced the porosity further, occurring as both pore-filling cement, as well as replacive cement.

**Sample Type:** Plug Trimend                    **Rock Classification (Pettijohn, 1975):** Sublitharenite

## Texture

| Texture | structureless | Grain size (modal) | fine sand (U) | Roundness | SA-SR |
|---|---|---|---|---|---|
| Sample heterogeneity | low | Grain size (min) | 31-62.5 µm | Sorting | MG-M |
| | | Grain size (max) | 500-710 µm | | |

**Remarks:** This sandstone sample is poorly consolidated.

## Compaction

| Grain contacts - Rigid | P | COPL (%) | 30 | IGV (%) | 21 |
|---|---|---|---|---|---|
| Grain contacts - Ductile | L | CEPL (%) | 3 | | |

**Remarks:** Compaction is low in this sample, even though some Feldspar grains are broken due to compaction (e.g. BSEM plate C).

## Detrital components (%)

| Monoquartz | 44.3 | Feldspar | 4.0 | Rigid RF | 3.7 | Microporous RF | 4.0 |
|---|---|---|---|---|---|---|---|
| Polyquartz | 12.0 | Leached feldspar | 3.7 | Ductile RF | 1.0 | Accessories | Tr |

**Remarks:** Feldspar is commonly recognized. Rock fragments are common and often leached.

## Authigenic components (%)

| Quartz | 1.0 | Grain rimming illite | 3.0 | Pore-filling kaolinite | 0.7 |
|---|---|---|---|---|---|
| Dolomite/Siderite | 0.3 | Grain rimming clay (mix) | 0.7 | Replacive kaolinite | 2.7 |
| Barite | Tr | Grain rimming chlorite | - | Replacive chlorite | - |
| | | Pore-filling clay (indet/mix) | - | Replacive clay (indet/mix) | - |

**Remarks:** Almost all quartz cement is replacive. The lack of quartz/carbonate/barite intergranular pore-filling cement partly explains the unconsolidated nature, together with the thin clay coating.

*Spatial relationships (Paragenetic sequence):*

- Clay coating outline shape of leached grain (predates leaching)
- Kaolinite dispersed through the sample (predates final compaction)
- Quartz cement in leached grains

## Point counted porosity (%)

| Intergranular | 16.3 | Intragranular | 1.3 |
|---|---|---|---|
| Oversized | 1.0 | Mouldic | Tr |
| Macroporosity (visible porosity) | | | 18.7 |
| Microporosity (He-porosity minus macroporosity) | | | 8.5 |

**Remarks:** Note the high macroporosity. Artificial fractures are not included.

## Reservoir properties

| He-Porosity (%) | 27.2 |
|---|---|
| Permeability (mD) | n/a |
| Grain density (g/cm$^3$) | 2.64 |
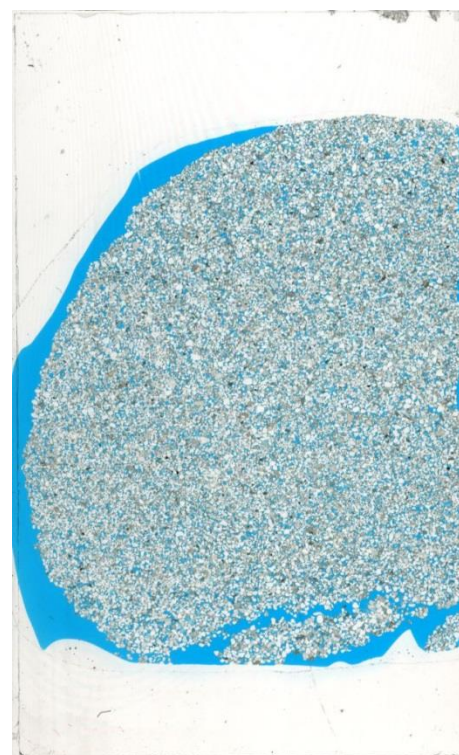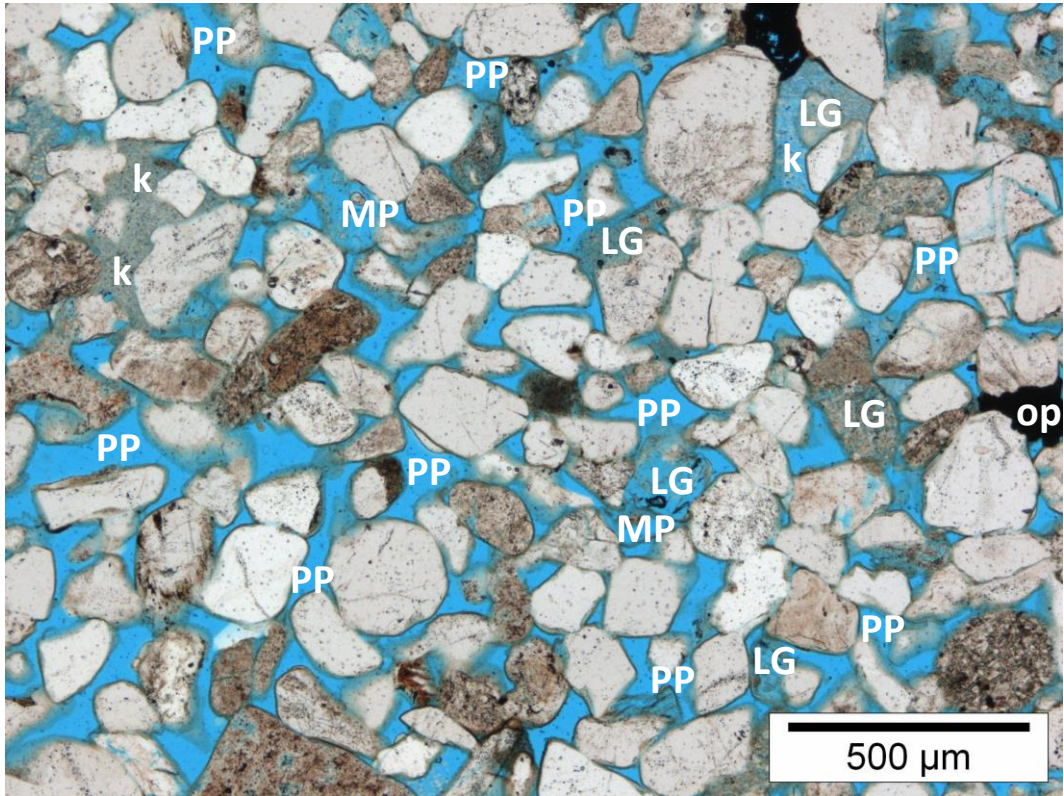


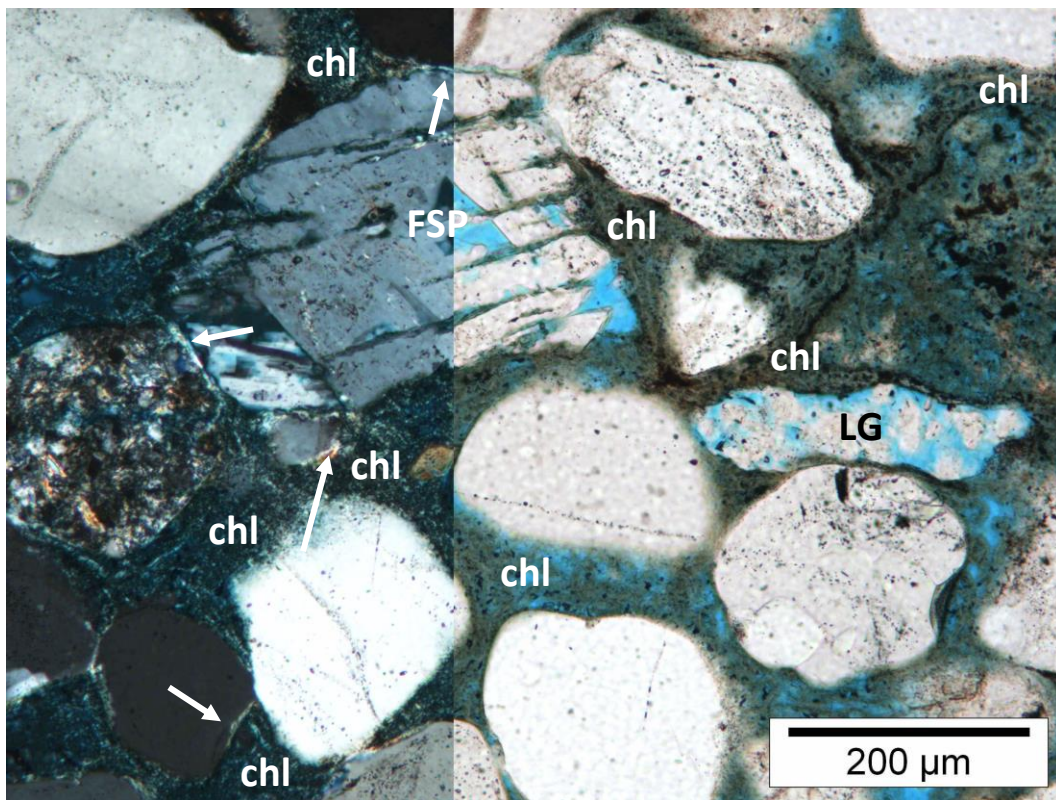*Thin section scan (width ~2.5 cm)*

**A. Magnification 45x**                                    **Plane Polarised Light**
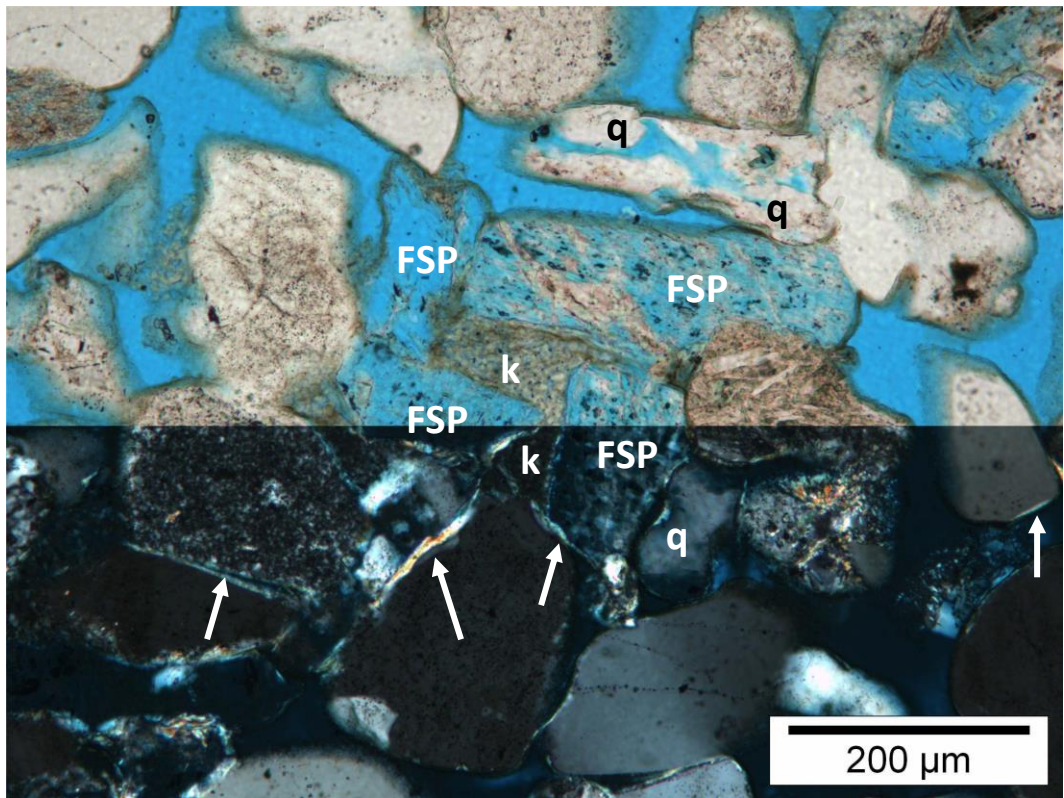


**B. Magnification 113x**                        **Plane Polarised Light/Crossed Nicols**

**Plate A:** This poorly consolidated sandstone comprises volumetrically relatively little authigenic clay. The illitic clay coatings are thin but continuous. Pores (PP) are moderate to well connected. The leached grains (LG) and mouldic pores (MP) were not significantly deformed after leaching. Note the opaque cement on the right (op) and the pore-filling authigenic kaolinite (k). **Plate B:** A cluster of leached feldspar grains (FSP) is shown, with in between authigenic kaolinite (k). Some of the leached grains are filled with authigenic quartz cement (q). The tangential illite rim (arrows) is identified in XPL (bottom half) by the high birefringence colours.

**Sample Type:** Plug Trimend                                    **Rock Classification (Pettijohn, 1975):** Sublitharenite

---

### Texture

| | | | | | |
|---|---|---|---|---|---|
| Texture | structureless | Grain size (modal) | fine sand (U) | Roundness | SA-SR |
| Sample heterogeneity | low | Grain size (min) | 62.5-88 µm | Sorting | MG |
| | | Grain size (max) | 350-500 µm | | |

**Remarks:** Coarse grains are absent in this sandstone sample.

### Compaction

| | | | | | |
|---|---|---|---|---|---|
| Grain contacts - Rigid | P | COPL (%) | 29 | IGV (%) | 23 |
| Grain contacts - Ductile | L-CC | CEPL (%) | 13 | | |

**Remarks:** The relatively high IGV and dominantly point rigid grain contacts indicate relatively low compaction.

### Detrital components (%)

| | | | | | | | |
|---|---|---|---|---|---|---|---|
| Monoquartz | 38.7 | Feldspar | 1.0 | Rigid RF | 6.7 | Microporous RF | 3.3 |
| Polyquartz | 11.3 | Leached feldspar | 2.7 | Ductile RF | Tr | Accessories | Tr |

### Authigenic components (%)

| | | | | | |
|---|---|---|---|---|---|
| Quartz | 0.3 | Grain rimming illite | 3.0 | Pore-filling kaolinite | 2.0 |
| Dolomite/Siderite | 5.3 | Grain rimming clay (mix) | 1.0 | Replacive kaolinite | 5.7 |
| Barite | - | Grain rimming chlorite | - | Replacive chlorite | - |
| | | Pore-filling clay (indet/mix) | 6.3 | Replacive clay (indet/mix) | 3.7 |

**Remarks:** Relatively common blotchy (PF) clay in the pores. This is likely a mixture of illite and chlorite. Kaolinite is common, as is PF carbonate.

*Spatial relationships (Paragenetic sequence):*

- Fe-dolomite at the outer rims of dolomite, visible in SEM (Fe-dolomite postdates Fe-poor dolomite)
- Dolomite in leached grain (postdates leaching)
- Barite overgrew dolomite and kaolinite (postdates dolomite and kaolinite)

### Point counted porosity (%)

| | | | |
|---|---|---|---|
| Intergranular | 5.0 | Intragranular | 1.7 |
| Oversized | 0.7 | Mouldic | 1.3 |
| Macroporosity (visible porosity) | | | 8.7 |
| Microporosity (He-porosity minus macroporosity) | | | 12.3 |

**Remarks:** Micropores occur mostly in the leached grains and authigenic clay.

### Reservoir properties

| | |
|---|---|
| He-Porosity (%) | 21 |
| Permeability (mD) | 31 |
| Grain density (g/cm$^3$) | 2.66 |

**Remarks:** Relatively low permeability, which is partly due to common PF clay.
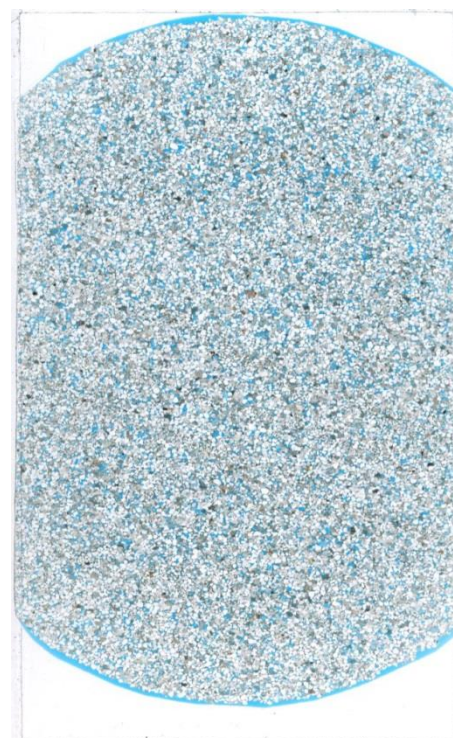


*Thin section scan (width ~2.5 cm)*
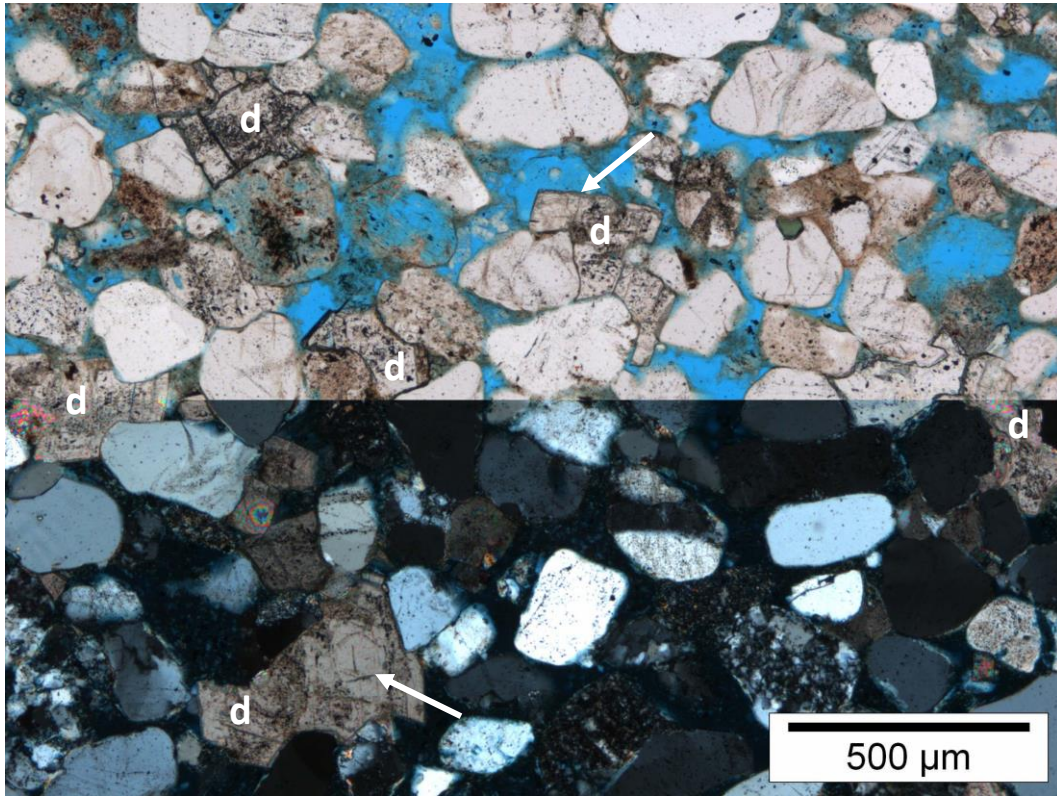
**A. Magnification 45x**                    Plane Polarised Light/Crossed Nicols
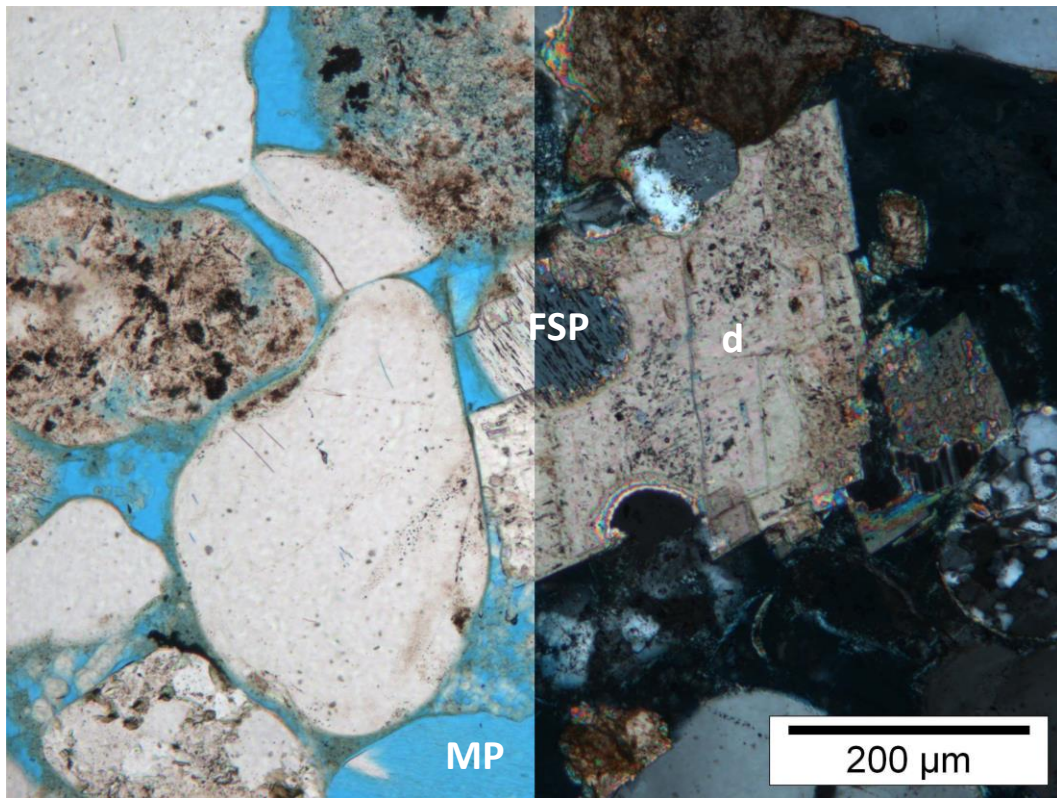


**B. Magnification 113x**                    Plane Polarised Light/Crossed Nicols

**Plate A:** By combining PPL images with XPL images, the commonly occurring dolomite (d; brownish in XPL) becomes apparent. Dolomite is mostly pore filling, even though locally, dolomite overprinted leached grains (arrows). The occurrence of dolomite and clay negatively influenced the reservoir quality. **Plate B:** Dolomite cement (d) engulfs a feldspar (FSP) grain. Note how clay occurs in between the detrital grains (arrows), including rock fragments (RF) and quartz (Q). The mouldic pore at the base of the image (MP) is free of authigenic clay. Clay coatings are commonly continuous at grain contacts.

**Sample Type:** Plug Trimend

**Rock Classification (Pettijohn, 1975):** Sublitharenite

## Texture

| | | | | | |
|---|---|---|---|---|---|
| Texture | laminated | Grain size (modal) | v.f sand (U) / m sand (L) | Roundness | SA-R |
| Sample heterogeneity | moderate | Grain size (min) | 31-62.5 µm | Sorting | MG-B |
| | | Grain size (max) | 710-1000 µm | | |

**Remarks:** Lamination is fairly distinct and pin stripe type. This is indicative of wind transport and deposition. No grading observed at this scale.

## Compaction

| | | | | | |
|---|---|---|---|---|---|
| Grain contacts - Rigid | P | COPL (%) | 34 | IGV (%) | 17 |
| Grain contacts - Ductile | L-CC | CEPL (%) | 8 | | |

**Remarks:** Compaction is relatively low, despite the low IGV. Mouldic pores are unaffected by (later stage) compaction.

## Detrital components (%)

| | | | | | | | |
|---|---|---|---|---|---|---|---|
| Monoquartz | 50.7 | Feldspar | 3.0 | Rigid RF | 6.3 | Microporous RF | 3.3 |
| Polyquartz | 12.7 | Leached feldspar | 1.3 | Ductile RF | 0.7 | Accessories | Tr |

**Remarks:** This sample has the highest monocrystalline quartz content of the sample set. Rock fragments are also common.

## Authigenic components (%)

| | | | | | |
|---|---|---|---|---|---|
| Quartz | 0.3 | Grain rimming illite | 6.3 | Pore-filling kaolinite | 0.3 |
| Dolomite/Siderite | 2.0 | Grain rimming clay (mix) | 1.3 | Replacive kaolinite | 2.0 |
| Barite | - | Grain rimming chlorite | 2.0 | Replacive chlorite | 1.3 |
| | | Pore-filling clay (indet/mix) | 1.0 | Replacive clay (indet/mix) | 0.7 |

**Remarks:** Grain rimming illite is thick and common. Other authigenic minerals are very sparse to sparse.

*Spatial relationships (Paragenetic sequence):*

- Clay coatings outline original shape of leached grain
- Leached grains are not significantly deformed (leaching postdates compaction)
- Chlorite and quartz in leached grain (postdates leaching)

## Point counted porosity (%)

| | | | |
|---|---|---|---|
| Intergranular | 4.0 | Intragranular | 0.7 |
| Oversized | - | Mouldic | Tr |
| Macroporosity (visible porosity) | | | 4.7 |
| Microporosity (He-porosity minus macroporosity) | | | 17.0 |

**Remarks:** The intergranular porosity is low, especially in the finer grained laminae.

## Reservoir properties

| | |
|---|---|
| He-Porosity (%) | 21.7 |
| Permeability (mD) | n/a |
| Grain density (g/cm$^3$) | 2.64 |

Due to the lamination, horizontal permeability is likely to be significantly higher than vertical permeability.
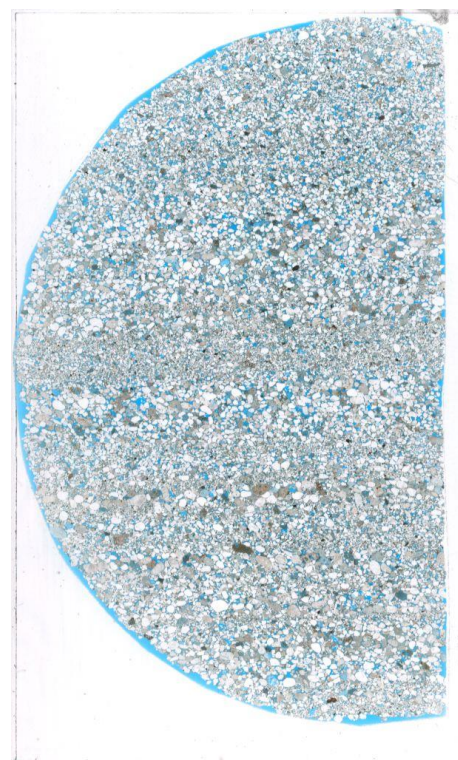


*Thin section scan (width ~2.5 cm)*
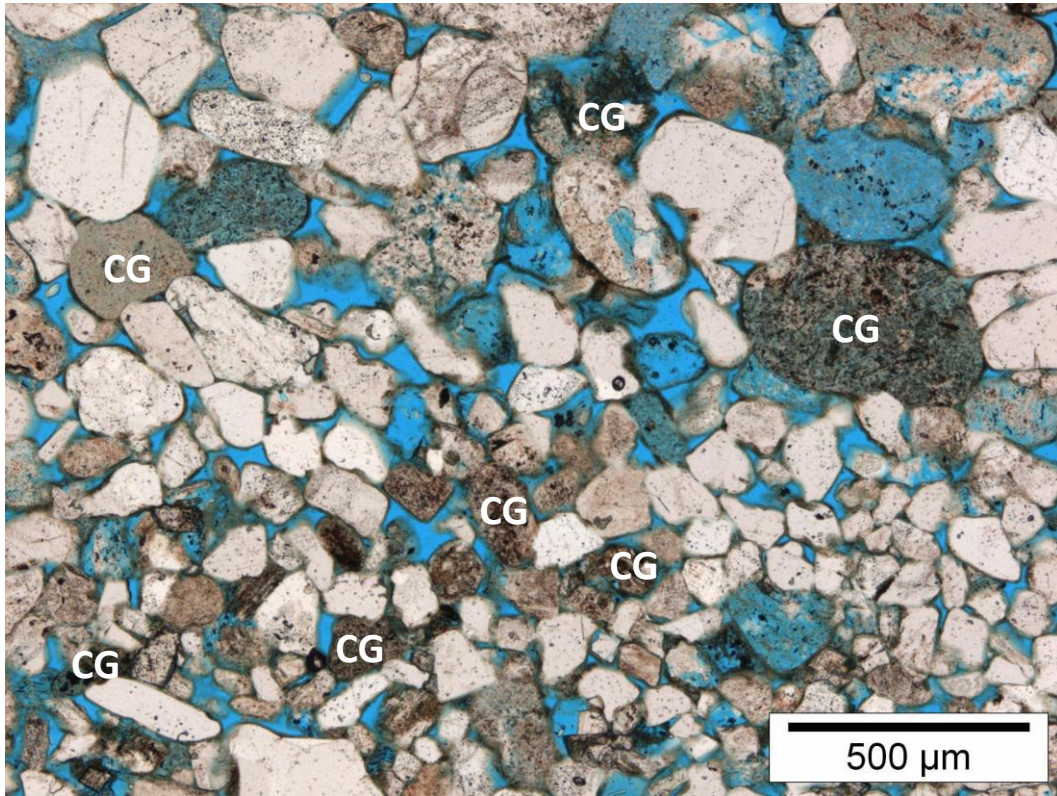
**A. Magnification 45x**     Plane Polarised Light
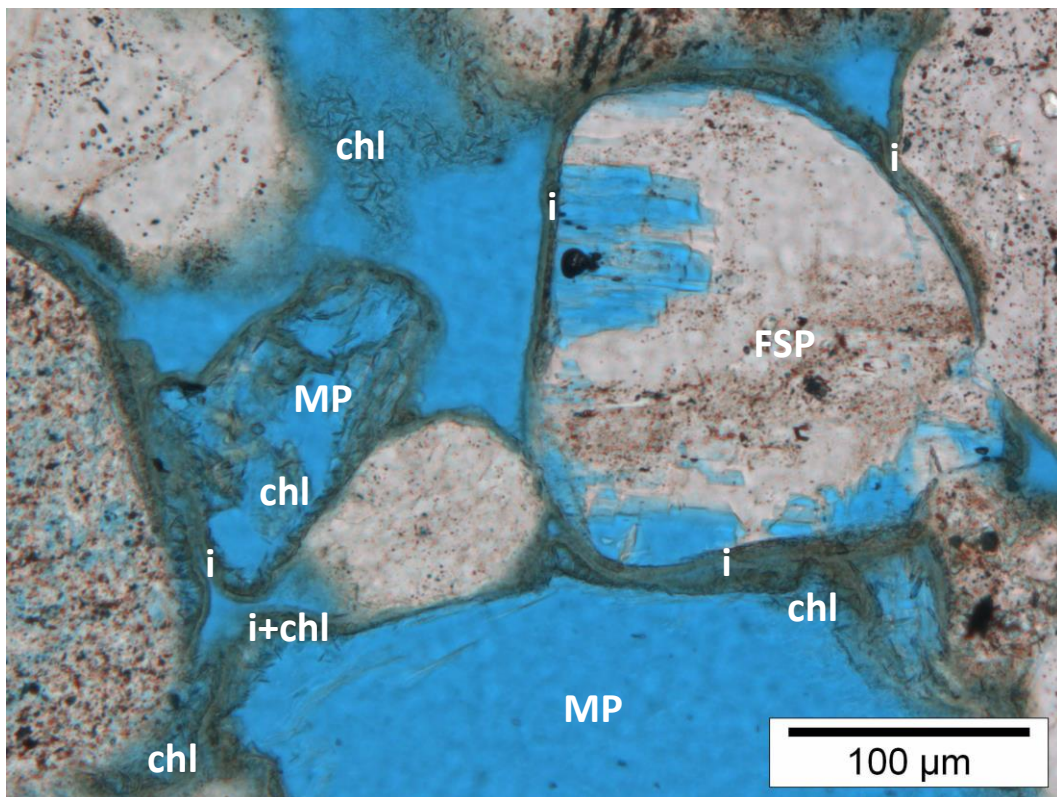


**B. Magnification 225x**     Plane Polarised Light

**Plate A:** This bimodally laminated sandstone sample (visible in the TS scan) is rich in clay-rich rock fragments (CG). The detrital grains (including the rock fragments) are covered with a thick clay coating. Therefore, pore throats are poorly connected. **Plate B:** This high magnification image (note the scale) shows the chlorite crystal structure (chl) as well as the finer crystalline tangential illitic rim (i). The feldspar grain (FSP) is partially leached, but the original shape is very well preserved. Note the mouldic pores (MP), also outlined by the clay rim. At the grain contacts coatings tend to be thin and mainly tangential illite.

**Sample Type:** Plug Trimend                                    **Rock Classification (Pettijohn, 1975):** Sublitharenite

## Texture

| | | | | | |
|---|---|---|---|---|---|
| Texture | faintly laminated | Grain size (modal) | medium sand (L) | Roundness | SA-SR |
| Sample heterogeneity | low to moderate | Grain size (min) | 31-62.5 µm | Sorting | P |
| | | Grain size (max) | 710-1000 µm | | |

**Remarks:** Thin, finer grained and slightly irregular laminae are present in this sample.

## Compaction

| | | | | | |
|---|---|---|---|---|---|
| Grain contacts - Rigid | P-L | COPL (%) | 35 | IGV (%) | 15 |
| Grain contacts - Ductile | CC | CEPL (%) | 6 | | |

**Remarks:** IGV is likely underestimated as the assumed initial depositional porosity of 45% was likely lower in this sample, due to the poor sort. Compaction appears to be low to moderate based on the grain contacts.

## Detrital components (%)

| | | | | | | | |
|---|---|---|---|---|---|---|---|
| Monoquartz | 42.0 | Feldspar | 4.7 | Rigid RF | 10.7 | Microporous RF | 1.3 |
| Polyquartz | 13.0 | Leached feldspar | 3.7 | Ductile RF | 1.3 | Accessories | Tr |

**Remarks:** The common rock fragments comprise mostly unidentified and igneous rock fragments. Feldspar is commonly identified as well.

## Authigenic components (%)

| | | | | | |
|---|---|---|---|---|---|
| Quartz | 1.7 | Grain rimming illite | 3.0 | Pore-filling kaolinite | 0.3 |
| Dolomite/Siderite | 2.3 | Grain rimming clay (mix) | 1.7 | Replacive kaolinite | 3.3 |
| Barite | - | Grain rimming chlorite | - | Replacive chlorite | - |
| | | Pore-filling clay (indet/mix) | 2.0 | Replacive clay (indet/mix) | 1.3 |

**Remarks:** Authigenic pore-filling minerals are relatively uncommon for this sample set. Dolomite and quartz are both intergranular pore-filling and replacive.

*Spatial relationships (Paragenetic sequence):*
- Quartz cement on grain fracture surface (postdates fracturing)
- (Fe-) dolomite and kaolinite overgrown by quartz cement
- Barite occurs in leached grains

## Point counted porosity (%)

| | | | |
|---|---|---|---|
| Intergranular | 5.7 | Intragranular | 1.3 |
| Oversized | 0.3 | Mouldic | Tr |
| Macroporosity (visible porosity) | | | 7.3 |
| Microporosity (He-porosity minus macroporosity) | | | 15.5 |

## Reservoir properties

| | |
|---|---|
| He-Porosity (%) | 22.8 |
| Permeability (mD) | n/a |
| Grain density (g/cm$^3$) | 2.66 |
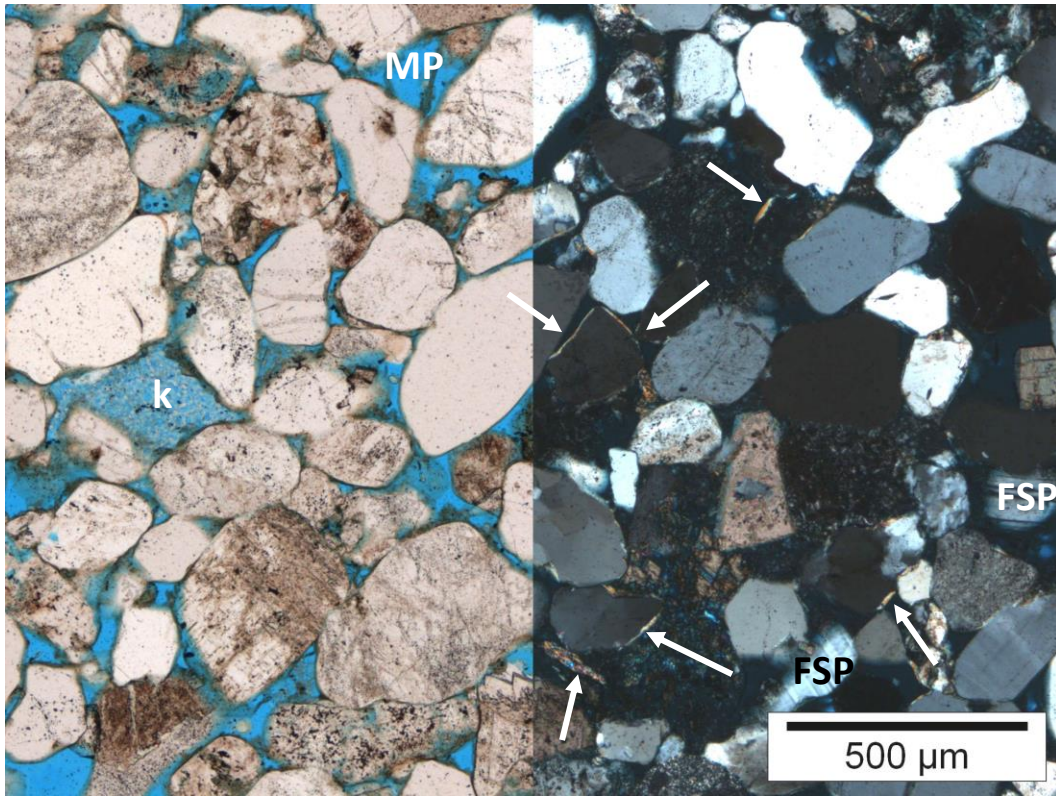


*Thin section scan (width ~2.5 cm)*

A. Magnification 45x     Plane Polarised Light/Crossed Nicols
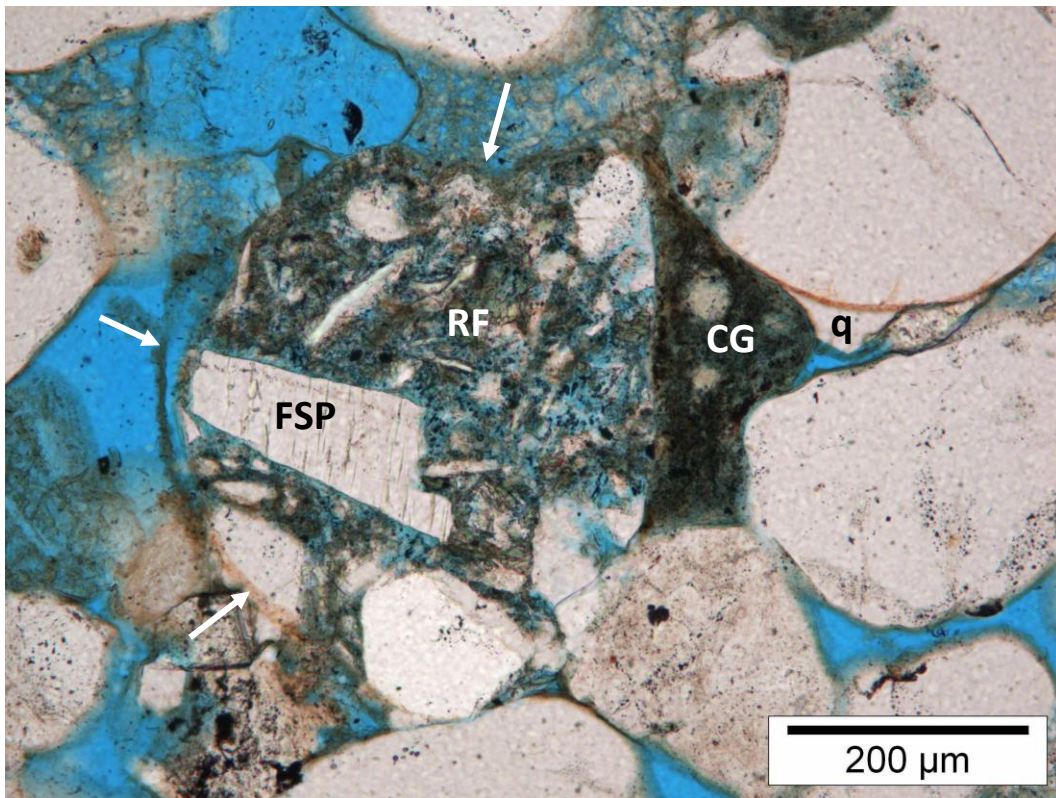


B. Magnification 113x     Plane Polarised Light

**Plate A:** This combined PPL/XPL image shows the high birefringence colour of the tangential clay rim, indicating this is illite (arrows). Also visible in XPL is the twinning of unleached feldspar grains (FSP; most likely plagioclase feldspar). In PPL, on the left side, kaolinite (k) and a mouldic pore (MP) are visible. **Plate B:** This cluster of various minerals is likely a (volcanic) rock fragment (RF) as it is outlined by a clay rim (arrows). This fragment contains elongated feldspar crystals (FSP). Note the strongly deformed clay-rich grain (CG) next to a quartz overgrowth (q).

**Sample Type:** Plug Trimend　　　　　　　　　　**Rock Classification (Pettijohn, 1975):** Sublitharenite

## Texture

| | | | | | |
|---|---|---|---|---|---|
| Texture | structureless | Grain size (modal) | fine sand (U) | Roundness | SA-SR |
| Sample heterogeneity | moderate to high | Grain size (min) | 31-62.5 µm | Sorting | MG-M |
| | | Grain size (max) | 710-1000 µm | | |

**Remarks:** The thin section sampled a dolomite cemented nodule.

## Compaction

| | | | | | |
|---|---|---|---|---|---|
| Grain contacts - Rigid | P | COPL (%) | 30 | IGV (%) | 21 |
| Grain contacts - Ductile | L-CC | CEPL (%) | 10 | | |

**Remarks:** Slightly higher CEPL than in other samples of the set due to dolomite cementation. Compaction is moderate to low.

## Detrital components (%)

| | | | | | | | |
|---|---|---|---|---|---|---|---|
| Monoquartz | 44.7 | Feldspar | 2.0 | Rigid RF | 7.3 | Microporous RF | - |
| Polyquartz | 10.0 | Leached feldspar | 1.3 | Ductile RF | Tr | Accessories | Tr |

## Authigenic components (%)

| | | | | | |
|---|---|---|---|---|---|
| Quartz | 2.0 | Grain rimming illite | 1.7 | Pore-filling kaolinite | 0.7 |
| Dolomite/Siderite | 5.7 | Grain rimming clay (mix) | 0.7 | Replacive kaolinite | 5.7 |
| Barite | - | Grain rimming chlorite | 0.3 | Replacive chlorite | 0.7 |
| | | Pore-filling clay (indet/mix) | 3.7 | Replacive clay (indet/mix) | 1.7 |

**Remarks:** Grain rimming clay (mix illite/chlorite) is relatively rare whereas pore-filling clay is slightly more common. Replacive kaolinite is micropore-rich. Dolomite is heterogeneously distributed.

*Spatial relationships (Paragenetic sequence):*
- Replacive illite occurs at the expense of leached grains (postdates leaching)
- $TiO_2$ and quartz occurs in leached grains (postdates leaching)

## Point counted porosity (%)

| | | | |
|---|---|---|---|
| Intergranular | 7.7 | Intragranular | 2.7 |
| Oversized | 0.3 | Mouldic | 0.3 |
| Macroporosity (visible porosity) | | 11.0 | |
| Microporosity (He-porosity minus macroporosity) | | 10.8 | |

**Remarks:** Macroporosity is low in the dolomite-cemented patch.

## Reservoir properties

| | |
|---|---|
| He-Porosity (%) | 21.8 |
| Permeability (mD) | 107 |
| Grain density (g/cm$^3$) | 2.65 |
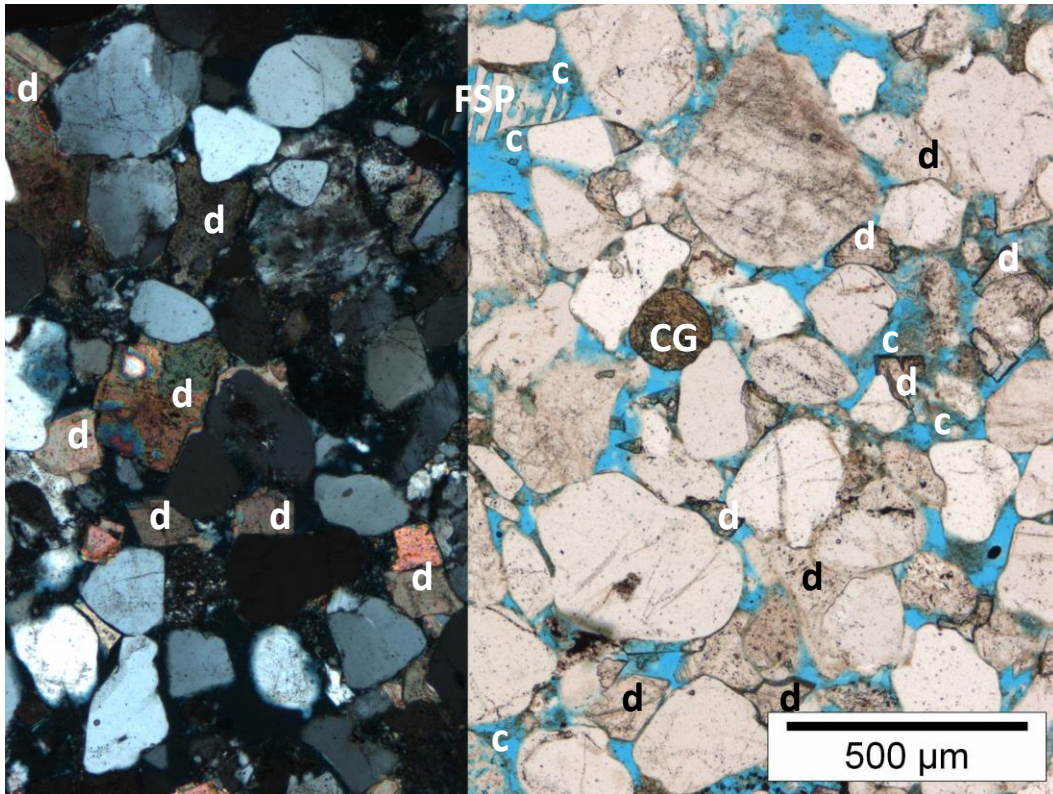


*Thin section scan (width ~2.5 cm)*

**A. Magnification 45x**                    **Plane Polarised Light/Crossed Nicols**
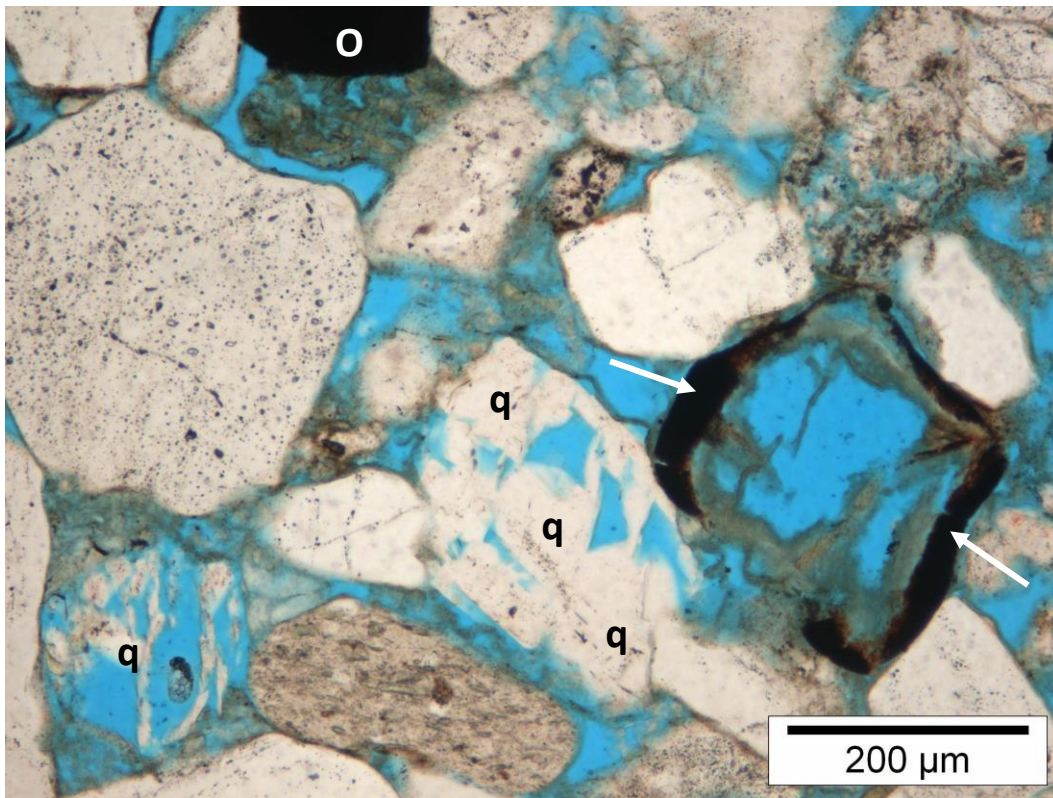


**B. Magnification 113x**                    **Plane Polarised Light**

**Plate A:** This sandstone sample contains a patch enriched in dolomite (d) cement (well visible in the TS scan; previous page). The dolomite locally reduces the reservoir quality significantly. Authigenic clay occurs as thin grain coatings (brown rim around grains) and as pore-filling authigenic fine-crystalline clay (c). Note the leached feldspar (FSP) and an undeformed clay grain (RF; possibly an altered igneous rock fragment). **Plate B:** Authigenic quartz (q) locally occurs in the leached grains. The leached grain (with intragranular pores; IP) on the right has a thick, possibly organic rim (arrows). Note the detached grain coatings and the opaque grain (O).

**Sample Type:** Plug Trimend      **Rock Classification (Pettijohn, 1975):** Sublitharenite

## Texture

| | | | | | |
|---|---|---|---|---|---|
| Texture | faintly laminated | Grain size (modal) | fine sand (U) | Roundness | SA-SR |
| Sample heterogeneity | low to moderate | Grain size (min) | 62.5-88 µm | Sorting | G-MG |
| | | Grain size (max) | 350-500 µm | | |

**Remarks:** Lamination is mostly visible by variations in clay content. Sand grain size variations are relatively subtle.

## Compaction

| | | | | | |
|---|---|---|---|---|---|
| Grain contacts - Rigid | P-L | COPL (%) | 28 | IGV (%) | 24 |
| Grain contacts - Ductile | L-CC | CEPL (%) | 16 | | |

**Remarks:** The presence of thick clay rims is a reason for the relatively high CEPL value. Compaction is low to moderate.

## Detrital components (%)

| | | | | | | | |
|---|---|---|---|---|---|---|---|
| Monoquartz | 46.3 | Feldspar | 2.7 | Rigid RF | 5.0 | Microporous RF | 1.0 |
| Polyquartz | 15.7 | Leached feldspar | Tr | Ductile RF | 0.3 | Accessories | Tr |

**Remarks:** Rock fragments are mostly unidentified and non-porous.

## Authigenic components (%)

| | | | | | |
|---|---|---|---|---|---|
| Quartz | 2.3 | Grain rimming illite | 4.7 | Pore-filling kaolinite | 1.0 |
| Dolomite/Siderite | 0.3 | Grain rimming clay (mix) | 4.3 | Replacive kaolinite | 1.3 |
| Barite | 0.7 | Grain rimming chlorite | - | Replacive chlorite | 0.3 |
| | | Pore-filling clay (indet/mix) | 9.3 | Replacive clay (indet/mix) | 1.3 |

**Remarks:** Authigenic (replacive) feldspar is identified in SEM. Grains are covered with a thick coating. Commonly, pores are filled with fine-crystalline clay. The coatings look like a mixture of illite and kaolinite (?). Booklet-shaped kaolinite is sparse.

*Spatial relationships (Paragenetic sequence):*

- Thick clay coatings outline original shape of leached grains
- Some leached grains appear slightly more compacted
- Quartz occurs in leached grains

## Point counted porosity (%)

| | | | |
|---|---|---|---|
| Intergranular | 1.7 | Intragranular | 0.3 |
| Oversized | - | Mouldic | 0.7 |
| Macroporosity (visible porosity) | | 2.7 | |
| Microporosity (He-porosity minus macroporosity) | | 15.0 | |

**Remarks:** Macroporosity is very low due to the thick clay coating.

## Reservoir properties

| | |
|---|---|
| He-Porosity (%) | 17.7 |
| Permeability (mD) | 7.0 |
| Grain density (g/cm$^3$) | 2.65 |

**Remarks:** The abundant pore-filling clay inhibits the permeability.
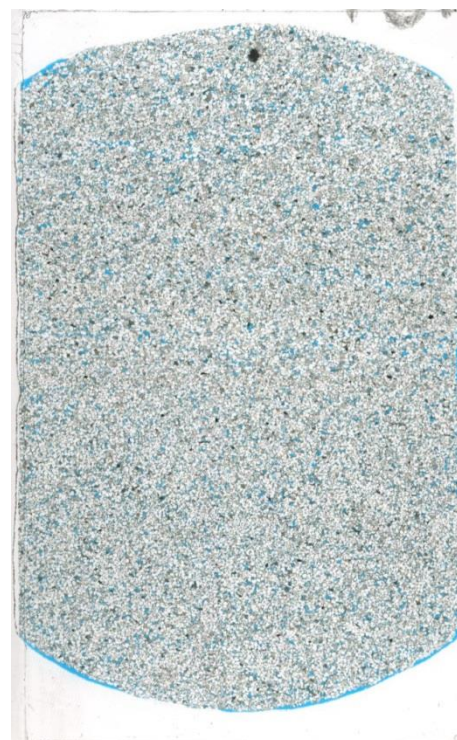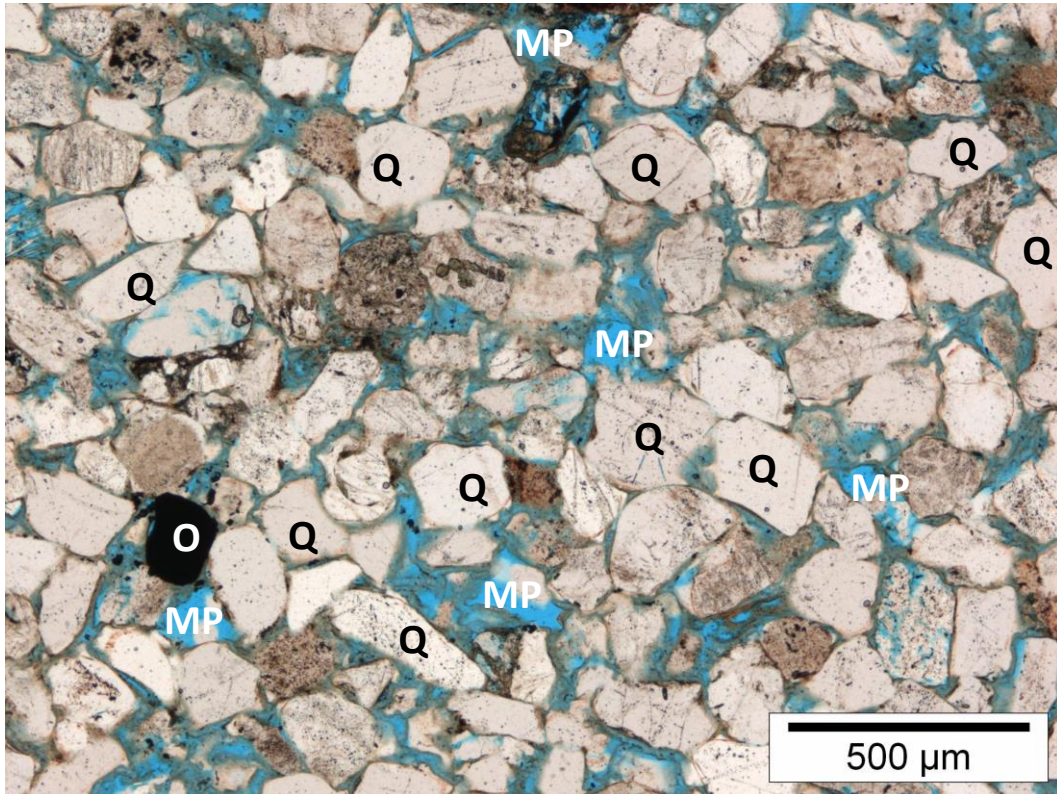


*Thin section scan (width ~2.5 cm)*

**A. Magnification 45x**                                                      **Plane Polarised Light**
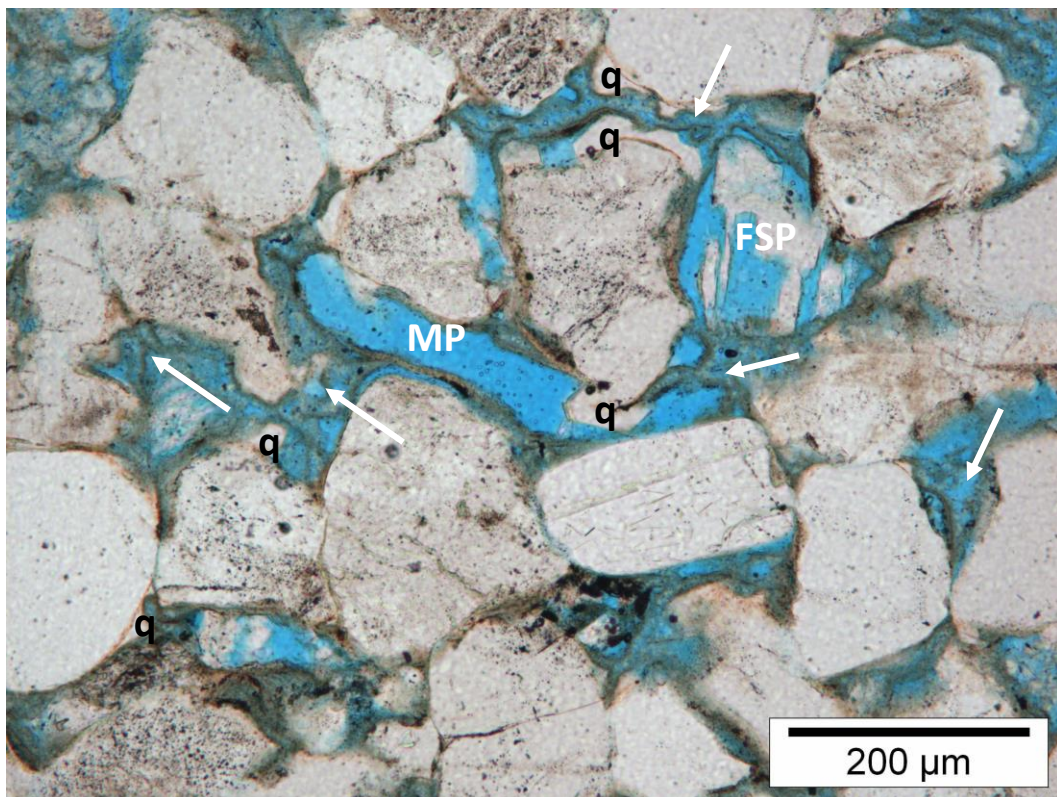


**B. Magnification 113x**                                                     **Plane Polarised Light**

**Plate A:** The macropores in this faintly laminated sandstone sample are mostly mouldic pores (MP), partially filled with authigenic quartz. Intergranular macropores are nearly absent. This is due to the relative close packing of the detrital grains (mostly quartz; Q but also e.g. an opaque grain; O) and thick clay coatings (arrows) that are partially detached from the grains they surround. **Plate B:** Detailed photo of a deformed mouldic pore (MP) and strongly leached feldspar grains (FSP). Illitic clay coatings are well preserved and regularly deformed (arrows), filling up intergranular pores. Some quartz cement occurs in between grains and the clay coatings (q).

**Sample Type:** Plug Trimend                     **Rock Classification (Pettijohn, 1975):** Sublitharenite

## Texture

| Texture | laminated | Grain size (modal) | f sand (L) / m sand (U) | Roundness | SA-SR |
|---|---|---|---|---|---|
| Sample heterogeneity | moderate | Grain size (min) | 31-62.5 µm | Sorting | MG-B |
| | | Grain size (max) | 500-710 µm | | |

**Remarks:** Poorly developed pin stripe type of lamination. This type of lamination is common in Aeolian deposits.

## Compaction

| Grain contacts - Rigid | P-L | COPL (%) | 29 | IGV (%) | 22 |
|---|---|---|---|---|---|
| Grain contacts - Ductile | L-CC | CEPL (%) | 8 | | |

## Detrital components (%)

| Monoquartz | 40.7 | Feldspar | 2.0 | Rigid RF | 7.3 | Microporous RF | 2.3 |
|---|---|---|---|---|---|---|---|
| Polyquartz | 12.0 | Leached feldspar | 3.3 | Ductile RF | 0.7 | Accessories | Tr |

**Remarks:** Accessory minerals include heavy minerals, glauconite and opaque minerals. Chert (included in the RF) is very sparse to sparse.

## Authigenic components (%)

| Quartz | 0.7 | Grain rimming illite | 4.7 | Pore-filling kaolinite | 0.7 |
|---|---|---|---|---|---|
| Dolomite/Siderite | 2.0 | Grain rimming clay (mix) | 1.0 | Replacive kaolinite | 5.0 |
| Barite | 0.3 | Grain rimming chlorite | 1.0 | Replacive chlorite | 0.7 |
| | | Pore-filling clay (indet/mix) | 1.3 | Replacive clay (indet/mix) | 1.3 |

**Remarks:** Grain rimming clay is mostly radial illite. Clusters of kaolinite are common.

*Spatial relationships (Paragenetic sequence):*
- Kaolinite could not pass clay coatings (kaolinite postdates coatings)
- Quartz engulfs kaolinite in leached grains (postdates leaching)

## Point counted porosity (%)

| Intergranular | 11.3 | Intragranular | Tr |
|---|---|---|---|
| Oversized | - | Mouldic | 0.7 |
| Macroporosity (visible porosity) | | | 12.0 |
| Microporosity (He-porosity minus macroporosity) | | | 9.7 |

**Remarks:** Intragranular macropores are not point counted. Due to the authigenic clay  and are almost all micropores.

## Reservoir properties
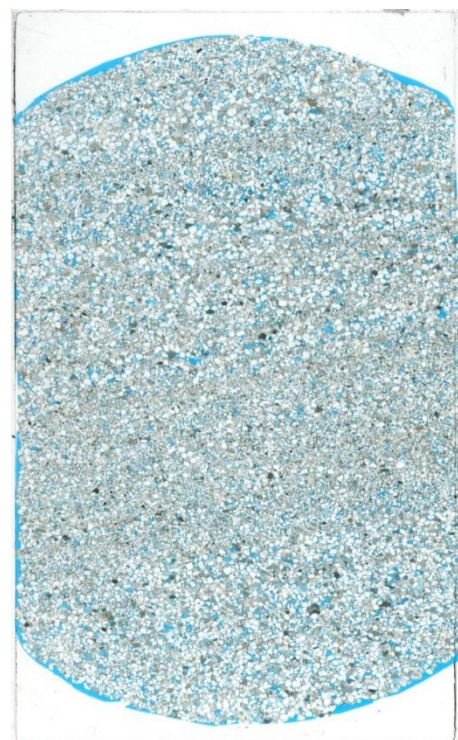
| He-Porosity (%) | 21.7 |
|---|---|
| Permeability (mD) | n/a |
| Grain density (g/cm$^3$) | 2.65 |



*Thin section scan (width ~2.5 cm)*
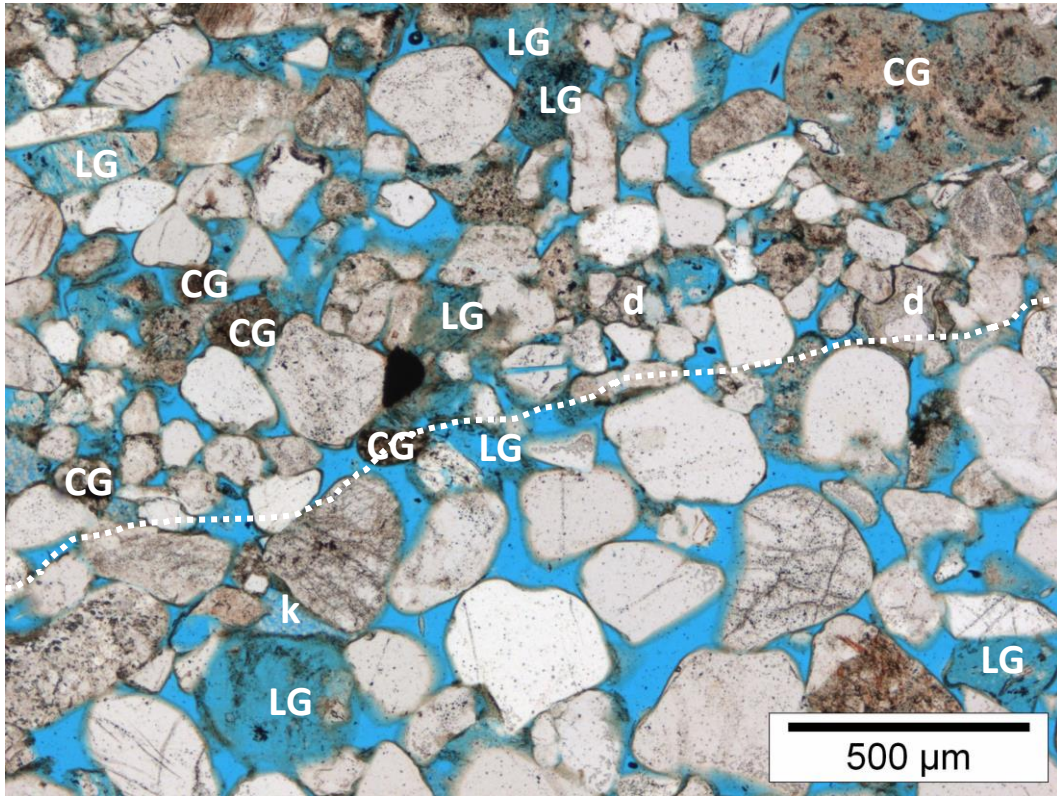
**A. Magnification 45x**                                    **Plane Polarised Light**
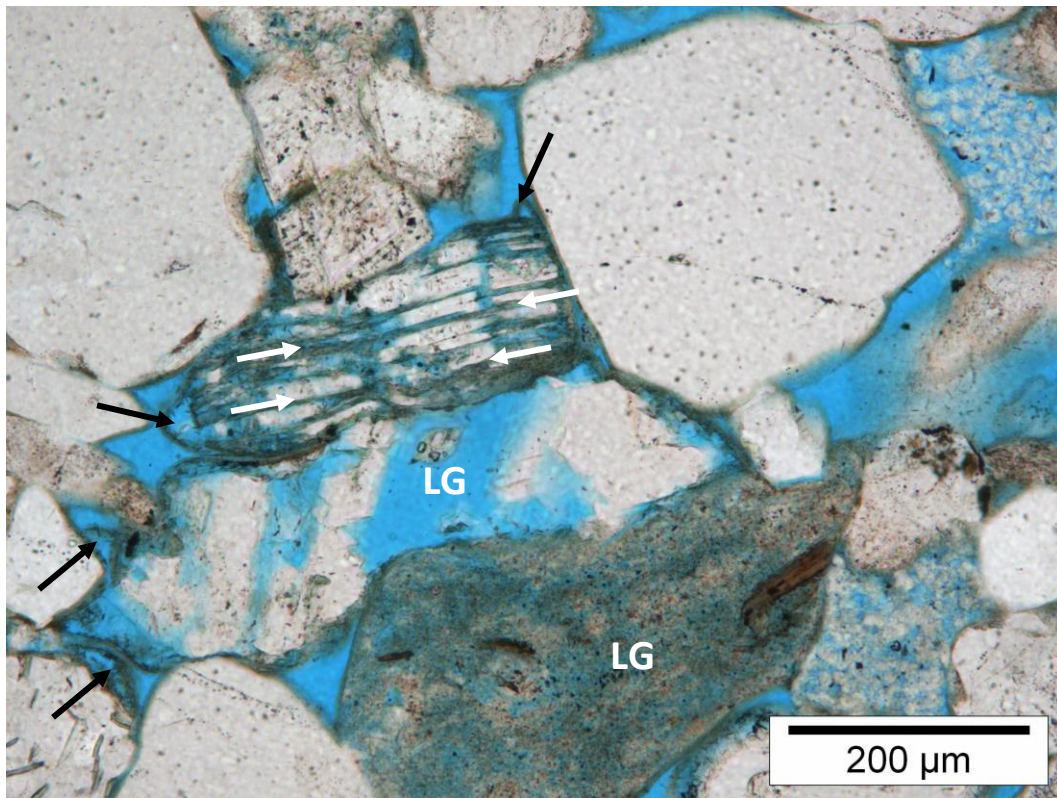


**B. Magnification 113x**                                    **Plane Polarised Light**

**Plate A:** The sandstone is grain size laminated (dashed line marks the orientation). The finer-grained laminae (top half) comprise most of the authigenic dolomite (d) and finer grained clay-rich grains (CG). Leached grains (LG) occur both in the coarser and finer laminae. Note the replacive authigenic kaolinite (k). **Plate B:** Illite (white arrows) occurs parallel to the cleavage of a leached feldspar grain. Some authigenic cement (quartz or feldspar) occurs in between. Note the deformed nature of the leached grains with secondary pores below (LG). Authigenic, chlorite-rich clay coatings are locally detached from the grains (black arrows).

**Sample Type:** Plug Trimend                    **Rock Classification (Pettijohn, 1975):** Sublitharenite

## Texture

| | | | | | |
|---|---|---|---|---|---|
| Texture | irregular lamination | Grain size (modal) | v.f sand (U) / m sand (L) | Roundness | SA-SR |
| Sample heterogeneity | moderate to high | Grain size (min) | 4-31 µm | Sorting | P-B |
| | | Grain size (max) | 710-1000 µm | | |

**Remarks:** Coarse grained quartz grains occur dispersed through the sample. Lamination is relatively pronounced.

## Compaction

| | | | | | |
|---|---|---|---|---|---|
| Grain contacts - Rigid | P | COPL (%) | 32 | IGV (%) | 20 |
| Grain contacts - Ductile | L-CC | CEPL (%) | 9 | | |

## Detrital components (%)

| | | | | | | | |
|---|---|---|---|---|---|---|---|
| Monoquartz | 45.7 | Feldspar | 2.3 | Rigid RF | 7.7 | Microporous RF | 1.7 |
| Polyquartz | 9.0 | Leached feldspar | 3.3 | Ductile RF | 2.0 | Accessories | 1.0 |

**Remarks:** The sample is enriched in heavy minerals (mostly zircon) in the finer grained laminae.

## Authigenic components (%)

| | | | | | |
|---|---|---|---|---|---|
| Quartz | 1.0 | Grain rimming illite | 2.3 | Pore-filling kaolinite | 0.3 |
| Dolomite/Siderite | 4.7 | Grain rimming clay (mix) | 0.7 | Replacive kaolinite | 2.3 |
| Barite | Tr | Grain rimming chlorite | - | Replacive chlorite | Tr |
| | | Pore-filling clay (indet/mix) | 2.3 | Replacive clay (indet/mix) | 2.7 |

**Remarks:** The clay rims arerelatively thin. Clay (most likely authigenic) is more common in the finer grained laminae.
Dolomite is dominantly pore-filling.

*Spatial relationships (Paragenetic sequence):*
- Some quartz cement on grain fracture surface
- K-feldspar cement engulfs kaolinite
- Fe-dolomite occurs in leached grains

## Point counted porosity (%)

| | | | |
|---|---|---|---|
| Intergranular | 7.0 | Intragranular | 0.7 |
| Oversized | 0.7 | Mouldic | 0.3 |
| Macroporosity (visible porosity) | | 8.7 | |
| Microporosity (He-porosity minus macroporosity) | | 9.4 | |

**Remarks:** Intergranular pores occur mostly in the clay-poor laminae.

## Reservoir properties

| | |
|---|---|
| He-Porosity (%) | 18.1 |
| Permeability (mD) | 53 |
| Grain density (g/cm³) | 2.66 |
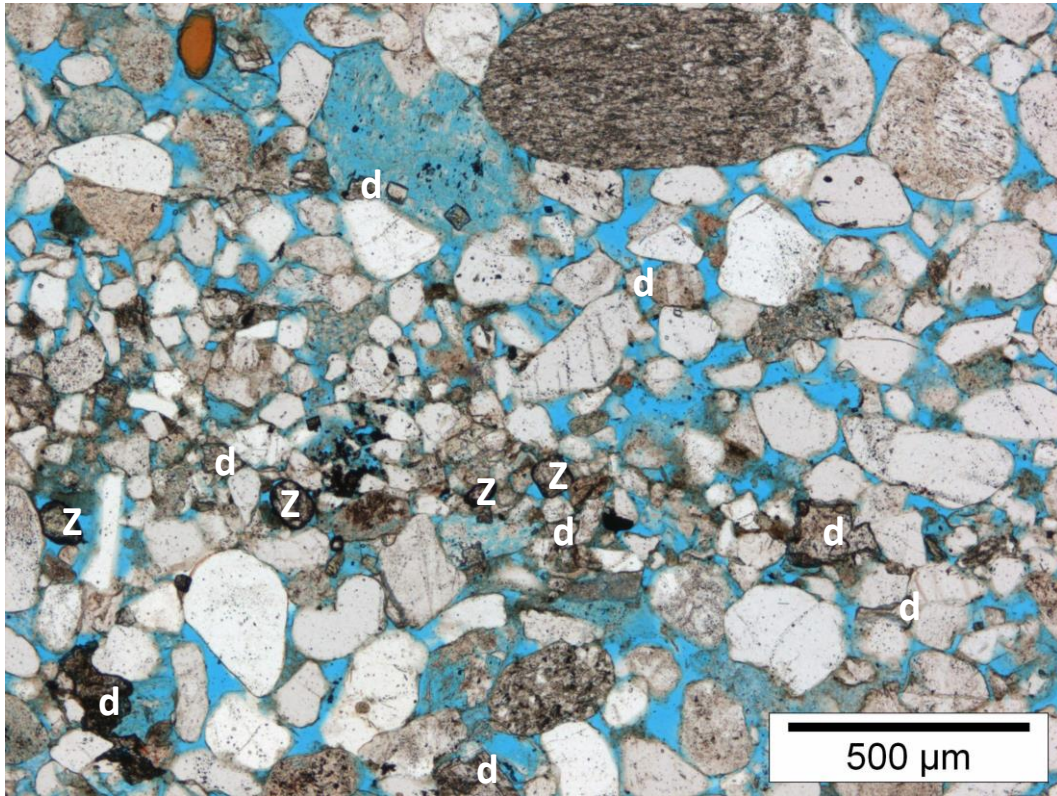


*Thin section scan (width ~2.5 cm)*

**A. Magnification 45x**                                                              **Plane Polarised Light**
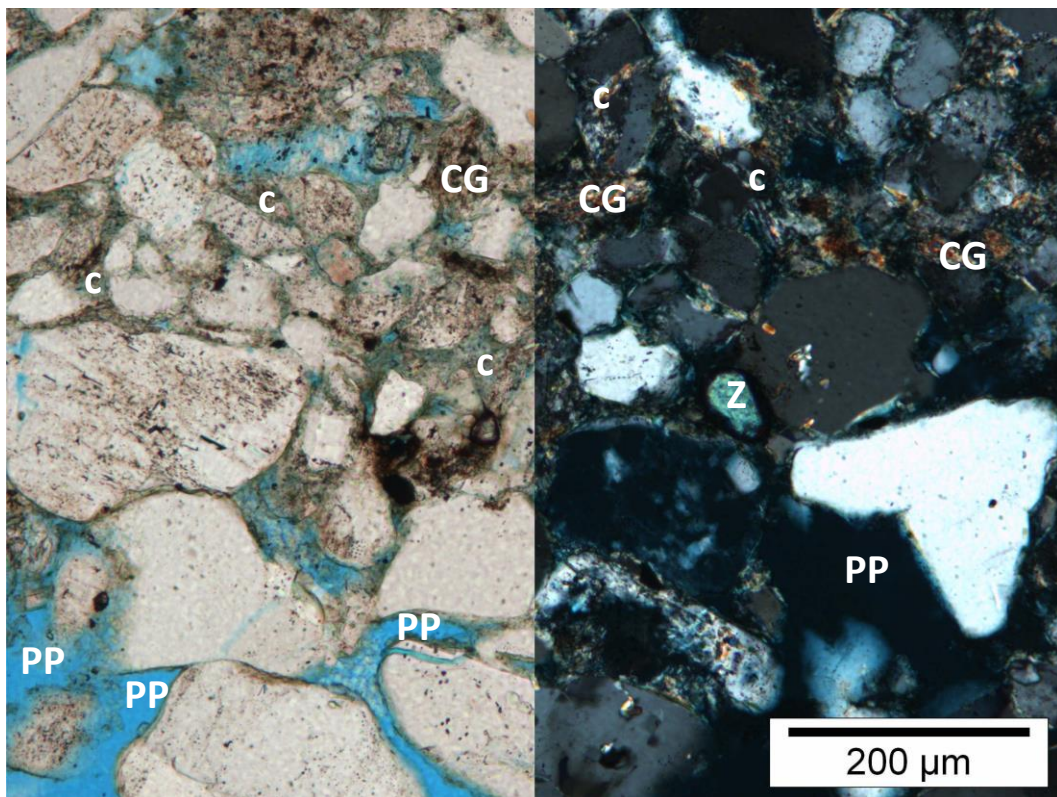


**B. Magnification 113x**                                          **Plane Polarised Light/Crossed Nicols**

**Plate A:** This laminated sandstone sample (see TS scan; page before) comprises laminae enriched in detrital heavy minerals (mostly zircon; Z) and authigenic pore-filling dolomite (d). The laminae are irregular and sorting in the entire sample is poor.
**Plate B:** Detailed photo of the boundary between a coarse-grained (base of photo) and fine-grained (top of photo) lamina. Intergranular macropores (PP) occur only in the coarse lamina. The fine lamina is rich in clay (c; mostly illite), which occurs both as detrital clay-rich grains (CG) and as authigenic clay.  Note the detrital zircon (Z).

**Sample Type:** Plug Trimend                **Rock Classification (Pettijohn, 1975):** Sublitharenite

## Texture

| Texture | laminated | Grain size (modal) | fine sand (U) | Roundness | SA-SR |
|---|---|---|---|---|---|
| Sample heterogeneity | low to moderate | Grain size (min) | 62.5-88 µm | Sorting | M |
| | | Grain size (max) | 1-1.41 mm | | |

**Remarks:** Lamination is mostly related to grain size variations. Individual laminae have a similar thickness. Together with the presence of mica and glauconite this could argue for a fluviatile nature of the sandstone, rather than aeolian.

## Compaction

| Grain contacts - Rigid | P | COPL (%) | 27 | IGV (%) | 25 |
|---|---|---|---|---|---|
| Grain contacts - Ductile | L | CEPL (%) | 15 | | |

**Remarks:** The abundant clay in the pores (including the clay rim) results in a relatively high CEPL. Compaction is low.

## Detrital components (%)

| Monoquartz | 38.7 | Feldspar | 3.3 | Rigid RF | 4.0 | Microporous RF | 0.3 |
|---|---|---|---|---|---|---|---|
| Polyquartz | 20.3 | Leached feldspar | 0.7 | Ductile RF | 0.3 | Accessories | Tr |

**Remarks:** Note the abundant to very abundant polycrystalline quartz grains. Rock fragments are sparse. Trace minerals include muscovite, glauconite and opaque mineral(s).

## Authigenic components (%)

| Quartz | 0.7 | Grain rimming illite | 1.3 | Pore-filling kaolinite | - |
|---|---|---|---|---|---|
| Dolomite/Siderite | 0.7 | Grain rimming clay (mix) | 1.0 | Replacive kaolinite | 2.7 |
| Barite | - | Grain rimming chlorite | 13.0 | Replacive chlorite | 1.7 |
| | | Pore-filling clay (indet/mix) | - | Replacive clay (indet/mix) | 1.3 |

**Remarks:** Chlorite forms thick rims, while quartz and dolomite cement are rare. Chlorite is locally completely pore-filling. Thin tangential illite coatings are identified as well.

*Spatial relationships (Paragenetic sequence):*

- Thick chlorite coating overgrew tangential illite
- Tangential illite and thick chlorite coats forms halos of where grains were leached out (coating predates leaching)

## Point counted porosity (%)

| Intergranular | 4.3 | Intragranular | 0.3 |
|---|---|---|---|
| Oversized | 0.3 | Mouldic | - |
| Macroporosity (visible porosity) | | | 5.0 |
| Microporosity (He-porosity minus macroporosity) | | | 15.8 |

**Remarks:** Some intergranular porosity between grain and clay rim.

## Reservoir properties

| He-Porosity (%) | 20.8 |
|---|---|
| Permeability (mD) | 41 |
| Grain density (g/cm³) | 2.66 |
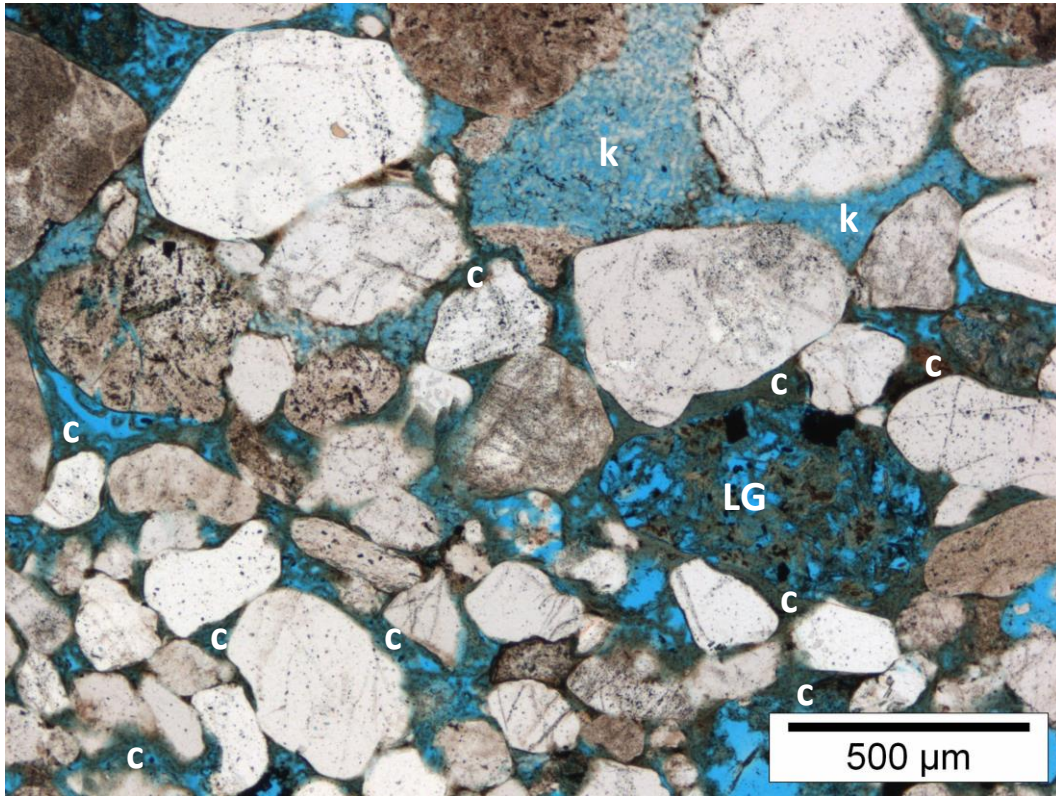


*Thin section scan (width ~2.5 cm)*

**A. Magnification 45x**                                    **Plane Polarised Light**



**B. Magnification 113x**                              **Plane Polarised Light/Crossed Nicols**

**Plate A:** The detrital grains in this laminated sandstone sample are covered with a very thick authigenic green clay rim, which is locally completely pore-filling (c). The clay rim comprises mostly chlorite. The clay is rarer in areas rich in kaolinite (k). Note the leached grain (LG) where the same greenish clay has formed. Poor connectivity is very poor. **Plate B:** XRD confirms the chlorite (chl) identification based on the birefringence colour (1st order, grey to pale green). Some tangential illite coating has formed prior to the chlorite (arrows; high birefringence). Note how the chlorite coating outlines leached grains (LG; including feldspar FSP).

**Sample Type:** Plug Trimend        **Rock Classification (Pettijohn, 1975):** Sublitharenite

## Texture

| | | | | | |
|---|---|---|---|---|---|
| Texture | laminated | Grain size (modal) | v.f sand (U) / f sand (U) | Roundness | SA-SR |
| Sample heterogeneity | moderate | Grain size (min) | 31-62.5 µm | Sorting | M |
| | | Grain size (max) | 500-710 µm | | |

**Remarks:** Lamina are regular, with the finer grained laminae being thinner compared to the coarser grained laminae.

## Compaction

| | | | | | |
|---|---|---|---|---|---|
| Grain contacts - Rigid | P-L | COPL (%) | 30 | IGV (%) | 21 |
| Grain contacts - Ductile | CC | CEPL (%) | 10 | | |

**Remarks:** Compaction is moderate, based on the grain contacts and the IGV. However, there is some evidence of localised chemical compaction (i.e. grain dissolution; see TS plate B).

## Detrital components (%)

| | | | | | | | |
|---|---|---|---|---|---|---|---|
| Monoquartz | 40.7 | Feldspar | 1.3 | Rigid RF | 7.7 | Microporous RF | 1.7 |
| Polyquartz | 18.0 | Leached feldspar | 1.3 | Ductile RF | 1.3 | Accessories | Tr |

**Remarks:** Note the high polycrystalline quartz content. Feldspar is very sparsely to sparsely recognised. Accessory minerals comprise muscovite and opaque mineral(s).

## Authigenic components (%)

| | | | | | |
|---|---|---|---|---|---|
| Quartz | 2.3 | Grain rimming illite | 0.3 | Pore-filling kaolinite | - |
| Dolomite/Siderite | 2.0 | Grain rimming clay (mix) | 0.7 | Replacive kaolinite | 2.0 |
| Barite | - | Grain rimming chlorite | 4.0 | Replacive chlorite | 1.7 |
| | | Pore-filling clay (indet/mix) | 1.0 | Replacive clay (indet/mix) | 0.7 |

**Remarks:** Quartz cement is pore-filling, as is most of the dolomite. Clay coatings are irregular (blotchy) and mostly chloritic.

*Spatial relationships (Paragenetic sequence):*

- Quartz cement engulfs kaolinite (postdates kaolinite)
- Some serrated grain contacts (chemical compaction postdates mechanical compaction)

## Point counted porosity (%)

| | | | |
|---|---|---|---|
| Intergranular | 7.0 | Intragranular | 1.7 |
| Oversized | 0.3 | Mouldic | - |
| Macroporosity (visible porosity) | | | 9.0 |
| Microporosity (He-porosity minus macroporosity) | | | 8.3 |

**Remarks:** The finer grained laminae have only rarely macropores.

## Reservoir properties

| | |
|---|---|
| He-Porosity (%) | 17.3 |
| Permeability (mD) | 11 |
| Grain density (g/cm$^3$) | 2.66 |

**Remarks:** Permeability is inhibited by the finer grained laminae and the blotchy clay coatings.
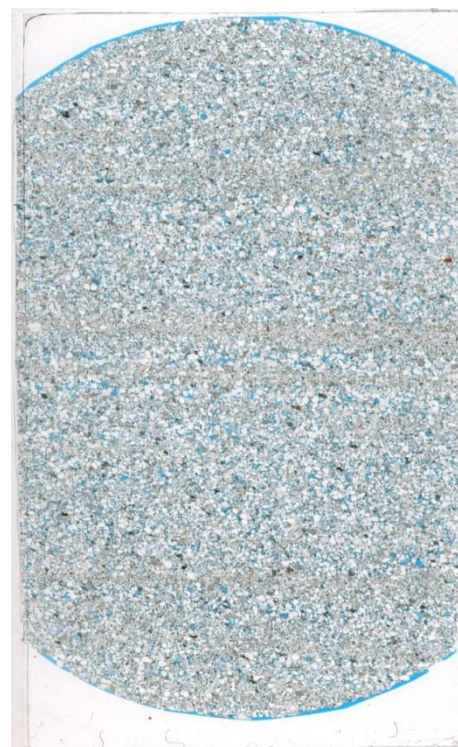


*Thin section scan (width ~2.5 cm)*
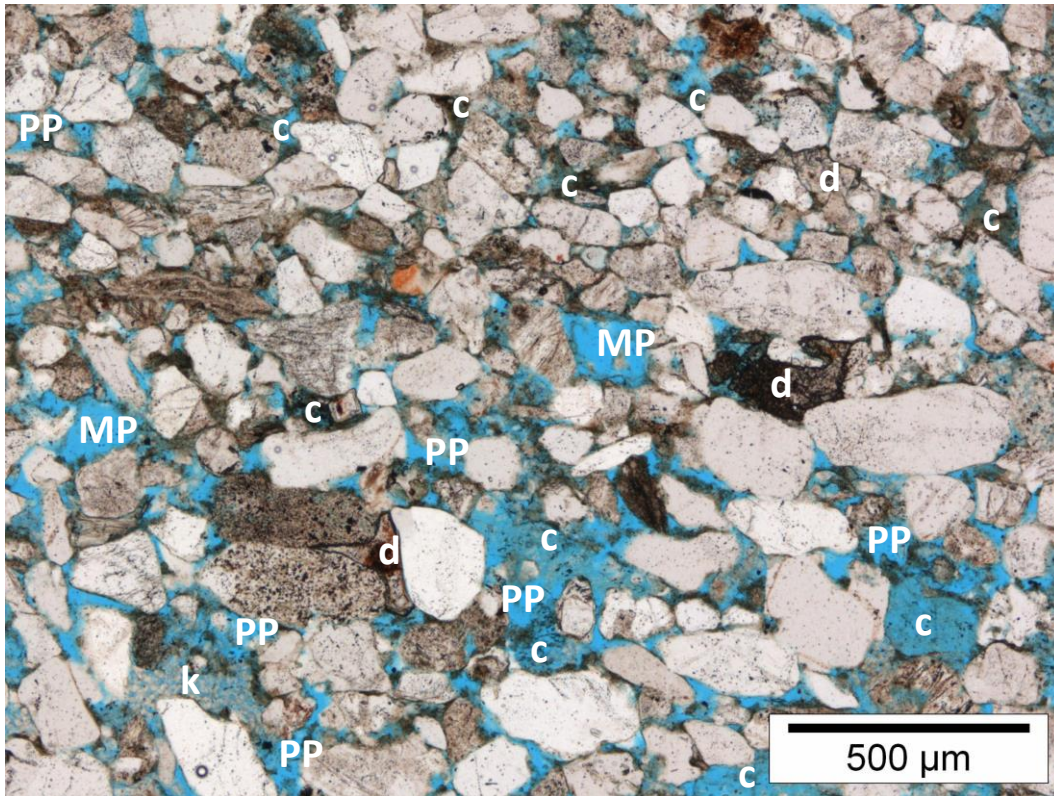
**A. Magnification 45x**       **Plane Polarised Light**
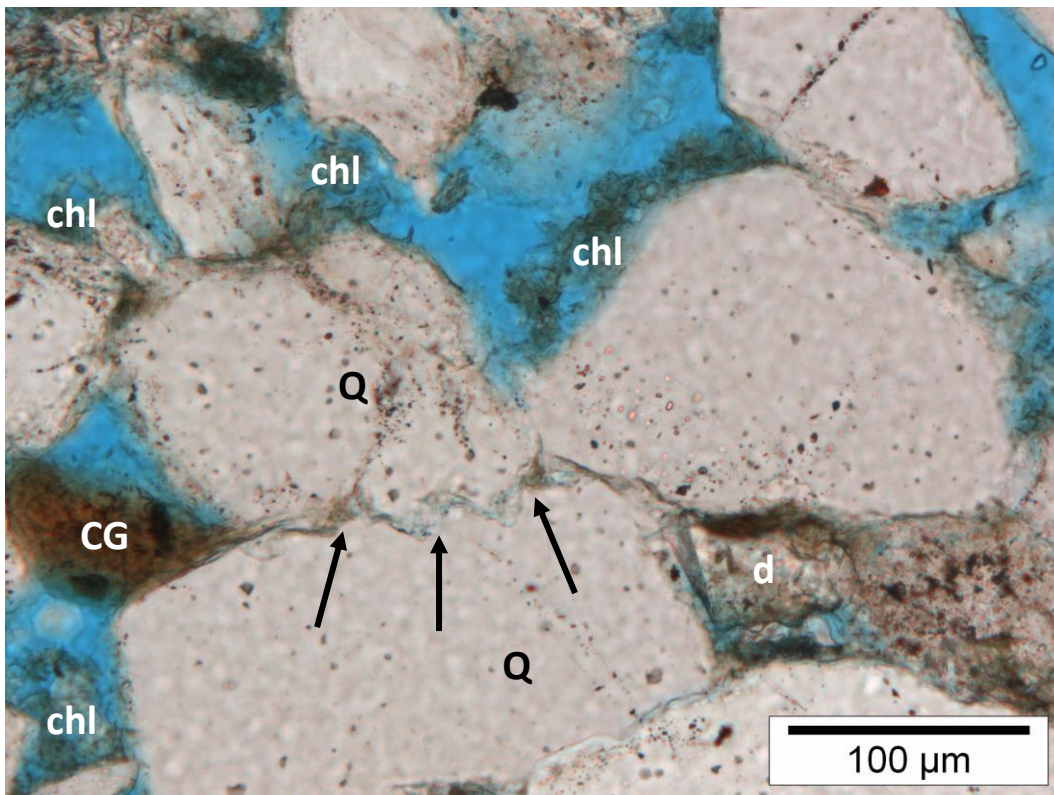


**B. Magnification 225x**       **Plane Polarised Light**

**Plate A:** The laminae in this fine grained sandstone are clearly visible on thin section scale (here horizontal), where the finer grained laminae have less and smaller macropores (mostly intergranular and mouldic pores; PP & MP) compared to the coarser grained laminae. The sample is relatively rich in authigenic clay (c (unidentified/mixed) & k (kaolinite)). Note the dolomite cement (d). **Plate B:** Detailed photo showing a stylolitic contact (arrows) between two quartz (Q) grains. A clay-rich grain is strongly deformed (CG). The pore-filling clay is mostly chlorite (chl), visible by the green colour and the (in 2D) fibrous nature. Also here, dolomite occurs (d).

**Sample Type:** Plug Trimend

**Rock Classification (Pettijohn, 1975):** Sublitharenite

## Texture

| Texture | laminated | Grain size (modal) | v.f sand (U) / m sand (L) | Roundness | A-SR |
|---|---|---|---|---|---|
| Sample heterogeneity | moderate to high | Grain size (min) | 31-62.5 µm | Sorting | P |
| | | Grain size (max) | 1-1.41 mm | | |

## Compaction

| Grain contacts - Rigid | P-L | COPL (%) | 30 | IGV (%) | 21 |
|---|---|---|---|---|---|
| Grain contacts - Ductile | L-PS | CEPL (%) | 11 | | |

**Remarks:** Clay grains, including a clay-intraclast, are strongly deformed. Leached grains are mostly undeformed. Hence leaching appears to postdate (most) compaction. The pebble sized intraclast indicates transport by water, which is consistent with the type of lamination and the mica content.

## Detrital components (%)

| Monoquartz | 46.3 | Feldspar | 2.7 | Rigid RF | 5.7 | Microporous RF | 1.0 |
|---|---|---|---|---|---|---|---|
| Polyquartz | 14.3 | Leached feldspar | Tr | Ductile RF | 1.3 | Accessories | 0.3 |

**Remarks:** Feldspar is relatively rare in this sample. Part of the ductile RF is a clay-rich intraclast (see TS scan). Accessories comprise muscovite, heavy minerals and opaque minerals.

## Authigenic components (%)

| Quartz | 2.0 | Grain rimming illite | 2.3 | Pore-filling kaolinite | - |
|---|---|---|---|---|---|
| Dolomite/Siderite | 2.0 | Grain rimming clay (mix) | 2.7 | Replacive kaolinite | 2.3 |
| Barite | 0.3 | Grain rimming chlorite | 1.7 | Replacive chlorite | 0.3 |
| | | Pore-filling clay (indet/mix) | 3.7 | Replacive clay (indet/mix) | 2.0 |

**Remarks:** Quartz and carbonate cement are both pore-filling and replacive. Sample is clay rich, occurring as grain rimming clay, pore-filling clay and detrital clay.

*Spatial relationships (Paragenetic sequence):*

- Quartz cement has overgrown clay coating
- Dolomite formed in leached grains
- Dolomite has overgrown kaolinite

## Point counted porosity (%)

| Intergranular | 5.0 | Intragranular | 0.7 |
|---|---|---|---|
| Oversized | - | Mouldic | Tr |
| Macroporosity (visible porosity) | | | 5.7 |
| Microporosity (He-porosity minus macroporosity) | | | 8.7 |

## Reservoir properties

| He-Porosity (%) | 14.4 |
|---|---|
| Permeability (mD) | 2.2 |
| Grain density (g/cm³) | 2.67 |

**Remarks:** The sample has a relatively poor reservoir quality.



*Thin section scan (width ~2.5 cm)*
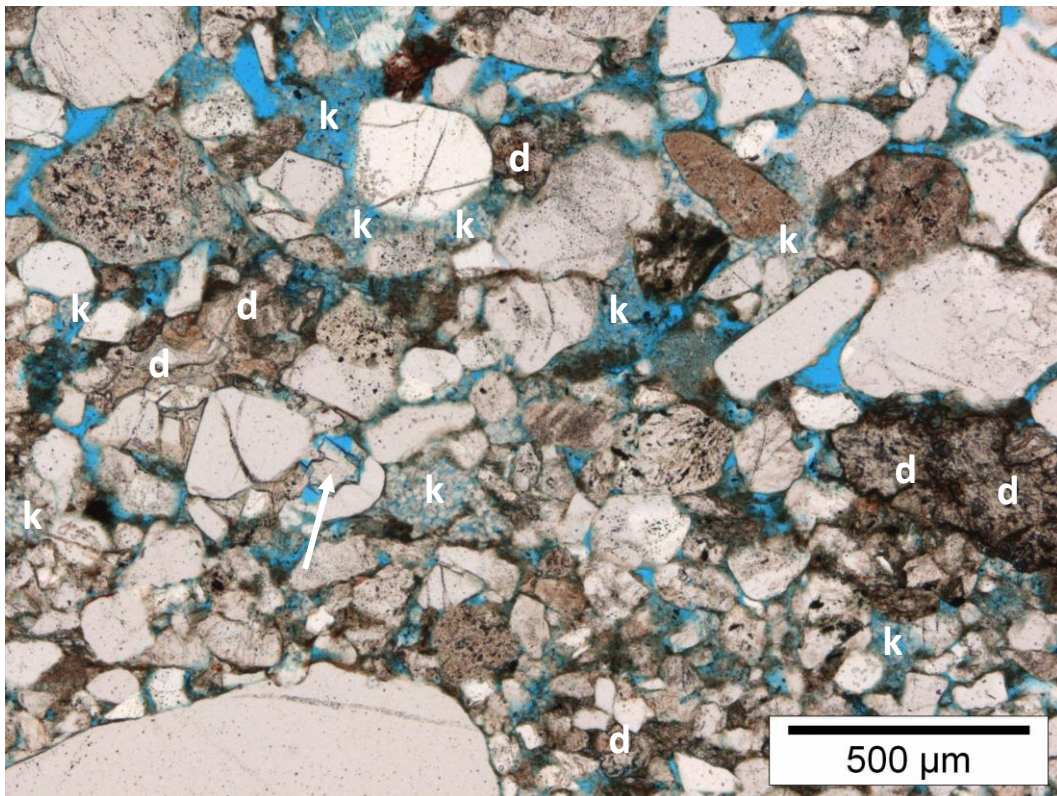
**A. Magnification 45x**　　　　　　　　　　**Plane Polarised Light**
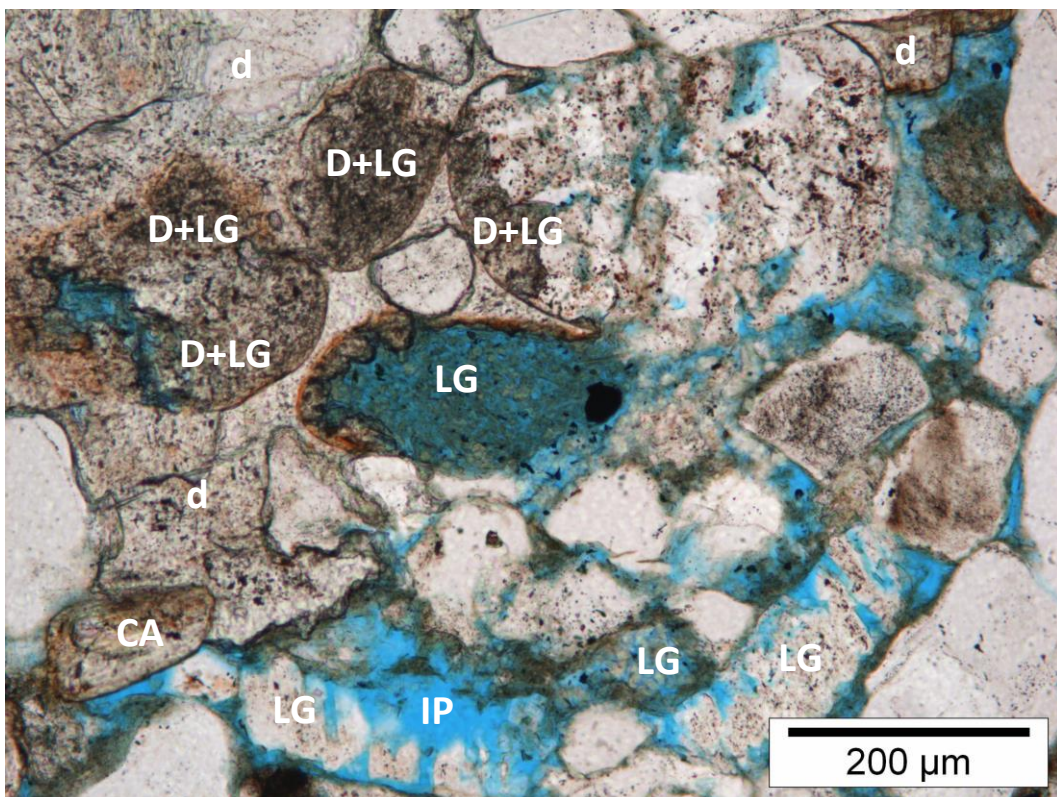


**B. Magnification 113x**　　　　　　　　　　**Plane Polarised Light**

**Plate A:** In this fine- to medium-grained sandstone, kaolinite (k), which has formed at the expense of most likely feldspar, occurs relatively commonly in the intergranular pores. Note the broken quartz grain with a large dolomite crystal that has formed in between the two halves (arrow) and the pore-filling dolomite (d). **Plate B:** Locally, dolomite cement (d) has grown in leached grains (d+LG), filling up pore spaces and fixing the framework. Note the carbonate grain (CA). Distinct clay rims are absent. Greenish authigenic clay outline leached grains (LG). Here, the largest (intragranular) macropores (IP) occur.

**Sample Type:** Plug Trimend

**Rock Classification (Pettijohn, 1975):** Sublitharenite

### Texture

| | | | | | |
|---|---|---|---|---|---|
| Texture | structureless | Grain size (modal) | medium sand (L) | Roundness | SR |
| Sample heterogeneity | low to moderate | Grain size (min) | 31-62.5 µm | Sorting | MG |
| | | Grain size (max) | 710-1000 µm | | |

**Remarks:** Very fragile and relatively coarse grained sandstone.

### Compaction

| | | | | | |
|---|---|---|---|---|---|
| Grain contacts - Rigid | P | COPL (%) | 31 | IGV (%) | 21 |
| Grain contacts - Ductile | L-CC | CEPL (%) | 8 | | |

### Detrital components (%)

| | | | | | | | |
|---|---|---|---|---|---|---|---|
| Monoquartz | 40.0 | Feldspar | 2.3 | Rigid RF | 7.3 | Microporous RF | 3.3 |
| Polyquartz | 18.3 | Leached feldspar | 2.3 | Ductile RF | 0.3 | Accessories | Tr |

**Remarks:** Note the relatively high content of polycrystalline quartz. Chert comprises 1.3% of the rock (included in the rigid RF).

### Authigenic components (%)

| | | | | | |
|---|---|---|---|---|---|
| Quartz | 0.3 | Grain rimming illite | 0.3 | Pore-filling kaolinite | 1.0 |
| Dolomite/Siderite | 3.0 | Grain rimming clay (mix) | 0.7 | Replacive kaolinite | 2.7 |
| Barite | 0.3 | Grain rimming chlorite | - | Replacive chlorite | 0.3 |
| | | Pore-filling clay (indet/mix) | 6.0 | Replacive clay (indet/mix) | 1.3 |

**Remarks:** The sparse dolomite is mostly intergranular pore-filling. Additionally replacive dolomite crystals occur. Intergranular pore-filling fine-crystalline clay (likely mostly chlorite) is common.

*Spatial relationships (Paragenetic sequence):*
- Some authigenic clay coating appears to cover kaolinite
- Leached grains show distinct fracturing (fracturing predates leaching)
- Dolomite occurs in leached grains

### Point counted porosity (%)

| | | | |
|---|---|---|---|
| Intergranular | 9.3 | Intragranular | 0.3 |
| Oversized | - | Mouldic | 0.3 |
| Macroporosity (visible porosity) | | 10.0 | |
| Microporosity (He-porosity minus macroporosity) | | 14.1 | |

**Remarks:** Both macroporosity and microporosity are relatively high.

### Reservoir properties

| | |
|---|---|
| He-Porosity (%) | 24.1 |
| Permeability (mD) | n/a |
| Grain density (g/cm$^3$) | 2.66 |
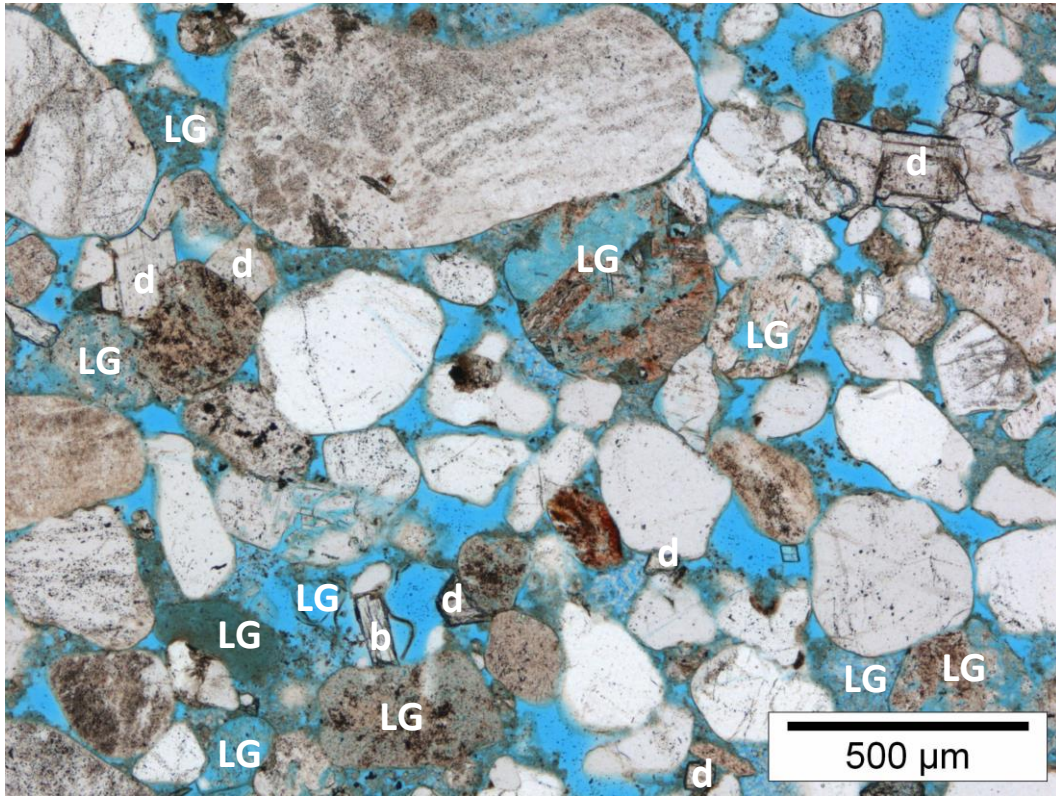


*Thin section scan (width ~2.5 cm)*

**A. Magnification 45x**                    Plane Polarised Light
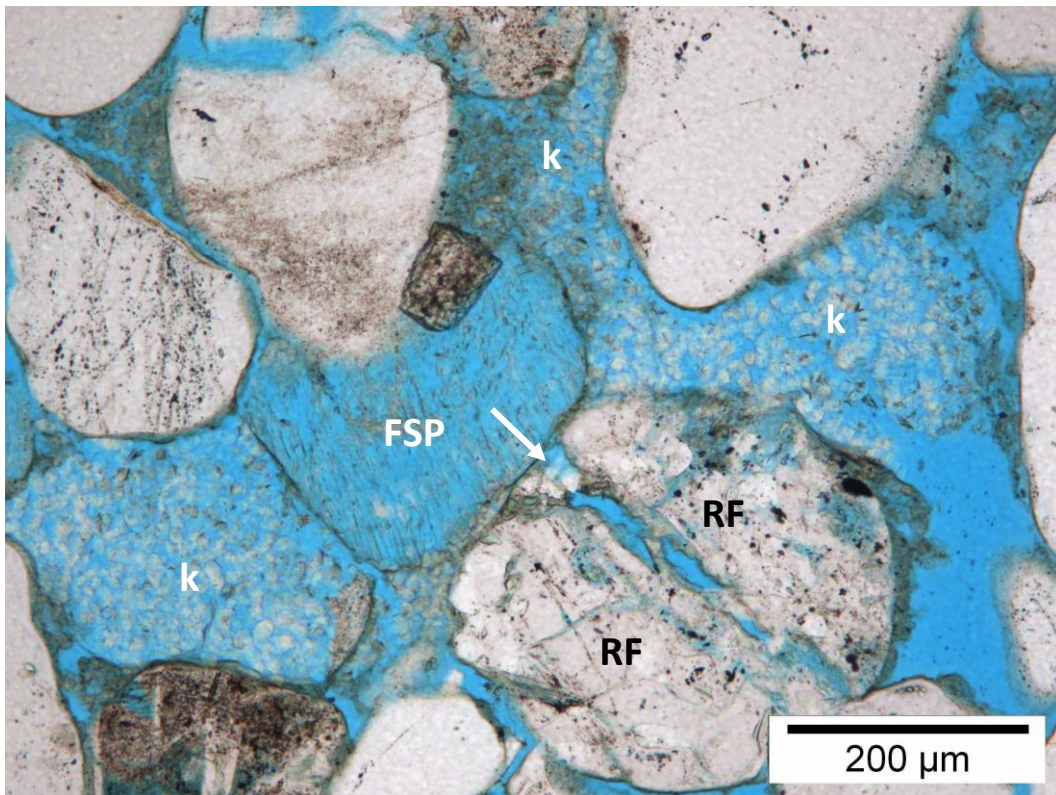


**B. Magnification 113x**                    Plane Polarised Light

**Plate A:** This friable sandstone is characterised by significant microporous leached grains (LG), which are partly filled with authigenic clay. Note the dolomite cement (d) which occurs throughout the sample, and the barite cement (b) which partially fills a mouldic pore. **Plate B:** The (sedimentary?) rock fragment (RF) is most likely fractured (arrow) prior to feldspar leaching (FSP), as otherwise the leached and microporous (fragile) feldspar would have been deformed more strongly instead of the rock fragment. Note the replacive kaolinite (k), which formed at the expense of two or possibly three grains.

**Sample Type:** Plug Trimend

**Rock Classification (Pettijohn, 1975):** Sublitharenite

## Texture

| Texture | laminated | Grain size (modal) | v.fine sand (U) | Roundness | SA-SR |
|---|---|---|---|---|---|
| Sample heterogeneity | moderate | Grain size (min) | 31-62.5 µm | Sorting | M |
|  |  | Grain size (max) | 710-1000 µm |  |  |

**Remarks:** Distinct lamination due to enrichment of clay in the finer grained laminae. Lamination is slightly wavy.

## Compaction

| Grain contacts - Rigid | P-L | COPL (%) | 29 | IGV (%) | 22 |
|---|---|---|---|---|---|
| Grain contacts - Ductile | CC | CEPL (%) | 13 |  |  |

**Remarks:** Traces of stylolitic contacts occur, which are macroscopically not visible in the TS scan. Mica is strongly deformed, indicating relatively strong compaction. IGV is however above average (of 20.5) for this sample set. Thus compaction is localized.

## Detrital components (%)

| Monoquartz | 47.7 | Feldspar | 3.0 | Rigid RF | 5.3 | Microporous RF | 0.3 |
|---|---|---|---|---|---|---|---|
| Polyquartz | 12.0 | Leached feldspar | 1.7 | Ductile RF | 1.3 | Accessories | Tr |

**Remarks:** Most rock fragments are indeterminable but quartz-rich. The traces of accessory minerals comprise muscovite, heavy minerals and opaque minerals.

## Authigenic components (%)

| Quartz | 2.0 | Grain rimming illite | 3.0 | Pore-filling kaolinite | - |
|---|---|---|---|---|---|
| Dolomite/Siderite | 5.0 | Grain rimming clay (mix) | 2.7 | Replacive kaolinite | 1.7 |
| Barite | - | Grain rimming chlorite | - | Replacive chlorite | 1.0 |
|  |  | Pore-filling clay (indet/mix) | 5.3 | Replacive clay (indet/mix) | 2.7 |

**Remarks:** Some of the clay is possibly detrital in origin. Nearly all of the sparse to common carbonate cement is intergranular pore-filling. Kaolinite is very sparse.

*Spatial relationships (Paragenetic sequence):*

- Quartz and replacive chlorite occurs in leached grains
- Kaolinite is engulfed by quartz (predates quartz cement)
- Apatite and quartz occur in leached grains (postdate leaching)

## Point counted porosity (%)

| Intergranular | 4.7 | Intragranular | - |
|---|---|---|---|
| Oversized | 0.3 | Mouldic | - |
| Macroporosity (visible porosity) |  | 5.0 | |
| Microporosity (He-porosity minus macroporosity) |  | 12.9 | |

**Remarks:** Intergranular pores are relatively small, especially in the finer-grained laminae.

## Reservoir properties

| He-Porosity (%) | 17.9 |
|---|---|
| Permeability (mD) | 14 |
| Grain density (g/cm$^3$) | 2.67 |
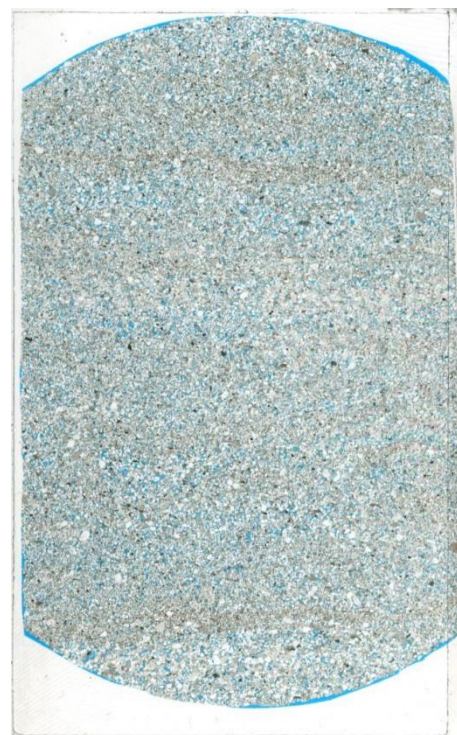


*Thin section scan (width ~2.5 cm)*
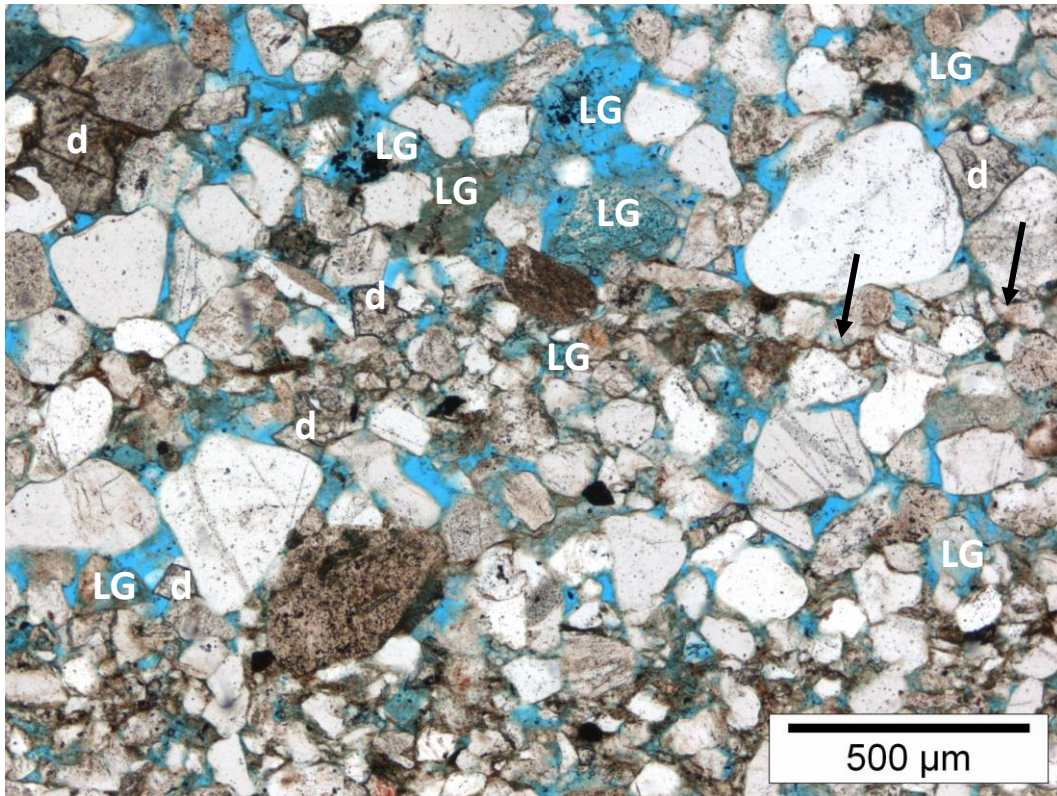
A. Magnification 45x                Plane Polarised Light
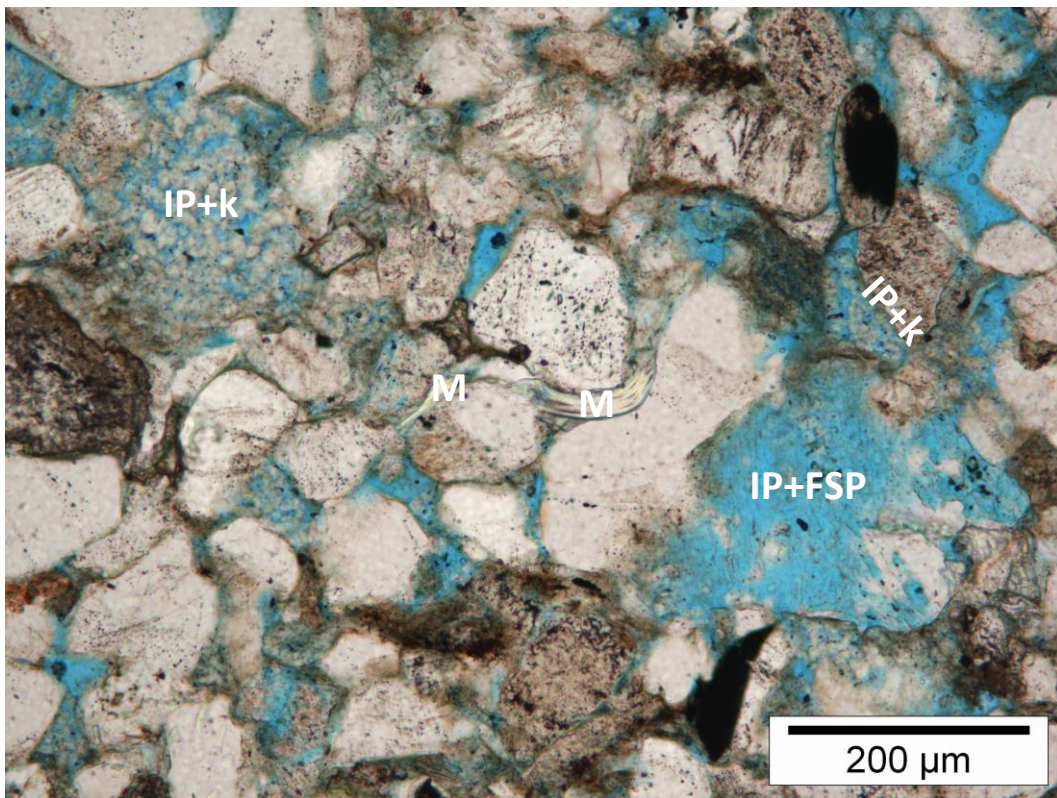


B. Magnification 113x                Plane Polarised Light

**Plate A:** This laminated fine-grained sandstone shows signs of relative strong compaction, including a stylolitic contact (arrows) and the long to concavo-convex grain contacts. Microporous leached grains (LG) did however not further collapse. Dolomite cement (d) locally formed in the intergranular pore spaces. **Plate B:** The muscovite (M) in the centre of the image is strongly deformed. The pores in this field of view are mostly secondary (dissolution) pores (IP), which formed at the expense of detrital feldspar (+FSP). Feldspar dissolution was accompanied by the formation of kaolinite (+k).

# Appendix 5: SEM and BSEM images

For abbreviations used in the images, see front page Appendix 4.
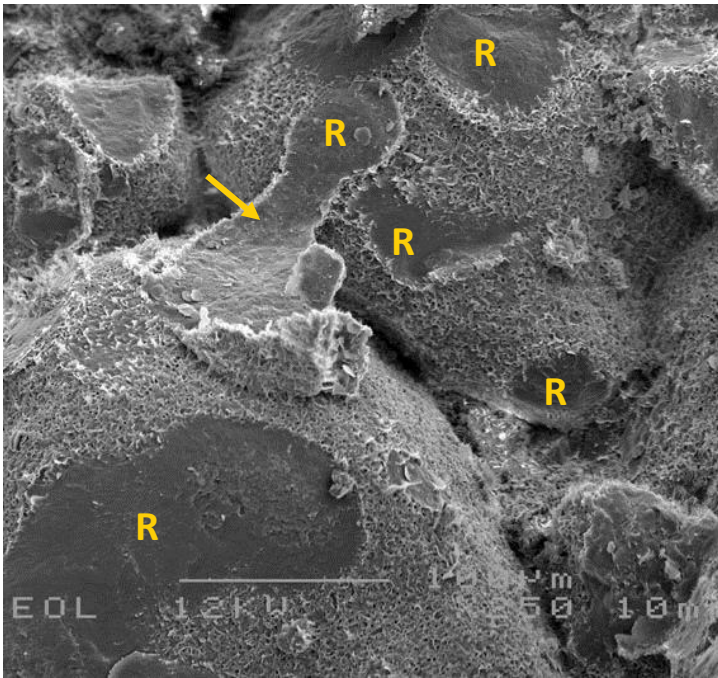
**A. Magnification 250x**

68µm
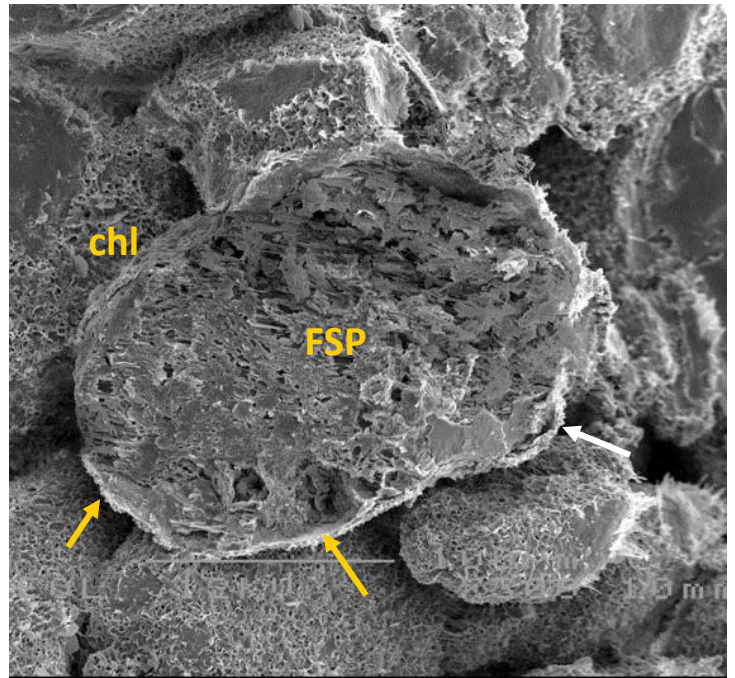
**B. Magnification 300x**

57µm
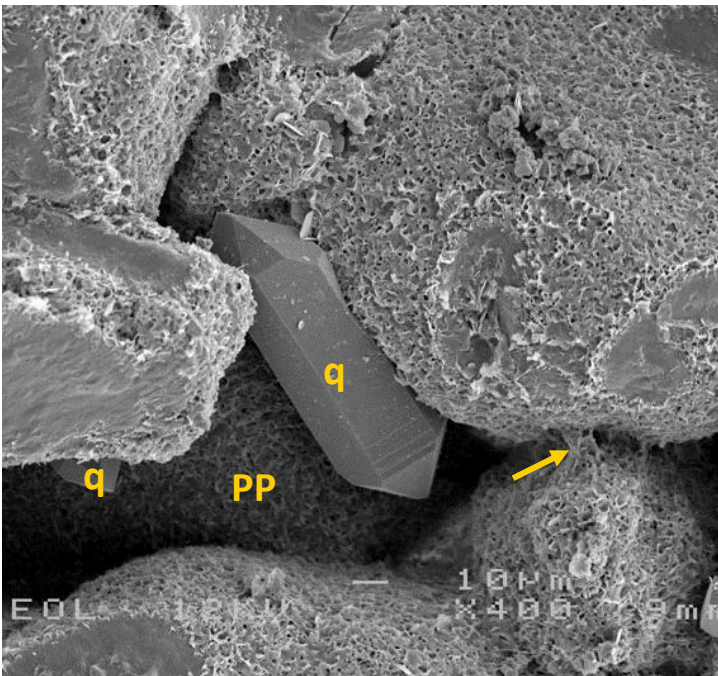
**C. Magnification 400x**

43µm
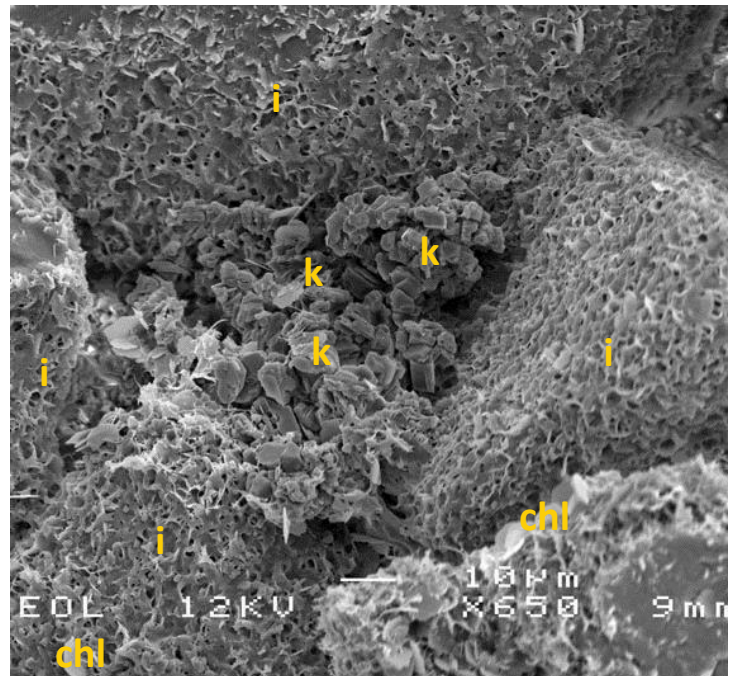
**D. Magnification 650x**

26µm

**Plate A:** Overview image showing the fine to medium grained detrital quartz grains covered with a thin illitic clay coating (fibrous material). Original grain contacts are visible by the clean surfaces, where grains were removed during sample preparation (R). Note the clay coating of a plugged out grain that bridges a pore (arrow). **Plate B:** Feldspar grains (FSP), which are abundant in the sample, are often leached. Micropores (dark in SEM) occur in between the remaining fibrous feldspar material. Also the feldspar grains are covered with a thin clay coating (arrows). Note the coarser grained authigenic platy chlorite (chl), which occurs together with the illitic clay coating. **Plate C:** Locally, well developed euhedral quartz cement (q) occurs.  The pore (PP) in which this authigenic quartz has formed is large. Note how the fibrous illite is pore bridging (arrow) and reducing the permeability. **Plate D:** Apart from the clay coating illite (i) and the less common chlorite (chl), authigenic kaolinite (k) also occurs. Kaolinite occurs mostly in clusters as it replaced a mineral, possibly an early leached feldspar. In between all authigenic clays, micropores occur.
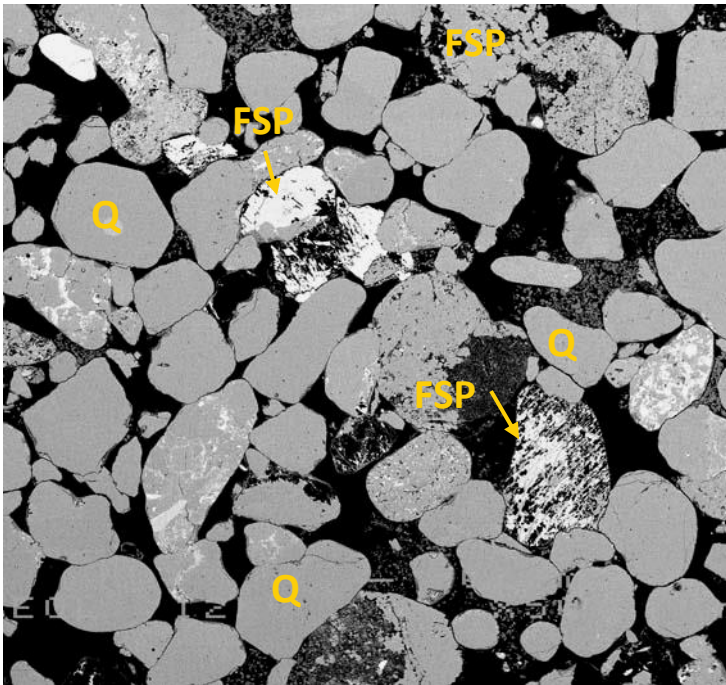
**A. Magnification 50x**
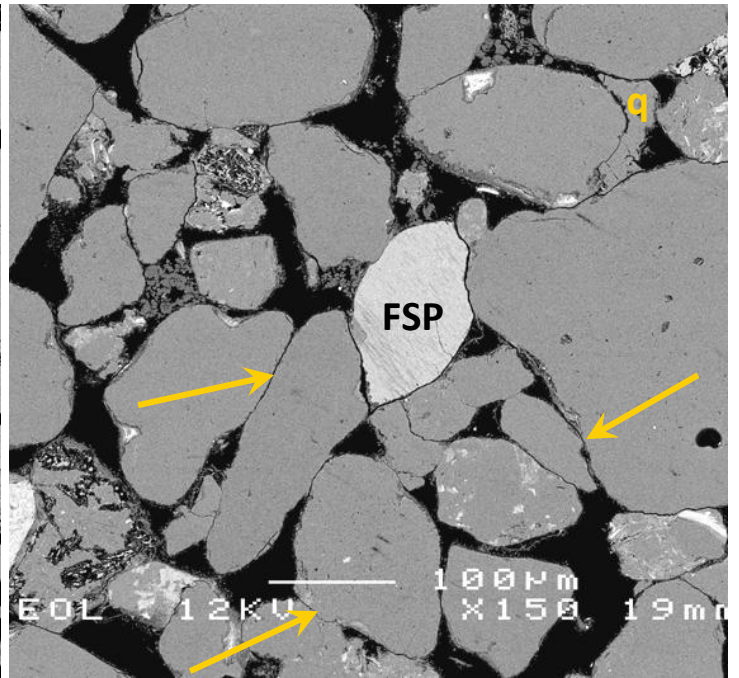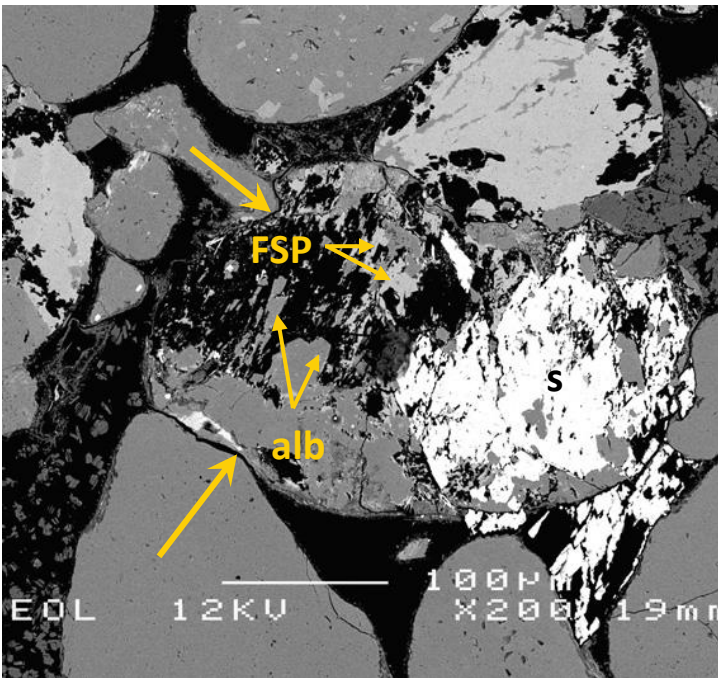
340μm

**B. Magnification 150x**

113μm

**C. Magnification 200x**

85μm
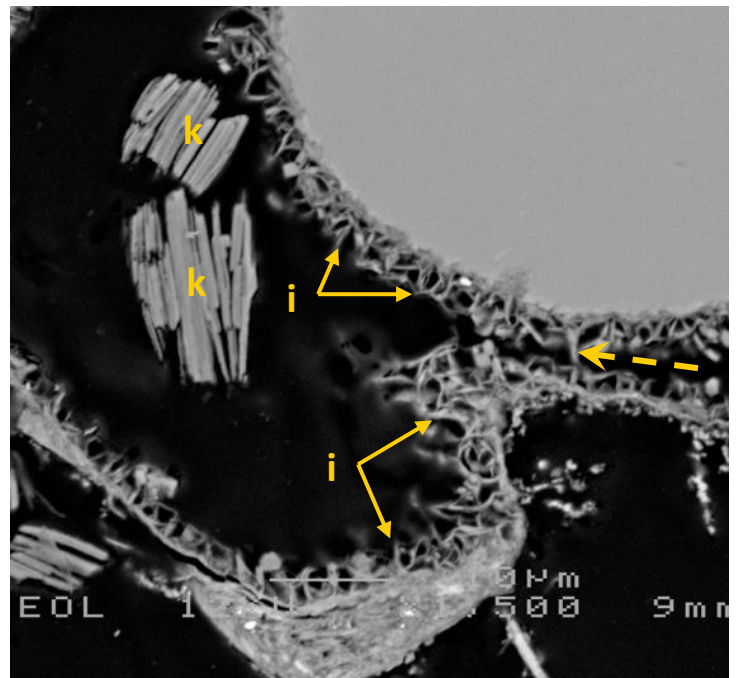
**D. Magnification 1500x**

11μm

**Plate A:** Overview of the fine-grained sublitharenite, in which quartz grains (Q) have point contacts. K-feldspar and albite grains (FSP) commonly have long or convex-concave contacts with quartz grains, particularly when partially dissolved. **Plate B:** Areas of poor sorting are characterised by tight grain packing and point to long grain contacts (solid arrows). K-feldspar grains (FSP), in contrast, have long or convex-concave grain contacts. Quartz cement is very rare (q). **Plate C:** Largely dissolved feldspar grain or rock fragment, which contains relict K-feldspar (FSP), as well as authigenic albite (alb) and siderite (s). Note indentations (solid arrows) of the grain outline by adjacent quartz grains. **Plate D:** Grain-coating clay minerals (i) occur as continuous radial crystals. The volume of these crystals is rather small, also compared with pore-filling kaolinite (k) but the chloritic to illitic clay may be pore-bridging in narrow pore throats (dashed arrows). EDX analyses of the clay crystals indicate predominantly illite with minor chlorite.
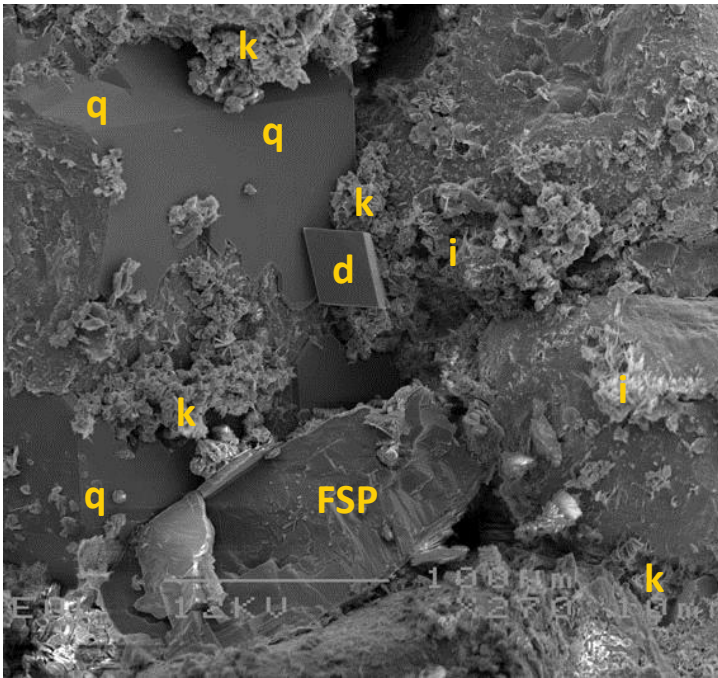
**A. Magnification 270x**

63µm
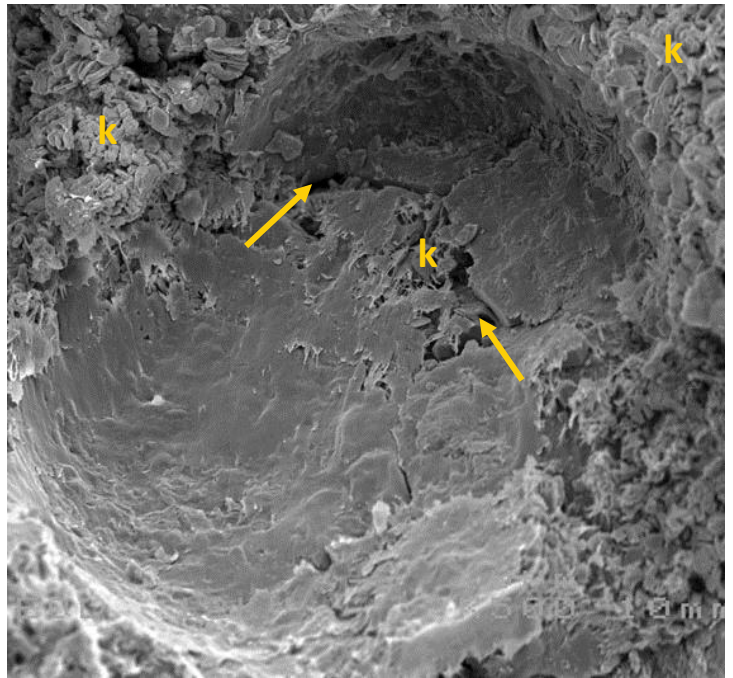
**B. Magnification 500x**

34µm
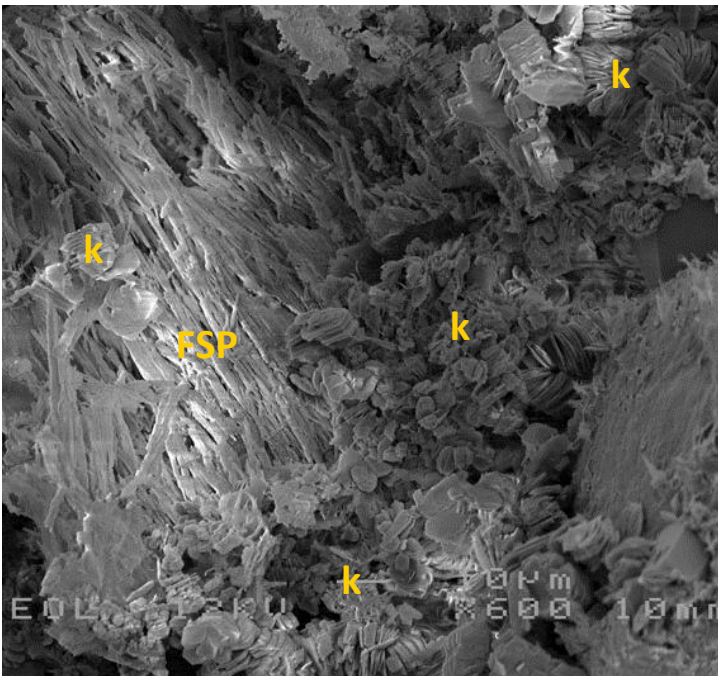
**C. Magnification 600x**

28µm
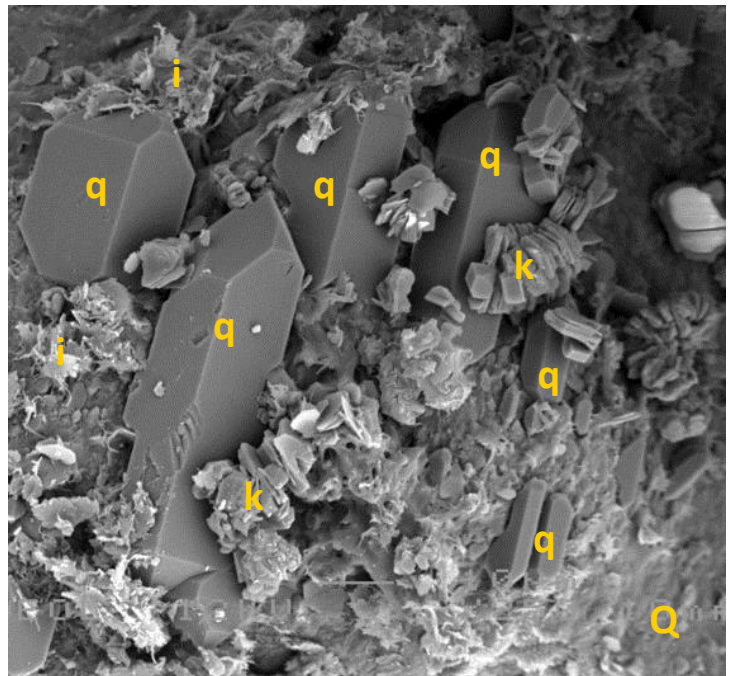
**D. Magnification 850x**

20µm

**Plate A:** This image shows dispersed kaolinite (k) booklets and illite (i) occurring together with authigenic quartz (q) and an authigenic dolomite (d) rhombus. Quartz cement is absent in areas more enriched in kaolinite and other authigenic clay (arrow). Clay coatings covering the detrital grains are however not very well developed. Note the well preserved alkali feldspar (FSP) grain. **Plate B:** The spatial relationship between clay minerals and the occurrence of micropores (arrows) are well visible in this area from which a grain was removed during sample preparation. Kaolinite (k) is relatively rich in micropores. **Plate C:** Residual feldspar (FSP) after grain leaching is very fibrous and prone to electron charging, hence the white colour. Closely associated to the feldspar is the presence of authigenic kaolinite (k), even though the kaolinite does not occur in between the feldspar fibres. **Plate D:** This relatively high magnification image shows microcrystalline quartz overgrowths (q) which cover a quartz grain (Q). Also here, kaolinite (k) and illitic (i) authigenic clay occur.
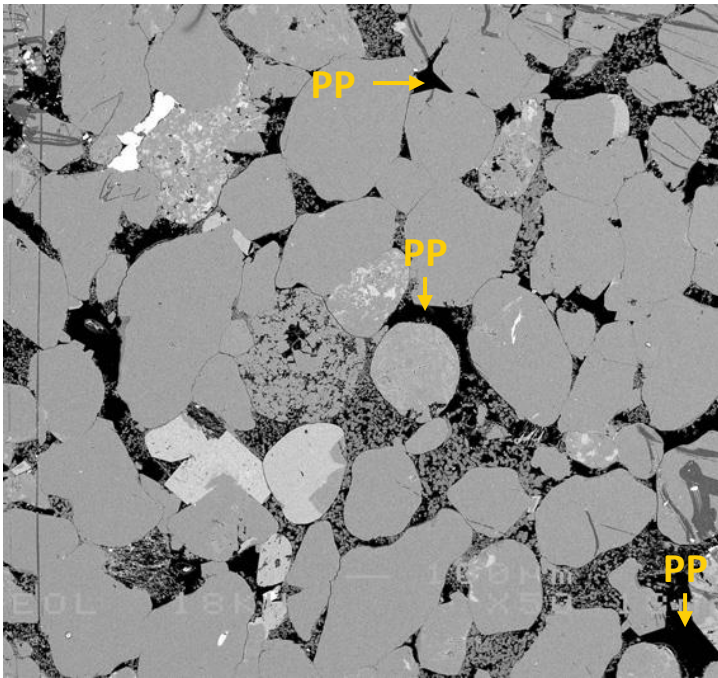
**A. Magnification 50x**
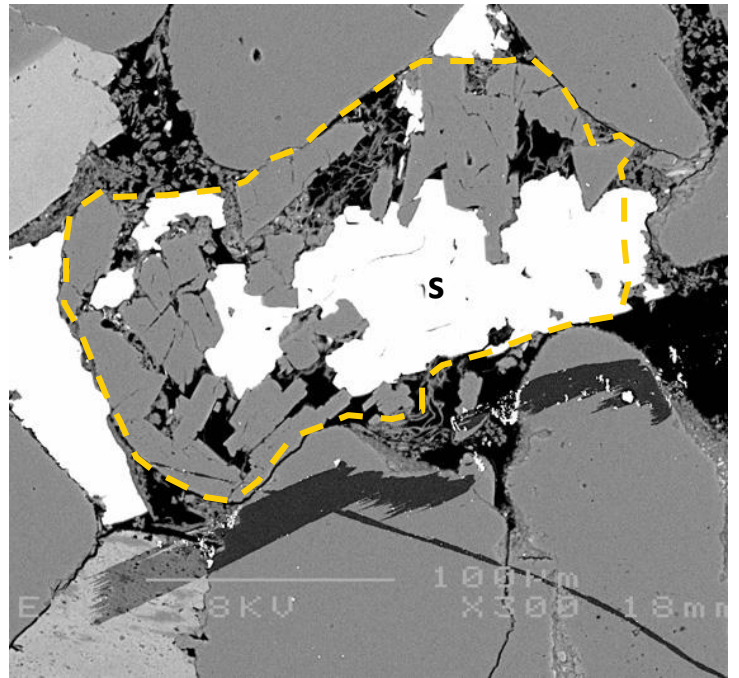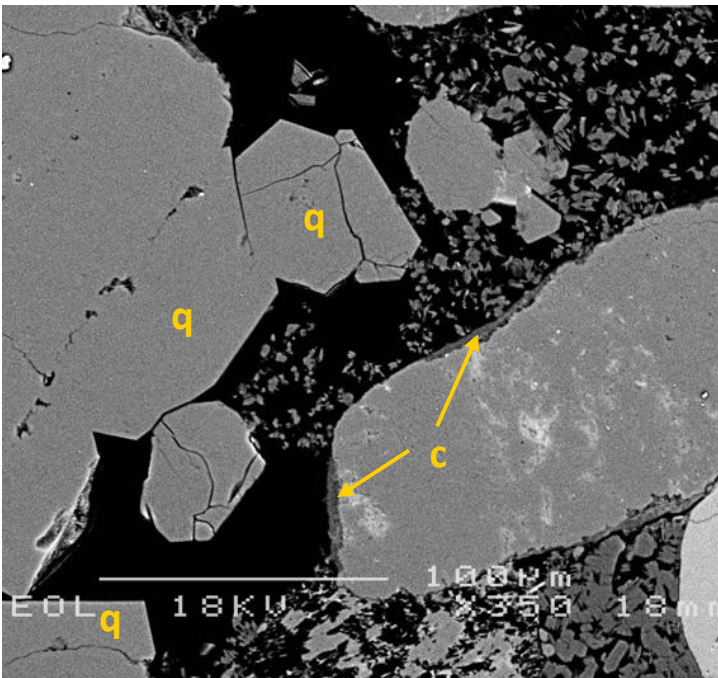
340μm

**B. Magnification 300x**

57μm

**C. Magnification 350x**

49μm
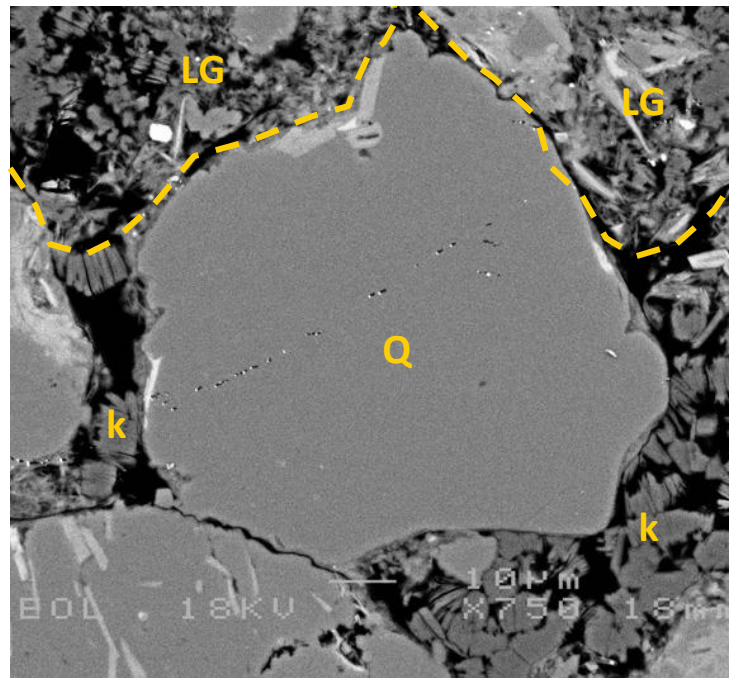
**D. Magnification 750x**

23μm

**Plate A:** Overview of the fine-grained sublitharenite, which shows a low amount of intergranular pores (PP). This is a result of a comparatively high degree of compaction, also visible by the relatively low IGV of 17.7 (sample set avg. is 20.5%). Pore spaces are commonly occupied by kaolinite (k). **Plate B:** Partially dissolved albite grain (outline indicated by dashed yellow line), which is deformed indicating ongoing compaction after leaching. The resulting secondary intragranular pores are largely filled by siderite (s). **Plate C:** Pore-filling quartz cement (q) is overall very sparse to sparse (2.0% vol.), but reduced pore sizes locally. Note the discontinuous tangential clay coatings (c) on some quartz grains. Clay coatings in general are very thin and irregular (cloudy). **Plate D:** Quartz grains (Q) have predominantly point or long grain contacts, while leached ductile grains are strongly indented (dashed line). Grain leaching (LG) left behind mixed authigenic illite, chlorite and kaolinite crystals. Kaolinite booklets (k) mainly occur in primary pores.
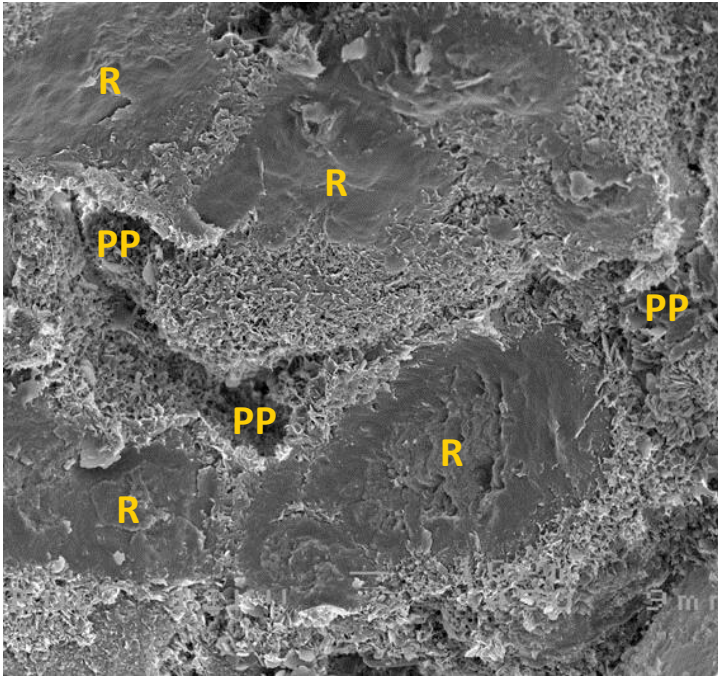
A. Magnification 450x

38µm
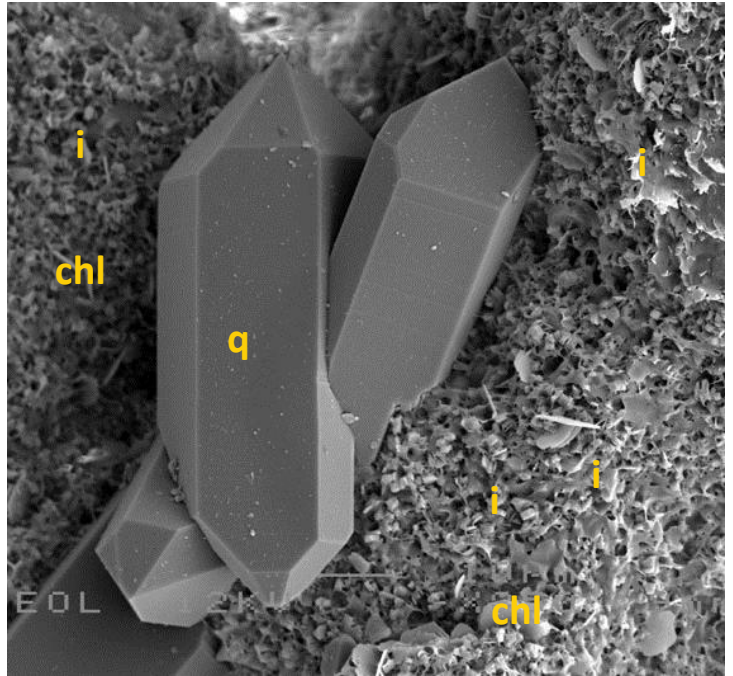
B. Magnification 850x
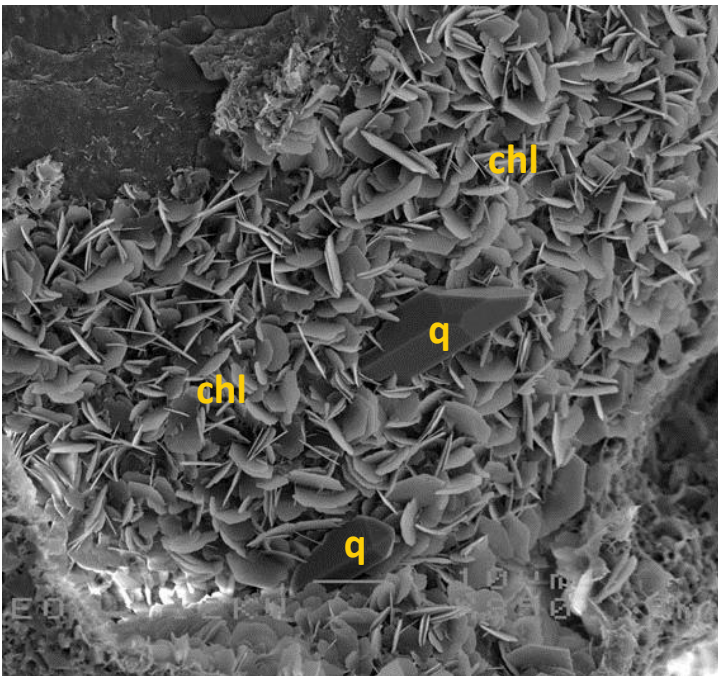
20µm

C. Magnification 850x

20µm
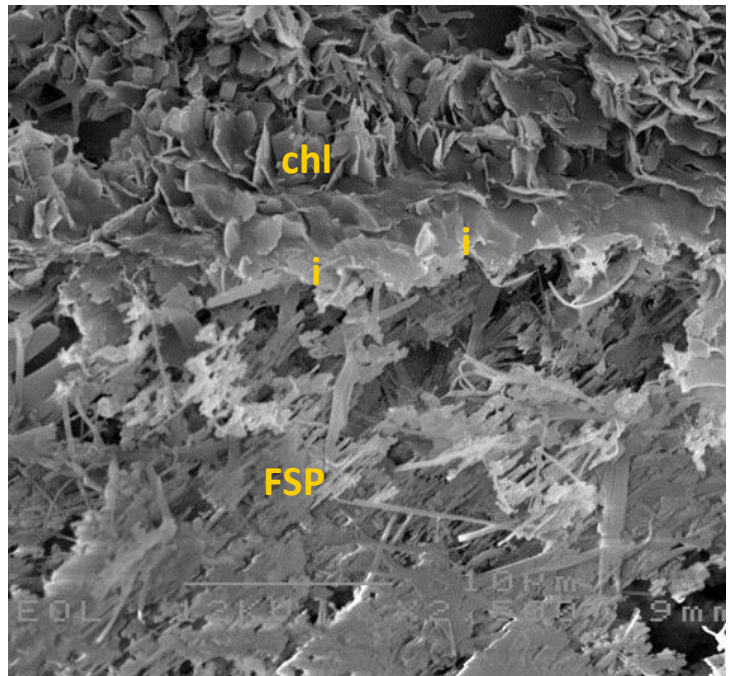
D. Magnification 2500x

7µm

**Plate A:** This image shows the relatively thick clay coatings covering the detrital grains. Due to these thick coatings, the true shape and size of the grains is difficult to identify. Despite the clay coating, intergranular pores (PP) remained relatively large. The more smooth surfaces are surfaces that were in contact with a plucked grain (R). **Plate B:** Locally, authigenic quartz crystals (q) have developed on grain surfaces. The clay minerals here are very fine crystalline, and most likely a mixture of illite (i) and chlorite (chl). **Plate C:** Locally, the chlorite (chl) has formed relatively large rosette shaped structures. These chlorite crystals have formed in open pore spaces, where growth was not hindered by other minerals or grains. Note that between the chlorite platelets, small quartz overgrowths (q) have formed. **Plate D:** This high magnification image shows the contact between a moderately to strongly leached, feldspar grain (FSP), composed of residual feldspar with micropores in between the feldspar fibres and the authigenic clay that is covering the detrital feldspar. The clay comprises illite (i) and chlorite (chl).
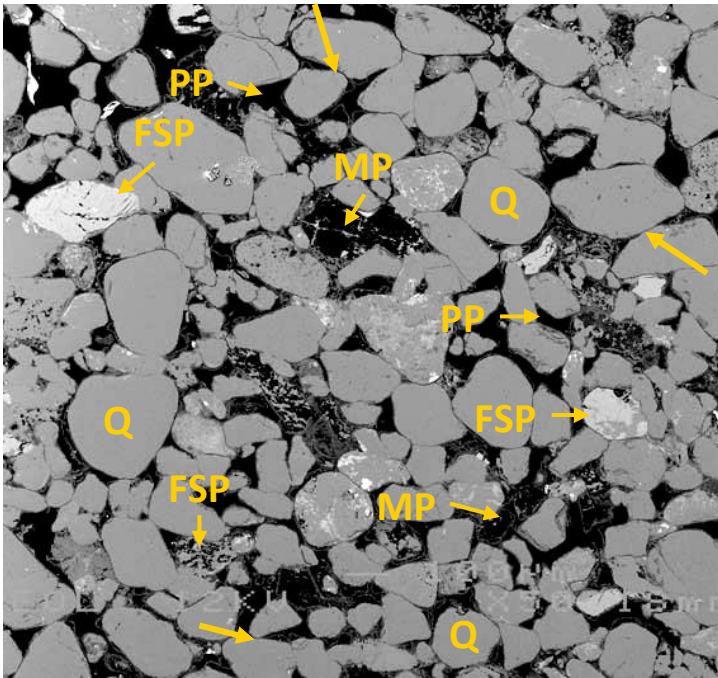
A. Magnification 50x
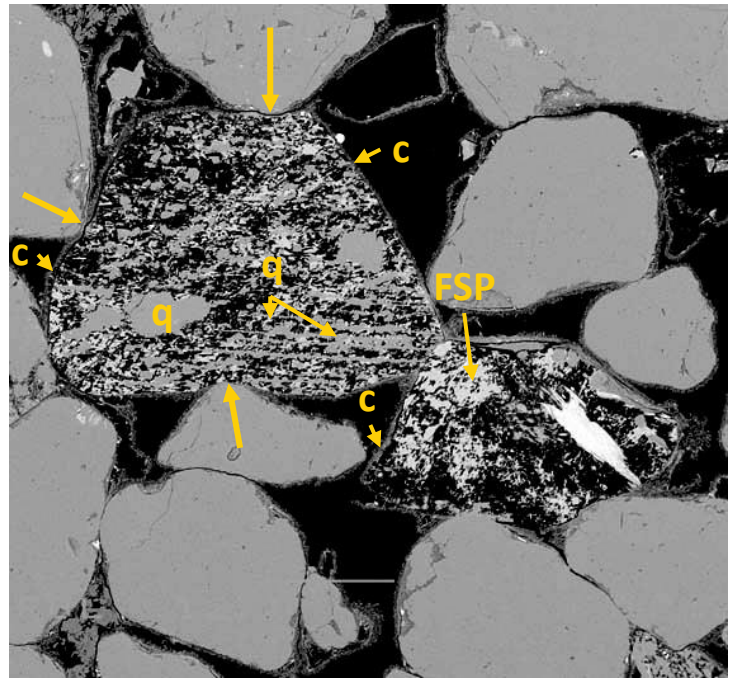
340µm

B. Magnification 200x

85µm
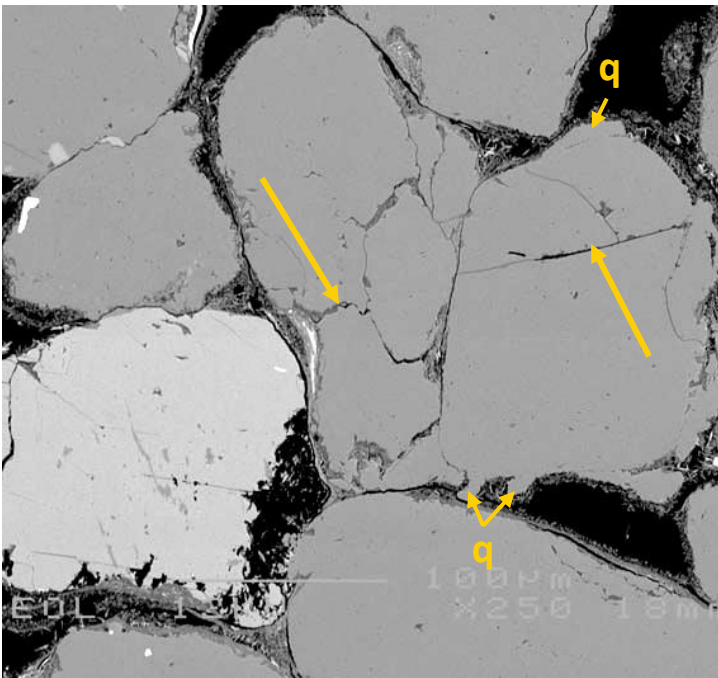
C. Magnification 250x

68µm
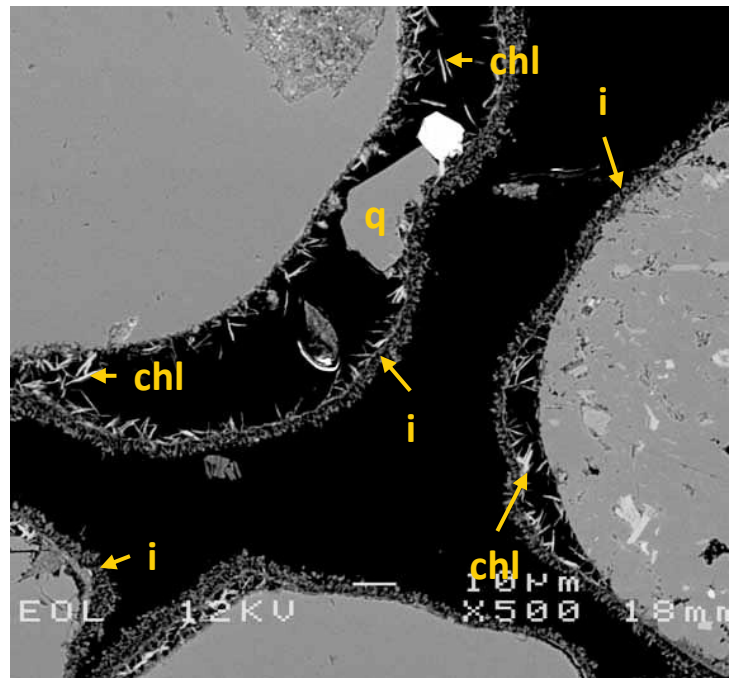
D. Magnification 500x

34µm

**Plate A:** Overview of the sublitharenite showing predominant point contacts (solid yellow arrows) between quartz (Q) and K-feldspar (FSP) grains. Primary intergranular pores (PP) are locally well interconnected, but many of the larger pores are secondary intragranular or mouldic (MP) pores. **Plate B:** The outlines of leached K-feldspar grains (FSP) are indicated by clay coatings (c). Unless completely dissolved, the feldspar grains contain ample micro-porosity between grain-replacive quartz (q) and kaolinite crystals (crystal size too small for highlighting). Note the local indentations (solid yellow arrows) of feldspar by quartz grains, despite the common point contacts observed in plate A. **Plate C:** In areas of dense grain packing, quartz grains may be fractured (solid yellow arrows). The overall volume of quartz overgrowths is limited; small authigenic outgrowths (q) are developed where clay coatings are disrupted. **Plate D:** Radial clay coatings, mostly composed of illite (i), are present on virtually all grain surfaces. The coatings are detached from the host grains (most likely due to compaction), providing space for authigenic clay growth (mixed chlorite and illite; chl) and quartz cementation (q).
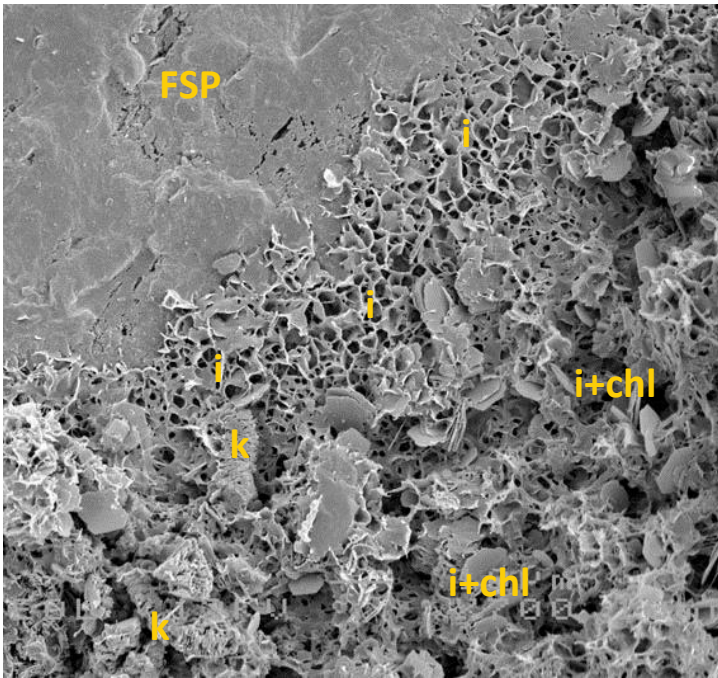
**A. Magnification 700x**

24μm
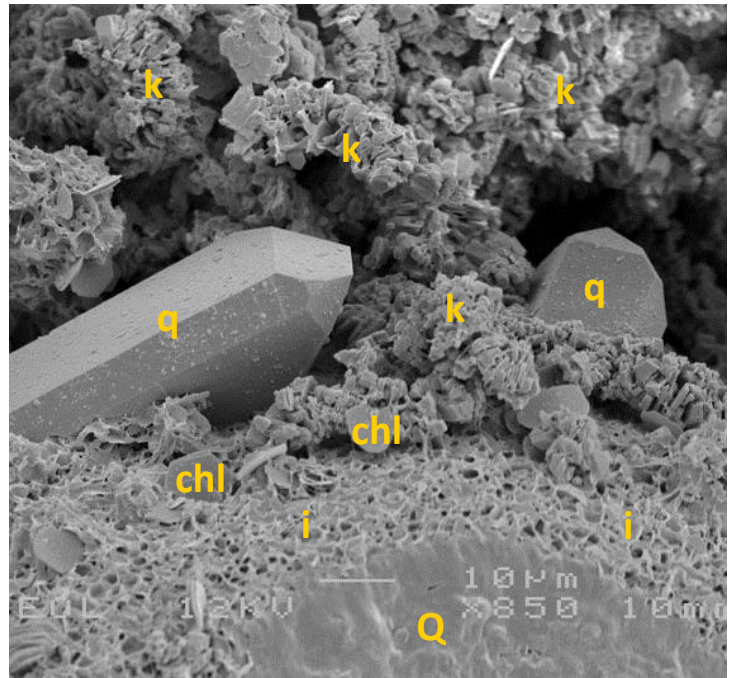
**B. Magnification 800x**

21μm
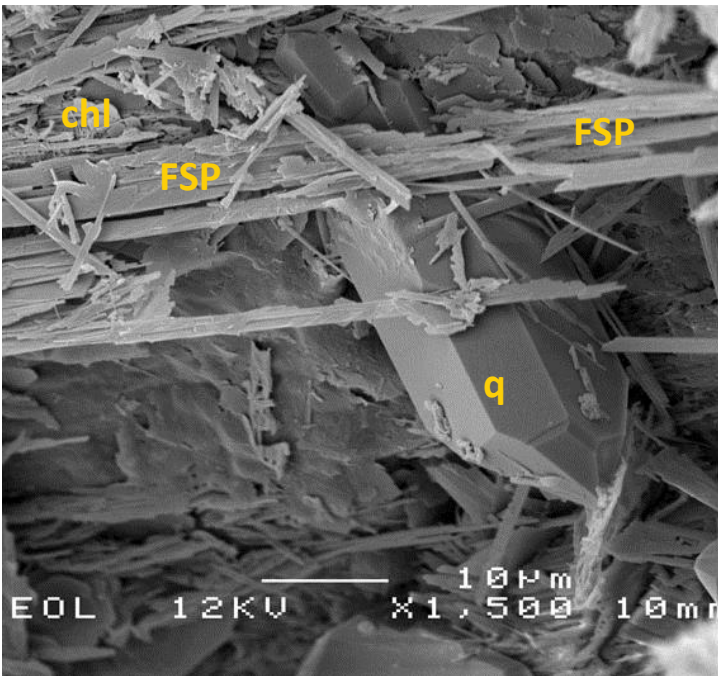
**C. Magnification 2000x**

9μm
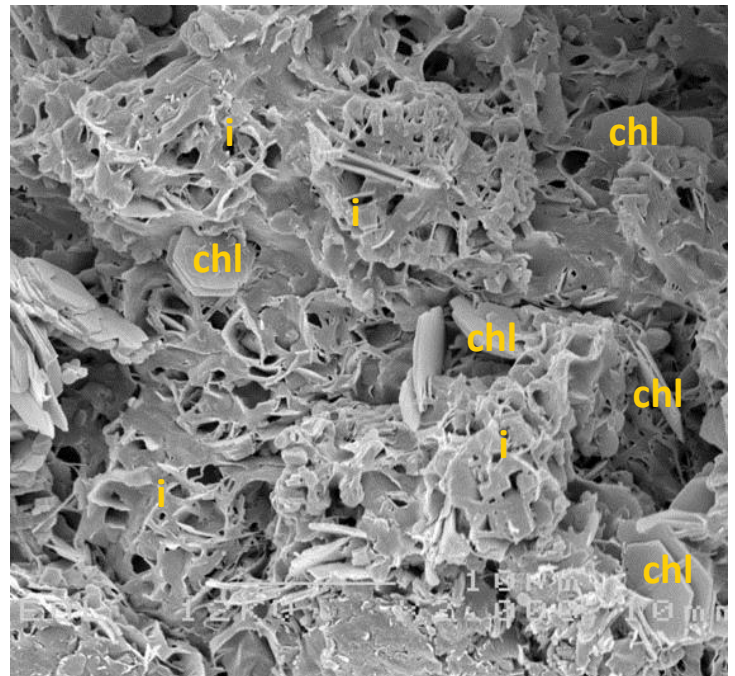
**D. Magnification 1500x**

11μm

**Plate A:** The intergranular pores in this sample are commonly filled with authigenic clays. This image shows an alkali feldspar grain (FSP) which is coated with honeycomb-shaped illite (i). This illitic coating is again covered with mixed authigenic illite and chlorite (i+chl). Also booklet shaped kaolinite (k) is present. In the displayed area, only micropores occur. **Plate B:** Locally, authigenic quartz crystals (q) formed, overgrowing the clay. Also on the quartz grain (Q) displayed here, an illite coating occurs (i), covered by a mixture of kaolinite (k) and chlorite (chl). Note how the quartz cement engulfs the clay (arrow). **Plate C:** A detailed image showing the inside of leached feldspar with remaining feldspar needles (FSP), as well as authigenic quartz (q). Some of the feldspar is replaced by chlorite (chl) and possibly some illite. **Plate D:** This high magnification image shows the texture of the fibrous illite, which occurs together with the coarser crystalline chlorite (chl). There are no signs of late stage (post clay formation) deformation within this clay-rich material.
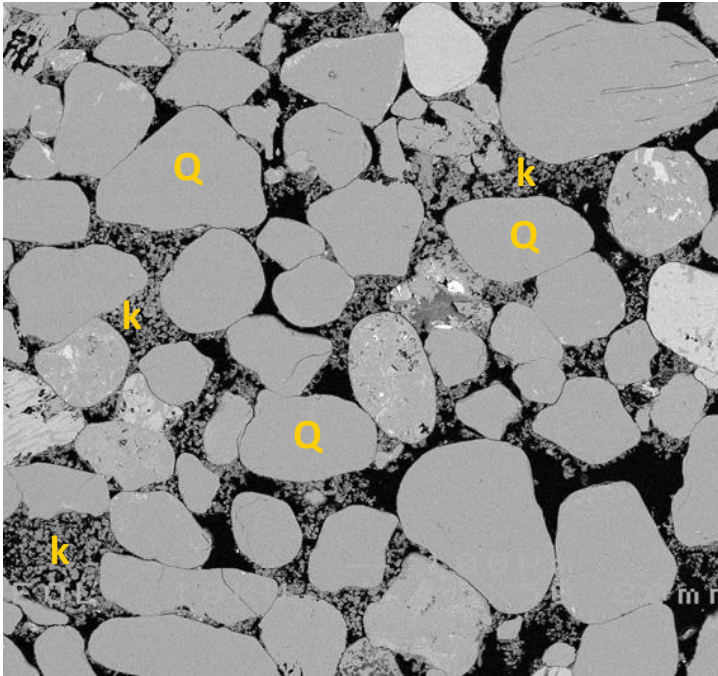
**A. Magnification 50x**

340μm
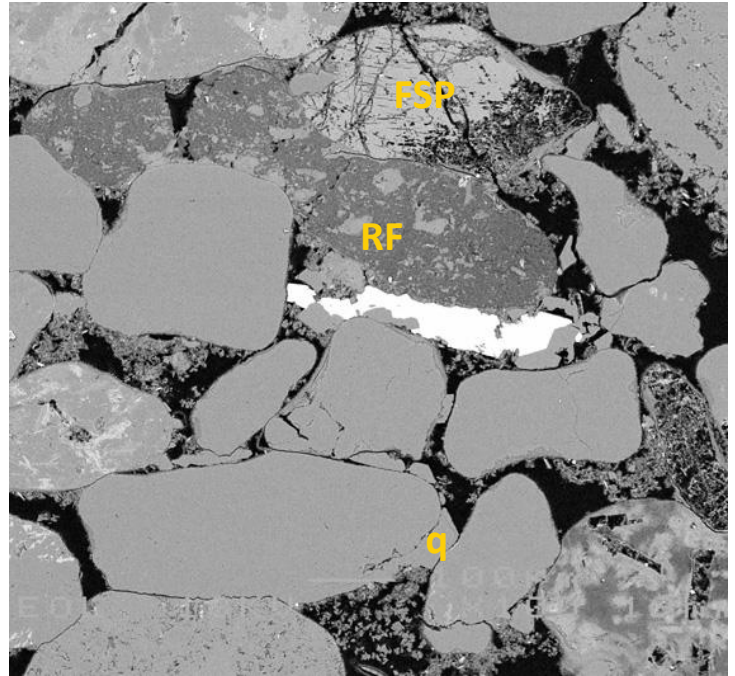


**B. Magnification 100x**
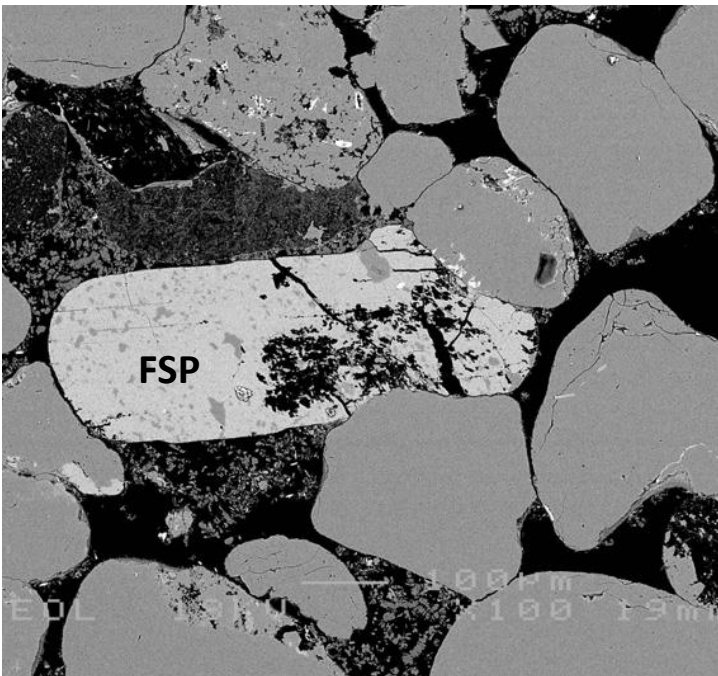
170μm



**C. Magnification 100x**

170μm



**D. Magnification 750x**

23μm

**Plate A:** Overview of this medium-grained sublitharenite showing subrounded quartz grains (Q). Note the common authigenic kaolinite clusters (k). **Plate B:** Ductile rock fragments (RF; composed of illite and larger chlorite crystals) and partially dissolved K-feldspar grains (FSP) accommodated strong mechanical compaction by deformation and fracturing. Quartz overgrowths (q) occur locally. **Plate C:** K-feldspar grain (FSP), which exhibits intragranular dissolution pores, is cross-cut by fractures. This indicates that dissolution and ongoing compaction occurred partially at the same time. Note also the concavo-convex contact to the adjoining quartz grains. **Plate D:** Radial illite grain coats (i) and more randomly oriented illite and chlorite crystals (chl) reduce pore throat sizes, particularly of smaller pores in the finer-grained laminae. The thickness of the clay coatings is intermediate compared to other samples of the set, as visible in Appendix 6.
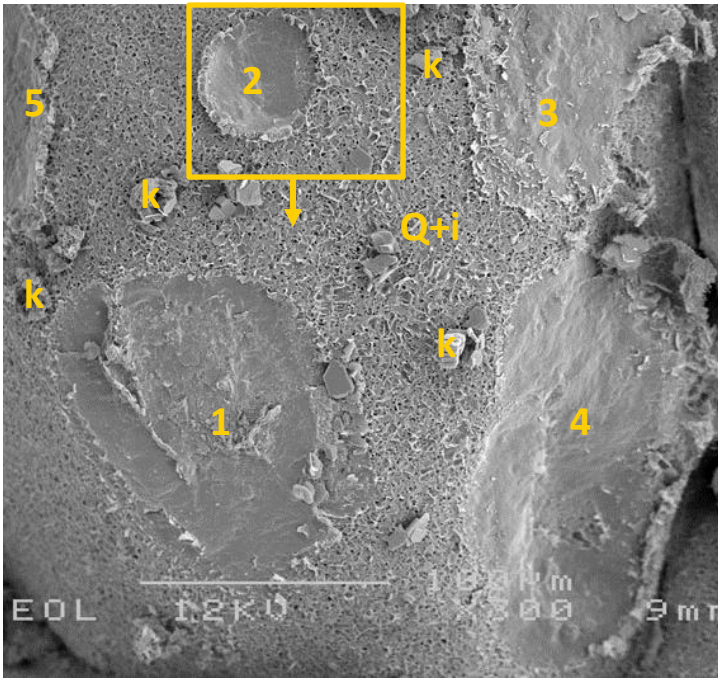
**A. Magnification 300x**
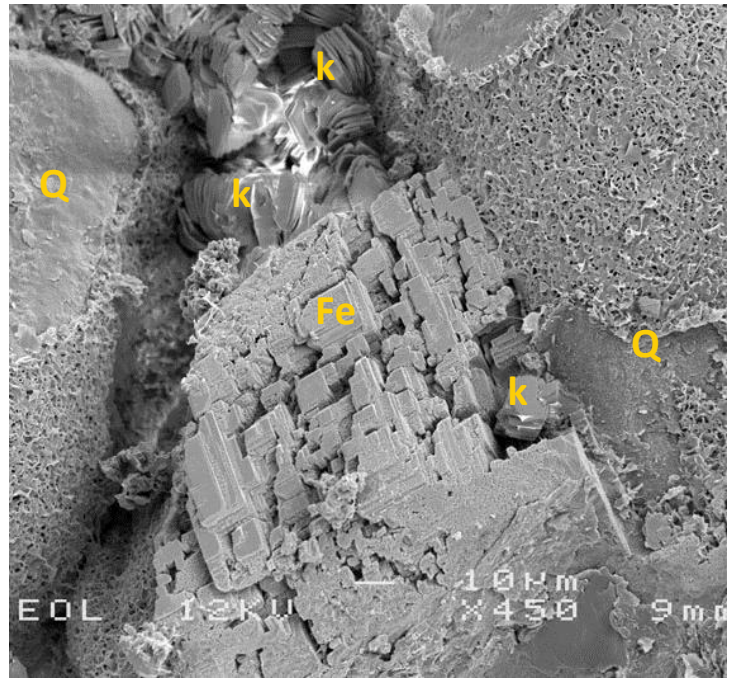
57µm

**B. Magnification 450x**

38µm
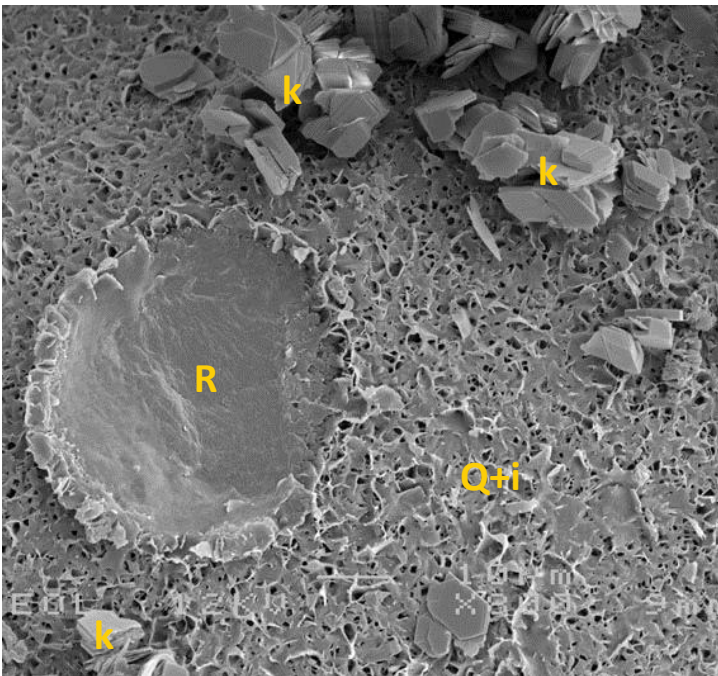
**C. Magnification 800x**

21µm
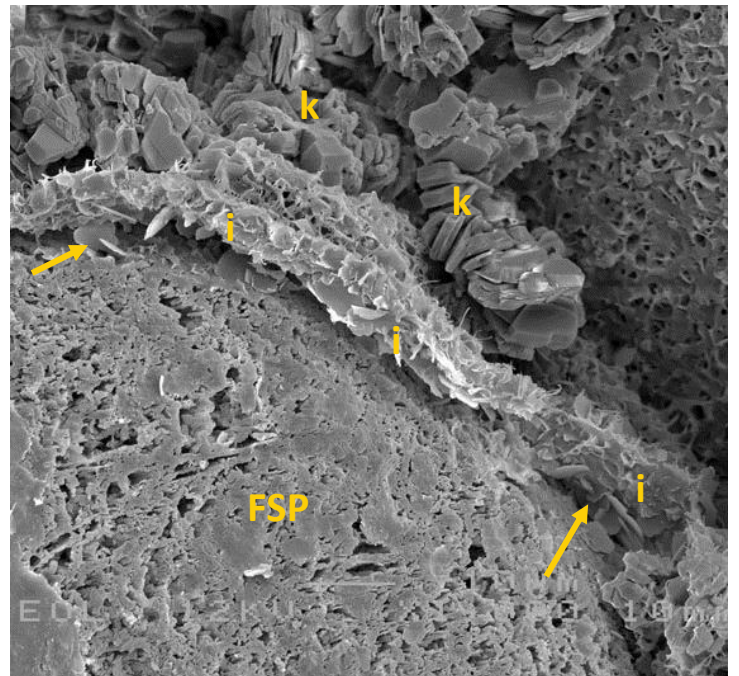
**D. Magnification 1000x**

17µm

**Plate A:** This coarse grained detrital quartz grain is covered with a thin layer of grain rimming clay (Q+i). Due to this grain rimming clay, the contact points with (in this field of view) 5 other grains (1-5) are well visible. Small clusters of kaolinite (k) occur on top of the grain rimming clay. The inset shows the area photographed in plate C. **Plate B:** Detailed image of authigenic cement that occurs in between two clay-covered quartz (Q) grains. The blocky cement is a Fe-rich intergranular carbonate (Fe; siderite?). Replacive kaolinite booklets (k) occur next to the pore-filling cement. **Plate C:** Detailed image of the inset of plate A, showing the imprint of a removed grain (R) and clustered vermicular kaolinite booklets (k). The surface of the quartz grain, which is covered with grain rimming clay (Q+i), was not in contact with another grain. The grain rimming clay appears to be mostly illitic. **Plate D:** The partially leached feldspar grain (FSP) contains isolated micropores (black). This grain is covered with grain rimming clay (i; illitic). The thickness of the rim is 3-4 µm. Some chlorite occurs in between the feldspar and the grain rimming clay (arrows). Note the authigenic kaolinite (k).
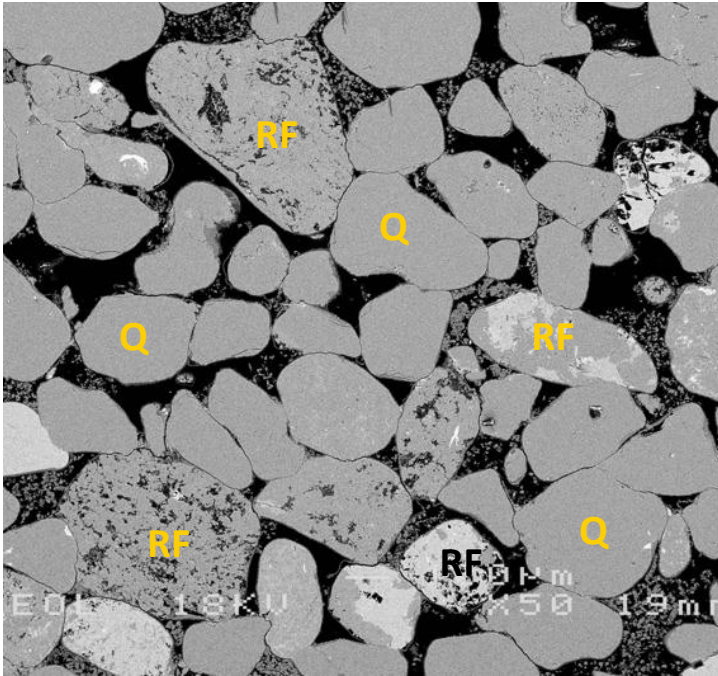
**A. Magnification 50x**
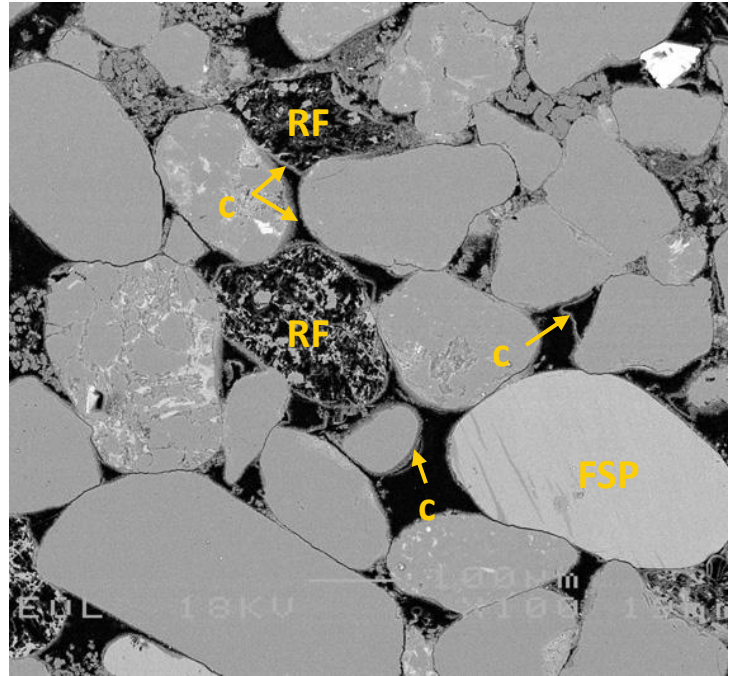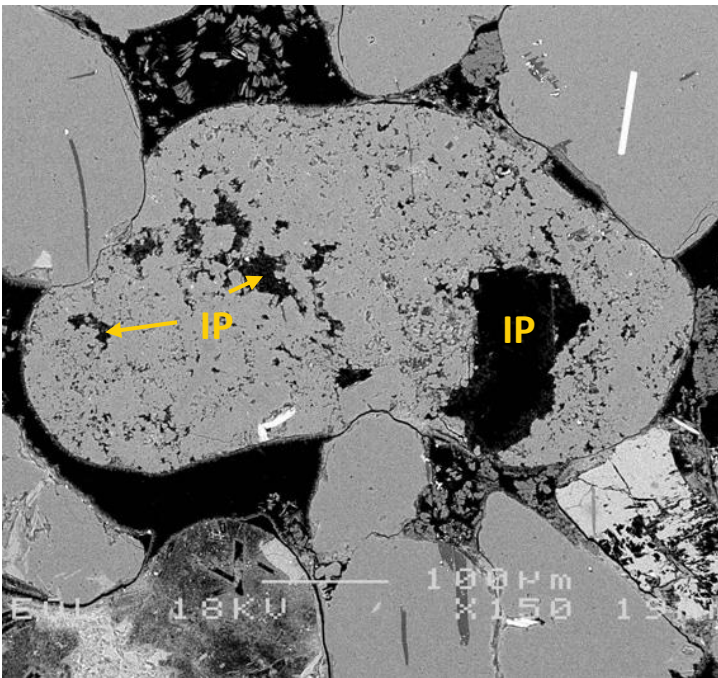
340µm



**B. Magnification 100x**

170µm



**C. Magnification 150x**

113µm
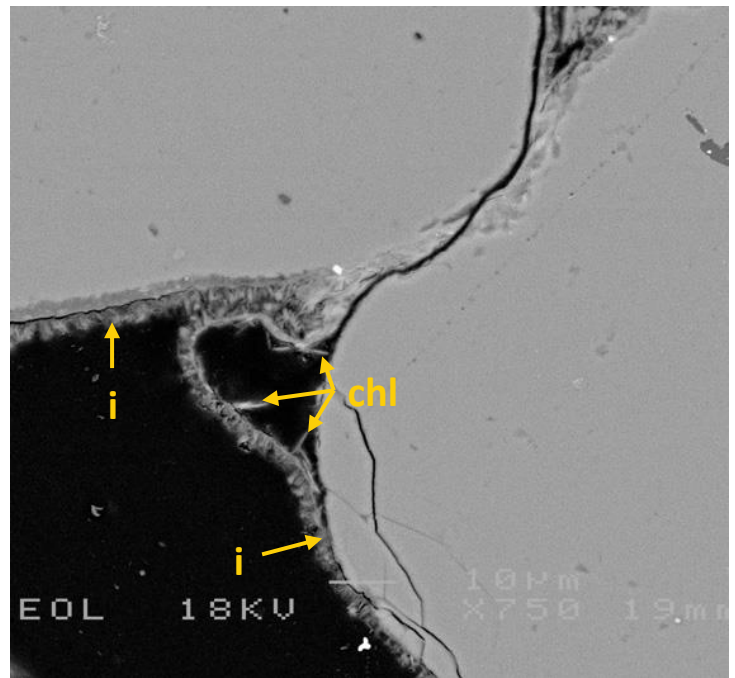


**D. Magnification 750x**

23µm

**Plate A:** Overview of this medium-grained sublitharenite being composed of quartz grains (Q) and abundant, partly microporous rock fragments (RF). **Plate B:** The sublitharenite is characterised by point to long contacts between rigid grains. K-feldspar grains (FSP) and leached grains (RF) may be indented by adjacent quartz grains. However, a fair content of intergranular pores (10.3% vol.) are present. **Plate C:** A deformed leached rock fragment indicates a comparatively high degree of compaction. Secondary intragranular pores (IP) developed through grain dissolution. **Plate D:** Clay coatings (i) are locally sheared off the grain surfaces near point or slightly convex-concave grain-to-grain contacts. EDX analyses of the clay crystals show a predominance of illite, but a minor Fe content indicates the presence of small amounts of chlorite. Chlorite crystals (chl) are visible on the inside of clay coatings; hence these may have formed later than the illite.
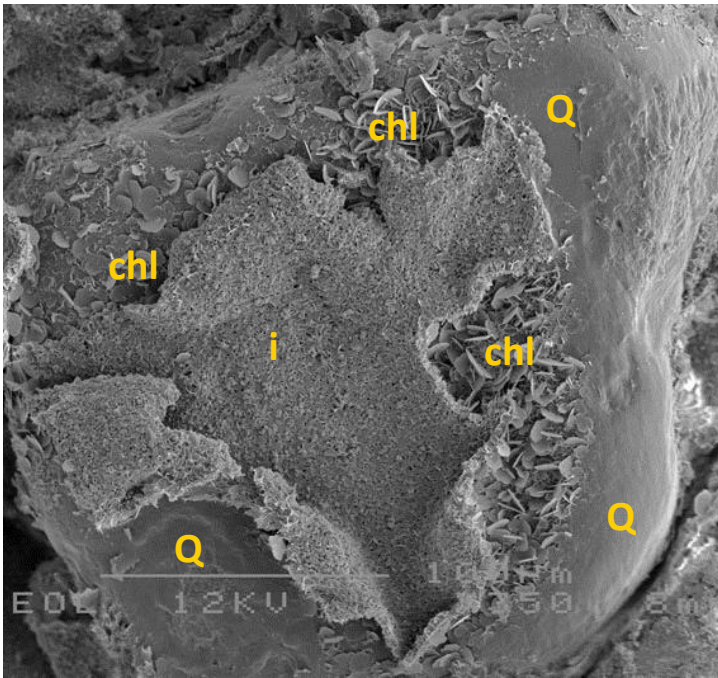
A. Magnification 350x
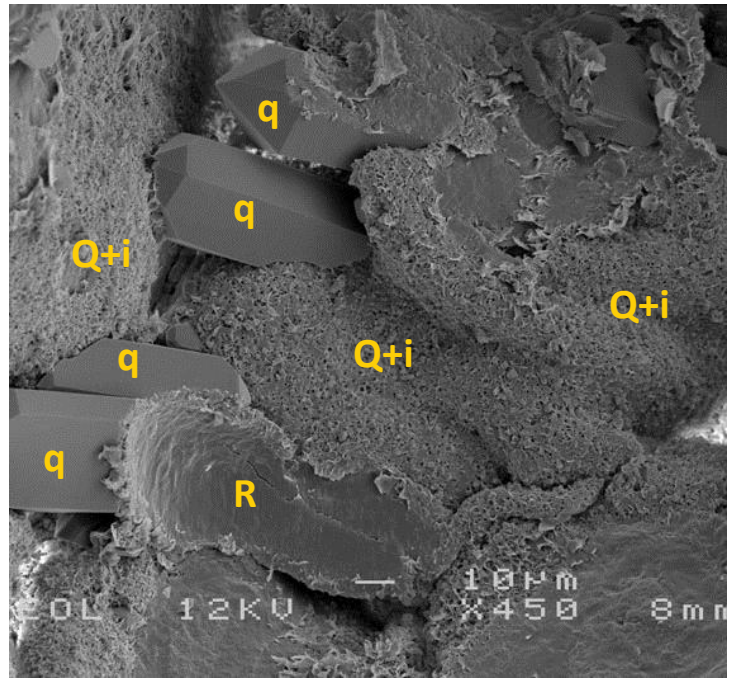
49µm



B. Magnification 450x

38µm
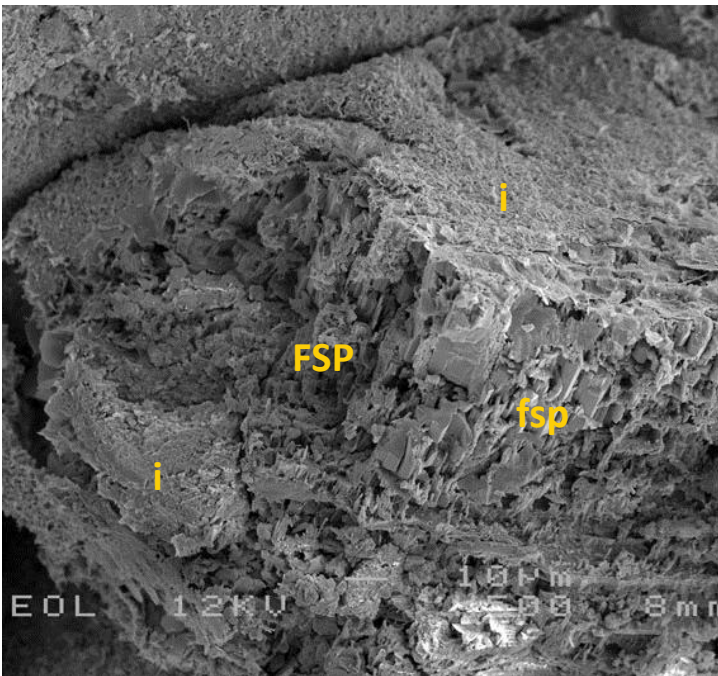


C. Magnification 500x

34µm
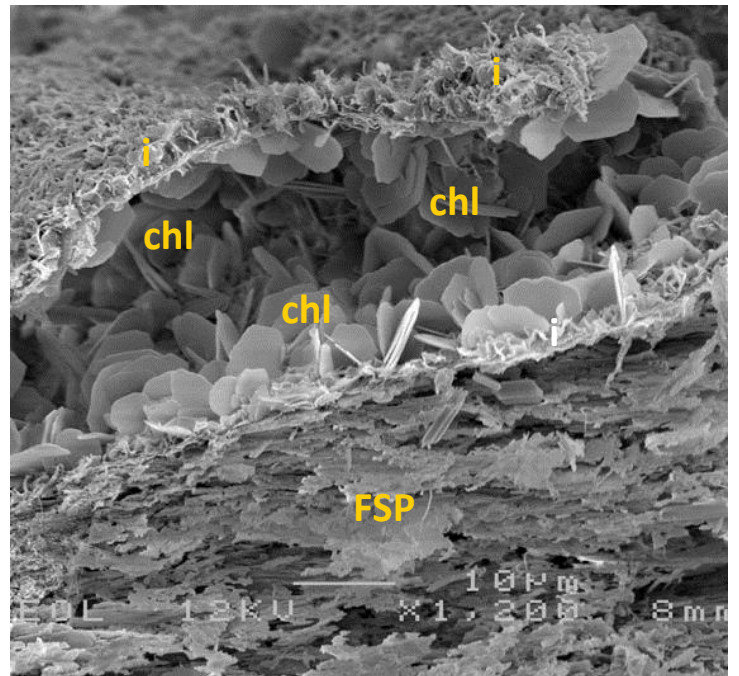


D. Magnification 1200x

14µm

**Plate A:** This coarse grained, well rounded quartz grain (Q) occurring in this fine grained sandstone is covered with two types of clay coating: 1) coarser crystalline rosette-shaped chlorite (chl) and 2) finer crystalline clay (i; illitic) located on top of the chlorite. Quartz overgrowths are not present on this grain. **Plate B:** A relatively thick illitic clay coating occurs on top of all detrital grains (Q+i). Locally, quartz outgrowths (q) formed in the relatively large pores. Note the imprint of the plucked grain (R). **Plate C:** This leached feldspar grain (FSP) is covered by the same illitic (i) clay coating as the detrital quartz grains. Leaching postdates the formation of the clay coating, as the coating did not penetrate the leached feldspar. Euhedral outlines indicate that in some places also newly formed feldspar occurs (fsp). **Plate D:** This high magnification image shows the relationship between microfibrous illitic clay coating (i), the rosette-shaped chlorite (chl) and residue of a partially leached feldspar (FSP). Apparently the illitic clay coating was pushed away (potentially due to continuous compaction) from the grain, creating space for the chlorite to form in between the detrital grain and the original illitic clay coating.
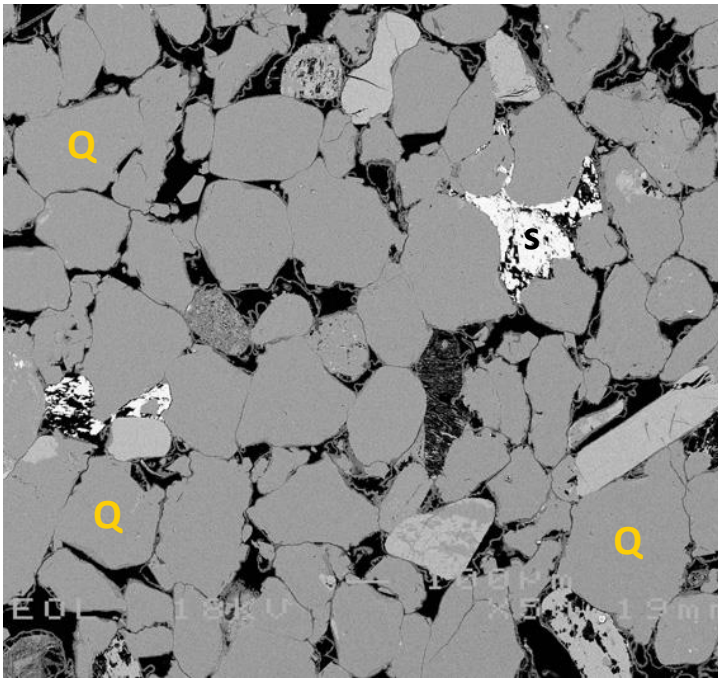
**A. Magnification 50x**
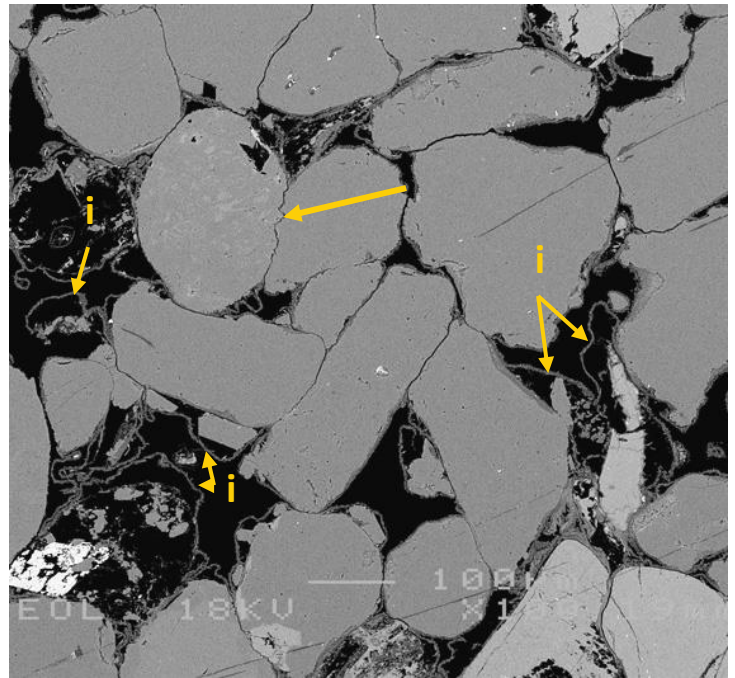
340μm



**B. Magnification 100x**

170μm
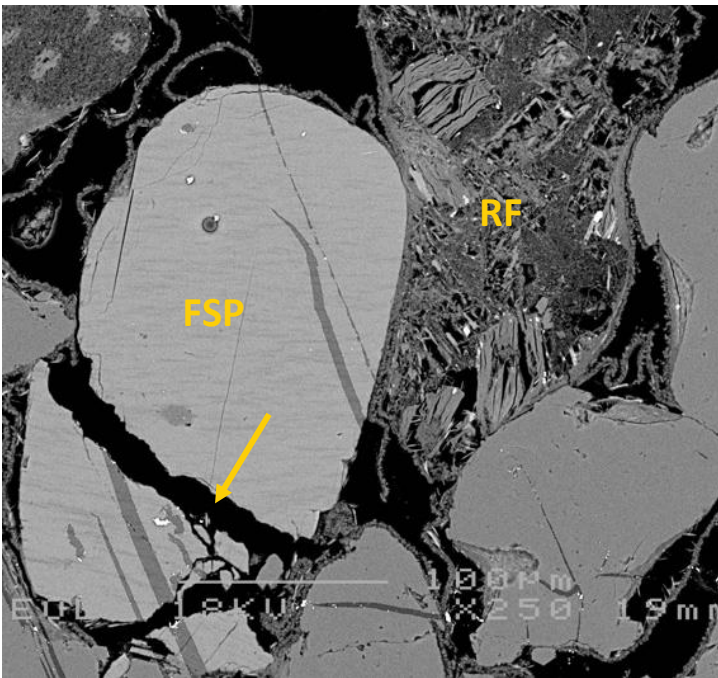


**C. Magnification 250x**

68μm
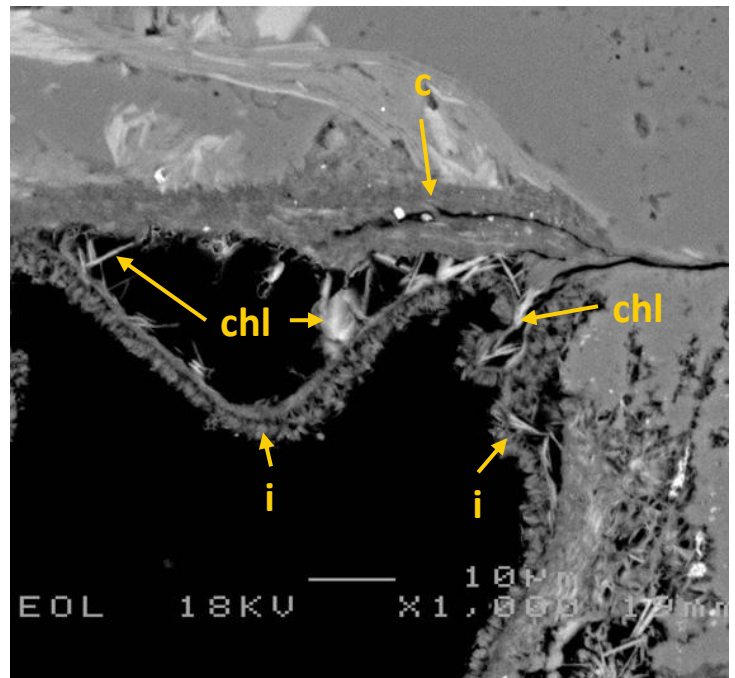


**D. Magnification 1000x**

17μm

**Plate A:** Overview of this fine-grained sublitharenite showing mainly subangular to subrounded quartz grains (Q; 48.0% vol.). Also note the patches of authigenic siderite (s). **Plate B:** The quartz grains have mainly point or long contacts. Convex-concave or slightly sutured contacts (solid yellow arrows) are present at rock fragments, indicating that locally chemical compaction occurred. Intergranular pores are commonly lined by radial authigenic illite (i) coatings. Quartz overgrowths (q) are developed where the clay coatings are detached from detrital grains. **Plate C** shows a fractured K-feldspar grain (FSP) and a deformed ductile rock fragment. The absence of authigenic clay or other cements in the main fracture (solid arrow) suggests that grain deformation occurred after the formation of authigenic clay coatings. **Plate D:** High-magnification view of a clay coating (i; EDX indicates predominance of illite with minor chlorite) that is detached from a relatively thick tangential clay coating. Needle-like (in 2D) chlorite crystals (chl) are present on the inside of the coatings.
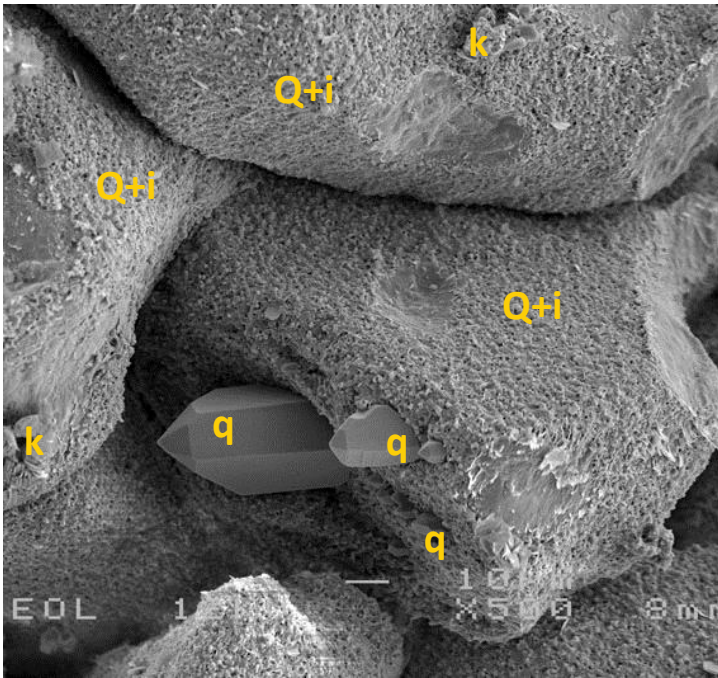
**A. Magnification 500x**
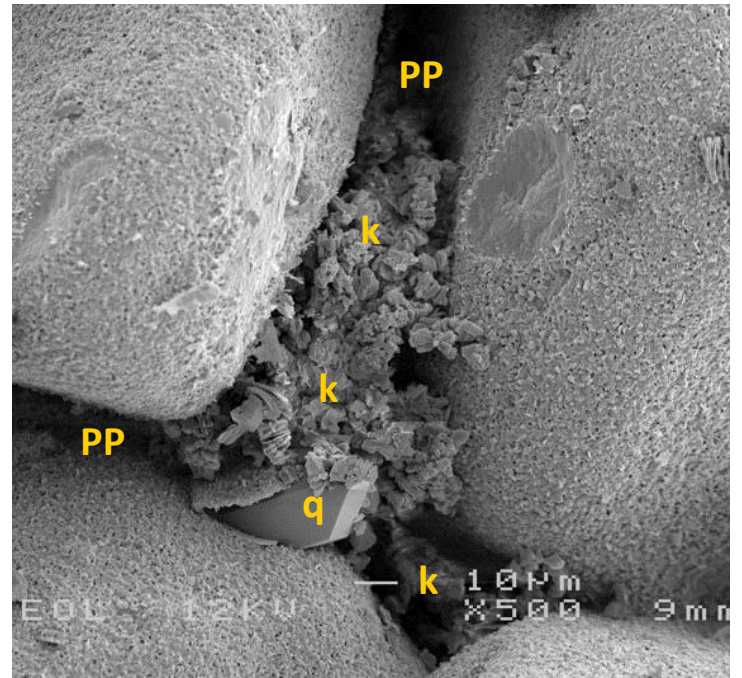
34µm

**B. Magnification 500x**

34µm
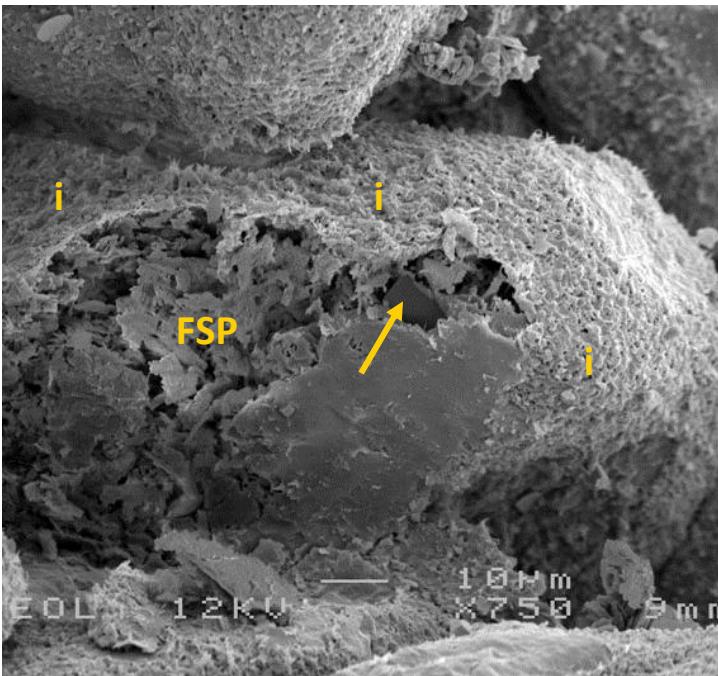
**C. Magnification 750x**

23µm
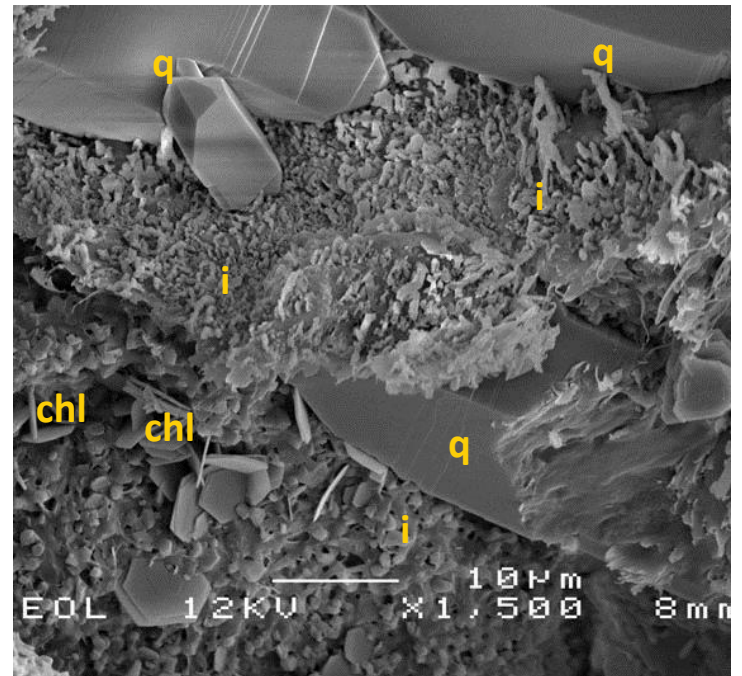
**D. Magnification 1500x**

11µm

**Plate A:** This moderately sorted, fine- to medium-grained sample is relatively free of intergranular clay other than thin authigenic clay rims (Q+i) and sparse authigenic kaolinite (k). Locally, well developed authigenic quartz outgrowths (q) grew into the large pore spaces. **Plate B:** Replacive kaolinite (k) occurs in this image together with authigenic quartz outgrowths (q). The permeability through this area is most likely good as pore and pore throat diameters (PP) as well as the micropores in between the kaolinite booklets are relatively large. **Plate C:** This strongly leached feldspar grain (FSP) is completely covered with authigenic clay coating (i), except for the area where a grain was plucked. This removal allows us to look inside the feldspar grain, showing that minor authigenic feldspar (?; arrow) has formed at the expense of the detrital feldspar. **Plate D:** This high magnification image shows that chlorite (chl) occurs rarely. Microquartz overgrowths (q) are also present, growing out of the illitic (fibrous) clay coating (i).
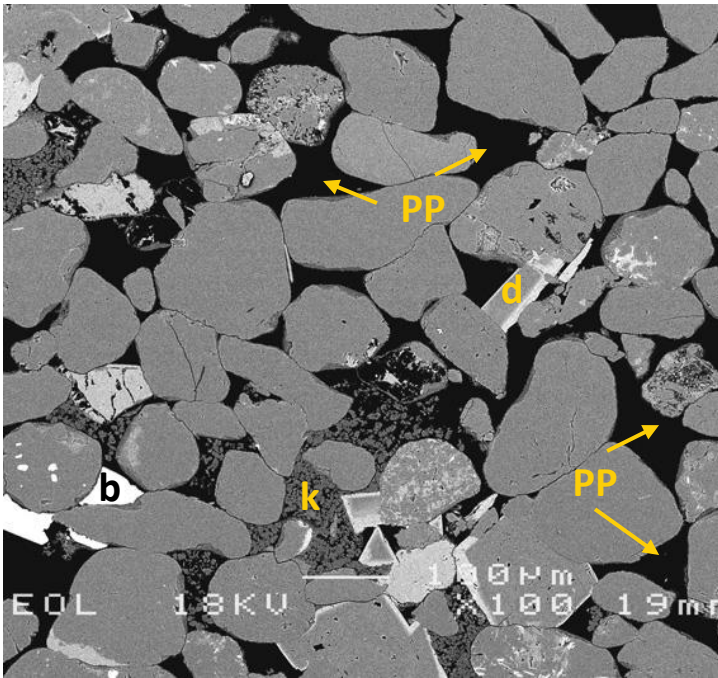
**A. Magnification 100x**
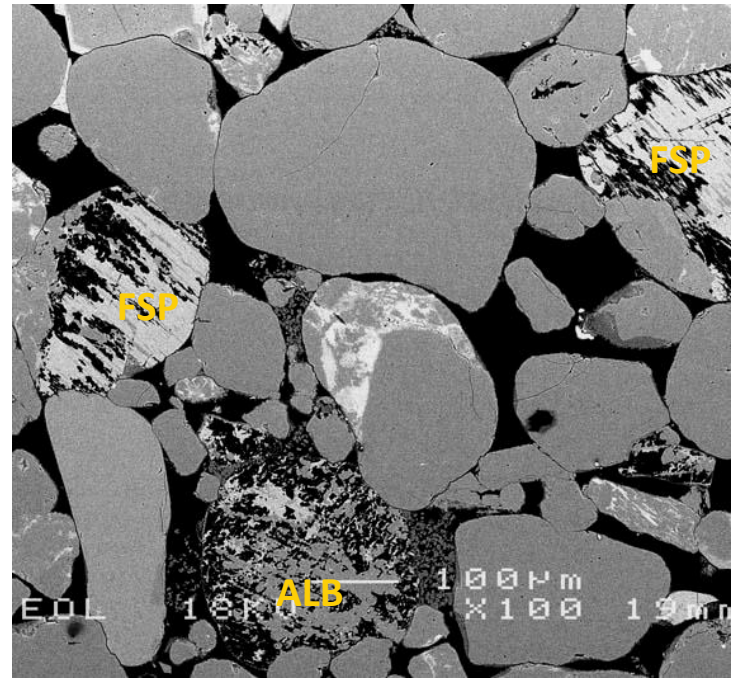
170μm

**B. Magnification 100x**

170μm
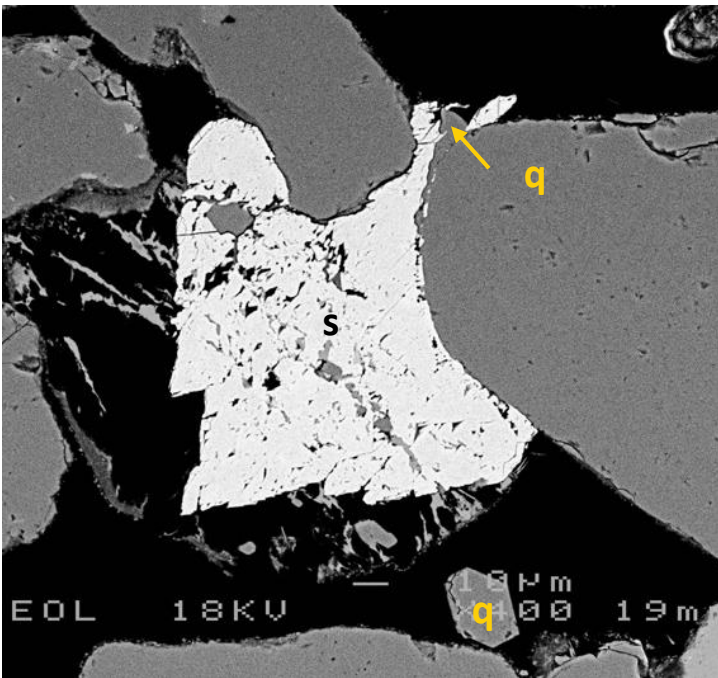
**C. Magnification 400x**

43μm
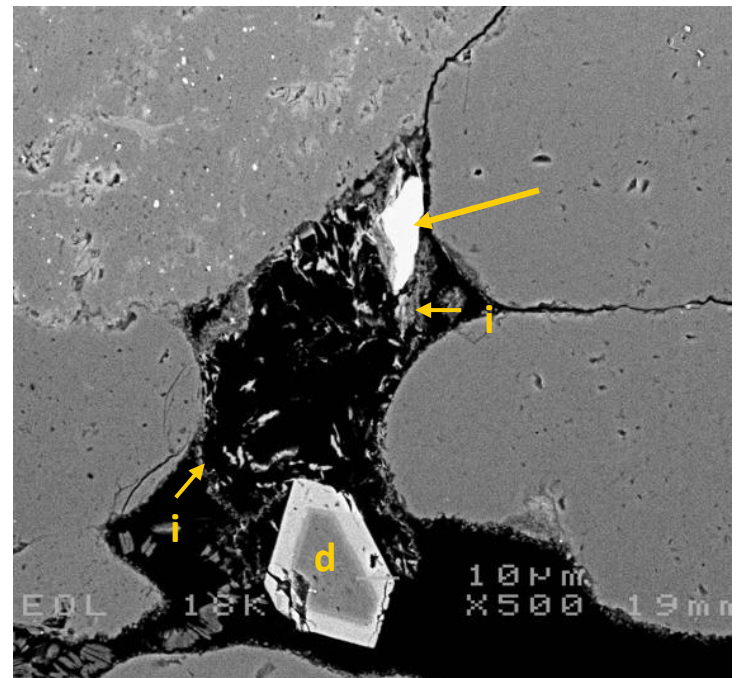
**D. Magnification 500x**

34μm

**Plate A:** Overview of a fine-grained lamina of this sublitharenite. Primary intergranular pores (PP) are moderately interconnected, although pores are locally blocked by kaolinite (k), dolomite (d) and traces of barite (b) cement. **Plate B:** Overview of a medium-grained lamina, which contains more K-feldspar (FSP) and albite (ALB) grains than the fine-grained lamina. The leaching of feldspar results in secondary intragranular and oversized pores and has a positive effect on reservoir quality. **Plate C:** Dissolved K-feldspar grains are also present within the fine-grained lamina. The grain in this field of view is partly replaced by siderite (s), which also fills pore throats between adjacent quartz grains, postdating minor quartz cement (q). **Plate D:** The deformed outline of this leached grain (containing apatite; solid arrow) is indicated by illite crystals (i). The long contacts between the rigid grains indicate locally a moderate to high degree of compaction. Note the authigenic pore-filling dolomite (d). Clay coats are relatively thin and mostly (radial) illitic.
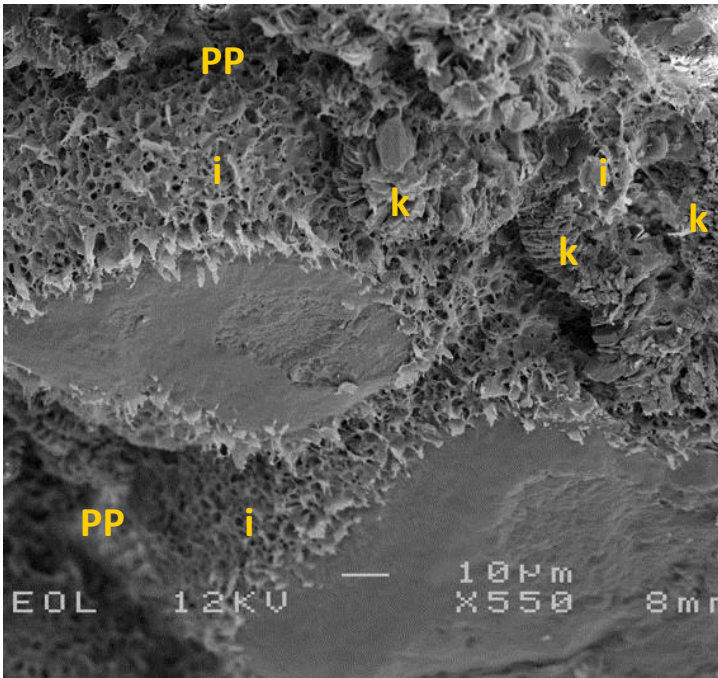
**A. Magnification 550x**

31μm
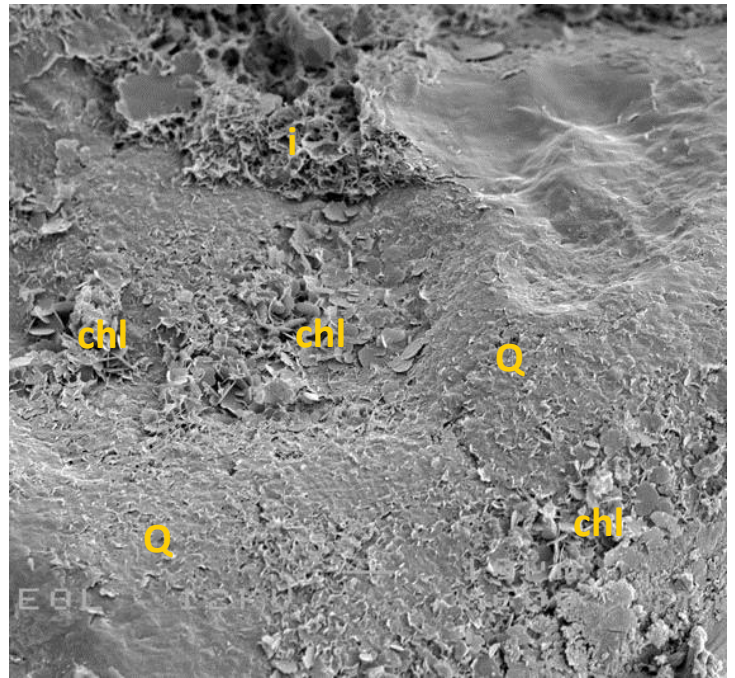


**B. Magnification 600x**

28μm
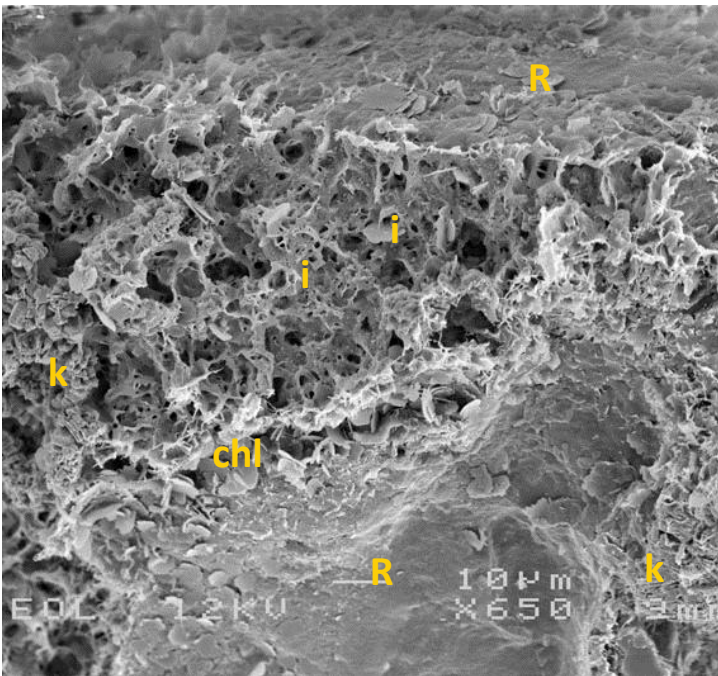


**C. Magnification 650x**

26μm
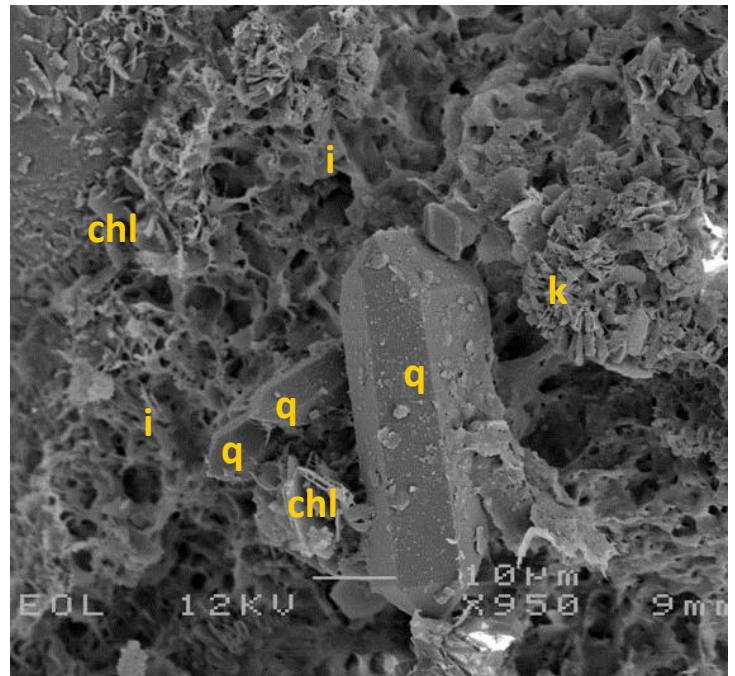


**D. Magnification 950x**

18μm

**Plate A:** Authigenic clay is common in this sample. Fibrous (illitic; i) clay coatings cover all grains and are relatively thick. Other authigenic clay visible in this field of view is booklet shaped kaolinite (k), mixed with more fibrous clay. The clay in the pore spaces (PP) does not show evidence of recent deformation as the original crystal shapes are preserved. **Plate B:** Other than the fibrous (illitic; i) clay coating visible in plate A, also authigenic chlorite (chl) locally covers the detrital grains (here quartz; Q). **Plate C:** The authigenic clay in this photo, which comprises chlorite (chl), kaolinite (k) and illite (i), has formed in such a way that locally only micropores occur (black in SEM). The permeability is therefore most likely strongly reduced. The more flat surfaces are contacts between grains, where the top grain was removed during sample preparation (R). **Plate D:** In the clay-rich (illite (i), chlorite (chl) and kaolinite (k)) intercrystalline spaces, small authigenic quartz crystals (q) formed.
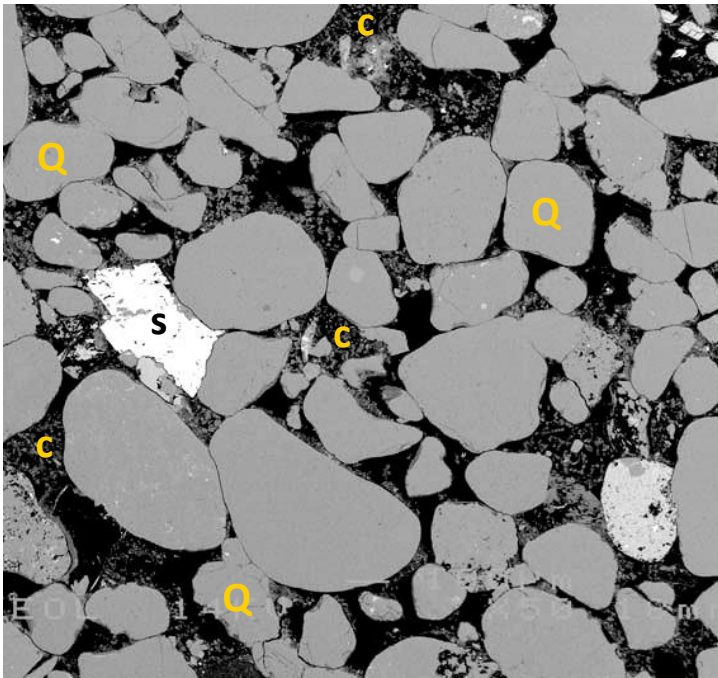
**A. Magnification 50x**

340μm
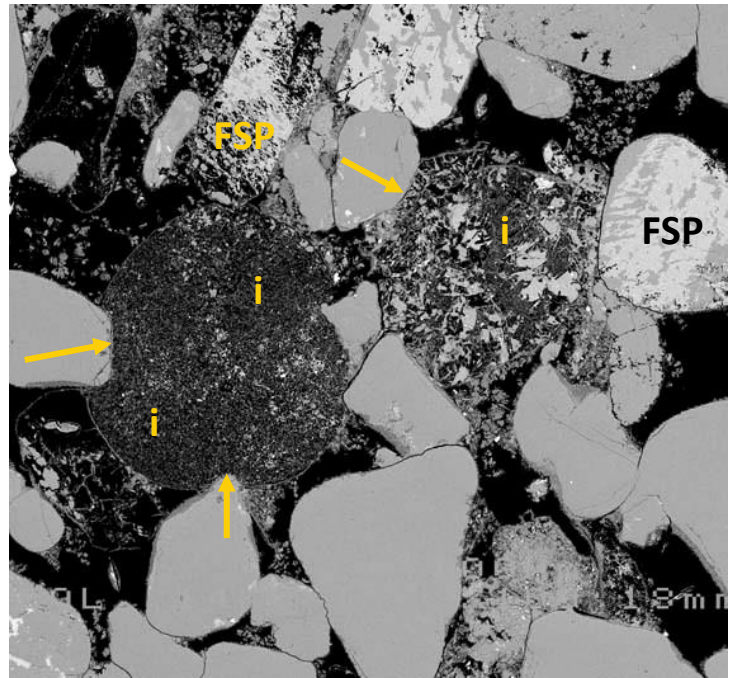


**B. Magnification 100x**

170μm
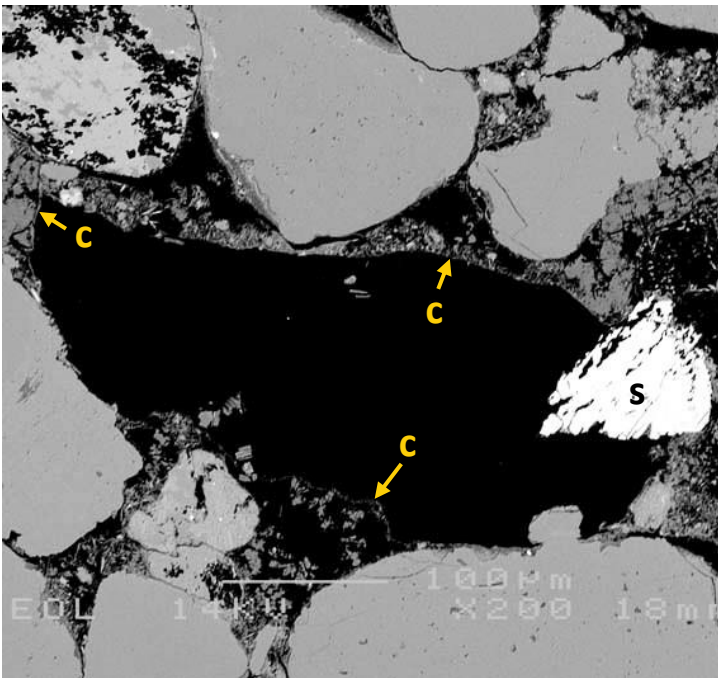


**C. Magnification 200x**
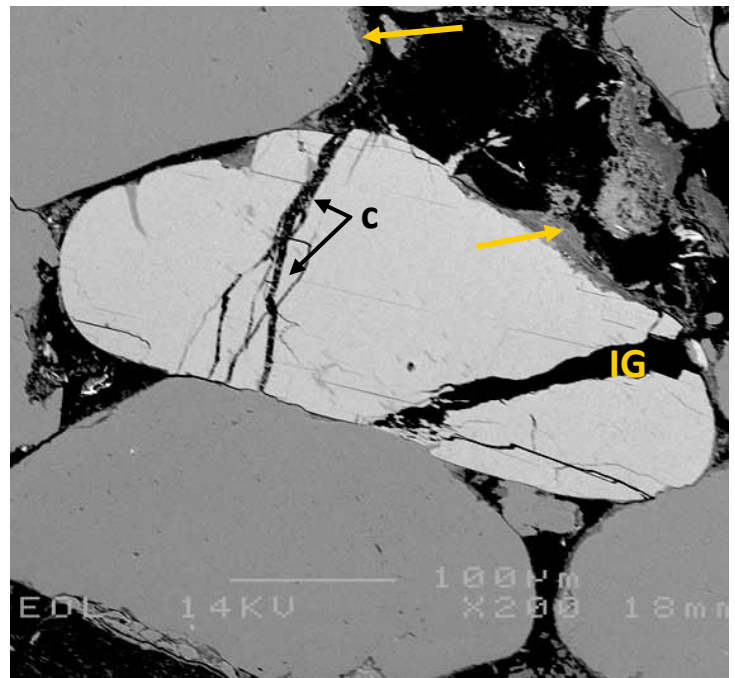
85μm



**D. Magnification 200x**

85μm

**Plate A:** Overview of the arenite, which is mainly composed of quartz grains (Q) and authigenic clay (c), including illite and kaolinite. Note the patch of siderite (s). **Plate B:** Leached grains are largely replaced by micro-crystalline illite (i). However, many feldspar grains (FSP; mixed albite (dark) and microcline (brighter)) are preserved. Note the indentations (solid yellow arrows) of the leached grain by quartz grains. **Plate C:** This mouldic pore is outlined by authigenic clay (c). The absence of clay crystals within the pore and its undeformed shape indicate that grain dissolution occurred largely after clay formation and mechanical compaction. Siderite (s) was also inhibited by the presence of a grain. **Plate D:** Fracturing of feldspar and other labile grains resulted in secondary fracture pores (IG), which may locally increase pore connectivity, although some fractures contain clay crystals (c). Note the variable thickness in clay coatings (arrows).
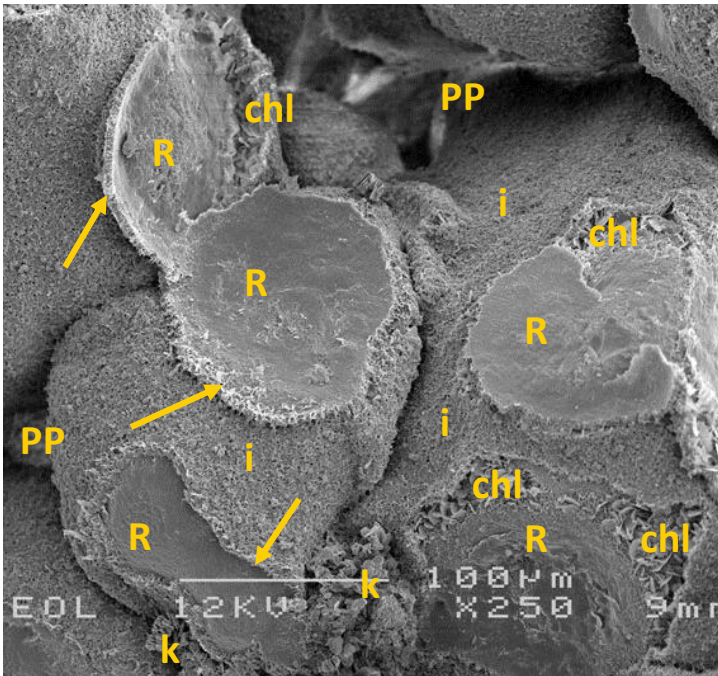
**A. Magnification 250x**
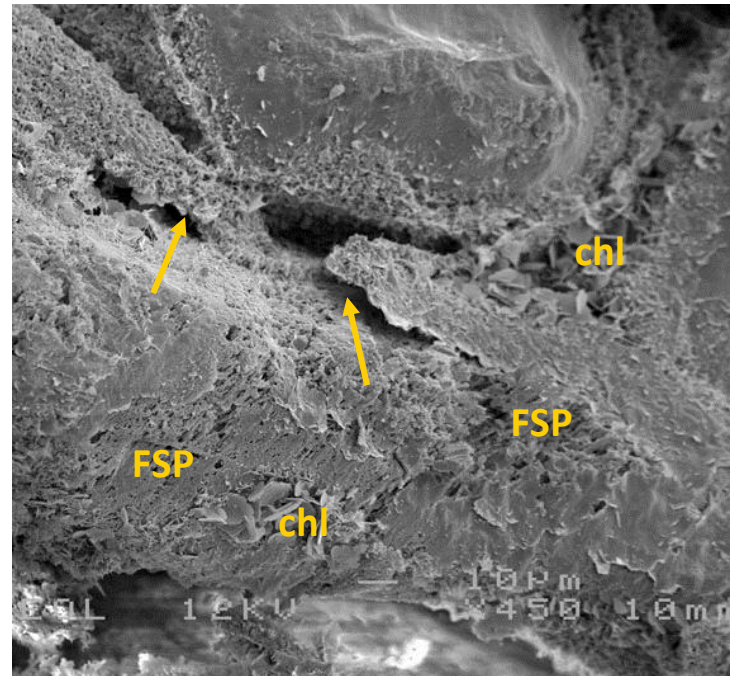
68μm

**B. Magnification 450x**

38μm
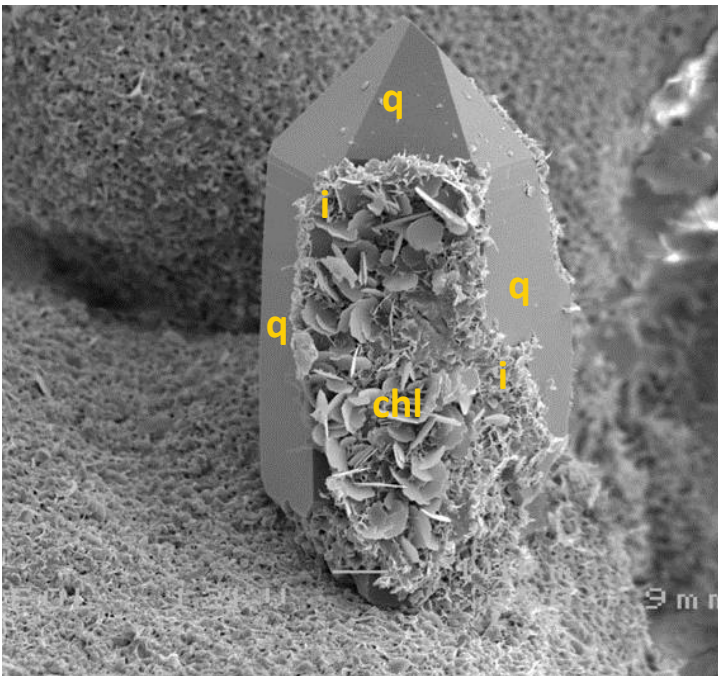
**C. Magnification 650x**

26μm
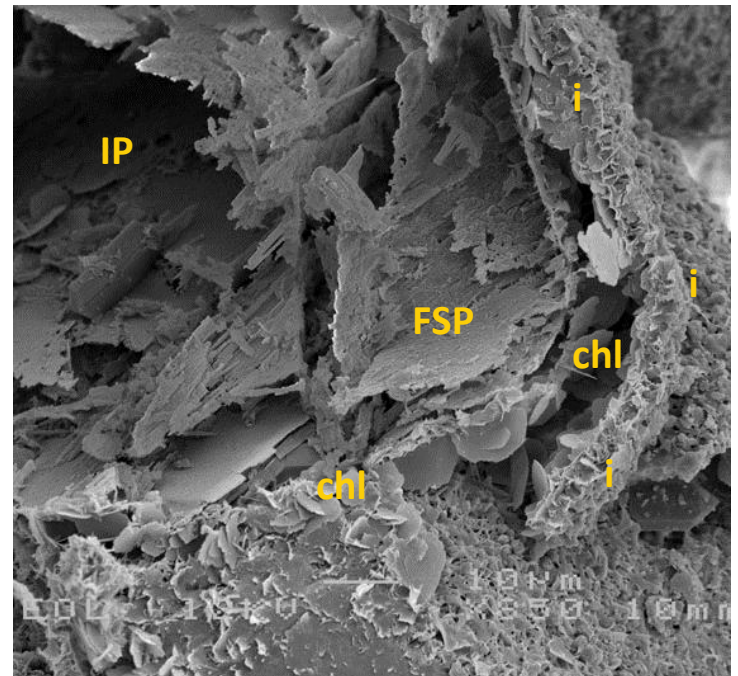
**D. Magnification 850x**

20μm

**Plate A:** This overview image clearly shows residual clay coatings from which grains were plucked (R), leaving a disrupted clay coating behind in the sample (arrows). Large intergranular pores are also very well visible here (PP). Clay coatings covering all detrital grains comprise illite (i; fine crystalline/fibrous) and chlorite (chl; rosette shaped, coarser). Locally, clustered replacive kaolinite occurs (k). **Plate B:** The authigenic illitic clay coating, covering a slightly leached feldspar (FSP) grain is separated from the detrital grain (arrow). Locally, authigenic chlorite (chl) occurs, also in between the detrital grain and the illitic clay coating. The detachment of the illite from the grain is possibly a compaction effect. The presence of chlorite in the areas between coating and grains indicates that the detachment predates chlorite formation. **Plate C:** Rarely it is visible that authigenic chlorite (chl) and finer-crystalline illite (i) cover quartz overgrowths (q), suggesting that the authigenic quartz crystal formed prior to the clay formed in a large open pore. **Plate D:** A detailed image of a nearly completely dissolved feldspar grain (FSP) covered by an illite (i) and chlorite (chl) coating. Intragranular (dissolution) pores (IP) are relatively large.
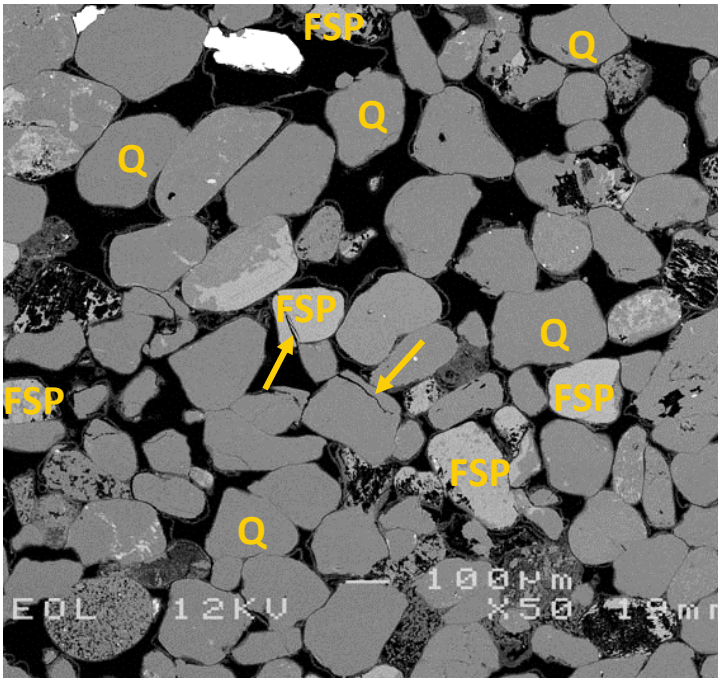
**A. Magnification 50x**
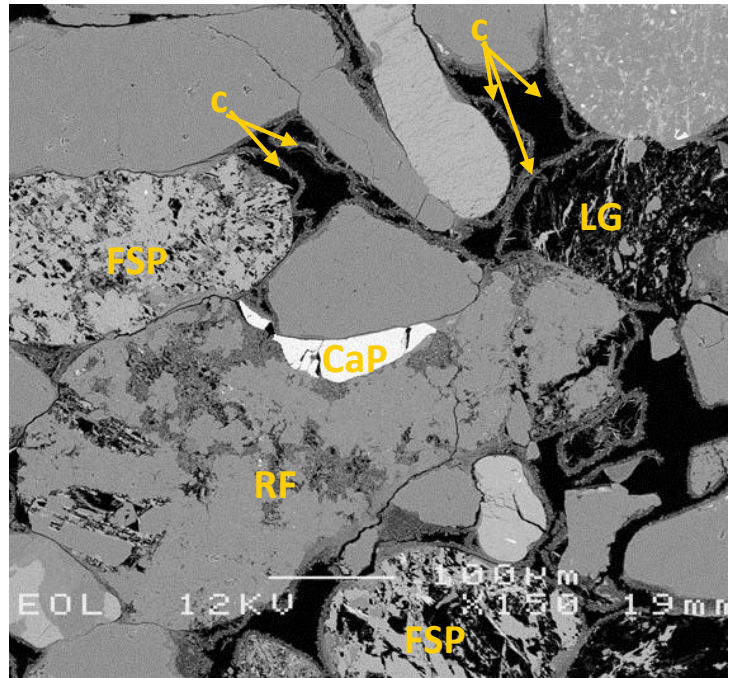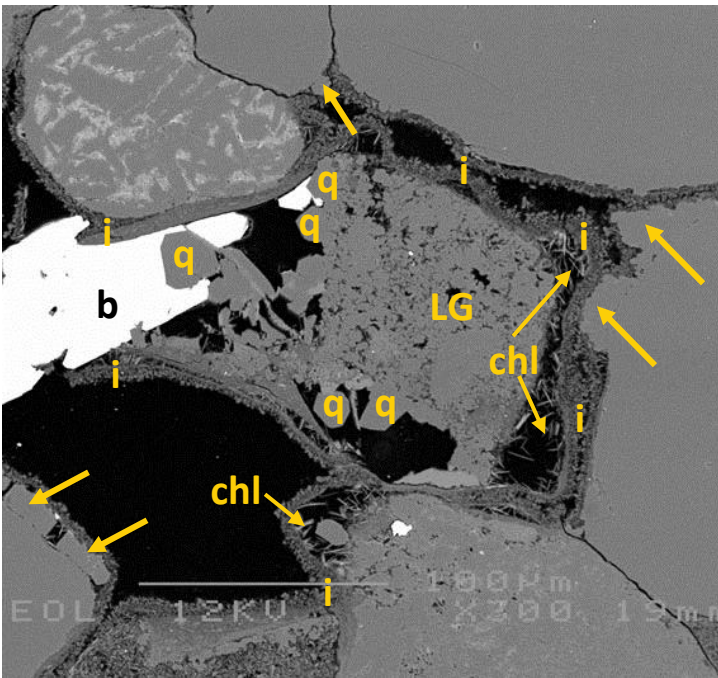
340µm



**B. Magnification 150x**

113µm



**C. Magnification 300x**

57µm
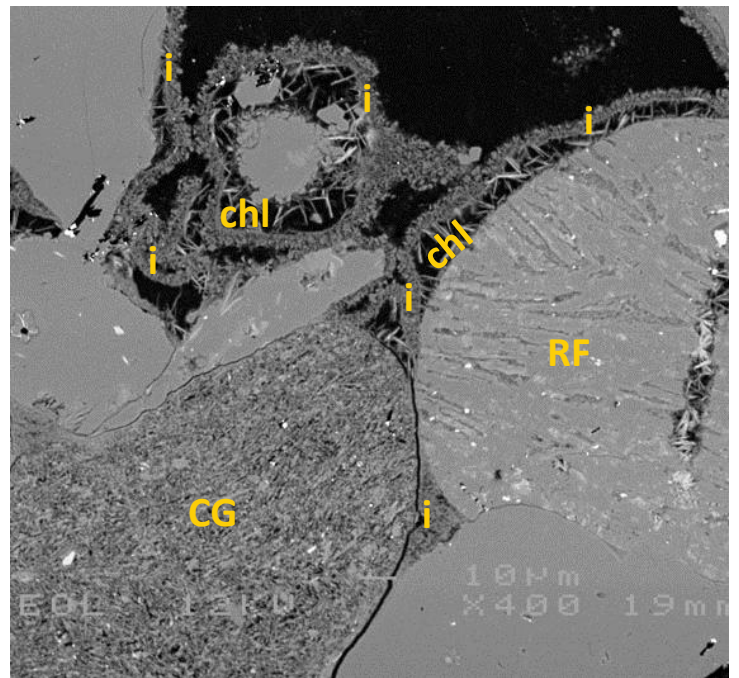


**D. Magnification 400x**

43µm

**Plate A:** This fine-grained sublitharenite contains dominantly quartz grains (Q) but also relatively common K-feldspar (slightly brighter; FSP). The porosity (black) is high in this field of view. Both a K-feldspar and a quartz grain are fractured due to compaction (arrows). **Plate B:** Both porous (leached) rock fragments (RF) and feldspar grains (FSP) are deformed due to compaction. The more strongly leached feldspar grains (LG) are not further deformed. Note the relatively thick and commonly detached illite-chlorite rims (c) and the calcium phosphate cement (apatite?; CaP). **Plate C:** The central part of this photo shows a leached grain (LG) with significant quartz (q) cement. The original grain is outlined by the thick illite (i) chlorite (chl) clay coating. Note the quartz overgrowths (arrows) that have formed in the places where the clay coating is detached. Barite (b) has formed after the quartz cement. **Plate D:** Relatively coarse crystalline chlorite in between the radial illite coating (i) and the detrital grains. These detrital grains include rock fragments (RF) and clay-rich grains (CG).
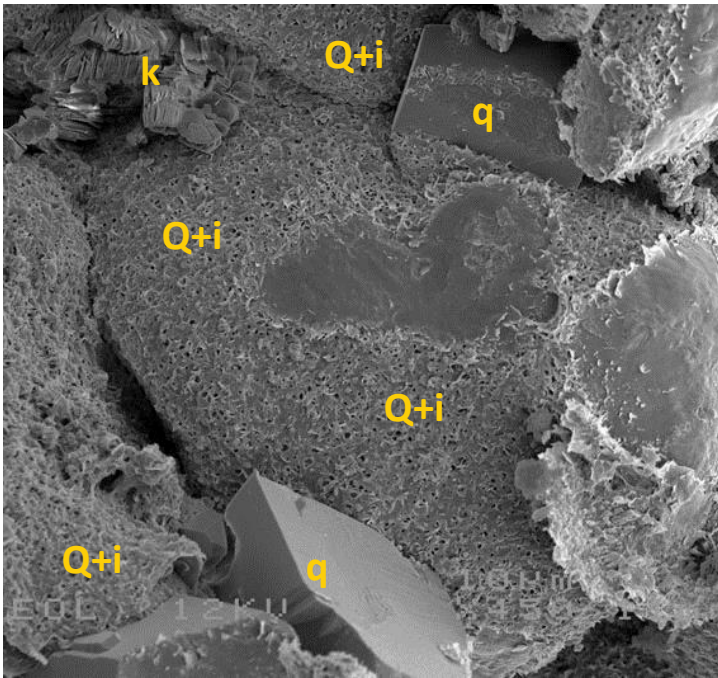
**A. Magnification 450x**

38µm
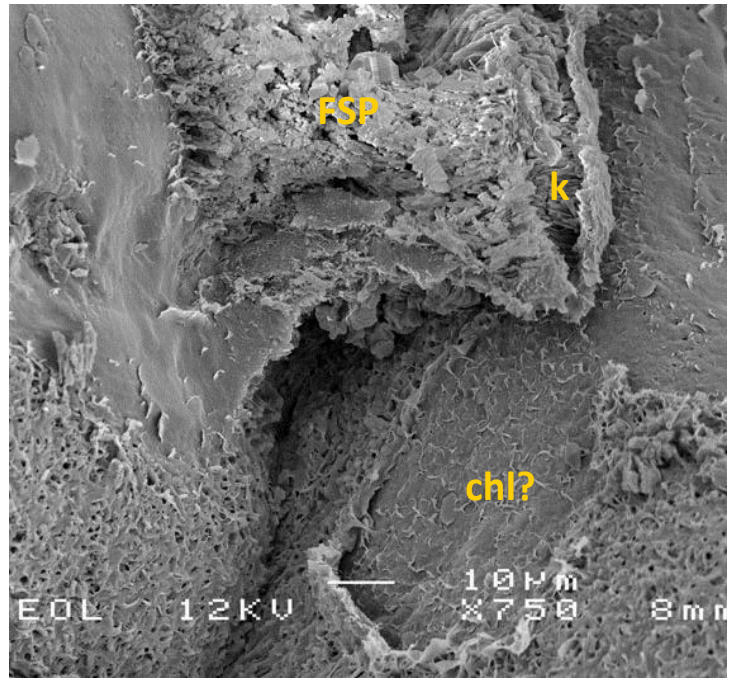


**B. Magnification 750x**

23µm
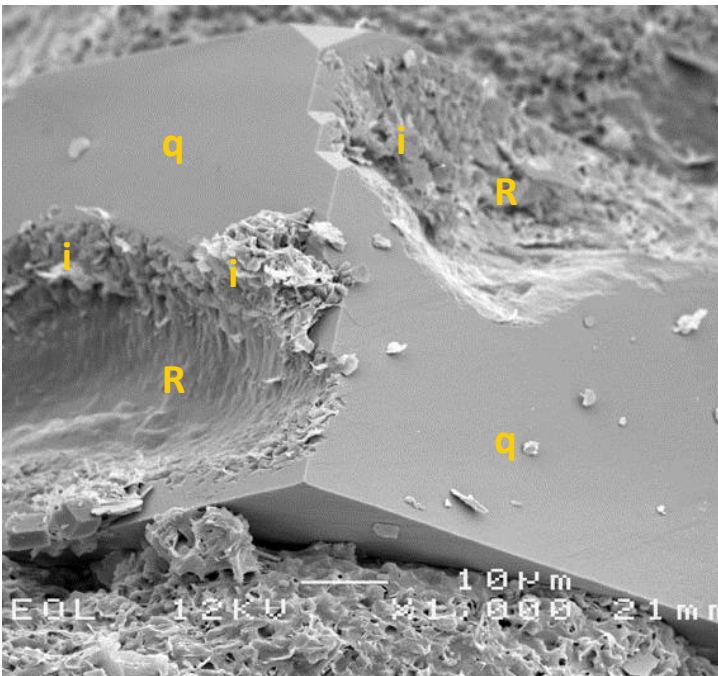


**C. Magnification 1000x**
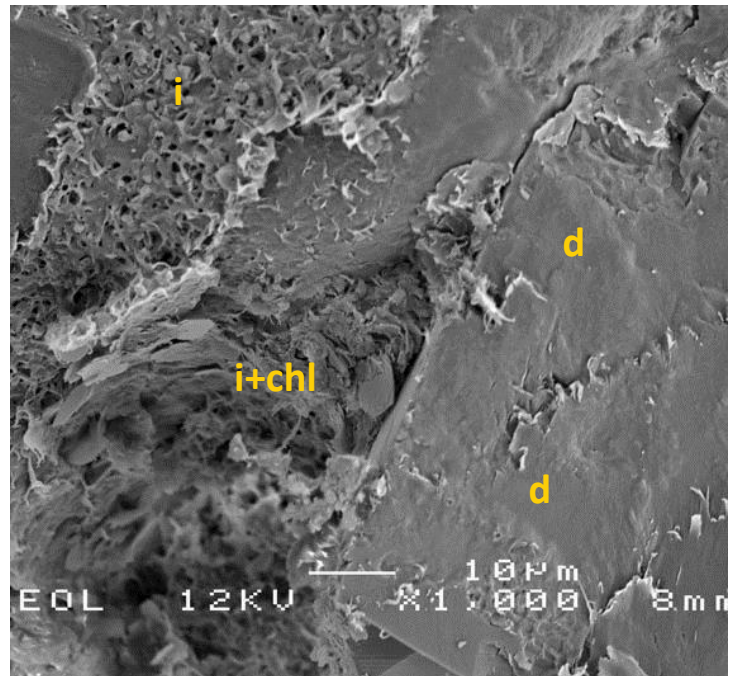
17µm



**D. Magnification 1000x**

17µm

**Plate A:** Authigenic illitic clay coatings are covering the detrital quartz grains (Q+i) and authigenic quartz (q) outgrowths locally form large euhedral crystals. In this field of view, the authigenic quartz has filled a substantial volume of the large pores. Authigenic kaolinite booklets (k) occur as well in this sample. **Plate B:** The top of the image shows a leached feldspar (FSP) which now comprises kaolinite (k). Even though most grain contacts are free of clay, sometimes a thin layer of possibly chlorite (chl?) is suggesting (tangential?) authigenic clay has formed prior to complete mechanical compaction. **Plate C:** This image shows imprints of two grains which were removed during sample preparation (R). During diagenesis, authigenic quartz (q) overgrowths are partially engulfing two plugged grains (R). Note the remaining clay coating (i) at the edges of where the grain used to be, showing that the coating predates quartz cement. **Plate D:** The microstructure of illitic clay coatings (i) differs from authigenic clay (illite) that resulted of grain leaching. The latter contains more randomly distributed illite+chlorite (i+chl). Locally, euhedral pore-filling dolomite (d) occurs.
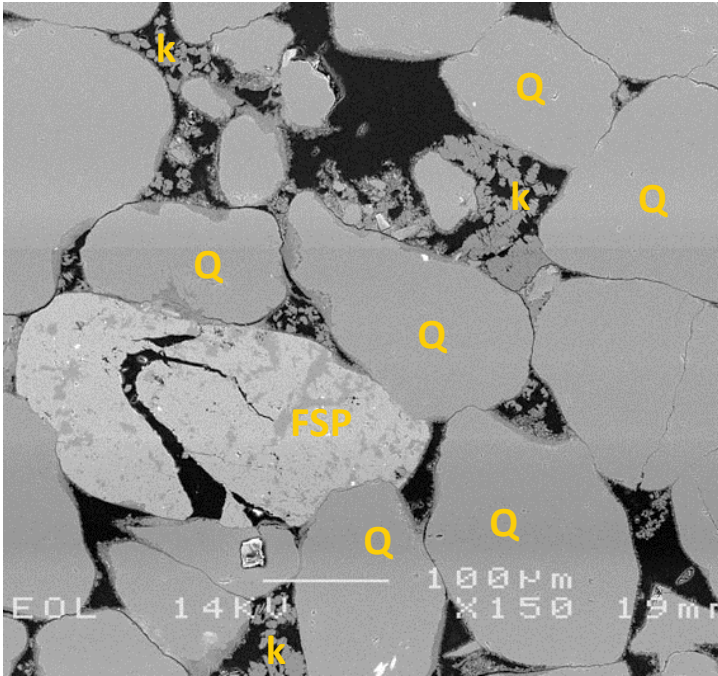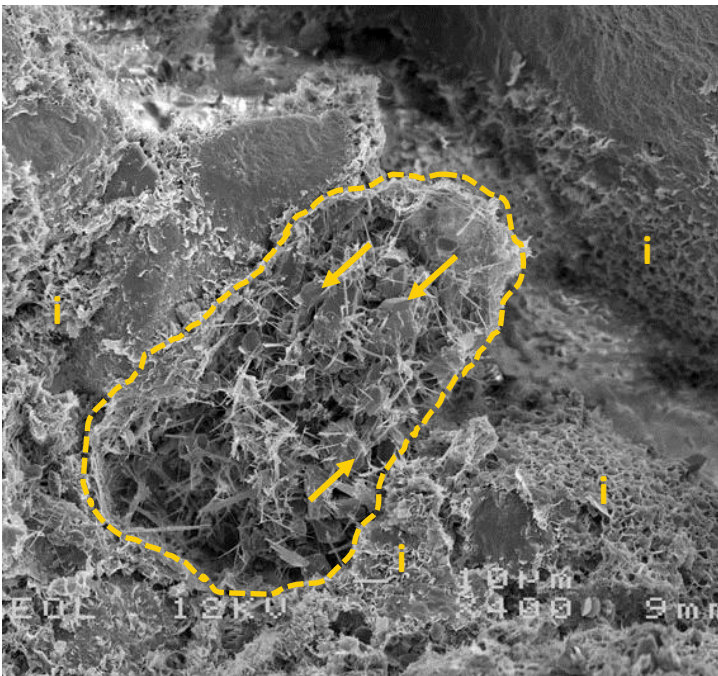
**A. Magnification 150x**
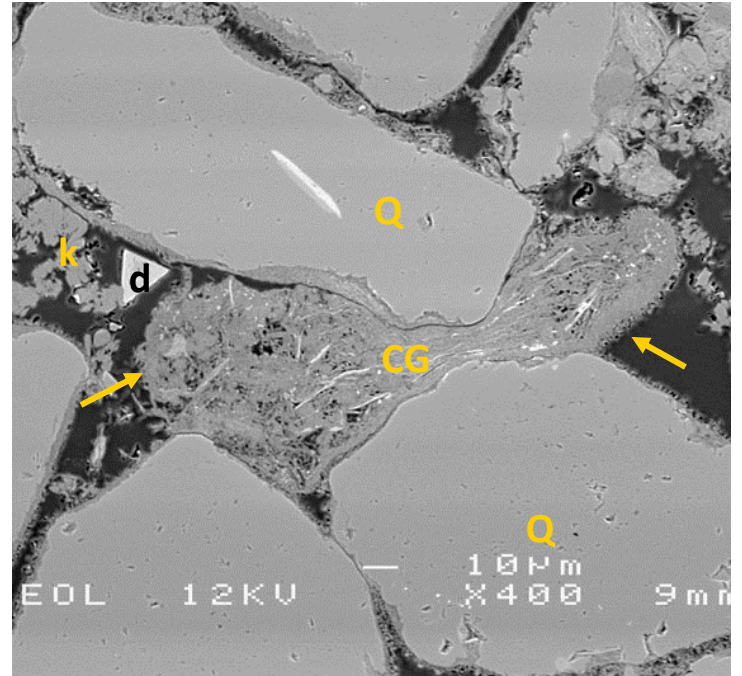
113µm



**B. Magnification 400x**

43µm
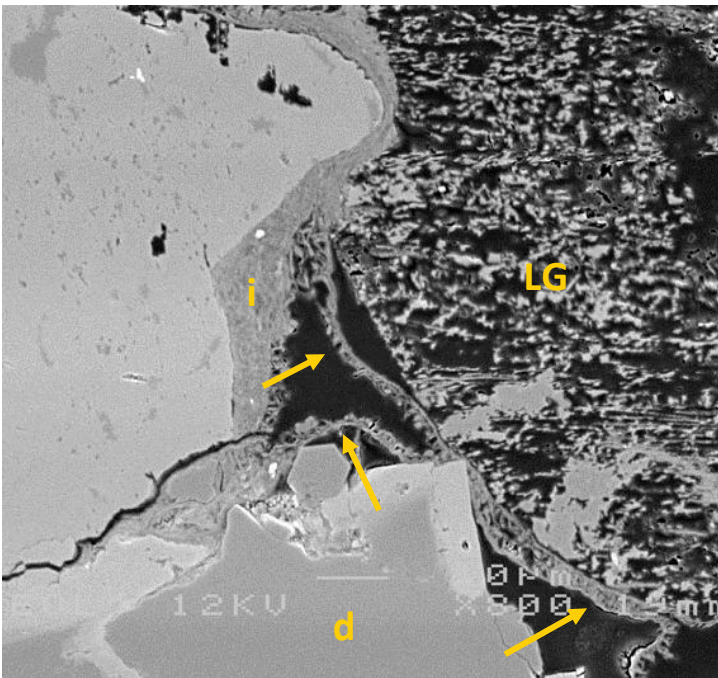


**C. Magnification 800x**

21µm
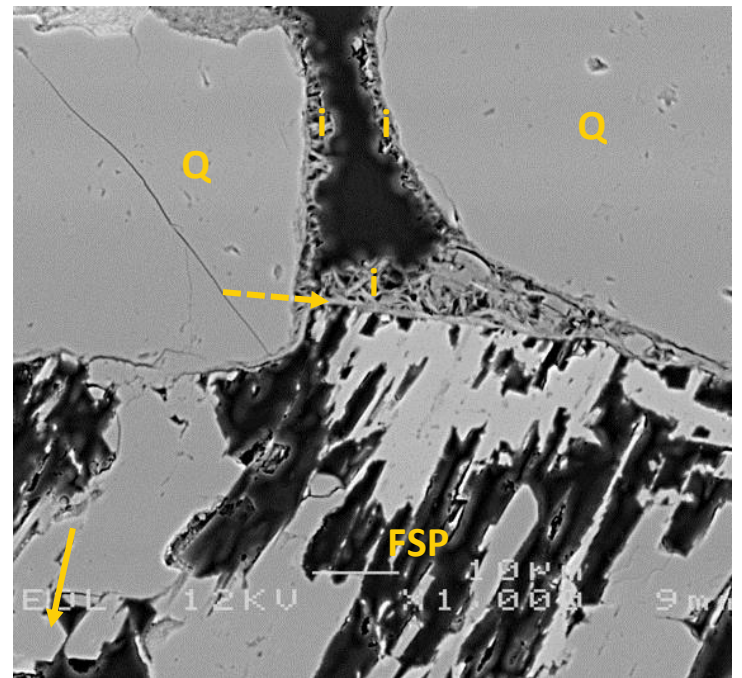


**D. Magnification 1000x**

17µm

**Plate A:** The feldspar grain (FSP; here K-feldspar) in this sublitharenite is broken due to compaction. The quartz grains (Q) are mostly unaffected. Kaolinite (k) occurs in clusters in between the quartz grains. All detrital grains have a thin continuous clay coating. **Plate B:** The clay-rich grain (CG) in the centre is squeezed in between quartz grains (Q) due to compaction. This clay-rich grain also has a thin radial clay coating (arrow). Note the euhedral authigenic dolomite crystal (d) next to vermicular kaolinite (k). **Plate C:** The thickness of the clay coating varies strongly. In the concave areas of a grain, thick tangential illite has formed (i), whereas in the convex areas, less clay occurs. Note the continuous, detached clay rim (arrow) next to the leached feldspar grain (LG) and the euhedral dolomite (d; present in a leached grain). **Plate D:** Detailed photo showing radial illite (i) covering both quartz grains (Q) and a leached feldspar grain (FSP). The brighter part of the feldspar is K-feldspar whereas the darker part (equal to quartz) is albite. Some of the feldspar might be authigenic as can be inferred from euhedral crystal shapes (arrow). Note the thin tangential illite rim (dashed arrow).
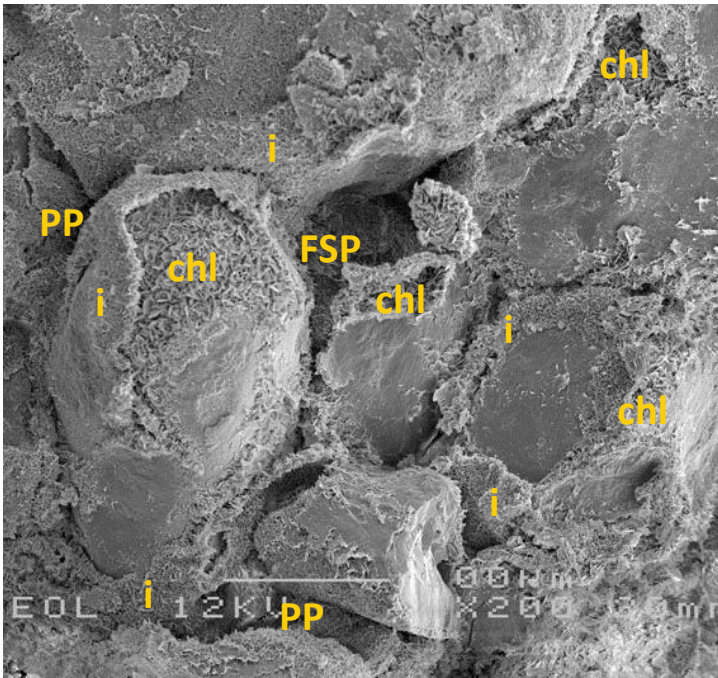
**A. Magnification 200x**

85µm
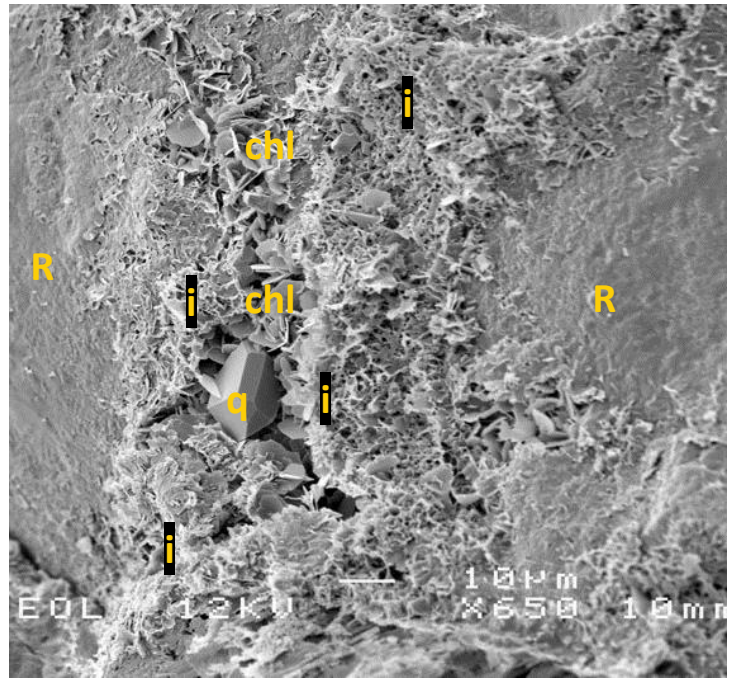


**B. Magnification 650x**

26µm
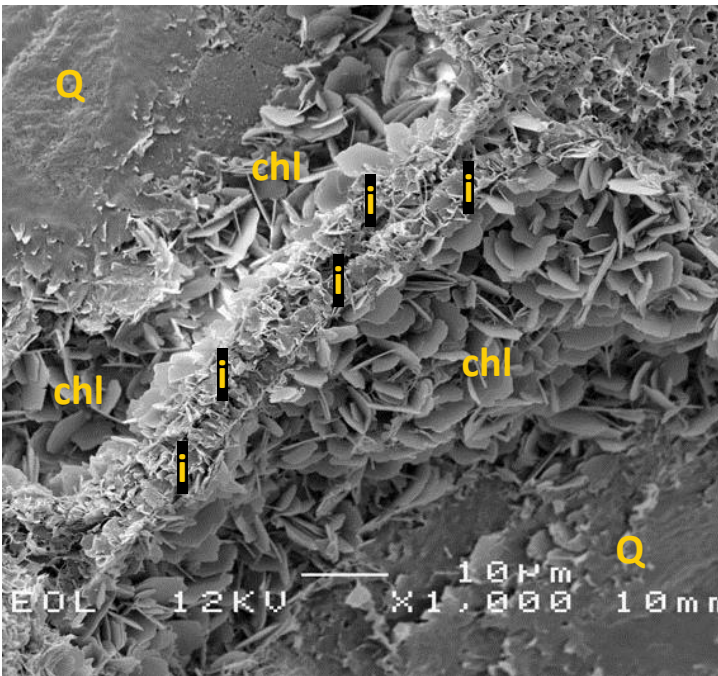


**C. Magnification 1000x**

17µm
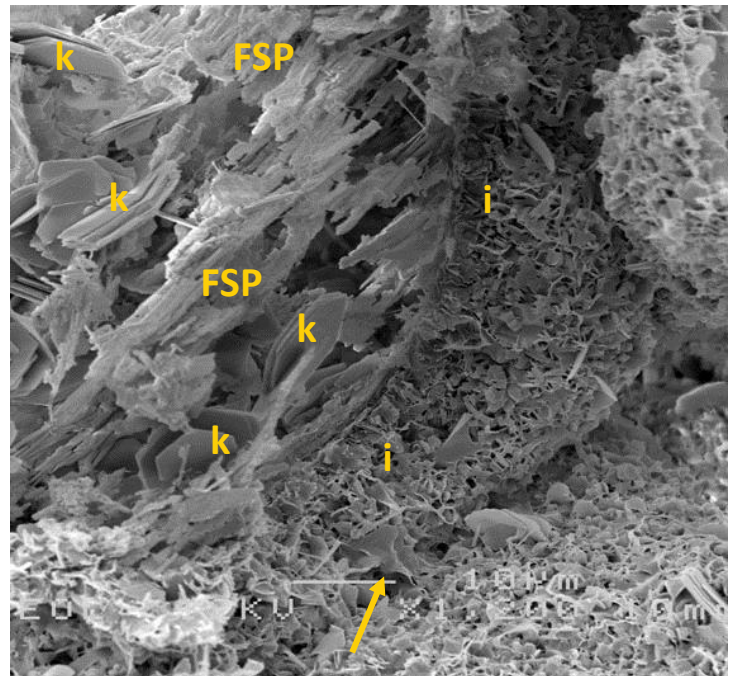


**D. Magnification 1200x**

14µm

**Plate A:** This poorly sorted, fine-grained sandstone has thick clay coatings covering the detrital grains. These clay coatings comprise rosette-shaped chlorite (chl) covered by more dense, very fine crystalline illite fibres (i). Even though the clay coatings reduce pore diameter, intergranular pores (PP) remained relatively large. Note the large pore, which is partially filled with leached feldspar (FSP). **Plate B:** Two grain contacts with plucked grains (R) are shown here. The former grain contacts are characterised by freely grown clay, comprising illite (i) on the outer rim, and chlorite (chl) in the centre. Note the euhedral quartz overgrowth (q). **Plate C:** This detailed image shows a rosette-shaped chlorite (chl) coating in contact with the detrital quartz (Q). Two thin (<5 µm) layers of tangential illite (i) coating are visible in the centre of the image. **Plate D:** Leached feldspar is best identified by the fibrous nature of the remaining feldspar (FSP). At the expense of the original feldspar, authigenic kaolinite (k) has formed. An illite rim (i) has formed around the feldspar grain, being similar to the grain coatings covering the quartz grains. Note that this illite is locally pore-bridging (arrow).
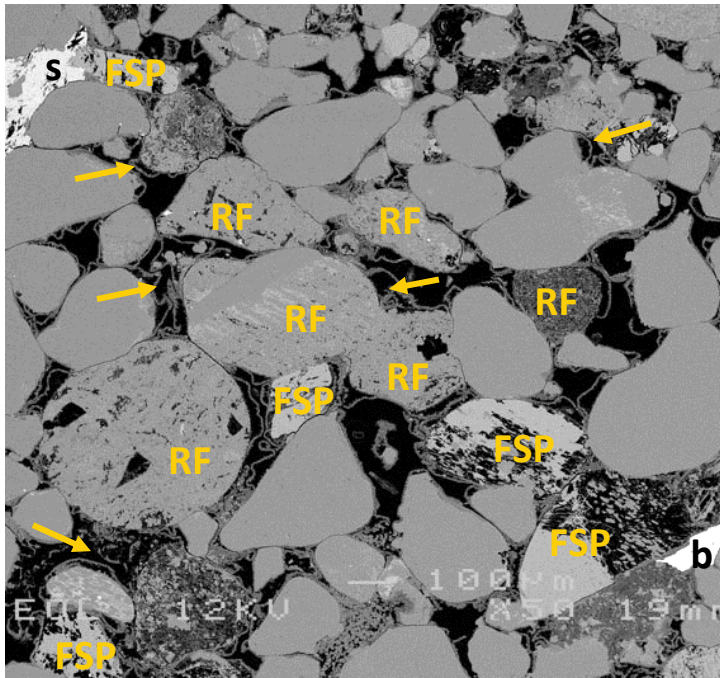
**A. Magnification 50x**
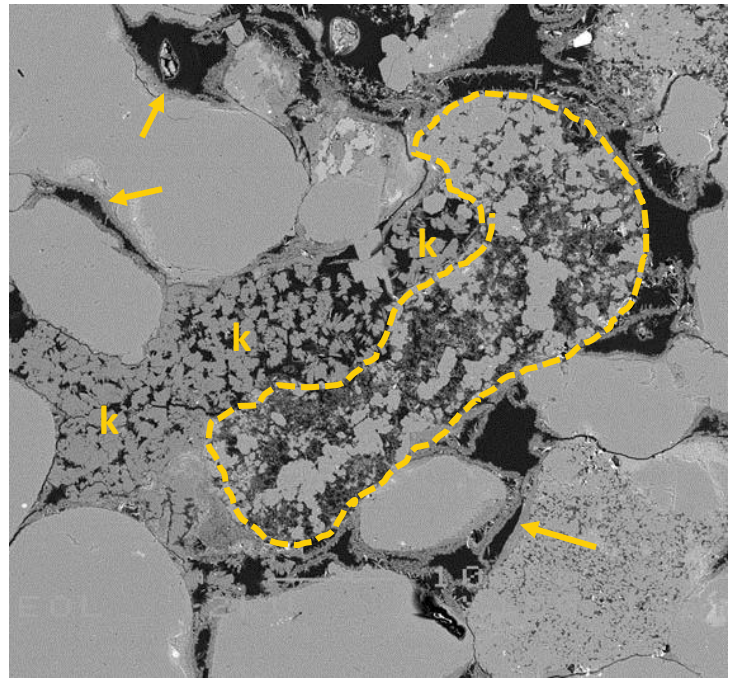
340µm

**B. Magnification 150x**

113µm
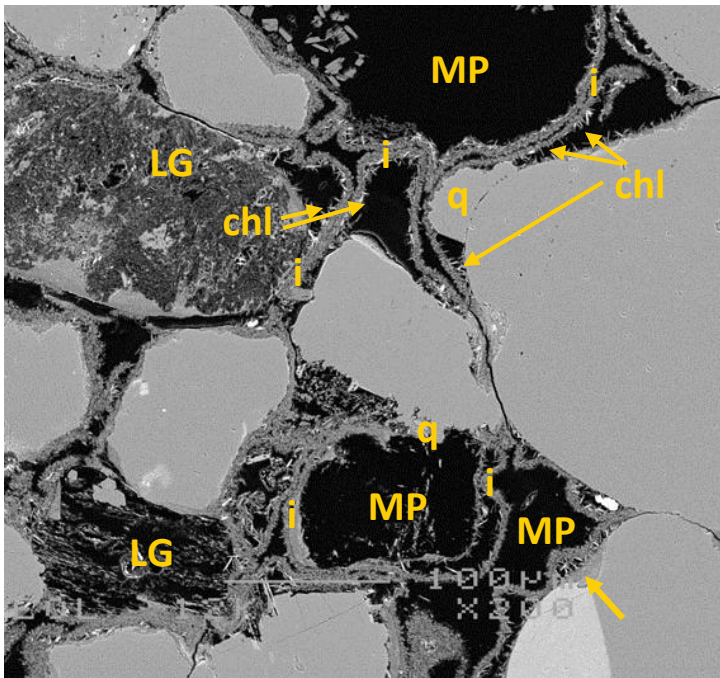
**C. Magnification 200x**

85µm
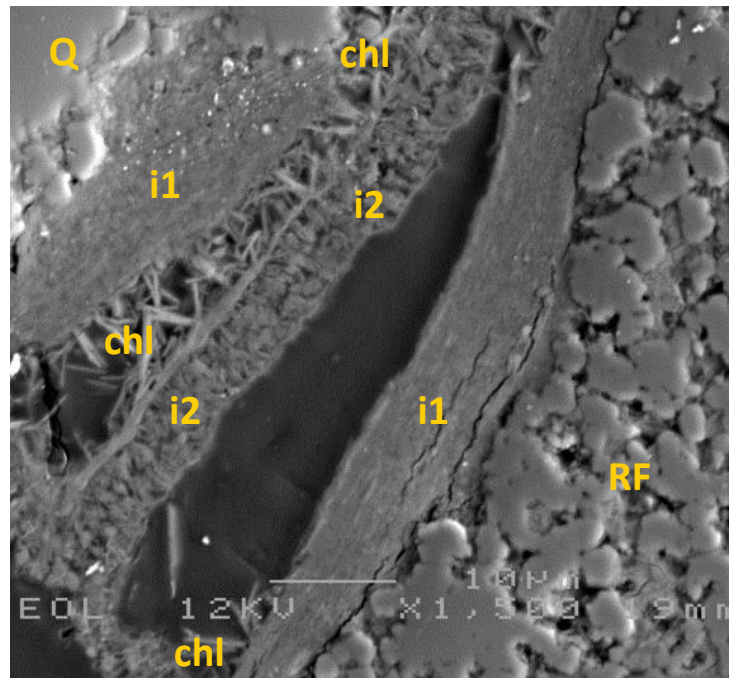
**D. Magnification 1500x**

11µm

**Plate A:** The rock fragments (RF) and K-feldspar grains (FSP) in this sublitharenite are often partially to strongly leached. Grain coatings, which are very thick, are commonly detached from the grains (arrows). Note that the clay coatings are mostly absent in between the rigid grains, indicating these have formed after (main) compaction. Locally, barite (b) and siderite (s) are present. **Plate B:** A leached and replaced (with quartz) detrital grain (dashed outline) is strongly deformed and occurs next to a large cluster of authigenic kaolinite (k). The kaolinite cluster (which replaced a detrital grain) is deformed, indicating that the kaolinite formed prior to maximum compaction. Clay coatings are locally very thick, especially in the concave areas of a grain (arrows). Around the kaolinite cluster, a clay coating could not be identified. **Plate C:** Multiple mouldic pores (MP) and strongly leached grains (LG) are outlined by thick clay coatings. This clay coating comprises tangential illite (arrow) in the concave areas, coarser crystalline chlorite (chl) and radial illite (i). Note the quartz cement that has formed in between the grains and the detached clay rim (q). **Plate D:** This high magnification image (taken with the SE detector) shows the details of the complex clay rims, including tangential illite (i1), radial illite (i2) and chlorite (chl), covering a rock fragment (RF) and a quartz grain (Q).
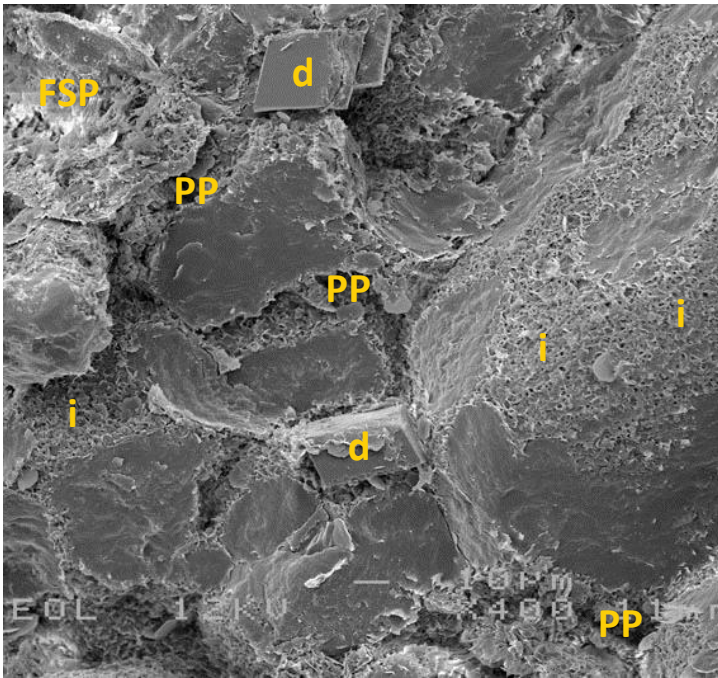
**A. Magnification 400x**

43μm
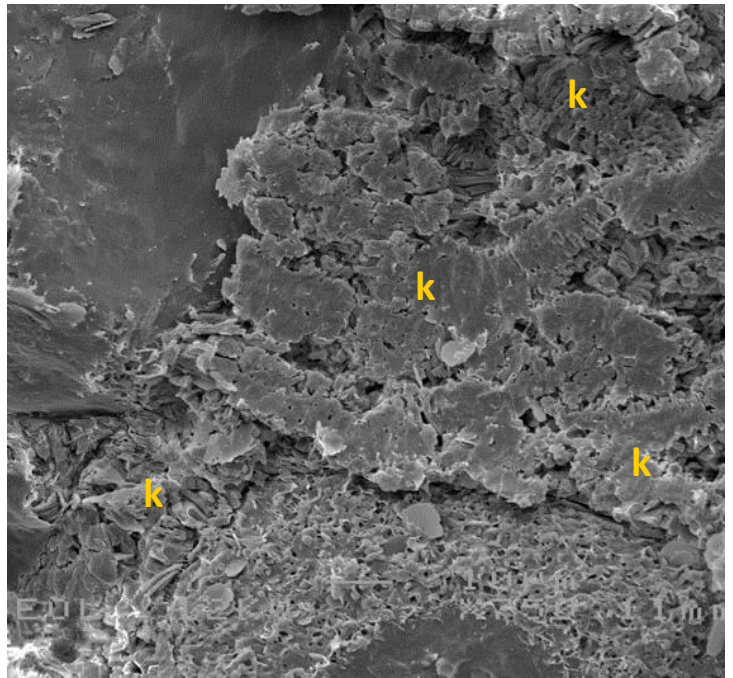


**B. Magnification 750x**

23μm
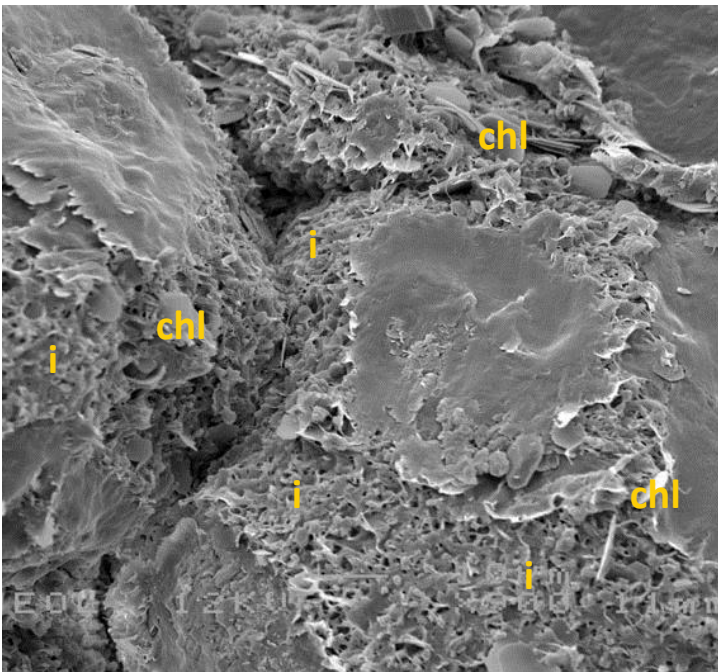


**C. Magnification 900x**

19μm
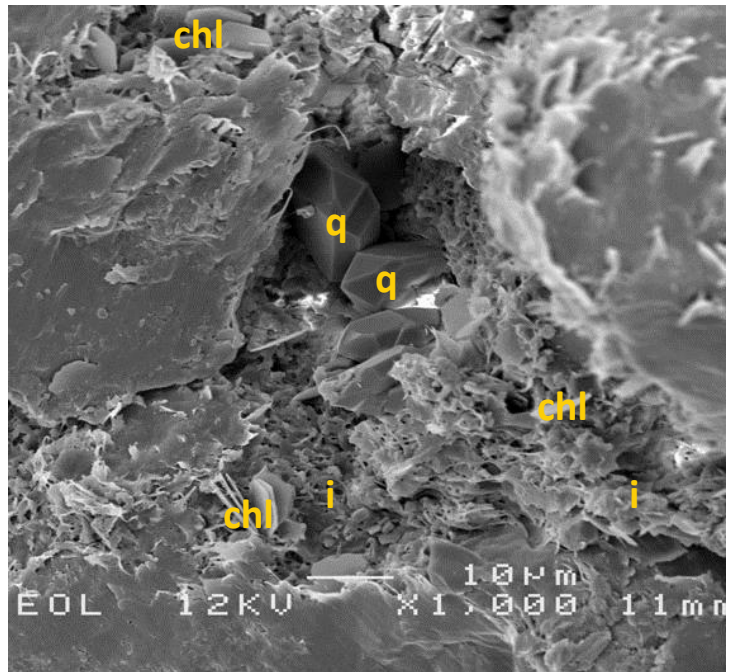


**D. Magnification 1000x**

17μm

**Plate A:** Overview photo of this poorly sorted sandstone, showing the small intergranular pores (PP). Sparse to common euhedral intergranular dolomite (d) formed, locally fixing the grain framework. Note the moderately leached feldspar (FSP) and the illitic clay coatings (i). **Plate B:** The kaolinite (k) in this photo has a flat surface as it was in contact with a (now plucked) grain. The micropore distribution in between the kaolinite platelets is well visible and shows that pore connectivity is poor. **Plate C:** Detailed view of several grains that are in contact with each other. The illitic clay coating (i) locally also contains chlorite (chl). There is no deformation of the coatings in between the grains and hence no evidence for compaction after the formation of the clay coatings. **Plate D:** Small authigenic quartz outgrowths (q) formed in the intergranular pore spaces. The white spots is due to artificial charging of the sample within the pore. Authigenic clay is a combination of chlorite (platy; chl) and illite (fibrous; i), with the chlorite being relatively coarse crystalline.
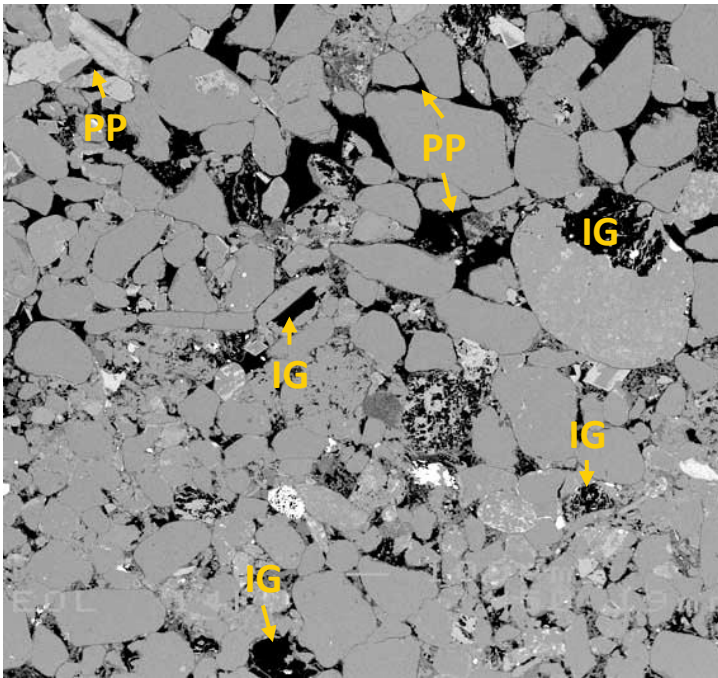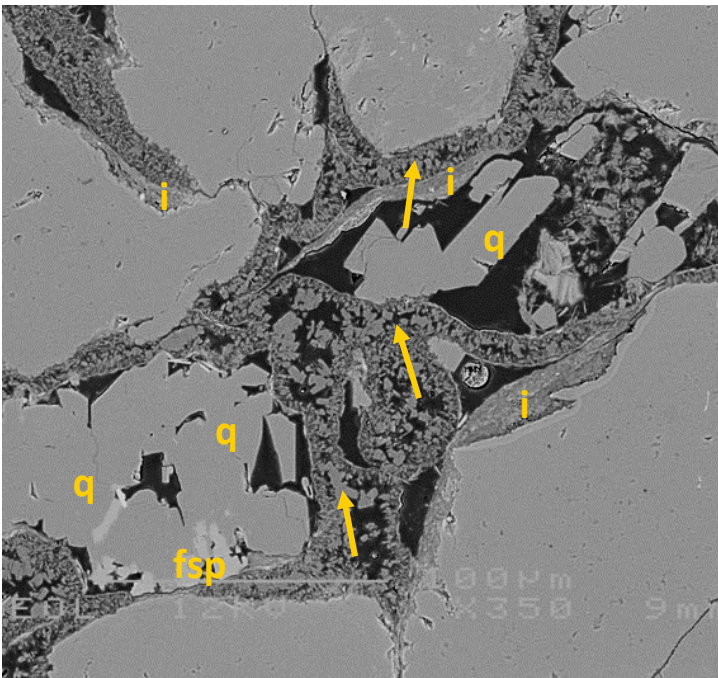
**A. Magnification 50x**

340µm
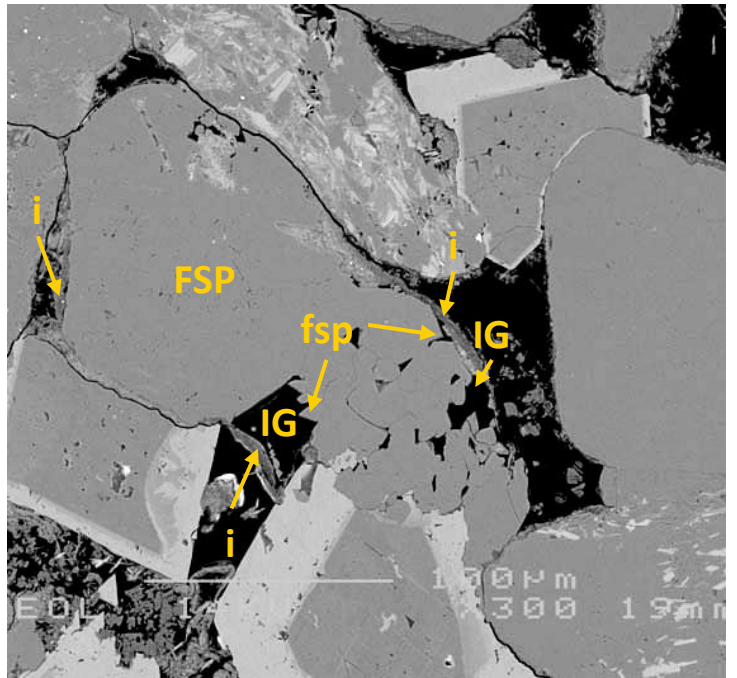
**B. Magnification 300x**

57µm
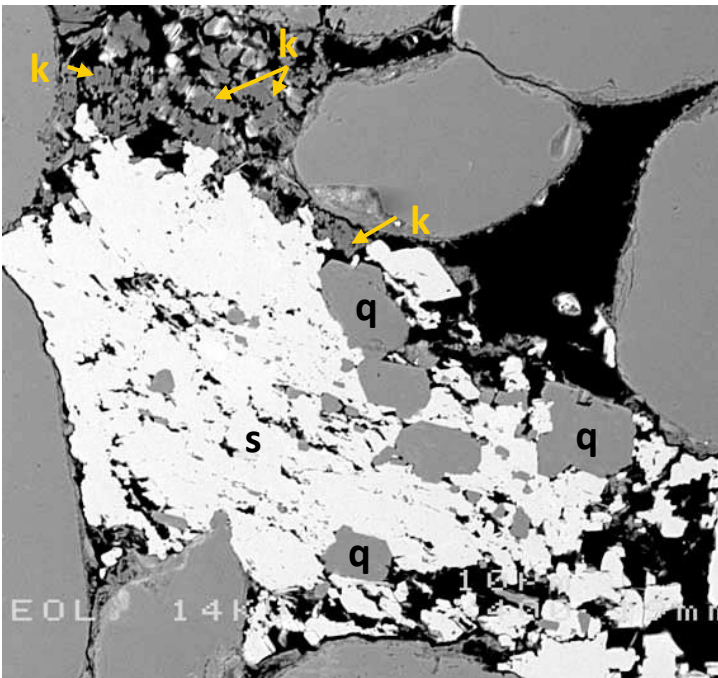
**C. Magnification 400x**
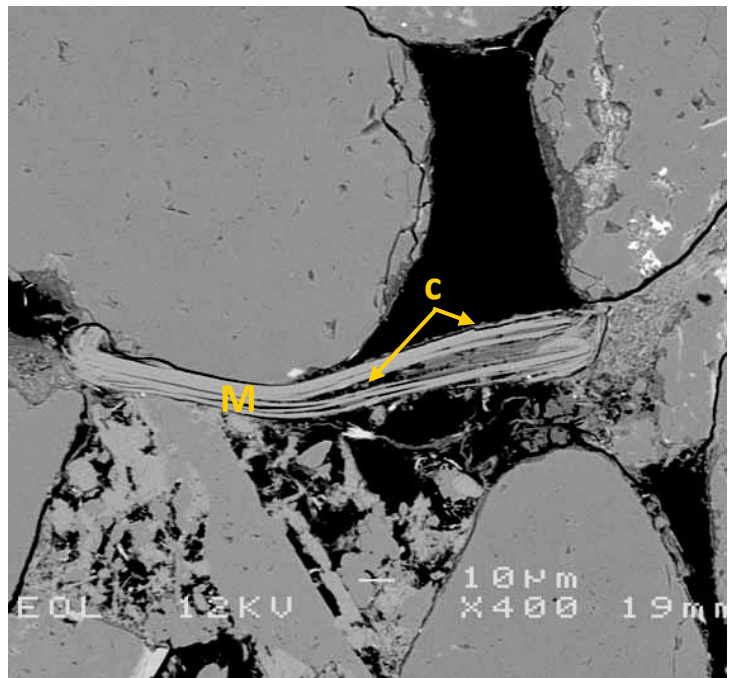
43µm

**D. Magnification 400x**

43µm

**Plate A:** The sublitharenite consists of medium-grained laminae (top) and fine-grained laminae (bottom). The medium-grained laminae contain both intergranular (PP) and secondary intragranular pores (IG), whereas fine-grained laminae contain mainly intragranular pores. **Plate B:** Within the fine-grained laminae, grain dissolution and authigenic mineral precipitation strongly altered the pore structure. The elongate sand grain in the centre of the image (indicated by tangential clay coating; i) is composed mainly of albite (FSP), but also shows intragranular pores (IG) as well as authigenic albite (fsp). Dolomite rhombohedra (d; ferroan towards the outside margin) fill intergranular and intragranular pores. **Plate C:** This oversized pore is filled by kaolinite (k), euhedral quartz (q) and later diagenetic siderite (s). The crystals replaced a detrital grain. Note that clay rims in this field of view are thin. **Plate D:** Particularly in the fine-grained laminae, a higher degree of mechanical compaction is indicated by deformed ductile grains such as this mica flake (M). A thin layer of authigenic clay coating (c) is developed at the grain surface and between the cleaved sheets of the grain.
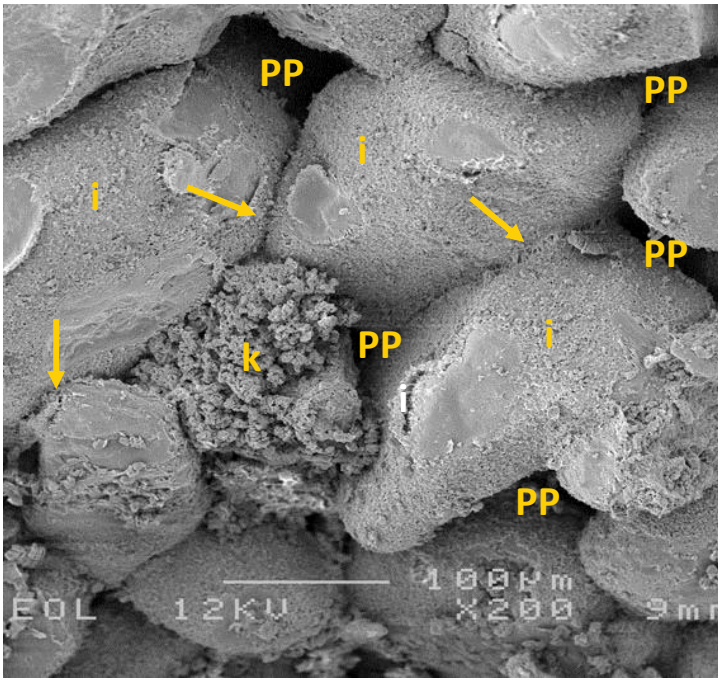
**A. Magnification 200x**
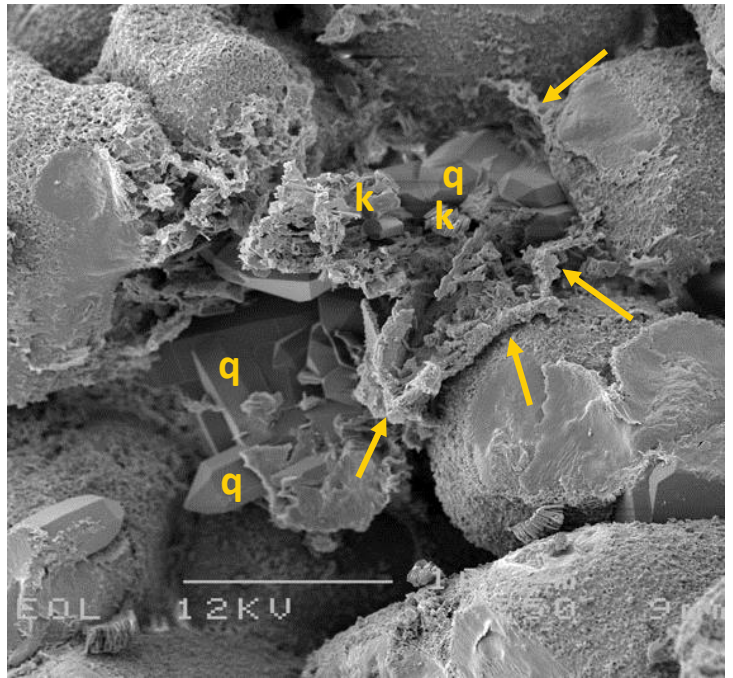
85µm



**B. Magnification 250x**
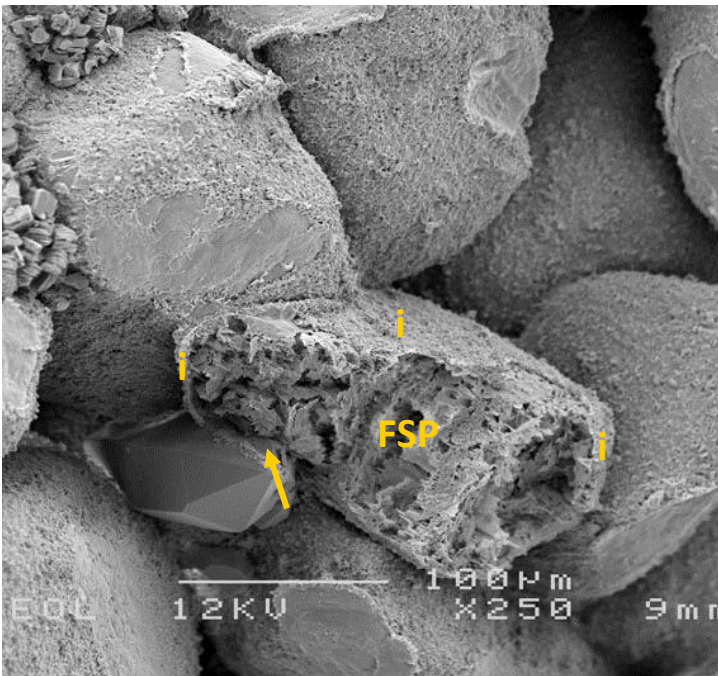
68µm



**C. Magnification 250x**

68µm
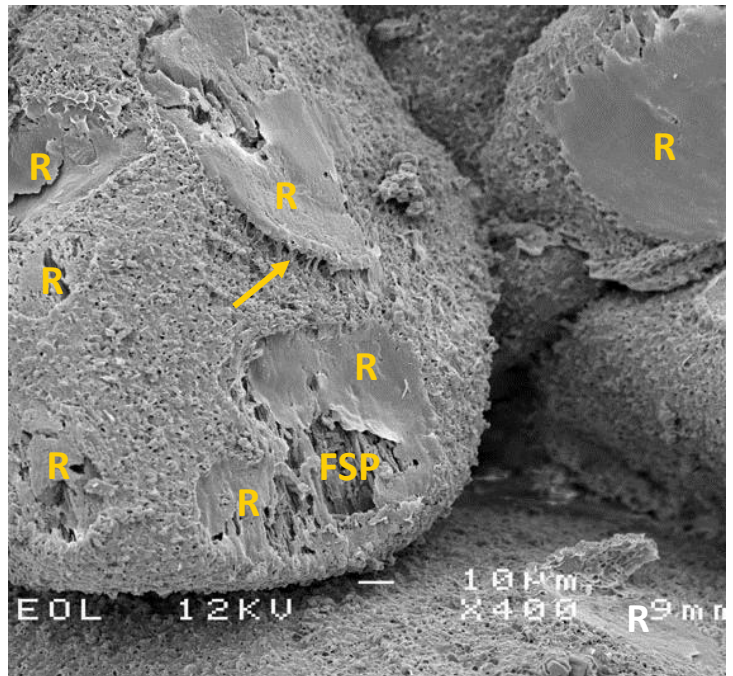


**D. Magnification 400x**

43µm

**Plate A:** This fine grained (U) sandstone is fragile due to the lack of common cementing phases. Intergranular pores (PP) are large and well connected. The detrital grains are covered with a continuous coating of fibrous illite (i), which is locally pore bridging (arrow), especially at pore throats. Replacive authigenic kaolinite (k) shows the approximate original shape of the replaced grain. **Plate B:** Remains of an authigenic clay rim (arrow) reveal that this patch is a leached grain which has been replaced by kaolinite (k) and quartz (q). **Plate C:** Feldspar is (according to XRD) common in this sample, and often strongly leached (FSP). The authigenic clay coating (i) is however continuous. Note how quartz cement overgrew this clay coating (arrow), forming both outside and within the coating. The leached feldspar grain is, despite the strong leaching, undeformed. **Plate D:** Several imprints of plucked grains are visible (R), revealing the slightly leached nature of the feldspar (FSP). Locally, some clay rims of the plucked grains remain, showing that the fibrous illite is pore bridging near the contacts (arrow).
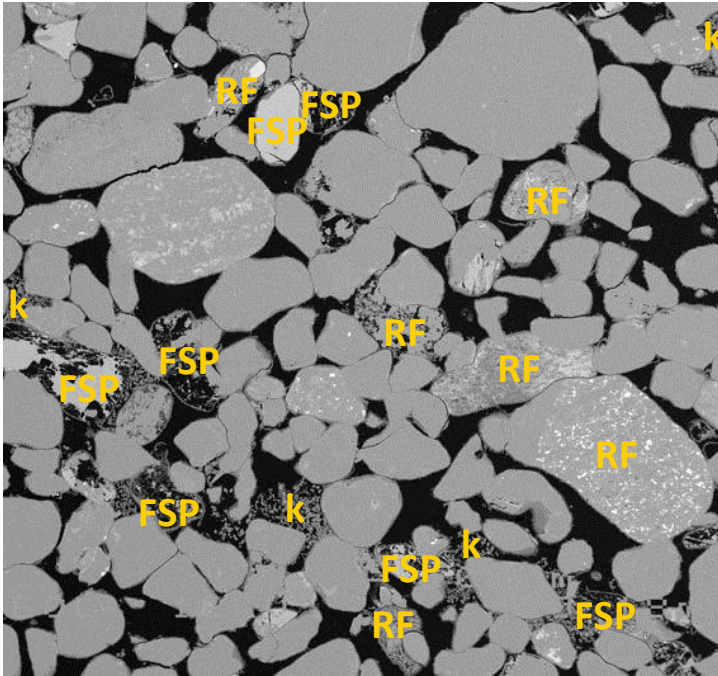
**A. Magnification 50x**

340µm
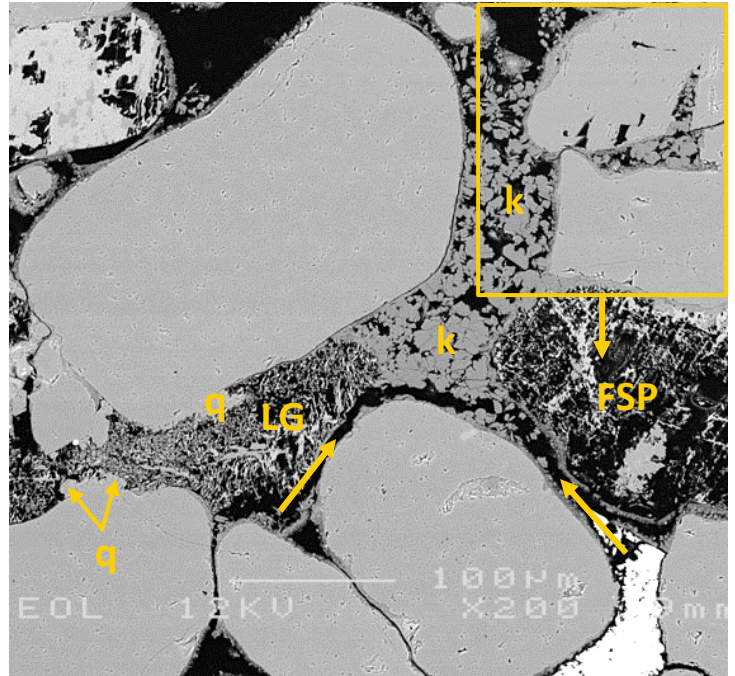
**B. Magnification 200x**

85µm
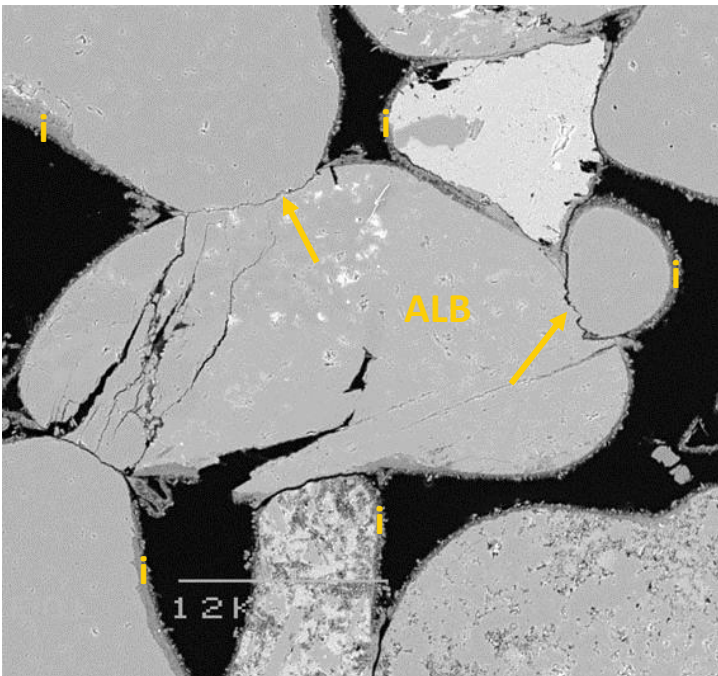
**C. Magnification 250x**

68µm
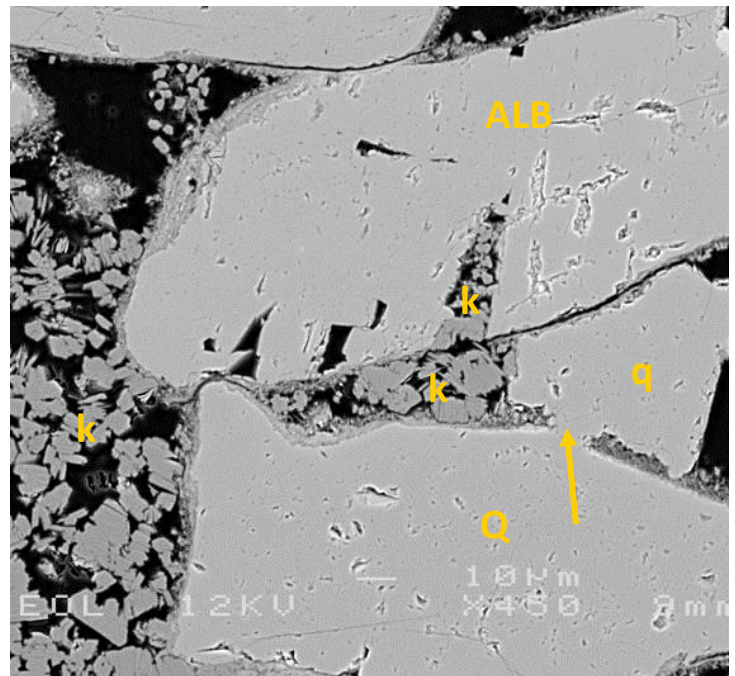
**D. Magnification 450x**

38µm

**Plate A:** This overview photo shows the high porosity of this sublitharenite. Most rock fragments (RF) are partially leached and/or deformed due to compaction. K-feldspar (FSP) is also commonly leached. Kaolinite (k) sparsely occurs as clusters.
**Plate B:** Quartz cement (q) locally formed in areas with leached grains (LG). Artificial dilatation of grains is visible as well (arrows) and due to sample preparation. Note how the dispersed kaolinite (k) outlines the strongly leached feldspar (FSP).
**Plate C:** This albite grain (ALB) is fractured due to compaction. All grains are covered with a continuous illite clay rim (i; both tangential as radial). Note that the clay rim is mostly absent in between the grain contacts, and that even some evidence for chemical compaction (pressure dissolution) is present (arrows). **Plate D:** Detailed photo from the inset of plate B, showing a fractured albite (ALB) grain with possibly some albite recementation as can be suggested from euhedral crystal outlines. Kaolinite (k) is present in the largest fracture. Note the quartz cement (q) that has formed on the detrital quartz grain surface (Q) where the clay rim (arrow) is interrupted.
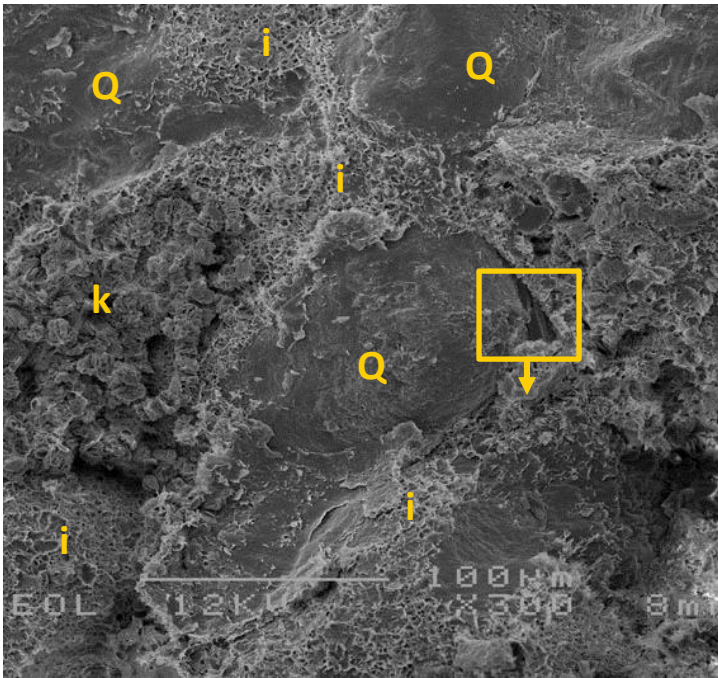
**A. Magnification 300x**

57µm
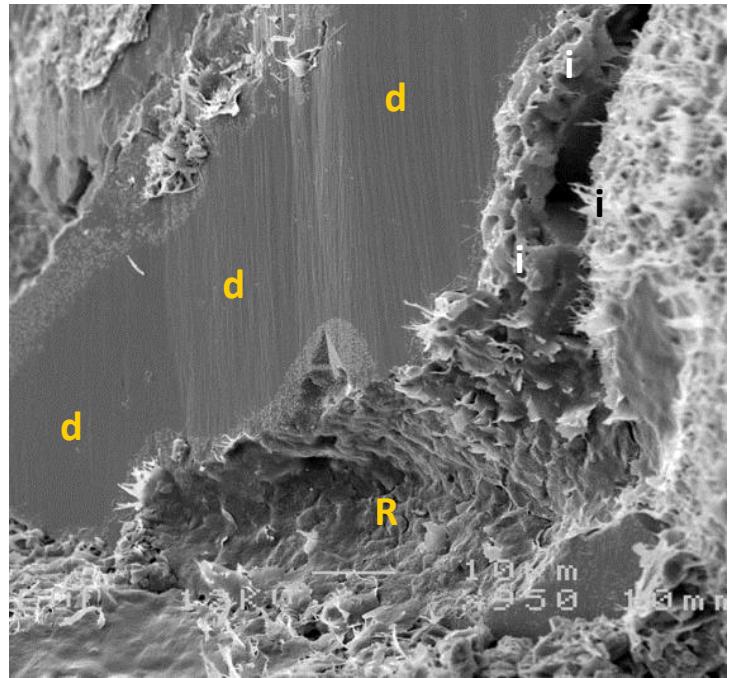
**B. Magnification 950x**

18µm
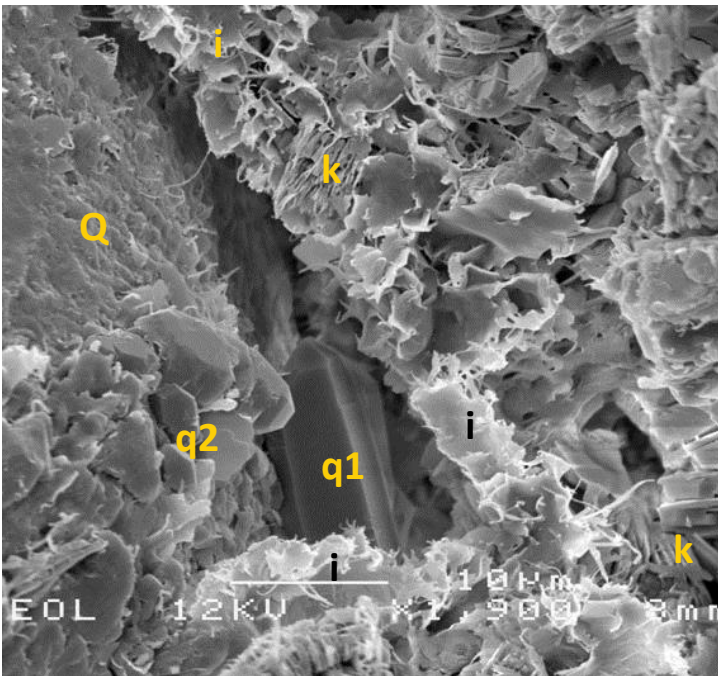
**C. Magnification 1900x**

9µm
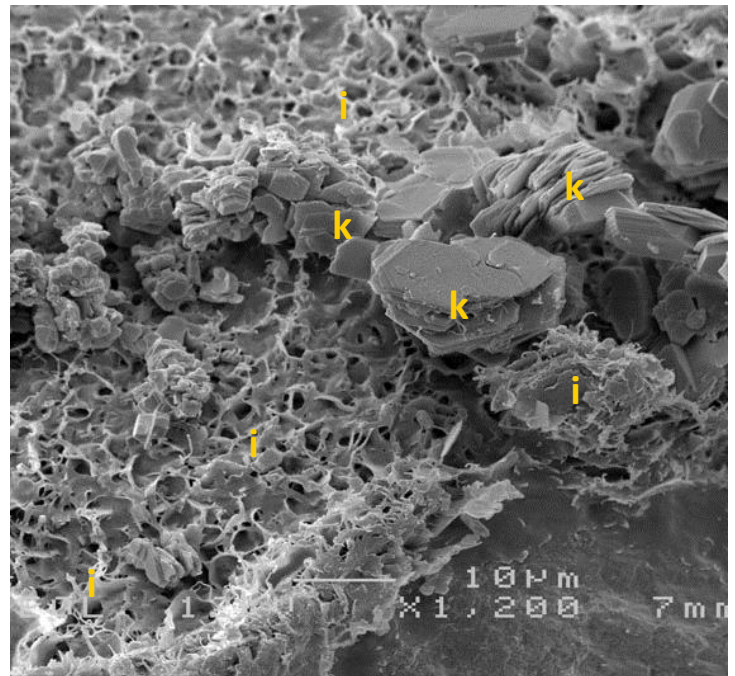
**D. Magnification 1200x**

14µm

**Plate A:** The detrital grains (mostly quartz; Q) of this sandstone sample are covered with a thick illitic clay coating (i). Macropores between individual grains are therefore absent. Relatively large micropores occur in between replacive kaolinite booklets (k). Both the kaolinite clusters as well as the illitic grain coating do not show evidence of compaction/deformation after the formation of authigenic clay minerals. **Plate B:** As is also visible in the thin section plates, dolomite (d) is locally completely pore filling. This dolomite is poor in Fe and overgrew now plucked grains (R). Note how the clay coating (i) on the right is partially detached from the detrital grain. **Plate C:** Detailed photo from the inset of plate A, showing that in between the clay coating (i) and the detrital quartz grain (Q), small authigenic quartz (q1) has formed. Also note the microscale overgrowths on top of the quartz grains (q2). Some kaolinite (k) occurs in between the illite. **Plate D:** Detailed photo of the radial illite coating (i) showing the honeycomb-like structure, as well as the fibres that grew out. The coarser authigenic clay crystals are kaolinite booklets (k), located on top of the illitic coating.
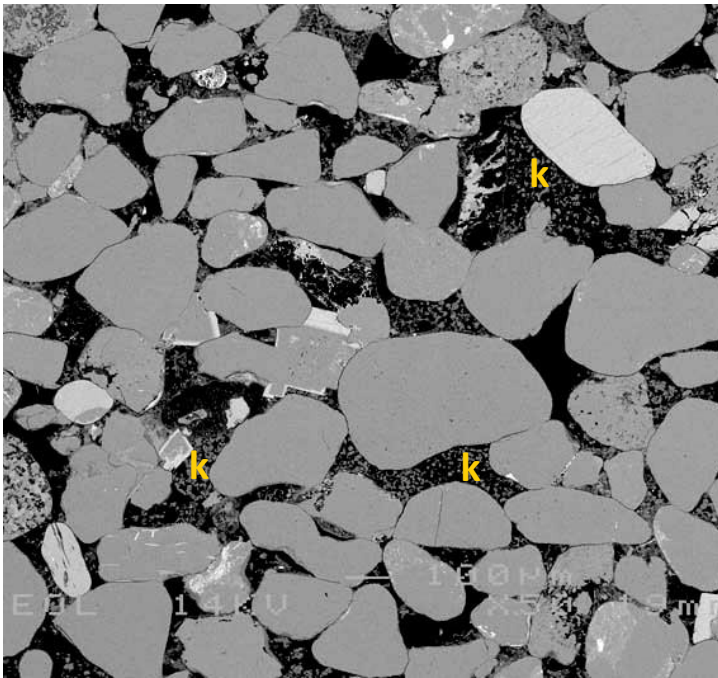
**A. Magnification 50x**
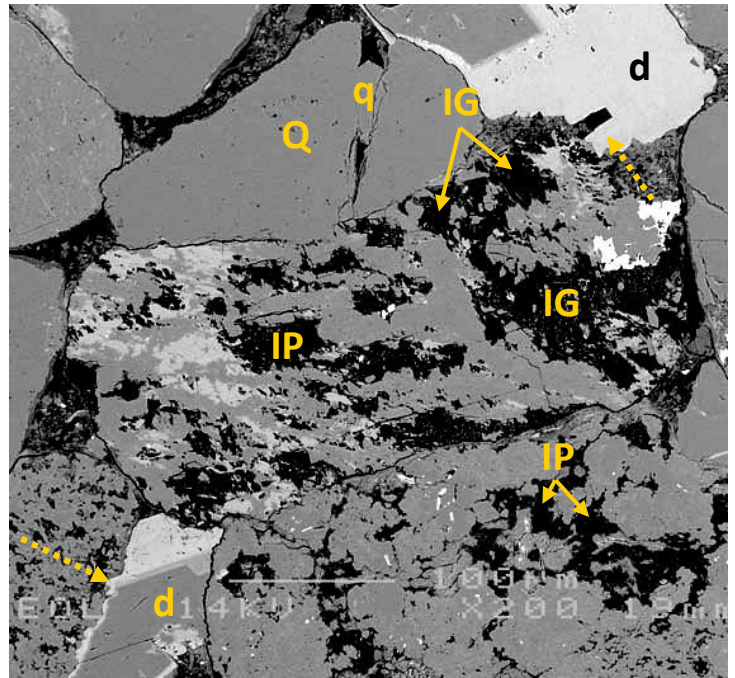
340μm



**B. Magnification 200x**
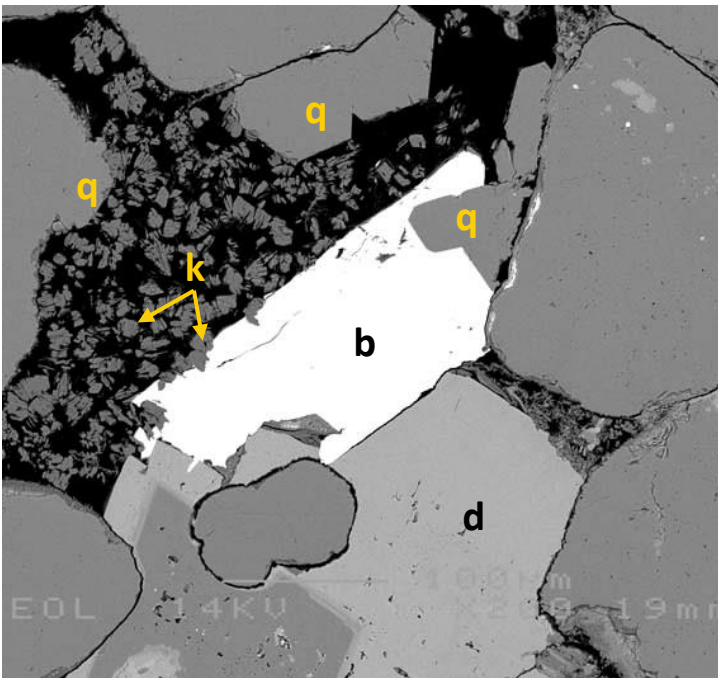
85μm



**C. Magnification 200x**

85μm
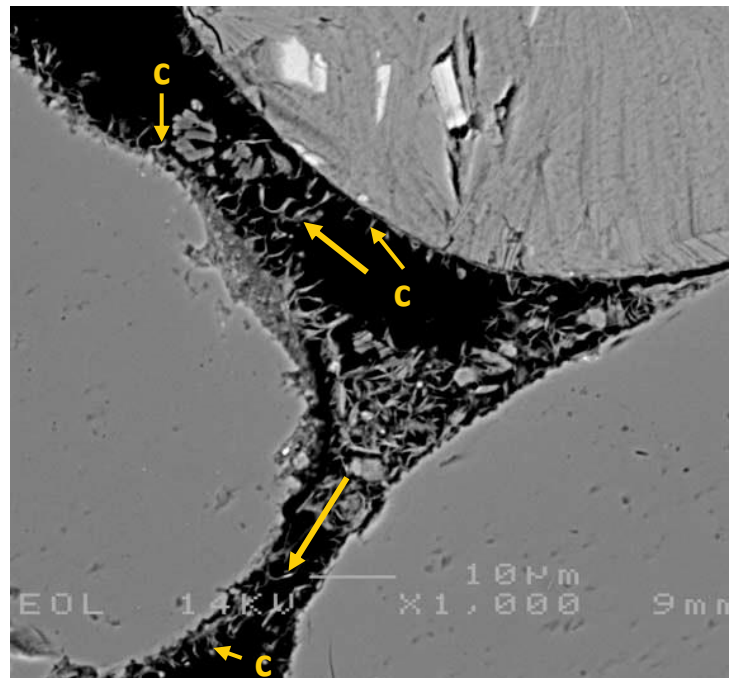


**D. Magnification 1000x**

17μm

**Plate A:** This fine-grained (upper) sublitharenite contains mainly subrounded quartz grains. Due to the moderately good sorting and predominant point contacts between quartz grains, the sandstone has a relatively high IGV (23%; avg. of this sample set is 20.5%). Note the patchy distribution of pore-filling kaolinite (k). **Plate B:** The leaching of feldspar grains created abundant secondary intragranular pores (IP) and micro-pores. Ferroan dolomite (d) mainly precipitated in primary pores, but also partly extends into secondary pores (dotted yellow arrows). Note the fractured quartz grain (Q), with authigenic quartz (q) on the fracture surface. **Plate C:** Spatial relationships indicate that kaolinite booklets (k) were likely the first authigenic crystals to form in this example, followed by quartz (Q), which is in turn enclosed by barite (b). Ferroan dolomite (d) also likely predates barite. **Plate D:** Radial clay coatings (c) surround detrital grains and reduce intergranular pore volume. Pore-bridging clay crystals (solid yellow arrows) also commonly block pore throats of smaller pores.
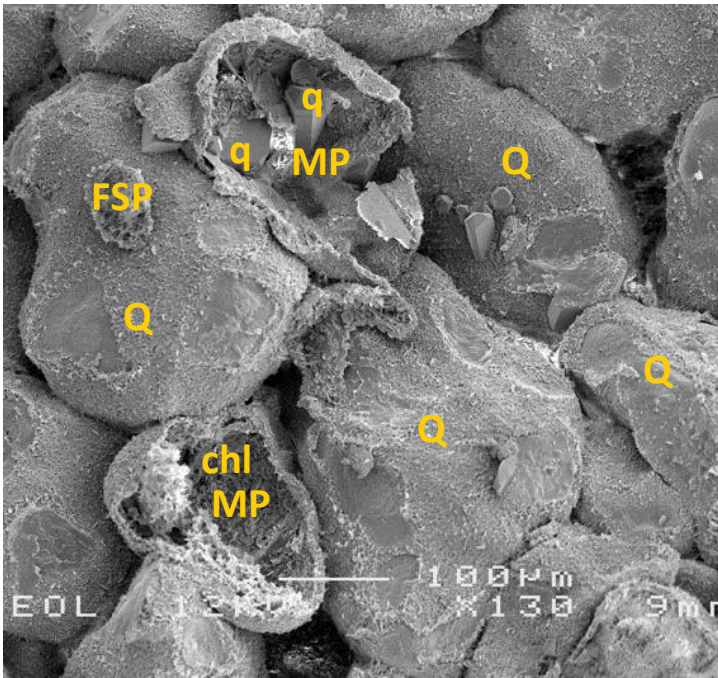
**A. Magnification 130x**

131µm
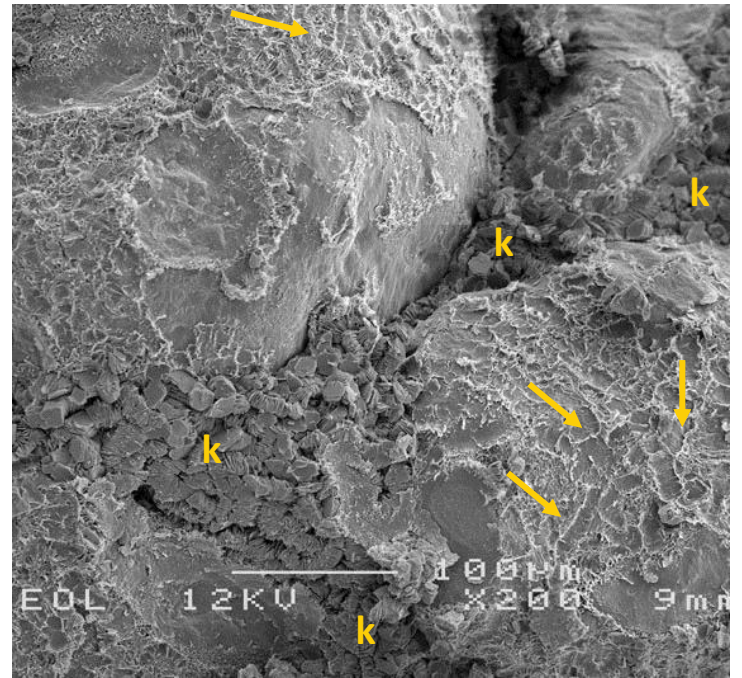
**B. Magnification 200x**

85µm
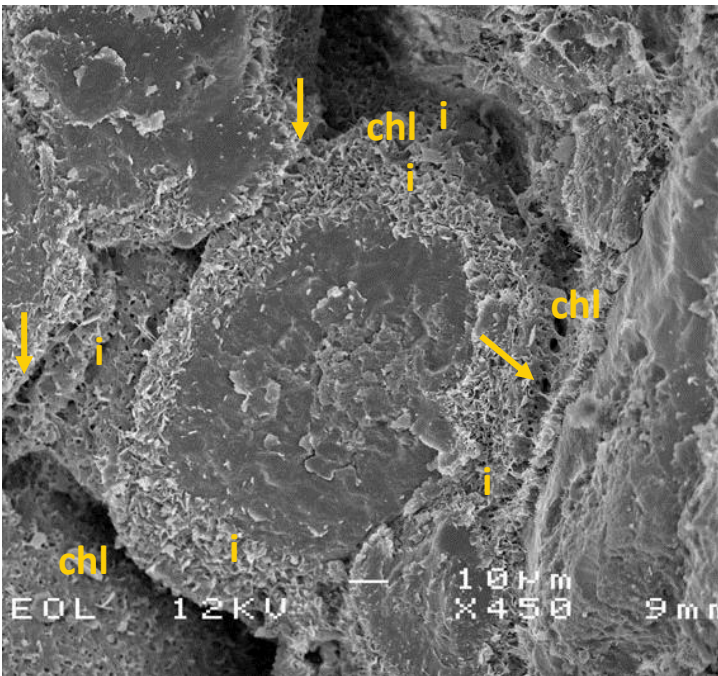
**C. Magnification 450x**

38µm
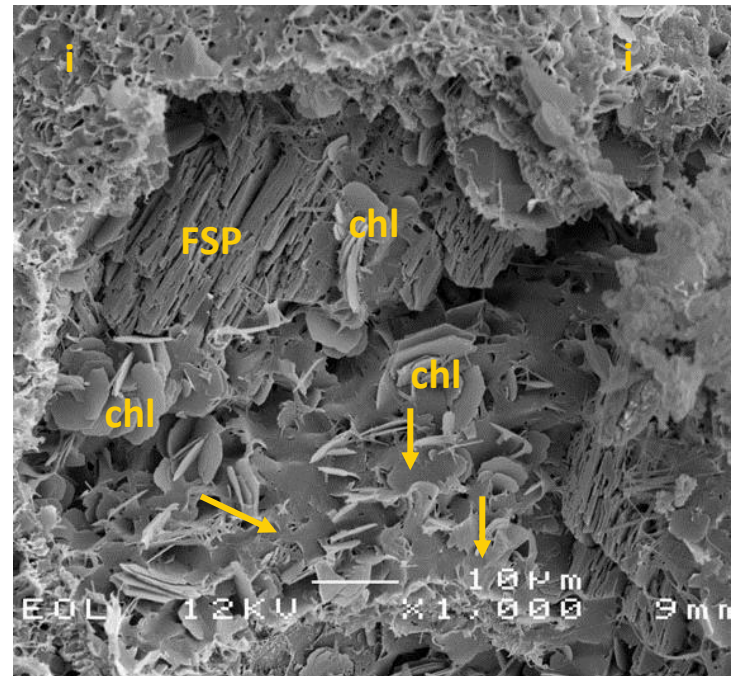
**D. Magnification 1000x**

17µm

**Plate A:** This laminated, very fine- to medium-grained sandstone contains, besides detrital quartz (Q), common feldspar grains. Some of these feldspar grains are completely leached, forming undeformed to slightly deformed mouldic pores (MP). Authigenic quartz (q; top leached FSP) and chlorite (chl; bottom leached FSP) formed in the mouldic pores. **Plate B:** Locally, pore-filling kaolinite (k) occurs in between the detrital grains. Note that the clay-rim covering the two large detrital grains is irregular, with imprints of what appears to be removed kaolinite (arrows). **Plate C:** This flat surface (due to removal of a grain) shows the pore-bridging nature of the grain-rimming clay (arrows). This grain-rimming clay is a combination of finer-crystalline fibrous illite (i) and more rosette-shaped coarser crystalline chlorite (chl). The clay rim thickness is ~5µm. **Plate D:** The partially leached feldspar grain (FSP) contains rosette-shaped chlorite (chl) mixed with more irregularly shaped (fibrous) illite (arrows)). Both appear to have formed at the expense of the feldspar. The illitic clay rim covering the former feldspar grain, is visible at the top and left part of the photo (i).
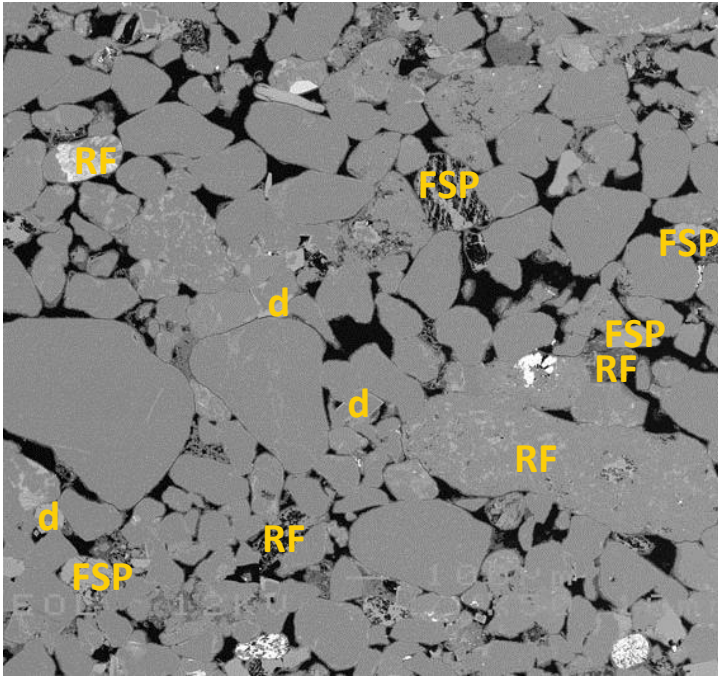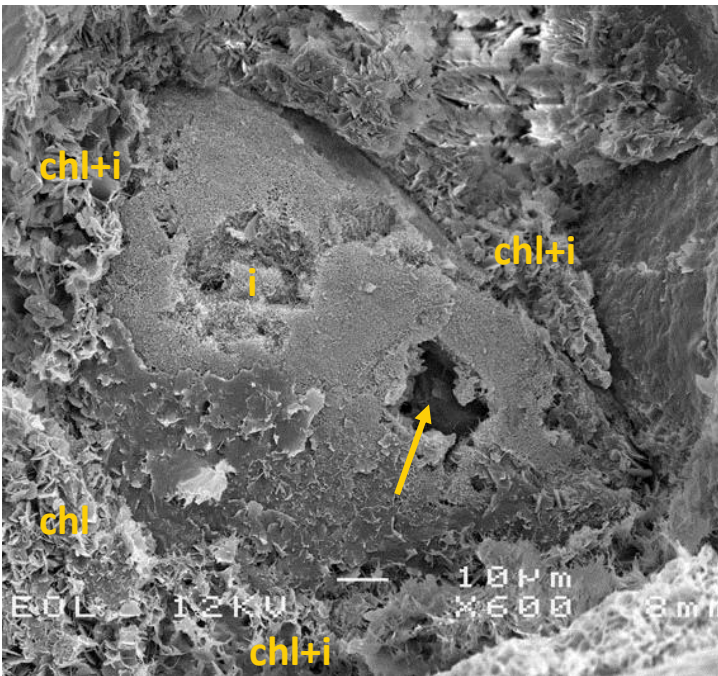
A. Magnification 50x

340μm
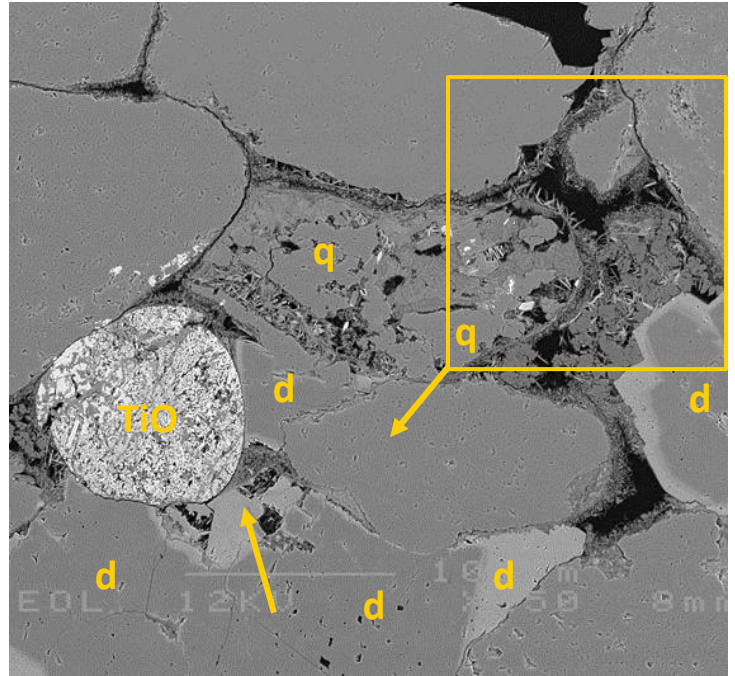
B. Magnification 250x

68μm
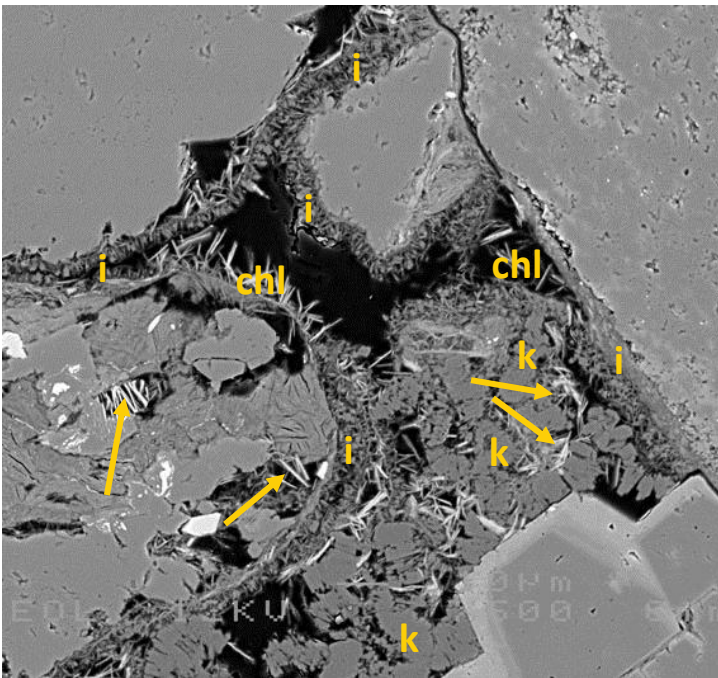
C. Magnification 600x

28μm
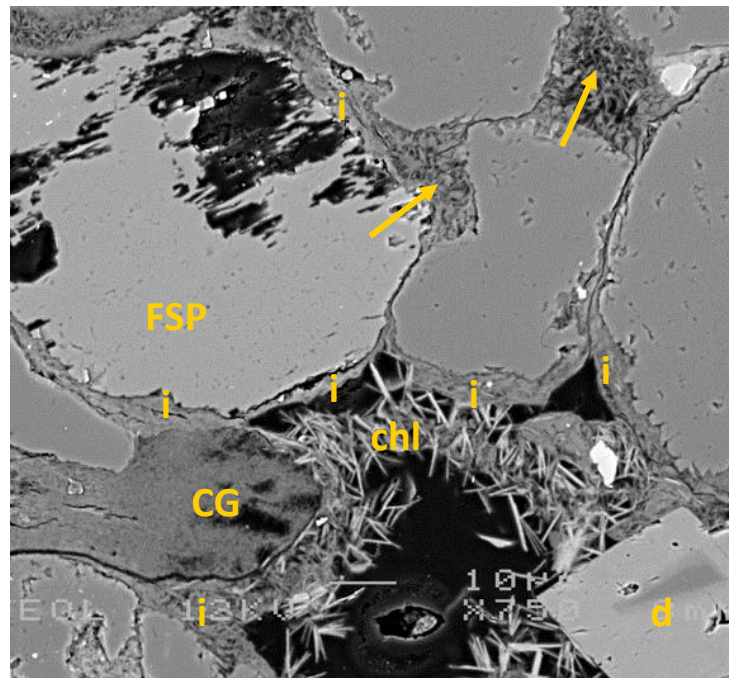
D. Magnification 750x

23μm

**Plate A:** This fairly heterogeneous, laminated sublitharenite contains common leached grains, including rock fragments (RF) and feldspar grains (FSP). Leached grains are not significantly deformed. Locally, pore-filling dolomite cement has formed (d), which is more iron-rich at the rims. **Plate B:** Rock fragments are commonly partially replaced with authigenic minerals; mostly quartz (q), but also locally with a bright TiO mineral (rutile?; TiO). Porosity in this field of view is significantly reduced by dolomite cement (d). More Fe-rich dolomite formed within a leached feldspar grain (arrow). **Plate C:** Detailed image from the inset in plate B, showing the clay rim of the detrital grains comprising chlorite (chl) and illite (i). The leached grains themselves are replaced by clay (illite?), chlorite (arrow) and/or kaolinite (k). There is no evidence of grain movement after clay rim formation as the clay crystals are not deformed. **Plate D:** All grains, including a leached K-feldspar grain (FSP) are outlined by a (mostly tangential) clay coating (i). Clay coatings are thick and locally fill up the pore space completely (arrows). Note the strongly deformed clay-rich grain (CG), dolomite and the authigenic chlorite (chl).
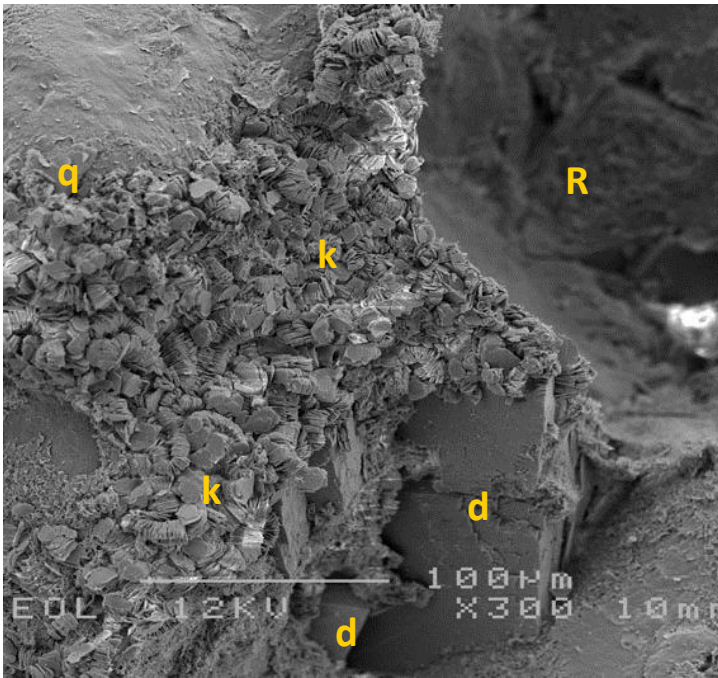
**A. Magnification 300x**

57µm
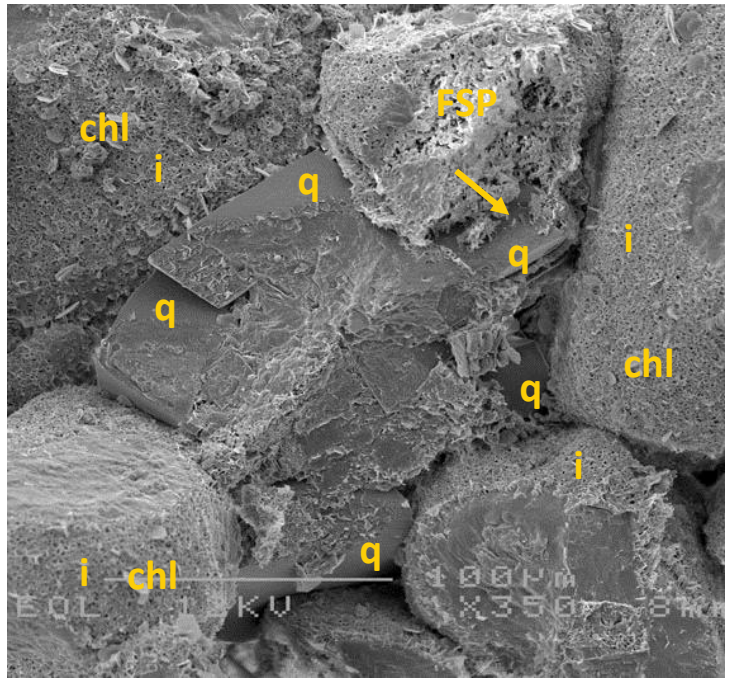


**B. Magnification 350x**

49µm
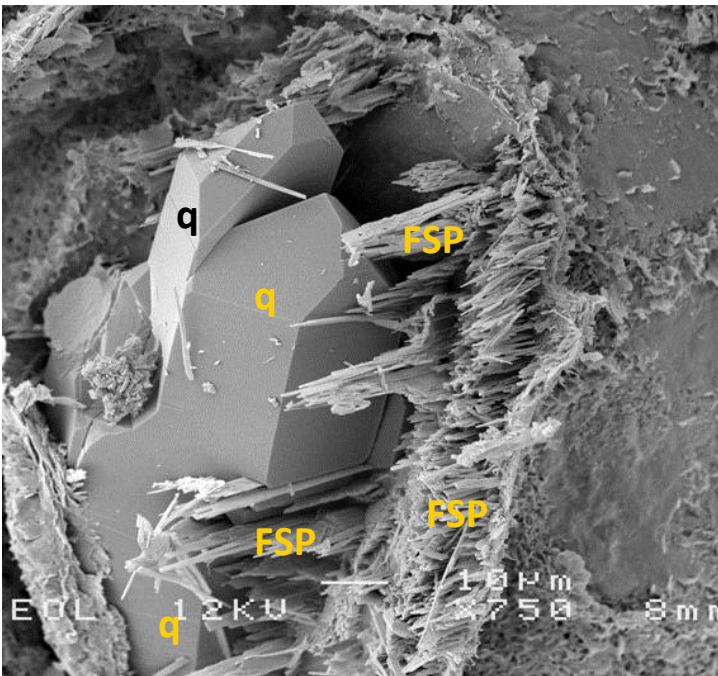


**C. Magnification 750x**

23µm
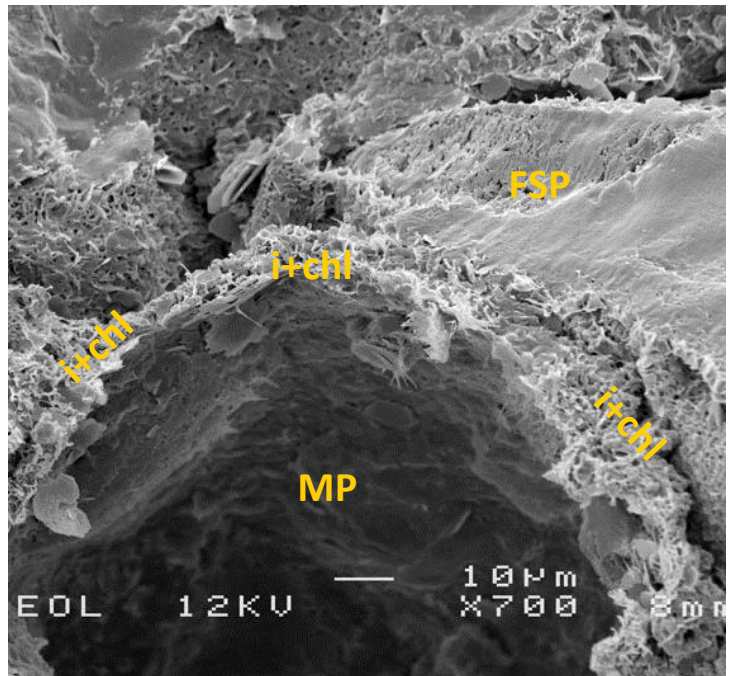


**D. Magnification 700x**

24µm

**Plate A:** This medium grained sandstone locally contains significant pore-filling kaolinite (k). The outlines of a plucked grain (R) are well visible by the shape of the kaolinite cluster. Traces of quartz overgrowths (q) occur. The cube-shaped cement next to the kaolinite is dolomite (d). **Plate B:** Quartz cement (identified with EDX) locally formed relatively large euhedral overgrowths (q), also filling secondary porosity (arrow) created by the leaching of feldspar (FSP). The authigenic clay rim comprises a combination of fine-crystalline fibrous illite (i) and coarser crystalline platy chlorite (chl). **Plate C:** Detailed photo of a leached feldspar (FSP; fibres remaining) that is almost completely replaced by quartz cement (q). Authigenic clay is absent within the leached feldspar. **Plate D:** Detailed image of the edge of a mouldic pore (MP). The clay rim is still intact and not deformed, indicating that compaction predates dissolution. The clay rim is relatively thick (>5µm) and comprises a mixture of illite and chlorite (i+chl). Note the feldspar grain (FSP) that only shows minor dissolution.
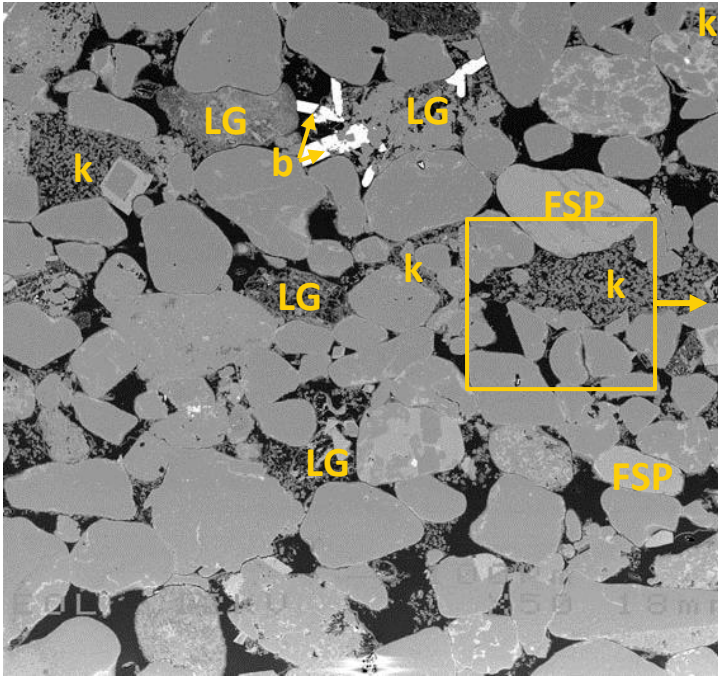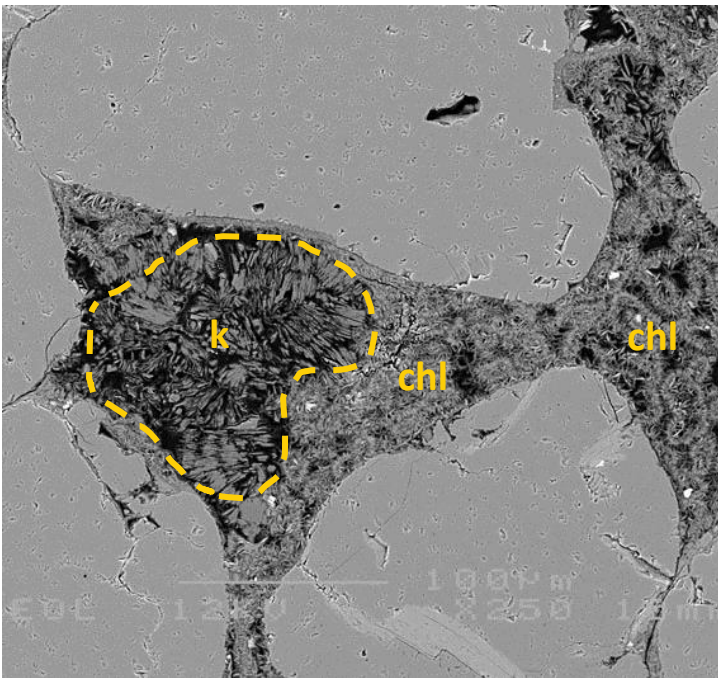
**A. Magnification 50x**

340μm
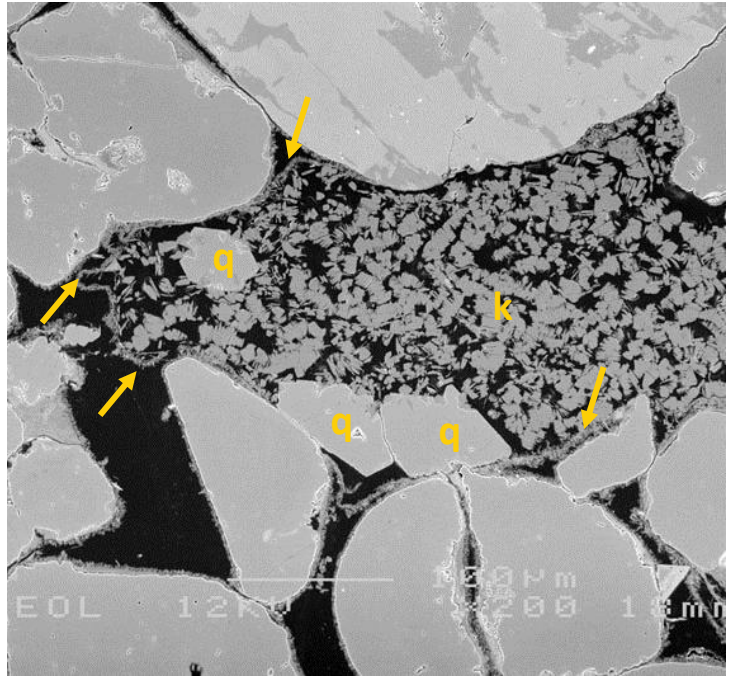
**B. Magnification 200x**

85μm
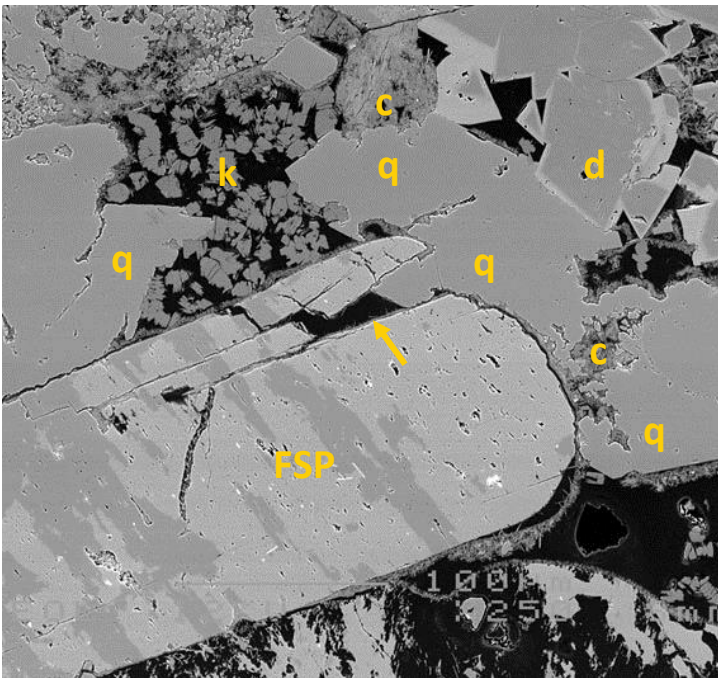
**C. Magnification 250x**
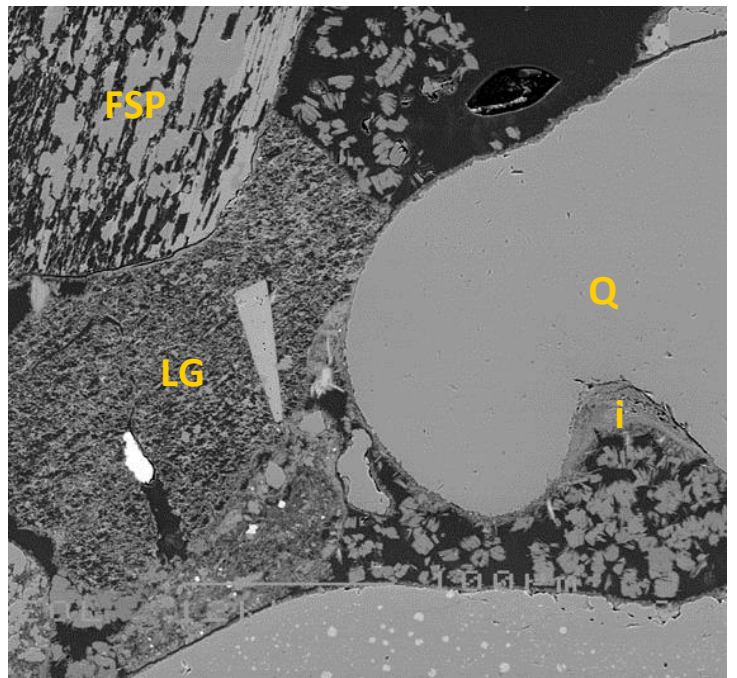
68μm

**D. Magnification 250x**

68μm

**Plate A:** This medium grained sandstone contains relatively common feldspar (FSP) and leached grains (LG). Barite (b) is partially filling the secondary pores of a leached grains, also overgrowing the clay rim (arrows). Kaolinite occurs in relatively large clusters (k). **Plate B:** Detailed view of a replacive kaolinite cluster from the inset in plate A. The kaolinite (k) is outlined by a thin and irregularly shaped illite rim (arrows). The kaolinite is locally engulfed by quartz cement (q). Whether the original grain was strongly deformed, or whether the deformation occurred after kaolinite formation cannot be said. **Plate C:** This feldspar grain (FSP; mix albite (dark) and K-fsp (light)) is fractured early during diagenesis, visible by the thin clay rim that occurs on the fracture surface (arrow) and the quartz cement that formed in between the parts (q). Note how the quartz cement is also engulfing presumably older dolomite (d), kaolinite (k) and other clay (c). **Plate D:** The quartz grain on the right (Q) has a thick tangential illite rim (i) covering the concave area. Elsewhere, the illite rim is thin. Leached grains comprise a feldspar grain (FSP) with secondary albite and illitic (replacing) leached grains (LG).
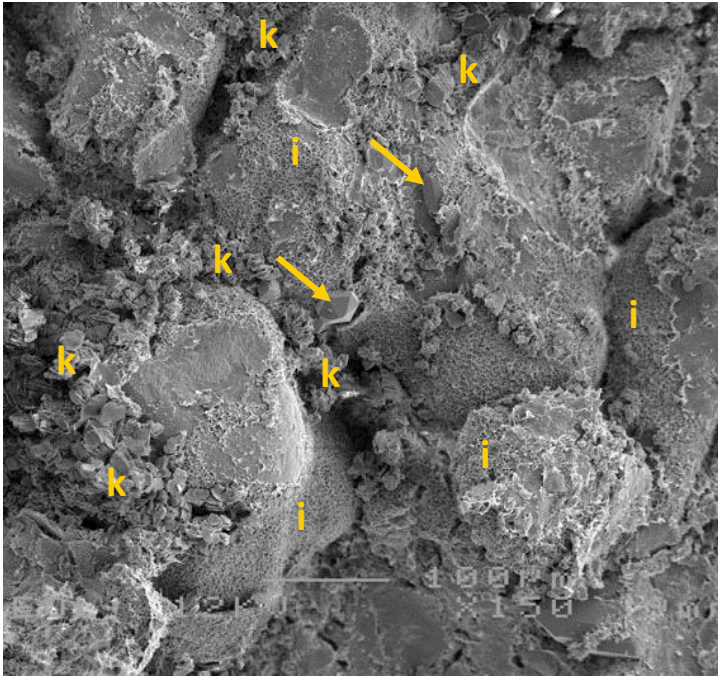
**A. Magnification 150x**
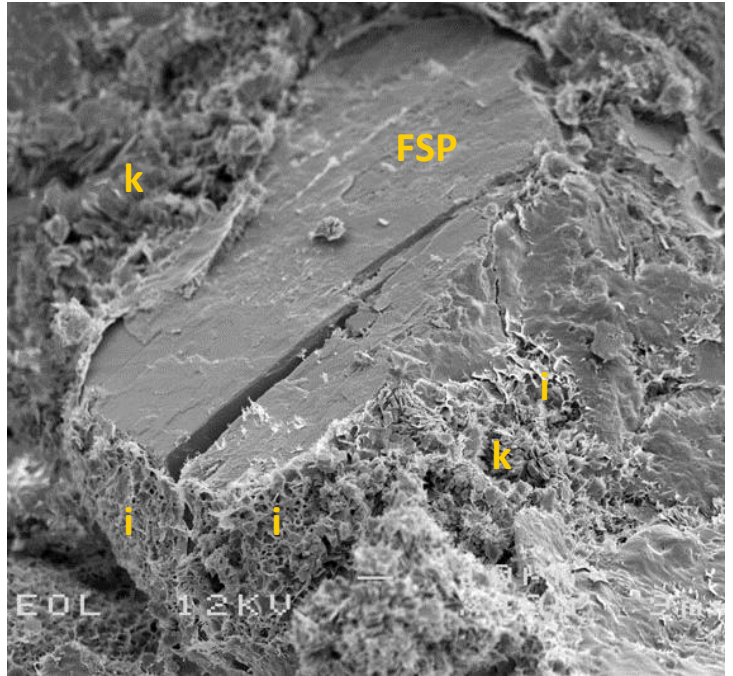
113μm

**B. Magnification 400x**

43μm

**C. Magnification 400x**

43μm
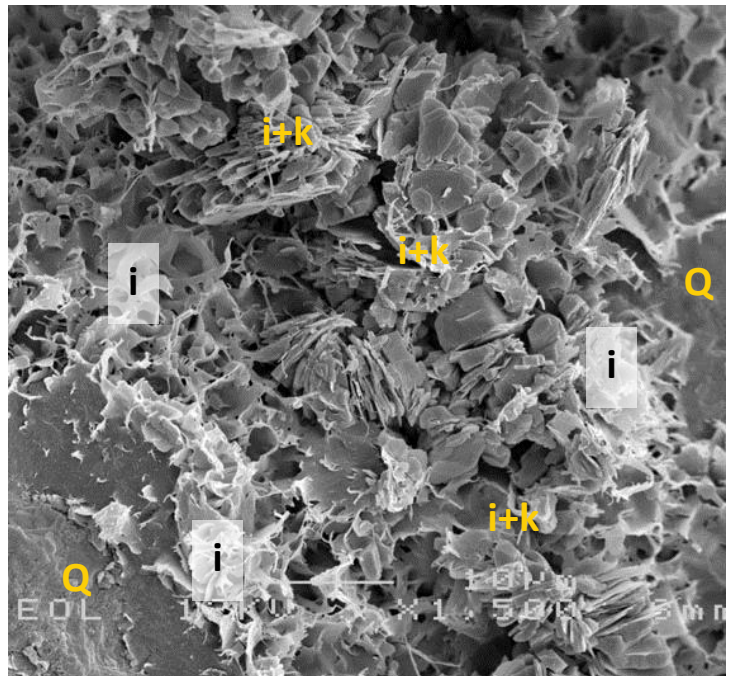
**D. Magnification 1500x**

11μm

**Plate A:** Overview image of this fine to medium grained sandstone showing kaolinite (k) dispersed in between the detrital grains. The detrital grains are covered with an illitic clay rim (i). Locally, small euhedral quartz outgrowths have formed (arrows). **Plate B:** This K-feldspar (FSP; determined with EDX) is broken along some cleavage planes. Whether this is due to compaction or artificial (due to sample preparation) is unknown, as there are no authigenic minerals on the fracture planes. The illitic clay rim (i) is also disrupted at the fractures. Note the authigenic kaolinite (k), which is locally mixed with the authigenic illite. **Plate C:** Recognisable by residual grain-rimming clay (mostly illite; i) is a strongly leached feldspar (outlined). The dissolution pore is now filled with illite(?) fibres oriented randomly, intergrown with replacive quartz cement (arrows). **Plate D:** Detailed image of quartz grains (Q) covered with honeycomb-like radial illite coating (i). The intergranular space is further filled with a mixture of illite and booklet shaped kaolinite (i+k), with in between only micropores. There is no evidence for more recent grain movement due to compaction as the fibres are not deformed.
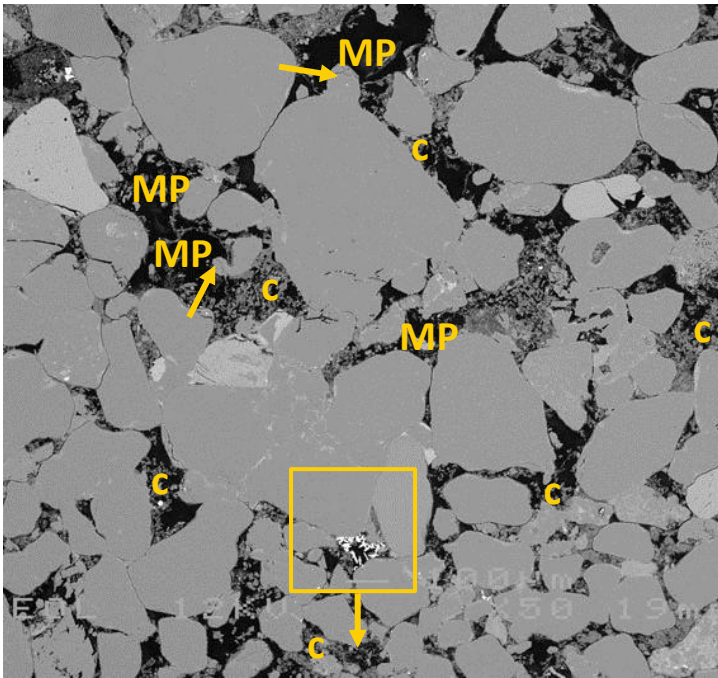
**A. Magnification 50x**

340µm
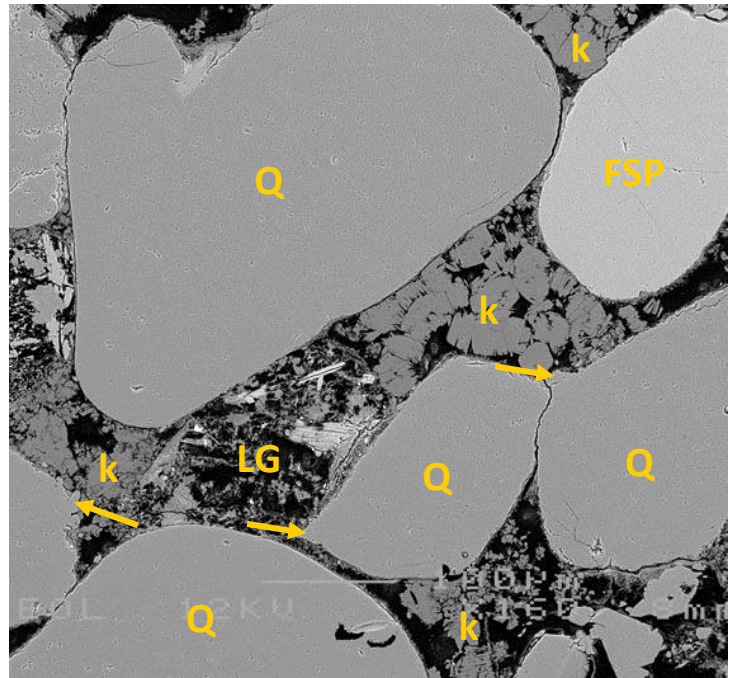
**B. Magnification 160x**

106µm
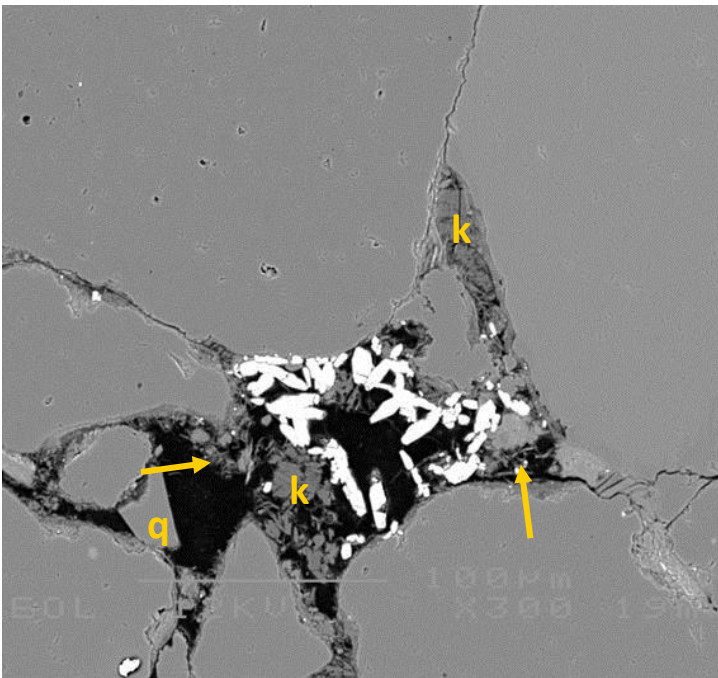
**C. Magnification 300x**

57µm
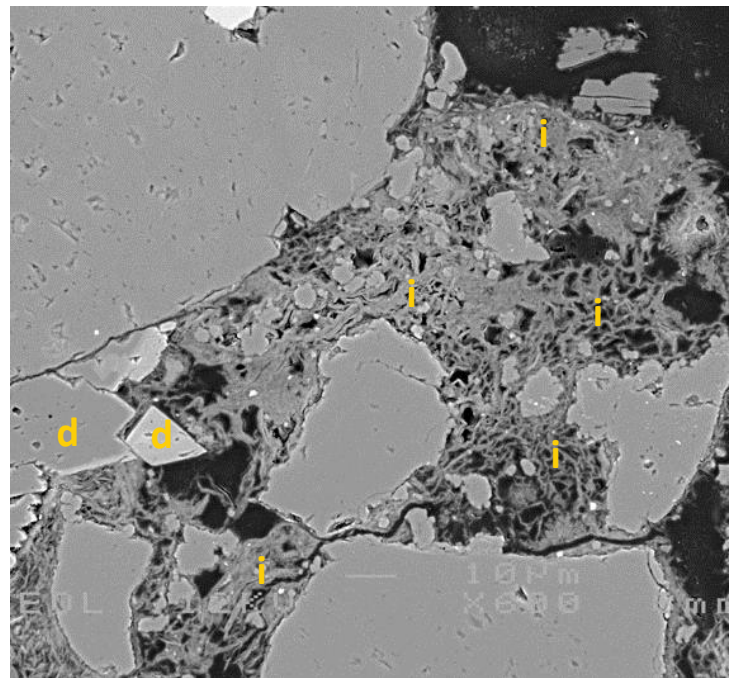
**D. Magnification 600x**

28µm

**Plate A:** This fairly heterogeneous, fine grained sandstone contains common intergranular authigenic clay (c). Most of this clay is replacive. Mouldic pores (MP) occur as well, and are outlined by a thin clay rim. Most mouldic pores are partially filled with quartz cement (arrows). **Plate B:** Authigenic kaolinite (k) occurs in clusters and has formed in a leached detrital grain. The detrital grains, including quartz (Q) and K-feldspar (FSP) have a very thin clay coating and quartz overgrowths are (in this field of view) very rare (arrows). Note the leached grain (LG) which is not deformed despite the lack of a framework structure in this 2D cut. **Plate C:** Detailed photograph if the inset of plate A, showing small replacive $TiO_2$ crystals (bright white; rutile?). Note the authigenic kaolinite (k) and more fibrous illite (arrows). Quartz cement (q) formed where clay is absent. **Plate D:** Zooming in on a leached grain shows the fibrous replacive illite (i) and euhedral dolomite (d). Replacive illite is different from the illite coating in that the fibre orientation is completely random. Therefore, there is no indication of what the former grain might have been.
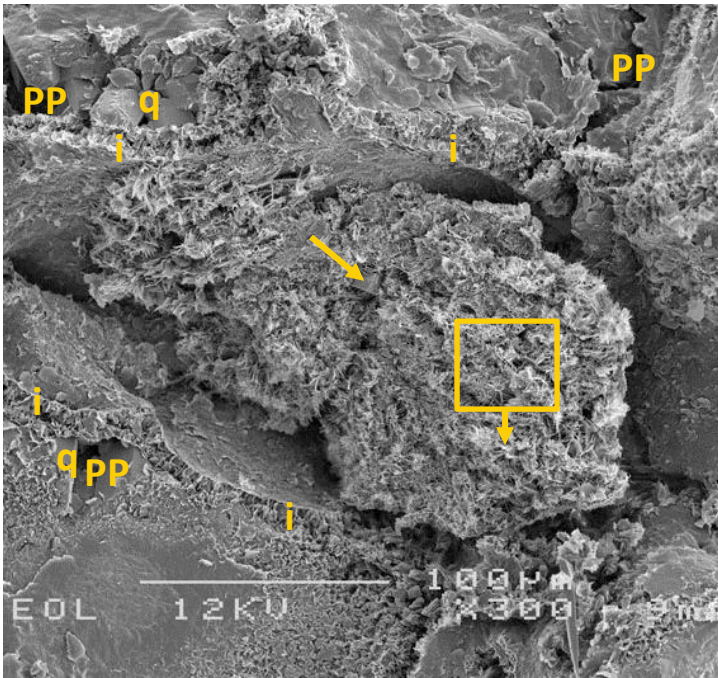
**A. Magnification 300x**

57μm
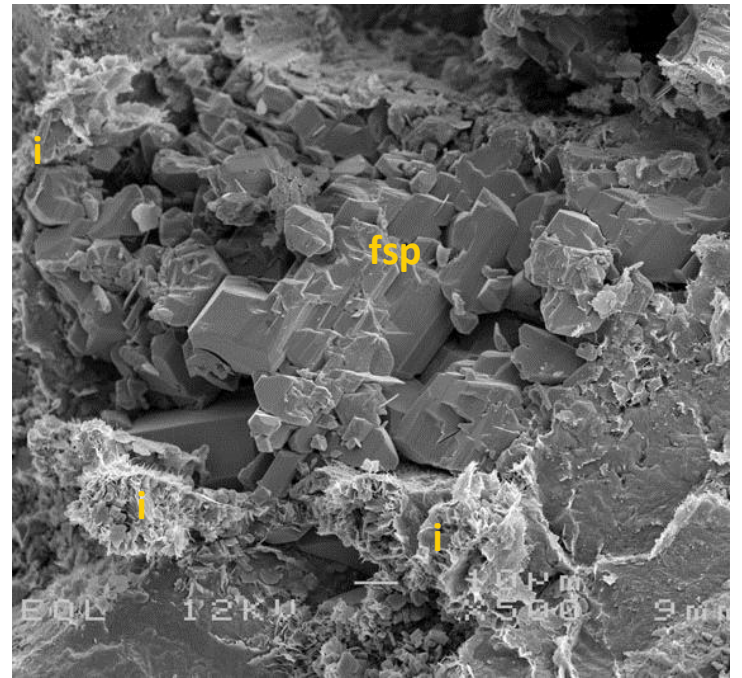
**B. Magnification 500x**

34μm
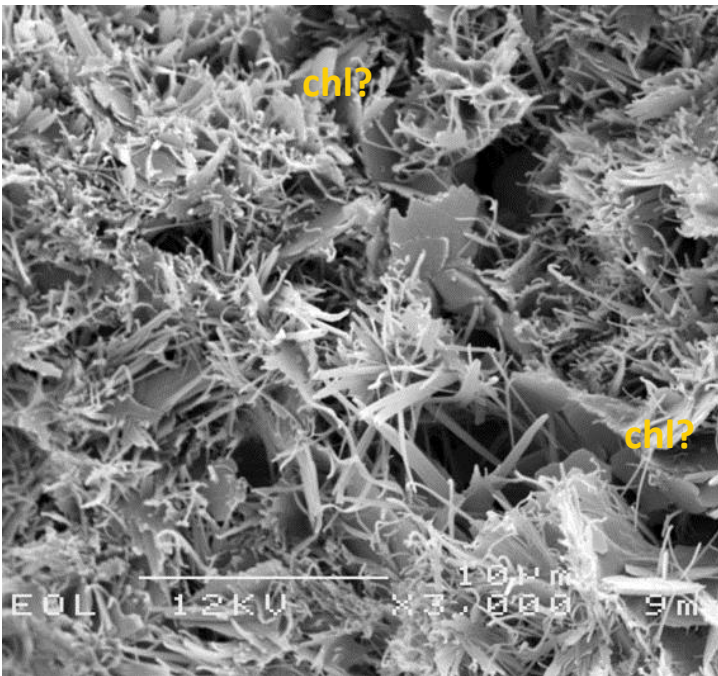
**C. Magnification 3000x**

6μm
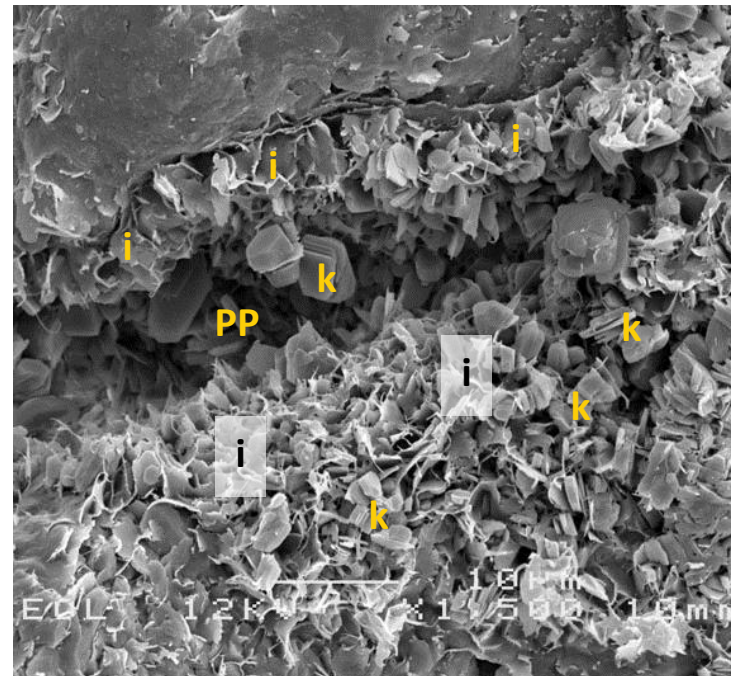
**D. Magnification 1500x**

11μm

**Plate A:** Primary intergranular pores are small (PP) in this fine to medium grained sandstone, Additionally, secondary (dissolution) pores occur, where the illitic clay rim (i) is outlining the shape of a partially dissolved grain. The grain is replaced by fibrous illite (e.g. within box) and minor dolomite cement (arrow). Note the traces of quartz cement (q). **Plate B:** Dissolved feldspar is locally partially recrystallized (fsp), forming euhedral authigenic feldspar (fsp) crystals (presumably) parallel to the original cleavage planes of the former feldspar grain. Note the irregular illite rim (i). **Plate C:** This high magnification photo is taken from the inset of plate A, showing the fibrous to platy nature of the illite, with significant micropores in between individual crystals. Possibly, some chlorite occurs as well (chl?). **Plate D:** The replacive illite in plate C has a clearly different texture compared to the illitic clay rim (i) shown in this photo. Here, the illite has grown parallel to each other, is honeycomb-shaped and mixed with kaolinite (k). The intergranular pore space (PP) in this image is small and there is no indication for movement between the detrital grains and deformation of the clays due to later stage compaction.
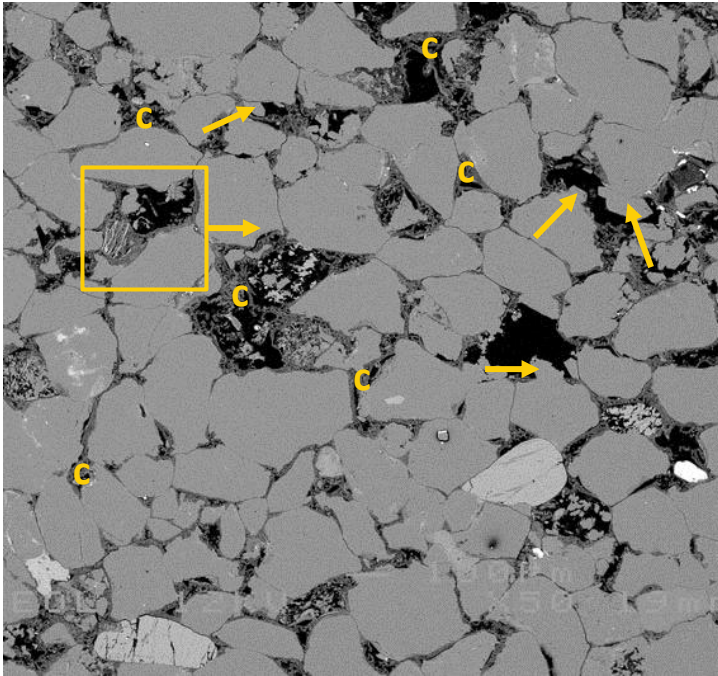
**A. Magnification 50x**

340μm
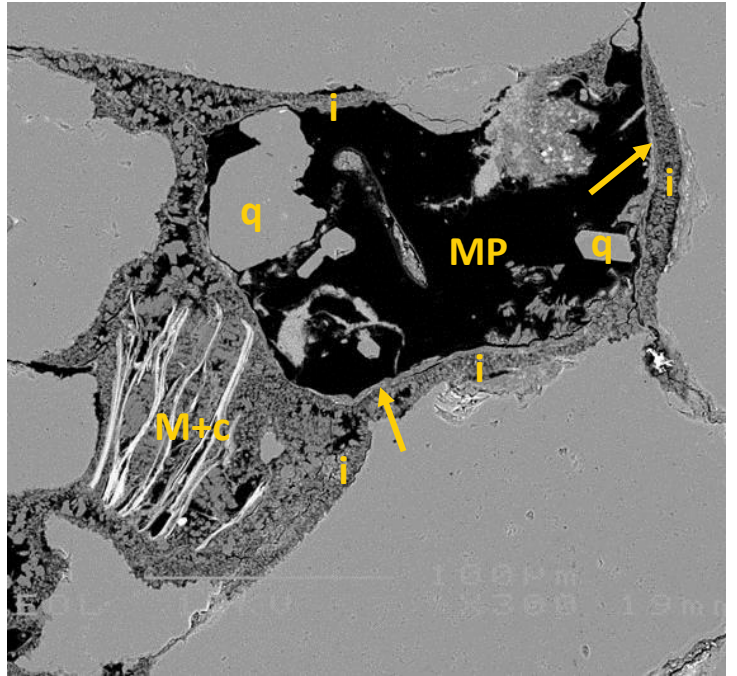


**B. Magnification 300x**

57μm



**C. Magnification 350x**

49μm
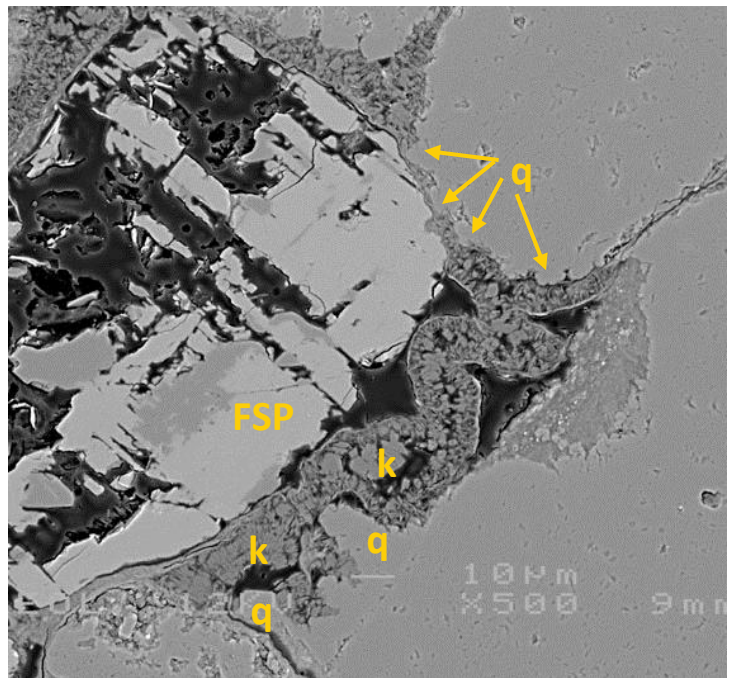


**D. Magnification 500x**

34μm

**Plate A:** The detrital quartz grains in this relatively well sorted sandstone are relatively angular. This is partly due to quartz cement (arrows), which is both a replacive and a pore-filling cement. The small intergranular spaces are mostly filled with a thick authigenic clay rim (c). **Plate B:** Detailed image from the inset in plate A, showing a partially quartz cemented (q) mouldic pore (MP) and an altered micaceous grain (M) with clay (+c) in between the long platelets. Note the thick (>10 μm) clay rim, which comprises both tangential (arrows) and radial illite (i). **Plate C:** Quartz (q) cement in mouldic pores can be very significant. Locally, also K-feldspar precipitated (fsp). Locally, the tangential illite is very thick (i), especially in the concave parts of grains. Next to the radial illite, a more blocky mineral (arrows; quartz? Dickite?) occurs. Intergranular pores are unconnected due to this thick clay rim and quartz cementation. **Plate D:** Locally, the illitic clay rim is crinckled. Here, kaolinite (k) occurs in between the illite coating. Note the irregular shape of the quartz grains and the very small to locally large quartz overgrowths (q). The feldspar (FSP) grain is strongly leached but not deformed.
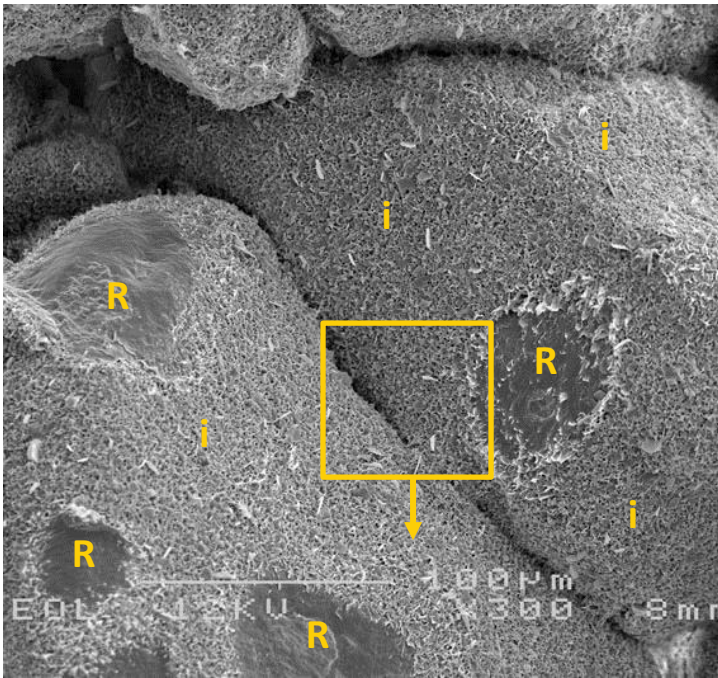
**A. Magnification 300x**

57µm
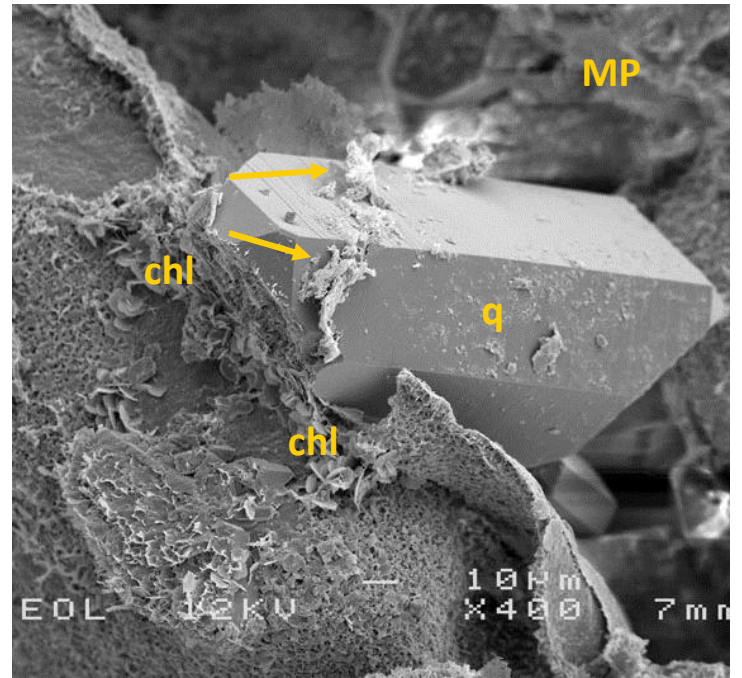


**B. Magnification 400x**

43µm
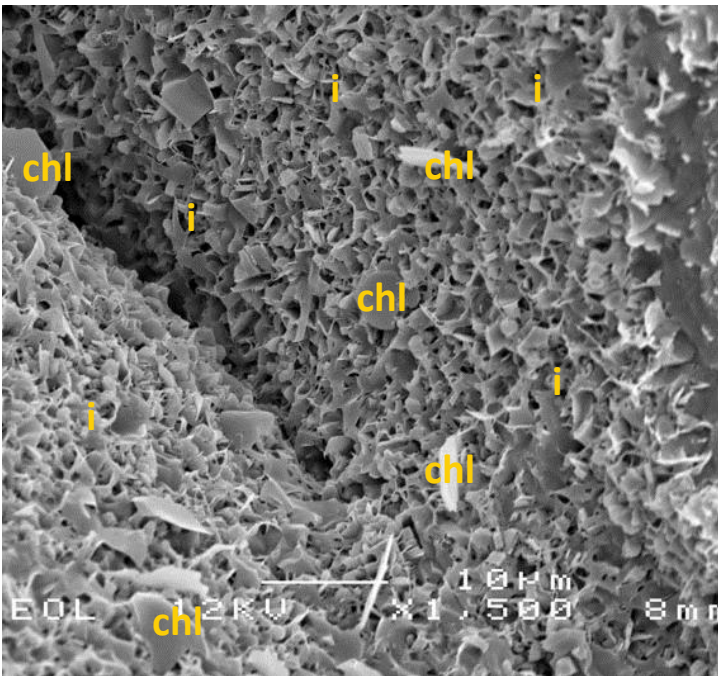


**C. Magnification 1500x**

11µm
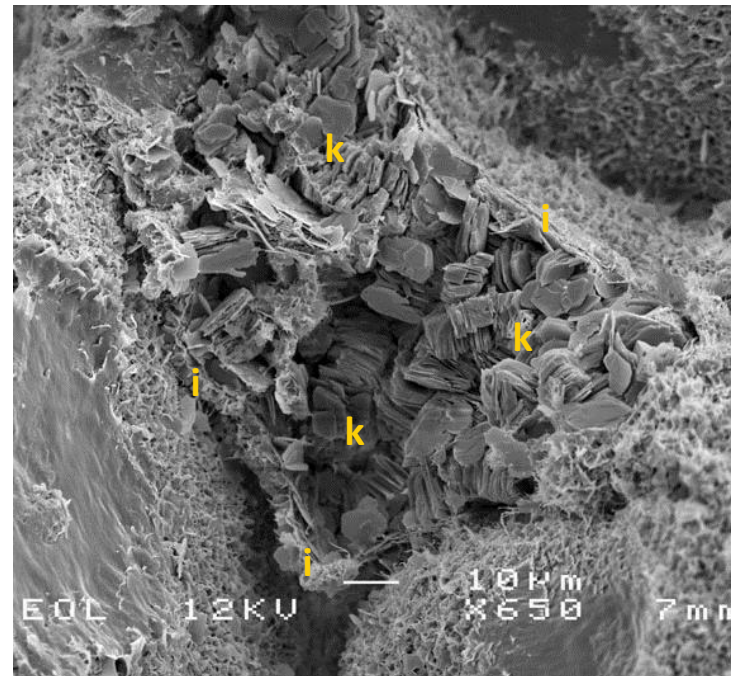


**D. Magnification 650x**

26µm

**Plate A:** The detrital grains in this fine to medium grained sandstone are uniformly covered with an illitic clay rim (i). The clay-free spots are grain to grain contacts, where the top grains were removed (R) during sample preparation. **Plate B:** In this mouldic pore (MP; right half of the image), a euhedral quartz outgrowth has formed (q). Note how the quartz crystal has overgrown the thin illitic clay rim (arrows). This clay rim is the only remainder of a completely leached grain, most likely a feldspar grain. Rosette-shaped chlorite (chl) occurs on top of the illitic clay rims. **Plate C:** This detailed image is from the outlined area in plate A, showing the details of the illitic honey-comb shaped clay coating (i) and the contacts between two detrital grains. Visible is that the illite rim is partially pore bridging and that later stage deformation did not occur, as the illite fibres remained intact. Coarser crystalline chlorite plates (chl) occur together with the illite rim. **Plate D:** Replacive kaolinite booklets (k) occur in this deformed and strongly leached grain, most likely an early leached feldspar. Remnants of the original grain are absent. Note the residual illitic clay rim (i) that formed around the grain prior to leaching.
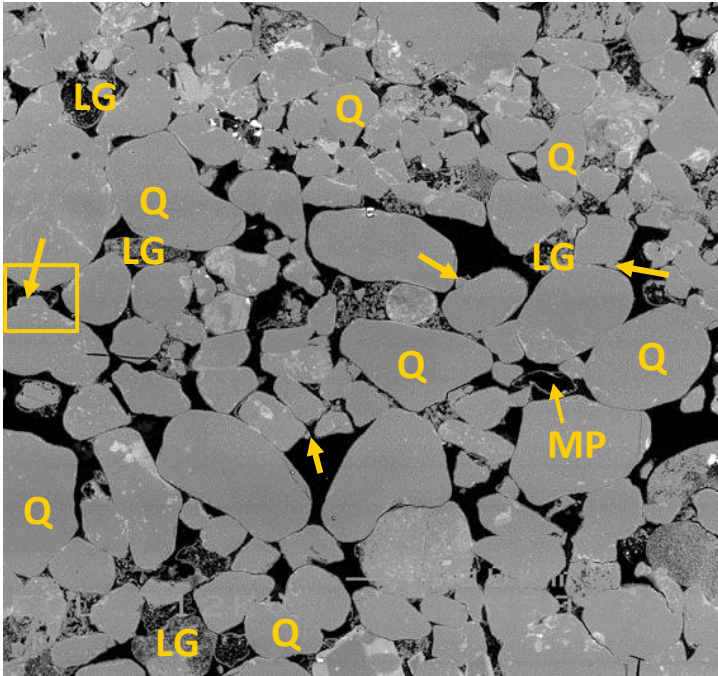
**A. Magnification 50x**

340µm
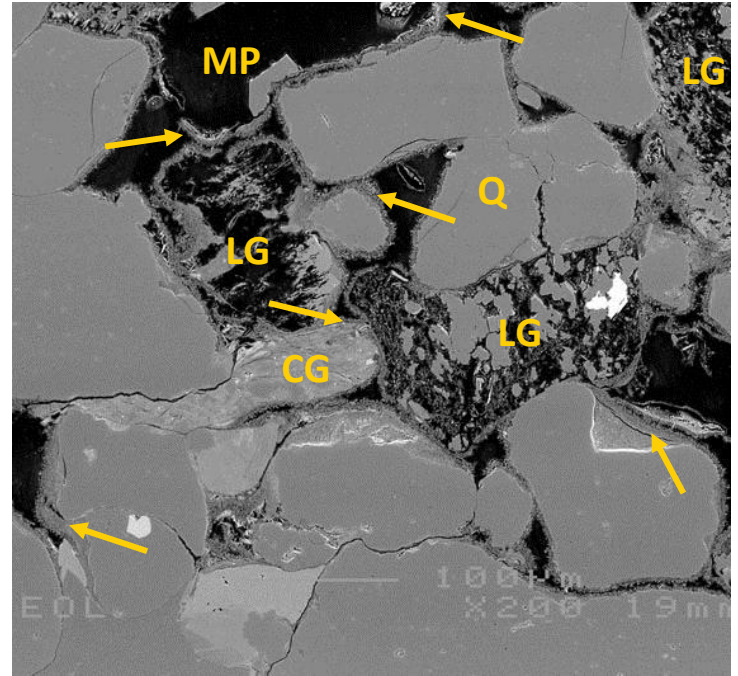


**B. Magnification 250x**

68µm
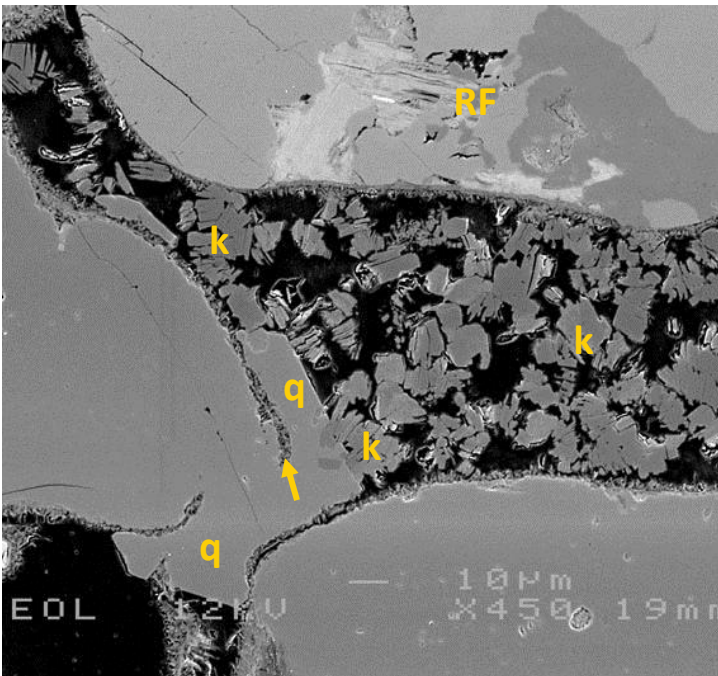


**C. Magnification 450x**

38µm
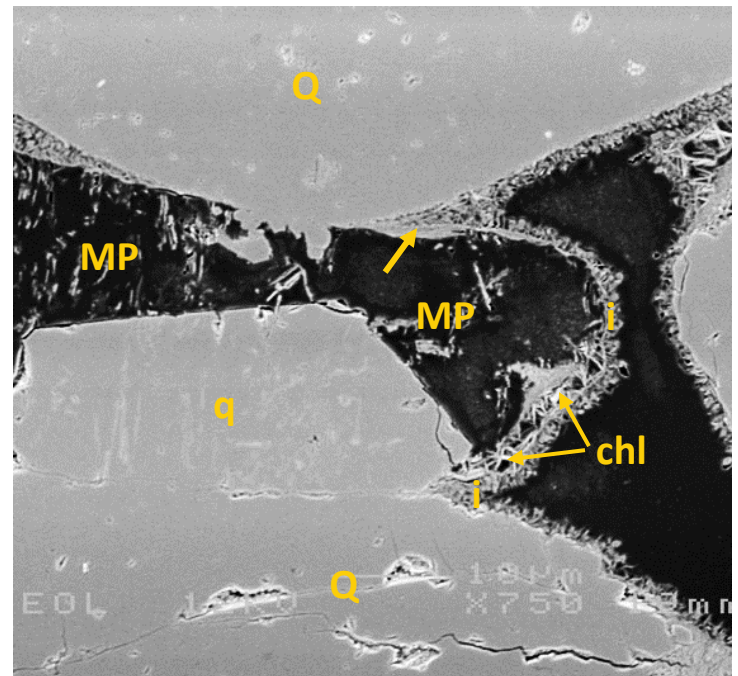


**D. Magnification 750x**

23µm

**Plate A:** In this fine- to medium-grained laminated sandstone, highly porous laminae (centre) alternate with less porous laminae (top/base). Leached grains (LG) and mouldic pores (MP) occur and are generally smaller than the detrital quartz grains (Q). Locally, euhedral quartz outgrowths formed (arrows). **Plate B:** Mechanical compaction is evident by the deformed clay-rich grain (CG) and the cracked quartz grain (Q). The deformation of the leached grains (LG) occurred most likely (partially) prior to leaching, as more deformation to even dissolution pore collaps is expected when compaction is after leaching. Note the thick clay rim (arrows) in this field of view, comprising both illite and chlorite. **Plate C:** The top of the image shows a mostly unleached igneous rock fragment (RF). Kaolinite (k) occurs in a cluster and is partially engulfed by authigenic quartz (q). It is striking that the quartz form at a place where the fairly thin illitic clay rim (arrow) was absent. **Plate D:** Detailed image showing a mouldic pore (MP) with remnants of the original feldspar cleavage. The contact between the completely leached feldspar grain and the quartz grains (Q) was virtually free of a clay rim, so that authigenic quartz (q) could grow into the mouldic pore. The illite rim is both tangential (arrow) and radial (i). Some chlorite (chl) occurs as well.
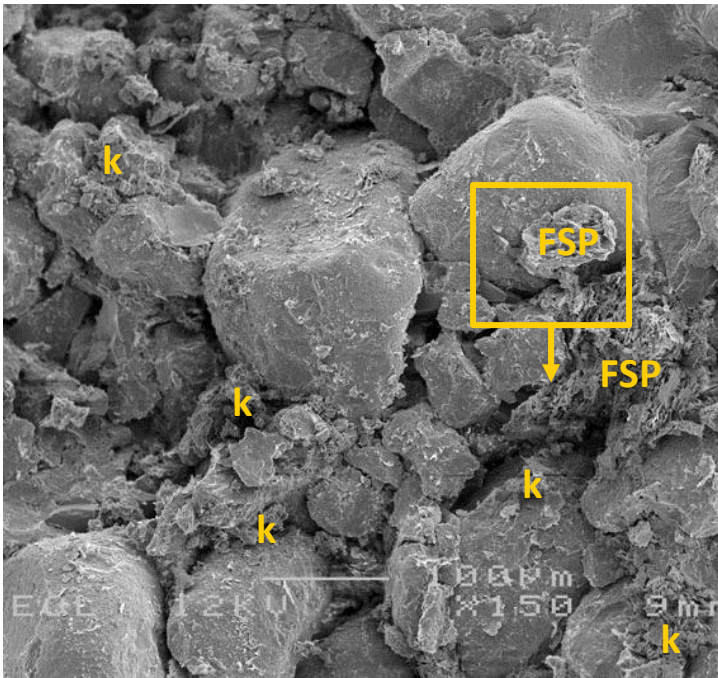
**A. Magnification 150x**

113µm
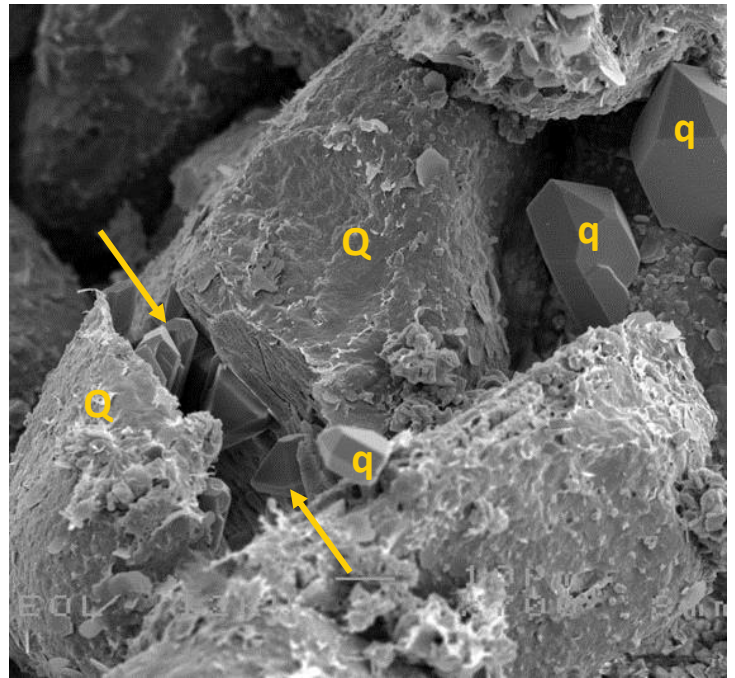


**B. Magnification 700x**

24µm
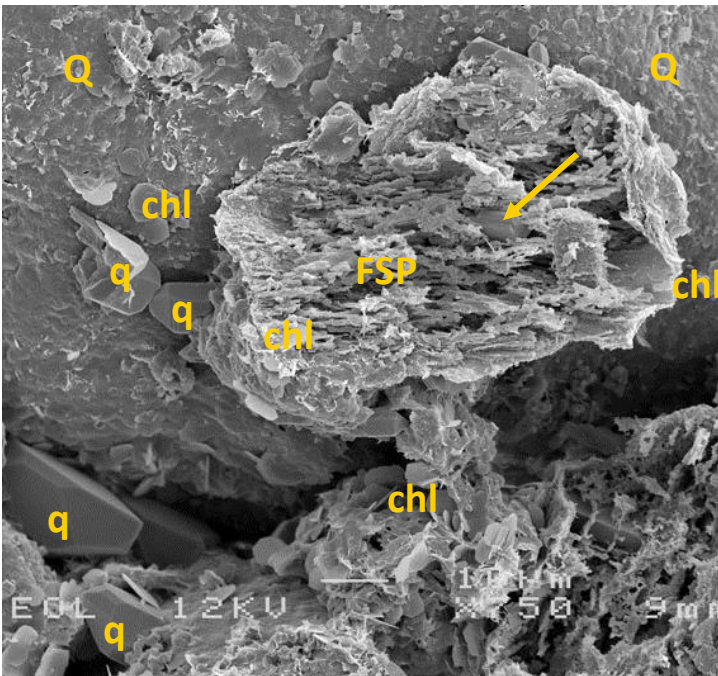


**C. Magnification 750x**

23µm
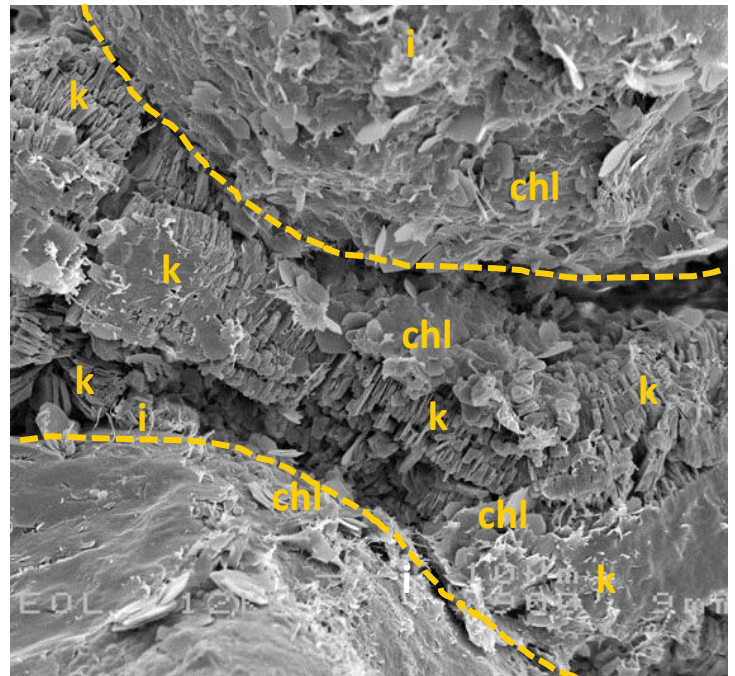


**D. Magnification 900x**

19µm

**Plate A:** This overview photo shows the poorly sorted nature of this sandstone. The coarser grains are well-rounded whereas the finer grains are more angular. Clay coatings are nearly absent. Intergranular clay is, in this field of view, mostly kaolinite (k). Note the strongly leached feldspar grains (FSP). **Plate B:** This photo shows the two halves of a broken quartz grain (Q), with euhedral quartz cement (arrows) on the fracture surfaces. This indicates that fracturing due to compaction predates (at least some) quartz cementation. This quartz grain was therefore not recently fractured. Also in the intergranular pores, euhedral quartz outgrowths have formed (q). **Plate C:** Zoomed photo from inset A, showing a strongly leached silt sized feldspar grain (FSP) on top of a detrital quartz grain (Q). Traces of authigenic feldspar occur in the feldspar grain (arrow). Note the absence of a continuous clay rim and the occurrence of quartz overgrowths (q) on the quartz grain. Authigenic clay comprises mostly chlorite (chl). **Plate D:** Closely packed kaolinite booklets (k) are wedged in between two detrital grains (dashed lines). Note the chlorite platelets (chl) and traces of fibrous illite (i) covering the detrital grains.
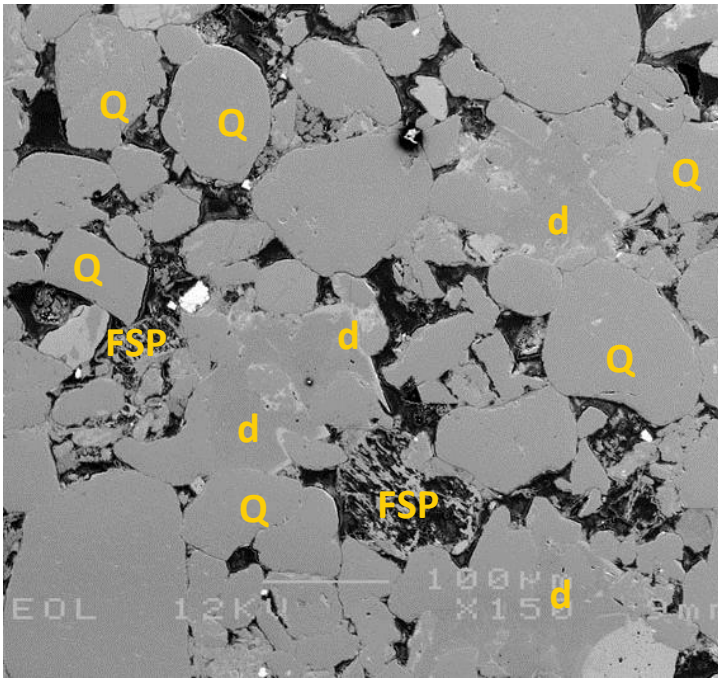
**A. Magnification 150x**
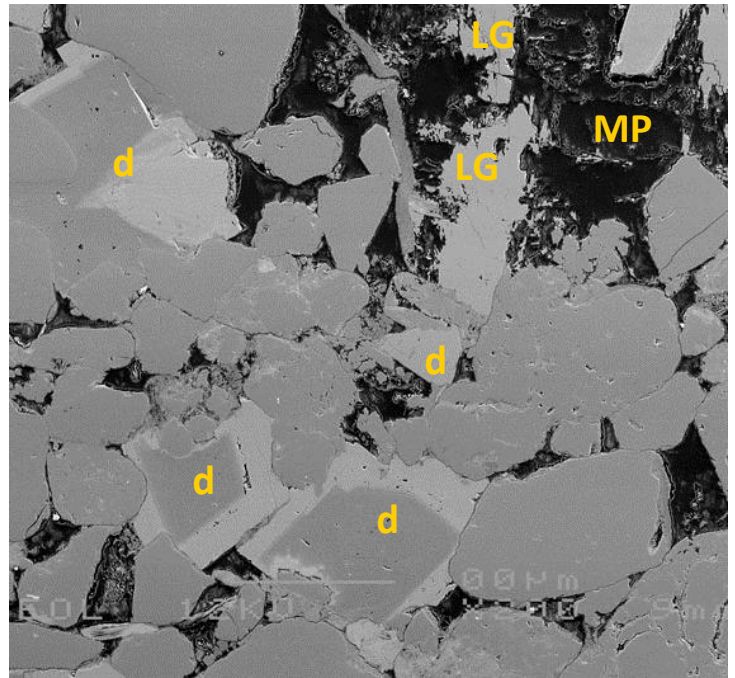
113µm

**B. Magnification 200x**

85µm
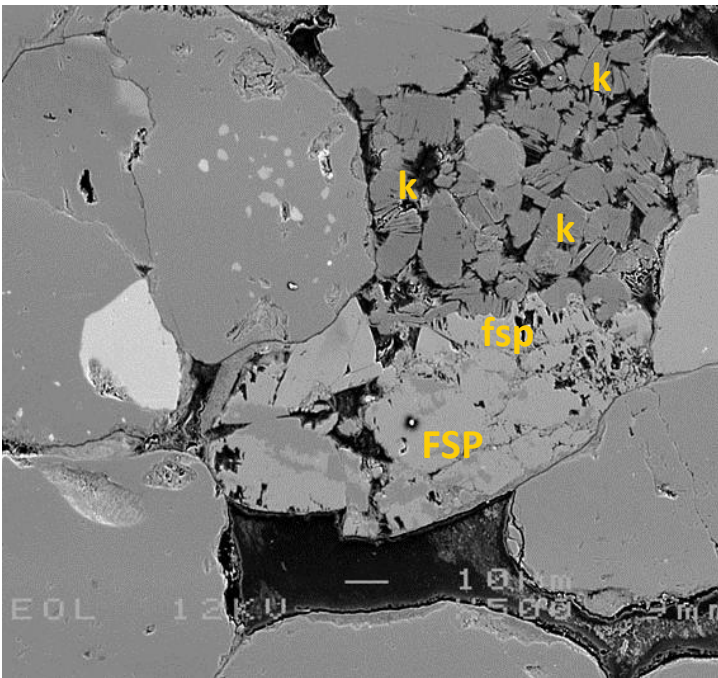
**C. Magnification 500x**

34µm
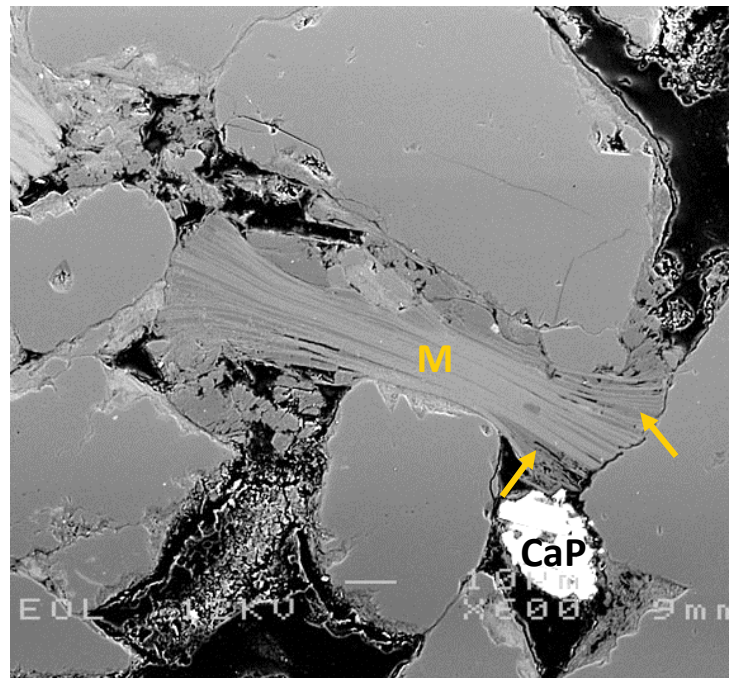
**D. Magnification 600x**

28µm

**Plate A:** This sublitharenite contains relatively common pore-filling dolomite (d), locally engulfing detrital grains. Also relatively common are leached feldspar grains, with K-feldspar (FSP) remaining. Despite the strong leaching, feldspar grains remained relatively undeformed. The irregular shape of some detrital quartz grains (Q) indicates that small quartz overgrowths do occur. **Plate B:** The dolomite cement (d), which is also common in this field of view, has a thick brighter rim which is more iron-rich. Multiple leached grains, including leached K-feldspar (FSP) and mouldic pores (MP) at the top of the image result in a large macropore. Elsewhere, pores are poorly connected. **Plate C:** A K-feldspar (FSP) grain was broken due to compaction, leached and partially replaced with kaolinite engulfing K-feldspar (fsp). This feldspar is wrapping around authigenic kaolinite (k) which formed at an earlier stage. Clay rims are mostly thin or absent. **Plate D:** Muscovite (M), which is an accessory mineral in the sample set, is slightly deformed and expanded. In between the muscovite platelets, kaolinite occurs (arrows). Note the bright authigenic apatite (CaP). The patchy nature of the pores is partially due to poor impregnation of epoxy resin.
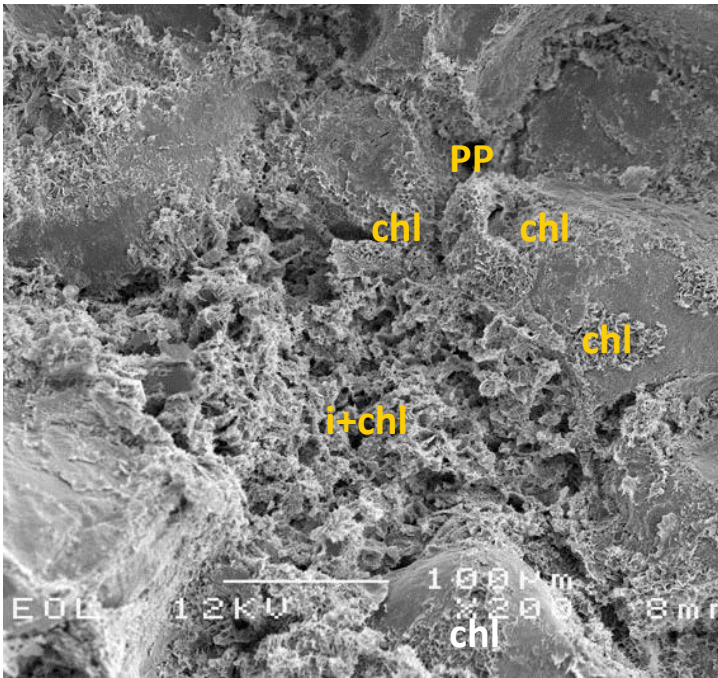
**A. Magnification 200x**

85µm
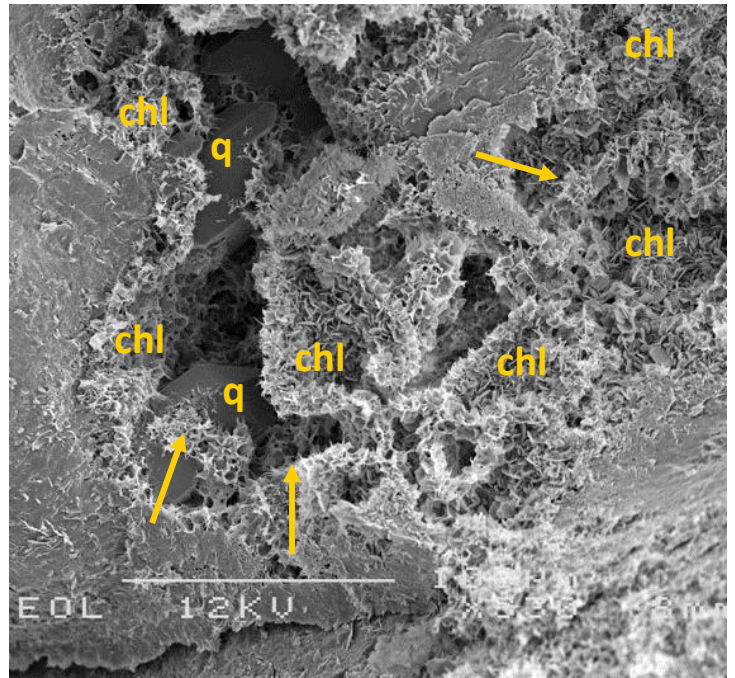
**B. Magnification 330x**

52µm

**C. Magnification 600x**

28µm
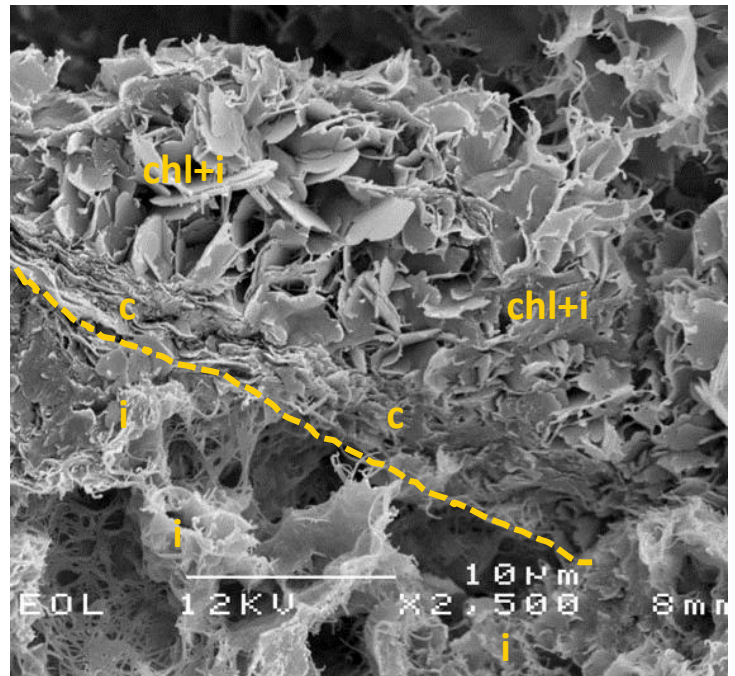
**D. Magnification 2500x**

7µm

**Plate A:** This sandstone comprises detrital grains covered with a discontinuous rim of radial clay, mostly chlorite (chl). In between the detrital grains, a strongly leached grain occurs, which now comprises mostly fibrous illite and chlorite (i+chl). Intergranular pores are often filled with authigenic chlorite-rich clay and are relatively small (PP). **Plate B:** Rosette-shaped chlorite (chl) occurs as, what appears to be detached clay coatings, partially filling up intergranular pores. Chlorite is locally mixed with illite, which is more fibrous (arrows). Note the quartz outgrowths (q), which have formed in the larger pores, indicating the texture as observed here formed prior to quartz cementation. **Plate C:** This fine grained detrital grain (feldspar?) has a very rough surface which is dissimilar to the chlorite (chl(+i; mixed with illite)) coating of the surrounding grains. The grain is partially leached and contains some fibrous illite (i) and chlorite (arrow). **Plate D:** This detailed image shows the boundary (dashed line) between a microporous leached feldspar grain, which is now filled with illite (i). Note the tangential clay coating (c; mostly illite), which is covered with rosette-shaped chlorite and fibrous illite (chl+i).
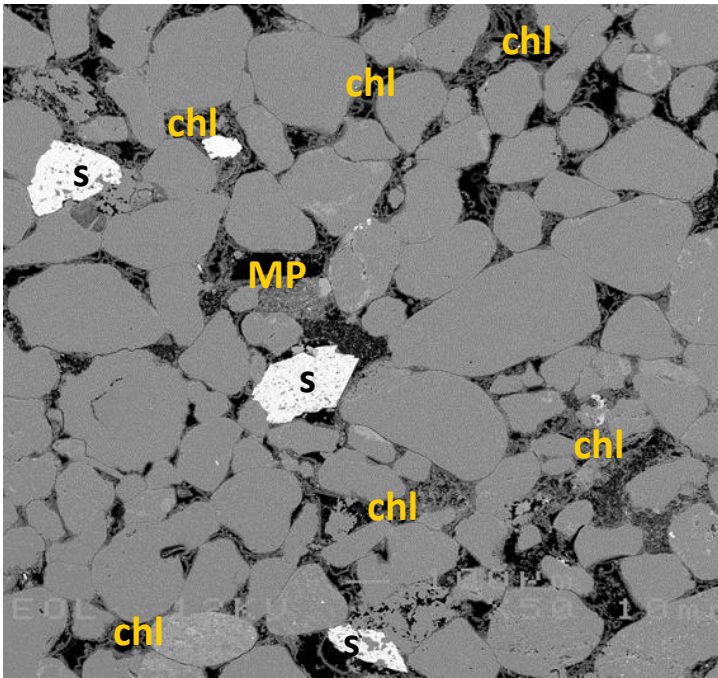
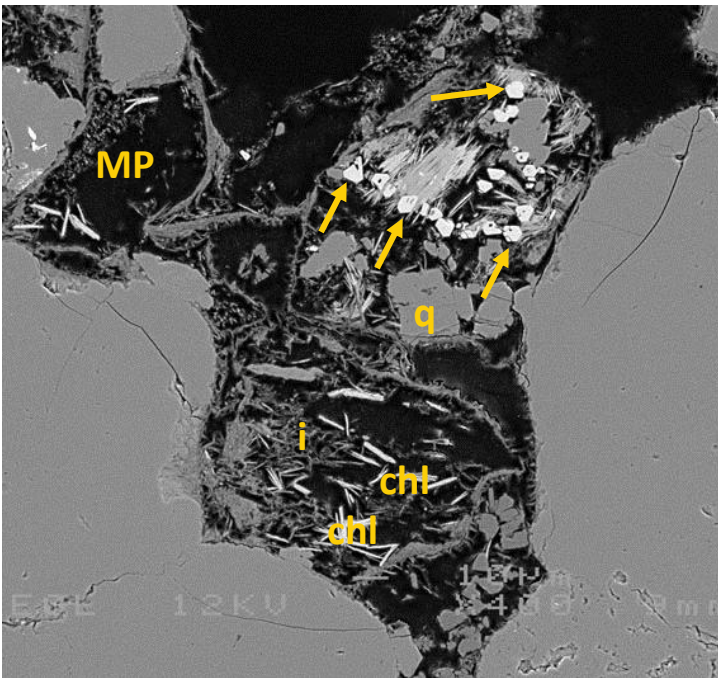**A. Magnification 50x**
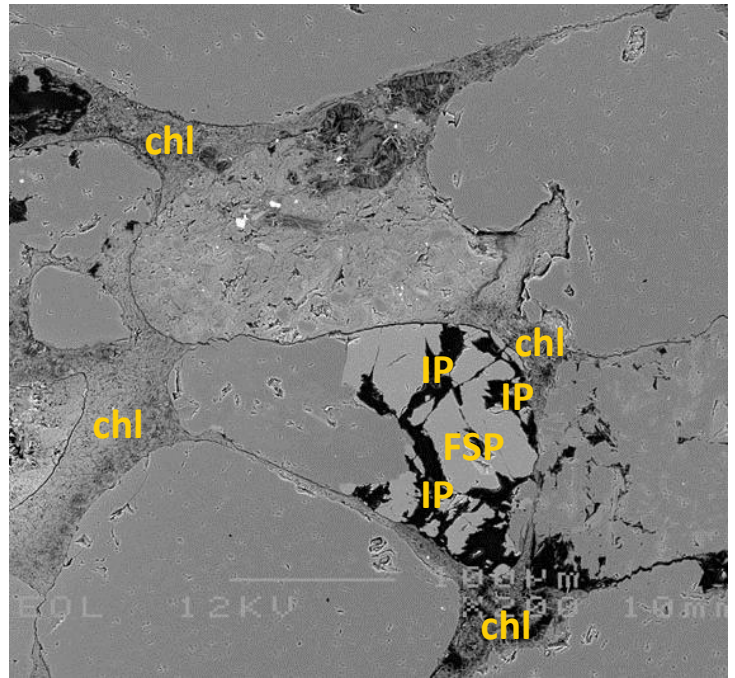
340µm

**B. Magnification 200x**

85µm

**C. Magnification 250x**

68µm
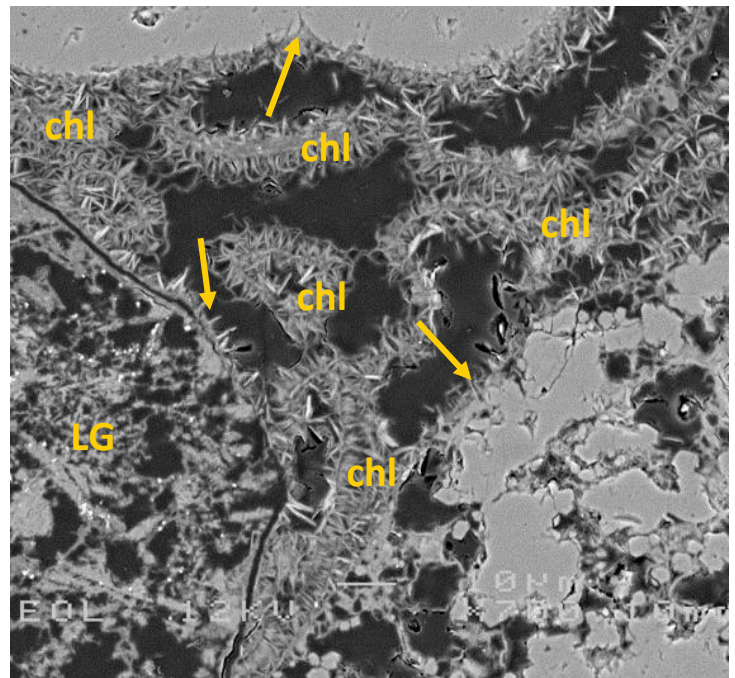
**D. Magnification 700x**

24µm

**Plate A:** This relatively quartz-grain rich sublitharenite contains patches of siderite (s) cement. An elongated mouldic pore (MP) occurs in the centre. Elsewhere, the larger intergranular pores are largely filled with thick radial chlorite, which reduces the permeability. **Plate B:** This photo shows that some macropores are secondary intragranular pores (IP) which formed in e.g. leached K-feldspar (FSP). Chlorite (chl; identified with EDX) is locally very closely packed, filling up the intergranular spaces. Individual clay rims are difficult to identify here. **Plate C:** Locally, leached grains (outlined) can be difficult to distinguish from the chlorite strings (chl) that have formed prior to grain leaching. The leached grain here is replaced by authigenic kaolinite (k). There are no macropores in this field of view, but common micropores. **Plate D:** Detailed photo of the chlorite (chl; fibrous in 2D) occurring in the intergranular spaces. Two different leached grains (LG) with possibly some illite are shown on the left and the right side of the image. The clay coating still attached to the detrital grains is also mostly chlorite (arrows).
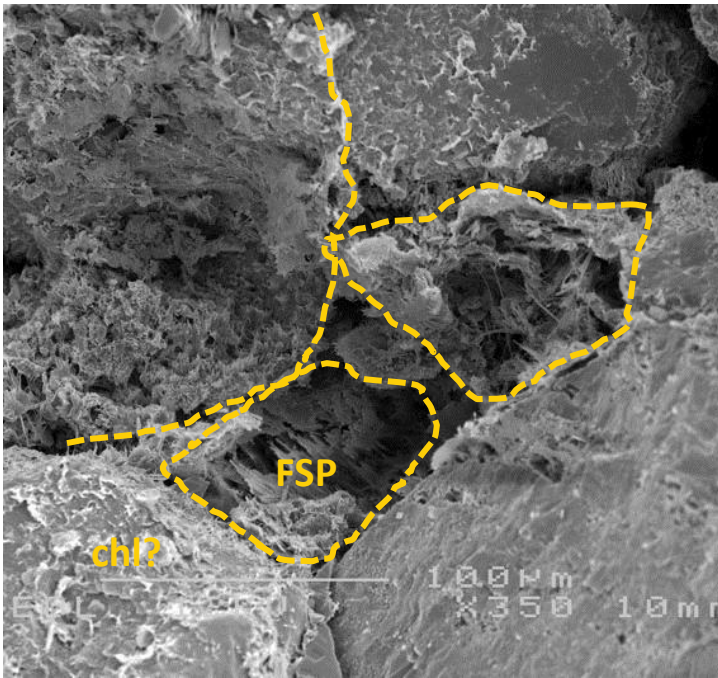
**A. Magnification 350x**
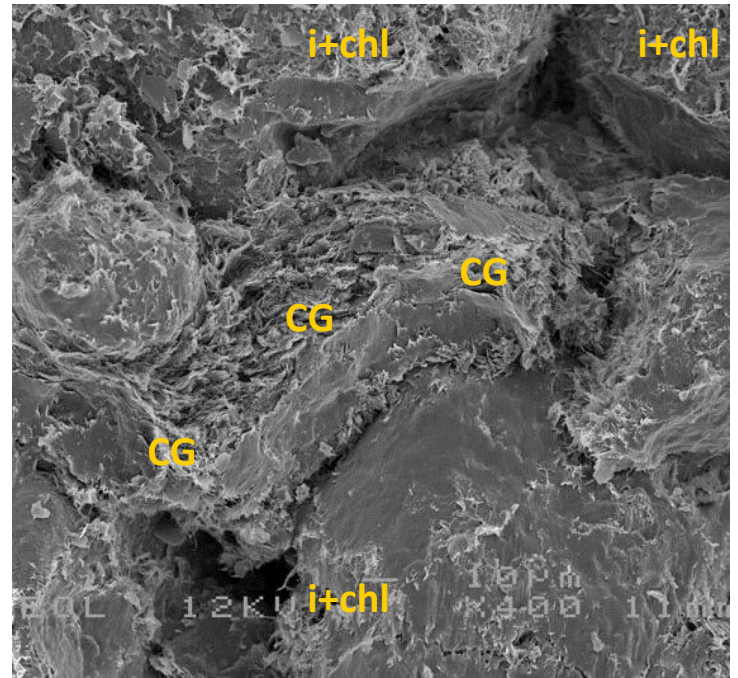
49μm



**B. Magnification 400x**

43μm
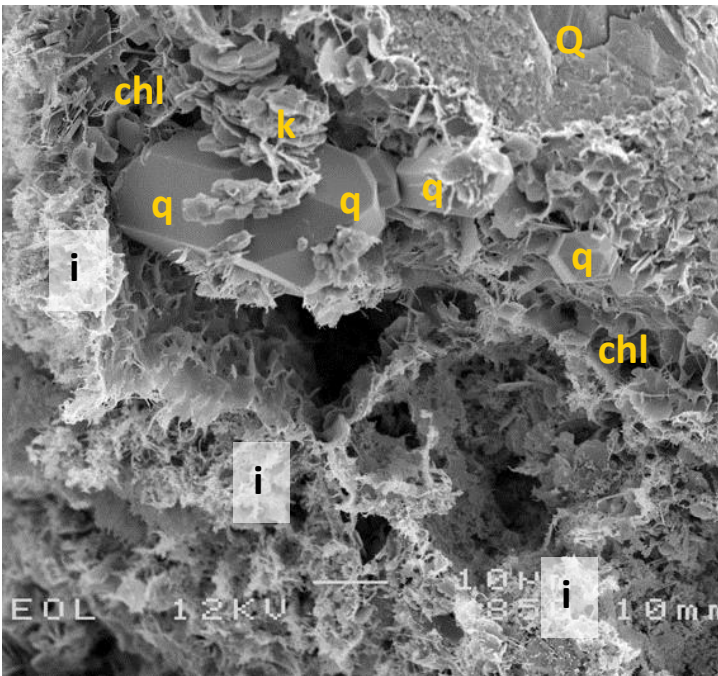


**C. Magnification 850x**

20μm
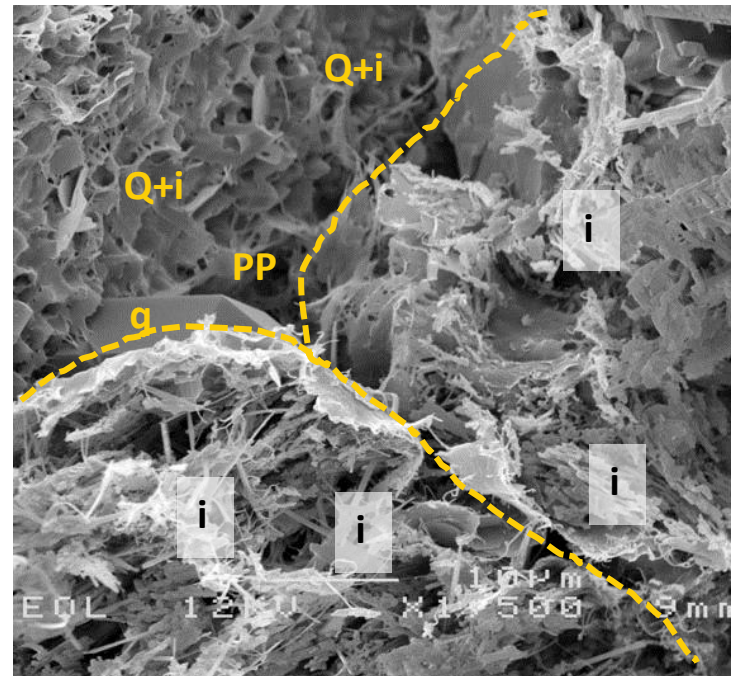


**D. Magnification 1500x**

11μm

**Plate A:** The authigenic clay in this sandstone appears to be most commonly a result of leaching of grains, mostly feldspar. In this field of view, at least 3 different leached grains are visible (outlines). One leached feldspar grain has residual lamellae (FSP). Authigenic clay in the leached grains is mostly illitic (i). Clay coatings around rigid detrital grains are flaky and most likely chloritic (chl?). **Plate B:** A clay grain (CG) is squeezed in between rigid grains due to compaction. The detrital clay in this grain is mostly illite, whereas the clay coating on this and other grains is a combination of illite and chlorite (i+chl). **Plate C:** Detailed photo of what appears to be a detached fibrous illitic clay coating (i). In between the coating and the detrital quartz grain (Q) authigenic quartz (q) is present. Minor amounts of kaolinite (k) and chlorite (chl) occur as well. **Plate D:** Another detailed photo of a small pore (PP) between two leached feldspar grains (outlines) and a quartz grain. The latter is coated with honeycomb-like illite (Q+i). In the pore, small authigenic quartz crystals have formed (q). Feldspar grains are converted to fibrous illite (i).
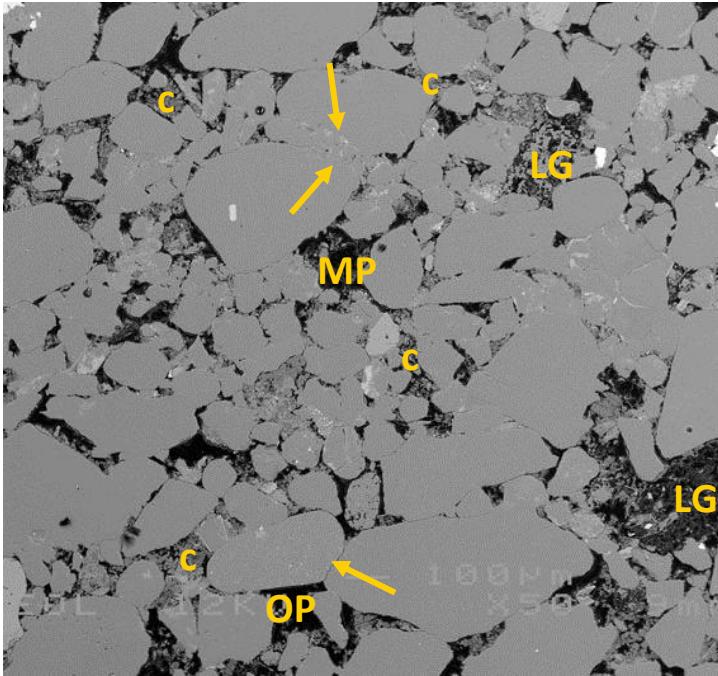
**A. Magnification 50x**

340µm
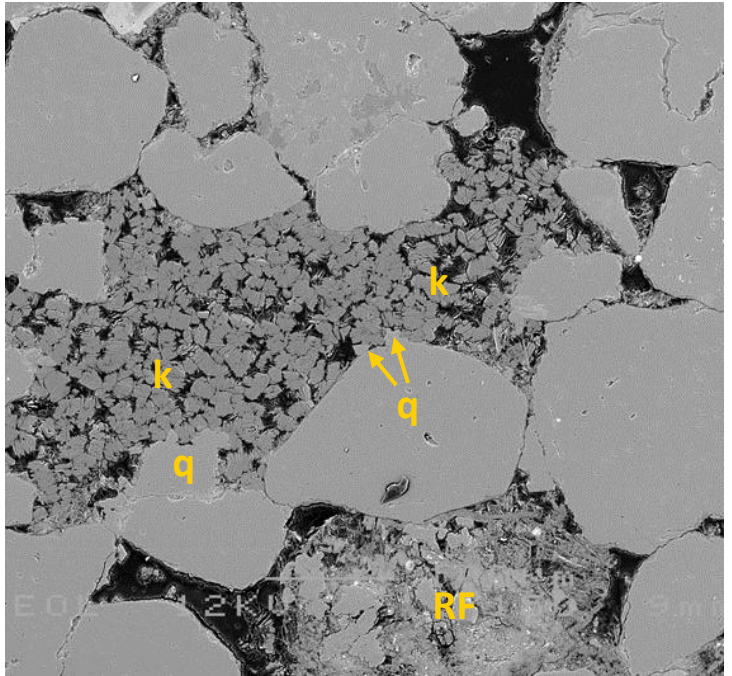
**B. Magnification 150x**

85µm
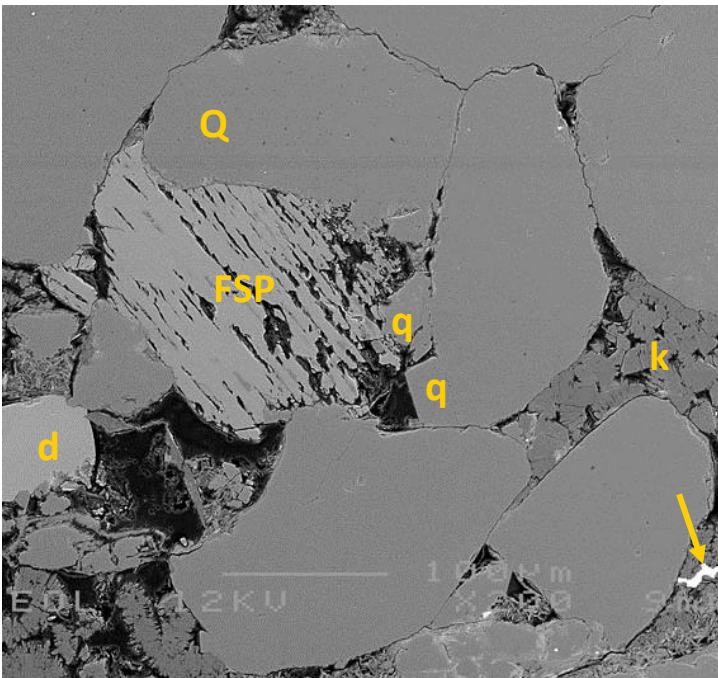
**C. Magnification 200x**

57µm
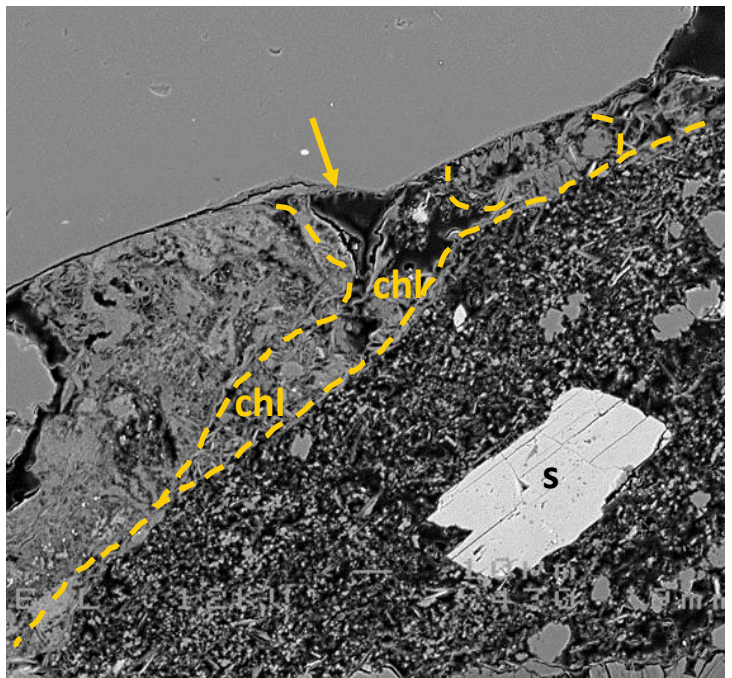
**D. Magnification 430x**

40µm

**Plate A:** The rock fragments in this relatively poorly sorted sublitharenite contain significant micropores due to leaching (LG). Locally, mouldic pores (MP) and oversized pores (OP) are present. Elsewhere, macropores are commonly filled with authigenic clay (c; some is kaolinite). Some serrated grain boundaries suggest local chemical compaction (arrows). **Plate B:** This image shows a large cluster of authigenic kaolinite (k), which is locally overgrown by quartz cement (q). This quartz cement gives the detrital grains an irregular shape, even though the grains themselves are relatively well-rounded. Note the microporous rock fragment (RF). Radial illite coating is absent (in this field of view) and tangential illite is uncommon. **Plate C:** The K-feldspar grain (FSP) is leached along the cleavage planes. Cleavage planes are not deformed, even though a quartz grain (Q) is indenting into the feldspar grain. The kaolinite in this image is relatively closely packed. Note the quartz (q), dolomite (d) and barite (arrow) cement that formed in the pores. **Plate D:** Three leached grains next to each other (outlined), with authigenic clay (mostly chlorite; chl) in between. Macropores are small. Note the siderite cement (s) and the thin clay rim (arrow).
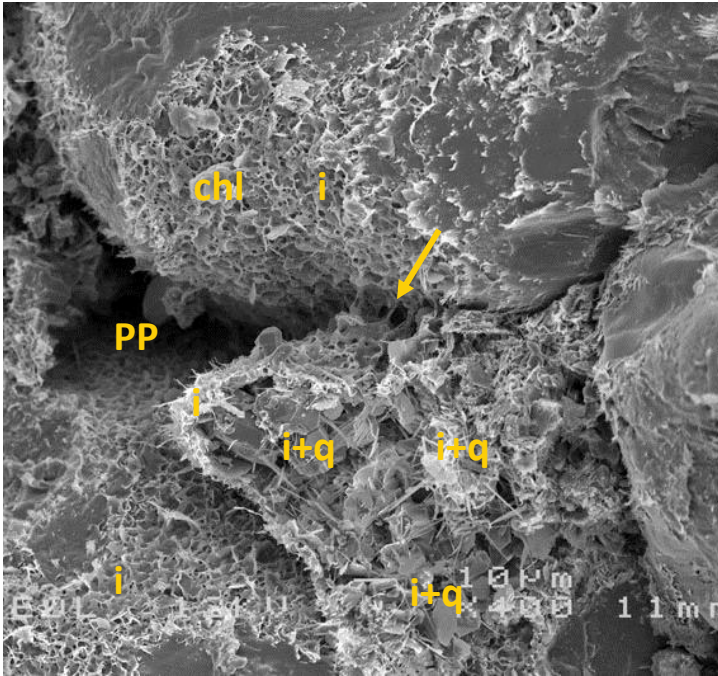
**A. Magnification 400x**

43µm
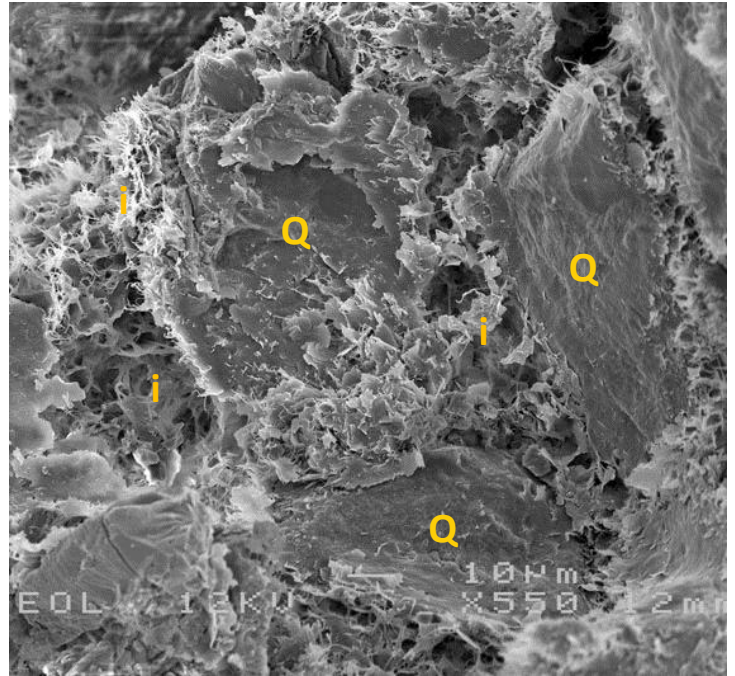
**B. Magnification 550x**

31µm
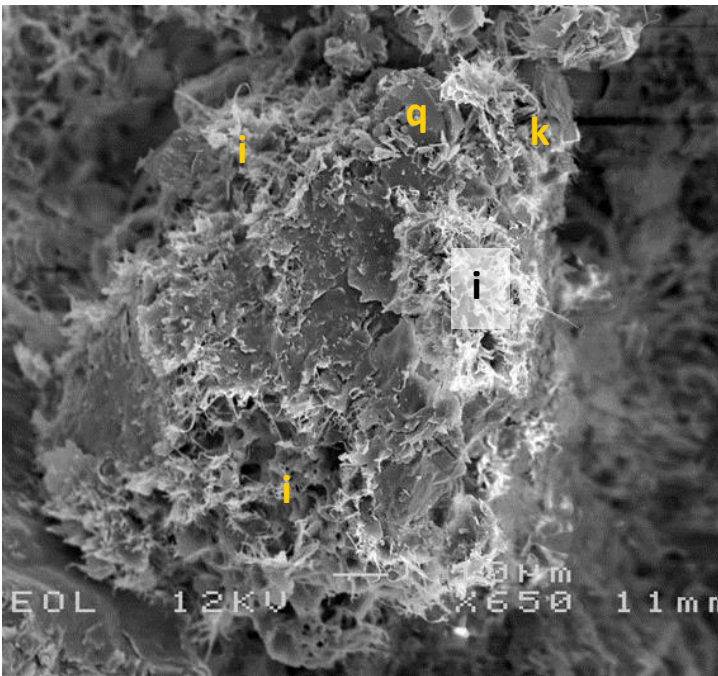
**C. Magnification 650x**

26µm
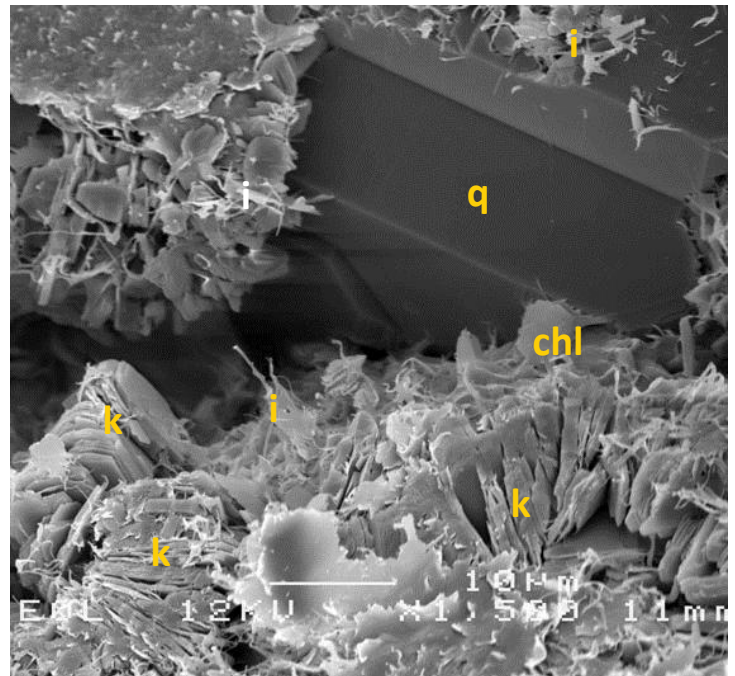
**D. Magnification 1500x**

11µm

**Plate A:** The detrital grains in this very fine to medium grained sandstone are covered with an illite (i) and chlorite (chl) clay rim. Intergranular pores (PP) locally remained relatively large. The photo also shows a leached grain (feldspar?) which now contains replacive fibrous illite and euhedral quartz (i+q). Note the illitic clay rim (i) around the original grain, and the pore-bridging illite (arrow). **Plate B:** Authigenic grain coating illite (i) around detrital quartz grains (Q) is reducing the reservoir quality significantly as it bridges all the pores, leaving no macropores. Since the illite fibres do not show signs of deformation, it is unlikely this sample has been deformed recently. **Plate C:** Due to the significant and irregularly shaped clay coatings (mostly illite; i), the detrital grains underneath the coating cannot be identified. Note the small quartz overgrowths (q) and authigenic kaolinite (k). **Plate D:** This detailed image shows the combination of fibrous illite (i), platy chlorite (chl) and booklet-shaped kaolinite (k), covering detrital grains. Note the pore-bridging quartz cement (q).
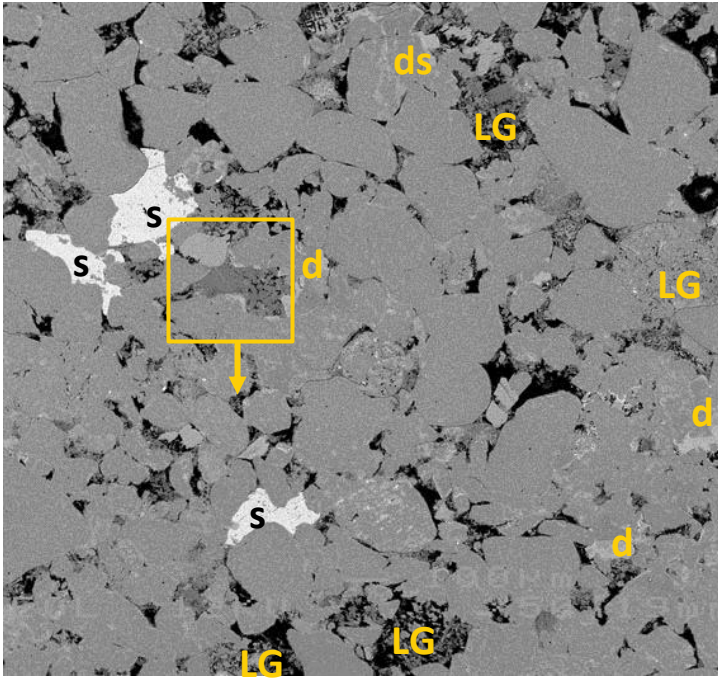
**A. Magnification 50x**

340µm
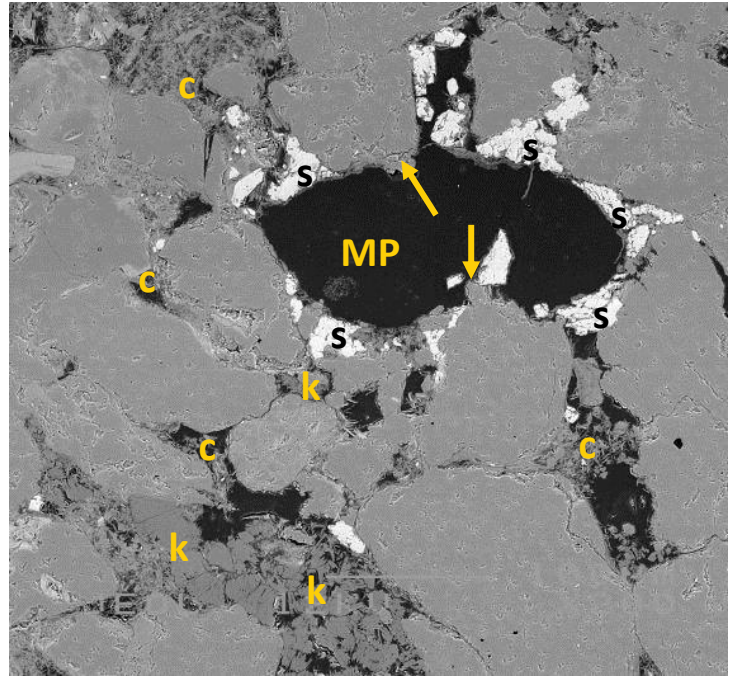
**B. Magnification 200x**

85µm
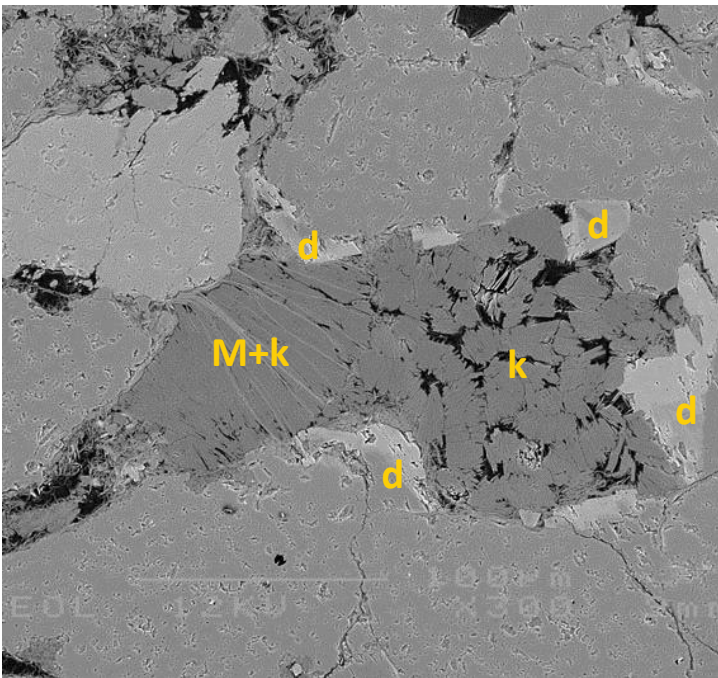
**C. Magnification 300x**

57µm
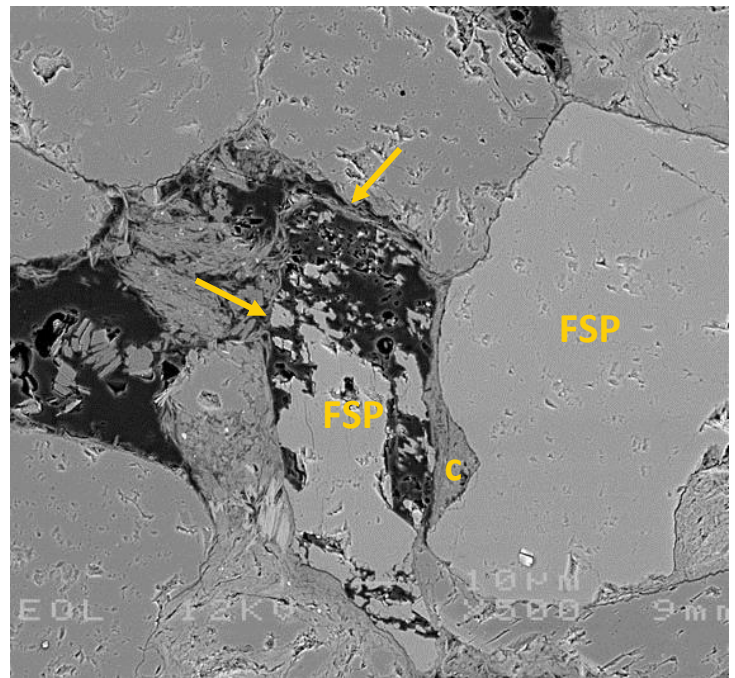
**D. Magnification 500x**

34µm

**Plate A:** The overview image of this sublitharenite shows the relative poor porosity compared to other samples from this well. This is partly due to siderite (s) and dolomite (d) cementation. Macropores (large black areas) are poorly connected. Note that leached feldspar grains and rock fragments (LG) often contain micropores. **Plate B:** The mouldic pore (MP) imaged here shows the outline of the original grain due to cementation of siderite (?; s) around it. Minor quartz cement (arrows) has formed in the mouldic pore. Smaller pores are commonly filled with clay (c) such as illite and chlorite. Locally, clustered kaolinite (k) occurs. Note the deformed muscovite (M). **Plate C:** Photo from the inset in plate A, showing densely packed kaolinite (k) with micropores (black). The kaolinite is engulfed by by dolomite (d) which is indication that the dolomite postdates kaolinite. The image also shows a mica that is mostly transformed to kaolinite (M+k?). **Plate D:** K-feldspar (FSP) can be either preserved (right) or strongly leached (centre). The leached feldspar is outlined by an illitic clay rim (arrows). The unleached feldspar has a thick clay (c) rim covering the concave part of the grain. Some clay might be pseudomatrix (i.e. squeezed clay due to compaction).
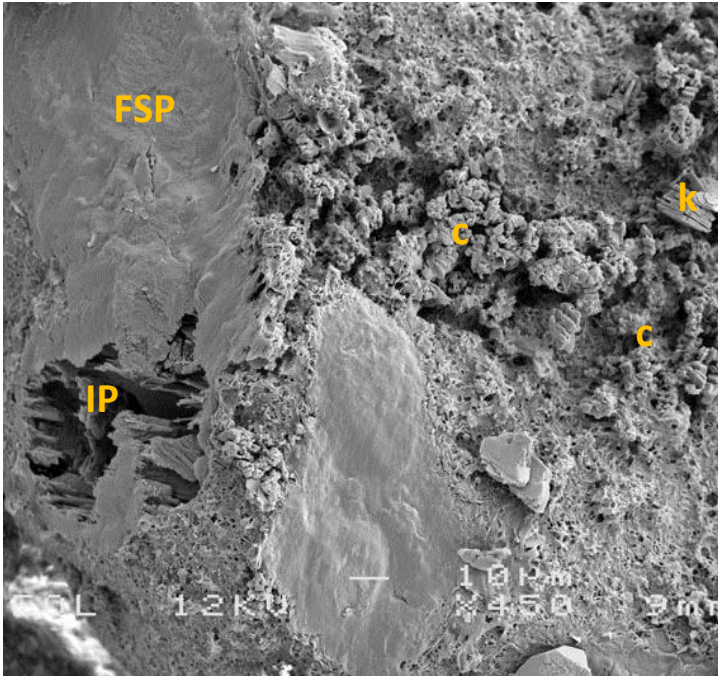
**A. Magnification 450x**
38μm
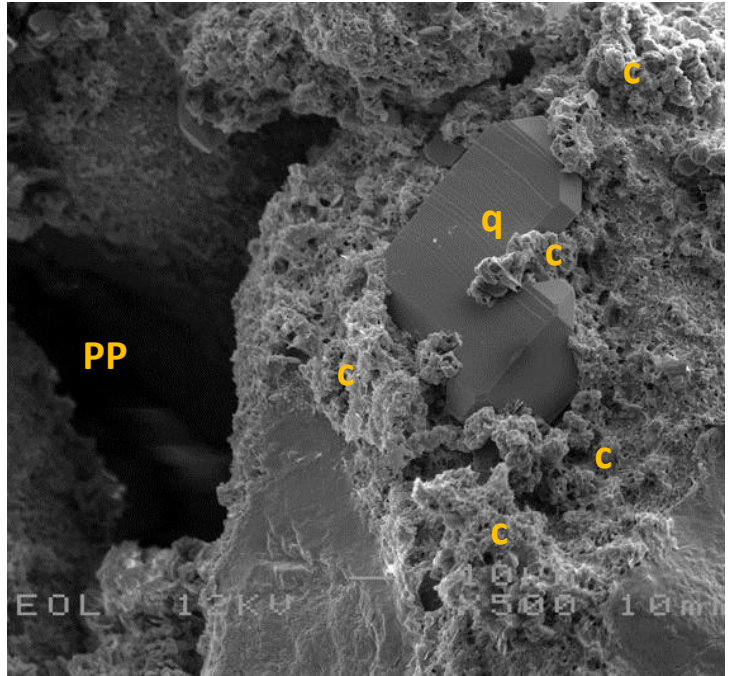
**B. Magnification 500x**
34μm
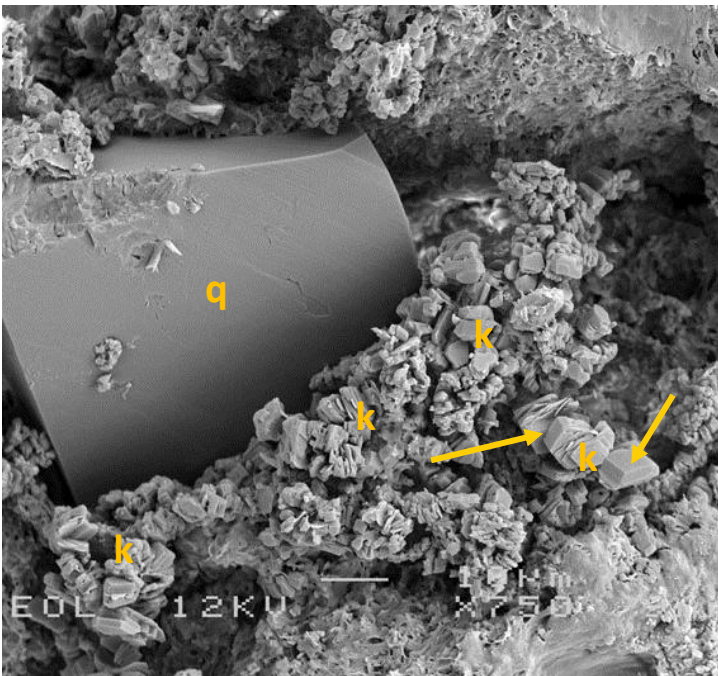
**C. Magnification 750x**
23μm
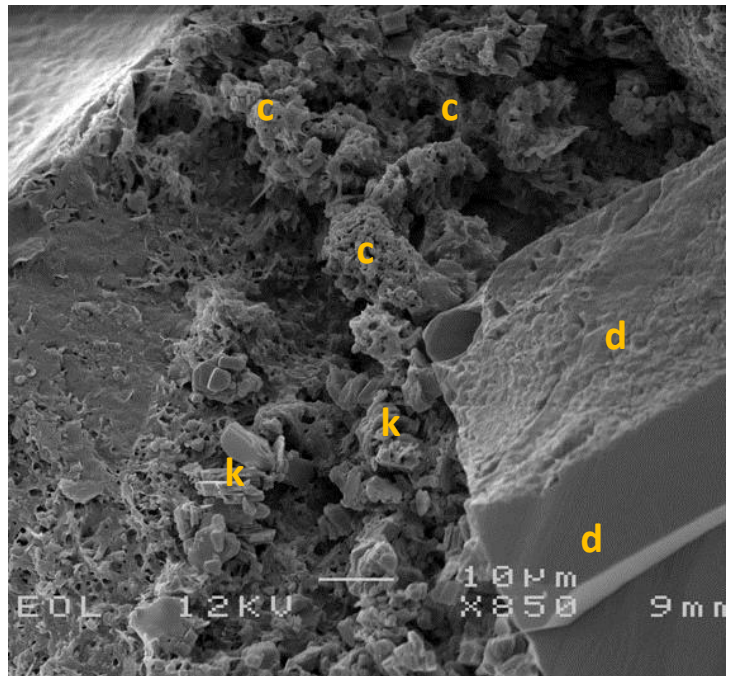
**D. Magnification 850x**
20μm

**Plate A:** This very fragile, medium grained sandstone comprises common feldspar according to XRD. As is visible in this photo, (plagioclase?) feldspar grains are locally partially leached (FSP), resulting in secondary intragranular porosity (IP). The illitic clay coatings (i), which are common in the sample set, are relatively thin in this sample. Fine crystalline, unidentified clay (c; possibly a mixture of clay minerals) occurs commonly on top of the illite clay coatings. Kaolinite (k) is coarser crystalline and relatively rare. Note that strongly leached feldspar grains were charging and could not be photographed. **Plate B:** Locally, euhedral quartz overgrowths (q) are present in between the fine crystalline clay (c). Intergranular pore spaces (PP) are large, despite the relatively common clay. **Plate C:** Locally, kaolinite (k) occurs more commonly in the intergranular pores. The authigenic kaolinite is replacive. Some of the thicker crystals are most likely dickite crystals (arrows), which is a polymorph of kaolinite. Also here, euhedral quartz outgrowths (q) occur. **Plate D:** Dolomite cement (d; here with some Ca and Fe according to EDX) is also present in the intergranular pore spaces. In this image, the fine crystalline clay occurs (c) together with kaolinite (k).
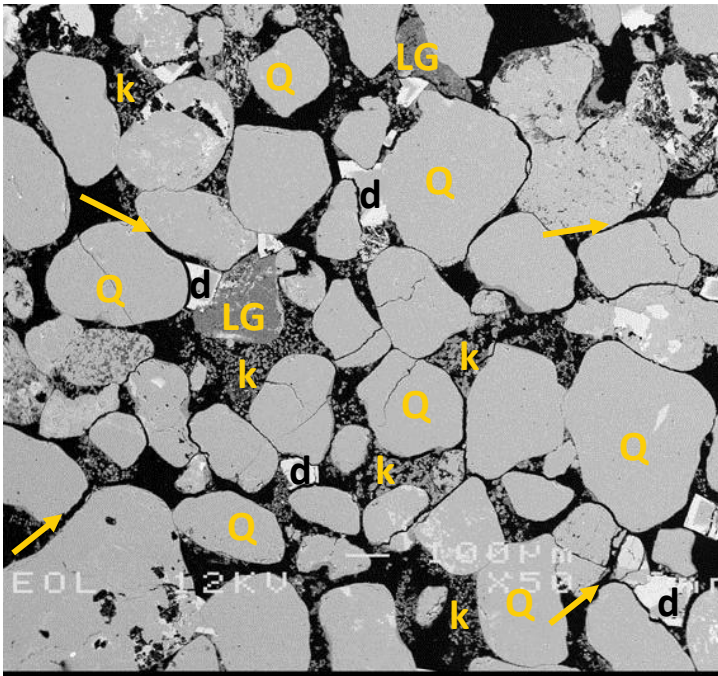
**A. Magnification 50x**
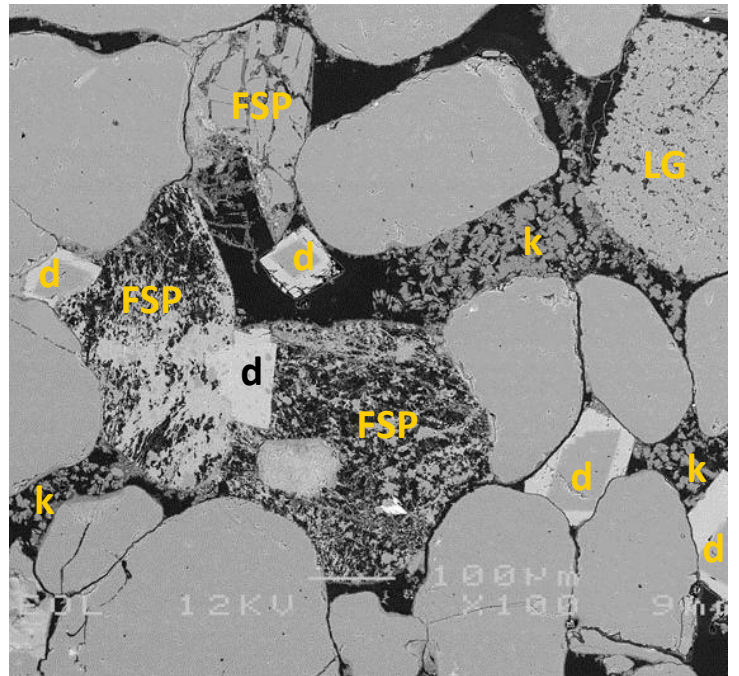
340μm

**B. Magnification 100x**

170μm
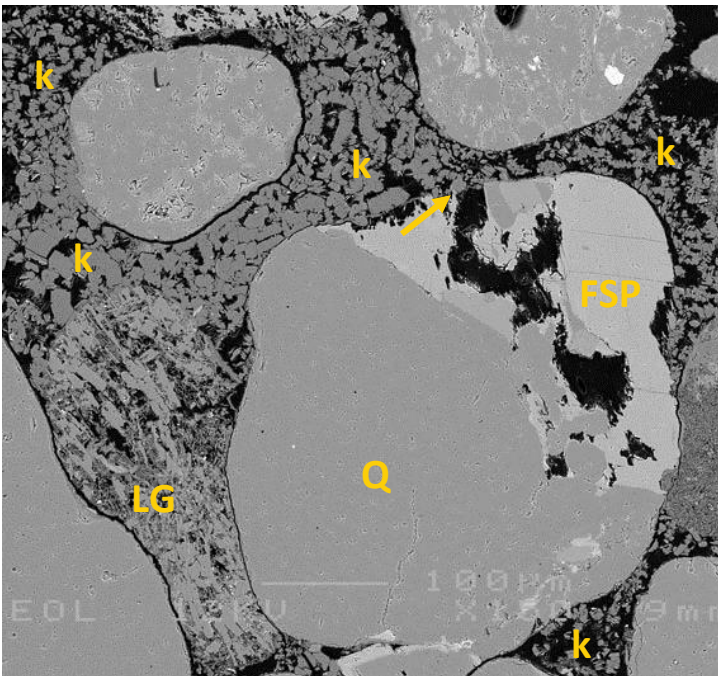
**C. Magnification 150x**

113μm
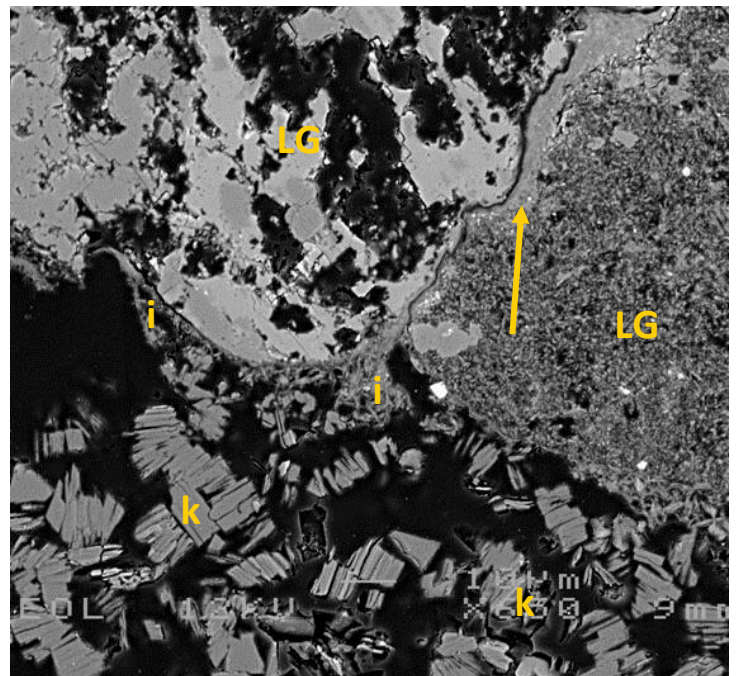
**D. Magnification 650x**

26μm

**Plate A:** This fairly well sorted, fragile sandstone sample contains predominantly detrital quartz grains (Q). Authigenic clay in this field of view is mostly kaolinite (k) and locally illite within leached rock fragment (RF). Patches of dolomite (d) cement occur, with thick brighter (Fe-rich) rims. Due to the poor consolidation, detrital grains are slightly dilatated from each other due to plugging or sample preparation, hence the large spaces between some detrital grains (arrows). **Plate B:** Various types of leached grains (LG) occur. Most are leached feldspar grains (FSP), with either K-feldspar or albite remaining. Note the clustered kaolinite (k) and the zoned dolomite (d). Locally, dolomite formed within the pores of the leached grains. **Plate C:** Detailed view showing a composite grain (possibly igneous) containing leached K-feldspar (FSP) and quartz (Q). Kaolinite (k) is filling pores, leaving only micropores. A very thin clay coating prevents the kaolinite to be squeezed into the secondary pores (arrow). Note the squeezed leached grain (LG). **Plate D:** Detailed view of the contact between two leached grains (LG). The contact is irregular, with a thick clay rim in between (arrow). Note the authigenic illite (i) and the kaolinite (k) in the larger pore.
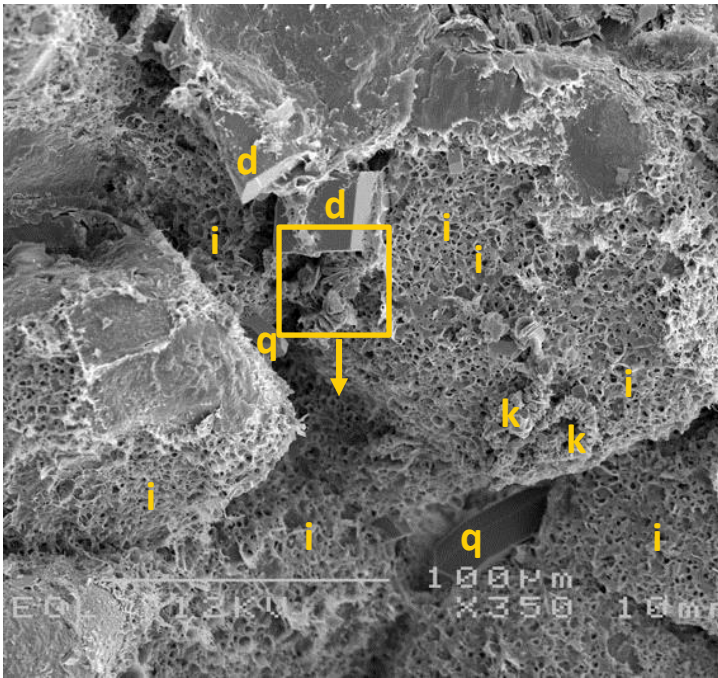
**A. Magnification 350x**

49µm
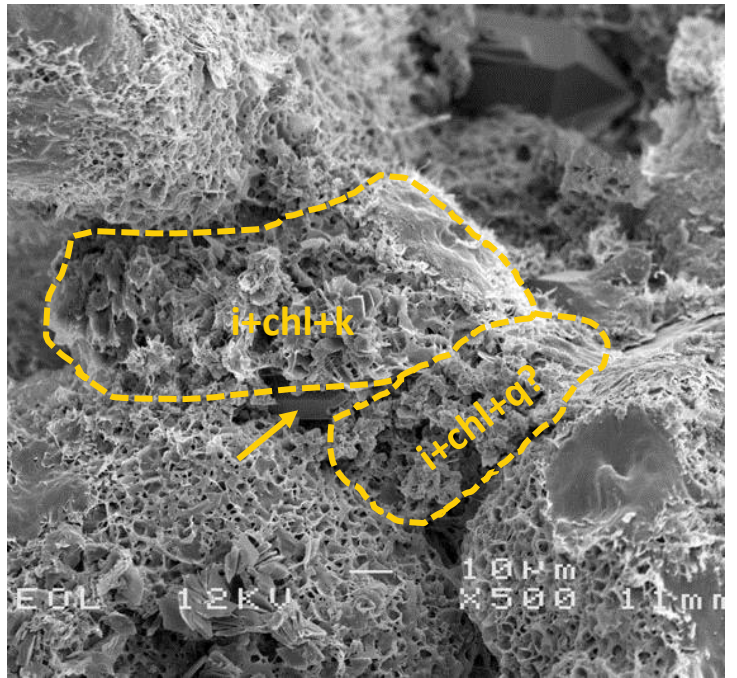


**B. Magnification 500x**

34µm
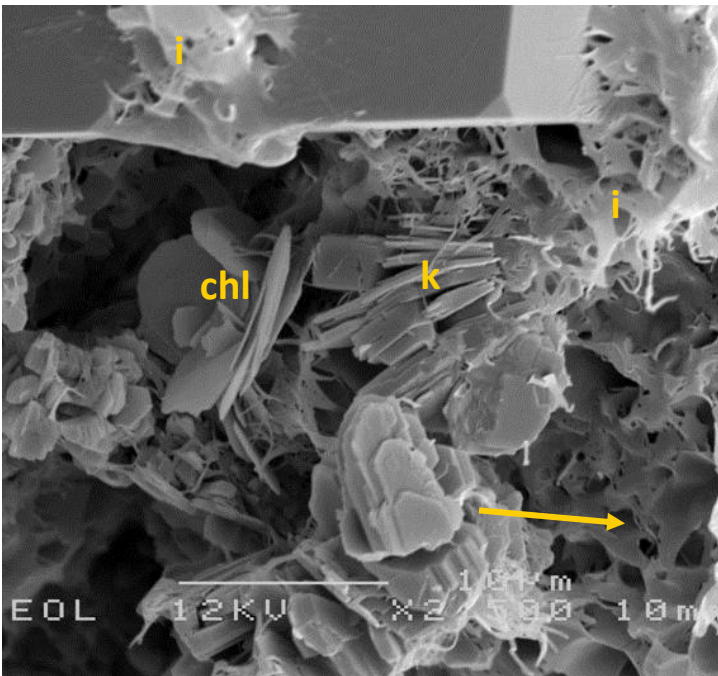


**C. Magnification 2500x**

7µm
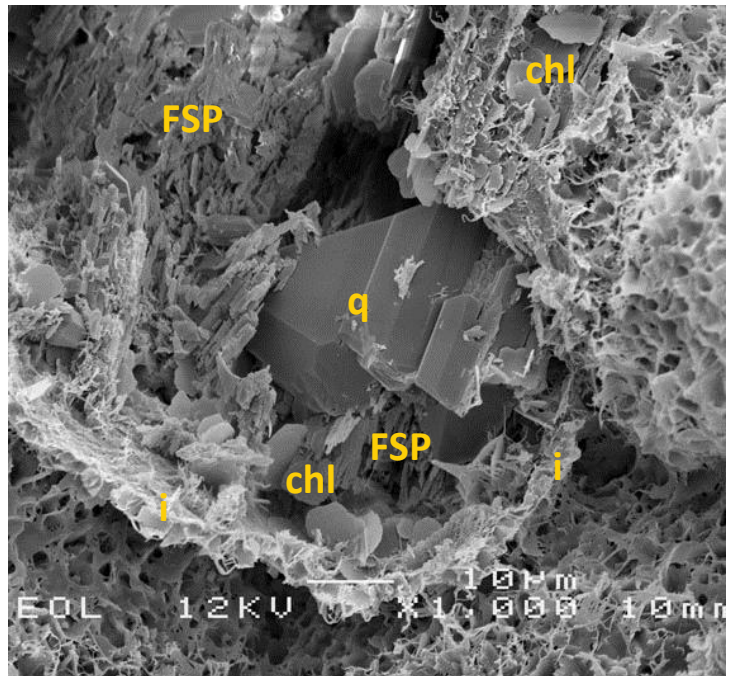


**D. Magnification 1000x**

17µm

**Plate A:** The detrital grains in this very fine grained sandstone have a continuous illitic (i) clay coating. The pore-filling cements in this sample comprise quartz (q) and dolomite (d; here Fe-rich). Also note the pore-filling booklet shaped kaolinite (k), covering the illitic clay coating. **Plate B:** This image shows two grains that are altered into clay (outlines). Grain 1 comprises a mixture of fibrous illite, platy chlorite and booklet-shaped kaolinite (i+chl+k), whereas grain two contains finer crystalline illite, chlorite and possibly some authigenic quartz (i+chl+q?). Note the authigenic quartz outgrowth (arrow) below grain 1. **Plate C:** High magnification image showing the details of the inset in plate A, where chlorite (chl), kaolinite (k) and illite (i) occur together. The illitic clay rim has a distinct honeycomb-like structure (arrow). **Plate D:** Authigenic quartz (q) has formed parallel to the (subvertical) cleavage plane of this leached feldspar grain (FSP). Note the chlorite crystals (chl) that have also formed at the expense of feldspar. The ~5µm thick illitic clay rim (i) has not been interrupted or deformed due to post-leaching compaction.
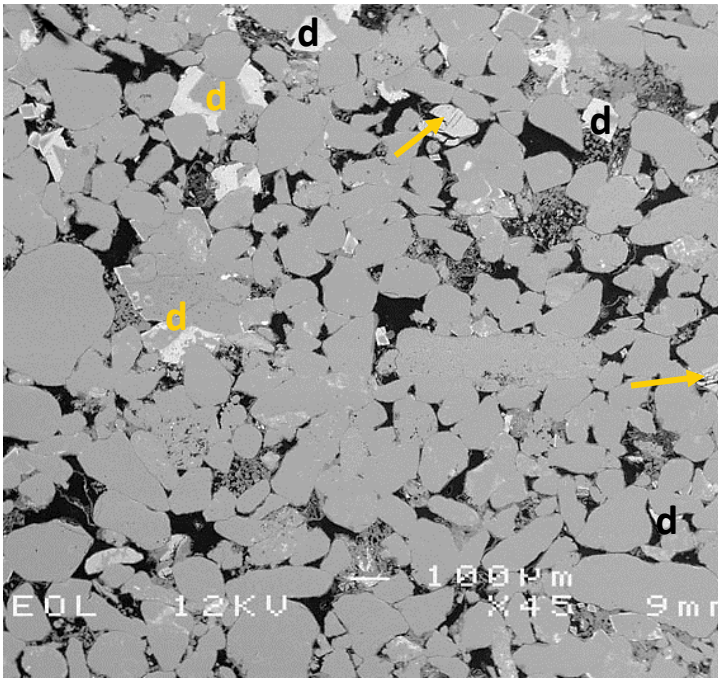
**A. Magnification 50x**

340µm
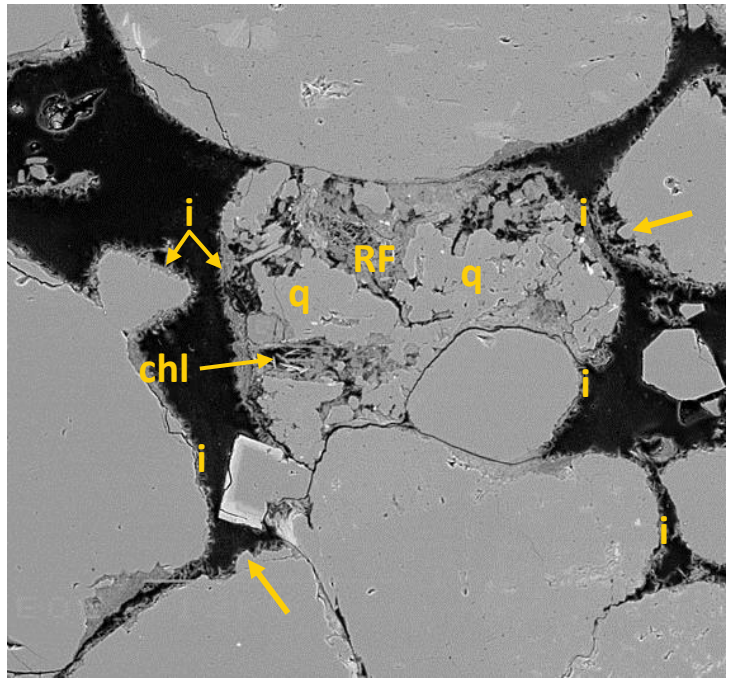
**B. Magnification 300x**

57µm

**C. Magnification 400x**

43µm
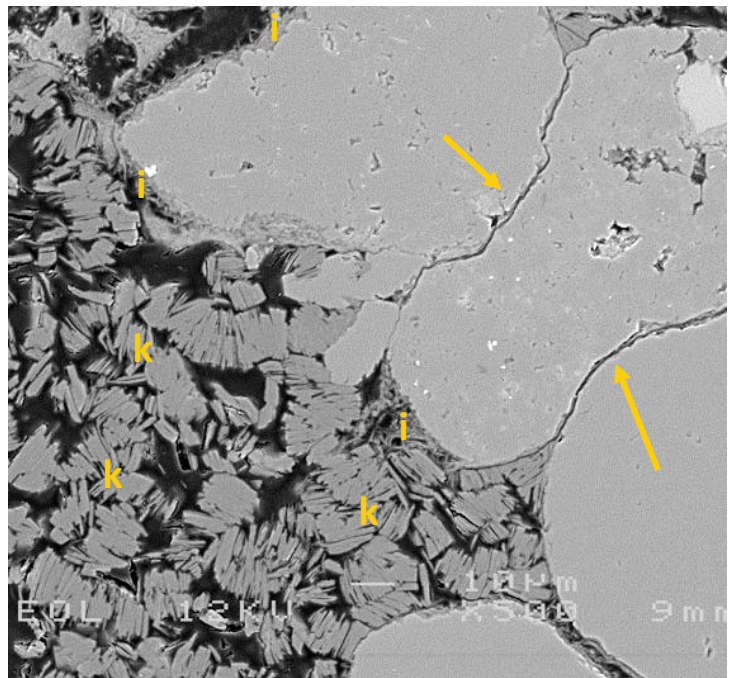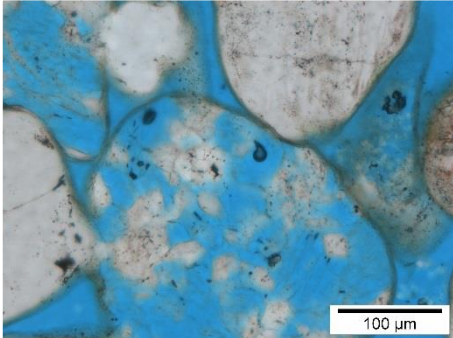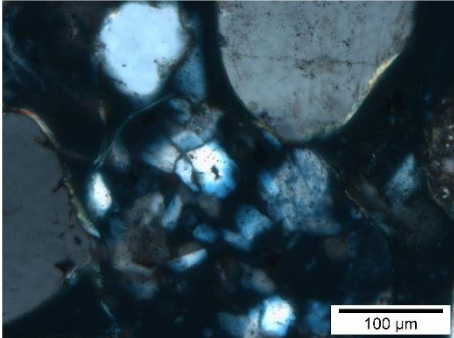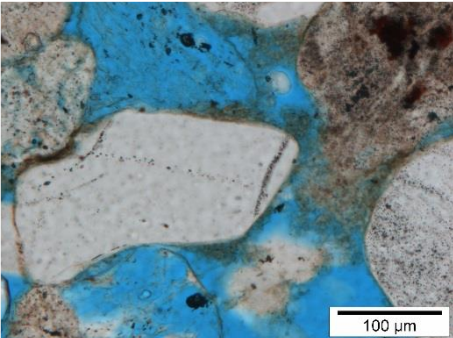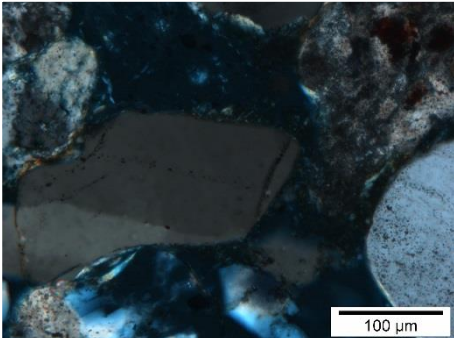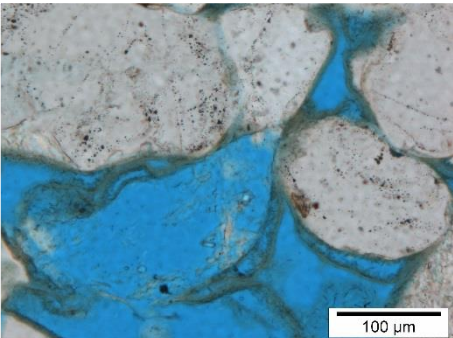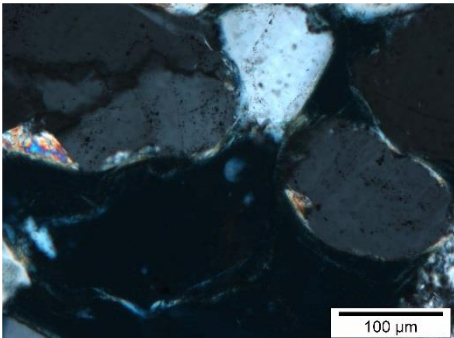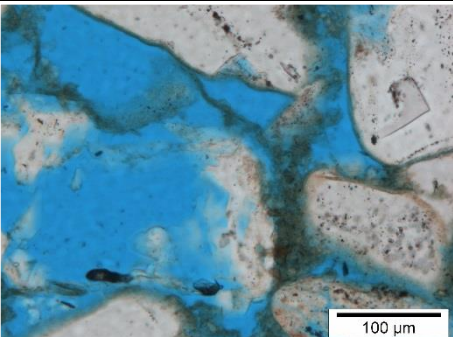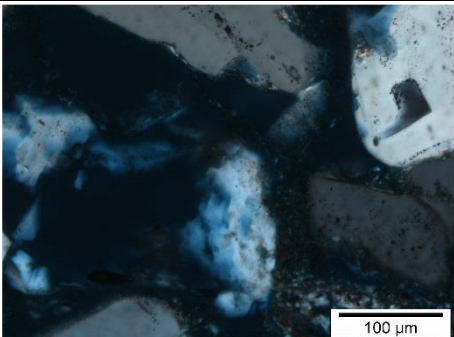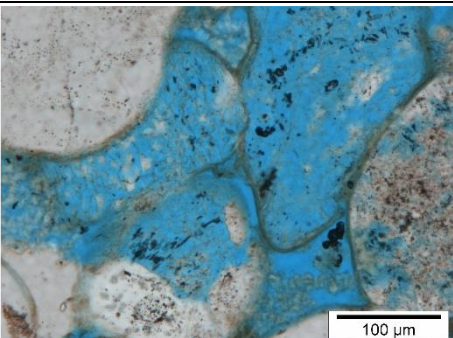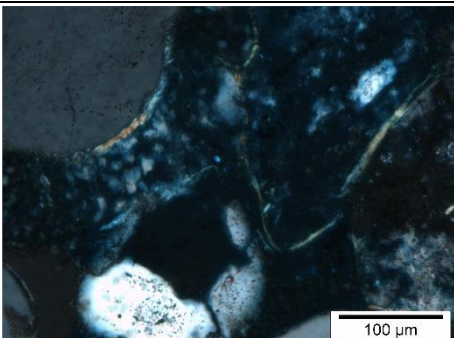
**D. Magnification 500x**
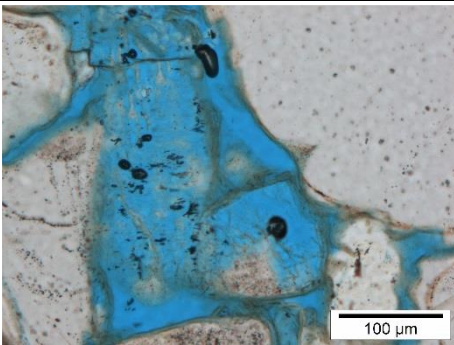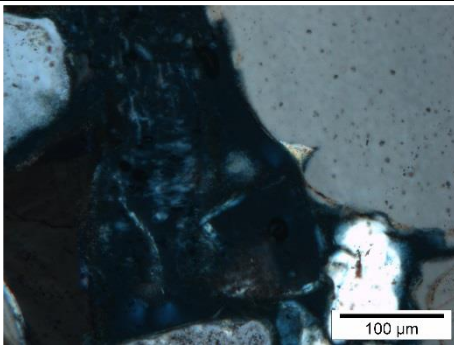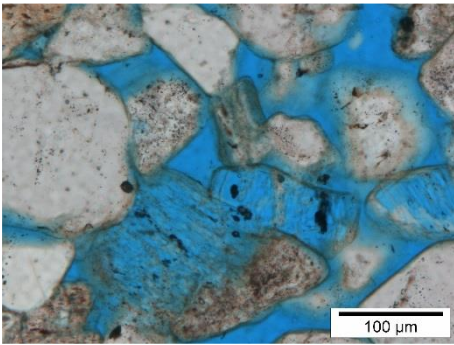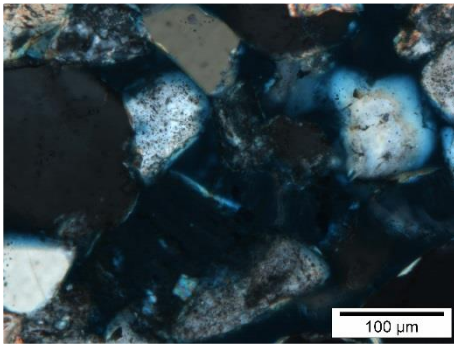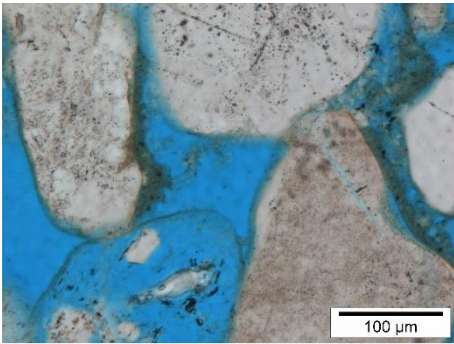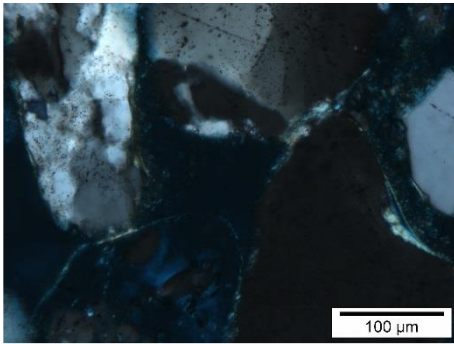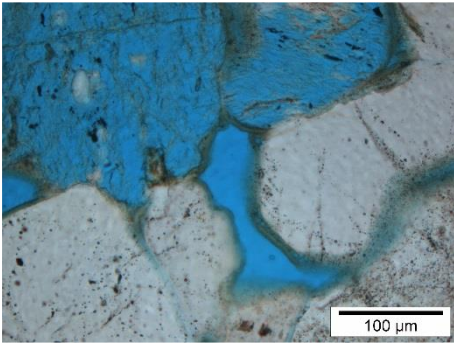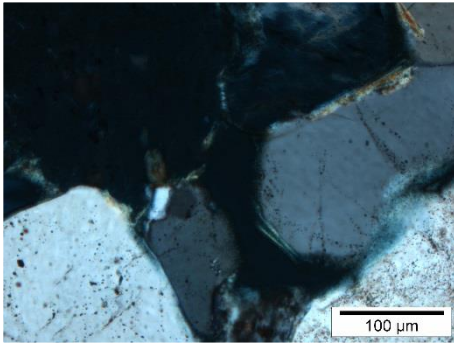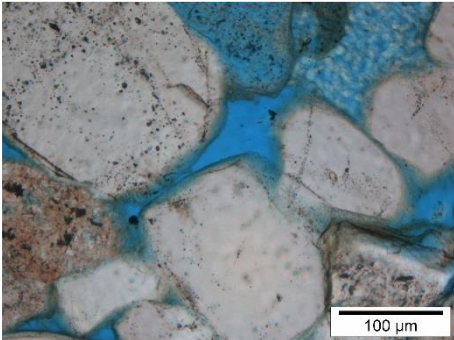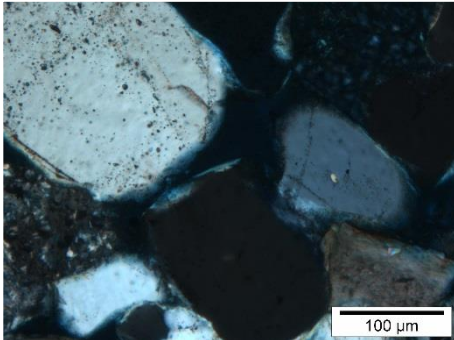
34µm
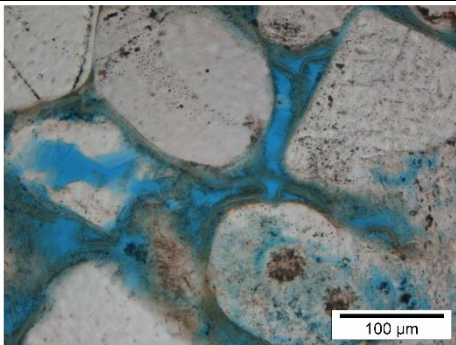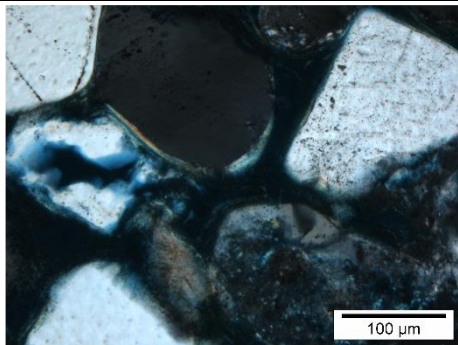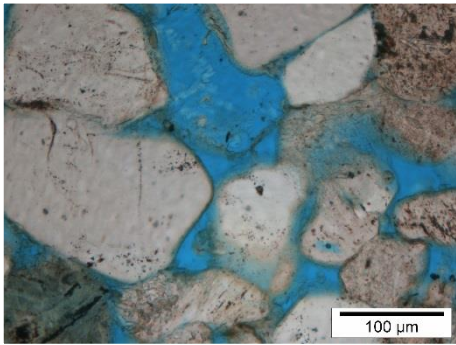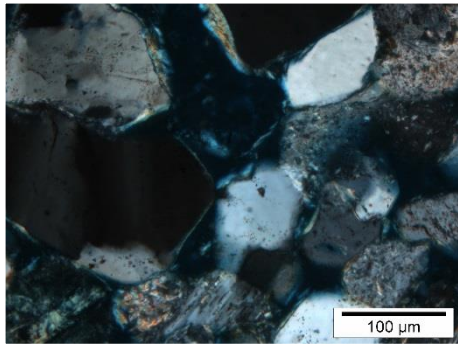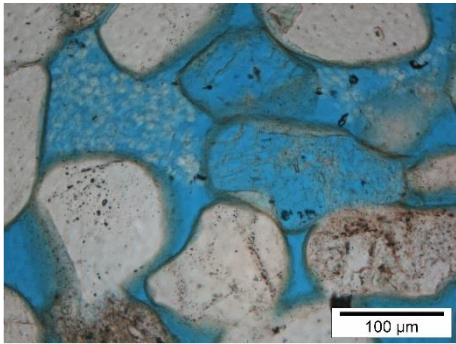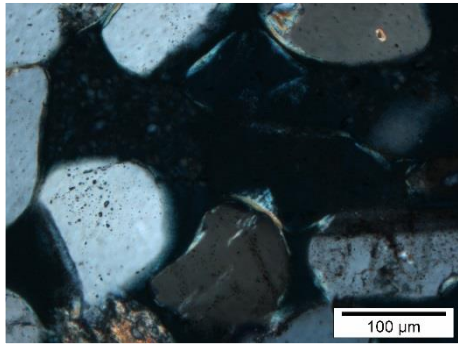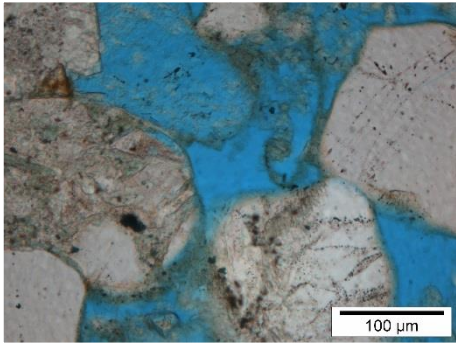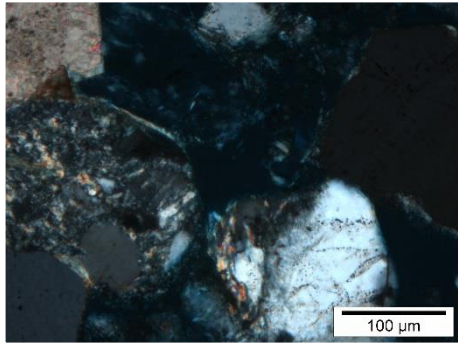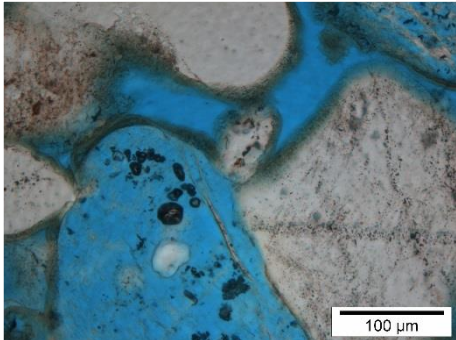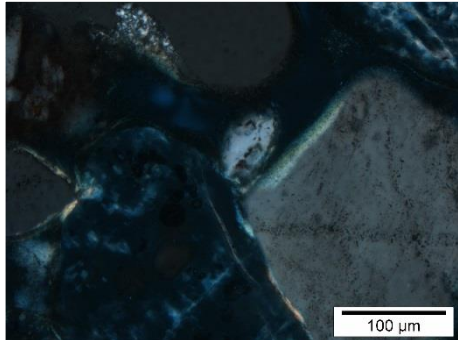
**Plate A:** The pores in this sublitharenite are relatively poorly connected, which is partly due to sparse to common pore-filling dolomite (d), relative strong compaction (also visible by the broken feldspar grains; arrows) and common pore-filling and replacive clay; including kaolinite (k). **Plate B:** Detailed view of a clay-rich (including authigenic chlorite; chl) rock fragment that appears to be partially replaced with quartz (q). The detrital grains, including this rock fragment, are covered with a thin clay coating, comprising tangential and radial illite (i). The tangential illite coating is thicker in the concave parts of grains. Note the small quartz outgrowths between a grain and its coating (arrows). **Plate C:** Locally, detrital grains are completely leached, leaving mouldic pores (MP) or only authigenic minerals, such as chlorite (chl), illite (i), quartz (q) and also apatite (arrows). The clay coatings outline the original grains. **Plate D:** The relatively strong compaction is visible by the concave-convex grain contacts (arrows). Porosity in this field of view is only microporosity in between the kaolinite (k) platelets. Note the illite clay coating (i), which is absent in between the grain contacts.
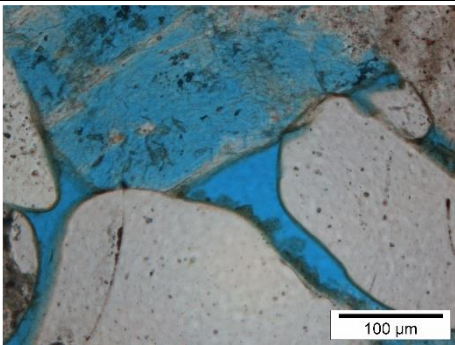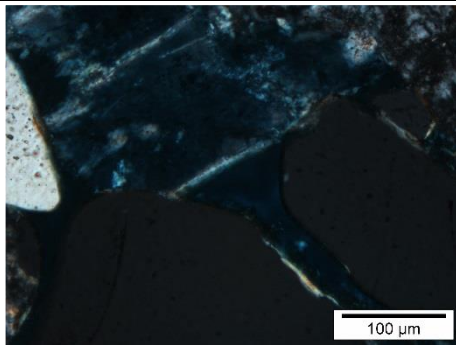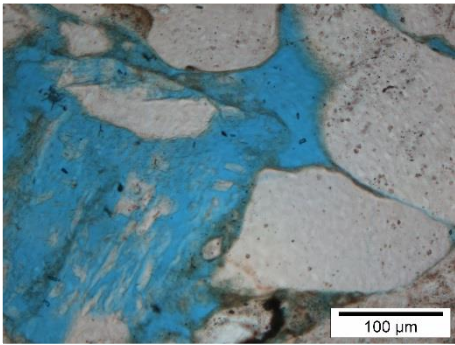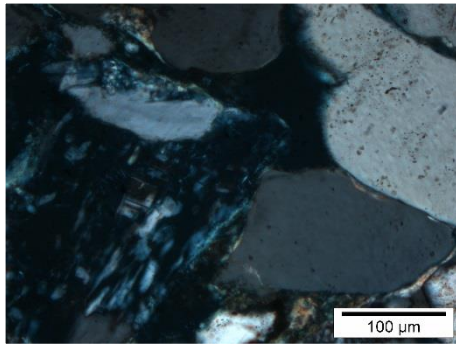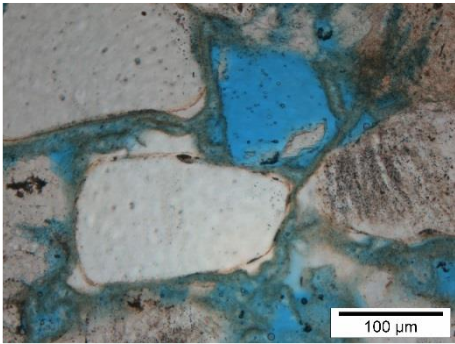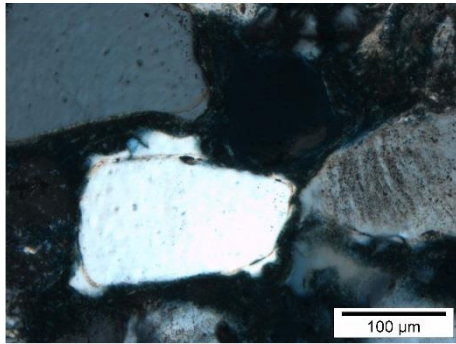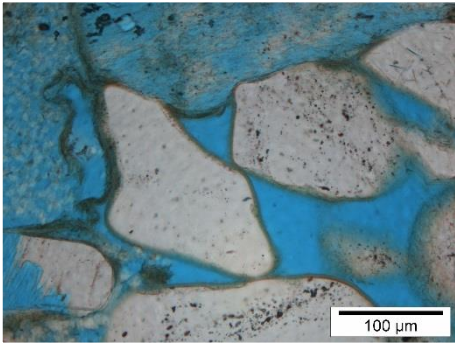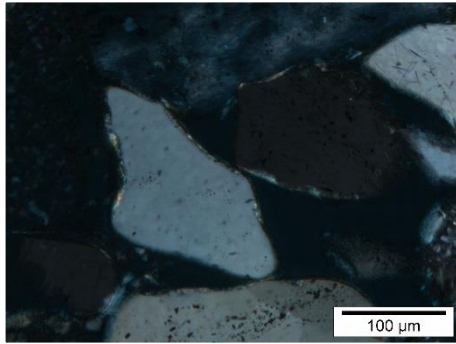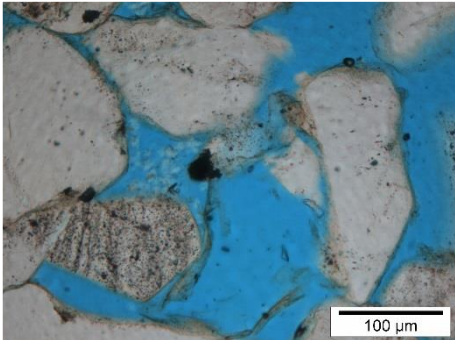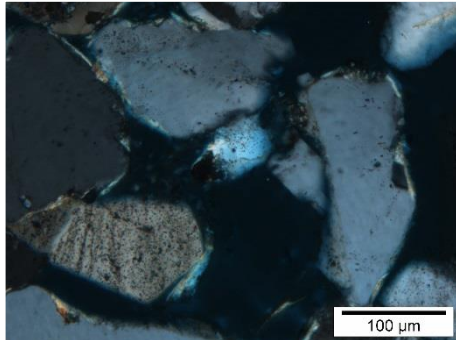
# Appendix 6: Clay coatings overview
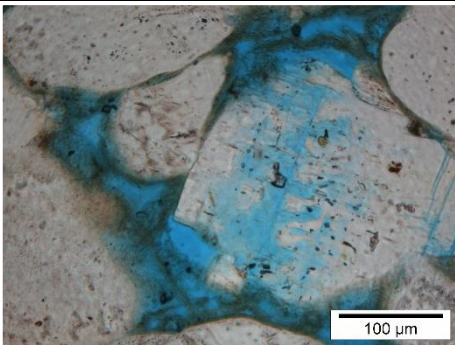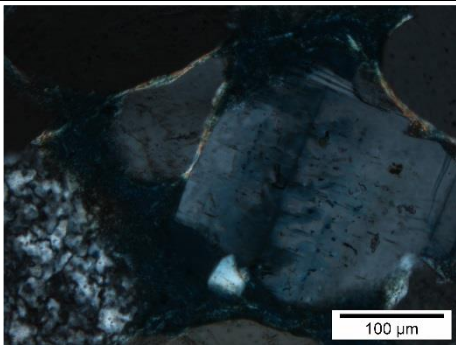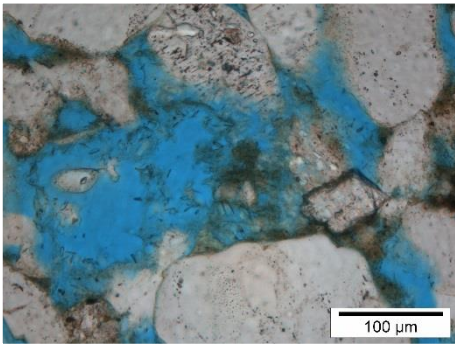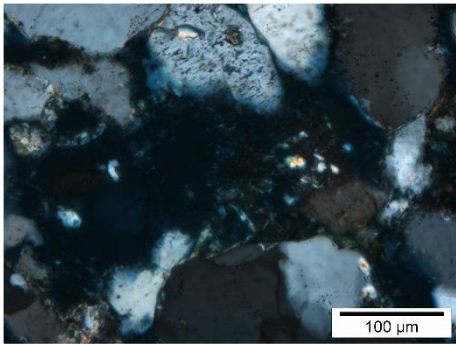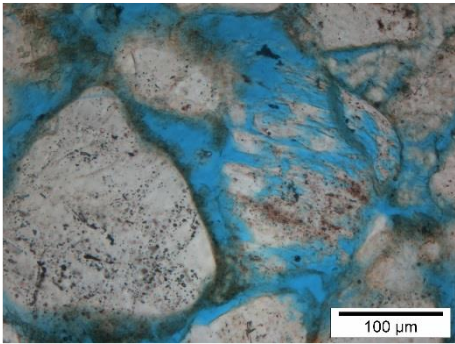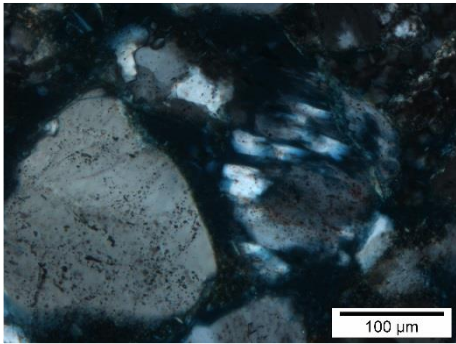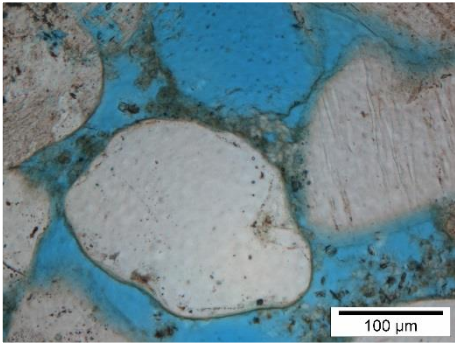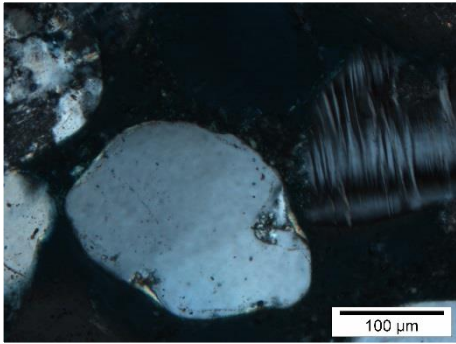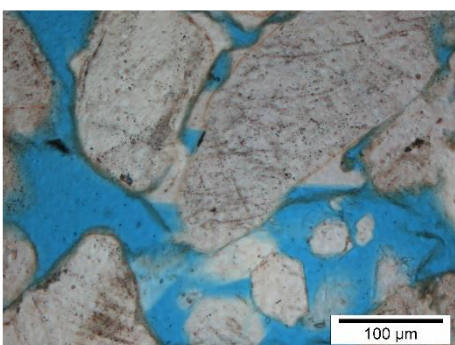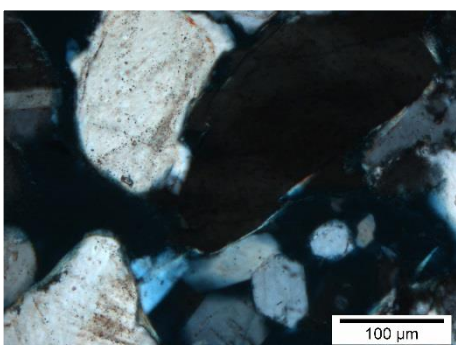
This appendix contains representative high magnification photographs and bullet point descriptions of the clay coatings present in the studied samples. Photographs are taken both in plane polarised light (PPL) and cross polarised light (XPL).

| # | Plane Polarised Light | Cross Polarised Light | Comments | XRD CF (%BW) |
|---|---|---|---|---|
| P1 |  |  | • Continuous<br>• Homogeneous<br>• Mixed illite/chlorite | • Ill: 47<br>• Kaol: 20<br>• Chl: 33 |
| P2 |  |  | • Irregular<br>• Clay clouds (pore-filling meshwork)<br>• Mixed illite/chlorite | • Ill: 43<br>• Kaol: 43<br>• Chl: 14 |
| P3 |  |  | • Double layered<br>• Chlorite in between illite<br>• Coating detached<br>• Locally quartz in between coating and grain | • Ill: 21<br>• Kaol: 20<br>• Chl: 59 |
| P4 |  |  | • Mostly continuous<br>• Relatively little tangential illite<br>• Meshwork chlorite (?) in the pores<br>• | • Ill: 58<br>• Kaol: 15<br>• Chl: 27 |
| P5 |  |  | • Continuous<br>• Rel. thick tangential illite<br>• Homogeneous<br>• Locally chlorite in between radial mixed clay | • Ill: 48<br>• Kaol: 23<br>• Chl: 29 |

| # | Plane Polarised Light | Cross Polarised Light | Comments | XRD CF (%BW) |
|---|---|---|---|---|
| P6 |  |  | • Mostly continuous<br>• Thin tangential illite<br>• Coating mostly illite<br>• Quartz cement between coating and grain | • Ill: 31<br>• Kaol: 27<br>• Chl: 42 |
| P7 |  |  | • Continuous<br>• Relatively thin<br>• Illite mixed with traces of chlorite | • Ill: 49<br>• Kaol: 35<br>• Chl: 16 |
| P8 |  |  | • Variable thickness<br>• Clay meshwork<br>• Illite mixed with chlorite. Locally chlorite only<br>• Note: clay-rich sample | • Ill: 36<br>• Kaol: 12<br>• Chl: 52 |
| P9 |  |  | • Continuous<br>• Relatively thick<br>• Thick tangential illite coating<br>• Chlorite in between and mixed with illite<br>• Locally detached | • Ill: 29<br>• Kaol: 27<br>• Chl: 43 |
| P10 |  |  | • Continuous<br>• Mostly illite<br>• Rarely detached | • Ill: 49<br>• Kaol: 34<br>• Chl: 16 |

| # | Plane Polarised Light | Cross Polarised Light | Comments | XRD CF (%BW) |
|---|---|---|---|---|
| P11 |  |  | • Thick and double layered<br>• Chlorite (common) in between illite<br>• Coating detached | • Ill: 14<br>• Kaol: 20<br>• Chl: 65 |
| P12 |  |  | • Mostly continuous<br>• Illite mixed with chlorite<br>• Locally thick tangential illite<br>• Note: sample contains clay-rich laminae | • Ill: 38<br>• Kaol: 22<br>• Chl: 41 |
| P13 |  |  | • Continuous<br>• Homogeneous<br>• Mostly illite<br>• Rarely detached | • Ill: 55<br>• Kaol: 38<br>• Chl: 7 |
| P14 |  |  | • Mostly continuous<br>• Variable thickness<br>• Clay clouds<br>• Mostly illite | • Ill: 47<br>• Kaol: 26<br>• Chl: 27 |
| P15 |  |  | • Continuous and thick<br>• Homogeneous<br>• Illite mixed with chlorite<br>• Rarely detached | • Ill: 34<br>• Kaol: 19<br>• Chl: 47 |

| # | Plane Polarised Light | Cross Polarised Light | Comments | XRD CF (%BW) |
|---|---|---|---|---|
| P16 |  100 µm |  100 µm | • Continuous<br>• Homogeneous thickness<br>• Some clay clouds<br>• Illite mixed with chlorite<br>• Rarely detached | • Ill: 39<br>• Kaol: 36<br>• Chl: 25 |
| P17 |  100 µm |  100 µm | • Mostly continuous<br>• Illite mixed with chlorite | • Ill: 39<br>• Kaol: 16<br>• Chl: 45 |
| P18 |  100 µm |  100 µm | • Double layered<br>• Illite mixed with kaolinite (?) and chlorite<br>• Commonly detached<br>• Locally quartz cement in between grain and coating | • Ill: 27<br>• Kaol: 25<br>• Chl: 49 |
| P19 |  100 µm |  100 µm | • Continuous<br>• Homogeneous thickness<br>• Illite mixed with chlorite | • Ill: 28<br>• Kaol: 33<br>• Chl: 39 |
| P20 |  100 µm |  100 µm | • Thin and locally absent<br>• Most illite is tangential.<br>• Remaining coating mosly chlorite | • Ill: 42<br>• Kaol: 14<br>• Chl: 45 |

| # | Plane Polarised Light | Cross Polarised Light | Comments | XRD CF (%BW) |
|---|---|---|---|---|
| P21 |  100 µm |  100 µm | • Heterogeneous, locally completely PF<br>• Most illite is tangential<br>• Commonly detached<br>• Chlorite mixed with tr. of illite | • Ill: 15<br>• Kaol: 3<br>• Chl: 82 |
| P22 |  100 µm |  100 µm | • Variable thickness<br>• Heterogeneous<br>• Chlorite mixed with tr. of illite | • Ill: 20<br>• Kaol: 5<br>• Chl: 85 |
| P23 |  100 µm |  100 µm | • Continous<br>• Variable thickness<br>• Illite mixed with chlorite<br>• Note the rel. common kaolinite. | • Ill: 46<br>• Kaol: 46<br>• Chl: 9 |
| P24 |  100 µm |  100 µm | • Mostly continuous<br>• Variable thickness<br>• Clay clouds<br>• Illite mixed with chlorite | • Ill: 33<br>• Kaol: 5<br>• Chl: 52 |
| P25 |  100 µm |  100 µm | • Continuous<br>• Homogeneous thickness<br>• Illite mixed with chlorite<br>• Rarely detached<br>• Locally quartz cement between grain and coating | • Ill: 52<br>• Kaol: 15<br>• Chl: 43 |

# Appendix 7: XRD Diffractograms

| G1220 Well | Sample No. | Sample No. NAM* | Depth (m)* | Sample Type | Whole Rock (%BW) | | | | | | | | | TOTAL % (WR) | Clay Fraction (%BW) | | | TOTAL % (CF) |
|---|---|---|---|---|---|---|---|---|---|---|---|---|---|---|---|---|---|---|
| | | | | | Quartz | Illite/Smectite | Kaolinite/Chlorite | Microcline | Albite | Dolomite | Fe-dolomite | Siderite | Barite | | Illite | Kaolinite | Chlorite | |
| ZRP-3A | P1 | R246 | 3582.5 | Trimend | 81 | 4 | 4 | 2 | 10 | 0 | 0 | Tr | 0 | 100 | 47 | 20 | 33 | 100 |
| ZRP-3A | P2 | R085 | 3542.3 | Trimend | 71 | 3 | 8 | 3 | 12 | 1 | 2 | Tr | 0 | 100 | 43 | 43 | 14 | 100 |
| ZRP-3A | P3 | R378 | 3615.5 | Trimend | 82 | 2 | 5 | 2 | 8 | 0 | 0 | Tr | Tr | 100 | 21 | 20 | 59 | 100 |
| ZRP-3A | P4 | R212 | 3574.0 | Trimend | 78 | 2 | 8 | 2 | 10 | 0 | 0 | 0 | 1 | 100 | 58 | 15 | 27 | 100 |
| ZRP-3A | P5 | R283 | 3591.8 | Trimend | 79 | 3 | 9 | 2 | 7 | 0 | 0 | Tr | Tr | 100 | 48 | 23 | 29 | 100 |
| ZRP-3A | P6 | R182 | 3566.5 | Trimend | 86 | Tr | 2 | 3 | 8 | 0 | 0 | Tr | 1 | 100 | 31 | 27 | 42 | 100 |
| ZRP-3A | P7 | R100 | 3546.0 | Trimend | 74 | 5 | 4 | 3 | 12 | 1 | 1 | 0 | Tr | 100 | 49 | 35 | 16 | 100 |
| ZRP-3A | P8 | R352 | 3609.0 | Trimend | 82 | 2 | 7 | 2 | 6 | 0 | 0 | Tr | 1 | 100 | 36 | 12 | 52 | 100 |
| ZRP-3A | P9 | R231 | 3578.8 | Trimend | 78 | 3 | 3 | 4 | 13 | 0 | 0 | 0 | 1 | 100 | 29 | 27 | 43 | 100 |
| ZRP-3A | P10 | R161 | 3561.3 | Trimend | 74 | 3 | 5 | 4 | 12 | 1 | 1 | Tr | 1 | 100 | 49 | 34 | 16 | 100 |
| ZRP-3A | P11 | R332 | 3604.0 | Trimend | 85 | 3 | 4 | 1 | 7 | 0 | 0 | Tr | 0 | 100 | 14 | 20 | 65 | 100 |
| ZRP-3A | P12 | R171 | 3563.7 | Trimend | 74 | 4 | 4 | 2 | 12 | 2 | 1 | 0 | Tr | 100 | 38 | 22 | 41 | 100 |
| ZRP-3A | P13 | R154 | 3559.3 | Trimend | 83 | 2 | 4 | 2 | 9 | 0 | 0 | 0 | Tr | 100 | 55 | 38 | 7 | 100 |
| ZRP-3A | P14 | R306 | 3597.5 | Trimend | 75 | 2 | 7 | 1 | 8 | 3 | 3 | Tr | 1 | 100 | 47 | 26 | 27 | 100 |
| ZRP-3A | P15 | R269 | 3588.3 | Trimend | 83 | Tr | 4 | 2 | 8 | Tr | 1 | Tr | 1 | 100 | 34 | 19 | 47 | 100 |
| ZRP-3A | P16 | R195 | 3569.8 | Trimend | 79 | 2 | 5 | 2 | 10 | 2 | 1 | 0 | Tr | 100 | 39 | 36 | 25 | 100 |
| ZRP-3A | P17 | R484 | 3642.0 | Trimend | 83 | 2 | 7 | 1 | 6 | Tr | Tr | Tr | 1 | 100 | 39 | 16 | 45 | 100 |
| ZRP-3A | P18 | R584 | 3667.0 | Trimend | 84 | 3 | 5 | Tr | 7 | 0 | 0 | 0 | 1 | 100 | 27 | 25 | 49 | 100 |
| ZRP-3A | P19 | R397 | 3620.2 | Trimend | 79 | 5 | 4 | 2 | 8 | 1 | 1 | Tr | 1 | 100 | 28 | 33 | 39 | 100 |
| ZRP-3A | P20 | R115 | 3549.8 | Trimend | 72 | 4 | 3 | 2 | 15 | 2 | 1 | 0 | 0 | 100 | 42 | 14 | 45 | 100 |
| ZRP-3A | P21 | R556 | 3660.0 | Trimend | 92 | Tr | 3 | Tr | 4 | 0 | 0 | Tr | 1 | 100 | 15 | 3 | 82 | 100 |
| ZRP-3A | P22 | R427 | 3627.7 | Trimend | 84 | 3 | 4 | 1 | 6 | 1 | Tr | Tr | 1 | 100 | 20 | 5 | 75 | 100 |
| ZRP-3A | P23 | R520 | 3651.0 | Trimend | 84 | 4 | 4 | Tr | 5 | 2 | 1 | Tr | 1 | 100 | 46 | 46 | 9 | 100 |
| ZRP-3A | P24 | R136 | 3555.1 | Trimend | 76 | 0 | 7 | 2 | 11 | 1 | 2 | Tr | Tr | 100 | 33 | 5 | 62 | 100 |
| ZRP-3A | P25 | R445 | 3632.3 | Trimend | 78 | 3 | 6 | 1 | 8 | 2 | 1 | Tr | 1 | 100 | 42 | 15 | 43 | 100 |

Tr = Trace amounts (<0.5%BW)          *Depth and sample no. obtained after draft

Semi-quantitative results of the whole rock (WR) and clay fraction (CF; <2μm) XRD analysis on sandstone and conglomerate samples from well ZRP-3A

The WR gives the relative weight percent (%BW) of each mineral in the bulk rock; the CF composition gives the %BW of each clay mineral in the extracted clay fraction.

For the methodology, see Appendix 1.

Counts

G1220_P1w

Position [°2Theta] (Copper (Cu))
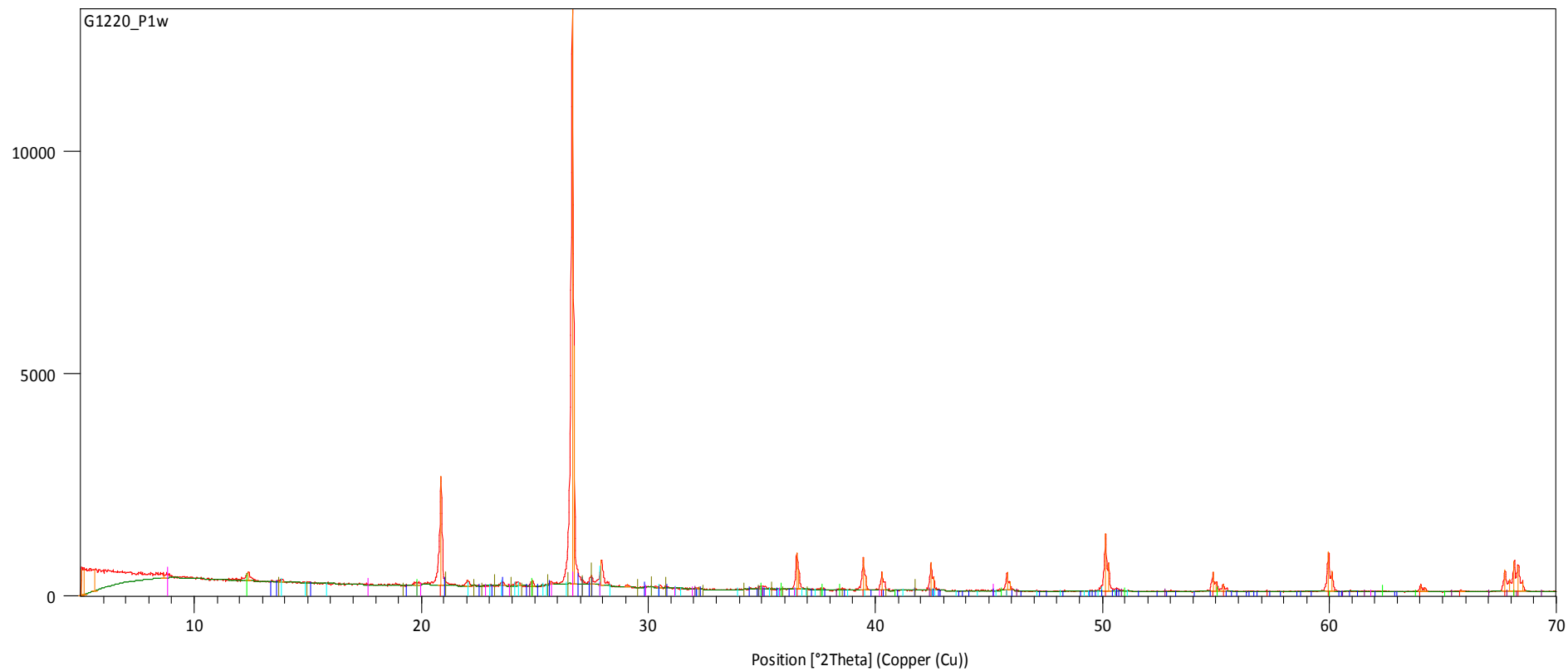
Peak List
Quartz, syn
Albite, ordered
Illite-2\ITM#1\RG
Orthoclase
Microcline, inter
Siderite
Kaolinite 1Md
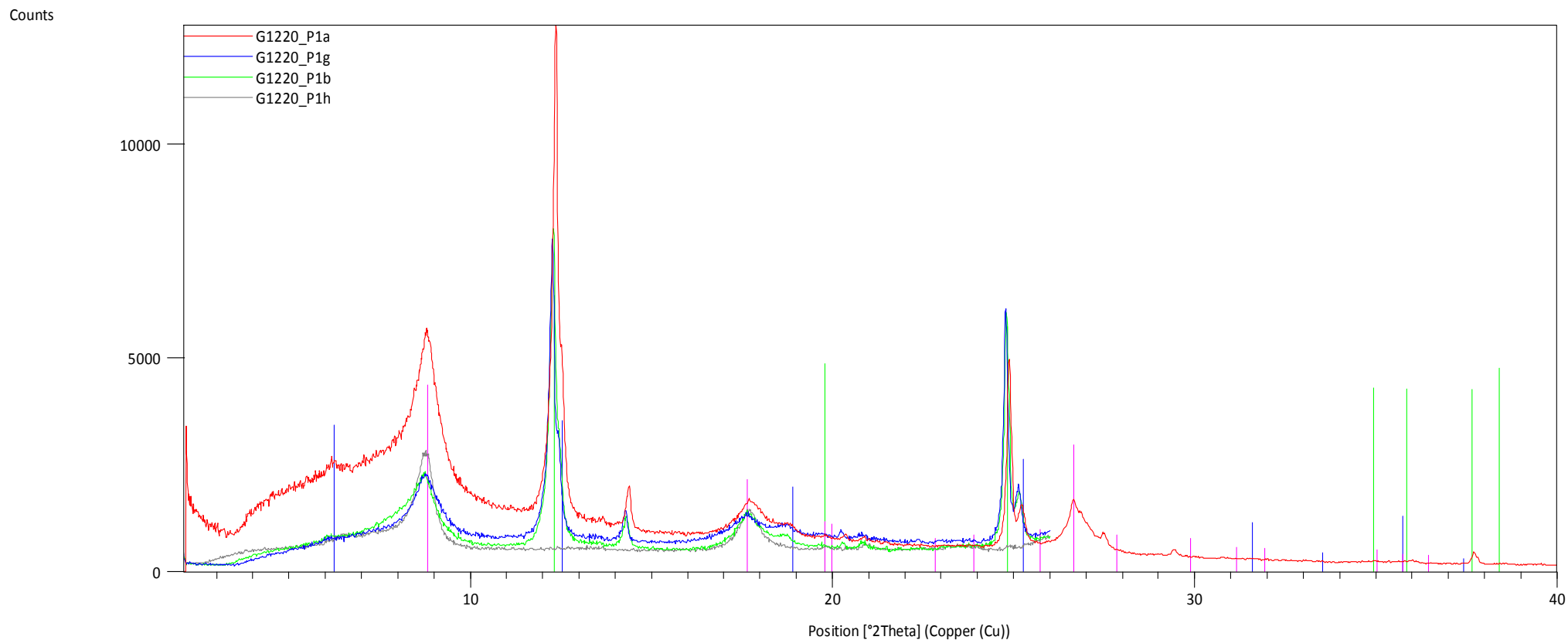
Counts



G1220_P3w

Position [°2Theta] (Copper (Cu))
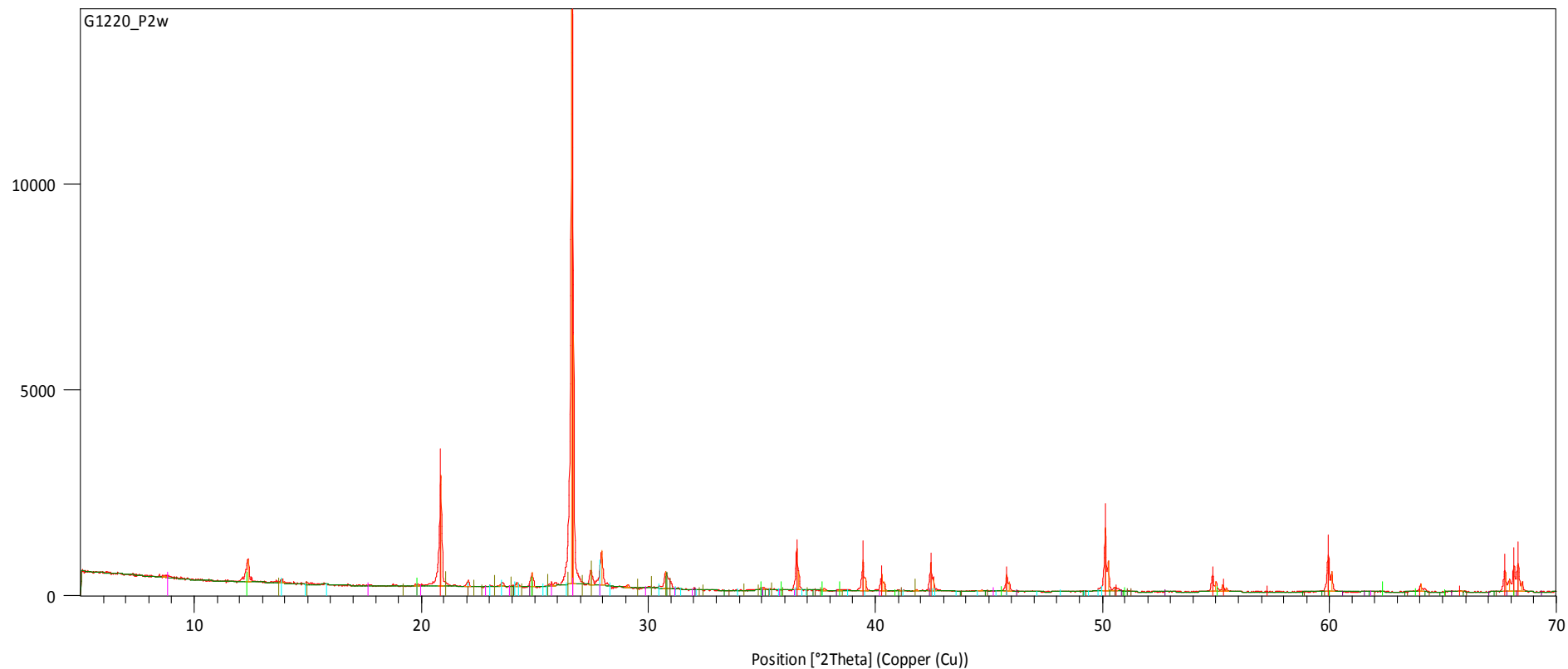
Peak List

Quartz, syn

Albite, ordered

Microcline, inter

Siderite

Barite

Kaolinite 1Md

Counts

20000

10000

0

G1220_P3a
G1220_P3g
G1220_P3b
G1220_P3h

Position [°2Theta] (Copper (Cu))

10     20     30     40
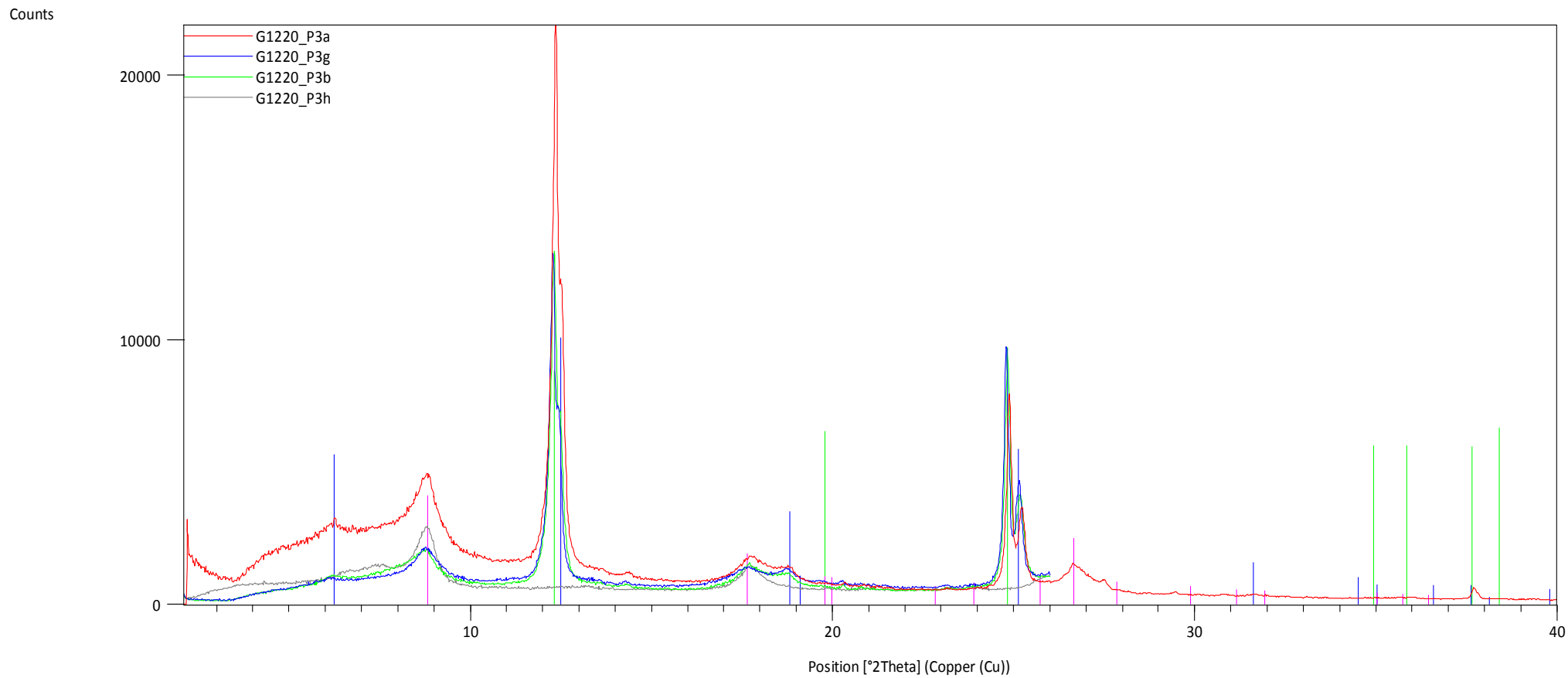
Peak List

Clinochlore-1\ITM#I#I#b\RG, ferroan

Kaolinite 1Md

Illite-2\ITM#1\RG
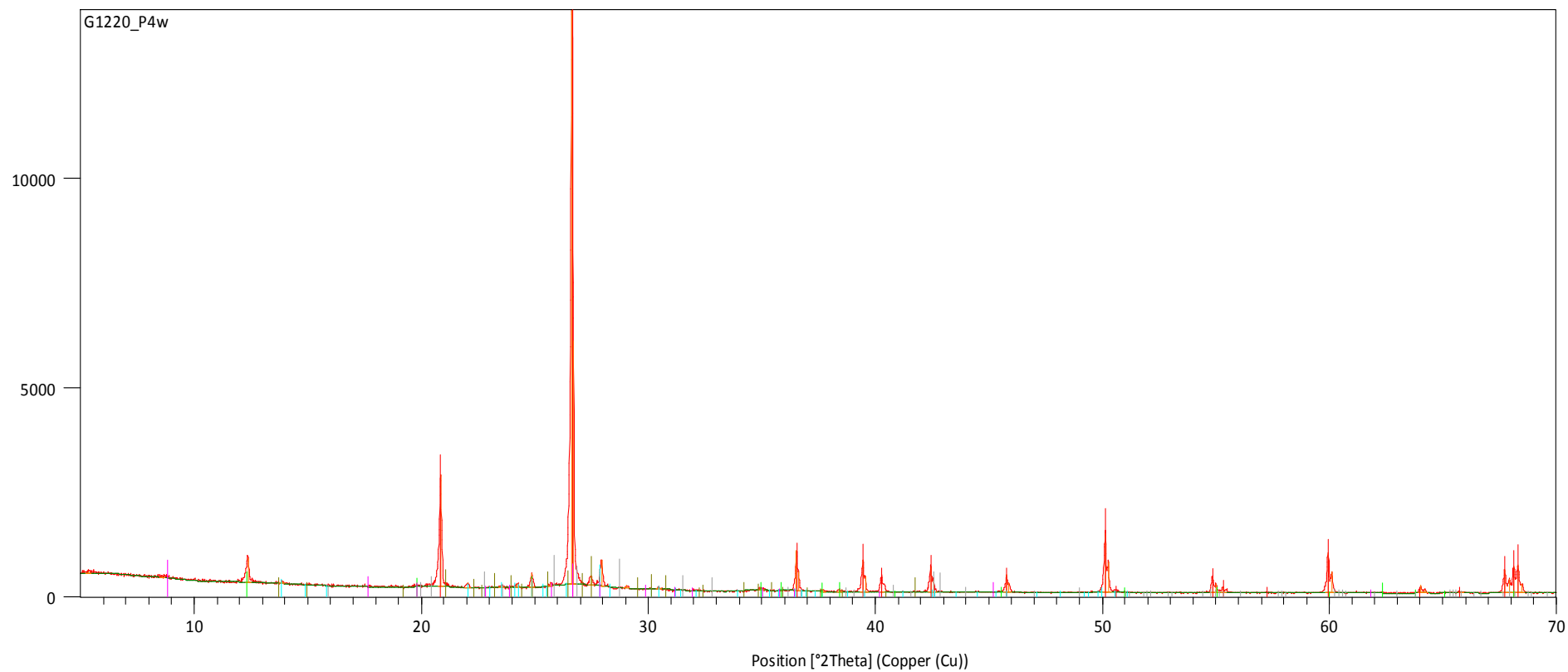
Counts



G1220_P4w

Position [°2Theta] (Copper (Cu))

Peak List

Quartz, syn

Albite, ordered

Microcline, inter

Kaolinite 1Md

Illite-2\ITM#1\RG

Barite

Counts

G1220_P4a
G1220_P4g
G1220_P4b
G1220_P4h

Position [°2Theta] (Copper (Cu))
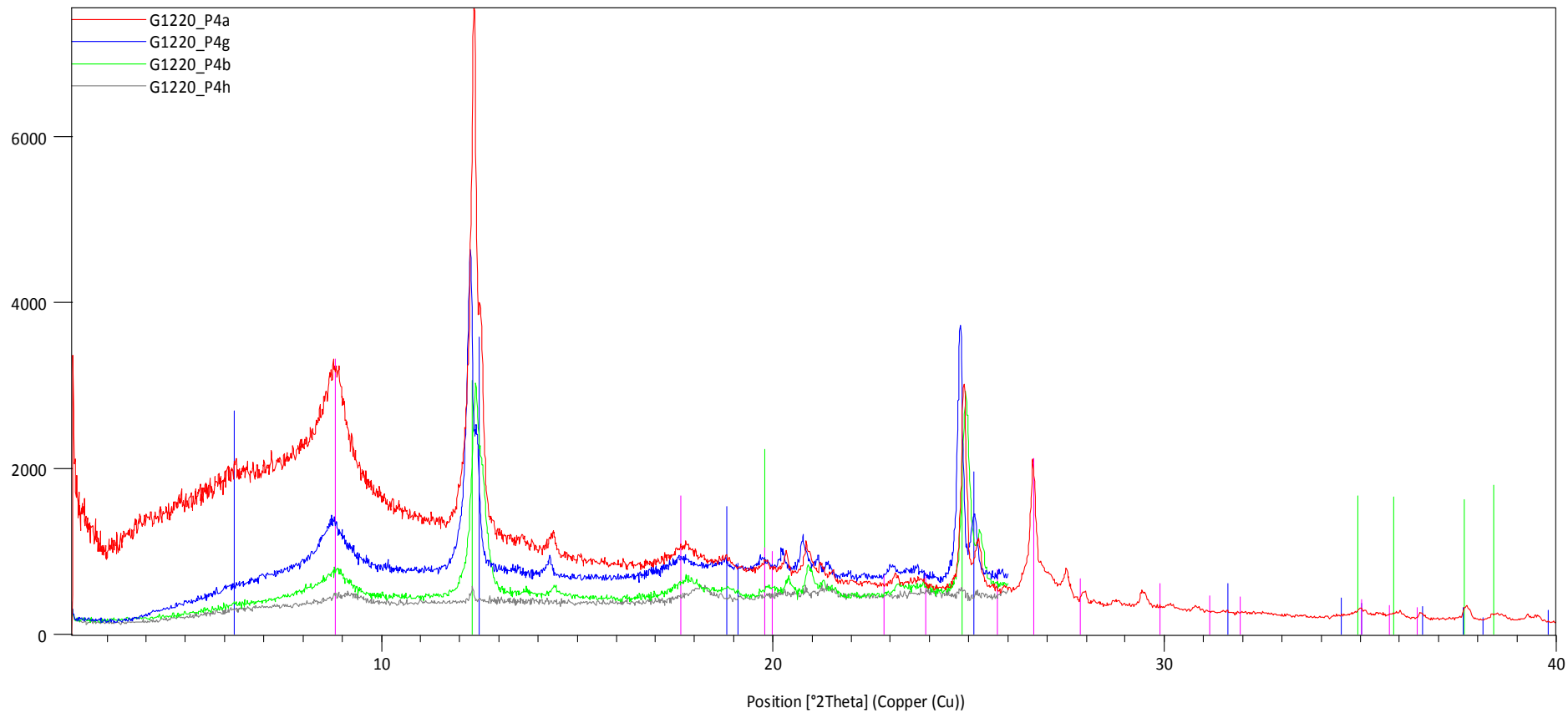
Peak List

Kaolinite 1Md

Clinochlore-1\ITM#I#I#b\RG, ferroan

Illite-2\ITM#1\RG

Whole Rock

Counts



G1220_P5w

Position [°2Theta] (Copper (Cu))
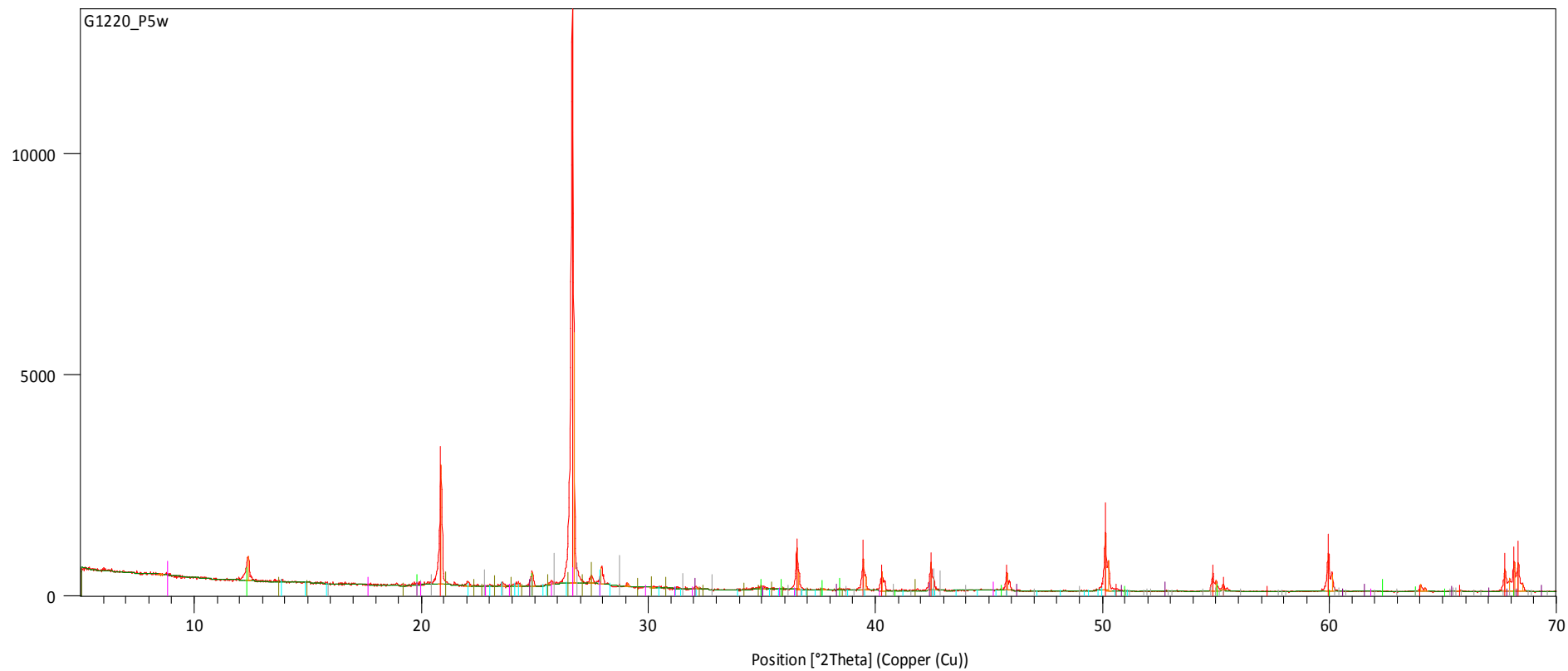
Peak List
Quartz, syn
Albite, ordered
Microcline, inter
Kaolinite 1Md
Barite
Illite-2\ITM#1\RG
Siderite

Counts

G1220_P5a
G1220_P5g
G1220_P5b
G1220_P5h

Position [°2Theta] (Copper (Cu))

Peak List

Clinochlore-1\ITM#I#I#b\RG, ferroan

Illite-2\ITM#1\RG

Kaolinite 1Md

Counts

G1220_P6a2
G1220_P6g
G1220_P6b
G1220_P6h

Position [°2Theta] (Copper (Cu))

Peak List

Clinochlore-1\ITM#I#I#b\RG, ferroan

Illite-2\ITM#1\RG

Kaolinite 1Md

Counts

G1220_P7w

10000

5000

0

10   20   30   40   50   60   70

Position [°2Theta] (Copper (Cu))

Peak List
Quartz, syn
Albite, ordered
Ankerite
Dolomite
Microcline, inter
Kaolinite 1Md
Illite-2\ITM#1\RG
Barite

Counts

G1220_P8w



Position [°2Theta] (Copper (Cu))

Peak List

Quartz, syn

Albite, ordered

Microcline, inter

Siderite

Kaolinite 1Md

Illite-2\ITM#1\RG

Barite

Counts

G1220_P9w



Position [°2Theta] (Copper (Cu))

Peak List

Quartz, syn

Albite, ordered

Microcline, inter

Kaolinite 1Md

Illite-2\ITM#1\RG

Barite

Counts



G1220_P10w

Position [°2Theta] (Copper (Cu))

Peak List
Quartz, syn
Ankerite
Dolomite
Albite, ordered
Microcline, inter
Illite-2\ITM#1\RG
Kaolinite 1Md
Barite
Siderite
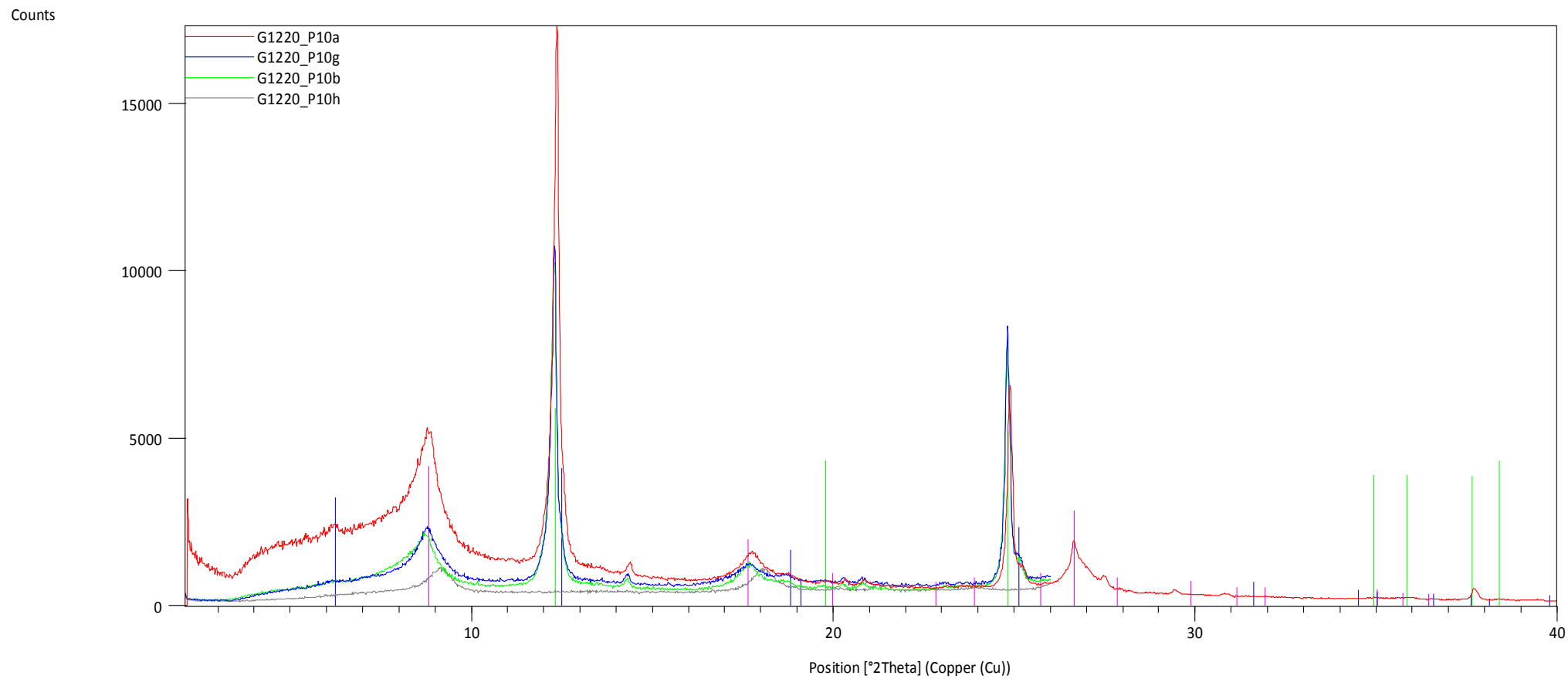
Counts



G1220_P11w

Position [°2Theta] (Copper (Cu))
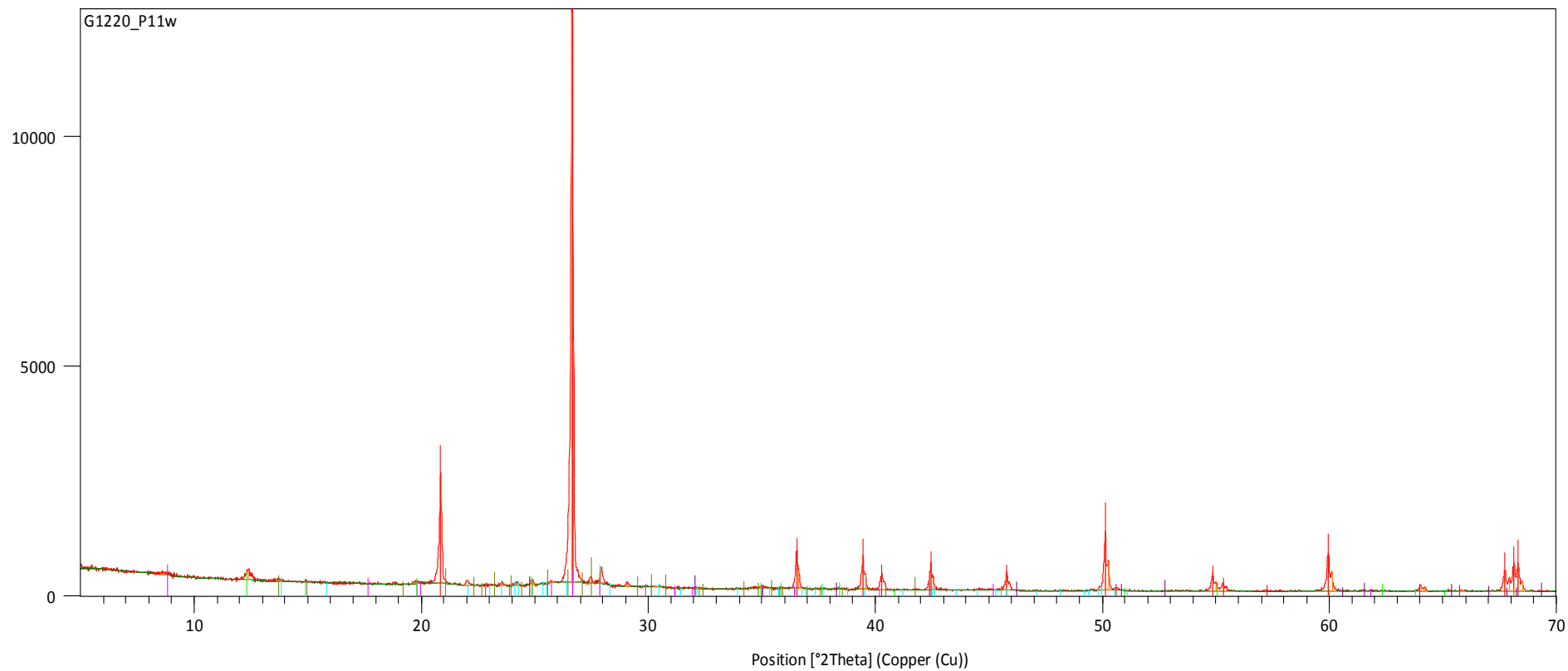
Peak List

Quartz, syn

Albite, ordered

Microcline, inter

Illite-2\ITM#1\RG

Kaolinite 1Md

Siderite
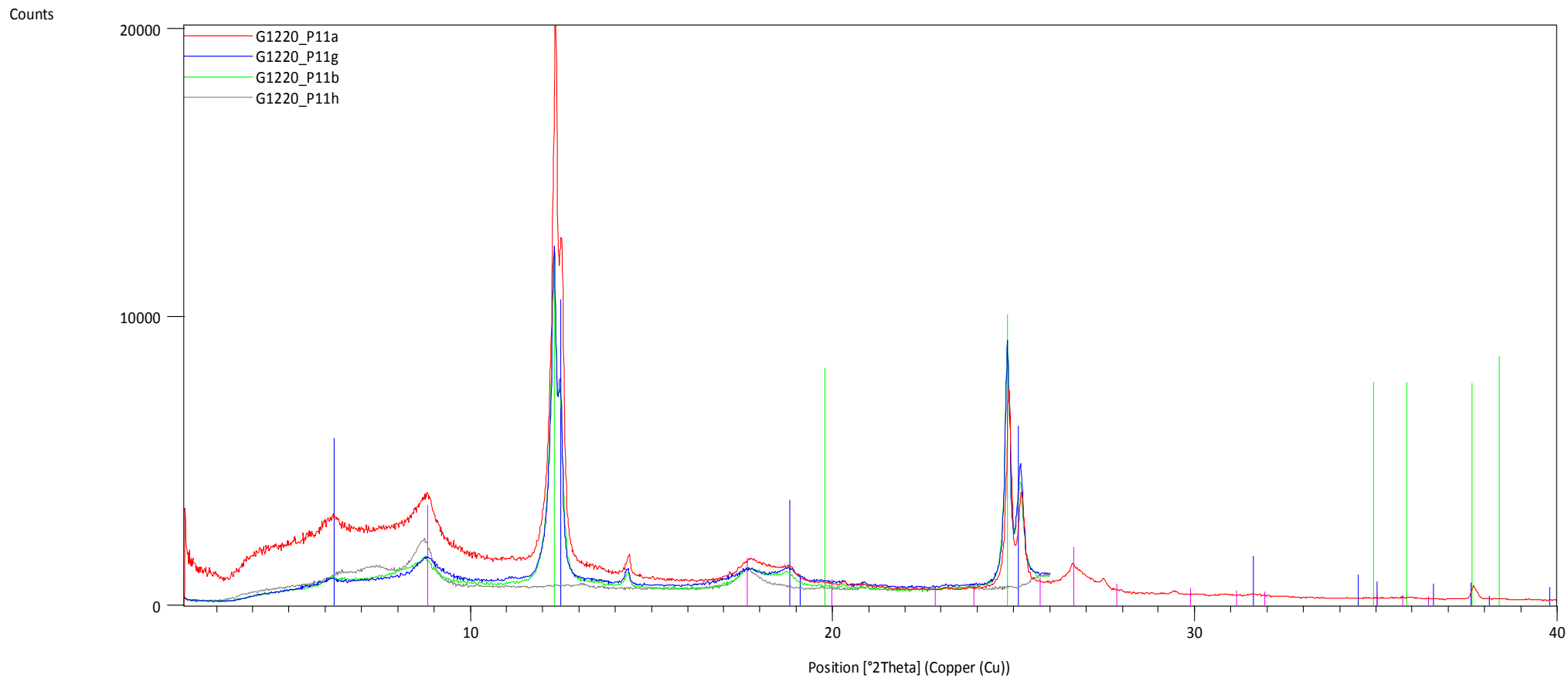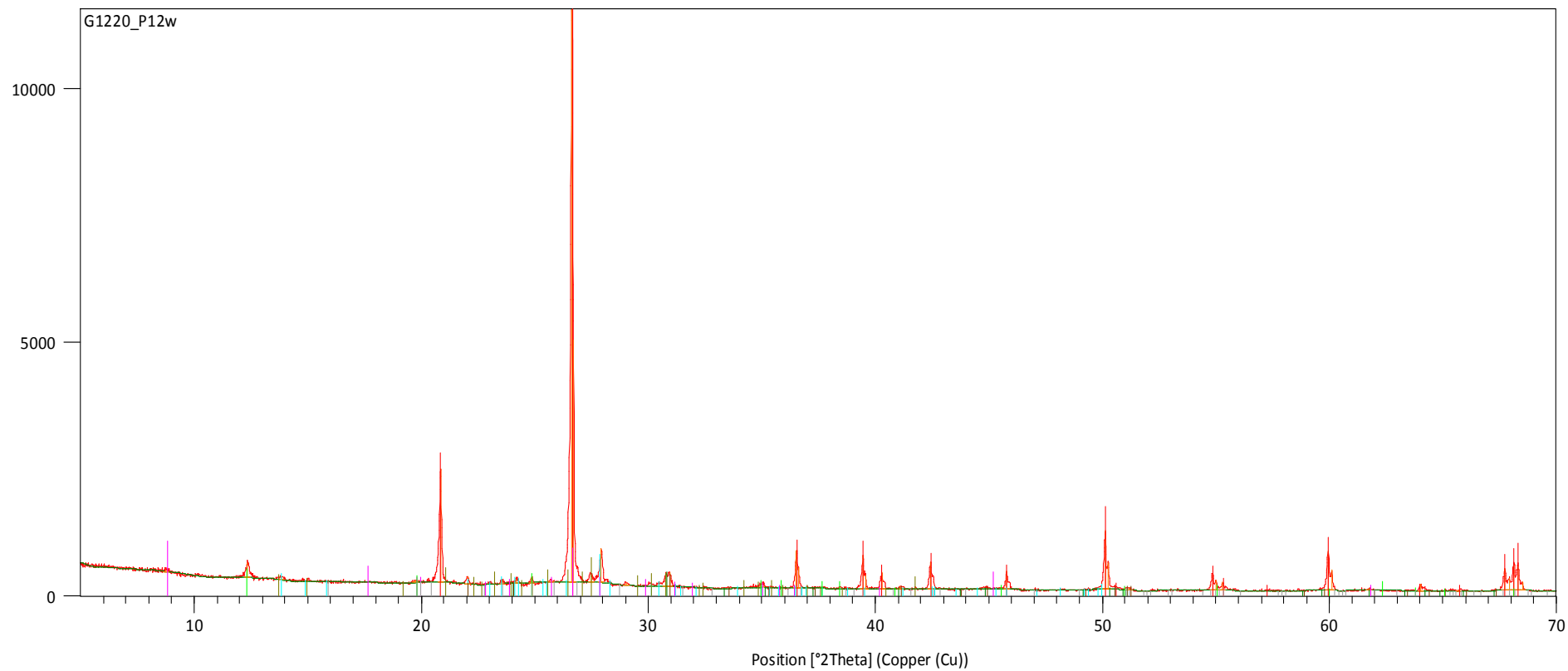
Counts

20000

10000

0

Position [°2Theta] (Copper (Cu))

Legend:
- G1220_P11a
- G1220_P11g
- G1220_P11b
- G1220_P11h

Peak List

Clinochlore-1\ITM#I#I#b\RG, ferroan

Illite-2\ITM#1\RG

Kaolinite 1Md

G1220_P12w

Counts

Position [°2Theta] (Copper (Cu))

Peak List
Quartz, syn
Albite, ordered
Ankerite
Dolomite
Microcline, inter
Illite-2\ITM#1\RG
Kaolinite 1Md
Barite

Counts

G1220_P13w

Position [°2Theta] (Copper (Cu))
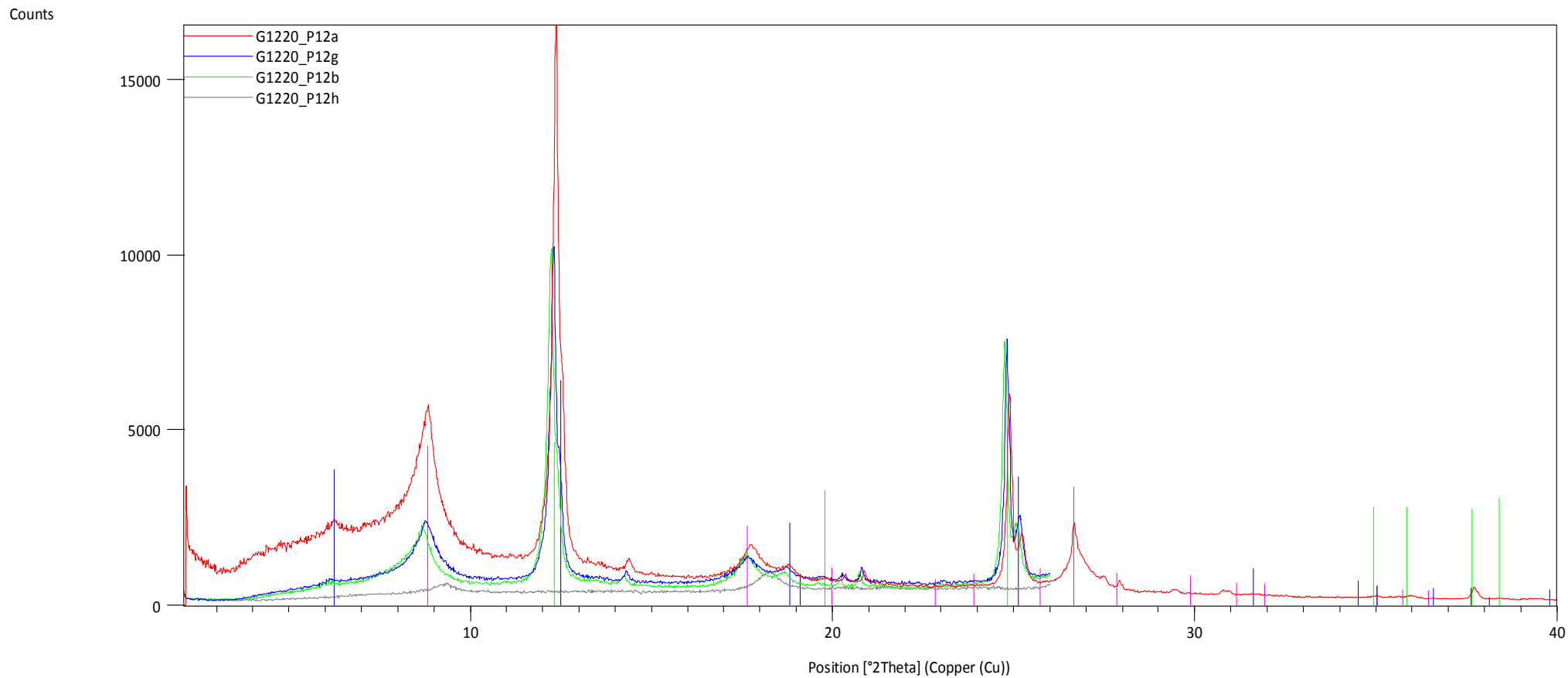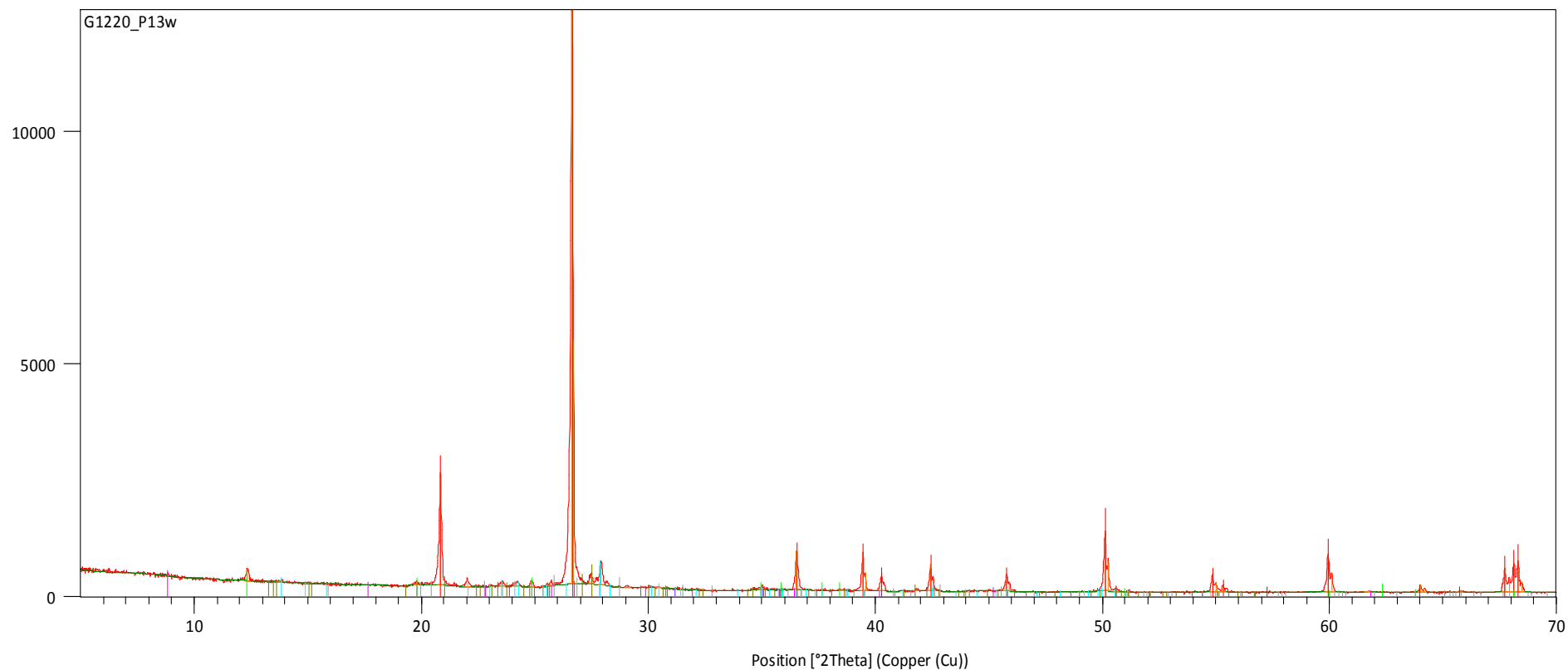
Peak List

Quartz, syn

Microcline, intermediate

Illite-2\ITM#1\RG

Kaolinite 1Md

Albite, ordered

Barite
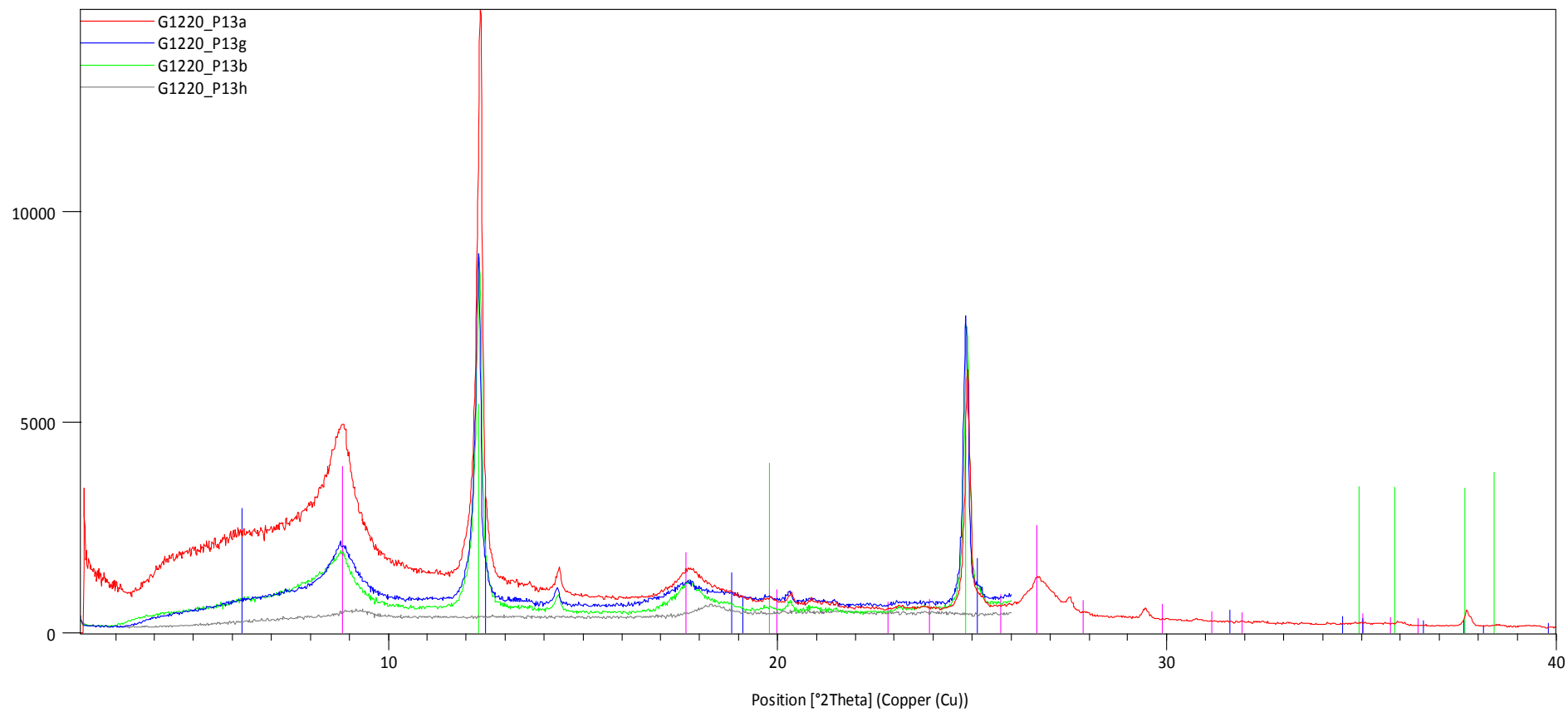
G1220_P14w

Counts

Position [°2Theta] (Copper (Cu))
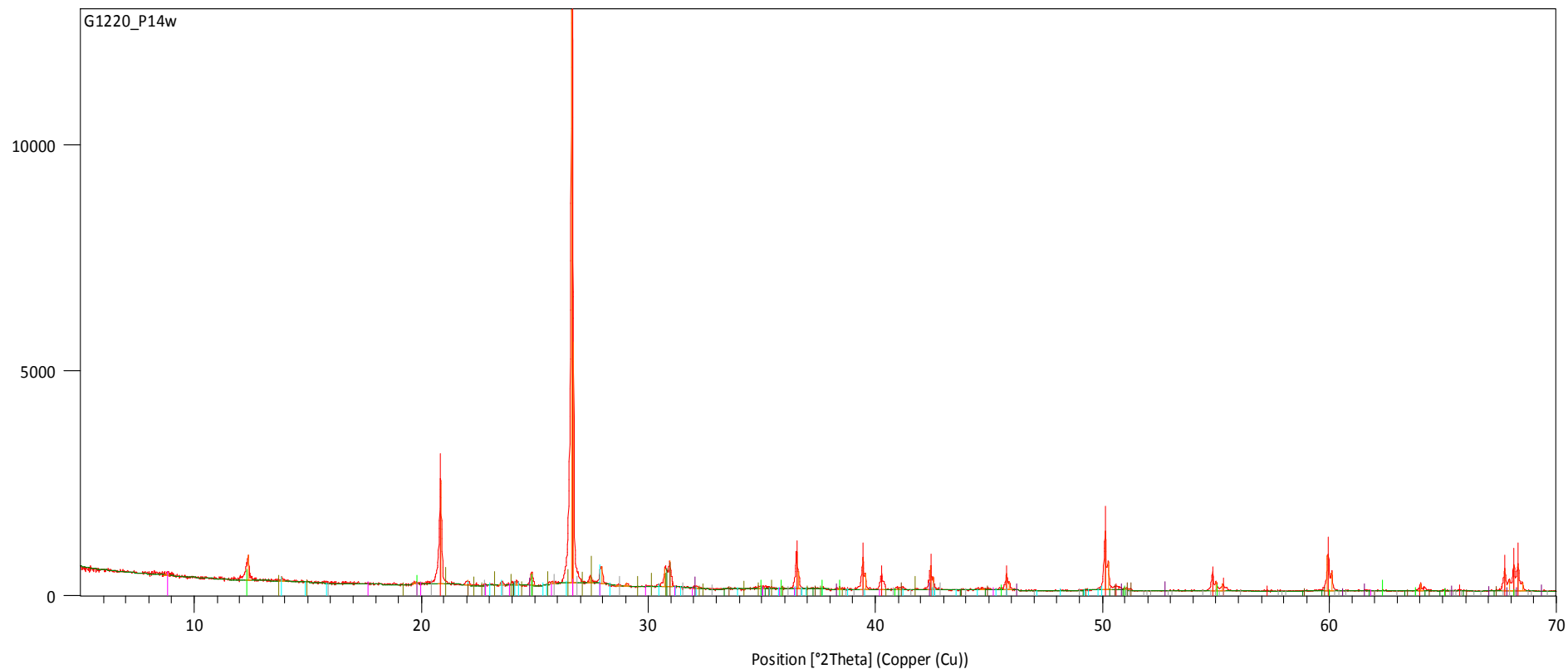
Peak List
Quartz, syn
Ankerite
Albite, ordered
Dolomite
Microcline, inter
Barite
Siderite
Kaolinite 1Md
Illite-2\ITM#1\RG
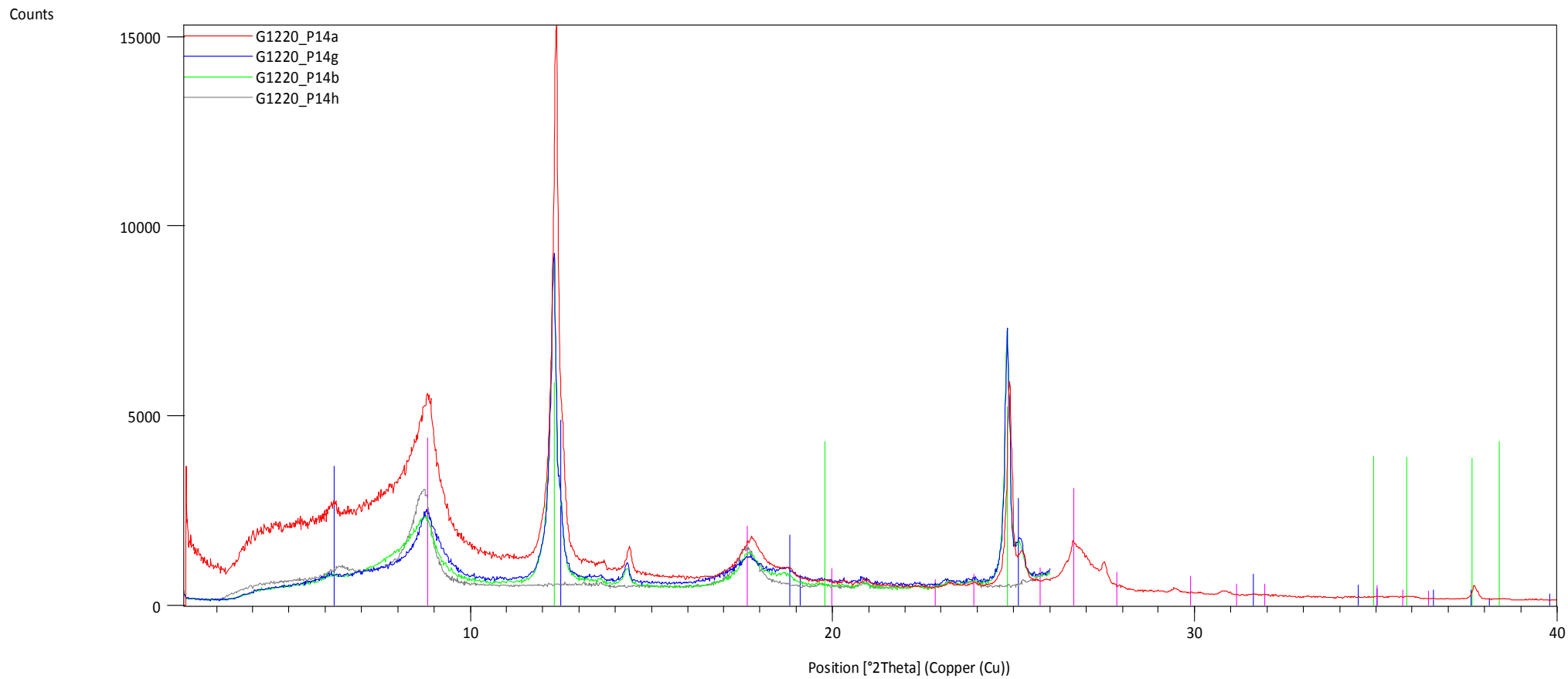
Counts

G1220_P15w



Position [°2Theta] (Copper (Cu))
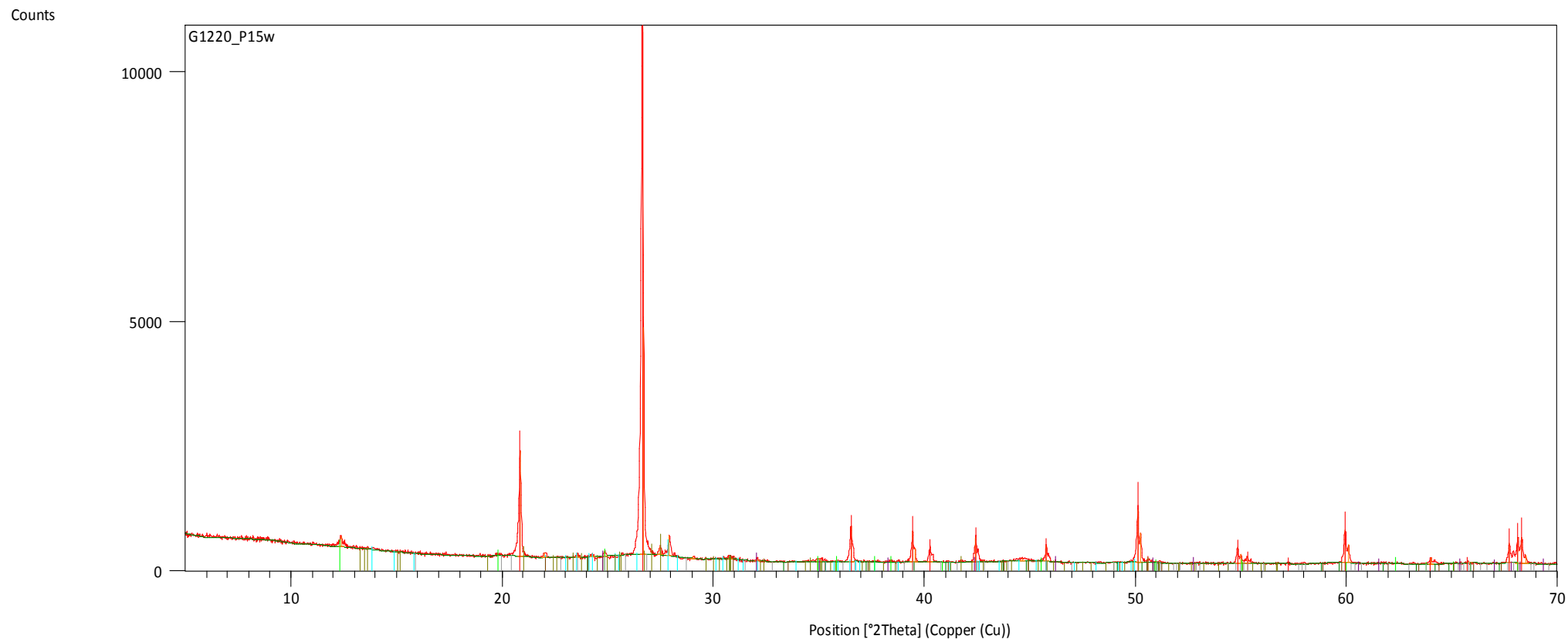
Peak List
Quartz, syn
Albite, ordered
Ankerite
Microcline, intermediate
Kaolinite 1Md
Dolomite
Barite
Siderite
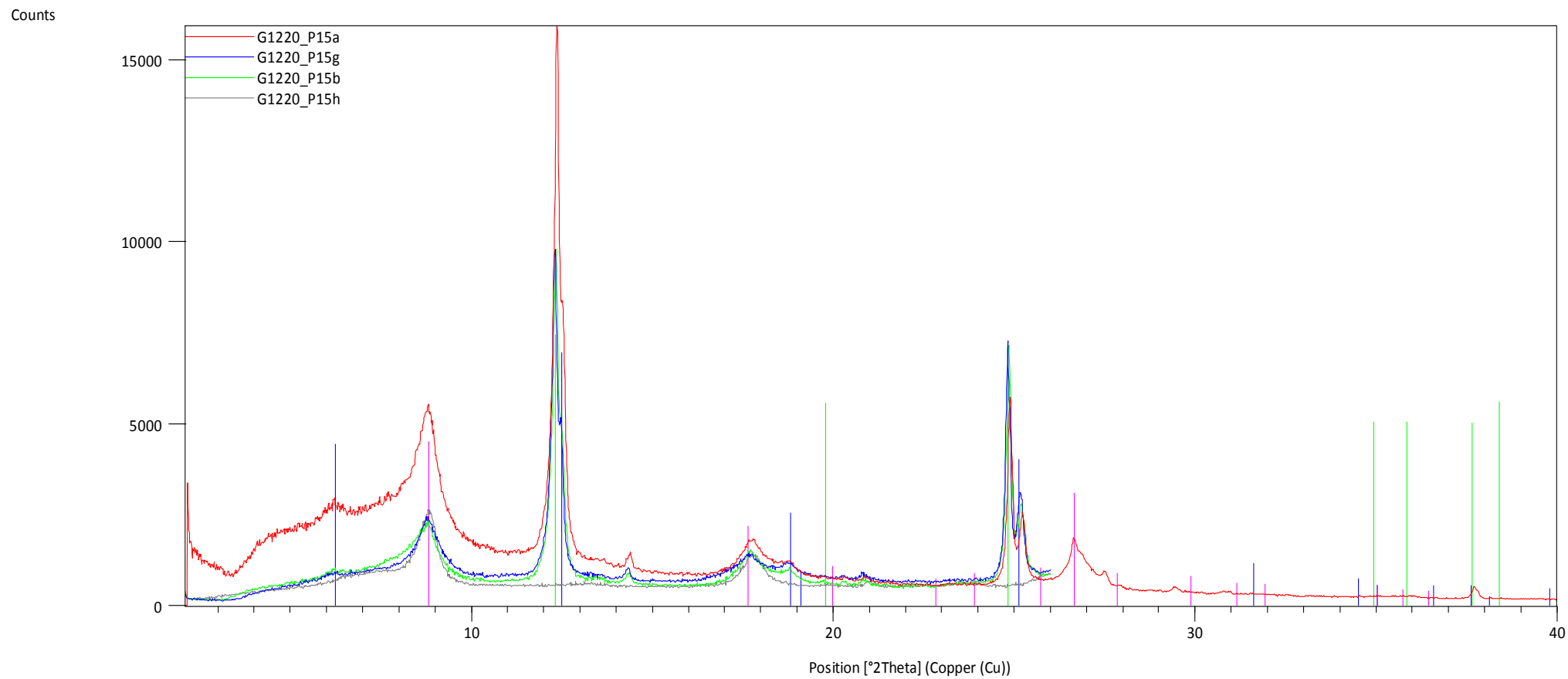
Counts



G1220_P16w

Position [°2Theta] (Copper (Cu))
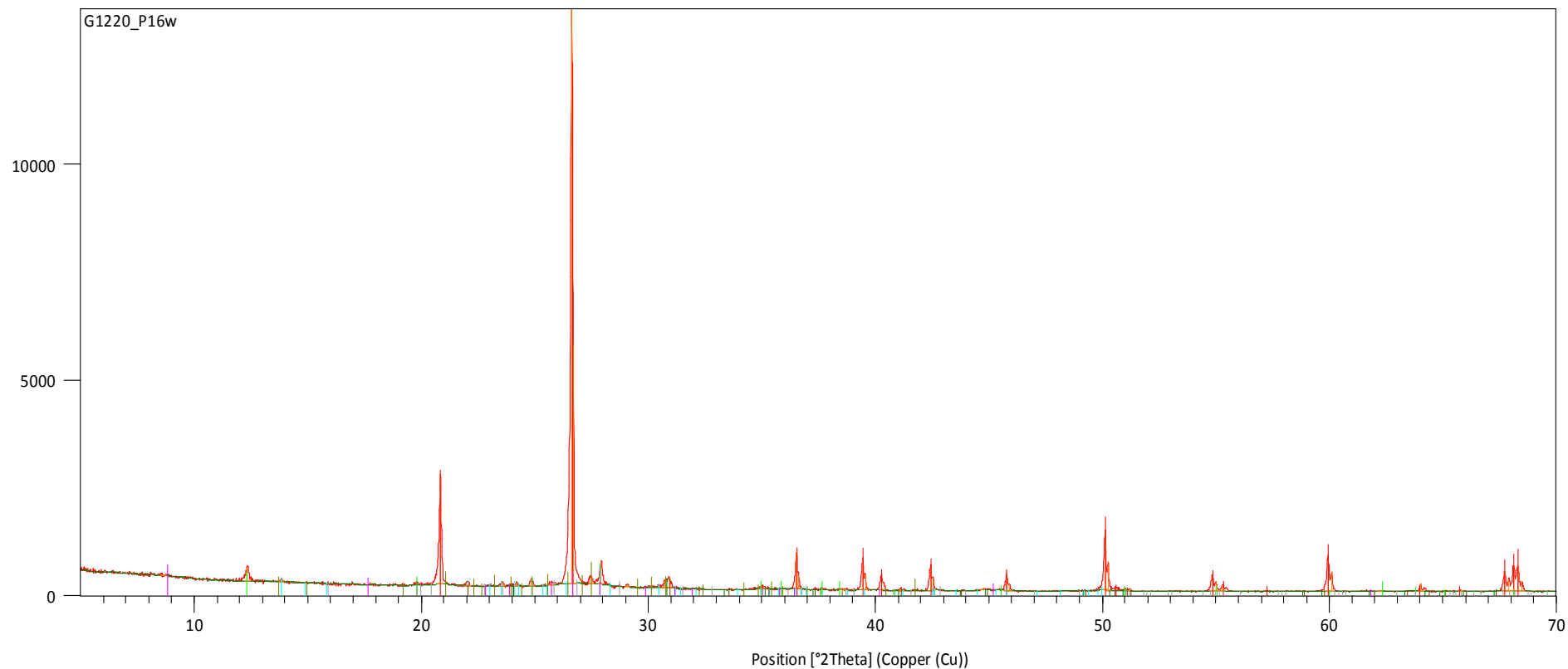
Peak List
Quartz, syn
Albite, ordered
Ankerite
Dolomite
Illite-2\ITM#1\RG
Kaolinite 1Md
Microcline, inter
Barite
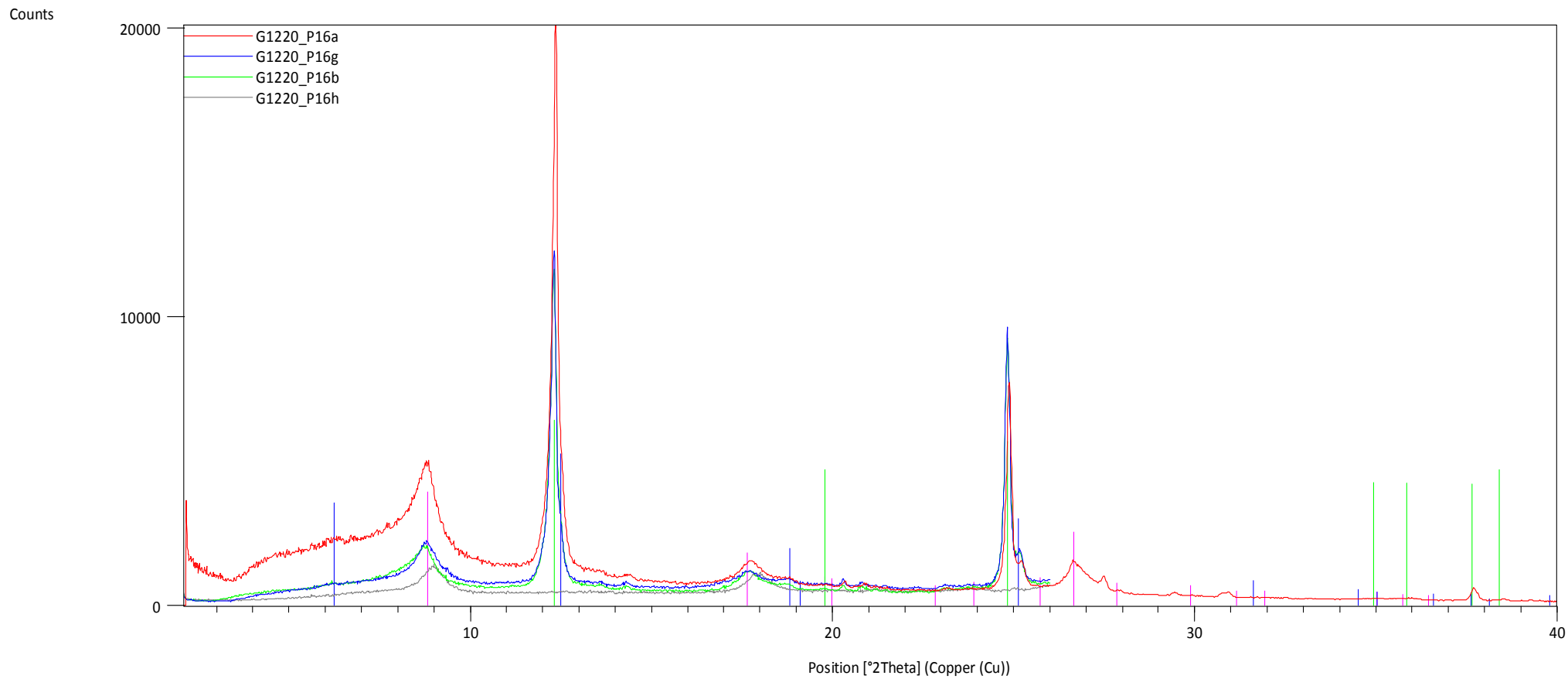
Counts



G1220_P17w

10000

5000

0

Position [°2Theta] (Copper (Cu))
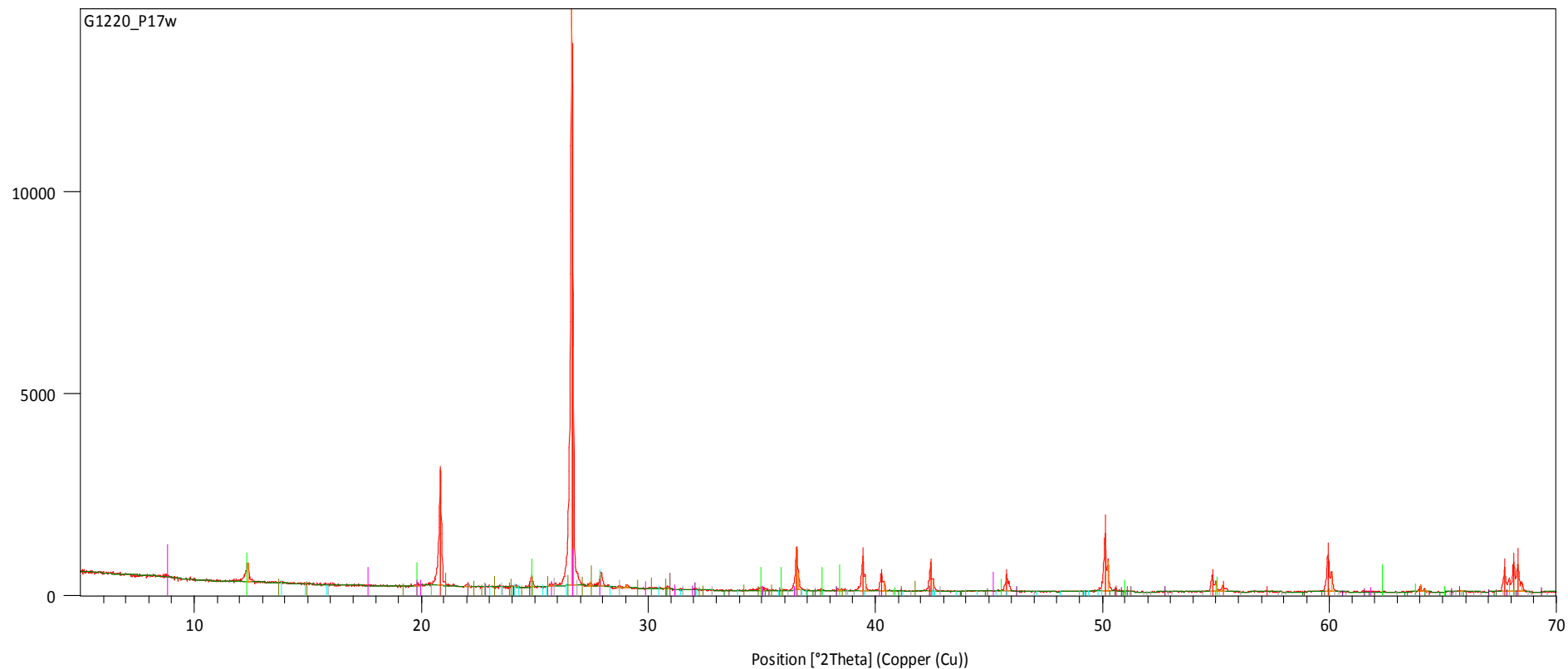
| | |
|---|---|
| Peak List | |
| Quartz, syn | |
| Albite, ordered | |
| Microcline, inter | |
| Barite | |
| Dolomite | |
| Ankerite | |
| Siderite | |
| Kaolinite 1Md | |
| Illite-2\ITM#1\RG | |
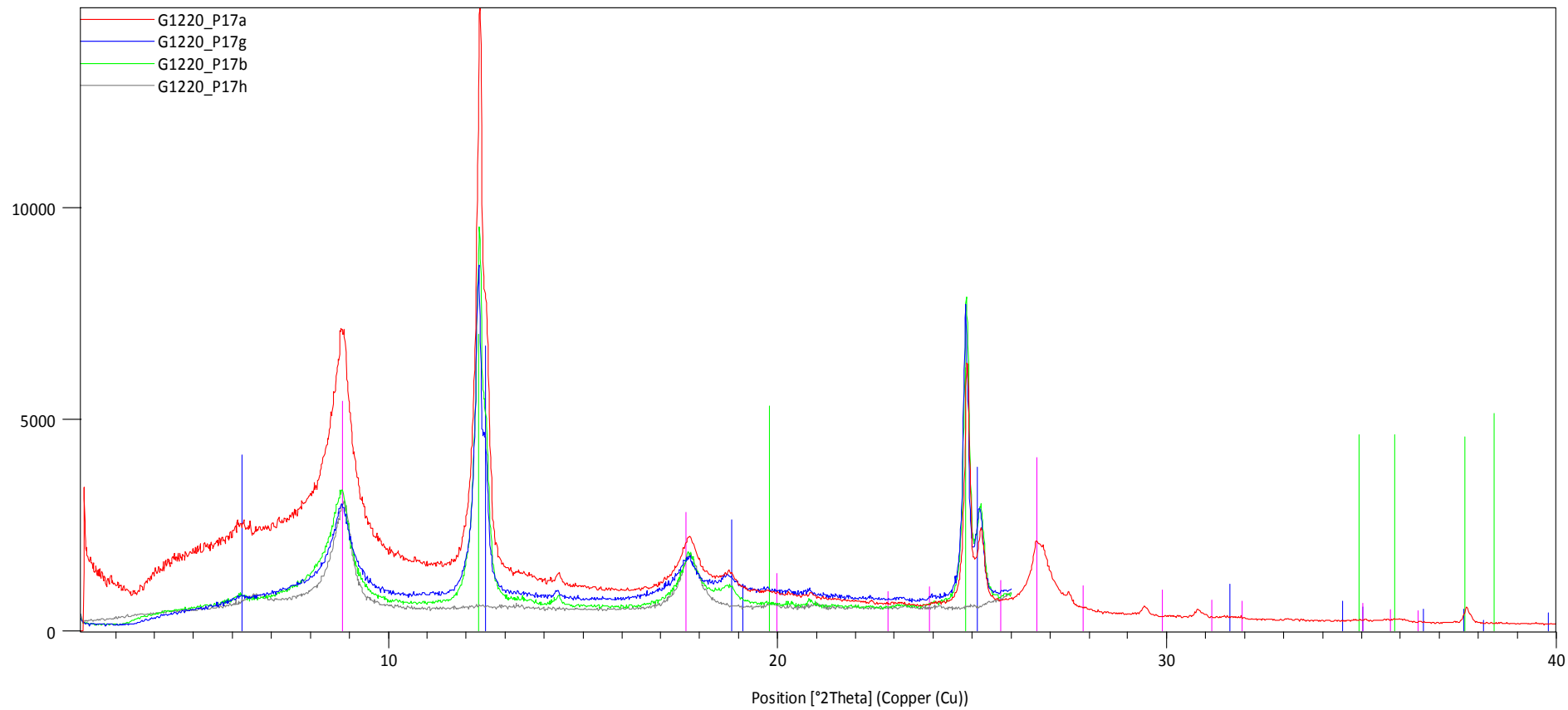
Counts



G1220_P18w

Position [°2Theta] (Copper (Cu))
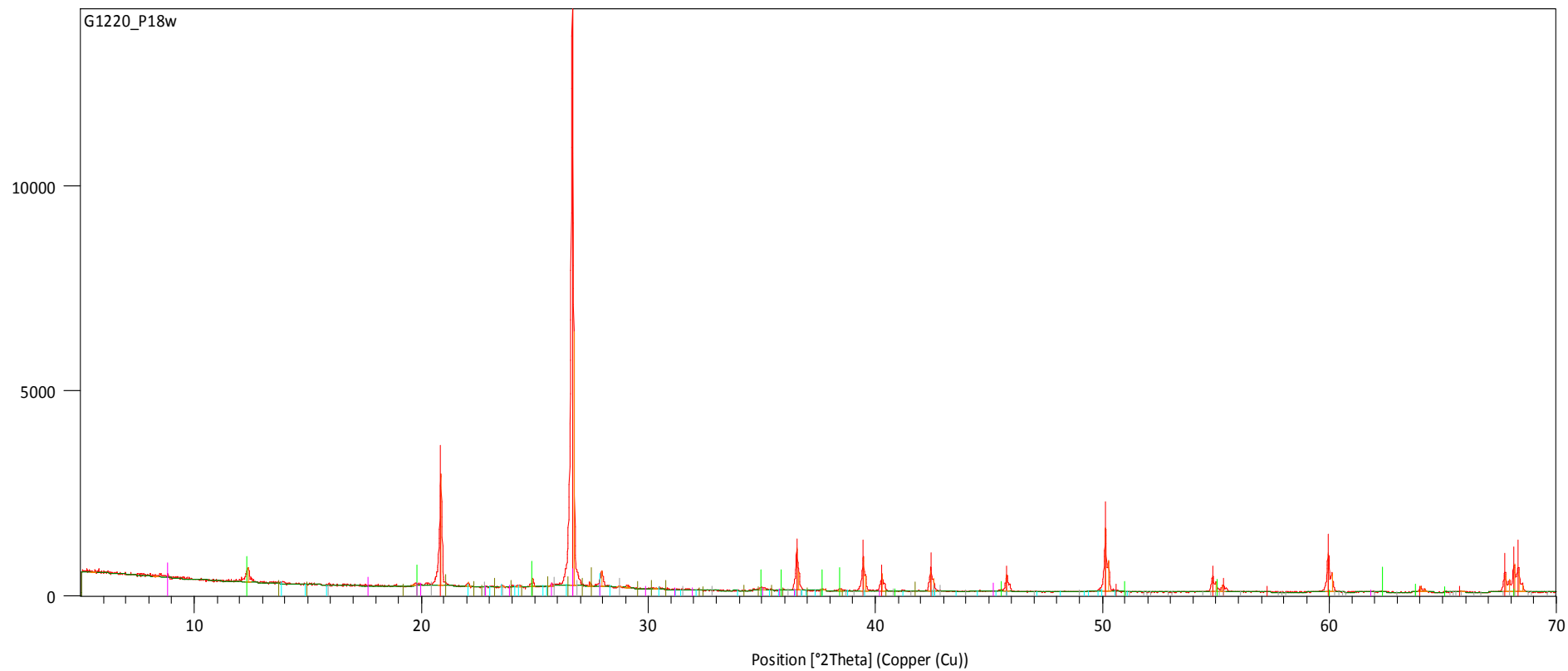
Peak List

Quartz, syn

Albite, ordered

Microcline, inter

Barite

Kaolinite 1Md
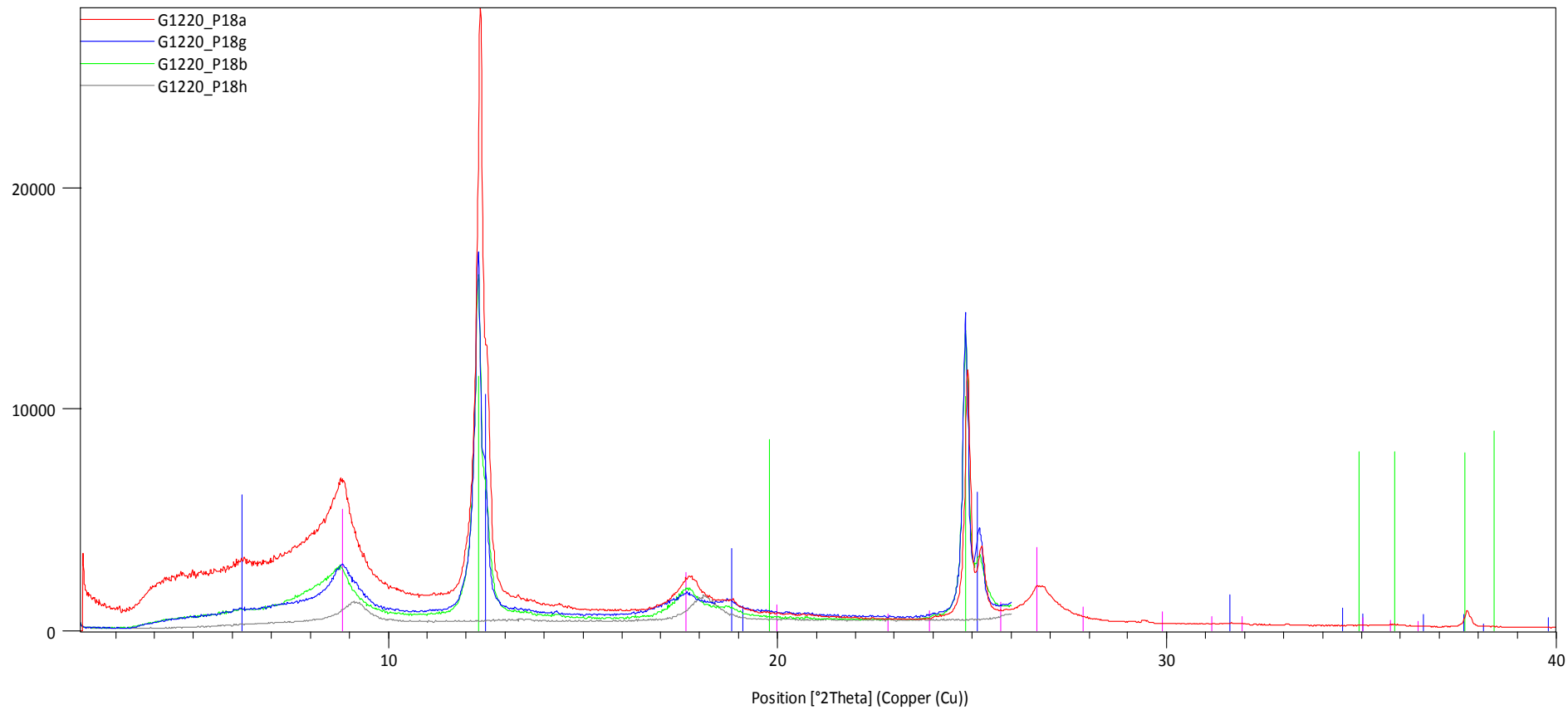
Illite-2\ITM#1\RG

Counts



G1220_P19w

Position [°2Theta] (Copper (Cu))
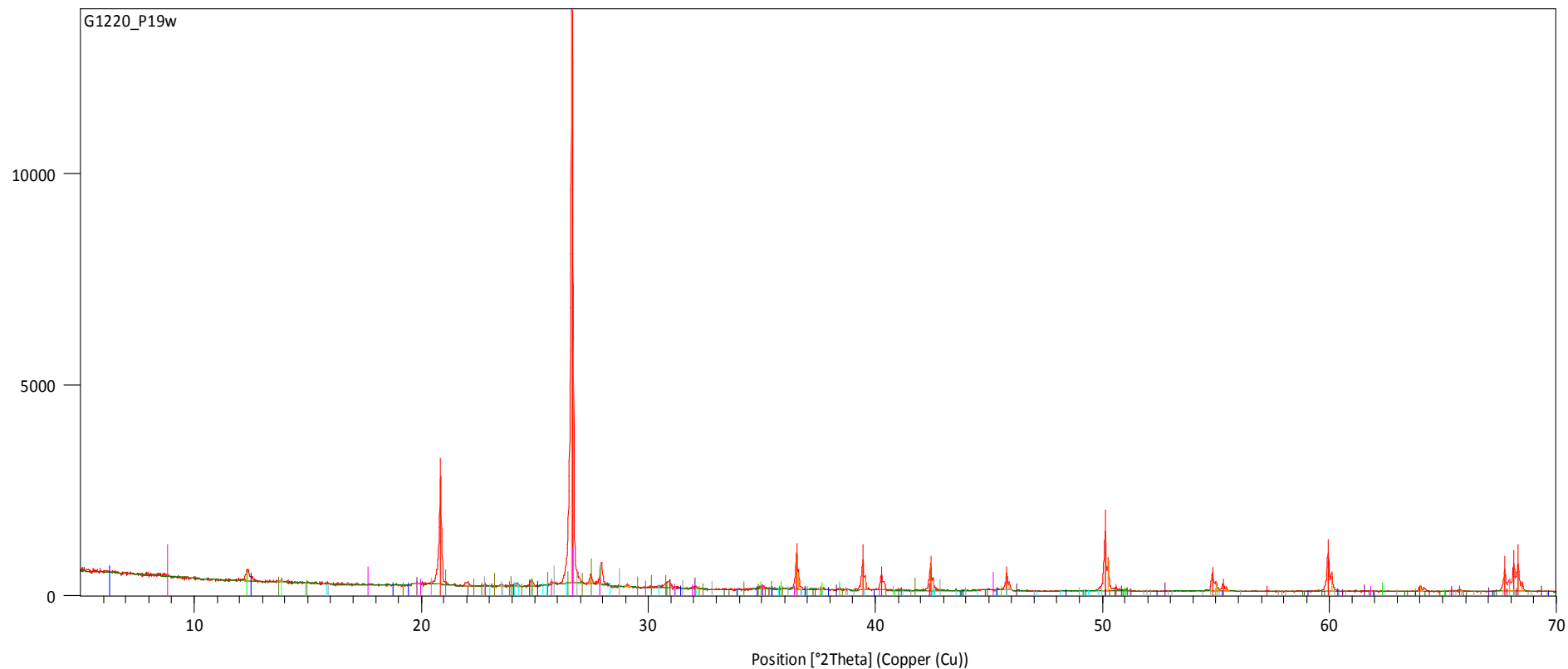
Peak List
Quartz, syn
Albite, ordered
Dolomite
Ankerite
Microcline, inter
Barite
Siderite
Kaolinite 1Md
Clinochlore-1\ITM#I#l#b\RG, ferrian
Illite-2\ITM#1\RG
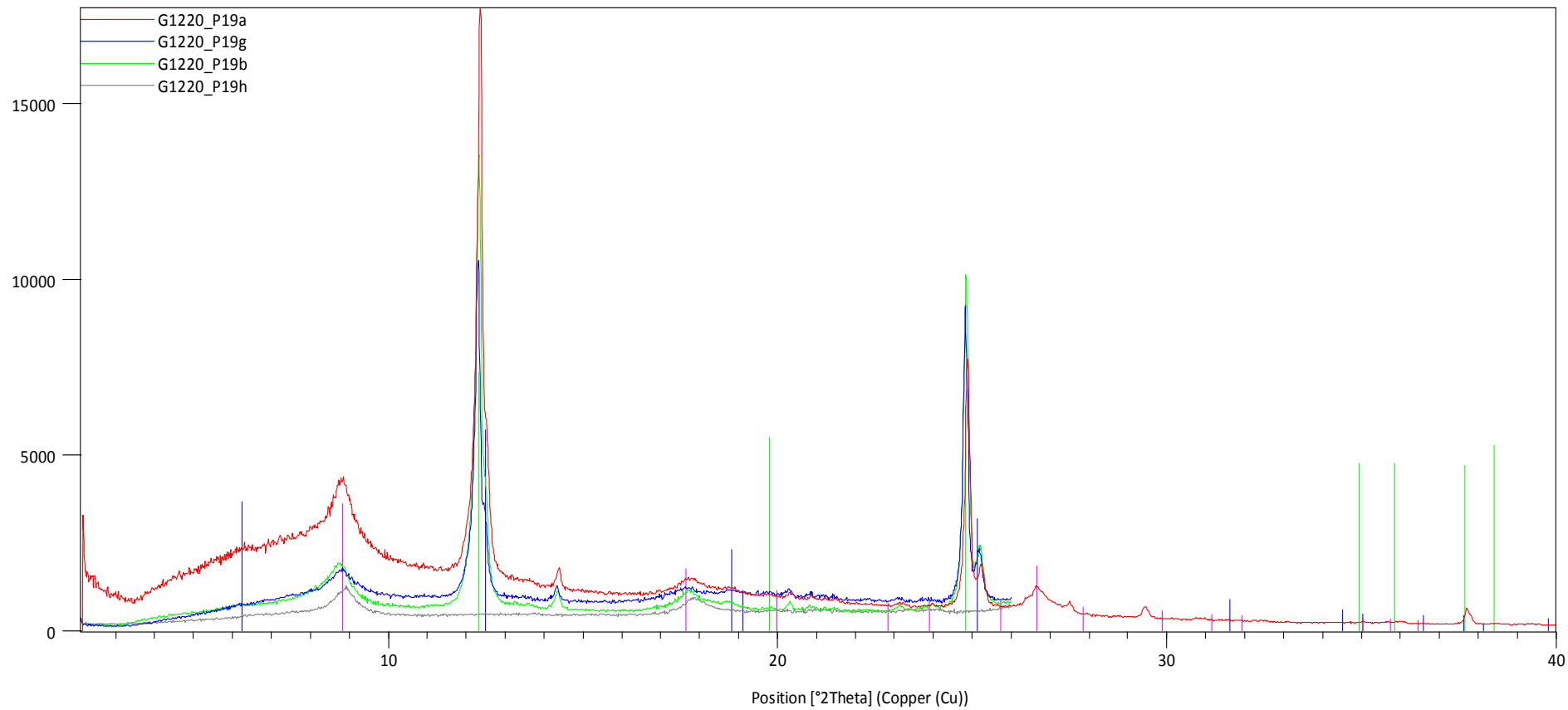
Counts

G1220_P20w

10000

5000

0

Position [°2Theta] (Copper (Cu))

10    20    30    40    50    60    70
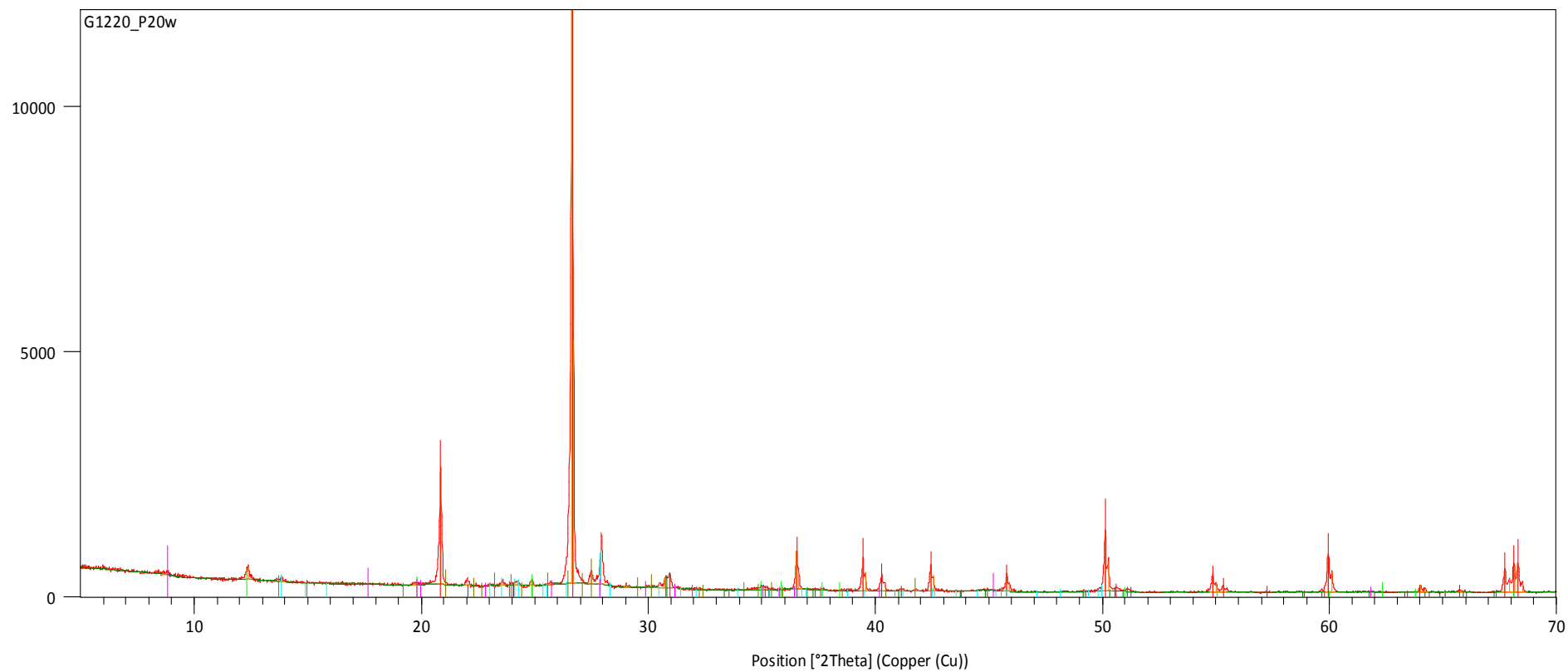
Peak List

Quartz, syn

Albite, ordered

Ankerite

Microcline, inter

Dolomite

Kaolinite 1Md
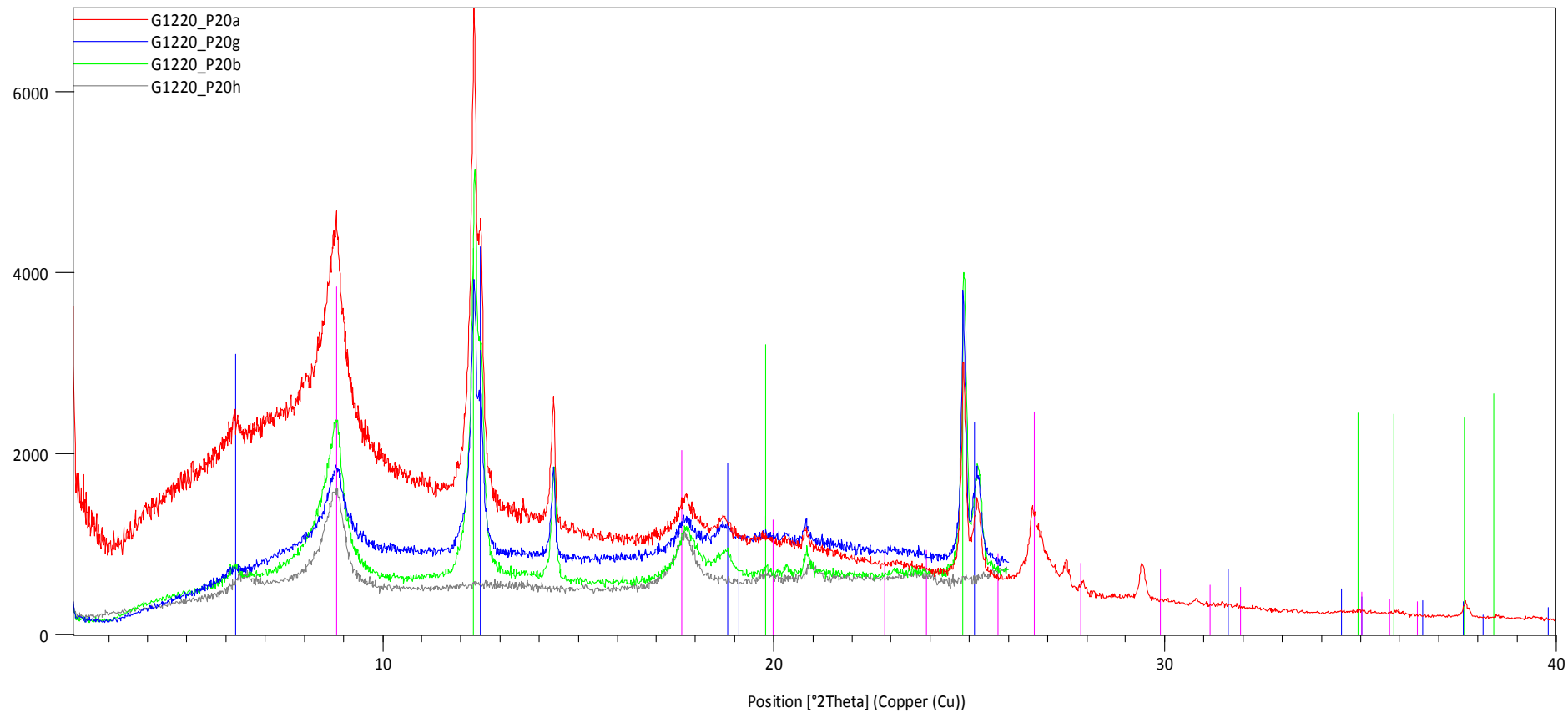
Illite-2\ITM#1\RG

Counts

G1220_P21w

10000

5000

0



Position [°2Theta] (Copper (Cu))
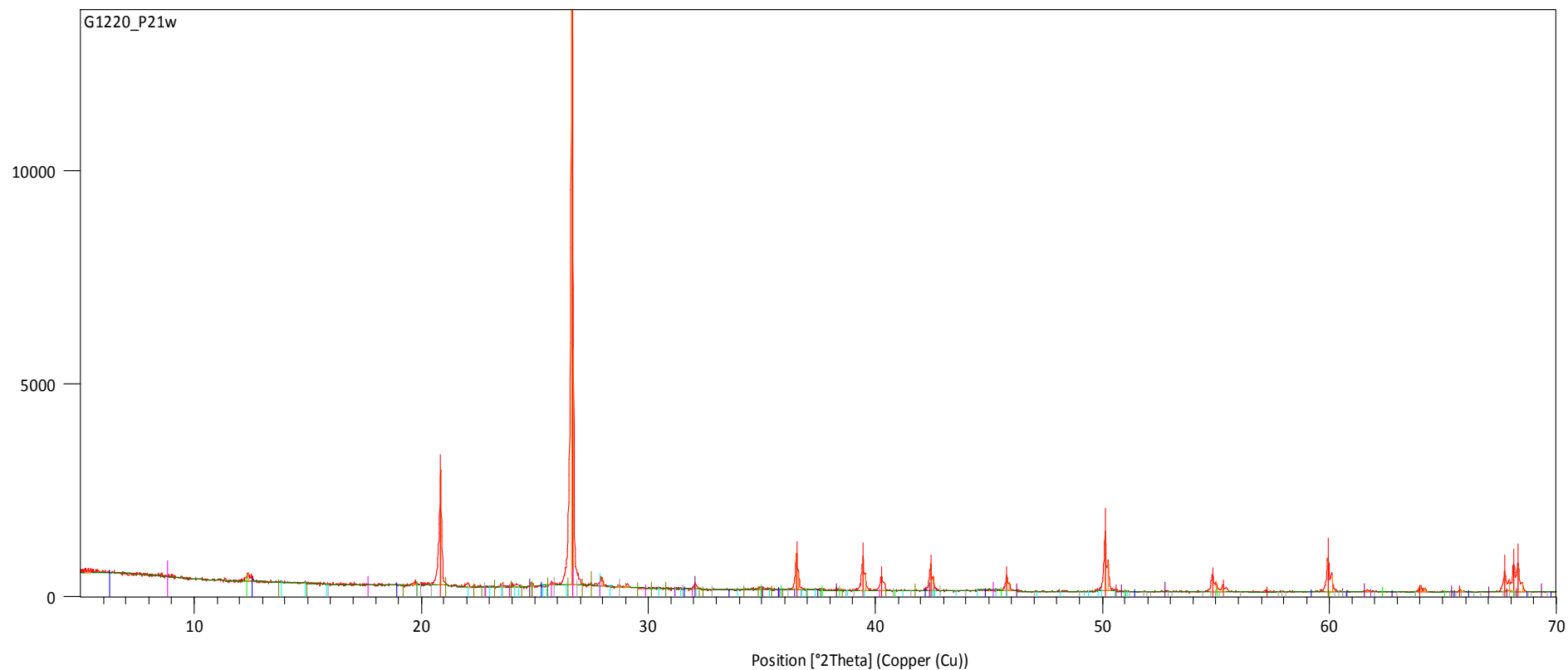
Peak List
Quartz, syn
Albite, ordered
Illite-2\ITM#1\RG
Kaolinite 1Md
Clinochlore
Siderite
Barite
Microcline, inter
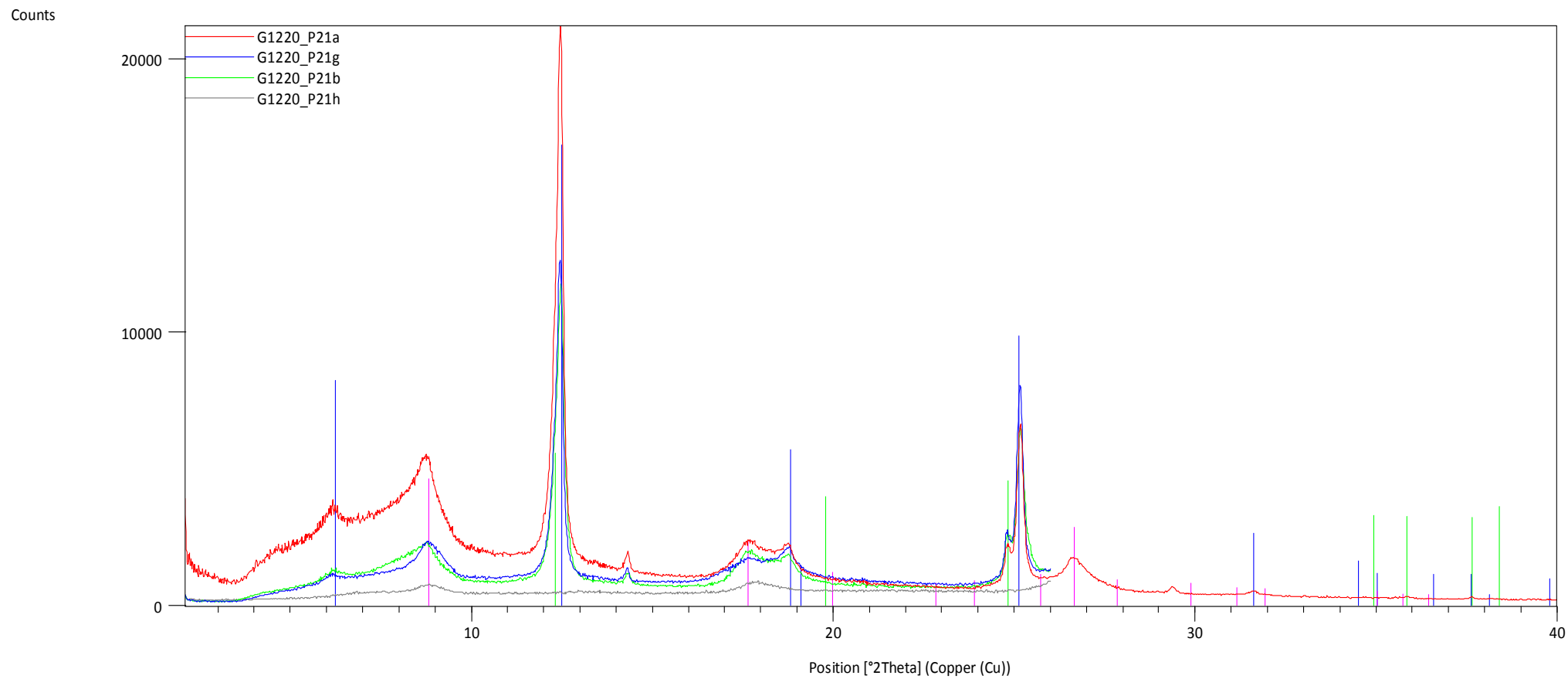
Counts



G1220_P22w

10000

5000

0

10        20        30        40        50        60        70

Position [°2Theta] (Copper (Cu))
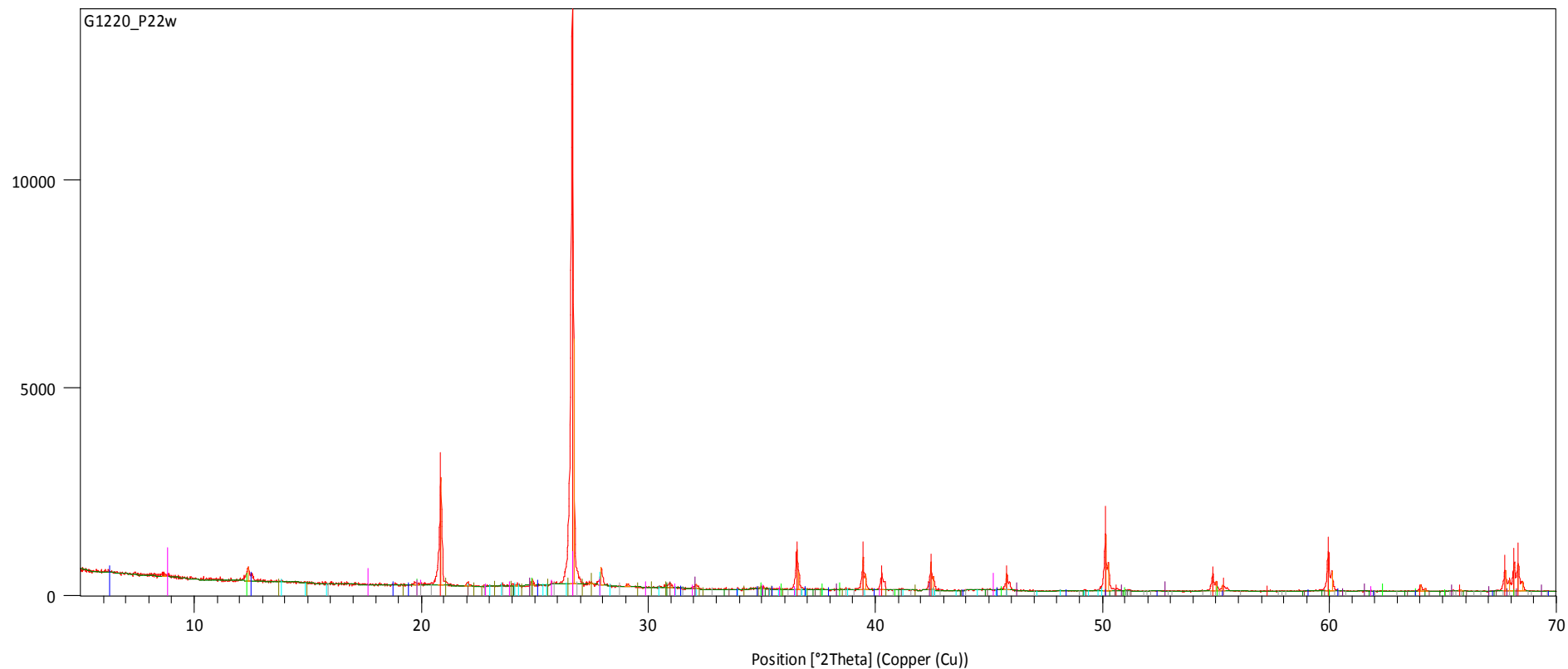
Peak List
Quartz, syn
Albite, ordered
Dolomite
Ankerite
Kaolinite 1Md
Illite-2\ITM#1\RG
Barite
Microcline, inter
Siderite
Clinochlore-1\ITM#I#I#b\RG, ferrian
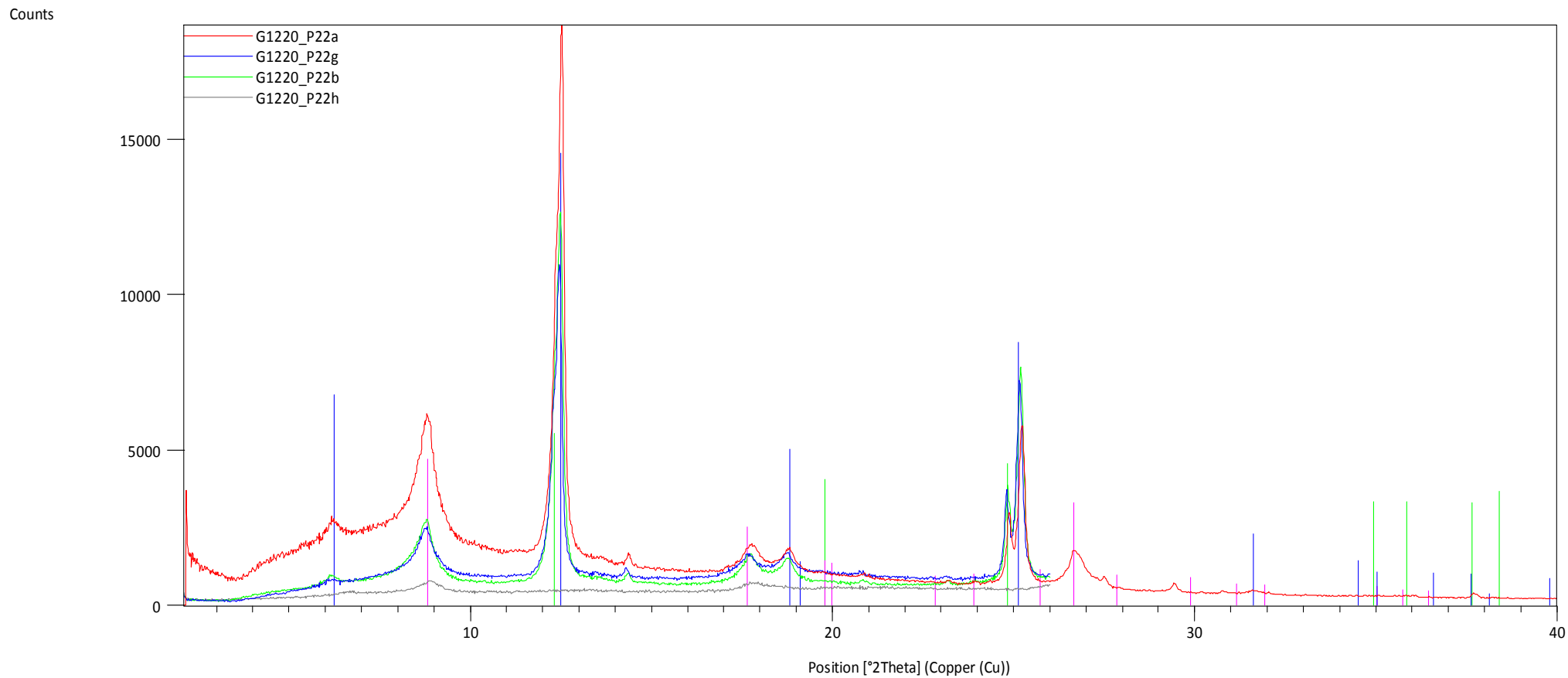
Counts

G1220_P23w



Position [°2Theta] (Copper (Cu))
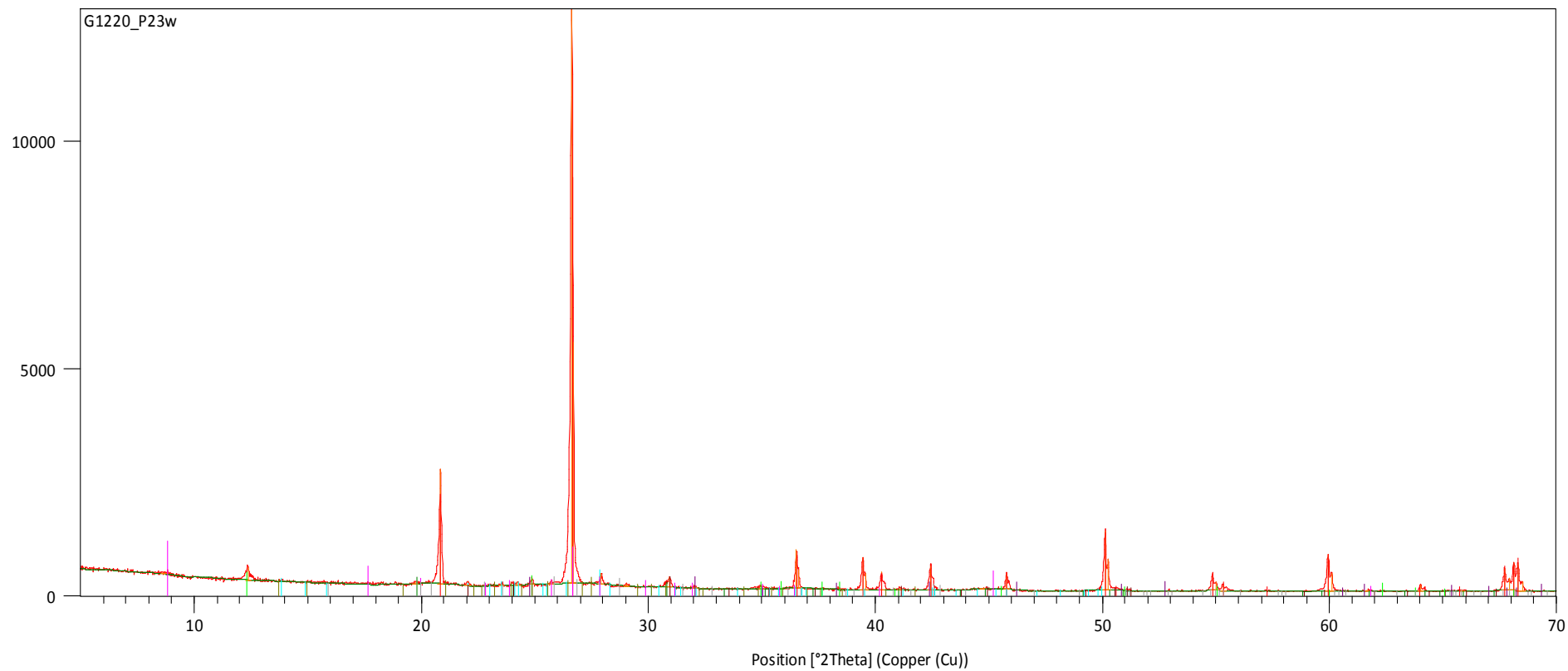
| Peak List |
| Quartz, syn |
| Ankerite |
| Albite, ordered |
| Illite-2\ITM#1\RG |
| Dolomite |
| Kaolinite 1Md |
| Barite |
| Microcline, inter |
| Siderite |
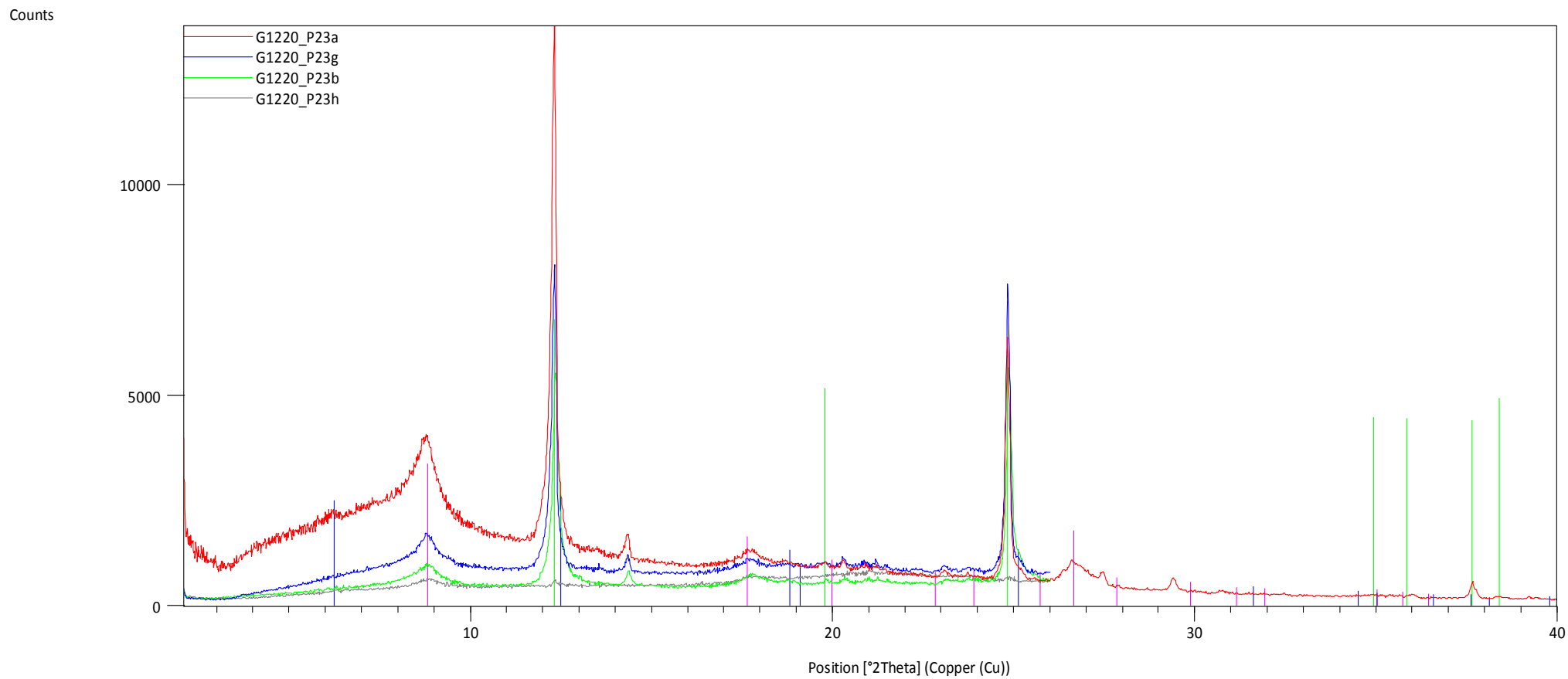
Counts



G1220_P24w

Position [°2Theta] (Copper (Cu))
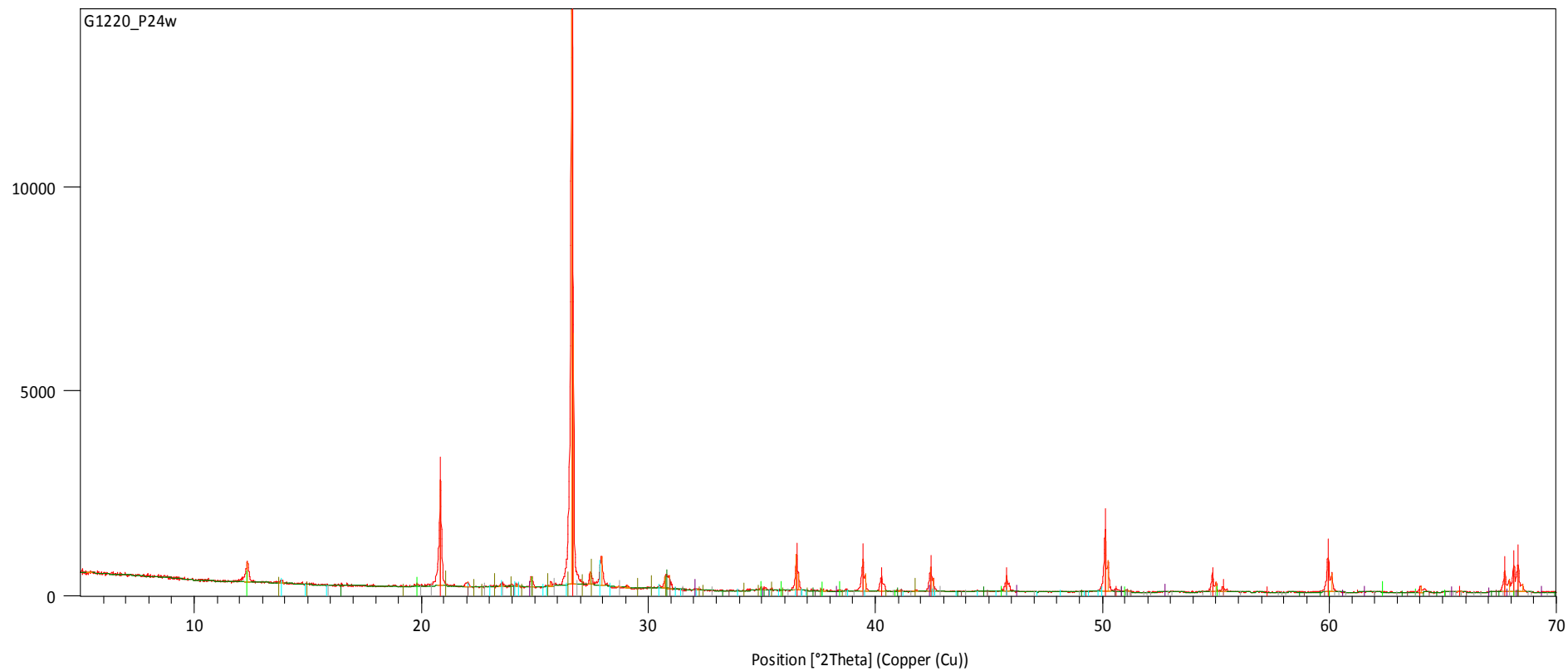
Peak List
Quartz, syn
Albite, ordered
Ankerite
Dolomite
Kaolinite 1Md
Barite
Microcline, inter
Siderite
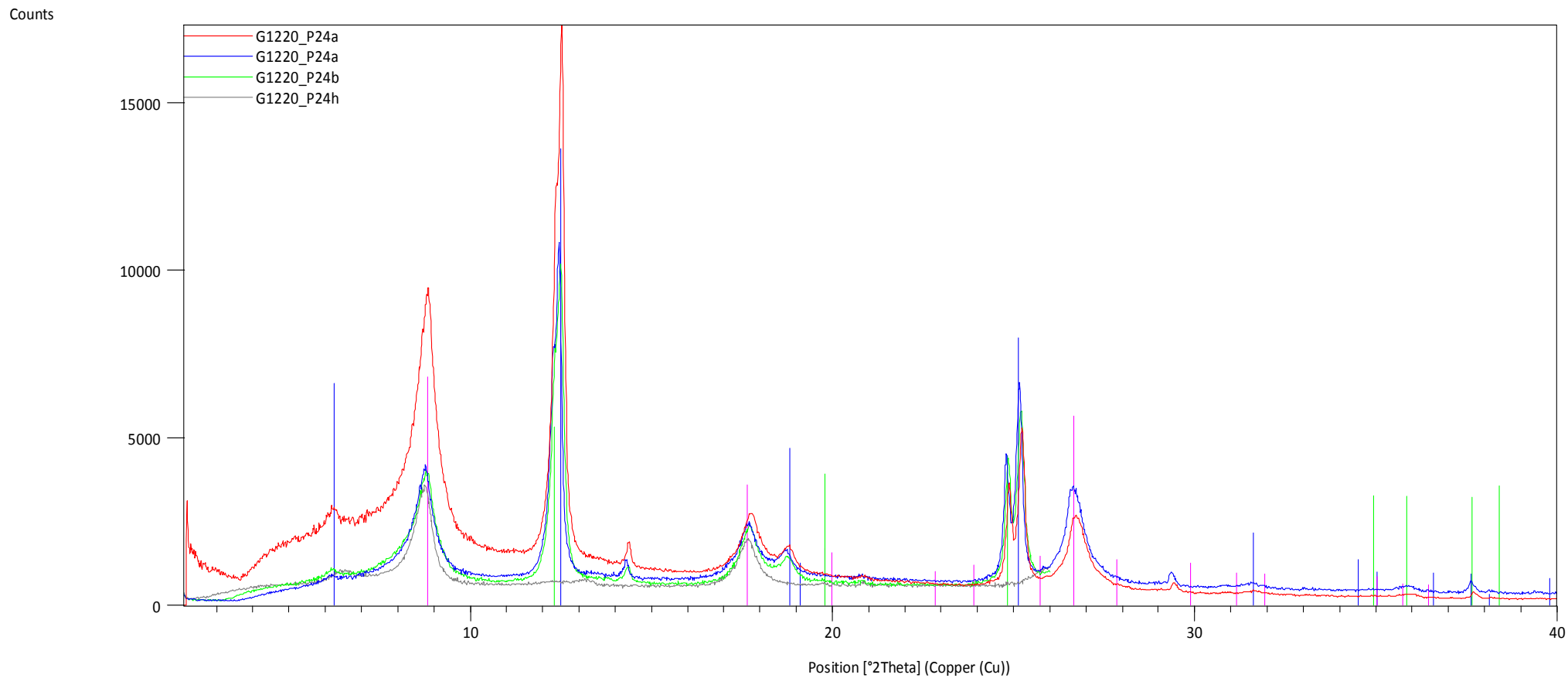
Counts

15000

10000

5000

0

G1220_P24a
G1220_P24a
G1220_P24b
G1220_P24h

10    20    30    40

Position [°2Theta] (Copper (Cu))

Peak List

Clinochlore-1\ITM#I#I#b\RG, ferroan

Illite-2\ITM#1\RG

Kaolinite 1Md

Counts

G1220_P25w



Position [°2Theta] (Copper (Cu))
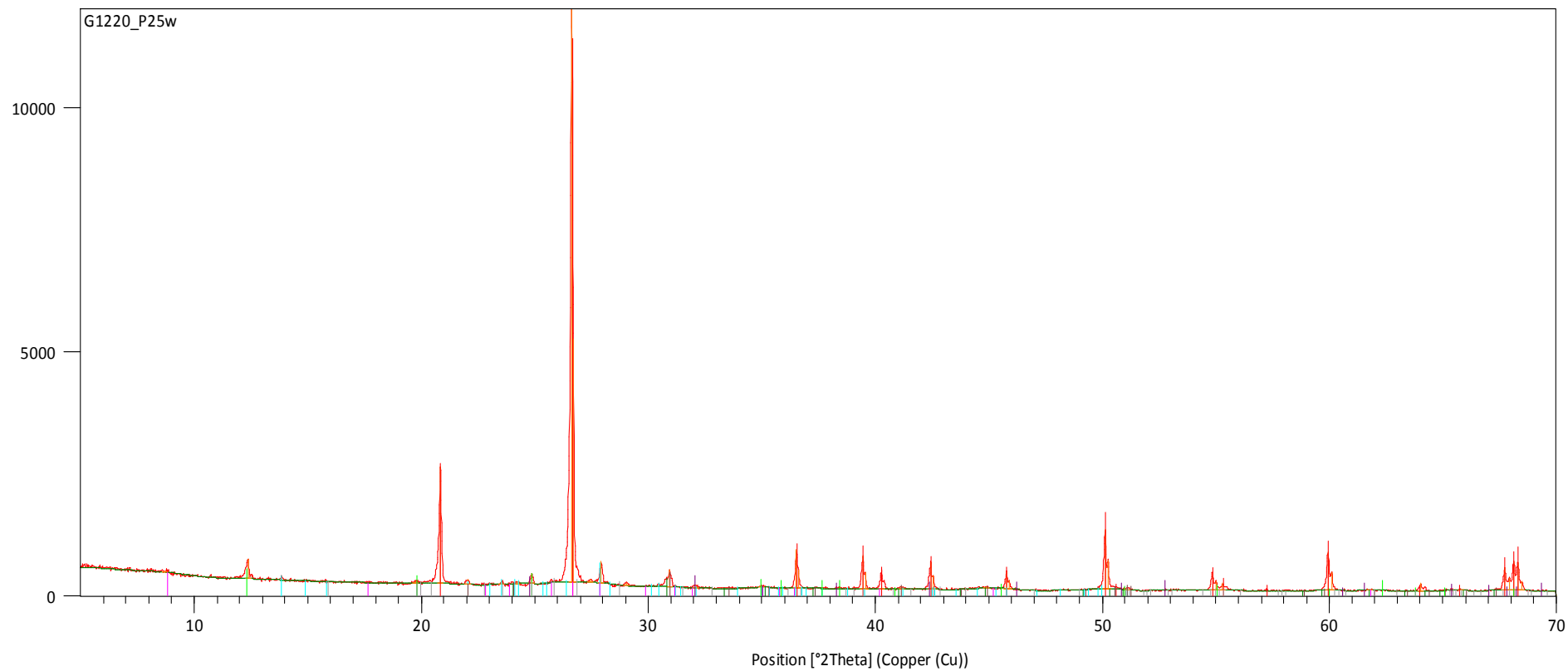
Peak List
Quartz, syn
Ankerite
Albite, ordered
Dolomite
Illite-2\ITM#1\RG
Kaolinite 1Md
Barite
Siderite